Anatomy of cast glass

The effect of casting parameters on the meso-level structure and macro-level structural performance of cast glass components

Bristogianni, T.

DOI
10.4233/uuid:8a12d0b1-fee2-47f1-9fa9-ff56ab2e84c1

Publication date
2022

Document Version
Final published version

Citation (APA)
Bristogianni, T. (2022). *Anatomy of cast glass: The effect of casting parameters on the meso-level structure and macro-level structural performance of cast glass components* . [Dissertation (TU Delft), Delft University of Technology]. https://doi.org/10.4233/uuid:8a12d0b1-fee2-47f1-9fa9-ff56ab2e84c1

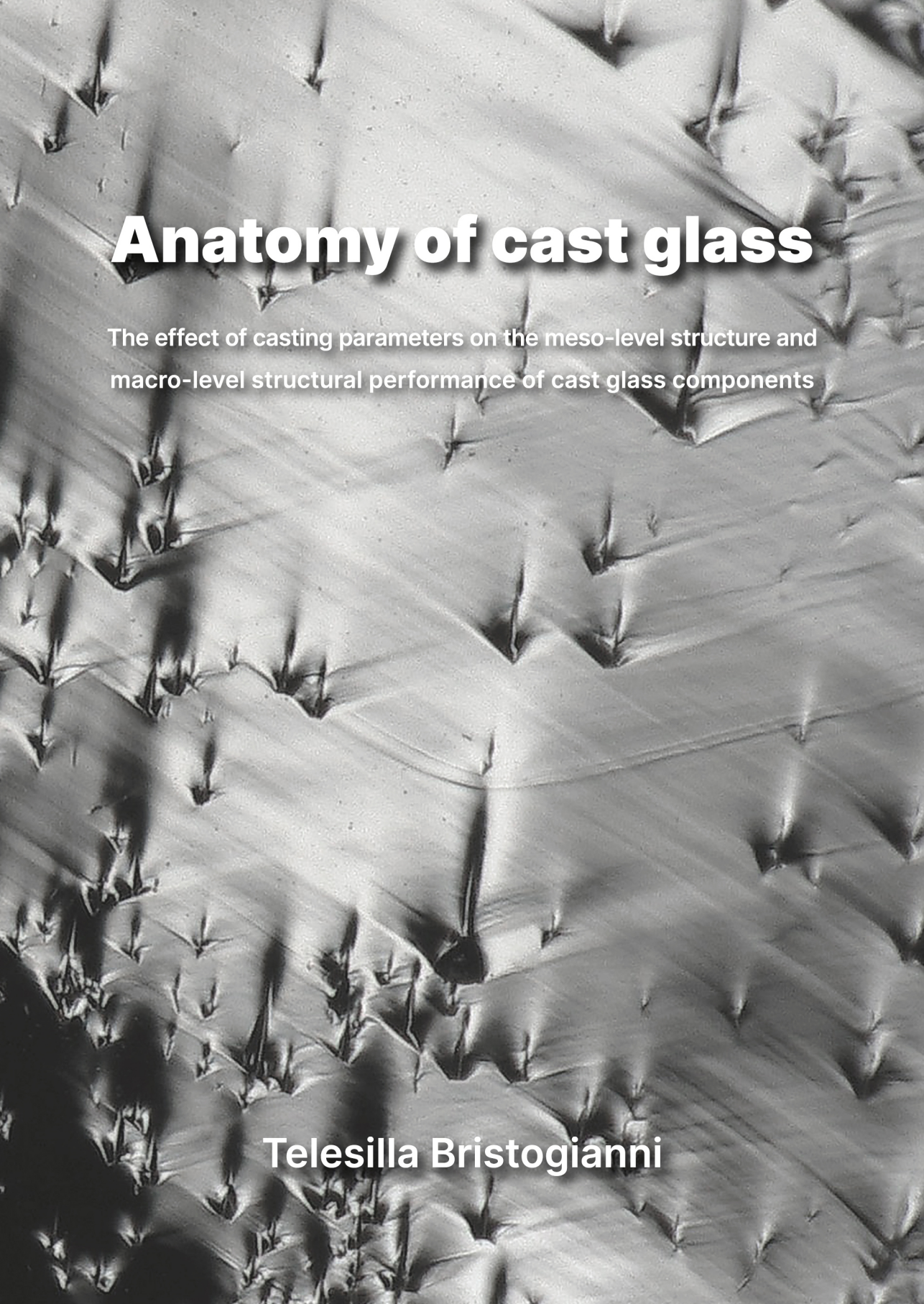

Anatomy of cast glass

The effect of casting parameters on the meso-level structure and macro-level structural performance of cast glass components

Telesilla Bristogianni

Anatomy of cast glass

The effect of casting parameters on the meso-level structure and macro-level structural performance of cast glass components

Anatomy of cast glass

The effect of casting parameters on the meso-level structure and macro-level structural performance of cast glass components

Dissertation

for the purpose of obtaining the degree of doctor

at Delft University of Technology,

by the authority of Rector Magnificus prof. dr. ir. T. H. J. J. van der Hagen

chair of the Board for Doctorates

to be defended publicly on

Friday, 25th of November 2022 at 12:30 o' clock

by

Telesilla BRISTOGIANNI

Master of Science in Building Technology, Delft University of Technology, The Netherlands

Master in Architectural Engineering, National Technical University of Athens, Greece

born in Athens, Greece

This dissertation has been approved by the promotors.

Composition of the doctoral committee:

Rector Magnificus	chairperson
Prof. ir. R. Nijsse	Delft University of Technology, promotor
Dr. ir. F. A. Veer	Delft University of Technology, promotor

Independent members:

Prof. Dr. ir. P. C. Louter	Delft University of Technology
Prof. Dr. M. Overend	Delft University of Technology
Prof. Dr. R. J. Hand	The University of Sheffield, UK
Dr. M. Prassas	Corning Incorporated, France
Dr. K. C. Datsiou	University of Hertfordshire, UK
Prof. Dr. ir. L. J. Sluys	Delft University of Technology, reserve member

Keywords: Cast glass, glass strength, glass defects, casting process, flexural strength, fracture resistance, glass recycling, meso-level structure, glass fractography

Printed by: Druk. Tan Heck, Delft

Cover by: T. Bristogianni
Cover image: Gull wings at the crack front of a split soda lime silica cast glass specimen.

ISBN: 9789068240740

An electronic version of this dissertation is available at *http://repository.tudelft.nl/*

To my parents and brother,

Ευτυχία, Πέτρος και Υπερίων

Previous page: Lead silica glass of various colours recycled by kiln-casting at 870ºC, using the flowerpot method.

Preface

Glass, in our daily experience, is clear, perfect, flawless. By habit, our eyes pass through the material and focus on the object behind, as if glass itself is absent, devoid of substance.

What a surprise to our eyes, when encountering a piece of cast glass for the first time! A multitude of imperfections creates pathways for our eyes to follow and marks for our eyes to stop. This world of imperfections, threaded into the amorphous structure of cast glass, forms unique identities and reminds us of the way each piece of glass was made. Imperfections are inherent to cast glass, adding beauty and subtracting strength; properties will vary per identity.

Through this dissertation, you are presented with a study of anatomy. Hundreds of cast glass specimens were created, sliced and observed, in search of these identities and the strength of cast glass. And though we may be far from mastering this knowledge, through the learning process, the wonderful potential of cast glass is starting to unfold in front of us.

Summary

Cast glass has great application potential in the architectural realm. By casting, freeform, volumetric glass components can be achieved that take full advantage of glass's significant compressive strength, facilitating in particular the load-bearing implementation of cast glass in the built environment. Only within the last two decades, have we seen the exploration of the structural potential of cast glass in a limited number of realized architectural projects such as the Atocha Memorial and the Crystal Houses façade. Despite the possibilities and attractiveness of cast glass, designers, engineers and developers are, from an early design stage, hesitant to employ cast glass; the limited available and craft-based manufacturing facilities, the uncertain quality of the product, the missing engineering data and quality control processes and the uncertainties linked with the structural application of cast glass, lead to discouraging high cost/ high risk solutions. Within the listed challenges and uncertainties, perhaps the most striking is our inability to answer the most obvious question: what is the strength of cast glass? A simple answer to this question does not exist, as the mechanical properties of cast glass vary from product to product, and are directly influenced by the employed chemical composition, thermal history, and casting process. Adding to this complexity, further questions over the mechanical properties and quality arise, once waste (contaminated) glass cullet and lower processing temperatures are used, in the efforts of reducing the environmental impact of cast glass components.

Focusing on this knowledge gap, the aim of this work is to develop an understanding of the effect of the casting parameters on the meso-level structure of cast glass, and thereupon of the relationship between this meso-level structure and the strength, stiffness and fracture resistance of cast glass components. Towards this aim, three main research questions are formed in this dissertation:

- What is the correlation between casting parameters and defect formation, and can the location and features of inhomogeneities and meso-level structures within the cast glass be controlled?
- How do inhomogeneities at the surface and in the glass bulk affect the strength, stiffness and crack propagation of cast glass components? Can the criticality of such defects be ranked according to their type, shape and arrangement and how does the chemical composition affect the strength and the response to stress concentrations around a flaw?
- Can waste glass cullet and lower forming temperatures be used for casting sustainable structural glass components, and what are the implications regarding the compositional varieties and contamination rates?

Tackling the posed research questions, this dissertation adopts an experimental approach based on physical prototyping and destructive and non-destructive testing. The research work is organized in three stages. Stage 1 involves the conduction of melting and casting experiments using various casting parameters, the study of the observed meso-level structures, and the correlation of these meso-level structures to the casting parameters. Lower processing

temperatures –achieved by using the kiln-casting method, and contaminated waste glass cullet are predominately used in order to intensify the creation of defects and meso-level structures in the glass, and facilitate the studying and correlation process. Characterization techniques such as X-Ray Fluorescence, X-Ray Diffraction, Differential Scanning Calorimetry, Cross polarization and microscopy are used to identify the obtained glasses and encountered defects. Stage 2 focuses on specimen prototyping and mechanical testing, with the aim to correlate the casting parameters to the obtained meso-level structures and further on to the resulting mechanical properties. The mechanical testing investigates to what extent the obtained flaws are affecting the flexural strength, stiffness and fracture resistance of the specimens. Experimental procedures include 4-point bending tests on 30x30x240mm and 20x30x350mm cast specimens made by using various silicate-based compositions and firing schedules, splitting tests on 50mm cubic specimens of similar characteristics and impulse excitation measurements. The size factor effect is also investigated by comparing the obtained experimental results. Fractographic techniques are used to interpret the critical defects and the interaction of the crack path with the encountered defects. Stage 3 gathers the conclusions of the prior research stages and drafts the outline for further work. Given the limited number of experimental data (the followed prototyping methods allowed for the casting and post-processing of only a small number of repetitions per specimen type) the conclusions of this work are of necessity qualitative. All results are indicative and not statistically valid for design purposes. Nonetheless, the obtained data are useful in establishing relationships between the flexural strength, stiffness and fracture resistance of the tested cast glass types, and their chemical composition, thermal profile and defect network.

The experimental work shows that by kiln-casting, a larger variety of chemical compositions can be cast, even at relatively low processing temperatures. As a consequence, a broad range of mechanical properties arises, especially when waste cullet is employed. Based on the casting parameters, combinations of different defects, grouped in meso-level structures, are commonly found in cast glass. Meso-level structures in the bulk are often tolerable, but if exposed at the surface, they play a strength reducing role according to their type, shape, orientation and interaction to other defects. Defects can be classified in intrinsic and extrinsic, with the latter being potentially more critical, depending on the variation in thermal expansion between the defect and the glass matrix. Extrinsic defects can be avoided by increasing the purity of the batch/cullet, while intrinsic defects are more challenging to avoid as they are inherently linked to the casting process. Intrinsic defects, specifically, are related to the consecutive interface transformations that occur above the glass transition temperature between deposited glass cullet pieces in a mould or within an accumulated coiling stream of poured glass inside a mould. Unless much higher temperatures leading to homogenization by diffusion and mechanically stirring are imposed, intrinsic meso-level structures retain a shape memory of the original cullet or pouring sequence. By adjusting the firing schedule and cullet type, shape and deposition method, meso-level structures can be deliberately engineered within a glass component. Inhomogeneous zones at the meso-level structure level in the form of cord, bubble veils or crystalline zones, however, do not form a barrier which is sufficient to arrest cracks. Crystalline zones and tack fused zones, on the other hand, can locally redirect a low energy crack.

Experimental testing further shows that the flexural strength of cast glass is defined mainly by its chemical composition and defect characteristics. The quality of the surface and proximity zone is of most crucial importance, while the inhomogeneities in the bulk rarely affect the mechanical performance, unless a high defect population is present. Subtle network alterations due to thermal history will not be usually noticed, but distinct defects related to the chosen thermal profile, such as crystallization or bubble veils, can significantly reduce the strength (by up to 75%) if exposed to the surface. The Young's modulus of cast glass is determined mainly by the chemical composition (bond strength and packing density), but the firing schedule may impose an alteration in the order of 3%. The fracture resistance of cast glass under a pressing sharp load is mainly dependent on the chemical composition and thermal history, and consists of two steps: crack initiation resistance -where an open network is favourable- and fracture propagation resistance- where a high surface fracture energy is required. Reverse ranking between flexural strength and fracture resistance is reported among different chemical compositions, due to the different fracture mechanisms involved between contact and far field stresses, showing that one type of test alone may be insufficient for determining the structural performance of a cast glass component. Nonetheless, the improvement of the surface by engineering composite glasses can improve both the flexural strength and fracture resistance of cast glass. Concluding on the experimental results, waste glass cullet and lower melting temperatures can still produce structurally reliable glass components.

Based on the conclusions of this work and its limitations, further testing is required to obtain a better understanding and hard numbers on the mechanical properties of cast glass. This does not only refer to a broader set of mechanical tests, repetition of the results and statistical prediction, but also to the development of defect mapping and characterization techniques, as well as testing procedures suitable for cast glass that overcome the challenges imposed by characterizing voluminous components. The results of this work also highlight the potential of developing composite cast glasses, using a combination of low and high grade compatible glasses, without compromising the strength. In fact, given that defects situated in the bulk of voluminous components are rarely activated during loading- impure cullet sources can be safely situated in the bulk, while stronger, purer glass streams are used to form the surface layer and are responsible for the strength and fracture resistance of the component. The further exploration of recycling by casting is perhaps of the outmost importance, as this technique enables the recycling of glass waste streams currently considered impossible to recycle, due to contrasting chemical compositions and embedded contamination. The recycling of a wider variety of commercial glass waste types, including specialty glasses, glass ceramics, quartz, aluminosilicate, and wired glass should be explored. For the successful implementation of cast glass in the built environment, and in particular in structural applications, any product and system development must be supported by manufacturing guidelines, test data, product certifications and quality control protocols.

Samenvatting

Gegoten glas heeft een groot en nog amper verkend potentieel binnen de architectuur. Door het gieten kunnen 3D glascomponenten worden gerealiseerd die ten volle gebruik maken van de aanzienlijke druksterkte van glas, waardoor met name de dragende toepassing van gegoten glas in de gebouwde omgeving wordt ontsloten. In de laatste twee decennia is de verkenning van het structurele potentieel van gegoten glas aangetoond in een beperkt aantal architectonische projecten, zoals het Atocha Memorial en de gevel van de Crystal Houses. Ondanks de mogelijkheden en aantrekkelijkheid van gegoten glas, aarzelen ontwerpers, ingenieurs en ontwikkelaars om gegoten glas toe te passen; de beperkt beschikbare en ambachtelijke productiefaciliteiten, de onzekere kwaliteit van het product, een gebrek aan technische data, niet gestandaardiseerde kwaliteitscontroleprocessen en de onzekerheden bij structurele toepassing van gegoten glas, leiden tot ontmoedigende oplossingen met zowel hoge kosten als hoge risico's. Binnen de opgesomde uitdagingen en onzekerheden is de meest in het oog springende misschien wel ons onvermogen om de meest basale vraag te beantwoorden: wat is de sterkte van gegoten glas? Een eenvoudig antwoord op deze vraag bestaat niet, aangezien de mechanische eigenschappen van gegoten glas van product tot product verschillen en worden beïnvloed door de gebruikte chemische samenstelling, de thermische geschiedenis en het gietproces. De complexiteit wordt nog verder vergroot omdat er vragen rijzen over de mechanische eigenschappen en de kwaliteit als (verontreinigde) glasscherven en lagere verwerkingstemperaturen worden gebruikt, om de milieu-impact van gegoten glascomponenten te verminderen.

Om dit gat in de kennis te helpen dichten beoogt dit werk inzicht te verwerven in het effect van de gietparameters op de meso-structuur van gegoten glas, en dus de relatie tussen deze materiaal meso-structuur en de resulterende sterkte, stijfheid en breukweerstand van gegoten glascomponenten. Met dit doel voor ogen zijn drie hoofdonderzoeksvragen geformuleerd:

- Wat is de correlatie tussen de gietparameters en het ontstaan van defecten; kunnen de locatie en kenmerken van defecten en meso-structuren in het gegoten glas worden gecontroleerd?

- Hoe beïnvloeden defecten aan het oppervlak en in de glasmassa de sterkte, stijfheid en scheurgroei van gegoten glascomponenten? Kan het effect van dergelijke defecten worden gerangschikt op basis van hun type, vorm en rangschikking en wat is de rol van de chemische samenstelling op de sterkte en de reactie op spanningsconcentraties rond een defect?
- Kunnen glasscherven en lagere verwerkingstemperaturen worden gebruikt voor het gieten van duurzame structurele glascomponenten, en wat zijn de implicaties met betrekking tot de samenstellingsvariëteiten en toelaatbare verontreinigingspercentages?

Om de gestelde onderzoeksvragen te beantwoorden, wordt in dit proefschrift een experimentele aanpak gehanteerd gebaseerd op fysische prototyping en zowel destructieve als niet-destructieve testen. Het onderzoekswerk is georganiseerd in drie fasen. Fase 1 omvat het uitvoeren van smelt-

en gietexperimenten met verschillende gietparameters, het bestuderen van de waargenomen meso- structuren, en de correlatie van deze meso-structuren met de gietparameters. Er wordt voornamelijk gebruik gemaakt van lagere procestemperaturen – mogelijk door in de oven zelf te gieten - en verontreinigde glasscherven om het ontstaan van defecten en mesoniveaustructuren in het glas te intensiveren, en het bestuderen en correleren te vergemakkelijken. Karakteriseringstechnieken zoals röntgenfluorescentie, röntgendiffractie, differentiële scanning calorimetrie, gebruik van gekruiste polarisatie filters en digitale microscopie worden gebruikt om de verkregen glazen proefstukken en aangetroffen defecten te karakteriseren. Fase 2 is gericht op het maken van prototypes van proefstukken en op mechanische proeven, met als doel de gietparameters te correleren aan de verkregen structuren op meso-niveau en de resulterende mechanische eigenschappen. De mechanische testen onderzoeken in welke mate de geproduceerde defecten de buigsterkte, stijfheid en breukweerstand van de proefstukken beïnvloeden. Experimentele procedures omvatten 4-punts buigproeven op 30x30x240mm en 20x30x350mm gegoten proefstukken; gemaakt door gebruik te maken van verschillende silicaat samenstellingen en bakschema's; te beproeven via splijtproeven op vergelijkbare 50mm brede kubusvormige proefstukken en impuls excitatie metingen. Het effect van de proefstuk grootte wordt ook onderzocht door de vergelijking van experimentele resultaten. Fractografische technieken worden gebruikt om de kritische defecten en de interactie van het scheurtraject met de aangetroffen defecten te interpreteren. Fase 3 verzamelt de conclusies van de voorgaande onderzoeksfasen en stelt de contouren op voor verdere werkzaamheden. Gezien het beperkte aantal experimentele gegevens (de tijdrovende gevolgde prototyping methodes lieten het gieten en na bewerken van slechts een klein aantal herhalingen per type proefstuk toe) zijn de conclusies van dit werk per definitie kwalitatief. Alle resultaten zijn alleen indicatief en niet statistisch bruikbaar voor ontwerpdoeleinden. Niettemin zijn de verkregen gegevens nuttig om verbanden te leggen tussen de buigsterkte, stijfheid en breukvastheid van de geteste gegoten glassoorten, en hun chemische samenstelling, thermisch profiel en het defectennetwerk.

Het experimentele werk toont aan dat door ovengieten een grotere verscheidenheid aan chemische samenstellingen kan worden gegoten, zelfs bij relatief lage procestemperaturen. Als gevolg daarvan ontstaat een breed scala van mechanische eigenschappen, vooral wanneer afvalglas wordt gebruikt. Op basis van de gietparameters worden in gegoten glas vaak combinaties van verschillende defecten aangetroffen, gegroepeerd in meso-structuren. Meso-structuren in de bulk zijn meestal niet kritisch, maar wanneer zij aan het oppervlak worden blootgelegd, verlagen ze de sterkte naar gelang van hun type, vorm, oriëntatie en interactie met andere defecten. Defecten kunnen worden ingedeeld in intrinsieke en extrinsieke defecten, waarbij de laatste potentieel kritieker zijn, afhankelijk van de variatie in thermische uitzetting tussen het defect en de glasmatrix. Extrinsieke defecten kunnen worden vermeden door de zuiverheid van het te smelten glas te verhogen, terwijl intrinsieke defecten moeilijker te vermijden zijn omdat zij inherent verbonden zijn met het gietproces. Intrinsieke defecten zijn een gevolg van de opeenvolgende grensvlaktransformaties die zich boven de glasovergangstemperatuur voordoen tussen afgezette glasscherven in een gietvorm of binnen een stroming van het gegoten glas in de gietvorm. Tenzij veel hogere temperaturen worden gebruikt die leiden tot een gehomogeniseerde smelt door diffusie en mechanisch roeren, behouden de

intrinsieke structuren op meso-niveau een vormgeheugen van de oorspronkelijke glasscherf of gietvolgorde. Door het verwarmingsschema, het type glasscherven, de vorm en de wijze van gieten aan te passen, kunnen doelbewust meso-structuren in een glascomponent worden aangebracht. Inhomogene zones binnen de meso-structuur in de vorm van koord, bubbelsluiers of kristallijne zones vormen echter geen barrière die scheuren tegen kan houden. Kristallijne en verdichte zones daarentegen kunnen een laag energetische scheur dwingen plaatselijk van richting te veranderen.

Experimentele proeven tonen verder aan dat de buigsterkte van gegoten glas hoofdzakelijk wordt bepaald door de chemische samenstelling en de kenmerken van de defecten. De kwaliteit van het oppervlak en de zone naast het oppervlak is van het grootste belang, terwijl de defecten in de bulk zelden een invloed hebben op de mechanische prestaties, tenzij er een groot aantal van defecten aanwezig is. Subtiele veranderingen van het glasnetwerk als gevolg van de thermische geschiedenis zullen meestal niet worden opgemerkt, maar defecten die verband houden met het gekozen thermische profiel, zoals kristallisatie of bubbelsluiers, kunnen de sterkte aanzienlijk verminderen (tot 75%) als zij aan het oppervlak aanwezig zijn. De Elasticiteitsmodulus van gegoten glas wordt hoofdzakelijk bepaald door de chemische samenstelling (bindingssterkte en pakkingsdichtheid), maar het bakschema kan een verandering in de orde van 3% tot gevolg hebben. De breukbestendigheid van gegoten glas onder een scherpe drukbelasting is voornamelijk afhankelijk van de chemische samenstelling en de thermische geschiedenis, en bestaat uit twee stappen: weerstand tegen scheurinitiatie - wanneer een open netwerk gunstig is - en weerstand tegen scheurvoortplanting - wanneer een hoge oppervlakte-breukenergie vereist is. Een omgekeerde rangschikking tussen buigsterkte en breukbestendigheid wordt gerapporteerd voor verschillende chemische samenstellingen, als gevolg van de verschillende breukmechanismen die betrokken zijn tussen lokale contact- en de globale spanningen, hetgeen aantoont dat één type test alleen onvoldoende kan zijn om de structurele prestaties van een glascomponent te bepalen. Niettemin kan verbetering van het oppervlak door engineering van een composietglas structuur zowel de buigsterkte als de breukweerstand van gegoten glas verbeteren. Uit de experimentele resultaten kan worden geconcludeerd dat glasscherven uit afvalglas en lagere smelttemperaturen nog steeds structureel betrouwbare glascomponenten kunnen worden gemaakt.

Op basis van de conclusies en de beperkingen van dit onderzoek zijn verdere tests nodig om een beter inzicht en harde cijfers te krijgen over de mechanische eigenschappen van gegoten glas. Dit heeft niet alleen betrekking op een bredere reeks mechanische proeven, herhaling van de resultaten en statistische voorspelling, maar ook op de ontwikkeling van technieken die gebreken in kaart kunnen brengen en karakteriseren, alsmede op testprocedures geschikt voor gegoten glas die de uitdagingen ondervangen die worden geschapen door het karakteriseren van 3D componenten. De resultaten van dit werk tonen verder aan dat het mogelijk is een composiet-gietglas te ontwikkelen, waarbij een combinatie van laag- en hoogwaardig compatibel glas wordt gebruikt, zonder dat dit ten koste gaat van de sterkte. Aangezien defecten in de bulk van 3D componenten zelden worden geactiveerd bij het belasten van het product, kunnen onzuivere glasscherven veilig in de bulk worden gesitueerd, terwijl sterkere, zuiverdere glasscherven

worden gebruikt om de oppervlaktelaag te vormen die verantwoordelijk is voor de sterkte en de breukweerstand van het component. De verdere ontwikkeling van recycling door in de oven gieten van glas is wellicht van het grootste belang, aangezien deze techniek het mogelijk maakt om afval glas dat momenteel niet gebruikt kan worden wegens de contrasterende chemische samenstelling en de ingesloten verontreinigingen toch te recyclen. Het recyclen van een grotere verscheidenheid aan commerciële soorten glasafval, met inbegrip van speciaal glas, glaskeramiek, kwarts, aluminosilicaat, en draadglas moet worden onderzocht. Voor een succesvolle toepassing van gegoten glas in de gebouwde omgeving, en met name in structurele toepassingen, moet elke product- en systeemontwikkeling worden ondersteund door productierichtlijnen, testgegevens, productcertificaten en protocollen voor kwaliteitscontrole.

Acknowledgements

This PhD journey was not an easy one, but I suppose this is part of the deal. For a long time this PhD dissertation was an evening and weekend activity, and time to work on it had to be claimed over other research and teaching tasks. And even though the first years I was working at TU Delft did not lead to a single page in this book, they were crucial for me to discover the world of cast glass. My promotor dr. Fred Veer after all had warned me the first day at work back in 2014 that it will take me 10 years to understand glass, while he handed over his copy of Zchimmer's Chemical Technology of Glass. The Crystal Houses research, the endless casting experiments at the lab, the supervision of students, the travelling and workshops, highlighted the topic I wanted to focus on: the imperfections of cast glass. The research that forms this dissertation started at mid-year 2017 with slow steps, when together with dr. Faidra Oikonomopoulou we received a 4TU Bouw Lighthouse grant to develop circular building components out of waste glass, took a more systematic character in mid-year 2018, and benefited by the hermitic lifestyle imposed by the Covid-19 pandemic to get completed.

So many people helped me through this learning process! I am more than grateful to my promotors dr. Fred Veer and Prof. Rob Nijsse for guiding me through this journey. Dear Fred, I cannot thank you enough for all the knowledge you passed on, the discussions and your ingenious suggestions when I got stuck, the immediate email replies on Sundays and evenings, your caustic humour, the freedom you gave me to explore, and for reviewing every single word in this dissertation. One can speculate for days on a problem, but you taught me the best way to find out about materials: break them. Dear Rob, you have been a mentor with the proper old-school meaning of the word. Thank you so much for the elevating, philosophical discussions, art expeditions and life lessons, for the sharp solutions you proposed, for persistently fighting to create an operational cast glass lab, for backing me up always, in fact for believing in me! I try to follow your most valuable advice, to enjoy whatever I have to do- it makes the process easier.

I want to thank my PhD committee for their valuable guidance. Thank you Prof. Russel Hand for your patience to go through the thesis, provide helpful feedback and correct each mistake! Prof. Christian Louter, thank you, not only for the meaningful remarks on my work, but most importantly for helping me throughout the years, out of genuine kindness. Prof. Mauro Overend, the generous support you showed me from the moment you came to Delft is moving. When in doubt, I seek for our in depth discussions and your advice, which always help me move forward. Dr. Corina Datsiou, thank you for being the meticulous reviewer to my journal publications. Your comments helped me improve as a researcher. Dear Michel Prassas, you opened the doors to the Corning facilities in France and US; two highly inspirational, overwhelming visits full of information that cannot be found in books. Yet, I doubt this dissertation would have been completed, had not Prof. Bert Sluys intervened in 2018 to alleviate me from auxiliary teaching and research activities, and to stir my work towards a more pure academic direction. Dear Bert, I am sincerely grateful for the support you gave me and for helping me structure the thesis and design concrete goals.

George Quinn played a crucial role as well in shaping the scientific content of the thesis. The received knowledge on mechanical testing and fractographic analysis was essential for conducting this work. Together with dr. James Varner, they gave valuable advice on how to test cast glass, and I would like to thank them for this.

Georgos Stamoulis has been a great support; he helped me design and perform the flexural tests with outmost accuracy. Always willing to help, with patience and good will, his calmness reassured me at times of peak stress. Dr. Clarissa Justino de Lima, apart from a good friend, you have been my chemical engineer fairy; I learned so many things from you, thank you very much! I am also thankful to Ruud Hendrikx for conducting all the XRF and XRD analyses involved in this dissertation. Ron Penners and Richard Idzes have been my daily –unofficial- support in the lab; I am so lucky to have your help and company around! My beloved Kees Bardolf had a solution for everything and would be always there for me. He tried to teach me that "almost perfect" is good enough; I am still processing this Kees. Peter de Vries, thank you so much for your flexibility and good will that made most of the experimental work possible at Stevin II.

This work would have taken a couple years more have it not been for my good friends and lab co-workers, who helped me with the casting and post-processing of specimens or simply alleviated me from other tasks so I can focus on writing. Rong Yu, you have been a soldier in the lab; one can really count on your hard work and creative ideas! My dear Mariska van der Velden, we worked together since 2017; you always surprised me with your innovative solutions that halved the time needed to get things done. Thank you for making the lab work so much fun! Lida Barou, you have been a cornerstone when we started developing the cast glass research, always delivering perfect work! My dear Tommaso Venturini, I am so thankful for your friendship. Your work at the lab touched an artisanal perfection, but your support as a friend has been way more important ever since! I would also like to thank our lab student assistants Menandros Ioannidis, Anna Maria Koniari and Anurag Sonar for their dedicated work on various research projects, which allowed me to focus on my PhD. Menandre, thank you so much for helping me out with the format of this dissertation. My colleagues at Stevin II Maiko van Leeuwen, Albert Bosman, Kees van Beek, Michele van Aggelen, Louis den Breejen, John Hermsen, Ton Blom, John van den Berg and Fred Schilperoort further supported and facilitated the experimental procedures at the lab, thank you so much! I am particularly grateful to Rein van den Oever, my ally when the Cast Glass Lab was just starting and the glass oven was a nuisance to all.

I am very thankful to Jiyong Lee, Katherine Rutecki, Hein van de Water and Dawn Bendick for teaching me how to kiln-cast and post-process glass. I would also like to thank Cor Wittekoek (Vlakglasrecycling), Danny Timmers (Maltha Glasrecycling Nederland), dr. Marco Zaccaria and François Boland (AGC Belgium), Brian Wittekoek (Coolrec), dr. Hans van Limpt (Sibelco), Bettina Sommer (Royal Leerdam Crystal), and Klaas Roelfsema (Schott) for providing me with valuable insights into the glass industry and with plenty of waste glass to experiment.

I am grateful to have received the help and support from my colleagues and friends at CiTG and BK. Jaap Meijer gave so many fights for me for which I am truly thankful, Roel Schipper always

gave me genuine advice, Pieter Ham made the coffee breaks fun, my office mate Sander Pasterkamp coloured the day with interesting facts and taught me how to deal with all the bureaucratic frustrations of this job, dr. Karel Terwel helped me improve my teaching skills, Chris Noteboom would enthusiastically brainstorm on the future applications of recycled cast glass, superwoman Anneke Meijer made everything possible, dr. Alessandro Cabboi always treated me with tasty Sardinian delicacies, and Marjo van der Schaaf and Iris Nederhof-van Woggelum flawlessly supported my working days at CiTG. My colleagues at BK had created a welcoming environment many years before I even started working there. Thank you Ate Snijder and Peter Eigenraam for the fun discussions on glass and structures and for the amazing travels in South Africa! I am also very grateful to Prof. James O' Callaghan for his inspiring advice and guidance over the years, and for the great and witty conversations over dinner. I want to thank Andrew Borgart, dr. Joris Smits, dr. Thaleia Konstantinou, Julia Schönwälder, dr. Simona Bianchi, dr. Michela Turrin, dr. Charalampos Andriotis, Silke Prinsse and Rik Rozendaal for the nice discussions and words of advice, and dr. Onno de Wit, Tessa Vermeulen, Francoise van Puffelen, Bas Vahl and Hans van Ginhoven for their helpful support. A special thank you goes to dr. Marcel Bilow, not only for his generous offer to photograph the PhD Defence ceremony, but for providing me with one of the most inspiring consultancies back in 2010 when I was studying Building Technology; you highlighted an out of the box route for dealing with materials and connections.

I am happy and honoured to have been part of the Crystal Houses crew and want to thank the fantastic van de Poppe brothers Marco and Ronald, Richard Van Het Ende, Gijs Rikken, Erwin ten Bricke, Ronald Jorissen, Ivano Massarotto and of course the man behind this unique project, Jack Bakker, for this wonderful experience.

Erik Muijsenberg, Prof. Jan Belis, Peter de Haan, Siebe Bakker, Adrian Betanzos and many more people have been kind and helpful to me over the last years! If I have forgotten a name or two, please excuse me; I am by nature thankful for the help I received, no doubt.

Having my MSc students at the lab was a meaningful learning experience for me, and all of them helped me progress as a researcher and teacher. I am particularly thankful to Giulia Maria Anagni, Isidora Matskidou, Ivneet Singh Bhatia, Ivo Sombroek, Robert Akerboom, Erwin Jacobs, Georgina Giassia, Shan Cindy Lei, Eliza Scholtens, Anna Eskes, Wilfried Damen and Naomi Schlösser for helping me deepen my knowledge in structural glass.

I would like to thank Jaap ten Hacken and Maria van Neer from the printing company Druk. Tan Heck for their commitment to printing this dissertation and for the good atmosphere. I am particularly grateful to Jaap for letting me try out different papers and colour prints, until the optimum result could be reached!

Of course, this journey would have been unbearable without the help of my friends. My dear Maria, thank you so much for patiently listening to my nagging for so many years, for your positivity and energy that motivated me to go on every time I had doubts, and for all the great and crazy times together that boosted my everyday life! Bob, you have a magic way of calming

me down and making me laugh with your unique sense of humour; our walks and microscope expeditions were a true highlight during the hard lockdowns for which I am grateful! Antonio thank you for being the friend I can always rely on; you are part of so many lovely memories here in Delft and I am lucky to be your friend. Marina and Kostas, so many times I showed up in your house with broken wings and left happy and warm-hearted! Your hospitality exceeds Homer's writings, and our discussions always broaden my perception; I cannot thank you enough. Eleni, thank you for the great company and support the last two years; together we survived the lengthy corona quarantines and made the most out of it! Wiebke, our museum visits and in depth discussions were a true point of inspiration for me. My beloved Iro, Thalia and Manolis, although you guys are far away, you are there for me. Luzma and Ale, Sylvia, Ale jr, Bernat and Nadjla thank you for the great gatherings, dinners and travels that made life so much more exciting and meaningful here in Delft. Alessandra and Stijn, it's been a pleasure getting to know you and I am looking forward to more good things to come. And a thank you to many more dear friends, who, due to the distance, I don't see as often as I hoped anymore; Yasemin, Kapo, Harshad, Aris, Cristian, Erik, Rangan, Jorge, Joao and Natasha, Dakis, Eirini, Panos and Foteini, Claire and Kostas.

And I am keeping for last the people who suffered along me the most and selflessly supported me on this journey on a daily basis, simply because I cannot think of words good enough to express my gratitude. My dear Faidra, the 20 years I know you, you voluntarily came to the rescue countless times; helping me complete my MSc thesis prototype when I had a fractured arm, giving me a crash-course in structural glass so I can pass my job interview at the TU, patiently listening to all my anxieties and coming up with Greek logic to dissolve them, pushing for my contracts, and so much more. And then there is the fun part! You dragged me all over the globe, on forced holidays (probably I wouldn't have taken breaks otherwise) and unforgettable experiences. Together we have been discovering the world and developing this unique cast glass research- as proper "Glass Queens"! Our friendship has been such a constant in my life that sometimes I forget you are not my sister. Thank you my dear Paranymph for all the things you have done!

This dissertation is rightfully dedicated to my family and their unconditional love. To my precious brother and Paranymph Hyperion who has been my life companion; you are my true alley in life, always helping me battle problems with your calmness, humour and cleverness. Dear Maritta, thank you for your warm support and for inspiring me! I am deeply grateful that you are taking such good care of me and my brother. Demi, you will get a kilo of boiled chicken including the broth as a thank you for absorbing my stress. My beloved dad, I take your support for granted and may forget to thank you, so now is a good opportunity. Thank you most of all for teaching me to question everything I am told, already from the age of 2, when you called cats "dogs" and dogs "cats". Mom, my dearest best friend, everything I accomplished is because of you. Exceeding the specifications of a "Greek mom", you have been omnipresent and tireless, a constant support. You have great patience to be re-living the same situation again and again since my kindergarten years- the stress for this PhD is not much different from other milestones. I got your passion, commitment, perseverance, patience and kindness as carry-over life skills and I love you to the moon!

Table of Contents


1

Previous page: Coiling threads of red glass within a clear glass, both of a modified soda lime silica composition, kiln-cast at 970°C using the flowerpot method.

Chapter 1: Introduction

There is another side of glass; a voluminous, colourful, defective, yet strong side (Figure 1.1). The industry's quest for ultra-thin, ultra-clear, ultra-strong glass has shifted our attention out of artisanal glass and its imperfections, and with this shift, we neglected the multifaceted character of the material and exiled it from our architectural world. Yet, among the various glass producing techniques, the oldest one- casting, escaped the attention of industrialization and is left in the hands of small-scale foundry craftsmen and glass artists who act empirically and intuitively, and a limited number of scientists and producers who focus on flawless specialty glass. As a result, cast glass products are, until this point, exclusive objects. Considering, however, the shaping possibilities and compositional freedom offered by this manufacturing technique, a wide variety of unexplored potential comes to the surface. The structural application of cast glass in the built environment is one of many directions, on which this dissertation will focus.

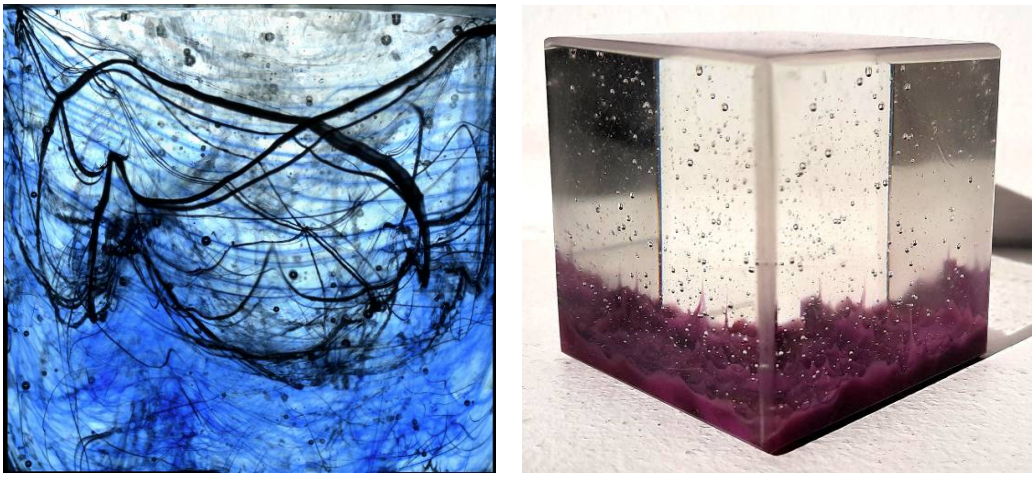

Fig. 1.1 The beauty of inhomogeneities in cast glass. 50mm cubic kiln cast specimens produced at TU Delft Glasslab from Leerdam crystal glass waste (left) and Bullseye art glass (right) at 870°C.

1.1 Problem statement

1.1.1 Cast glass components for structural applications: a new field

Advances in glass technology and engineering have changed the way we think of glass in buildings over the last 30 years. Considering the material's high compressive strength[1] and the

[1] The literature concerning the applied use of float glass will report a compressive strength of 1000MPa (Saint-Gobain); a value useful to an engineer newly introduced to glass to compare the material to other standard construction materials such as steel or concrete. However, the actual failure strength of glass is invariably referring to the tensile strength of the material and is related to the strength of its bonds and to its inherent flaws. Although theoretically a typical silicate glass could reach a strength of 32GPa (Shelby 2005 based on equation by Orowan 1934), in practice strength values between 14-70MPa are reported for common glass products and reach a maximum of 2.1GPa for freshly drawn glass fibers (Varshneya 2013). In other

constantly improving safety strategies (e.g. chemical and thermal tempering, lamination), glass is nowadays more and more trusted in load-bearing structures, escaping the traditional limitation of the material in cladding applications. The world of structural glass, however, evolves around the technological achievements of the float glass industry and the engineering progression on the testing, calculation and assembly of planar glass elements. As the majority of realised structural glass projects, scientific publications, regulations[2] and engineering manuals[3] concern float glass, the architectural expression of such structures is governed by the aesthetics and shape limitations of float glass.

The use of cast glass elements in buildings made its appearance in the second half of the 19th century, with the popular application of semi-prismatic light vaults in pavements of metropolitan cities (Fagan 2015, Hayward 1871, Trollope 1872, Sullivan 1898). In the 1930s, colourful cast glass pieces (circa 30mm thick) were introduced as an infill in concrete walls, known as the "Dalle de Verre" technique (Boon 2017). Cast glass has also figured in buildings in the form of monumental art installations such as the NYC Rockefeller Center glass murals "Wisdom, Sound and Light" by Lee Lawrie in 1934 (Dyer and Gross 2001) and "Rhythm of Infinity" by Denise Amses and Chris Cosma in 2000 (Amses), or the "Ice Falls" at the lobby of Hearst Tower in NYC 2006 by James Carpenter Design Associates (John Lewis Glass), (Figure 1.2). But the use of cast glass as a load-bearing component came into the picture with the completion of projects such as the Crown Fountain in Chicago 2004 (Krueck Sexton Partners 2004), the Atocha Memorial in Madrid 2007 (Paech and Göppert 2008), the Optical House in Hiroshima 2012 (Nakamura & NAP 2012), the Crystal Houses Façade in Amsterdam 2016 (Oikonomopoulou et al. 2015, 201a) and the Davidson-Gerson Gallery of Glass in Dearborn 2017 (James Carpenter Design Associates Inc. 2017), (Figure 1.3).

words, typical commercial glass will fail due to tension at much lower stress values than 1000MPa. Therefore, the term "high compressive strength" refers here to a predominantly compressive loading condition that prevents the breaking of bonds and opening of the glass network. If the tensile forces applied in this component are minimum, then we can assume a high (compressive) strength.

[2] The reader is referred to the building codes DIN 18008, EN 16612:2019, NEN 2608:2014 and ASTM E1300-00

[3] As a reference see the "Structural use of glass in buildings" (O'Regan 2014), "Structural Use of Glass" (Haldimann et al. 2008), "Glass Construction Manual" (Schittich et al. 2007), "Glass Structures" (Wurm 2007) and "Glass in Structures" (Nijsse 2003).

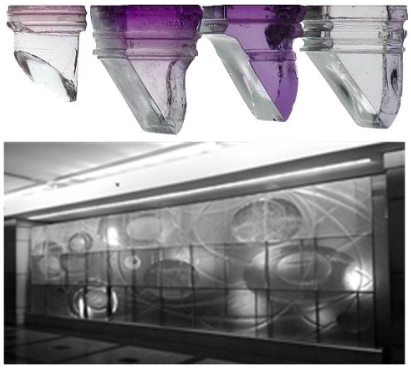

Top: Solarized “Vault Lights” used in street pavements at the end of the 19th century; image by glassian.org

Bottom: Rhythms of Infinity sculpture at the Rockefeller Center, NYC (2000).

“Dalle de Verre” window at the former Station Post Office in Rotterdam, made by Louis van Roode in 1955.

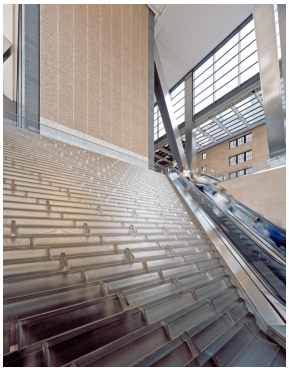

“Ice falls” Hearst Tower NYC (2006); image by James Carpenter Design Associates, Inc. and John Lewis.

Fig. 1.2 The non-structural architectural use of cast glass in buildings over the last two centuries.

The Crystal Houses Façade in Amsterdam (2016); image by MVRDV

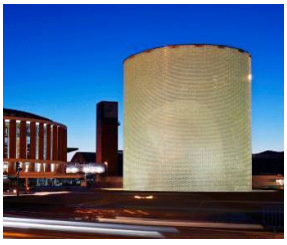

Top: Crown Fountain Tower in Chicago (2004).

Bottom: Monumento 11M in Madrid (2007); image by sbp Engineers.

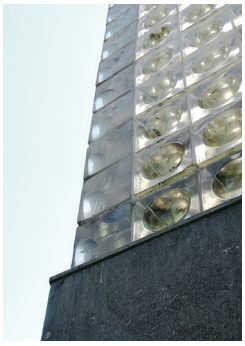

Top: Heesen’s Glass Tower in Leerdam (1976).

Bottom: Optical Glass House in Hiroshima (2012); image by Hiroshi Nakamura & NAP

Fig. 1.3 Examples of structural cast glass applications in the architectural realm.

Oikonomopoulou (2019) argues on the multiple potential arising from the structural implementation of cast glass in architecture. These originate from the shaping freedom provided by this manufacturing technique in combination with the robustness of the resulting voluminous components. In this manner, freeform, fully-transparent load-bearing compressive structures can be realised that due to their geometry resist buckling and subsequent failure at low tensile stresses. The Crystal Houses façade in Amsterdam celebrates the architectural qualities and structural capacity of a self-supporting adhesively bonded cast glass brick façade that circumvents the use of any metal substructure. Suggesting a sustainable direction in the architectural use of glass, the "Re^3 Glass" project (Oikonomopoulou and Bristogianni 2019) proposes demountable structures out of cast glass components that employ currently non-recyclable waste glass. All the environmental benefits of this proposal are linked to the forming and compositional flexibility associated with the casting technique. Further on, Barou et al. (2019) explore the consolidation of historic monuments by replacing the missing components of a ruin with cast glass components. Oikonomopoulou et al. (2020) showcase the shape optimization and material savings to be achieved by implementing form-finding algorithms in the design, and by developing novel moulding methods (Figure 1.4). Hybrid cast glass and concrete structures have been investigated at TU Delft, a glass brick vault was assembled by robotic arms (Parascho et al. 2020, Oikonomopoulou and Bristogianni 2022), the use of cast glass in the extreme weather conditions of Greenland is being researched (Oikonomopoulou et al. 2022), as seen in Figure 1.5; we are only beginning to grasp the possibilities of cast glass. Just by wandering through the collection of renowned museums of glass art such as the "Corning Museum of Glass" (see 2001 catalogue publication) or "Le Mus Verre" (see 2016 catalogue), one can immediately understand the numerous, yet to come, expressions of colour and form that the use of architectural cast glass of the future will bring (Figure 1.6).

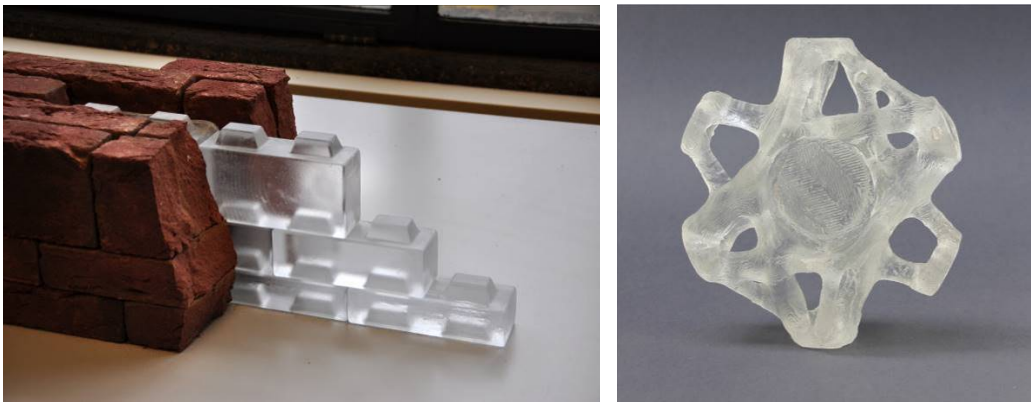

Fig. 1.4 Cast glass components developed at the TU Delft Glasslab, exploring the potential of casting in achieving complex geometries. Left: prototype for the 3TU.Bouw Lighthouse project "Restorative Glass" (Oikonomopoulou et. al 2017), right: topologically optimized cast glass node developed by Damen, W. (2019).

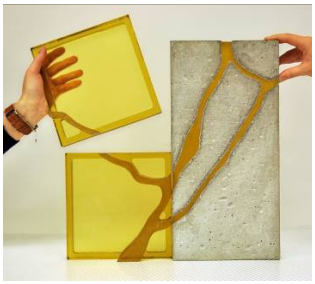

Hybrid concrete and cast glass component developed for MVRDV and Bvlgari by the TU Delft Glass Lab (2017).

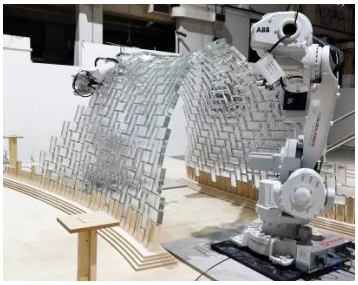

Robotically assembled cast glass vault developed by SOM and Princeton University c.r.e.A.te lab and Form Finding Lab, in consultation with TU Delft Glass Lab (2020); image by SOM.

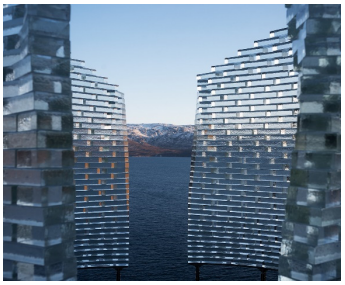

Unesco cast glass pavilion in Sarfannguit, Greenland, in progress (2021). Designed by Konstantin Ikonomidis. Glass Engineering by TU Delft Glass Lab. Image by Julien Lanoo.

Fig. 1.5 The versatile character of cast glass.

Julia Buckingham “Crown Block” Sculpture; image by the artist for Global Views.

Sculpture by Aleš Vašíček; image by the artist.

Richard Whiteley “Leaver” Sculpture, 2016; image by the artist.

Fig. 1.6 Glass art as a pool of inspiration for stretching the architectural expression of cast glass. Julia Buckingham’s work can inspire colourful columns that offer a gradient of transparency, Ales Vasicek’s sculpture could be envisioned as a free form wall of variable thickness -offering mass optimization, while Richard Whiteley work helps visualize the introduction of voids that could have thermal benefits in a cast glass façade.

1.1.2 Challenges hindering the structural use of cast glass

Cast glass structural applications in the built environment are quite rare, despite the architectural and structural potential of this manufacturing process. Although the success of projects such as the Crystal Houses has attracted architects to the use of cast glass, several impediments prevent new projects from taking off. These obstacles can be summarized to the following points:

- Casting foundries specializing in architectural glass are limited
- Glass casting is far from an industrialized process; it is mainly practiced in small-scale foundries, in an artisanal manner
- The manual casting and post-processing of glass results in a labour-intensive, time-demanding and thus expensive product
- There is a lack of standards regarding the production and quality control process
- There are no testing procedures or standards developed specifically for determining the mechanical properties of cast glass
- There is a critical knowledge gap concerning the strength of cast glass. The relation between chemical composition, casting process and occurring manufacturing flaws is neither straightforward nor well defined
- Most engineers lack the knowledge and experience of how to design and calculate a cast glass structure. There are also no standard solutions developed for connecting cast glass components for outdoor structural applications. Design values are missing, not only of the strength of cast glass but also of the strength of adhesively bonded cast glass assemblies
- The structural application of cast glass in most cases requires some form of testing and certification to comply with building permit regulations
- There is a general mistrust in the use of glass structurally; therefore it is commonly assumed that cast glass will break easily, either by accident or due to vandalism, even though it is more impact resistant than commonly used concrete or terracotta bricks
- There is no established demand for cast glass to motivate investment from the industry and research from the scientific community.

So the limited production facilities, the uncertain quality of the product, the missing engineering data, the involved risks in the structural application of cast glass, the high costs involved and the non-established market, discourage the majority of the designers, engineers and developers from using cast glass in buildings. For those pursuing it nonetheless, the requirement of research data to validate the design is almost inevitable. Moreover, to overcome the engineering uncertainties, cast glass structures tend to be over-dimensioned, and are linked, therefore, with an uneconomical use of material. In case of a fracture of a cast glass component in a realized structure, the term “spontaneous failure” is often used to mask the uncertainties surrounding errors during product manufacturing, engineering and application (Figure 1.7).

Public sculpture, Wertheim.

Crown Fountain, Chicago.

Crystal Houses, Amsterdam.

Fig. 1.7 Cases of cast glass failure in realized structures. Improper component annealing, the presence of inclusions and other inhomogeneities, insufficient polishing, erroneous choice or thickness of adhesive, or damage incurred during installation are the most common reasons behind such failures.

For the realisation of optimum, reliable and aesthetically pleasing cast glass structures, there is a clear need for regulations and manuals that span the total of the design, engineering, production process, quality control, and application of cast glass. This is a major undertaking, given that cast glass is currently under-defined in all the above mentioned aspects. For example regarding production, there may be numerous publications by the artistic community (Thwaites 2011, Cummings 1997, Beveridge et al. 2005, TechNotes and TipSheets by Bullseye Glass co., Whittingham 2019, Stone 2010, Lundstorm 1989, Knoppert 2011) mainly on how to kiln-cast or fuse glass, where empirical knowledge, glass recipes and firing schedules are shared, but the literature from the scientific and industrial side is limited, either due to confidential proprietary knowledge or simply due to lack of research on the specific field. Up to a great extent, the work of Zschimmer (1913), Shand (1955), Vogel (1985), Shelby (2005) and Varshneya (2013) can serve as a solid basis for navigating in a range of topics such as batch calculation, annealing schedules, moulding techniques and mechanical properties, but these books are not written from the point of view of the casting manufacturing process. Similarly, there are numerous books, articles and dissertations discussing the formation of defects during batch melting (e.g. refractory contamination, variable heat flow leading to non-molten compounds, poor homogenization) and glass forming (Bartuška 2008, Aldinger and de Haan 2019, Aldinger and Collins 2016, Clark-Monks and Parker 1980, Peddle 1927, van Dijk 1994), but in plurality these are written from the point of view of the float and container glass industry. As a simple example to demonstrate how far we are standing from a controlled glass casting process, typing the keyword “cast iron” in the search of the ASTM standards web-database will return 89 active standards, concerning different types of iron (ASTM International, 2022). These standards provide guidelines for product manufacturers and end-users that ensure consistent high quality castings, effective quality control and proper product application. The result for “cast glass” in the same database is zero regulations. Specifications for other glass types, however, do exist; EN572:2004 and ASTM

C1036 – 16 provide specifications for float, wired, patterned drawn sheet and channel glass, ASTM C1048 - 18 for heat-strengthened and fully tempered flat glass, and ASTM C1172 – 19 for laminated architectural flat glass, to name a few. But perhaps the most glaring indication of this knowledge gap is the inability to give an answer to the most recurring and obvious question: what is the strength of cast glass? Without an answer, the engineering of cast glass will continue to be founded on uncertainty.

1.1.3 Casting parameters and component geometry define the material properties of cast glass

What differentiates cast glass from other types of glass (e.g. float, drawn, blown), is in principle the set of defects it acquires from the casting process- which differ from other production processes (Figure 1.8)- in combination with its geometrical characteristics. As a result, a change in the casting parameters or a redesign in the product's shape, can alter the mechanical properties. This justifies the variability among cast glass products, as –without norms and guidelines- it is a challenge to control the quality of the resulting component and predict its properties. As an example, the vertical glass slabs produced at John Lewis Glass studio (CA, USA) vary greatly from the Poesia glass bricks (Italy), due to the different chemical composition, pouring method followed, cooling scheme and component size (Figure 1.9).

Bullseye window piece, Kloster in Trier, Germany. This is the centrepiece of crown glass, a hand-made flat glass produced by spinning a bowl-shaped blown piece of glass. Memory of this centrifugal action can be seen in the spiral cord, which is dominant in the piece.

Blown bottle (≈18th century) used for Haarlemmerolie, The Netherlands. The elongated elliptical bubbles are indicative of the blowing action and the act of gravity.

Hand-made wired glass in the Van Ravesteyn House, Utrecht (1932). Evidence of a corrugated roller pushing the wire net in the viscous glass can be seen on the surface of the panel as body marks (wrinkles).

Fig. 1.8 Each glass production technique, and in particular non-industrialized processes, are associated with a specific set of defects.

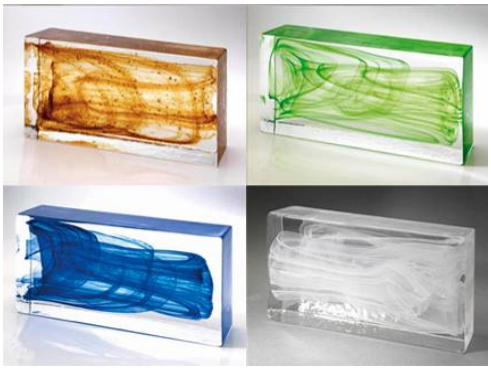

Top: Casting of a replacement piece for the “Ice Falls” installation at John Lewis Glass Studio (2017). The kiln is situated above the casting area, and a thin thread of molten glass flows down to the mould, at atmospheric conditions, while the mould is rotated to get equally filled up.

Bottom: Panel cast at John Lewis Glass Studio following the described technique. The flow of the molten glass thread as it fills up a vertical, moving mould is portrayed in the glass meso-level structure.

Top: Casting of a Crystal Houses brick at Vetreria Resanese (2014); image by F. Oikonomopoulou. The thread of molten glass is much thicker and significantly closer to the mould, in comparison to the John Lewis casting example. This results in a much coarser meso-level structure.

Bottom: Poesia bricks produced by Vetreria Resanese containing a colour swirling that suggests the manner the glass was poured inside the mould.

Fig. 1.9 Differences in the characteristics of the molten glass thread (size, distance, movement of mould or ladle) will result in a different flow, and therefore a different glass meso-level structure.

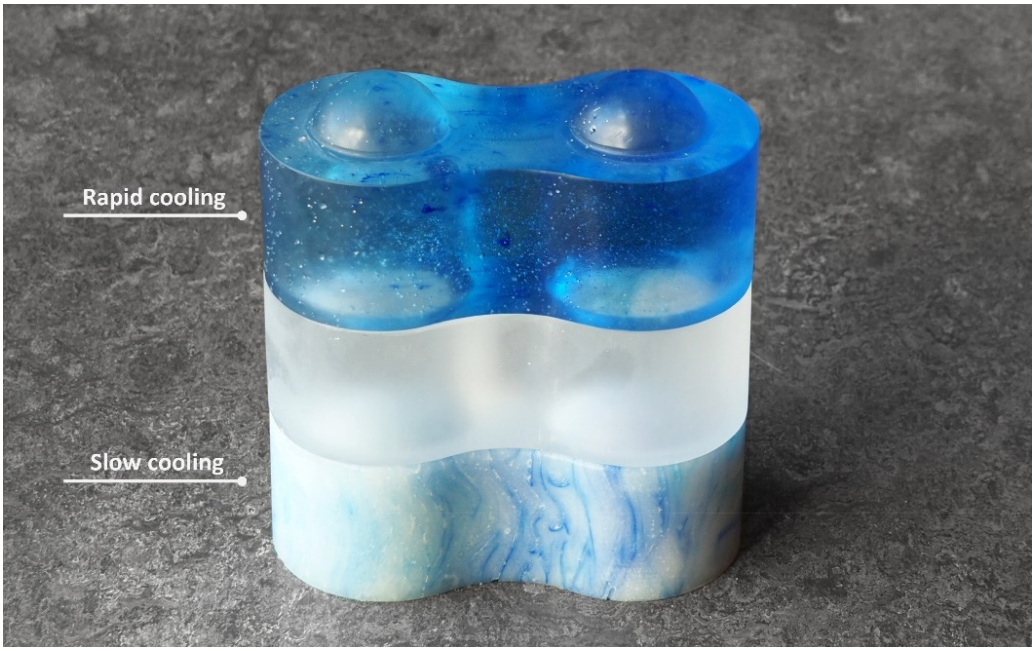

Fig. 1.10 Glass prototype produced at TU Delft, showing that a change in parameters can significantly alter the mechanical and physical properties of cast glass. In this case, the top and bottom component have been kiln-cast using the same glass cullet yet a different firing schedule (a top temperature of 860ºC and a slower cooling has been used for the crystallized component at the bottom, in comparison to a 950ºC top temperature for the blue, transparent component).

Yet, controlling the quality of the final cast glass product is beyond following a list of rules and optimal parameters (although such rules would certainly help). In fact our inability to control the process is aligned with our lack of understanding of the meso-level structure of cast glass and how this is formed. Knowledge gaps in the physiochemistry of glass and our current inability to experimentally investigate the structure of glass at high temperatures- a molecular liquid at this state- create the danger of borrowing the concepts, theory and terminology assigned to atomic liquids (e.g. molten metal) to explain how glass is formed. As a characteristic example, a clear solidification point is assumed in the literature for each individual glass recipe. In actual fact, glass undergoes a series of transitions from a hot mass containing small enough molecules that they can flow under gravity (casting) to an intermediate phase where the molecules are large enough that the glass mass cannot flow under gravity but can deform under pressure (hot bending), to the point where the glass molecules become so large that they cannot move freely. During the increase of molecular weight with the decrease of the temperature, glass gradually changes its flow pattern from almost Newtonian at high temperatures to non-Newtonian at lower temperatures[4]. When casting, the top temperature and corresponding forming viscosity we choose

[4] In a non-Newtonian fluid, the viscosity is a function of the shear strain rate. According to Varshneya (2013), glass will exhibit a pseudoplastic non-Newtonian behaviour (shear thinning) at high shearing stresses. Simmons and Simmons (1989) show that a soda lime silica glass can exhibit such behaviour at very

in relation to the glass recipe, the time we keep the glass at this temperature, the manner we feed the glass to the mould and the forces applied (e.g. gravity, mechanical pressure) are determining parameters of the properties of the final product. Batching defects, volatilisation of some elements and refractory corrosion intensify the problems and increase the chance of inclusions and cord. A different mould shape could imply different heat flows within the liquid glass mass, which results in distinct glass flow behaviours and chemical reactions, and eventually in inhomogeneities. Moreover, the use of a different kiln can alter the result, even if the same firing schedule is used. Further on, the selected cooling rate will determine whether the liquid glass will transition to a totally amorphous, rigid structure or if it will crystallize and to what extent (Figure 1.10). The annealing process is crucial in defining the glass product, not only in the evident manner of stress relief, but also in the level the glass will compact itself. Focusing on the transition of the supercooled liquid to a rigid solid, the assignment of a specific Glass Transition Temperature (T_g) to a given glass composition is a characteristic misconception, as well as an accepted convenience to experimental procedures, given that in reality, the T_g in glass refers to a transformation range and not to a point of abrupt transition. In this temperature range, a slower or faster cooling can increase or decrease the density of the glass structure accordingly (Varshneya 2013) and affect its mechanical properties (Gross and Tomozawa 2008, Striepe et al. 2013). Moreover, the annealing of a glass at a slightly lower temperature within this transition range will also lead to an increase of the material's density (Tool 1945, Babcock 1977).

So it starts to become evident that not only the glass composition is responsible for the physical and mechanical properties of glass, but also the element of time in relation to the applied heat and external forces. For simplification purposes, the parameters affecting the cast glass properties can be grouped into five main categories (Figure 1.11), while Figure 1.12 lists the relevant sub-parameters:

low strain rates at 530ºC, but will require much higher strain rates at 900ºC to escape the Newtonian behaviour. Glass is an incompressible Newtonian fluid at forming temperature (Babcock 1977, de Waal and Beerkens 1997, Groot et al. 2009).

1) **Glass composition**: the chemical composition will determine the quality of the glass network but also define the physical properties related with glass forming (e.g. viscosity, density)
2) **Contamination**: this can originate from batch/cullet impurities or from refractory and mould contamination of the melt
3) **Thermal history**: The firing schedule will determine the level of homogenization, crystallization, network cross-linking and stress-elimination of the glass. Temperature gradients can contribute to local inhomogeneities and stress
4) **External forces**: Gravity, pressure and mechanical stirring can alter the level of homogenization of the glass and the level of network compacting
5) **Geometry**: This refers not only to the mould geometry but also to the geometrical characteristics associated with casting, whether this is static (by depositing cullet inside the mould) or dynamic (by pouring molten glass in the mould).

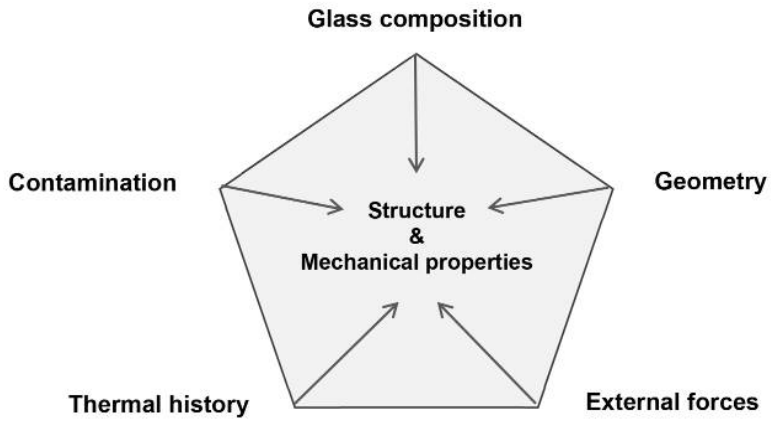

Fig. 1.11 Main parameters affecting the properties of cast glass.

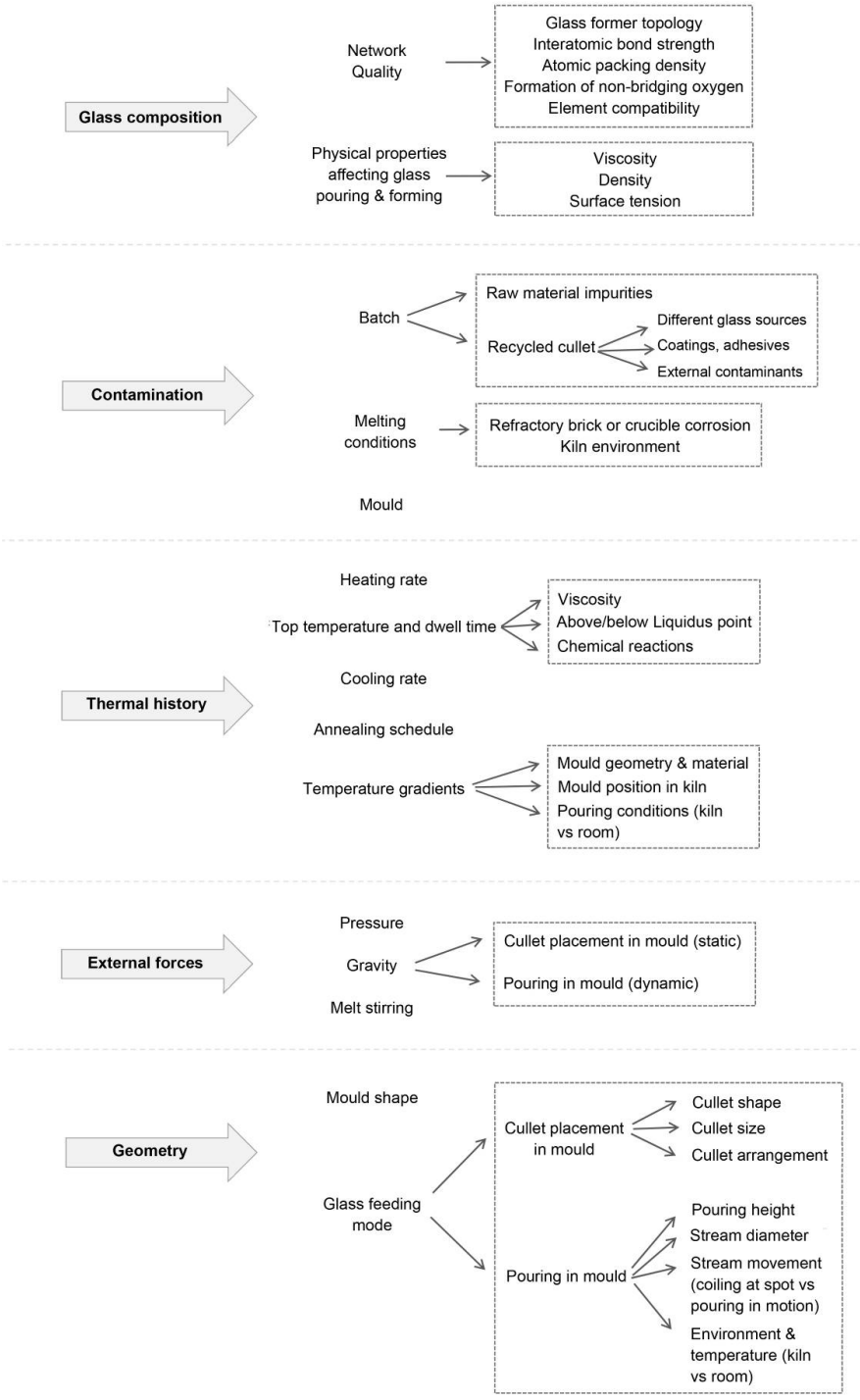

Fig. 1.12 Sub-parameters affecting the quality of cast glass.

The majority of the above mentioned parameters and linked problems are to a point relevant to other glass production techniques, but the voluminous and often free-form character of cast glass products- the parameter "Geometry"- intensifies the difficulty of achieving homogeneity and multiplies the chances of defect-formation. By reviewing different commercial cast glass objects produced during the last hundred years by various foundries, the population of defects -especially in the bulk- is striking (Figure 1.13). In that sense, discussions about singularities in cast glass are not very relevant, as in actual fact we are dealing with a combined statistical population of different types of flaws. Such a population of defects and inhomogeneities is often enough to create a random or organized "meso-level structure" in the bulk of the cast glass product. This meso-level structure is linked with the commonly used high forming viscosity (e.g. 10^3-10^4 dPa·s) of the melt, which slows down the Brownian motion[5] in the liquid, preventing homogenization. In fact, the higher the forming viscosity, the more the meso-level structure of cast glass is a reminiscent of the component's forming history, retaining a form of shape memory of how the material was poured or fused inside the mould (Figures 1.9, 1.14-1.16).

Glass column produced by John Lewis Glass Studio.

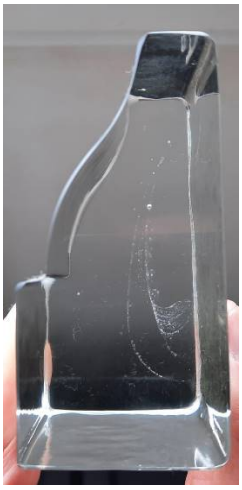

Corbel cross-section produced by Vetreria Resanese.

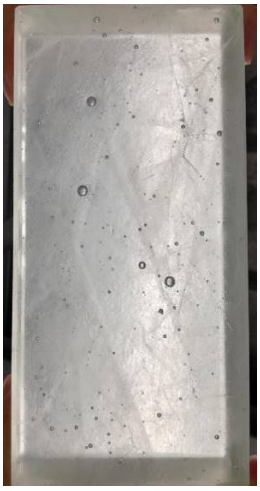

Glass brick from recycled cullet produced by Interstyle.

Fig. 1.13 Cast glass products are often characterised by a network of defects.

[5] The term "Brownian motion" describes the irregular movement of particles in a liquid as a result of random collisions by molecules of the medium. This diffusive motion allows two miscible liquids to eventually mix without the requirement of stirring (March and Tosi 2002).

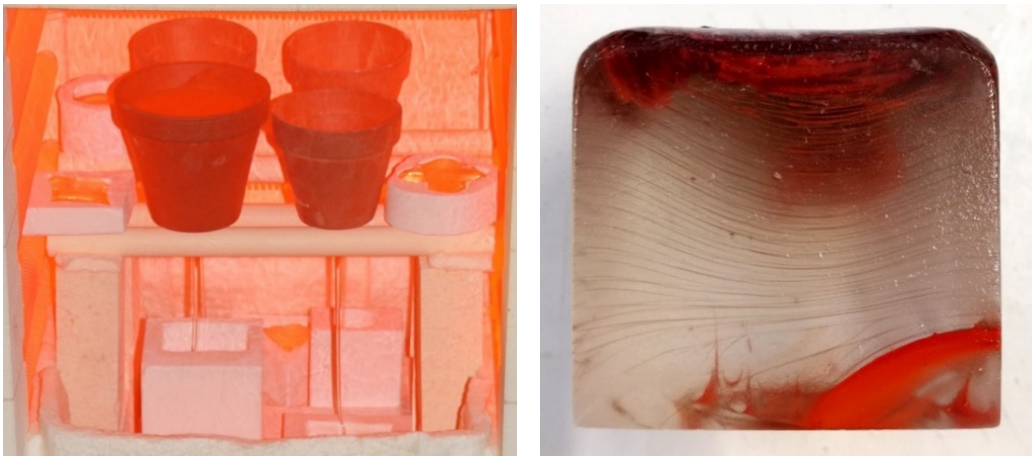

Fig. 1.14 Kiln-casting process followed at the TU Delft Glasslab: a viscous thread of glass slowly flows from the flowerpot down inside the mould as the kiln reaches the selected top temperature (left). The movement of the glass thread can be seen in the marks left on the glass-mould surface (right image shows the side view of the component, prior to polishing) but also in the cord present in the bulk of the glass component.

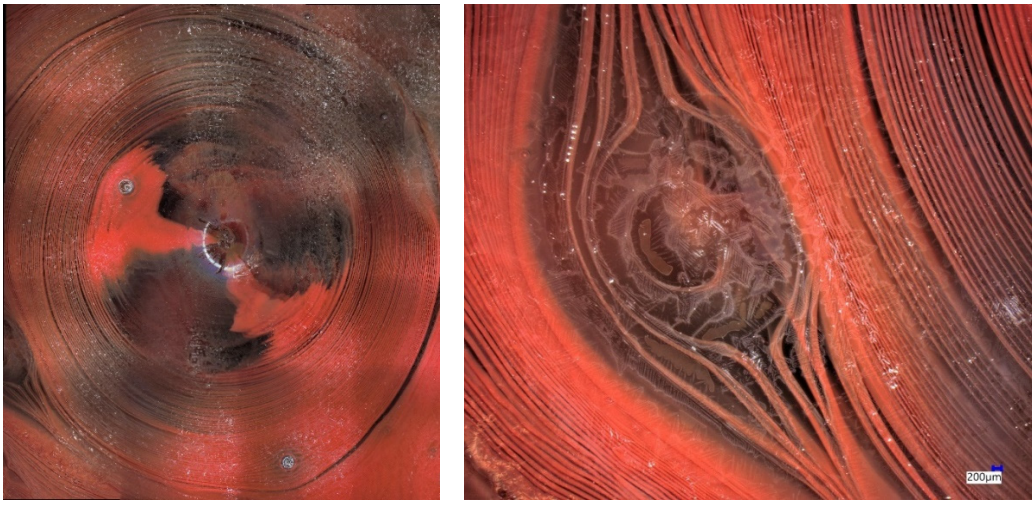

Fig. 1.15 Top surface of a kiln-cast specimen produced at the TU Delft Glasslab following the flowerpot method. The addition of colour helps tracing the spiral movement of glass while filling the mould (left). The spiral structure often overlaps with other structured layers -such as the crystallization film developed at the top surface- or gets interrupted by the uprising movement of bubbles (right).

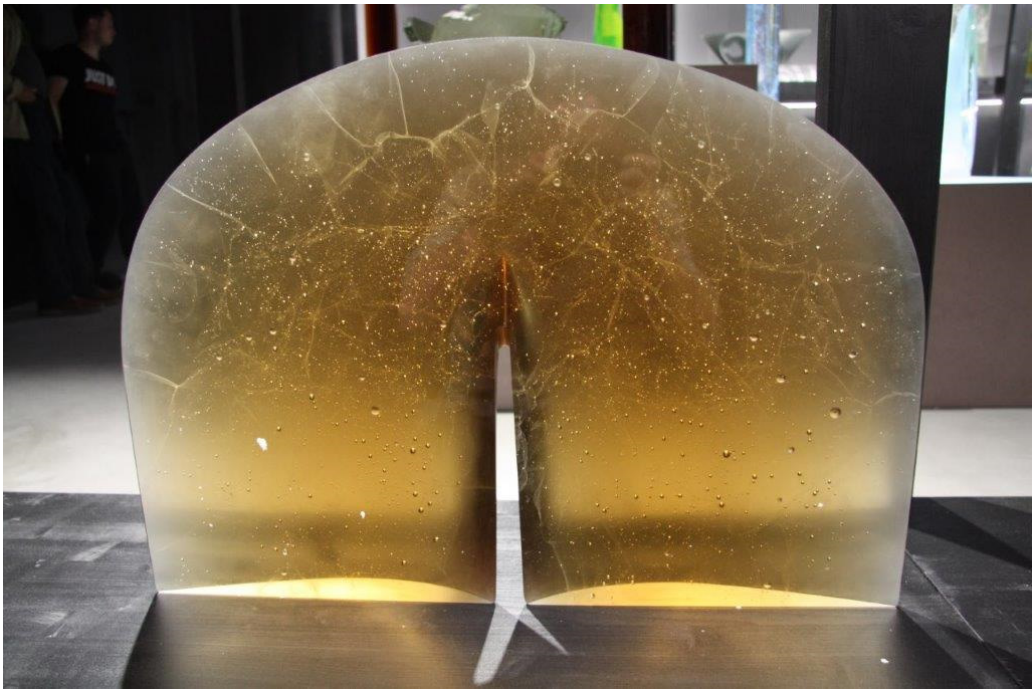

Fig. 1.16 Kiln-cast sculpture by Aleš Vašíček. The network of defects forming a meso-level structure in a kiln-cast component is directly linked to the manner the glass billets were placed inside the mould prior to kiln-casting and attributed to the high kinematic viscosity of glass at top casting temperature that prevented homogenization.

Yet, Peddle (1927) argues that glass defects are a necessary evil; there is always a compromise the producer needs to make, as a truly perfect glass would imply an unrealistic market price. It would be naïve to expect that all cast glass foundries would adopt the meticulous casting process followed at the Corning Bagneaux-sur-Loing premises: top quality raw materials and careful batching, three step melting process including degassing and melt-stirring, pouring of the melt within a controlled kiln-environment, upward movement of the mould to avoid cording, etc. This would theoretically sky-rocket the price of an already expensive at the moment product (cast glass is often priced around 8-16 euro per kilo). So it is worth posing the question: what would be an acceptable level of defects in cast glass products that would still allow their structural application in buildings while maintaining a marketable price? Accepting an amount of flaws in the cast product further sparks the discussion; are all defects equal but some more equal than others? Identifying the critical flaw types from the tolerable or negligible types would help target the production and quality control process. Moreover, how is the location of a specific type of flaw affecting the strength of the cast component? From a completely aesthetic point of view though, the presence of defects in cast glass can even be considered appealing to architects and designers, due to the greater visual expression they offer.

So considering the voluminous nature of cast glass, more manufacturing flaws are expected. An increase of glass-melt volume makes it more challenging to control the level of homogeneity. However, if a distinction is made between surface-distributed (s) and bulk-distributed flaws (b),

then the volume ratio Vs to Vb is much smaller in cast glass than in thin-walled glass elements (e.g. float, blown glass). This is important if we consider that the effective flaw zone of a voluminous cast glass object is mainly concerning the object's surface and immediate bulk surrounding. In practice, the structural application of such a voluminous component is most commonly related to a bending or compression load, which means a maximum tensile force along one or more of the components' surfaces, either directly or through buckling. As a result, only a small ratio of flaws is exposed to tension, and thus seem to be affecting the cast glass product, in comparison to a thin window glass where almost all its cross-section can be critical. Therefore, simplistically, one could argue that the defects in the meso-level structure (bulk) of glass are less critical.

What happens however in the case of a different load case, such as uni-axial tension or thermal shock? More questions arise regarding the extent the stiffness of the component is affected in respect to the population of flaws, or if alterations in the crack propagation of the material are caused due to certain defects. Could in that sense weak zones be formed in the bulk that promote crack propagation? Yet prior to understanding the effect of different defects to the mechanical properties of cast glass components, the causality of these defects needs to be determined.

1.1.4 Defects in cast glass and the need of correlation to the casting process

Different glass defect classifications exist in literature, helping with the assessment of the severity of each defect and the detection of its cause of formation, with the aim to avoid its reoccurrence. Below the major classification systems are listed (see work by Aldinger and de Haan 2019, Bartuška 2008), based on different characteristics such as:

- **Chemical**: Crystalline, Glassy or Gaseous
- **Location**: Surface vs Volume distributed
- **Defect Severity**: Critical, Functional, Stress inducing, Strength reducing, cosmetic
- **Process stage**: Batch, forming, post-processing, handling, storing
- **Defect frequency:** Rare, occasional, repeating

The most typical defects encountered during quality control of cast glass components include stones, cord, crystallized interfaces, bubbles, internal stresses, and surface damage due to mould contact, post-processing and handling (Figures 1.17-1.19). The criticality of these defects is not only related to their particular characteristics versus the glass matrix properties (e.g. composition, thermal expansion coefficient, toughness, modulus of elasticity, size), but also to their location in the cast component (surface vs bulk), their association with other flaws (e.g. "kissing" bubble occurrence[6]) and the externally imposed stress-field on the component (e.g. mechanical loading, thermal shock etc).

[6] Bubbles are considered relatively harmless smooth pores, yet Quinn (2016) uses the term "kissing" to draw our attention to incomplete bubble volumes that touch the exterior surface or another bubble close to the surface of the glass or ceramic object. Such occurrences can be strength-limiting.

Piece of glass (ownership of J. Varner) retrieved from a glass furnace, showcasing the most common encountered melting defects such as devitrification stones, bubbles, cord and colour streaks.

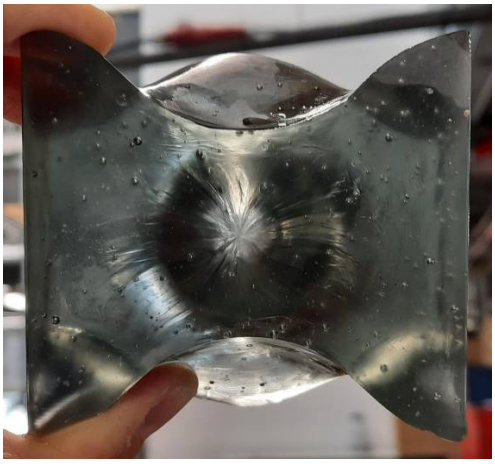

Kilncast component out of old television screens (CRT) produced at the TU Delft Glasslab. The component has a prominent cord structure at the center, and noticeable gas bubbles.

Fig. 1.17 Typical defects encountered in glass, associated with the melting process.

Surface crystallization developed along the side surface of a kiln-cast component, which was in contact with the silica-plaster investment mould (TU Delft Glasslab). The higher than usual alkali content (18% wt) and aluminium oxide (3.4 wt%) of this soda lime silica glass by Lamberts could be responsible for the extended reaction to the mould material.

Top surface of a kiln-cast component out of recycled float glass produced at the TU Delft Glasslab. Creasing, crystallization patterns, bubbles, and colour streaks are characteristic of the glass surface to kiln-atmosphere exchange reactions.

Fig. 1.18 Glass surface contamination at the mould to glass and kiln-atmosphere to glass interface.

Glass frame for the Crystal Houses, produced by Vetreria Resanese, exhibiting deep lap marks. The improper flow of the molten glass at the bottom of the mould could be attributed to a non-sufficiently heated mould surface.

Pressed cast glass brick for the Atocha Memorial produced by Schott. Chill marks from the pressing process are evident at the top surface of the component.

Cast glass column by John Lewis Glass Studio exhibiting an intense "orange peel" structure at its surface, due to contact with a non-sufficiently heated mould.

Fig. 1.19 Surface flaws in cast glass as a result of the mould to molten glass reaction.

To familiarize the reader with some of the above mentioned -less self-explanatory- defects, a stone is a crystalline inclusion in the glass matrix, which causes optical disturbance and often strain and fracture to the glass object. Evans (1982) assesses the probability of fracture caused by such inclusions, by the level of deviation of the thermal expansion coefficient in combination with the elastic modulus (E) and fracture toughness of the inclusion versus those of the matrix. For example, a highly contracting inclusion with high E, will detach from the matrix acting like a void (not a threat), however, a similarly high contracting defect of low stiffness and toughness will remain attached to the matrix, leading to fracture. Cord, on the other hand, is a glassy inclusion of different composition from the matrix. Usually cord leads to an optical disturbance caused by the refractive index difference between the inclusion and the matrix, yet in some cases, an additional difference in the thermal expansion coefficient leads to stresses that cannot be removed during annealing, impacting therefore the strength of the glass (Clark-Monks and Parker 1980). Interestingly enough though, a compositional inhomogeneity in the molten state that would typically end up as a glassy inhomogeneity (cord) in the cooled glass object, can also turn out becoming a crystalline inhomogeneity, if the thermal conditions support it (Figure 1.20). This occurs if part of the glass melt shows excess or deficiency of a particular compound, and the firing and cooling schedule promotes the separation of this compound from the glass melt and the formation of crystals (Peddle 1927).

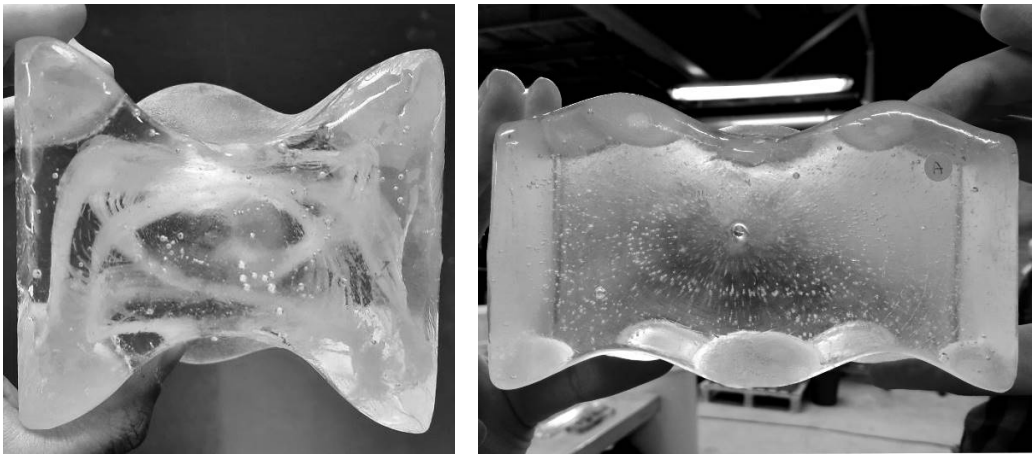

Fig. 1.20 Components kiln-cast at 970ºC with the flowerpot method at the TU Delft Glasslab, using Schott B270 glass cullet. In the component on the left, a crystallization zone has evoked along the swirling pattern of molten glass, possibly due to cullet contamination in combination with a favourable thermal condition associated with the location of the mould in the kiln. The component at the right image shows a similar swirling structure, composed by cord and bubbles, yet no crystallization appears along this path, due to lack of favourable conditions.

This phenomenon can be easily observed when re-melting soda lime silica glass cullet inside a mould: initially, as the temperature increases past the softening point, the cullet pieces sag to each other, eliminating the void space in-between. A further temperature increase will cause the surface of each piece to become more fluid and tack-fuse to its adjacent surface. These fluid zones start to differ from their corresponding bulk zones, as the glass there has a lower kinematic viscosity so various diffusive actions can take place, locally altering the composition. Moreover, due to the lower viscosity, the growth of crystal nuclei is favoured, and the longer the glass cullet stays in this condition the more crystal formation and growth is stimulated. If however this stage is quickly passed and an extra increase in the temperature is applied, then these fluid interfaces will simply appear as inhomogeneities in the melt and end up as cord in the super-cooled glass object. The position of the cord corresponds to the initial positioning of the cullet pieces (Figures 1.21-1.22), and only with higher temperatures -where a low kinematic viscosity is reached ($<10^2$dPa·s)- diffusion and the uprising movement of bubbles (Figure 1.23) take over to erase this shape memory and homogenize the melt.

Fig. 1.21 Casting process and prototypes for the “Sarcophagus for Her Majesty the Queen of Denmark”, cast by the Zdeněk Lhotský Studio and exhibited at the Museum of Decorative Arts in Prague in 2019. On the top left image, the kiln-casting method followed can be seen, with the organized feeding of the mould with glass rods (image extracted from the documentary “Sarkofág pro královnu”). All other images are depicting the prototypes and are made by the author in Prague. The top right image shows the top view of the prototype where the linear reminisce of the rods can be seen, as a subtle translucent veil. The bottom left image shows a side view of the prototype, with the translucent veil structure situated at the bottom, while at the top (more exposure to heat), a subtle honeycomb structure of bubbles can be observed at the prior connection zones of the rods. The bottom right image shows a much smaller prototype (possibly better heated), where the honeycomb structure has dissolved and transformed into a 3dimensional cord structure. In these images, three consecutive stages from fusion to homogenization can be seen (translucent veil/crystallization to bubble veil to cord), as the temperature locally increases.

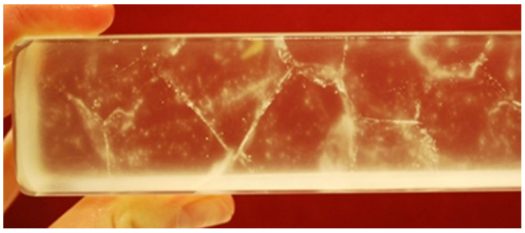

Recycled borosilicate beam kiln-cast at the TU Delft Glasslab (Scholtens, 2019) at 1120ºC, showing a meso-level structure of hexagonal form.

Placement of cullet (borosilicate rods by Schott) inside the investment mould, for the kiln-casting of the sample on the left.

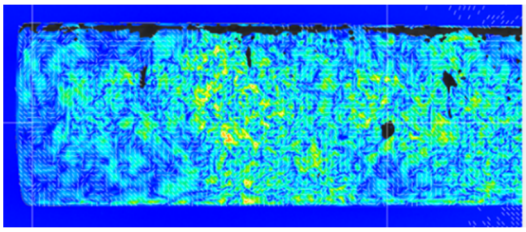

Stress distribution in a recycled borosilicate beam, kiln-cast at the TU Delft Glasslab at 1120ºC from coarse cullet (Scholtens, 2019). The polarized image has been taken by the author using an Ilis StrainScope Flex polariscope.

Cullet distribution inside the mould prior to casting the sample on the left.

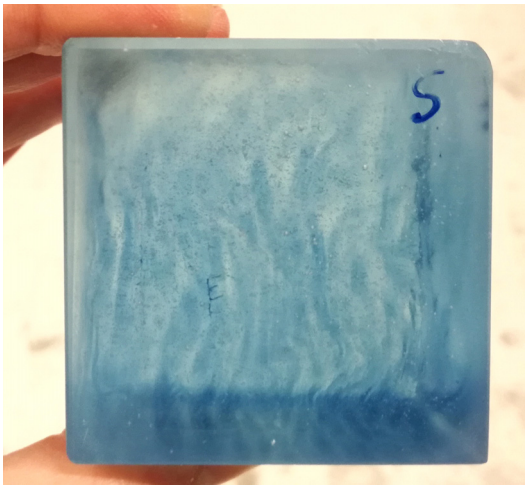

Vertical meso-level structure composed by cord, colour streaks, and air inclusions, in a recycled mirror sample kiln-cast at the TU Delft Glasslab at 1120ºC. The vertical meso-level structure is linked to the manner the mirror pieces were introduced in the mould.

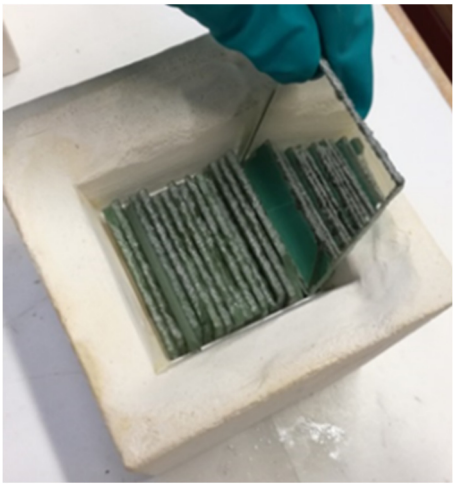

Arrangement of mirror pieces in an investment mould prior to casting the sample on the left.

Fig. 1.22 Association between the frozen-in meso-level structure in cast glass specimens (left column) and the cullet distribution inside the investment mould prior to casting (right column).

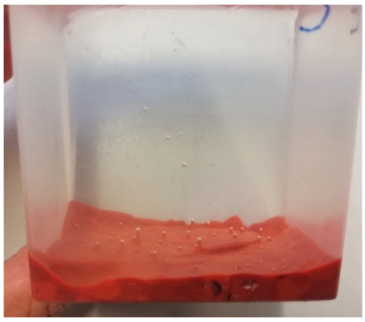

Kiln-cast at 870ºC for 10hr

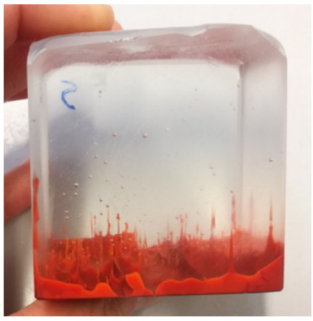

Kiln-cast at 970ºC for 20hr

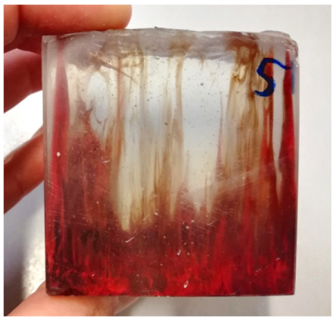

Kiln-cast at 1120ºC for 10hr

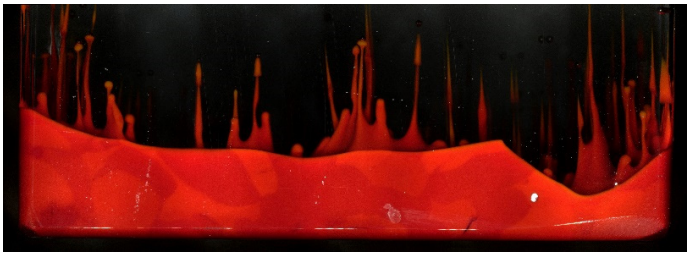

Microscope image of the 970ºC/20hr sample

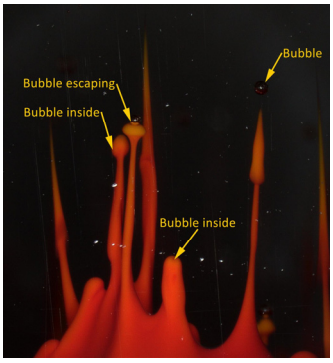

Close-up on the bubble movement

Fig. 1.23 Kiln-casting experiments at the TU Delft Glasslab exploring the mixing of two different (compatible) glasses (see Tables A1a,b in Appendix A for more details). In all specimens, the red cullet is introduced at the bottom of the investment mould, while transparent cullet is placed on top (B270 Schott glass), and the mould is slowly heated up to the selected top temperature. Computed tomography scans suggest a minor density differential between the two glasses, with the red being slightly denser. However, melting experiments show that the red glass is less viscous and more volatile at working temperatures than the clear glass. The red glass tends to have an uprising movement, which is minimal at a high viscosity (e.g. at 870ºC) but more prominent when the temperature increases by 250ºC. If the specimen is kept at 1200ºC for 10hr, then the red colour volatizes completely. The microscope images show how the uprising movement of bubbles (air trapped between the cullet pieces at the bottom of the mould) aids the transfer of the less viscous red glass through the transparent melt.

Considering the intertwined character of crystalline and glassy defects, it is meaningful to summarize the main types of compositional inhomogeneities and their causes during the forming and cooling of glass. As seen in Figure 1.24, these can be listed as:

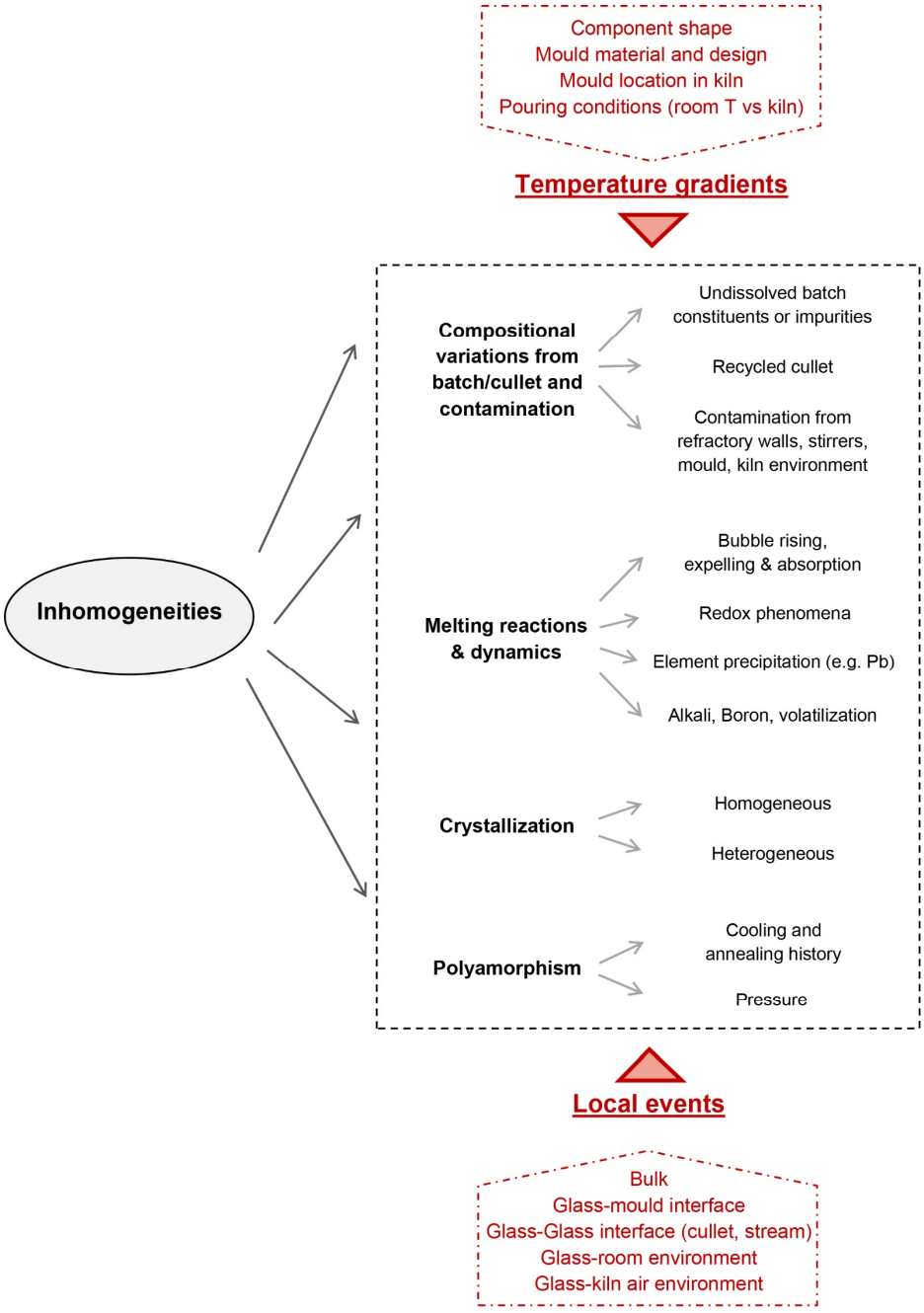

Fig. 1.24 Main types of compositional inhomogeneities in cast glass.

- **Compositional variations from batch/cullet and contamination:** this could involve undissolved batch constituents (e.g. error in batch calculation, improper batch mixing, coarse grain size used), or inhomogeneities in the cullet, if recycled material is employed. Further contamination during the melting and forming process affects the homogeneity of the glass. Main contaminants can originate from the contact of the melt with the furnace's refractory walls, stirrers, mould and kiln environment. Certain glass melts (e.g. the high temperature melting aluminosilicate) can be particularly corrosive[7] to the refractory walls or mould, leading to a higher level of contamination. As Martlew (2005) states, glass-forming melts at high temperatures are almost never in equilibrium with their vapour phase or their containing crucibles. Thus, volatilization and reaction with the crucible are anticipated. Moreover, the redox state of the glass melt will depend on the partial pressure of the gases[8] found above it.

- **Inhomogeneities resulting from melting reactions and dynamics**: various melting reactions during melting, forming and cooling (e.g. Figures 1.25-1.26) which involve the movement of gases, the evaporation of volatile components (e.g. alkali oxides, B_2O_3), the reduction or oxidation of transition metal and rare earth ions that impact the colour (e.g. reduced ferrous oxide FeO gives a green/blue colour to glass vs oxidised ferric oxide Fe_2O_3 that gives yellow/green, see Peddle 1927, Zschimmer 1913, Bray 2001), and the separation by reduction and precipitation of heavier compounds (e.g. PbO, see work by Inano 2012 and co-workers 2018).

- **Crystallization:** this describes the nucleation and growth of crystalline formations from a supercooled melt. The nuclei either exist in the batch or are formed during heating/cooling due to component reactions. Crystallization can be categorized as homogeneous (intrinsic) or heterogeneous (assisted). According to Cormier (2017), homogeneous crystallization has an equal probability of occurring in any part of the melt due to a thermally activated fluctuation in density, composition, or entropy. The crystalline phase has the stoichiometry of the initial glass- something that in practice only occurs in a limited number of compositions of short/medium range order, where the low-dimensionality of the system allows such structural rearrangements. On the other hand, heterogeneous crystallization commences on a preferential site, this being a pre-existing surface (e.g. the wall of a mould), a previously nucleated element, impurities, bubbles etc.

- **Polyamorphism:** this phenomenon assumes various short-range non-crystalline ordering forms in an amorphous structure, some denser, with a higher level of cross-linking than

[7] According to Peddle (1927), glasses rich in basic constituents (e.g. PbO, Na_2O, CaO, Li_2O, MgO, BaO) need to be melted in highly-aluminous clay refractories while highly acidic glasses (e.g. SiO_2, B_2O_3) should be molten in silica-rich clay refractories. If an improper choice is made -to use here the example of a silicate glass rich in basic oxides glasses- it will be observed that at melting temperatures, the silica content (acid) is not enough to satisfy the basic content, so the latter will extract silica from the refractory wall.
[8] Such as oxygen, nitrogen, water vapour etc.

others. This has been observed in glassy metals and only computationally proven for silica. Pressure and heat-treatment are responsible for these different packing phases.

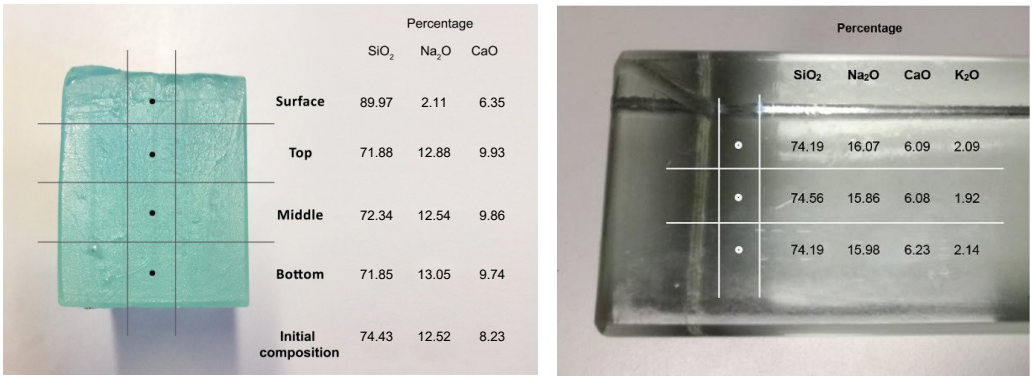

Fig 1.25 Chemical composition determined by X-Ray fluorescence in segments extracted from a recycled float glass component (left, kiln-cast at the TU Delft Glasslab) and a Poesia brick (right, hot-poured at Vetreria Resanese). The Poesia brick, produced at a higher temperature and from purer materials, has a high degree of compositional homogeneity. The kiln-cast recycled component shows more compositional variations within the bulk, and a striking depletion of alkali at the top surface, due to the prolonged dwell time at top temperature (1120ºC).

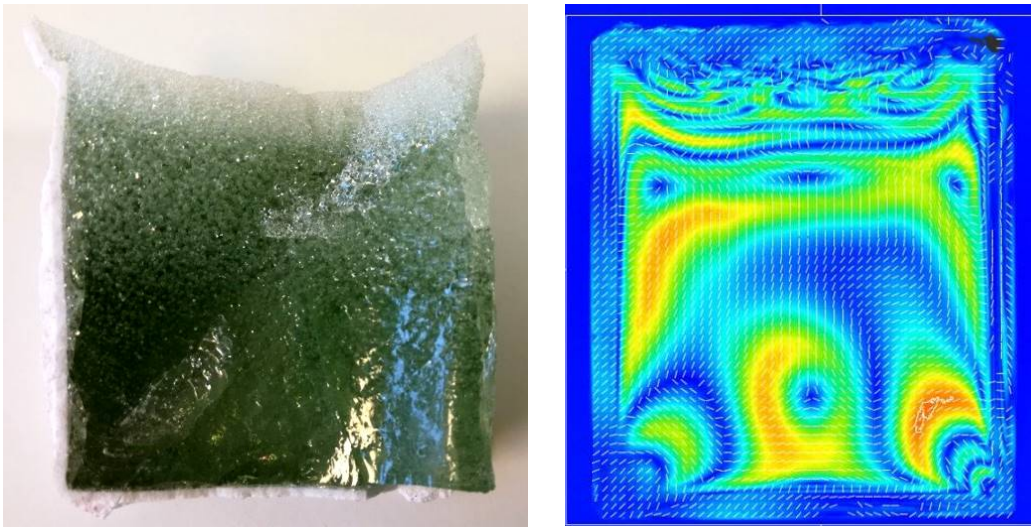

Fig. 1.26 Inhomogeneities resulting from melting reactions observed in kiln-cast specimens at the TU Delft Glasslab. Left: side cross-section of a recycled fiberglass specimen (1120ºC), characterized by a gradient increase of bubble concentration towards the top surface. The great population of bubbles is related to the powder form of the cullet and the high viscosity of the melt at top temperature. Right: stress concentration observed through the side view of a recycled borosilicate specimen (1120ºC) using an Ilis StrainScope polariscope. Given the volatile character of B_2O_3, intense cord is created at the top side of the specimen.

Temperature gradients and local events will promote or suppress the manifestation of the above inhomogeneities. Temperature fluctuations can be imposed by various reasons, such as the heat flow at the melting furnace, the shape of the glass component, the type and material of the mould, the pouring conditions (e.g. within a kiln vs at atmospheric conditions), or the location of a mould in the annealing kiln. For example, the pouring of molten glass into a cold mould, exposes the exterior of the glass stream to an abruptly cold temperature; depending on the viscosity of the glass and the diameter of the stream, this temperature drop could lead to an obvious layering or cord in the glass component. Once the glass melt is poured in the mould, different conditions and transfer phenomena will apply at the glass zone in contact with the mould than the one in contact with the kiln air or room atmosphere and so forth. This stresses the role that fluctuating local conditions play during glass forming and annealing.

Glass defects have been well documented in literature, mainly focusing on float and container glass, as well as optical and specialty glass. As previously mentioned, one can borrow the developed defect characterizations, classifications, causations and definitions for describing the formation of defects in cast glass, yet an additional importance needs to be adhered to the role of geometry, and thus to the creation of meso-level structures out of a combination of manufacturing flaws. In this process of determining casting related defects, an interesting new direction arises, this of glass recycling by casting. In 2017, the Re^3 Glass project commenced (Oikonomopoulou and Bristogianni 2019), with the aim to recycle currently non-recyclable glass by casting (Figures 1.27-1.28). Currently, apart from the successful closed-loop recycling of container glass in Europe, the rest of the glass products are in their majority downcycled or landfilled. This comes down to the lack of infrastructure for the collection, separation and treatment of glasses different in composition and surface treatment than container glass, and the distrust of glass producers to contaminate their furnaces with recycled cullet. The project, therefore, benefiting from the flexibility of glass casting and the small scale of typical glass foundries, has been focusing on the casting of a wide range of commercial waste glass products, in their “as received” form and at relatively high viscosities that are linked with lower forming temperatures and thus energy savings and CO_2 emission reductions. As glass technology progresses and novel glass compositions, together with new coating, heat-treatment, lamination and adhesion systems are introduced in the market, novel, un-documented types of defects are expected to come forward during their recycling process.

Fig. 1.27 Prototype for the Re^3 Glass project, kiln-cast at the TU Delft Glasslab. The interlocking building components are cast out of waste artware glass. The kiln-casting at a low temperature, below the liquidus point of this glass (870ºC), and the slow cooling lead to the partial crystallization of the glass, and thus marble like appearance of the components.

Fig. 1.28 Re^3 Glass prototypes kiln-cast at the TU Delft glass at 1120ºC out of car windshields (left), containers (middle) and oven-doors (right). The remelting of commercial glass waste in its "as-received" form introduces a rich pallet of defects in the glass network. The severity of such flaws is uncertain.

It is therefore evident that, on top of the knowledge deficit of the various aspects of the mechanical properties of homogeneous, well-manufactured cast glass, further uncertainties are added due to the random and non-random distributions of the combination of inherent and newly-introduced defects.

1.1.5 Defining the mechanical properties of cast glass

Glass is intrinsically strong due to its covalent and ionic bonds, but for the same reason is also brittle (Lawn and Marshall 1979). It cannot exhibit any form of plastic flow or permanent deformation below T_g and will thus fail abruptly when the applied tensile stress (locally) exceeds its capacity, usually at built-up stress concentration around a flaw. The strength of glass is thus defined by the fracture toughness in combination with the size, orientation and criticality of the worst present defect. This applies if the glass object is uniformly subjected to a constant tensile stress, a condition that usually neither in real-world applications nor in mechanical testing procedures actually occurs. Given the stress gradients commonly developing in a strained glass component, the glass will fail –in tension- by the flaw that will first reach the critical stress intensity factor K_{Ic} (fracture toughness). Formulae for slender elliptical flaws and sharp flaws subjected to far field stresses were developed by Griffith (1920)[9] and Irwin (1957)[10]. Here the strength of the component is related to the fracture toughness and inversely related to the size and criticality factor of the defect. However, in most loading scenarios (either in laboratory testing[11] or in application scenarios), it is mainly the defects situated at the glass surface that will determine the strength. Littleton remarked that "we never test the strength of glass: all we test is the weakness of its surface", and experimentally showed that the etching of glass beams in hydrofluoric acid etched away the micro-cracks at the surface, resulting in a glass specimen with high tensile strength values, stronger than those of nickel steel (Preston 1942). Preston (1942) later on indicated the effects of moisture and temperature on glass strength, due to static fatigue, and rephrased Littleton stating that "we do not test the properties of the glass at all, but only those of the surrounding atmosphere". Indeed static, dynamic and cyclic fatigue in glass is a commonly reported phenomenon, often mentioned in the literature as "environmentally assisted slow crack growth" (see work by Charles 1958a-c, Wiederhorn and Bolz 1970, Doremus, 1974, Varner 1996, Haldimann 2006, Brokmann et al 2021 to name a few). The opening of a pre-existing crack at a glass surface requires an applied stress and a reactive species that will chemically attack the bonds at the crack tip. Usually water, in liquid of vapour form, plays the role of the reactive medium, and temperature can assist or slow down the travelling of water through the crack. Mould (1967) mentioned the extreme range of fracture stresses (200:1) on superficially identical samples, and

[9] Griffith (1920) developed the formula below, with σ_f= fracture strength, E= Young's modulus, γ_f= fracture energy and c= radius of an elliptical flaw:

$$\sigma_f = \sqrt{\frac{2 \cdot E \cdot \gamma_f}{\pi \cdot c}} \quad (1)$$

[10] Irwin's equation (1957) relates the fracture strength σ_f to the fracture toughness K_{Ic}:

$$\sigma_f = \frac{K_{Ic}}{Y \cdot \sqrt{c}} \quad (2)$$

Where Y= stress intensity shape factor, a dimensionless geometric parameter based on the shape of the flaw, and c= size of the flaw, and specifically, half its length if the flaw is situated in the bulk, or full its length if it is situated at the surface.

[11] Typical strength testing methods for glass include 3- and 4-point flexure, biaxial "Ring on Ring", uni-axial compression and direct tension, while diametral compression (Brazilian Disk) is less common.

calculated[12] the instantaneous and static fatigue strength of soda lime silica glass in relation to the surface flaw depth. He assigned a $0.3x10^6$ -$2x10^6$ psi (2.1-13.8 GPa) strength to pristine, as drawn glass, for a corresponding flaw depth range of up 10^{-6} -$5x10^{-8}$ inches ($2.54x10^{-6}$ -$12.7x10^{-8}$ cm). This strength would drop to $0.1x10^6$ -$0.7x10^6$ psi (0.7-4.8 GPa) respectively due to fatigue. A visibly damaged and fatigued glass on the other hand, would have a strength as low as $0.001x10^6$ psi (0.007 GPa) for a 10^{-2} inches ($2.54x10^{-2}$ cm) flaw depth. Thus, the strength of glass is the combined result of fracture toughness, surface quality and environmental conditions under loading.

In the field of structural glass, there are multiple documents exploring the strength of float glass in relation to surface flaws either due to machining (Veer 2007, Veer and Rodichev 2011, Vandebroek et al. 2012 and 2014, Lindqvist 2013, Kleuderlein et al. 2016, Sable and Kalnins 2017, Bukieda et al. 2020), external damage (Kašiarová et al. 2005, Swab et al. 2013), and weathering (Datsiou and Overend 2017a-b, Ronchetto 2019). As an example, Datsiou and Overend (2017a) experimentally showed a 68% reduction in the mean strength of annealed glass, after artificial ageing by sand abrasion (coaxial double ring tests on 150x150mm specimens). Veer and Zuidema (2003) tested annealed float glass 400x40mm specimens of 3, 6 and 8mm thickness in 3-point bending, with different edge qualities, from manually cut to machine cut and polished. As anticipated, the Weibull derived design strength of a manually cut 6mm specimen was significantly lower (38MPa), than the strength corresponding to the machine cut and fully polished specimen (70MPa). An interesting remark is the reduction of the strength with the increase of specimen thickness (from 55MPa to 32MPa). This is not only attributed to the size factor, but to the fact that the crack growth process cutting the glass is rougher in thicker specimens, increasing the caused damage, which is not sufficiently removed by polishing. This exposes the complexity of scaling up a structural component, even for a few millimetres. Vandebroek et al. 2012 performed in-plane 4-point bending tests using 550x50x4mm annealed float glass specimens (20 per series) with either cut or polished edge finishing, and loading them either at a high stress rate (≈55MPa/s) or a low stress rate (≈0.55MPa/s). The reported tensile strength corresponding to a linearly increasing loading was ranging from 68-127MPa for specimens with polished edges and tested using a fast stress rate, to 28-48MPa for specimens with cut edges and tested using a slow stress rate. Vandebroek et al. (2014) performed similar in-plane 4-point bending tests (stress rate ≈0.06MPa/s), studying float glass specimens (30 per series) of 2 sizes (550x62.5mm and 1100x125mm), of 4 or 8mm thickness, and with cut or ground edges, and evaluated the accuracy of analytical prediction models in deriving the strength reduction due to the size effect. The reported mean values showed a range from 40.9-56.2MPa, with the larger specimens being weaker than the smaller counterparts (e.g. the mean strength value for the 4mm/ground edge/small series was 48.1MPa while for the 4mm/ground edge/large

[12] Below the equation used for this calculation, based on the work of Inglis (1913) and Orowan (1955):

$$\sigma\sqrt{c} = K \quad (3)$$

Where σ = strength, c = surface flaw depth and K is a constant. Equation (3) is in essence equation (2) with the geometrical parameter Y omitted. Inglis suggests that this relationship is valid to a high approximation regardless of the general shape of the surface flaw, as long as a uniform stress is applied and the crack tip is elliptical.

series was 41.5MPa). Regarding the variation in strength per thickness, it was found that the specimens with cut edges were stronger in the 4mm series than the 8mm one, yet the opposite occurred for the specimens with the ground edges, which proved stronger in the 8mm series. Bukieda et al. (2020) performed in-plane 4-point bending tests using 1100x125x10mm float glass specimens with different edge finishing characteristics and reported a wide range of bending strength values, specifically 35.03-103.77MPa (59-87MPa mean strength with an average of 16.5MPa standard deviation). Variations in the reported bending strength values must also be expected when a different testing method is employed. For example, in antithesis to the 4-point bending method that tests the edge quality, the coaxial double ring test neglects the edges and tests the quality of the surface. Especially in the case of the coaxial double ring test with small test surface areas (EN 1288-5), the reported bending strength values can be 300% higher than those reported by the 4-point bending test (EN 1288-3) or the coaxial double ring test with large surface areas (EN 1288-2) (Feldmann et al. 2014). The very familiar to engineers 45MPa value of the characteristic bending strength for float glass (EN 572-1:2012), derives in fact from testing employing the favourable coaxial double ring method (EN 1288-5). Castori and Speranzini (2016) performed coaxial double ring tests on 100x100mm float glass specimens of 4, 5, 6, or 8mm thickness, using a stress rate of ≈2MPa/s and reported a mean bending strength range from 134-216MPa. Haldimann (2006) performed coaxial double ring tests on 200mm square annealed float specimens of 6mm thickness, at different testing speeds and surface conditions. The samples tested in ambient temperature conditions, showed a 55MPa average strength (with a 16.6MPa standard deviation SD) when tested at a 0.21MPa/s rate versus 103MPa (SD= 28.5MPa) for the hundred times higher rate of 21MPa/s. The dried and coated samples (to approximate inert conditions) on the other hand, showed an average strength of 85MPa strength (SD= 20MPa) for the slow testing rate (0.21MPa/s)[13]. So not only the randomness in the population of flaws but also the external testing factors add to the complexity of experimentally defining a design strength for glass. Persson et al. (2020) attempted to correlate the mapping of large surface cracks in glass specimens by Nonlinear Acoustic Wave with the components failure strength, in order to establish an non-destructive quality control method that predicts the strength of glass. Several strength prediction mathematical models have also been developed –either microscopic (assuming pre-existing flaws) or macroscopic based (see the work of Kinsella providing an extensive overview of the prevailing models) with the Weibull distribution being the most commonly applied model.

The above examples and many more found in the literature show the broadness of the reported bending strength values for float glass, which depend (assuming homogeneous and sufficiently annealed float glass samples) on the edge and surface quality, the size and thickness of the specimens and number of tests per series, and on the experimental set-up and conditions. In addition, one should account for additional complexity when the characteristic strength value (5% fractile value) is reported, as the accuracy of this value depends on the mathematical prediction model applied and the number of tested specimens. Overall, the elusive character of the strength

[13] Average and standard deviation values calculated based on the data provided by Haldimann (2006) in Appendix C.1, and for a number of 10 tested samples per series.

of glass and the succeeding uncertainties for determining reliable design values in structural glass engineering lead often to unsafe (over-confident) estimations or to the use of an increased material factor that compensates for the above uncertainties.

Moreover, given the high level of homogeneity of float glass and its slender proportions (area to thickness ratio), it is a logical consequence that the majority of scientific structural glass research concentrates on the role the surface and edges play in determining the strength. It is unclear, however, if we can assume the same for a voluminous cast glass component. The much higher population of flaws, often of more than one type and occurring along the totality of the glass volume, in relation to the prominent nature of the bulk of a cast glass component, raise questions about the effect they have on the strength. It also pinpoints that mechanical testing targeting the surface quality, such as micro- or nano-hardness or an indentation fracture toughness test, would only provide information for the tip of the iceberg in this case. In a similar fashion, it is common to consider one value for the Young's (E) modulus or Poisson's ratio of glass, but what really happens when a bulk glass is characterized by distinct inhomogeneities along the bulk? Several formulae have been developed that link typical different but homogenous glass compositions with the E modulus (Makishima and Mackenzie 1973), Poisson's ratio (Makishima and Mackenzie 1975), fracture toughness (Rouxel 2017), and Vickers hardness (Yamane and Mackenzie 1974), yet to what extent are these relevant to inhomogeneous cast glass, given that the inhomogeneities and flaws at meso-level structure level together with the actual thermal history gradient seem to have a prominent role upon the resulting glass composition?

The testing of cast glass in fact requires the design of new experimental methods, which focus on the equal activation of defects at both the surface and in the bulk. This is however a daring step if first a comparison of cast glass with float is not established by standard testing methods. This comparison should eventually generate the needed tools for specialized testing procedures for cast glass. Even if a specific experimental method (e.g. 4-point bending) targets the specimen's surface, there is still a lot to be learned simply by comparing the performance of a defective cast glass specimen with that of a pure homogeneous float glass specimen. Moreover, fractographic analysis of the interaction of the crack front with the flaws it encounters in the bulk, can reveal information about the impact these flaws have on the surrounding glass matrix.

1.1.6 Intensification of the casting flaws as a telltale method

For purposes of correlation of the casting parameters to the created defects and for the understanding of the role of these volumetrically distributed defects to the mechanical properties of the cast glass component, it is meaningful to examine cast glass of different levels of homogeneity. Casting using batch materials of different grades of purity and at different viscosities can increase or reduce the amount of inhomogeneities. Experimentation with various chemical compositions and thermal histories can in addition provide information about the response of the created glass network (bond strength and atomic packing density) to the imposed inhomogeneities during mechanical loading. So in contrast to the holy grail of glass science- that

of total glass homogeneity- this work deliberately opts to employ glass batches with impurities and high forming viscosities, in order to introduce distinct meso-level structures that facilitate the studying of the above mentioned relationships (Figure 1.29). For this purpose, waste glass of various different sources, compositions and contamination types is employed, contributing to the random creation and distribution of a rich pallet of flaws.

Fig. 1.29 Kiln-casting method followed at the TU Delft Glasslab, employing low temperatures/high kinematic glass viscosities that intensify the creation of casting defects in the glass.

The casting of these glass cullet qualities at different temperatures and cooling rates will further freeze structures that correspond to different viscosities, revealing how diffusion evolves with temperature during glass forming and how inhomogeneities form glass meso-level structures. As an example, the mixing of transparent and red-coloured Ø25mm glass spheres is presented, at different temperatures and configurations within a 50mm cubic mould (Figures 1.30-1.32). It becomes evident that at low forming temperatures (in this case 970°C), the glass spheres and their corresponding molecules follow the "Cage principle" for dense liquids: the molecules are confined by their neighbouring molecules and will not diffuse or flow to the other side of the liquid as there is not enough energy for such movement. Therefore, if we focus on the movement of the clear spheres inside the square mould (all volumetrically and compositionally equal), these will deform into cube-like shapes to fill-up the space corresponding to them by the boundaries set by the mould and adjustment spheres (see the sample in Figure 1.30 containing only clear spheres as a reference). The red sphere, being less viscous at this temperature due to its different composition and it having a lower surface tension than the clear spheres, will travel further in between the space of the clear spheres. Yet only minimum interdiffusion will occur at the border of the clear and red spheres due to the low temperature. With the increase of the temperature (e.g. 1120°C), diffusion between the clear and red glass will be facilitated significantly. Any differential between the spheres, concerning density and viscosity, will promote this diffusion. Differentials in viscosity can also occur within the same type of glass sphere, if there is a variable heat flow within the mould, for example due to its position inside the kiln. Other movements such as bubble rising or capillary movement along the mould will contribute as well to the material

transfer and mixing (Figure 1.23). The higher the temperature, the longer the dwell time, and the more the instabilities (viscosity, density etc.) are, then the higher the mixing rate (Figure 1.33). However, unless the temperature is much more increased to a corresponding viscosity of perhaps 10-10^2 dPa·s and/or a mechanical stirring is imposed, it cannot be expected that a glass melt containing two or more distinct compositions, will inherently mix (Figure 1.34). Inhomogeneities are therefore to be expected when cullet of different sources is used and once contamination is present in the batch/cullet. This is particularly dominant in the case of glass recycling and specifically in the use of waste glass for casting.

Fig. 1.30 Kiln-casting experiment at 970ºC, using two layers of Ø25mm clear glass spheres introduced inside the investment mould (left). The top (middle) and bottom (right) aspect of the cast specimen suggest the equal filling of the mould space by each sphere.

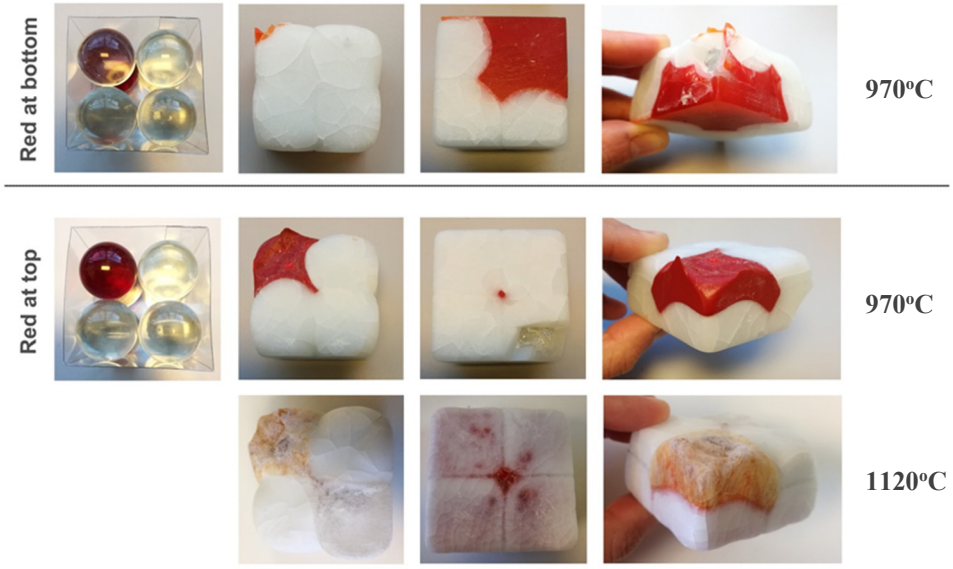

Fig. 1.31 Kiln-casting experiment, using two layers of Ø25mm clear glass spheres and replacing one clear sphere with a red one. The red sphere has a lower surface tension and viscosity than the clear one, therefore it starts to fill up the space between the clear spheres before they start to deform (see prototypes cast at 970ºC). With an increase in temperature, diffusive movements will be more prominent, and the red colour will distribute further along the mould, mixing with the clear glass.

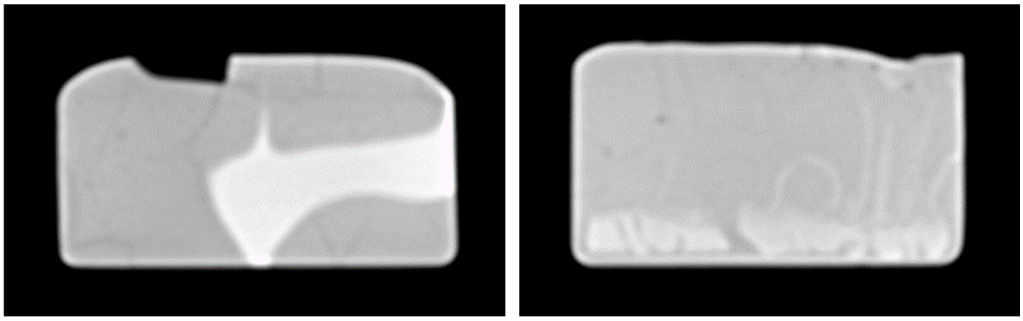

Fig. 1.32 Cross-section of a 970ºC/red sphere at top (left) and 1120ºC/red sphere at bottom (right) specimen, as seen in a computed tomography (CT) scan. The red glass appears as white (denser) in the image. With an increase in temperature, the red colour flows and covers the bottom of the mould, and then starts an uprising movement, seen as white vertical fingers.

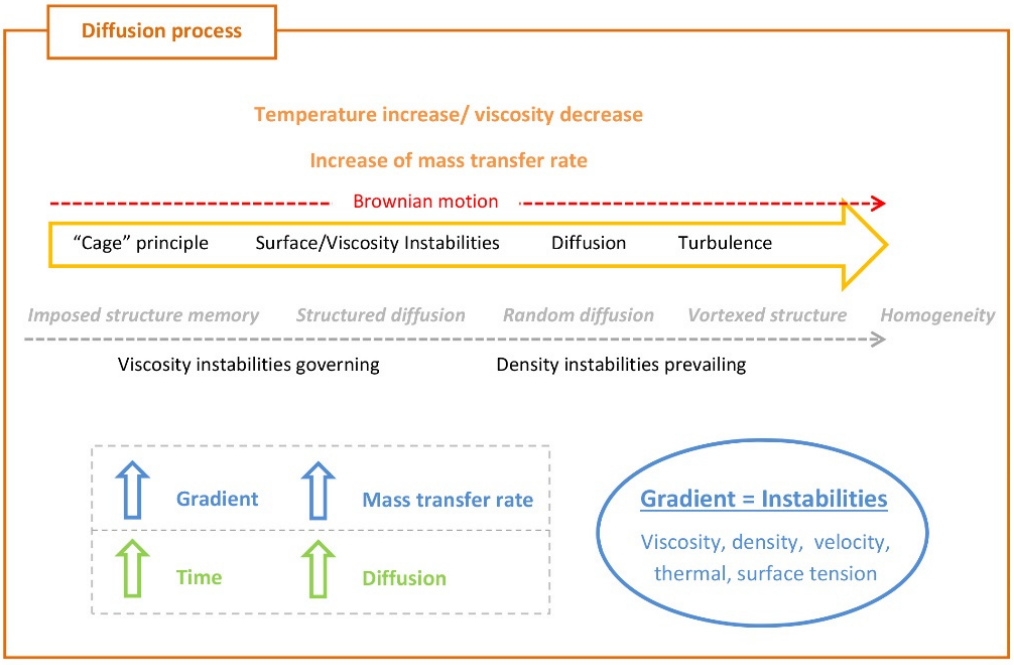

Fig. 1.33 The diffusion process between two glasses is powered by the temperature and the level of instabilities between the two compositions.

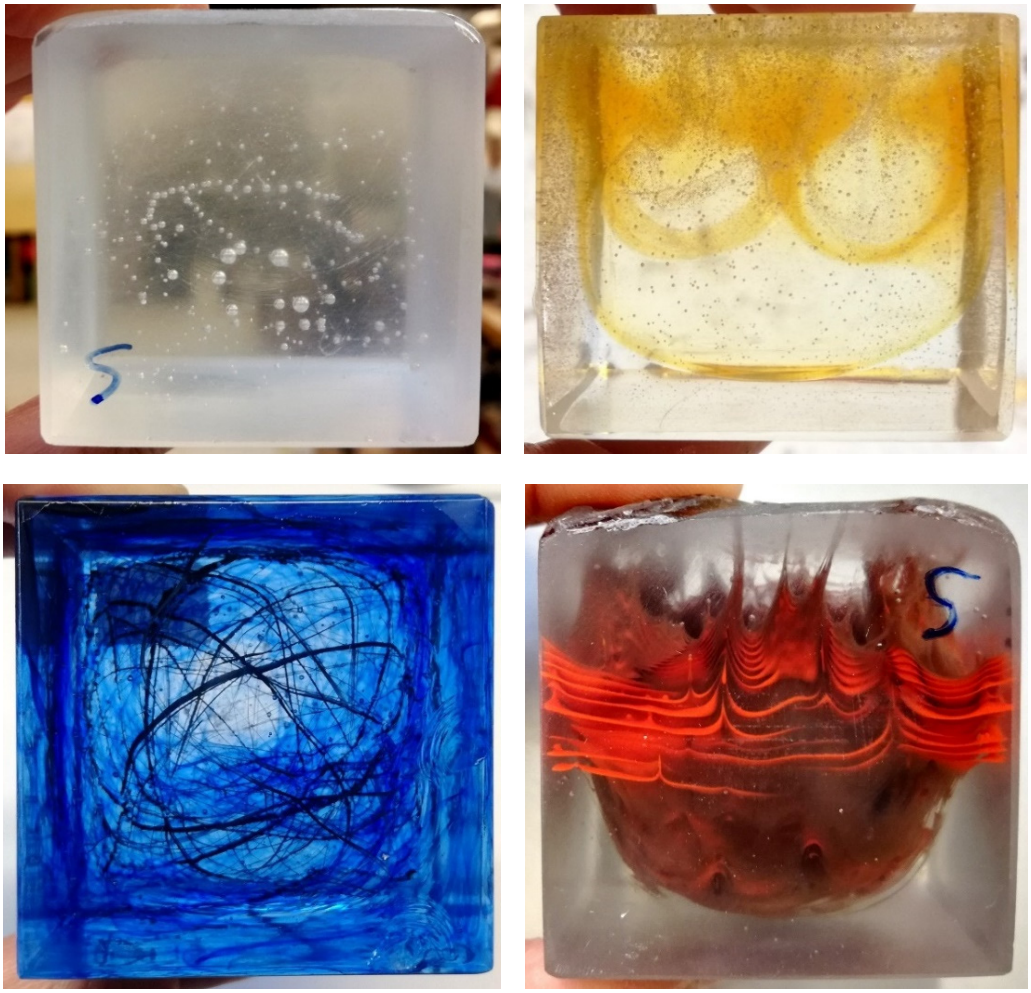

Fig. 1.34 Kiln-cast specimens employing different silicate base glasses. The specimens on the left column are kiln-cast at 870ºC, preserving in this manner a characteristic swirling meso-level structure that originates from the coiling of the glass thread inside the mould. The increasing temperature used in the specimens to the right (970ºC) allows for diffusion and convection to take place, especially if the glass (in this case the yellow and red glass) have volatile components. Yet, total homogenization of the glass mixture will not readily occur at these viscosities in reasonable holding times in the oven.

It is of particular interest to investigate the effect of inhomogeneities in the glass network appearing as localized events, distinct zones with hard boundaries or diffused zones blended through diffusion to the hosting glass (Figure 1.35). In this manner, light can be shed to the performance of glasses with localized or gradient shifts in the mechanical properties. Such results could inform about the risks present in cast glass products perceived as homogeneous, yet they contain subtle defects that are overlooked during quality control inspection.

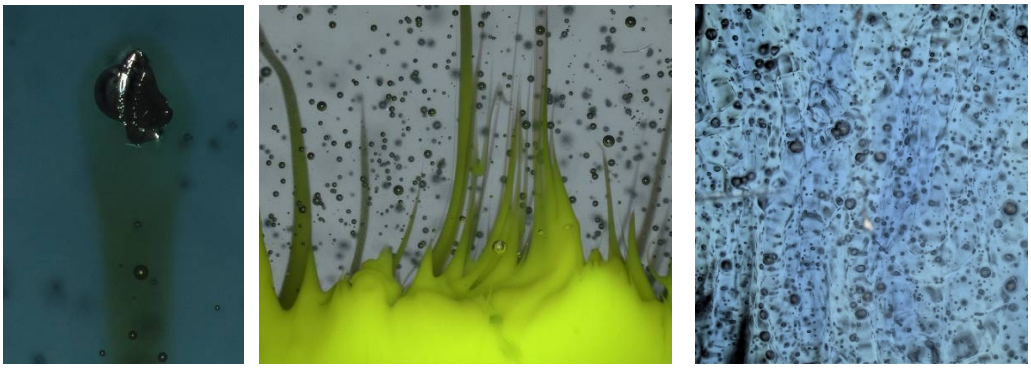

Fig. 1.35 Microscope images of kiln-cast specimens, showing a localized singularity (left), a hard interface (middle) and blended inhomogeneities (right).

The experimental approach is preferred at this stage over a computational prediction model. The creation of different flaws is a complex, multi-parameter phenomenon that first requires extensive physical testing, in order to determine the laws for flaw occurrence and the correlation with casting parameters. An attempt of by-passing the experimental stage at this point would simply lead to inaccurate results.

1.2 Research questions

Considering the above argumentation, a set of main research questions is formed, related to the strength of cast glass as a function of its flaw population and the casting process followed for its creation.

- What is the correlation between casting parameters and defect formation? Further on, how do glass meso-level structures develop as a result of the casting process? Can the location and features of inhomogeneous zones be controlled? In that sense, can weak or strong zones be engineered in the glass bulk?
- How do inhomogeneities at the surface and in the glass bulk affect the strength and stiffness of cast glass components? To what extent do they affect the crack propagation path and can a terminal crack be arrested by crystalline zones in the bulk? Can the criticality of such defects be ranked according to their type, shape and arrangement? What is the role of the chemical composition to the strength and response to stress around a flaw?
- Can waste glass cullet be used for casting and what are the implications regarding the compositional varieties and contamination rates? Moreover, to what extent can we employ lower forming temperatures in order to achieve sustainable structural glass components?

1.3 Aim and objectives

The aim of this work is to develop an understanding of the effect of the casting parameters on the meso-level structure of cast glass, and thereupon of the relationship between this meso-level structure and the strength, stiffness and fracture resistance of cast glass components. Towards this goal, several objectives are set:

- Experiment by casting different glass recipes -of pure or contaminated quality, employing variable casting parameters
- Correlate the casting parameters to the resulting meso-level structure and defects
- Control the development of specific meso-level structures in a cast glass component
- Experimentally validate the strength, stiffness and fracture resistance of various cast glass specimens and associate the properties to the meso-level structure characteristics
- Provide a distinction regarding the criticality of the different observed defects, as well as the effect of flaw location (surface vs bulk) on strength and crack propagation
- Comprehend the negative results from using improper casting procedures and initiate a discussion for the need of establishing production standards for the manufacturing of safe and reliable structural cast glass components
- Inform glass technologists and engineers on the quality control process required for the safe application of cast glass components in structures.

1.4 Methodology and outline of the dissertation

This dissertation is at its core based on the methodology of physical prototyping and testing. The research adopts the exploratory "Cook and look" method, which is commonly used by glass scientists to develop and test new glass compositions. Destructive and non-destructive mechanical testing methods are used, to acquire information about the different quality levels of cast glass. The research work –outlined in Figure 1.36- is organized in three stages as following:

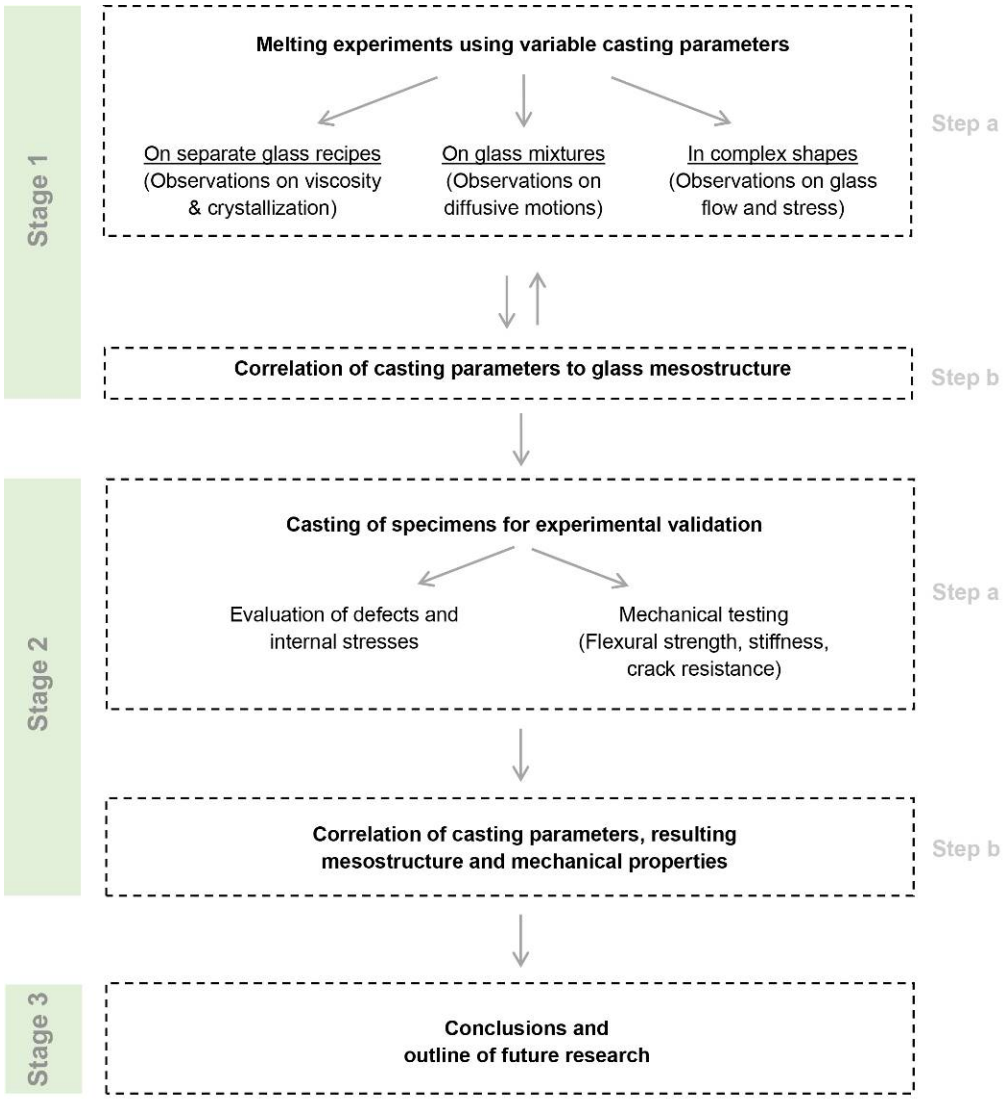

Fig. 1.36 Outline of experimental work.

Stage 1: This stage involves two steps, (a) the conduction of melting and casting experiments using various casting parameters and (b) the study of the observed meso-level structures and their correlation to the casting parameters. According to the results of step (b), further melting experiments are conducted focusing on the new aspects brought into surface. The melting experiments in step (a) are divided into three categories:

(i.) the casting of different glass recipes individually: this category contributes to the understanding of the thermal profile of main glass compositions of commercial interest. The tests reveal at what temperatures each glass family can be molten, poured,

crystallized and annealed. This shows if they are suitable candidates for glass casting (Figure 1.37). The results of this research are presented in Chapter 2.

Fig. 1.37 Study on the casting potential of different commercial glass waste sources, in the context of the Re^3 Glass project; image by F. Oikonomopoulou.

(ii.) the casting of glass mixtures of the same or different compositional families: this category explores the diffusive motions occurring during the mixing of two different glass recipes. The mixing of glasses with minor compositional variations (e.g. same glass family, yet different colour, viscosity and density characteristics) as well as glasses with significant differences (e.g. lead glass versus soda lime silica glass) is studied. The aim is to understand how inhomogeneities and internal stresses are built up or blended in, in relation to the mixing method (e.g. premixed cullet vs separate positioning of each cullet type), casting process (e.g. pouring vs depositing cullet in the mould) and the shape characteristics of the different cullet types used (see Figures 1.38-1.40 as a reference). This step serves as an understanding for the author of how meso-level structures are created in cast glass, so that the most characteristic specimens out of recycled cullet can be created. Therefore the most important conclusions of this category will be presented in the specimen preparation and assessment sections of Chapters 3-5. An overview of the diffusion experiments on similar compositions can be found in Tables A1a-b and A2 in the appendix, while studies on the mixing of distinct compositions can be found in the paper by Anagni et al. (2020).

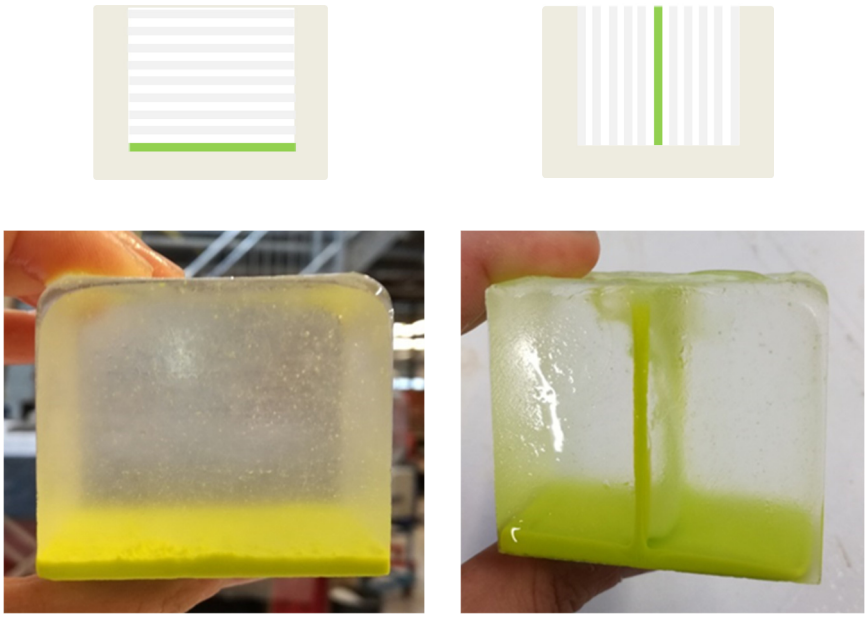

Fig. 1.38 Study of the mixing behaviour of two compatible glasses (Bullseye glass 3mm sheets, clear and opaque green colour) at 970ºC, at different cullet distributions (left: green glass placed at the bottom of the mould, right: green glass vertically placed at the middle. The sketches and images above show the side view of the cullet configuration followed inside the moulds and of the final kiln-cast components). The two glasses do not readily mix at the given temperature, and therefore the green glass, by being denser, tends to occupy the bottom part of the mould in both cases.

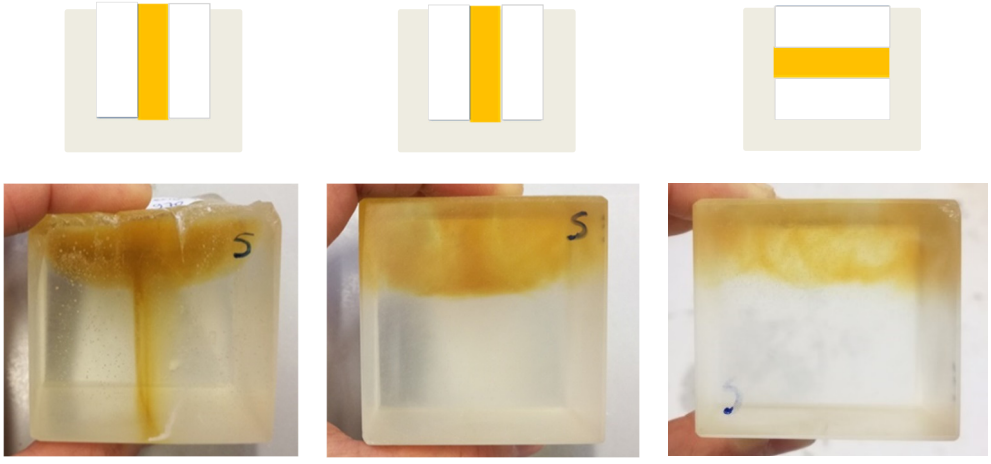

970ºC 1120ºC 1120ºC

Fig. 1.39 Study of the mixing behaviour of two compatible glasses (Poesia glass, cut in 16mm strips, clear and amber colour) at different temperatures and cullet distributions. The sketches and images above show the side view of the cullet configuration followed inside the moulds and of the final kiln-cast components. The amber glass is quite volatile (the colour is acquired by the –volatile- sulphur in the composition) and will tend to rise at the top of the mould regardless the configuration. The specimen kiln-cast at a lower temperature (970ºC) captures the upward movement of the amber glass.

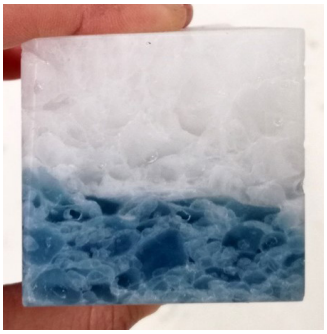

970ºC

Blue cullet placed at the bottom of the mould

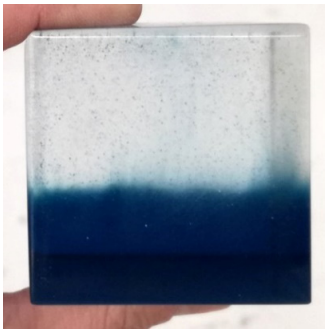

1120ºC

Blue cullet placed at the bottom of the mould

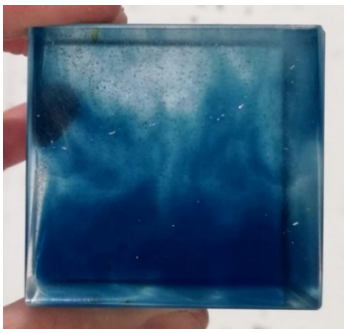

1120ºC

Blue cullet placed at the top of the mould

Fig. 1.40 Study of the mixing behaviour of two compatible glasses (AGC float glass cullet, clear and blue colour) at different temperatures and cullet distributions. The images above show the side view of the final kiln-cast components. The specimen to the right shows how the positioning of the cullet –in combination with the increase in temperature- can assist the diffusive mixing of the two glasses.

(iii.) The casting of complex shapes: This category explores the flow of relatively or highly viscous molten glass inside a mould of complex shape. It focuses on the concentration of flaws (e.g. bubbles, cord) due to mould undercuts and size variations, and the development of internal stresses (see Figures 1.41-1.42 as reference). The results of this category point out an additional complexity in the creation of meso-level structures, which is not present in the creation of specimens of orthogonal geometry (used for the mechanical testing), yet is very much relevant to the production of freeform cast glass components for building applications. Studies on this aspect are found in Appendix B (Bristogianni et al., 2016, Bristogianni et al., 2017), as well as in the MSc thesis work of Barou (2016), Sombroek (2016), Akerboom (2016), conducted under the author's supervision.

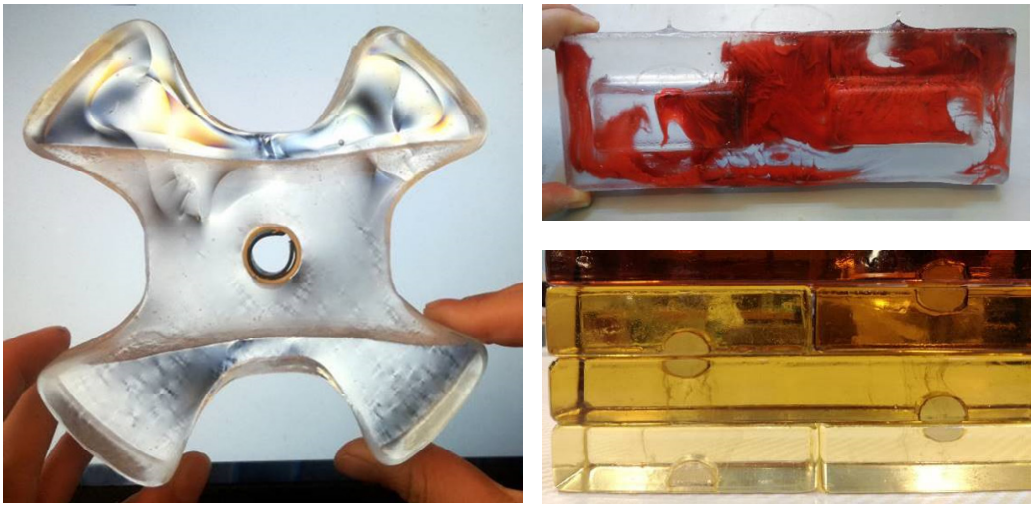

Fig. 1.41 Study of the flow of glass in complex mould shapes and the concentration of flaws due to geometry. Cross-polarization techniques (left) can indicate the regions of stress concentration but also the flow of the molten glass during casting and how this movement is related to stress. The use of colour (top right image) can also assist to the understanding of glass flow. The image to the bottom right (prototype developed for MVRDV and Bvlgari by the TU Delft Glasslab) shows repetitive flaw patterns associated with the undercut connection detail of the glass bricks.

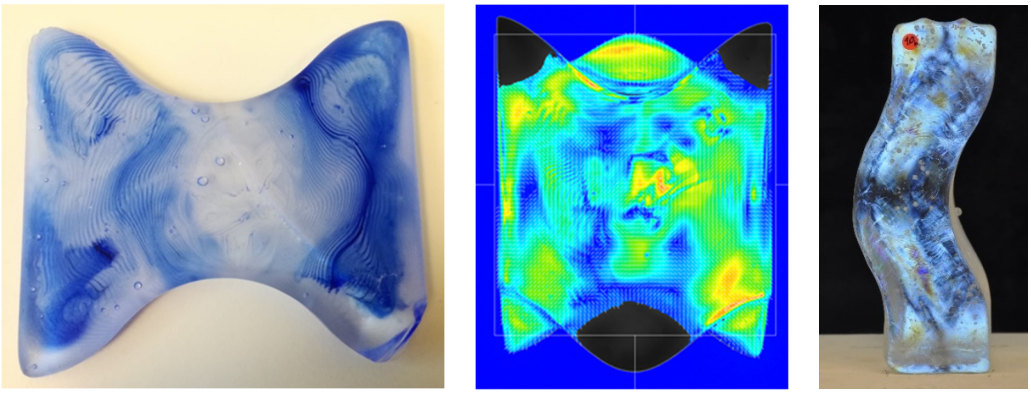

Fig. 1.42 Study of viscous glass flow in complex shapes, using colour (left) and polarization techniques (middle: image by Ilis StrainScope polariscope, right: image through cross-polarized films).

Further on in step (b), the obtained meso-level structures are analysed with the help of digital microscopy, cross polarized light techniques, and computed tomography (CT) scanning, and linked to the employed casting parameters. This knowledge and observations are employed for the creation of a wide range of specimens for the purposes of Stage 2 (Figures 1.43-1.44).

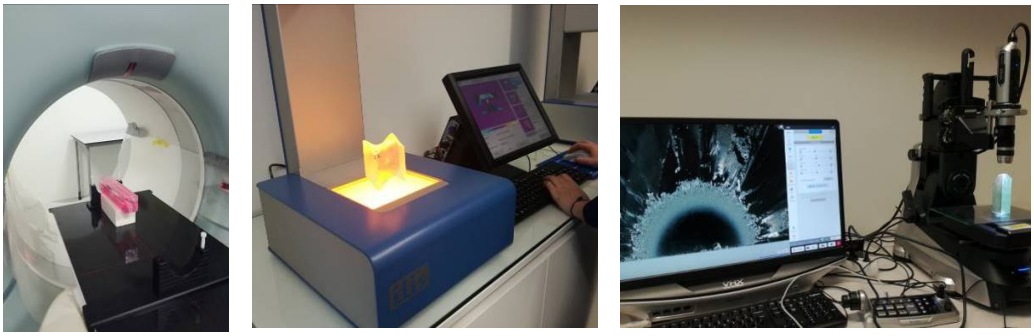

Fig. 1.43 Various techniques explored in this dissertation for the mapping of defects and inhomogeneities in glass components: Computerized Tomography (CT) Scanning to evaluate density differentials, stress birefringence measurement using an Ilis StrainScope polarimeter, and digital microscopy. With the use of a VHX-7000 Digital Microscope (right image), surface defects, defects at the fracture plane of specimens and, where possible, defects in the bulk could be evaluated.

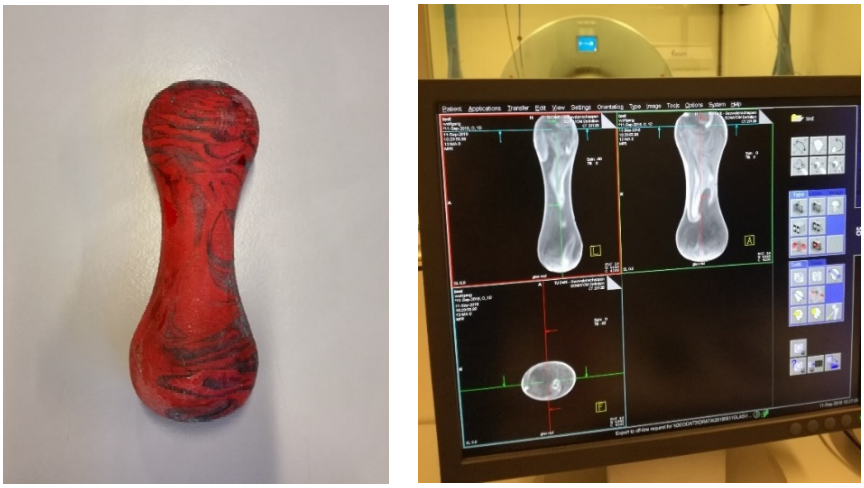

Fig. 1.44 CT scanning of a glass specimen showing the layering of the black and red glass in the interior of the sample.

Stage 2: This stage involves the prototyping and mechanical testing, with the aim to correlate the casting parameters to the obtained meso-level structures and further on to the mechanical properties. Prior knowledge acquired from the experimental work of Stage 1 is used as a basis in order to cast distinct specimens, covering a variety of flaws and meso-level structures. First step of the process (a) involves the documentation of the observed meso-level structures and correlation to the casting parameters. This process is described in the initial part of Chapters 3, 4 and 5 of this dissertation. Thereafter, the mechanical testing follows (step b), investigating to what extent the obtained flaws are affecting the flexural strength (Chapter 3 and 4), stiffness (Chapter 3 and 4) and fracture resistance (Chapter 5) of the specimens. Non-destructive and destructive experiments are employed towards this goal (e.g. see Figure 1.45). The size factor effect is also investigated by comparing the experimental results presented in Chapter 3 and 4.

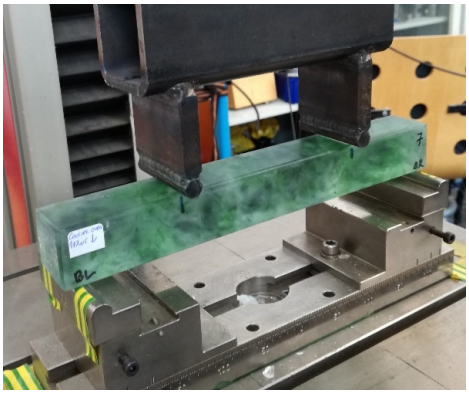
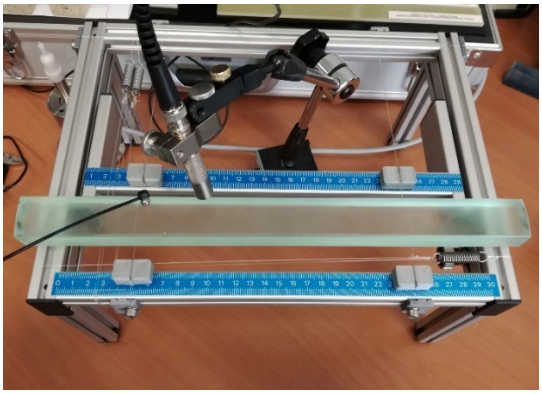

Fig. 1.45 Destructive (left, 4-point bending test) and non-destructive (right, Impulse Excitation test) experimental procedures followed in this dissertation.

Stage 3: This stage gathers the conclusions of the prior research stages and drafts the outline for further research (Discussion, Conclusions and Recommendations, Chapters 6-8).

Chapters 2-5 are based on the peer-reviewed journal articles Bristogianni et al. 2018, Bristogianni et al. 2020, and Bristogianni et al. 2021 (a), (b) respectively.

1.5 Societal and Scientific Relevance

This dissertation aims to contribute to a wider use of cast glass in the architectural realm. It intends to inspire trust to engineers, architects, designers and the general public on cast glass as a structural material and glass casting as a reliable and promising production technique. Cast glass can unlock the geometrical and colour limitations currently imposed by the prevailing glass production techniques, and introduce novel architectural expressions that advance the quality of the built environment and our interior spaces (Figures 1.46-1.47). But more importantly, cast glass- even with cast-in inhomogeneities- has a high compressive strength. Trusting cast glass, similarly to how we trust concrete, could supply the building industry with a new building unit. A unit based on sand- an abundant material on this and other planets- which can be endlessly recycled without loss of quality. Furthermore, proving that cast glass, even when it is produced out of waste glass resources and at lower temperatures, has good load-bearing properties, can have a significant decrease in the environmental footprint of the material. Simultaneously, the structural cast glass market could absorb an important volume of currently discarded glass, providing a good solution to the problem of accumulating glass waste. Therefore, information provided in this dissertation on what types of waste glass sources can be used, at which percentages and the firing schedules required can aid the industry in the recycling by casting process. Together with all other findings and casting suggestions, valuable tools are to be provided to the cast glass foundries but also to the quality control engineers working with cast glass.

In terms of scientific contribution, this work aspires to shed light on the strength of cast glass and how this is defined by the inhomogeneities included and developed during the casting process. In this attempt, valuable side questions regarding the documentation of defects in a 3-dimensional (freeform) glass component and the non-destructive and destructive testing of the mechanical properties are posed, opening a discussion about the validation methodology to be adopted in the field of structural cast glass. The importance of geometry and thermal history during the casting process are brought into attention over the effect of chemical composition, revealing important factors that affect the quality of cast glass that are often overseen. Insights on how meso-level structures can be engineered to our advantage are also provided. The information on the relation between the mechanical properties and the complexities of cast glass meso-level structure in the literature is up to this point unclear and unidentified. This dissertation is only a first explorative step in a scientifically unmapped territory.

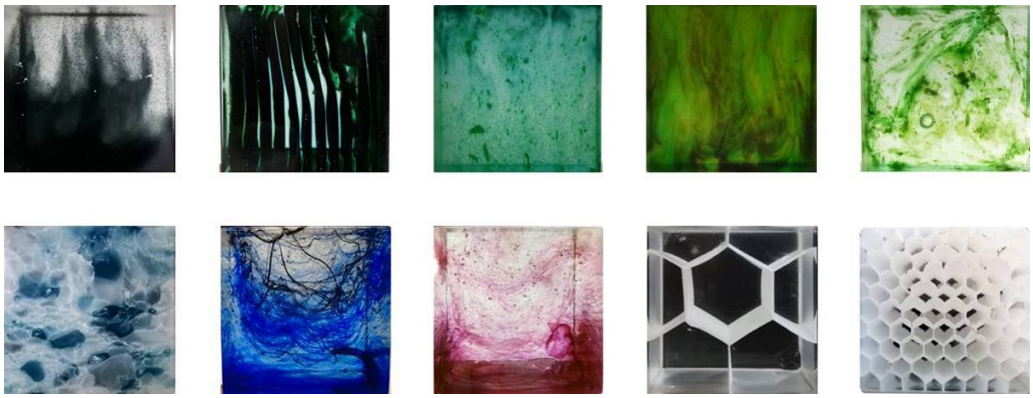

Fig. 1.46 Enabling the safe, structural use of inhomogeneous, recycled cast glass in architecture is one of the main aspirations of this work. Depicted here a series of recycled specimens kiln-cast at the TU Delft Glasslab.

Fig. 1.47 Re^3 Glass prototype showcasing the aesthetical potential of shape and colour and the environmental benefits or recycled cast glass.

References

Akerboom, R.: Glass Columns, exploring the potential of free standing glass columns assembled from stacked cast elements. Architecture and The Built Environment, Delft University of Technology (2016)

Aldinger, B.S., Collins, B.K.: Color Atlas of Stones in Glass. American Glass Research, Butler, PA (2016)

Aldinger, B.S., de Haan, P.W.: Color Atlas of Glass Container Defects. American Glass Research, Butler, PA (2019)

Amses, D.: Public Work. www.deniseamses.com/publicwork.

Anagni, G.M., Bristogianni, T., Oikonomopoulou, F. Rigone, P., Mazzucchelli, E.S.: Recycled Glass Mixtures as Cast Glass Components for Structural Applications, Towards Sustainability. Paper presented at the Challenging Glass 7: Conference on Architectural and Structural Applications of Glass, Ghent University,

Babcock, C.L.: Silicate Glass Technology Methods. John Wiley & Sons, USA (1977)

Barou, L.: Transparent Restoration. Architecture and The Built Environment, Delft Univestity of Technology (2016)

Barou, L., Oikonomopoulou, F., Bristogianni, T., Veer, F. and Nijsse, R.: Structural glass: A new remedial tool for the consolidation of historic structures. Heron 62 (2019)

Bartuška, M.: Glass defects. Glass Service Inc. and Práh, Prague (2008)

Beveridge, P., Domenech, I., Pacual, E.: Warm Glass: A complete Guide to Kiln-Forming Techniques: Fusing, Slumping, Casting. Lark Books, (2005)

Boon, L.: Glas in Beton in Nederland. (2017)

Bray, C.: Dictionary of glass : materials and techniques, Second ed. A & C Black; University of Pennsylvania Press, London; Philadelphia (2001)

Bristogianni, T., Oikonomopoulou, F., Veer, F.A., Nijsse, R.: Design and production of a structural cast glass element for a transparent dome. In: Zingoni, A. (ed.) Insights and Innovations in Structural Engineering, Mechanics and Computation : Proceedings of the 6th International Conference on Structural Engineering, Mechanics and Computation, SEMC, Cape Town 2016, pp. 1662-1667. CRC Press

Bristogianni, T., Oikonomopoulou, F., Veer, F., Snijder, A., Nijsse, R.: Production and Testing of Kiln-cast Glass Components for an Interlocking, Dry-assembled Transparent Bridge. Paper presented at the Glass Performance Days 2017 Conference Proceedings, Tampere (2017)
Bristogianni, T., Oikonomopoulou, F., Justino de Lima, C.L., Veer, F.A., Nijsse, R. : Structural cast glass components manufactured from waste glass: Diverting everyday discarded glass from the landfill to the building industry. Heron 63 (1/2 Special issue: Structural Glass) (2018)
Bristogianni, T., Oikonomopoulou, F., Yu, R., Veer, F.A., Nijsse, R.: Investigating the flexural strength of recycled cast glass. Glass Structures & Engineering (2020). doi:10.1007/s40940-020-00138-2
Bristogianni, T., Oikonomopoulou, F., Veer, F., Nijsse, R.: Exploratory Study on the Fracture Resistance of Cast Glass. International Journal of Structural Glass and Advanced Materials Research 5 (2021). doi:10.3844/sgamrsp.2021.195.225
Bristogianni, T., Oikonomopoulou, F., Veer, F.A.: On the flexural strength and stiffness of cast glass. Glass Structures & Engineering 6(2), 147-194 (2021). doi:10.1007/s40940-021-00151-z
Brokmann, C., Kolling, S., Schneider, J.: Subcritical crack growth parameters in glass as a function of environmental conditions. Glass Structures & Engineering 6(1), 89-101 (2021). doi:10.1007/s40940-020-00134-6
Bukieda, P., Lohr, K, Meiberg, J., Weller, B.: Study on the optical quality and strength of glass edges after the grinding and polishing process. Glass Structures & Engineering 5(3), 411-428 (2020). doi:10.1007/s40940-020-00121-x
Bullseye Glass co.: Methods & Ideas. http://www.bullseyeglass.com/methods-ideas/index-of-articles.html
Castori. G., S., E.: Experimental and Numerical Investigation of the Bending Strength of Glass In: Belis, Bos, Louter (ed.) Challenging Glass 5 – Conference on Architectural and Structural Applications of Glass, Ghent University 2016
Charles, R.J.: Dynamic Fatigue of Glass. Journal of Applied Physics 29(12), 1657-1662 (1958). doi:10.1063/1.1723019
Charles, R.J.: Static Fatigue of Glass. I. Journal of Applied Physics 29(11), 1549-1553 (1958). doi:10.1063/1.1722991
Charles, R.J.: Static Fatigue of Glass. II. Journal of Applied Physics 29(11), 1554-1560 (1958). doi:10.1063/1.1722992
Clark-Monks, C., and Parker, J.M.: Stones and Cord in Glass. Society of Glass Technology, Sheffield (1980)
Cormier, L.: The classical nucleation theory. In: Neuville, D., Cormier, L., Caurant, D., Montagne, L. (ed.) From glass to crystal. Nucleation, growth and phase separation: from research to applications. EDP Sciences, London, UK (2017)
Cummings, K.: Techniques of Kiln-Formed Glass. University of Pennsylvania Press, (1997)
Damen, W.: Topologically Optimised Cast Glass Grid Shell Nodes. Architecture and the Built Environment, Delft University of Technology (2019)
Datsiou, K.C., Overend, M.: Artificial ageing of glass with sand abrasion. Construction and Building Materials 142, 536-551 (2017). doi:https://doi.org/10.1016/j.conbuildmat.2017.03.094
Datsiou, K.C., Overend, M.: The strength of aged glass. Glass Structures & Engineering 2(2), 105-120 (2017). doi:10.1007/s40940-017-0045-6
de Waal, H., Beerkens, R.G.C. : NCNG Handboek voor de Glasfabricage TNO-TPD-Glastechnologie, (1997)
Doremus, R.H.: Static Fatigue in Glass. In: Bishay, A. (ed.) Recent Advances in Science and Technology of Materials: Volume 2. pp. 203-206. Springer US, Boston, MA (1974)
Dyer, D.a.G., D.: The Generations of Corning: The Life and Times of a Global Corporation. Oxford University Press, New York (2001)
Fagan, E.: Building Walls of Light: the Development of Glass Block and its Influence on American Architecture in the 1930s. Columbia University (2015)
Feldmann, M., Kaspar, R., Abeln, B., Gessler, A., Langosch, K., Beyer, J., Schneider, J., Schula, S., Siebert, G., Haese, A., Wellershoff, F., Cruz, P., Belis, J., Colvin, J., Morgan, T., Ensslen, F., Eliasova, M., Šulcova, Z., Royer-Carfagni, G., Galuppi, L., Grenier, C., Hoegner, H., Kruijs, R., Louter, C., Manara, G., Neugebauer, J., Rajcic V., Zarnic, R.: Guidance for European Structural Design of Glass Components. In: Dimova, S., Pinto Vieira, A., Feldmann, M., Denton, S. (ed.). JRC86637. European Commission, Luxembourg, (2014)
Griffith, A.A.: The phenomena of rupture and flow in solids. Philosophical Transactions of the Royal Society of London. 221(582-593), 163-198 (1920). doi:10.1098/rsta.1921.0006
Groot, J.A.W.M., Mattheij, R.M.M., Laevsky, K.Y.: Mathematical modelling of glass forming processes. In: CASA-report, vol. 09-07. Eindhoven University of Technology, The Netherlands, (2009)
Gross, T.M.a.T., M.: Fictive temperature-independent density and minimum indentation size effect in calcium aluminosilicate glass. 104(6), 063529 (2008). doi:10.1063/1.2985907
Haldimann, M.: Fracture strength of structural glass elements: analytical and numerical modelling, testing and design. École Polytechnique Fédérale de Lausanne (2006)
Haldimann, M., Luible, A., Overend, M.: Structural Use of Glass. IABSE-AIPC-IVBH, Zürich (2008)
Hayward, E.L.: Improvement in Pavement Lights. UK Patent (1871)
Inano, H.: Effect of Alkali Metal Oxide on Pb Recovery from the Waste CRT Glass by Reduction Melting Method. In, Dordrecht 2012. Design for Innovative Value Towards a Sustainable Society, pp. 896-900. Springer Netherlands
Inano, H., Tomita, K., Tada, T., Hiroyoshi, N.: Lead generation and separation mechanisms from lead silicate glass by reduction-melting. Journal of the Ceramic Society of Japan 126(8), 595-601 (2018). doi:10.2109/jcersj2.18090
Inglis, C.E.: Stresses in a Plate Due to the Presence of Cracks and Sharp Corners. SPIE Milestone Series 137, 3-17 (1913)

Irwin, G.R.: Analysis of Stresses and Strains near the End of a crack Traversing a Plate. Journal of applied Mechanics Vol. 24, pp. 361-364 (1957)
James Carpenter Design Associates Inc.: Davidson-Gerson Gallery of Glass. www.jcdainc.com/projects/davidson-gerson-gallery-of-glass?view=slider#3 (2017).
John Lewis Glass: Hearst Water Cascade. http://johnlewisglass.com/our-work/for-architects/hearst-water-cascade/.
Kašiarová, M., Rouxel, T., Sangleboeuf, J.C., Houérou, V.: Fractographic Analysis of Surface Flaws in Glass. Key Engineering Materials 290 (2005). doi:10.4028/www.scientific.net/KEM.290.300
Kinsella, D.: Modelling of Annealed Glass Fracture. Lund University (2018)
Kleuderlein, J., Ensslen, F., Schneider, J.: Study on edge strength of float glass as a function of edge processing. Stahlbau 85, 149-159 (2016)
Knoppert, M.: Glasbewerken. Glasatelier Knoppert, Den Haag (2011)
Krueck Sexton Partners: Crown Fountain. https://ks.partners/projects/crown-fountain/ (2004).
Lawn, B.R., Marshall, D.B.: Hardness, Toughness, and Brittleness: An Indentation Analysis. 62(7-8), 347-350 (1979). doi:10.1111/j.1151-2916.1979.tb19075.x
Lindqvist, M.: Structural Glass Strength Prediction Based on Edge Flaw Characterization. École Polytechnique Fédérale de Lausanne (2013)
Lundstrom, B.: Glass Casting and Moldmaking: Glass Fusing, Book 3. Vitreous Publications Inc., (1989)
Makishima, A., Mackenzie, J. D.: Direct calculation of Young's modulus of glass. Journal of Non-Crystalline Solids 12(1), 35-45 (1973). doi:10.1016/0022-3093(73)90053-7
Makishima, A., Mackenzie, J.D.: Calculation of bulk modulus, shear modulus and Poisson's ratio of glass. Journal of Non-Crystalline Solids 17(2), 147-157 (1975). doi:10.1016/0022-3093(75)90047-2
March, N.H., Tosi, M.P.: Introduction to Liquid State Physics. World Scientific, (2002)
Martlew, D.: Viscosity of Molten Glasses. In: Pye, L.D., Montenero, A., Joseph, I. (ed.) Properties of Glass-Forming Melts. CRC Press (2005)
Mould, R.E.: The Strength of Inorganic Glasses. In: Proceedings of the Fourth Symposium on Fundamental Phenomena in the Materials Sciences, Boston, MA 1967. Fracture of Metals, Polymers, and Glasses, pp. 119-149. Springer US
Nakamura, H., NAP: Optical Glass House. www.nakam.info/en/works/optical-glass-house/ (2012).
Nijsse, R.: Glass in Structures. Birkhäuser, Basel (2003)
Oikonomopoulou, F., Veer, F., Nijsse, R., Baardolf, K.: A completely transparent, adhesively bonded soda-lime glass block masonry system. Journal of Facade Design and Engineering 2 (2015). doi:10.7480/jfde.2014.3-4.909
Oikonomopoulou, F., Bristogianni, T., Barou, L., van Hees, R., Nijsse, R., Veer, F., Schellen, H., van Schijnde, J.: Restorative glass: reversible, discreet restoration using structural glass components SPOOL - Journal of Architecture and the Built Environment 4(2) (2017)
Oikonomopoulou, F., Bristogianni, T., Veer, F.A., Nijsse, R.: The construction of the Crystal Houses façade: challenges and innovations. Glass Structures & Engineering 3(1), 87-108 (2018). doi:10.1007/s40940-017-0039-4
Oikonomopoulou, F., Bristogianni, T., Barou, L., Veer, F.A., Nijsse, R.: The potential of cast glass in structural applications. Lessons learned from large-scale castings and state-of-the art load-bearing cast glass in architecture. Journal of Building Engineering 20, 213-234 (2018). doi:10.1016/j.jobe.2018.07.014
Oikonomopoulou, F.: Experimental and numerical investigation of an interlocking system out of osteomorphic cast glass components. In: Unveiling the third dimension of glass: Solid cast glass components and assemblies for structural applications. A+BE | Architecture and the Built Environment, (2019)
Oikonomopoulou, F., Bhatia I.S., Damen, W., van der Weijst, F., Bristogianni, T. : Rethinking the Cast Glass Mould. Paper presented at the Challenging Glass 7, Ghent University, (2020)
Oikonomopoulou, F., Bristogianni, T.: Adhesive solutions for cast glass assemblies: ground rules emerging from built case studies on adhesive selection and experimental validation. Glass Structures & Engineering 7(2), 293-317 (2022). doi:10.1007/s40940-022-00178-w
Oikonomopoulou, F., Bristogianni, T., van der Velden, M., Ikonomidis, K.: The adhesively-bonded glass brick system of the Qaammat Pavilion in Greenland: From research to realization. Architecture, Structures and Construction 2(1), 39-62 (2022). doi:10.1007/s44150-022-00031-2
O'Regan, C.: Structural use of glass in buildings. IStructE Ltd, London (2014)
Orowan, E.: The mechanical strength properties and the real structure of crystals. Z. Kristallographie 89, 327-343 (1934)
Orowan, E.: Energy Criteria of Fracture. Welding Research Supplement 34, 157 (1955)
Paech, C., Göppert, K.: Innovative Glass Joints – The 11 March Memorial in Madrid. Paper presented at the Challenging Glass, Conference on Architectural and Structural Applications of Glass, Delft (NL), (2008)
Parascho, S., Han, I., Walker, S., Beghini, A., Bruun, E., Adriaenssens, S.: Robotic vault: a cooperative robotic assembly method for brick vault construction. Construction Robotics 4 (2020). doi:10.1007/s41693-020-00041-w
Peddle, C.J.: Defects in Glass. Glass publications ltd, London (1927)
Persson, K., Haller, K., Karlsson, S., Kozłowski Non-destructive testing of the strength of glass by a non-linear ultrasonic method. In: Belis, B.L.E. (ed.) Challenging Glass 7, Gent (2020)
Preston, F.W.: The Mechanical Properties of Glass. Journal of Applied Physics 13(10), 623-634 (1942). doi:10.1063/1.1714811

Quinn, G.D.: NIST Recommended Practice Guide: Fractography of Ceramics and Glasses, 2nd edition. (2016)
Ronchetto, E.A.: The effects of fatigue and weathering on the failure behavior of commercial soda-lime-silicate glass. Missouri University of Science and Technology (2019)
Rouxel, T.: Fracture surface energy and toughness of inorganic glasses. 137, 109--113 (2017). doi:10.1016/j.scriptamat.2017.05.005
Sable, L., Kalnins, K.: Verification of available glass mechanical properties against recommendation by the draft Eurocode design practice. Technology of Inorganic Materials 68(1) (2017). doi:doi.org/10.5755/j01.ct.68.1.18872
Saint-Gobain: Mechanical Properties of Glass. https://uk.saint-gobain-building-glass.com/en-gb/architects/physical-properties.
Schittich, C., Staib, G., Balkow, D., Schuler, M., Sobek, W.: Glass Construction Manual. Birkhäuser, Munich (2007)
Scholtens, E.: Recycling borosilicate glass for a facade system assembled of dry-interlocking cast glass components implemented in Casa da Música. Architecture and the Built Environment, Delft University of Technology (2019)
Shand, E.B.: Glass Engineering Handbook. Corning Glass Works, USA (1955)
Shelby, J.E.: Introduction to Glass Science and Technology. The Royal Society of Chemistry, UK (2005)
Simmons, J.H., Simmons, C. J. : Nonlinear viscous flow in glass forming. American Ceramic Society Bulletin 68, 1949-1955 (1989)
Sombroek, I.: Structural cast glass; A research process of design and experiment towards a feasible geometry for a cast glass element. Architecture and The Built Environment, Delft University of Technology (2016)
Stone, G.: Firing Schedules for Glass- The Kiln Companion. Igneous Glassworks, (2010)
Striepe, S., Potuzak, M., Smedskjaer, M.M., Deubener, J.: Relaxation kinetics of the mechanical properties of an aluminosilicate glass. Journal of Non-Crystalline Solids 362, 40-46 (2013). doi:https://doi.org/10.1016/j.jnoncrysol.2012.11.017
Sullivan, E.J.: Illuminating Lens for Sidewalks. US Patent, US603799A (1898)
Swab, J.J., Thies, S.R., Wright, J.C., Schoenstein, J.A., Patel, P.J.: Influence of Surface Scratches on the Flexure Strength of Soda-Lime Silicate and Borosilicate Glass. Experimental Mechanics 53(1), 91-96 (2013). doi:10.1007/s11340-012-9674-5
Thwaites, A.: Mould Making for Glass. A&C Black, (2011)
Tool, A.Q.: Relaxation of stresses in annealing glass. Journal of Research of the National Bureau of Standards 34, 199 (1945)
Trollope, A.: Improvement in Vault-Covers. USA Patent, US134447A (1872)
Vandebroek, M., Belis, J., Louter, C., Van Tendeloo, G.: Experimental validation of edge strength model for glass with polished and cut edge finishing. Engineering Fracture Mechanics 96, 480-489 (2012). doi:https://doi.org/10.1016/j.engfracmech.2012.08.019
Vandebroek, M., Louter, C., Caspeele, R., Ensslen, F., Belis, J.: Size effect model for the edge strength of glass with cut and ground edge finishing. Engineering Structures 79, 96-105 (2014). doi:https://doi.org/10.1016/j.engstruct.2014.08.004
van Dijk, F.A.G.: Glass defects originating from glass melt/fused cast AZS refractory interaction. Technische Universiteit Eindhoven (1994)
Varner, J.R.: Fatigue and Fracture Behavior of Glasses. In: Fatigue and Fracture, vol. 19. p. 0. ASM International, (1996)
Varshneya, A.K.: Fundamentals of inorganic glasses, 2nd ed. Society of Glass Technology, Sheffield , UK (2013)
Veer, F.A., Zuidema, J.: The Strength of Glass, Effect of Edge Quality. In: Glass Processing Days, Tampere, Finland 2003, pp. 106-109
Veer, F.A.: The strength of glass, a nontransparent value. Heron 52 (2007)
Veer, F.A., Rodichev, Y.: The structural strength of glass: Hidden damage. Strength of Materials 43, 302-315 (2011). doi:10.1007/s11223-011-9298-5
Whittingham, A.: Glass Casting. The Crowood Press Ltd, (2019)
Wiederhorn, S.M., Bolz, L.H.: Stress Corrosion and Static Fatigue of Glass. Journal of the American Ceramic Society 53(10), 543-548 (1970). doi:https://doi.org/10.1111/j.1151-2916.1970.tb15962.x
Wurm, J.: Glass Structures. Birkhäuser, Germany (2007)
Yamane, M., Mackenzie, J.D.: Vicker's Hardness of glass. Journal of Non-Crystalline Solids 15(2), 153-164 (1974). doi:10.1016/0022-3093(74)90044-1
Zschimmer, E.: Chemische Technologie des Glases. Glaswerks Schott & Genossen, Jena (1913)

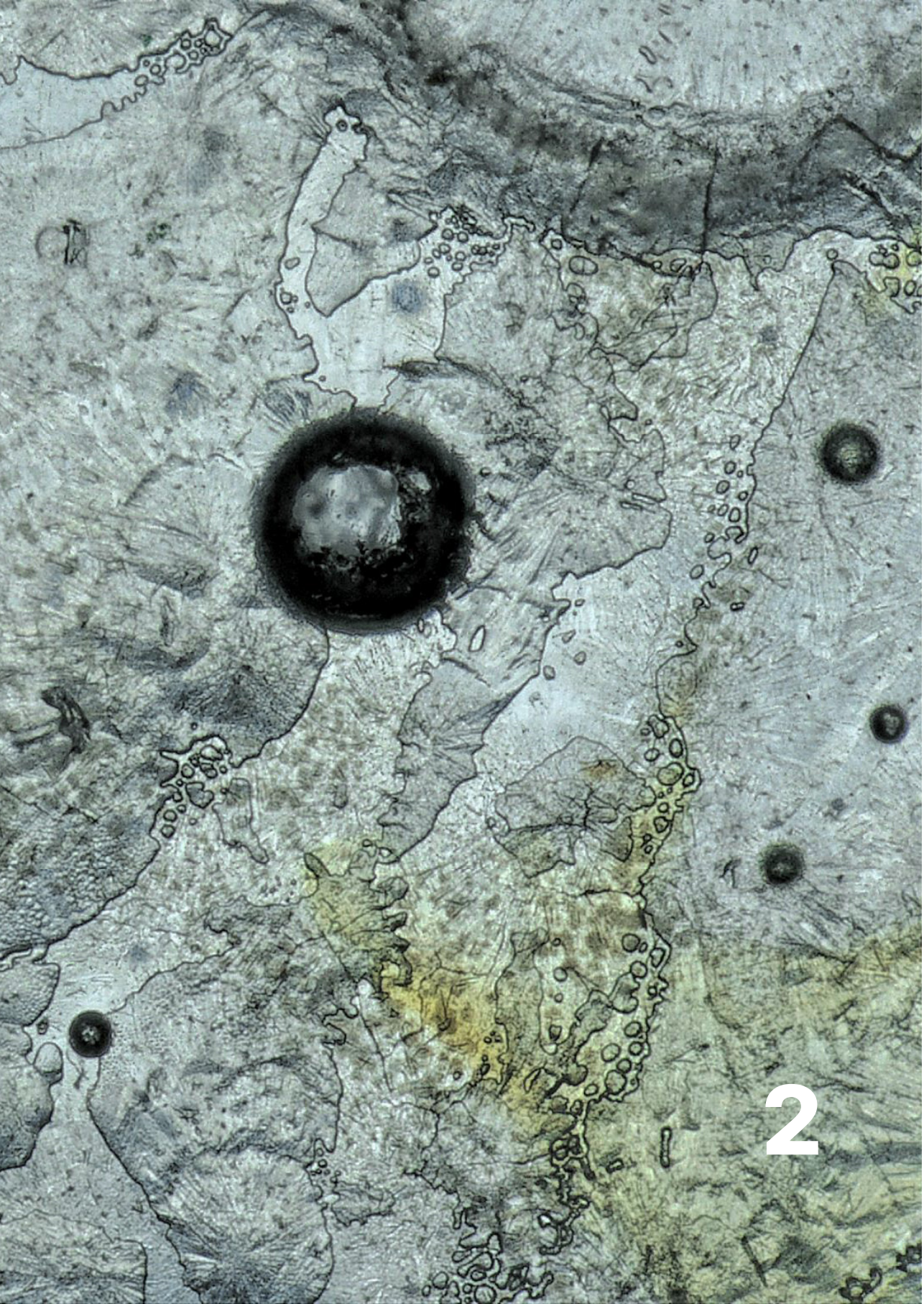
2

Previous page: Top surface crystallization observed at a recycled, float glass specimen, kiln-cast at 1120 °C.

Chapter 2: Casting potential of silicate based glass waste

Based on

Bristogianni, T., Oikonomopoulou, F., Justino de Lima, C.L., Veer, F.A., Nijsse, R. : Structural cast glass components manufactured from waste glass: Diverting everyday discarded glass from the landfill to the building industry. Heron 63 (1/2 Special issue: Structural Glass), 57-102 (2018)

Aim and context

To define the thermal profile of common commercial glass compositions and examine if they are suitable candidates for glass casting. Chapter 2 forms the basis for the design and preparation of glass specimens involved in the experimental work described in Chapters 3, 4 and 5.

Abstract

Although in theory glass can be endlessly re-melted without loss in quality, in practice only a small percentage gets recycled, mainly by the packaging industry. Most of the discarded glass fails to pass the high quality standards of the prevailing glass industry -due to coatings, adhesives, other contaminants or incompatibility of the recipe- and ends up in landfill. However, using discarded glass in cast components for building applications can be a good way to reintroduce this waste to the supply chain. Such components can tolerate a higher percentage of inclusions, without necessarily compromising their mechanical or aesthetical properties. This chapter explores the potential but also the limitations of recycling glass in order to obtain load-bearing components. First, an overview is provided regarding which types of glass reach the recycling plants and the which not, arguing on the reasons behind this selection. Afterwards, a series of experiments is presented, exploring the possibilities of recycling everyday glass waste, from beer bottles and *Pyrex*® trays to mobile phone screens. Each type of glass waste is cast at different temperatures and firing/cooling rates to define its flow capability and risk of crystallization. The tests reveal at what temperatures each glass family can be molten, poured, crystallized and annealed. The above information is linked to the X-ray fluorescence (XRF) analyses of the samples prior to recycling. The results point out the types of glass with potential in structural applications, and the overall feasibility of the concept.

Authors' contribution on the relevant published journal article

Bristogianni, T.: Research concept, organization, sample preparation, conduction of experiments, data analysis, writing of the paper. Oikonomopoulou, F.: Research concept and discussion, paper review. Justino de Lima, C.L.: DSC analyses and discussion. Veer, F.A.: supervision of research, discussion, paper review. Nijsse, R. : supervision of research.

Acknowledgements

I would like to thank the co-authors of the above mentioned paper for their valuable contribution in this chapter. I would also like to thank Prof. Jiyong Lee and Katherine Rutecki from the School of Art and Design at Southern Illinois University (SIU), and glass artist Joshua Hershman for their inspiring guidance and technical knowledge in kiln-casting. Ruud Hendrikx (3mE, TU Delft) was of significant help, providing with all the XRF and XRD analyses. I am also grateful to Lida Barou (CiTG, TU Delft), Mariska van der Velden (CiTG, TU Delft), Kees Baardolf (BK, TU Delft), Ron Penners (CiTG, TU Delft), and Tommaso Venturini (BK, TU Delft) for their meaningful assistance in the TU Delft Glass Laboratory. Finally, I would like to thank Annissa Flickinger, Glenn Miner, Paul W. Bush, Patrick J. Kenny from Vitro Architectural Glass for providing us with glass samples and valuable input.

2.1 Introduction

The term glass recycling is almost a synonym to the sole recycling of glass bottles and containers for the purposes of the food packaging industry. The glass packaging industry has significantly invested in the infrastructure for the collection, sorting and processing of glass bottle and container waste, and this has resulted in high percentages of waste recovery and recycling, such as a mean of 73.2% in 2015 in the European Union (Eurostat 2016). Glass waste is however a broader term including overall everyday household waste (ex. tableware, ovenware, lighting), building waste (ex. windows, glass tiles), electronic waste (ex. Liquid Crystal Displays and Cathode Ray Tubes), automotive industry waste (ex. laminated windshields) and industrial/laboratory waste to name a few. The percentages of recovery and closed-loop recycling of non-packaging glass waste are rather low (ELVIROS 2004)[14]. Such glass objects are considered non-recyclable either due to contamination from coatings, adhesives, laminates or even hazardous substances, or due to the labour intensive demounting process required (ex.

[14] For example, in the case of the flat glass industry, which includes the building and automotive sector, post-consumer discarded flat glass is seldom recycled back into flat glass products; instead it is down-cycled to glass bottles, processed into low-value products or landfilled (Hestin et al. 2016). Even in the Netherlands, where, through the establishment of the "Vlakglas Recycling Nederland" Foundation, the highest percentage of Construction and Demolition (C&D) glass recycling in Europe is achieved (80%), the majority of the collected glass is either down-cycled into bottles (42.8%), or processed into aggregates and insulation products such as glass wool (41.2%). Only 7.5% of the collected float glass is recycled back into the same product (Vlakglas Recycling Nederland 2020).

Window panes, computer screens) (Dyer 2014). The food packaging industry does not accept contaminated glass cullet that will affect the taste of the products, similarly, the float industry rejects such glass, as it is responsible for the creation of stones and other flaws and reduces the transparency of their glass panes while also increasing the risk of failure due to inclusions such as nickel sulphide (NiS). Since this glass cannot meet the strict criteria to be reused for the same purpose (closed-loop recycling), it either ends up in landfills or gets down-cycled (open-loop recycling) into aggregate in concrete, ceramic or pavement products, into abrasive or into foam insulation (Silva et al. 2017; Dyer 2014). What is more, tons of non-contaminated glass waste are simply discarded or down-cycled due to the mismatch in their recipe with that of glass packaging. In other words, the lack of facilities and automated processes for separation and handling of different types of glass is- to a great extent- responsible for the rejection of this waste from the closed-loop recycling.

Cast glass technology for structural applications can be a strategy for tackling the problem of glass waste rejection due to contamination or glass composition. Cast glass has already been applied in load-bearing applications, such as the self-supporting glass façade of the Crystal Houses in Amsterdam (Oikonomopoulou et al. 2017). On the one hand, building components out of cast glass can tolerate more flaws[15] than a piece of float glass or a drinking bottle, without compromising the strength or aesthetic quality. On the other hand, the relatively smaller scale of the cast glass factories and often lack of automation leave more room for experimentation. In contrast to the giants of glass processing and their strict specifications, cast glass producers have more freedom in altering the firing schedules and the glass recipes.

The scope of this chapter is the categorization of prevailing types of glass waste and the understanding of their value as a raw source for the casting of glass building components. Not only are the mechanical properties of the final product important, but also the suitability and easiness of a waste glass type to be cast in the first place. To elaborate on the aforementioned suitability, it should be noted that for each composition, a different liquidus temperature region and minimum cooling rate apply. These parameters need to be taken into account during casting in order to obtain glass, or in other words, to sustain the amorphous structure of the liquid melt when this transitions to a solid component. A glass formed at temperatures just below this region and cooled down at slower rates, carries the risk of crystallization (Pye 2005). As a consequence, according to the heating and cooling conditions, a portion or all the material will be structured in crystals, and the end product will have altered properties. Such crystallized materials, for example, lose the property of transparency and become more impact resistant than their amorphous alternative (Cormier 2017). Therefore, the parameters defining each type of glass waste should facilitate the casting process, implying that high liquidus temperatures or extremely

[15] Experimental testing on cast glass components at the TU Delft Glass & Transparency Lab indicate that a few air bubbles or inclusions (ex. ceramic stones) within the bulk of the components- that do not exceed a diameter of a millimeter- are not critical for the structural performance Similar bubbles or stones in a glass pane of 6 or 8mm thickness would significantly reduce the strength of the product, but also its aesthetic quality (a perfectly clear transparent pane is expected). For similar aesthetic reasons, colour shifts are rejected from the industry and consumers, but can be of aesthetic value in cast glass elements.

fast cooling rates are not realistic for the mass production of building components of a competitive price.

2.2 Categorization of everyday glass waste

2.2.1 Prevailing glass families

By clustering the commercial glass waste into families of similar chemical composition, we can set guidelines on how to handle each piece of glass waste and what to expect from the resulting product. Specifically, we can define the working and annealing temperature range, the easiness of crystallization, the coefficient of thermal expansion and the possibility of combination with similar glass waste sources. We can also predict the characteristics of the finished products in terms of mechanical, optical and thermal properties.

Everyday glass waste was therefore categorized in the following six families: soda lime silica, soda potassium lime silica, lead crystal, lead-free crystal, borosilicate and alkali-aluminosilicate glass (Figure 2.1). Within the soda lime silica category- which is also the most prevailing one- three subcategories were set in relation to the manufacturing process of the glass objects, since the production method fine tunes the basic soda lime silica recipe. These subcategories are: automated blown, mouth-blown and float glass. Other types of specialty glasses are not included in this research as their contribution to the problem of glass waste is negligible.

Fig. 2.1 Main families of commercial glasses.

Table 2.1 provides a list of properties for each family of commercial glass. This list will be further used in this research as a guideline for determining the handling temperatures during the casting of the different glass waste types.

Table 2.1 (part a): Properties of commercial glasses.

Properties of various types of commercial glasses				
Glass family	Lead crystal	Lead-free barium strontium		Soda lime silica (mouth-blown)
Glass name	Schott LF5	CRT colour panel	Corning 9068 (Colour TV panel)	Cristalica, Spruce Pine
Young's modulus E in GPa	59			
Thermal expansion coefficient a (20°C;300°C) in 10^{6} K^{-1}	10.6	9.7-10.9	9.9	10
Density in g/cm^3	3.22	2.75-2.79	2.69	
Forming temperature (viscosity= 10^{4} dPa·s) in °C				995
Forming temperature (viscosity= 10^{5} dPa·s) in °C				879
Forming temperature (viscosity= 10^{6} dPa·s) in °C				792
Softening point (viscosity= $10^{7.6}$ dPa·s) in °C	585		688	692
Annealing point (viscosity= 10^{13} dPa·s) in °C	411	501	503	515
Strain point (viscosity= $10^{14.5}$ dPa·s) in °C			462	486
Sources	*(SCHOTT 2014b)*	*(Mear et al. 2006)*	*(Campbell et al 1990)*	*(Spruce Pine Batch)*
		(Shelby 2005)	*(Seward III et al. 2001)*	

Glass family	Soda lime silica (float)		Soda lime silica (glass bottles)	Soda potassium lime silica
Glass name	PPG Starphire	Kimble R6	Common glass container	Schott B270
Young's modulus E in GPa	73.1		70-75	71.5
Thermal expansion coefficient a (20°C;300°C) in 10^{6} K^{-1}	9.03	9.3	9	9.4
Density in g/cm^3	2.5		2.52	2.55
Forming temperature (viscosity= 10^{4} dPa·s) in °C		984		1033
Forming temperature (viscosity= 10^{5} dPa·s) in °C		871		915
Forming temperature (viscosity= 10^{6} dPa·s) in °C		789		827
Softening point (viscosity= $10^{7.6}$ dPa·s) in °C	710	694		724
Annealing point (viscosity= 10^{13} dPa·s) in °C	547	527	548	541
Strain point (viscosity= $10^{14.5}$ dPa·s) in °C	513	486		511
Sources	*(Precision Glass and Optics)*	*(Martlew 2005)*	*(Shelby 2005)*	*(Knight Optical)*
	(Specialty Glass Products)	*(Brockway 1981)*		

Table 2.1 (part b): Properties of commercial glasses.

Glass family	Borosilicate		Alkali-Aluminosilicate	Alkaline Earth Aluminosilicate
Glass name	Schott DURAN®	"Pyrex" KG-33	Corning Gorilla Glass 5	EZ-1
Young's modulus E in GPa	64		76.7	
Thermal expansion coefficient a (20°C;300°C) in 10^{6} K^{-1}	3.3	3.3	7.88	4.2
Density in g/cm^{3}	2.23	2.23	2.43	2.52
Forming temperature (viscosity= 10^{4} dPa·s) in °C	1260	1248		1204
Forming temperature (viscosity= 10^{5} dPa·s) in °C		1072		1094
Forming temperature (viscosity= 10^{6} dPa·s) in °C		946		1010
Softening point (viscosity= $10^{7.6}$ dPa·s) in °C	825	805	884	915
Annealing point (viscosity= 10^{13} dPa·s) in °C	560	565	623 ($10^{13.2}$ dPa·s)	715
Strain point (viscosity= $10^{14.5}$ dPa·s) in °C	518	513	571 ($10^{14.7}$ dPa·s)	670
Sources	*(SCHOTT 2017)*	*(Doremus 1994)*	*(CORNING 2017)*	*(Doremus 1994)*
	(Abrisa Technologies 2014)	*(Martlew 2005)*		*(Martlew 2005)*
		(Campbell et al 1990)		*(Campbell et al 1990)*

2.2.2 Selection of glass waste samples

According to the above categorization, characteristic samples from each type of glass family were collected and analyzed with a Panalytical Axios Max WD-XRF spectrometer in order to define their glass composition. The Panalytical set of Omnian standards were used for calibration, as well as several NIST SRM standards and pure (p.a.) compounds. The results can be seen in Table 2.2. In short, the following samples were analyzed per category:

- Soda lime silica/ blown, automated: Beer/wine/soda bottles, drinking glasses
- Soda lime silica/ mouth-blown: artifacts from the glass blowing studio at Southern Illinois University
- Soda lime silica/ float: window glass, waste glass from furnace clean-up
- Soda potassium lime silica: optical lenses, tableware
- Lead crystal: tableware
- Lead-free crystal: CRT screen (panel)
- Borosilicate: laboratory tubes
- Alkali-aluminosilicate: mobile phone screens

Table 2.2 (part a): Composition of selected waste glass by category (XRF analysis). The reported values are normalised to 100%.

Soda-lime silica glass											
Blown, automated: Glass Bottles											
Green beer bottle (Stella)		Green beer bottle (Heineken)		Light green wine Bottle (from USA)		Clear wine bottle (Riesling)		Clear (Coca cola)		Clear (Spa)	
Compound name	Content (wt%)	Compound name	Content (wt%)	Compound name	Content (wt%)	Compound name	Content (wt%)	Compound name	Content (wt%)	Compound name	Content (wt%)
SiO_2	73.34	SiO_2	72.094	SiO_2	73.36	SiO_2	72.543	SiO_2	73.529	SiO_2	73.994
Na_2O	12.41	Na_2O	12.039	Na_2O	12.704	CaO	11.266	Na_2O	12.008	Na_2O	11.255
CaO	9.925	CaO	10.704	CaO	11.313	Na_2O	10.953	CaO	10.813	CaO	10.934
Al_2O_3	1.598	MgO	2.24	Al_2O_3	1.22	MgO	2.03	MgO	1.899	MgO	1.917
MgO	1.454	Al_2O_3	1.514	K_2O	0.455	Al_2O_3	1.683	Al_2O_3	1.184	Al_2O_3	1.3
K_2O	0.517	K_2O	0.419	MgO	0.382	K_2O	0.689	K_2O	0.211	K_2O	0.225
Fe_2O_3	0.341	Fe_2O_3	0.368	Fe_2O_3	0.323	P_2O_5	0.244	S	0.168	S	0.121
Cr_2O_3	0.175	Cr_2O_3	0.208	Cr_2O_3	0.051	S	0.163	Fe_2O_3	0.062	Fe_2O_3	0.09
BaO	0.055	MnO	0.169	TiO_2	0.047	CeO_2	0.114	BaO	0.027	Cl	0.043
TiO_2	0.051	S	0.056	S	0.043	Fe_2O_3	0.071	Cl	0.027	TiO2	0.033
S	0.029	TiO_2	0.047	BaO	0.021	TiO_2	0.065	P_2O_5	0.021	BaO	0.028
MnO	0.026	Cl	0.039	Cl	0.017	BaO	0.048	PbO	0.02	SrO	0.015
PbO	0.018	BaO	0.029	ZrO_2	0.015	MnO	0.034	SrO	0.013	P_2O_5	0.015
SrO	0.016	SrO	0.019	P_2O_5	0.015	Cl	0.03	ZrO_2	0.01	ZrO_2	0.013
P_2O_5	0.015	ZrO_2	0.018	MnO	0.012	SrO	0.021	ZnO	0.008	PbO	0.011
ZrO_2	0.014	PbO	0.013	SrO	0.011	ZrO_2	0.02			ZnO	0.006
ZnO	0.006	P_2O_5	0.011	PbO	0.005	PbO	0.017				
CuO	0.005	ZnO	0.01	ZnO	0.004	ZnO	0.012				
NiO	0.003	Rb2O	0.002	Rb_2O	0.001						
Rb_2O	0.002										

Table 2.2 (part b): Composition of selected waste glass by category (XRF analysis). The reported values are normalised to 100%.

Soda-lime silica glass											
Blown, automated: Glass Bottles								Blown, automated: Drinking glass		Mouth-blown glass	
Wine bottle mix								Champagne glass		Spruce Pine transparent blue	
1. Clear		2. Light blue		3. Light green		4. Green					
Compound name	Content (wt%)	Compound name	Content (wt%)	Compound name	Content (wt%)	Compound name	Content (wt%)	Compound name	Content (wt%)	Compound name	Content (wt%)
SiO_2	73.356	SiO_2	72.628	SiO_2	73.358	SiO_2	71.124	SiO_2	73.241	SiO_2	71.768
Na_2O	11.882	Na_2O	11.761	CaO	11.888	Na_2O	12.903	Na_2O	12.682	Na_2O	14.288
CaO	9.878	CaO	9.746	Na_2O	11.477	CaO	11.072	CaO	10.883	CaO	6.834
MgO	2.165	MgO	3.129	Al_2O_3	1.305	Al_2O_3	2.875	Al_2O_3	1.621	Al_2O_3	2.306
Al_2O_3	1.261	Al_2O_3	1.603	MgO	1.013	K_2O	0.882	MgO	1.277	CuO	2.038
K_2O	0.639	K_2O	0.661	K_2O	0.397	Fe_2O_3	0.446	S	0.149	Fe_2O_3	0.835
SrO	0.203	S	0.19	Fe_2O_3	0.257	MgO	0.239	TiO_2	0.052	ZnO	0.759
BaO	0.184	Fe_2O_3	0.144	TiO_2	0.073	Cr_2O_3	0.211	Cl	0.027	K_2O	0.38
S	0.143	TiO_2	0.049	Cr_2O_3	0.062	TiO_2	0.07	K_2O	0.025	BaO	0.355
ZrO_2	0.085	Cl	0.026	BaO	0.047	P_2O_5	0.045	P_2O_5	0.022	Sb_2O_3	0.161
Fe_2O_3	0.069	P_2O_5	0.022	S	0.025	Cl	0.044	ZrO_2	0.013	MgO	0.133
TiO_2	0.045	ZrO_2	0.017	SrO	0.021	S	0.038	SrO	0.008	ZrO_2	0.046
Cl	0.031	ZnO	0.009	ZrO_2	0.02	BaO	0.025			Co_3O_4	0.04
ZnO	0.024	PbO	0.008	Cl	0.018	SrO	0.017			S	0.04
P_2O_5	0.021	SrO	0.006	PbO	0.016	ZrO_2	0.009			SrO	0.012
PbO	0.013			ZnO	0.011					P_2O_5	0.005
				P_2O_5	0.01						
				Rb_2O	0.003						

Table 2.2 (part c): Composition of selected waste glass by category (XRF analysis). The reported values are normalised to 100%.

Soda-lime silica glass											
Mouth-blown glass				Float glass							
Spruce Pine transparent orange		Spruce Pine transparent clear		PPG Starphire (extra clear)		PPG clear		PPG furnace waste aquamarine		PPG furnace waste light green	
Compound name	Content (wt%)	Compound name	Content (wt%)	Compound name	Content (wt%)	Compound name	Content (wt%)	Compound name	Content (wt%)	Compound name	Content (wt%)
SiO_2	73.144	SiO_2	74.61	SiO_2	74.563	SiO_2	74.214	SiO_2	73.108	SiO_2	67.41
Na_2O	15.393	Na_2O	13.595	Na_2O	13.323	Na_2O	12.438	Na_2O	14.346	Na_2O	13.676
CaO	7.093	CaO	7.356	CaO	8.905	CaO	10.029	CaO	7.888	Al_2O_3	8.828
Al_2O_3	2.058	Al_2O_3	2.037	MgO	3.006	MgO	2.859	MgO	3.947	CaO	5.943
ZnO	0.886	ZnO	0.908	S	0.105	Al_2O_3	0.142	Al_2O_3	0.311	ZrO_2	2.975
BaO	0.411	BaO	0.45	Al_2O_3	0.035	Fe_2O_3	0.124	S	0.159	MgO	0.431
K_2O	0.411	K_2O	0.388	Fe_2O_3	0.015	S	0.084	Fe_2O_3	0.087	TiO_2	0.213
MgO	0.258	Sb_2O_3	0.218	Cl	0.014	K_2O	0.043	K_2O	0.078	Fe_2O_3	0.171
Sb_2O_3	0.223	MgO	0.157	K_2O	0.012	P_2O_5	0.038	TiO_2	0.035	S	0.101
Fe_2O_3	0.027	Er_2O_3	0.123	P_2O_5	0.01	Cl	0.024	ZrO_2	0.014	SrO	0.089
ZrO_2	0.024	S	0.062	ZrO_2	0.007	SrO	0.005	Cl	0.013	K_2O	0.073
S	0.023	Fe_2O_3	0.054	SrO	0.005			P_2O_5	0.009	HfO_2	0.055
PbO	0.021	Cl	0.016					SrO	0.005	P_2O_5	0.02
SrO	0.012	SrO	0.013							Cl	0.015
Cl	0.01	P_2O_5	0.007								
P_2O_5	0.005	Ag_2O	0.005								

Table 2.2 (part d): Composition of selected waste glass by category (XRF analysis). The reported values are normalised to 100%.

Soda potassium lime silica glass (optical glass)			
Schott B270 lenses		Czechoslovakia bowl	
Compound name	Content (wt%)	Compound name	Content (wt%)
SiO_2	71.802	SiO_2	82.632
Na_2O	10.138	Na_2O	6.488
K_2O	6.275	CaO	4.146
CaO	5.168	K_2O	3.2
ZnO	2.198	MgO	2.755
Al_2O_3	2.083	S	0.281
TiO_2	1.765	Al_2O_3	0.219
Sb_2O_3	0.403	Cl	0.1
MgO	0.041	TiO_2	0.06
BaO	0.03	Fe_2O_3	0.045
Cl	0.022	PbO	0.028
S	0.018	P_2O_5	0.023
P_2O_5	0.017	ZnO	0.01
Fe_2O_3	0.016	ZrO_2	0.009
ZrO_2	0.008	Rb_2O	0.004
SrO	0.006	Br	0.002
Rb_2O	0.005		
PbO	0.005		

Lead Crystal					
Schott LF5 lead crystal		G210		Crystal D'Arques 24% Lead Bowl	
Compound name	Content (wt%)	Compound name	Content (wt%)	Compound name	Content (wt%)
SiO_2	53.731	PbO	47.002	SiO_2	63.229
PbO	36.643	SiO_2	44.714	PbO	24.799
K_2O	5.387	K_2O	3.936	K_2O	7.753
Na_2O	3.771	Na_2O	3.296	Na_2O	2.842
Al_2O_3	0.198	S	0.231	CaO	1.2
S	0.134	Sb_2O_3	0.215	S	0.075
CaO	0.114	CaO	0.212	Al_2O_3	0.051
NiO	0.018	Al_2O_3	0.203	ZrO_2	0.026
P_2O_5	0.005	Cl	0.086	Fe_2O_3	0.024
		MgO	0.06		
		Fe_2O_3	0.046		

Table 2.2 (part e): Composition of selected waste glass by category (XRF analysis). The reported values are normalised to 100%.

Alkali-barium silicate glass	
CRT computer screen (panel)	
Compound name	Content (wt%)
SiO_2	61.505
SrO	8.056
BaO	8.039
Na_2O	7.21
K_2O	6.776
ZrO_2	3.587
Al_2O_3	2.304
CaO	1.109
TiO_2	0.378
Sb_2O_3	0.343
MgO	0.296
S	0.153
Fe_2O_3	0.095
CuO	0.055
Cl	0.028
ZnO	0.027
P_2O_5	0.023
NiO	0.018

Borosilicate glass			
Schott lab glassware			
Compound name	Content (wt%)	Compound name	Content (wt%)
Boron not measured therefore Si content appears high		Duran composition according to (Heimerl 1999)	
SiO_2	*93.024*	SiO_2	80
Na_2O	3.548	B_2O_3	13
Al_2O_3	2.725		
K_2O	0.513		
Cl	0.051		
ZrO_2	0.049		
Fe_2O_3	0.036		
TiO_2	0.033		
P_2O_5	0.012		
ZnO	0.005		
SrO	0.002		
Rb_2O	0.002		

Alkali-aluminosilicate glass	
Mobile phone screen thin glass	
Compound name	Content (wt%)
SiO_2	63.062
Al_2O_3	12.958
K_2O	11.12
MgO	6.235
Na_2O	5.603
ZrO_2	0.843
CaO	0.062
S	0.039
Fe_2O_3	0.027
Cl	0.017
TiO_2	0.014
HfO_2	0.013
P_2O_5	0.006
SrO	0.002

2.3 Recycling experiments and interpretation of the results

2.3.1 Experimental set-up

In this section, an explanation of the set-up parameters is provided. Regarding the casting method for the sample production, the two techniques listed below were followed, according to the maximum operating temperature needed:

a) Kiln-casting employing investment silica-plaster moulds (Figure 2.2a, b). For this method, one kiln is used for the melting and annealing of the glass and therefore, the feeding of the moulds with glass takes place inside the kiln (kiln used: ROHDE ELS 200S). Three different types of moulds were produced:

- Crystalcast M248, powder to water volume ratio 2.75:1. The product consists of cristobalite, quartz and gypsum (Gold Star). For firings above 1000°C, the crystalcast moulds are reinforced by an exterior layer of heat-resistant concrete.
- Ransom & Randolph (R&R) Glass Cast 910, powder to water mass ratio 10:2.8. The product consists of cristobalite, quartz, mullite, calcium sulfate and fibrous glass (Ransom & Randolph).
- Heat-resistant concrete coated with a 1mm thick layer of Mold Mix 6 by Zincar, which is a high alumina putty coating with glass reinforcement fibers (ZRCI 2017). Two layers of EKamold® spray are applied as top coating. This product is an ethanolic coating based on hexagonal boron nitride (ESK 2013). This mould was used for a firing at 1250°C.

The glass was introduced in the moulds either directly ("free-set", see Figure 2.2d) or indirectly by being placed in terracotta flowerpots that were positioned above the moulds (Figure 2.2e). The heating ramp was set at 50°C/hr. Regarding the quenching applied to prevent the crystallization of the components, the samples are either manually quenched below their softening point, by opening and closing the kiln door in repetition or mechanically by setting the kiln controller at the "As Fast As Possible" function. The later cooling process requires more time versus the manual, abrupt quenching.

b) Melt-quenching technique employing high-alumina crucibles and steel moulds (Figure 2.2c). This method is preferred in this research for castings above 1250°C, due to the high thermal and chemical resistance of the alumina crucibles. For this method, two kilns are needed for the melting (Carbolite HTF 17/10) and annealing (ROHDE ELS 200S) of the glass respectively. The glass is melted in Coors™ high-alumina crucibles (Figure 2.2f) and poured at atmospheric conditions in steel moulds that are preheated at 500°C. Upon quenching, the samples are placed in the annealing oven together with the steel mould. The heating rate used was 17.5C°/min.

An overview of the casting experiments including the casting set-up and the results is provided in Table 2.3.

(a) (b) (c)

(d) (e) (f)

Fig. 2.2 (a) Kiln-casting at 1120ºC in a ROHDE ELS 200S kiln using Crystalcast moulds with glass directly placed inside the moulds (free-set). (b) Kiln-casting at 1120ºC in Crystalcast moulds employing the flowerpot technique. (c) Hot pouring at 1450ºC in a steel mould. (d) Cullet directly placed inside a Crystalcast mould (free-set), prior to kiln-casting. (e) Terracotta flowerpots filled with glass cullet and placed above Crystalcast moulds. (f) High-alumina crucibles placed in a Carbolite HTF 17/10 kiln.

Table 2.3 (part a): Overview of the conducted casting experiments.

Most pictures are taken before post-processing so surfaces in contact with the investment mould may be still translucent

Glass type	Data	Before firing	Casting temperature in °C									
			860	940	950	970	1120	1200	1250	1350	1450	1500
Lead Crystal	Crystal D' Arques 24% Lead											
	Mould type				Crystalcast M248							
	Casting method				Kiln-casting							
	Glass feeding				Free-set on mould							
	Quenching				Abrupt: door open							
	Homogeneous melt				Yes							
	Crystallisation				No							
	Top surface creasing				Minimal							
	Transparency				Yes							
Alkali barium silica	CRT computer screen (panel)				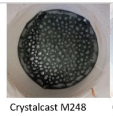	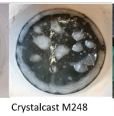	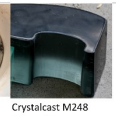					
	Mould type				Crystalcast M248	Crystalcast M248	Crystalcast M248					
	Casting method				Kiln-casting	Kiln-casting	Kiln-casting					
	Glass feeding				Free-set on mould	Flowerpot method	Free-set on mould					
	Quenching				Abrupt: door open	Kiln-operated	Abrupt: door open					
	Homogeneous melt				Yes	Yes	Yes					
	Crystallisation				Top surface dotted (water soluble)	Top surface, linear	Top surface dotted (water soluble)					
	Top surface creasing				No	No	No					
	Transparency				Yes	Yes	Yes					
Potassium soda lime silica	Czechoslovakia bowl											
	Mould type				Crystalcast M248							
	Casting method				Kiln-casting							
	Glass feeding				Free-set on mould							
	Quenching				Abrupt: door open							
	Homogeneous melt				Yes							
	Crystallisation				No							
	Top surface creasing				Intense							
	Transparency				Yes							
Soda lime silica (blown)	Spruce Pine transparent blue		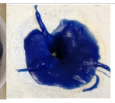									
	Mould type		R&R Glass-Cast 910									
	Casting method		Kiln-casting									
	Glass feeding		Flowerpot method									
	Quenching		Kiln-operated									
	Homogeneous melt		Yes									
	Crystallisation		Full									
	Top surface creasing		No									
	Transparency		No									

Table 2.3 (part b): Overview of the conducted casting experiments.

Glass type	Data	Before firing	Casting temperature in °C									
			860	940	950	970	1120	1200	1250	:350	1450	1500
Soda lime silica (blown)	Spruce Pine transparent orange		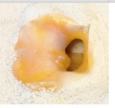									
	Mould type		R&R Glass-Cast 910									
	Casting method		Kiln-casting									
	Glass feeding		Flowerpot method									
	Quenching		Kiln-operated									
	Homogeneous melt		No (different hues of orange used)									
	Crystallisation		Full									
	Top surface creasing		No									
	Transparency		No									
Soda lime silica (blown)	Spruce Pine transparent clear and blue		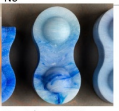									
	Mould type		Crystalcast M248		Crystalcast M248							
	Casting method		Kiln-casting		Kiln-casting							
	Glass feeding		Flowerpot method		Flowerpot method							
	Quenching		Kiln-operated		Kiln-operated							
	Homogeneous melt		No (different colour zones)		No (different colour zones)							
	Crystallisation		Full		No							
	Top surface creasing		No		No							
	Transparency		No		Yes							
Soda lime silica (float)	PPG Starphire (extra clear)						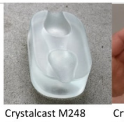					
	Mould type		R&R Glass-Cast 910				Crystalcast M248	Crystalcast M248				
	Casting method		Kiln-casting				Kiln-casting	Kiln-casting				
	Glass feeding		Flowerpot method				Free-set on mould	Free-set on mould				
	Quenching		Kiln-operated				Abrupt: door open	Abrupt: door open				
	Homogeneous melt		No				Yes	Yes				
	Crystallisation		Full				No	Top surface only				
	Top surface creasing		No				Yes	No				
	Transparency		No				Yes	Yes				
Soda lime silica (float)	PPG clear											
	Mould type							Crystalcast M248				
	Casting method							Kiln-casting				
	Glass feeding							Free-set on mould				
	Quenching							Abrupt: door open				
	Homogeneous melt							Yes				
	Crystallisation							Top surface only				
	Top surface creasing							No				
	Transparency							Yes				

Table 2.3 (part c): Overview of the conducted casting experiments.

Glass type	Data	Before firing	Casting temperature in °C									
			860	940	950	970	1120	1200	1250	1350	1450	1500
Soda lime silica (float-furnace waste)	PPG furnace waste aquamarine							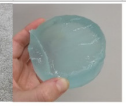				
	Mould type		R&R Glass-Cast 910				Crystalcast M248	Crystalcast M248				
	Casting method		Kiln-casting				Kiln-casting	Kiln-casting				
	Glass feeding		Flowerpot method				Free-set on mould	Free-set on mould				
	Quenching		Kiln-operated				Abrupt: door open	Abrupt: door open				
	Homogeneous melt		No				Yes	Yes				
	Crystallisation		Yes				No	Top surface only				
	Top surface creasing		Yes				Yes	Yes				
	Transparency		No				Yes	Yes				
Soda lime silica (float-furnace waste)	PPG furnace waste light green											
	Mould type		Terracotta (sample did not flow down to the investment mould)									
	Casting method		Kiln-casting									
	Glass feeding		Flowerpot method									
	Quenching		Kiln-operated									
	Homogeneous melt		Yes									
	Crystallisation		No									
	Top surface creasing		No									
	Transparency		Yes									
Soda-lime silica (drinking glass)	Champagne glass											
	Mould type				Crystalcast M248							
	Casting method				Kiln-casting							
	Glass feeding				Free-set on mould							
	Quenching				Abrupt: door open							
	Homogeneous melt				No/ fusion lines							
	Crystallisation				Full							
	Top surface creasing				Minimum							
	Transparency				No							

Table 2.3 (part d): Overview of the conducted casting experiments.

Glass type	Data	Before firing	Casting temperature in °C									
			860	940	950	970	1120	1200	1250	1350	1450	1500
Soda lime silica (bottle glass)	Clear wine bottle (Riesling)											
	Mould type					Crystalcast M248 (sample could barely flow down to the investment mould)						
	Casting method					Kiln-casting						
	Glass feeding					Flowerpot method						
	Quenching					Kiln-operated						
	Homogeneous melt					Yes						
	Crystallisation					Full						
	Top surface creasing					-						
	Transparency					No						
Soda lime silica (bottle glass)	Clear bottle (Spa)											
	Mould type							Crystalcast M248				
	Casting method							Kiln-casting				
	Glass feeding							Free-set on mould				
	Quenching							Abrupt: door open				
	Homogeneous melt							Yes				
	Crystallisation							Top surface				
	Top surface creasing							No				
	Transparency							Yes				
Soda lime silica (bottle glass)	Green beer bottle glass (Stella:860°C, Heineken:970°C, 1120°C, 1200°C)	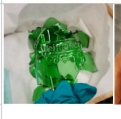					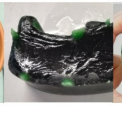	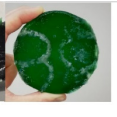				
	Mould type		Terracotta (sample did not flow down to the investment mould)			Terracotta (sample could barely flow down to the investment mould)	Crystalcast M248	Crystalcast M248				
	Casting method		Kiln-casting			Kiln-casting	Kiln-casting	Kiln-casting				
	Glass feeding		Flowerpot method			Flowerpot method	Free-set on mould	Free-set on mould				
	Quenching		Kiln-operated			Kiln-operated	Abrupt: door open	Abrupt: door open				
	Homogeneous melt		No			No	Yes	Yes				
	Crystallisation		Full			Full	No	Top surface only				
	Top surface creasing		-			Yes	Yes	Minimum				
	Transparency		No			No	Yes	Yes				

Table 2.3 (part e): Overview of the conducted casting experiments.

Glass type	Data	Before firing	Casting temperature in °C									
			860	940	950	970	1120	1200	1250	1350	1450	1500
Soda lime silica (bottle glass)	Light green wine Bottle (from USA)											
	Mould type		Terracotta (sample did not flow down to the investment mould)									
	Casting method		Kiln-casting									
	Glass feeding		Flowerpot method									
	Quenching		Kiln-operated									
	Homogeneous melt		No									
	Crystallisation		Full									
	Top surface creasing		-									
	Transparency		No									
Soda lime silica (bottle glass)	Mix wine bottle glass (powder - cullet)							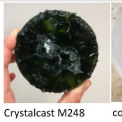				
	Mould type			Crystalcast M248		Crystalcast M248		Crystalcast M248	coated with Mold Mix 6	Stainless steel	Stainless steel	
	Casting method			Kiln-casting		Kiln-casting		Kiln-casting	Kiln-casting	Coors high-alumina	Coors high-alumina	
	Glass feeding			Free-set on mould		Free-set on mould		Free-set on mould	Free-set on mould	crucible)	crucible)	
	Quenching			Abrupt: door open		Kiln-operated		Abrupt: door open	Abrupt: door open	In atm. conditions	In atm. conditions	
	Flux agent			10% CNa2O3		No		No	No	No	No	
	Homogeneous melt			No		No		Yes	due to the shrinkage of	Yes		
	Crystallisation			Yes		Yes		Top surface only	No	No		
	Top surface creasing			No		-		Yes	No	-	-	
	Transparency			No		No		Yes	Yes	in air bubbles)	Yes	
Soda lime silica (bottle glass)	Mix clear bottle (50% coca cola + 50% spa per mass)											
	Mould type					Crystalcast M248						
	Casting method					Kiln-casting						
	Glass feeding					Free-set on mould						
	Quenching					Kiln-operated						
	Homogeneous melt					Yes						
	Crystallisation					Yes						
	Top surface creasing					-						
	Transparency					No						

Table 2.3 (part f): Overview of the conducted casting experiments.

Glass type	Data	Before firing	Casting temperature in °C									
			860	940	950	970	1120	1200	1250	1350	1450	1500
Borosilicate	Schott lab glassware DURAN											
	Mould type						Crystalcast M248	Crystalcast M248				
	Casting method						Kiln-casting	Kiln-casting				
	Glass feeding						Free-set on mould	Free-set on mould				
	Quenching						Kiln-operated	Abrupt: door open				
	Homogeneous melt						Yes	Yes				
	Crystallisation						Top surface	Locally at top surface only				
	Top surface creasing						No	No				
	Transparency						Yes	Yes				
Aluminosilicate glass	Mobile phone screen thin glass											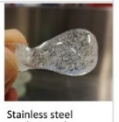
	Mould type					Crystalcast M248			Crystalcast M248			Stainless steel
	Casting method					Kiln-casting			Kiln-casting			Coors high-alumina crucible)
	Glass feeding					Free-set on mould			Free-set on mould			In atm. conditions
	Quenching					Kiln-operated			Abrupt: door open			Yes
	Homogeneous melt					Yes			Reaction with mould			
	Crystallisation					No			Porous structure			No
	Top surface creasing					No			-			-
	Transparency								No			Yes (but high content of air bubbles)

2.3.2 Casting experiments of the selected glass waste families

Table 2.3 presents the results of the castings of samples from the six selected glass families at different temperatures. The samples are initially evaluated on their workability. As the collection of samples includes glasses that have been developed for other production techniques (automated-blowing, float line, automated draw etc.), implications are expected when attempting to cast them, especially with the- slower- method of kiln-casting. Ideally, the glass samples should be able to flow and homogenize at temperatures below 1000°C, both to increase the energy savings but also to simplify the prerequisites of their mould. The aim of this research is thus to identify the glasses that have both lower working temperatures and a resistance to crystallization from the glasses that are difficult to cast and which will need extra attention. For this identification step, each glass is cast individually. The following observations and conclusions can be gathered for each glass family:

- Soda lime silica/ blown, automated (Container glass such as beer/wine/soda bottles, drinking glasses):
  These glasses are developed for the automated blowing process, therefore they need to be stiff enough to keep their shape once blown in a mould. Although this prerequisite decreases the workability of the glass, this fact is counteracted by the mechanically applied air pressure for the moulding. This attribute was prevailing during the casting of these glasses (key results seen in Figure 2.3), since the samples needed temperatures higher than 1000°C in order to flow and homogenize. Moreover, all samples were very susceptible to crystallization below the liquidus temperature. Abrupt quenching was necessary to avoid full crystallization and to confine the problem only to the top surface. Specifically, samples cast at 860°C would not flow but only partially fuse, and would appear fully crystallized with mechanical quenching. At 950°C the drinking glass sample failed to homogenize and crystallized despite its fast cooling. Likewise, the samples cast at 970°C and mechanically quenched were crystallized and incomplete, as the glass could not easily flow from the flowerpot down to the mould. It should be noted, however, that samples appearing to be fully crystallized, proved to contain glassy zones within their body, when sliced in two and observed along their cross section. Only when cast at 1120/1200°C and abruptly cooled down to 600°C were the resulting samples transparent. This transparency was evident after the top crystallized surface[16] and the bottom surface in contact with the investment mould were polished.

[16] Unless a nucleating agent is added in the glass melt to promote bulk crystallization, usually crystallization starts from the glass surface. Airborne dust is often the main trigger. In addition, volatilization of various components from the glass melt alters the composition at the outer layer. Particles from the mould found on that altered surface could also act as nucleating sites (Müller 2000).

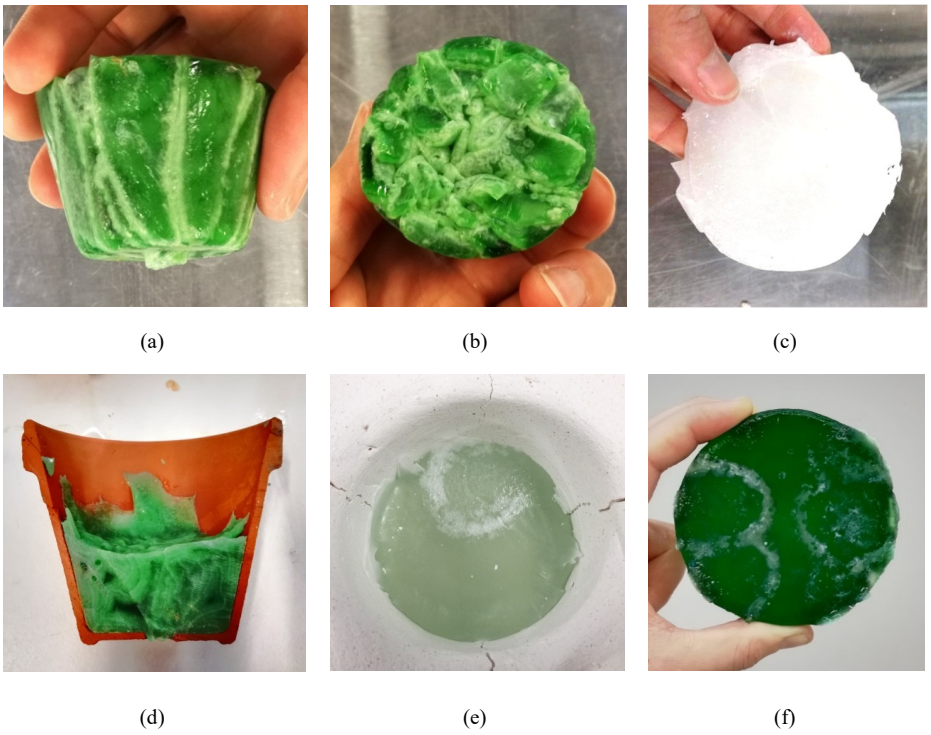

(a) (b) (c)

(d) (e) (f)

Fig. 2.3 (a), (b) Beer bottle starting to fuse inside the flowerpot, at 860°C, (c) drinking glass, crystallized at 950°C, (d) beer bottle fused inside the flowerpot and partially crystallized, (e) clear bottle cast at 1200°C with top surface crystallization linked to the contact of the glass to the mould, (f) beer bottle cast at 1200°C.

From the XRF data obtained, we can observe that all above tested glasses have a similar composition. Mainly we see a range of 71.12-73.99 per weight percentage (wt%) of SiO_2, 10.95-12.90 wt% Na_2O, and 9.74-11.88 wt% CaO. Calcium oxide (CaO, lime) is increasing the softening point and the sagging temperature, thus the observed high viscosity of the samples (Zschimmer 2013). Although this is required for the automated blowing process, the increased softening point impedes the casting. The high percentage of lime is also responsible for the susceptibility to crystallization. According to Zschimmer, lime percentages above 10% promote devitrification. This is to be taken into account when working with this glass sub-family.

It should be also mentioned that although the tested glasses have almost the same composition and viscosity, their colour affects their setting time. Kitaĭgorodskiĭ et al. (1934) and Burch et al. (1938) proved that glasses with identical basic composition and viscosity characteristics, differ regarding their working range. Specifically, dark coloured glasses, due to their greater heat loss by radiation rate, tend to set much faster than the equivalent transparent or light coloured samples. Holscher et al. (1943) suggest chromium emerald green glasses of basic composition SiO_2 74.0 wt%, Na_2O 16.0 wt%, CaO 10.0 wt%, Fe_2O_3 0.035 wt% and Cr_2O 0.25 wt% to be one of the most rapid cooling

systems after dark green Fe-Mn systems. In our tested samples that could be easily verified by the intense luminosity of these samples at 1200°C in comparison to the transparent ones (Figure 2.4). The fast setting of darker colours should be considered when the hot-pouring method is employed.

Fig. 2.4 Kiln-casting experiment at 1120°C, portraying the differences in luminosity among the various coloured samples.

Experiments with mixing different container samples together were also conducted in order to define their compatibility. The glass recycling industry separates soda lime silica containers from numerous different producers into similar colours. The segregated cullet is then successfully recycled together with new raw material. In that sense, casting two different clear bottles together was expected to work well at temperatures corresponding to viscosities of $10^{1.5\text{-}2.5}$ poise, which are achieved in the melting tanks. For typical soda lime silica glasses (Kimble R-6 used as reference), a $10^{2.5}$ viscosity would correspond to 1254°C (Martlew 2005). Therefore it was opted to test the combination at a lower temperature, namely 970°C. The sample, placed in a flowerpot, was kept at top temperature for 2 hours and then mechanically quenched. A small part of the glass mixture flowed down the mould and despite the fact that the glass was fully crystallized, it was homogenized and did not crack during annealing (Figure 2.5a). Regarding the glass mass that remained in the flowerpot, this could be observed by cutting the pot in half (Figure 2.5c). There, zones of crystallized glass of almost same thickness (similar to the thickness of the bottles) are fused together. A few glassy regions are also observed. It is interesting to see that the zone of glass in contact with the flowerpot- which heats up and cools down faster- is more homogeneous and has a different micro-pattern of crystallization (Figure 2.5b).[17] Regardless of the above, none of the glass masses cracked, proving that this combination is also feasible at temperatures below 1250°C.

[17] In comparison to the previously described high temperature tests at 1200-1250ºC, in this case the glass shards reach a state just above the softening point that allows them to compact within the

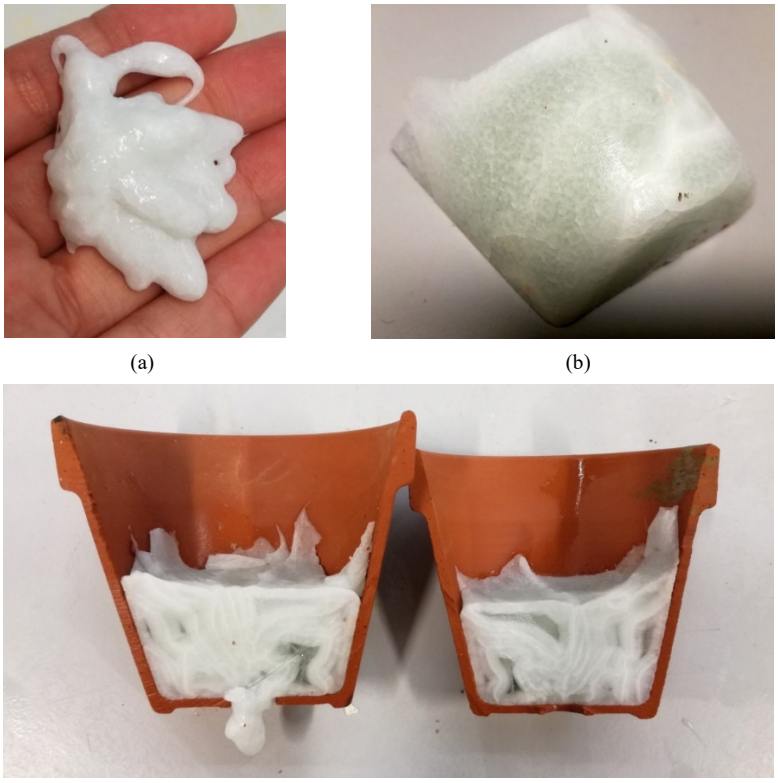

(a) (b)

(c)

Fig. 2.5 Results from the kiln-casting of two different types of clear bottles at 970°C. (a) Droplets that flowed from the flowerpot down to the mould, (b) glass part that fused inside the flowerpot. In this picture, the surface in contact with the flowerpot is seen, (c) flowerpot cut in half, showing the layering of the fused glass and the glassy areas within the crystallized mass.

The mixing of different colours of container glass (wine bottles) was also tested, in various sizes from powder to small and medium sized shards (Figure 2.6). The XRF analysis of 4 different samples showed strong compositional similarity despite the colour shifts. The mix of wine bottles was fired at various temperatures between 940°C - 1450°C. At 970°C the sample would partially fuse and still keep the integrity and colours of the individual pieces. This comes in antithesis with the above mixture of clear bottles (similar recipes to the wine bottles) that homogenized at the same temperature. In this case, the differences in colour/exact recipe, seem to require higher temperatures. Nonetheless, the sample did not crack upon annealing. Adding 10% of fluxing agent (in

flowerpot. Moreover, there is a difference observed within the bulk of each individual shard and its exterior surface. The bulk is overall cooler than the exterior surface and has a high viscosity that acts as a kinetic barrier for the formation of crystals. The exterior, however, heats up first and has a reduced viscosity that allows the fusion with the adjacent shards. This viscosity simultaneously allows the formation of crystals, thus the crystallization observed in these areas.

this case Na_2CO_3) in the powdered mix and firing it at 940°C helped the melting of the top surface but did not result in a homogenized sample. The sample was homogenized at the tests conducted from 1200°C and above. Higher temperatures are required for the homogenization of this combination.

In general, despite the challenges to cast this sub-family described in this chapter, glass container waste is still the most prevailing one. In that sense, it is worth exploring the derailing of sorted- yet discarded by the packaging industry -glass waste, from the landfill to the building sector. As an advantage, the iron in the green and amber (combined with Sulfur) glasses can provide excellent UV-radiation protection (Shelby 2005) and should thus be considered for use in facades.

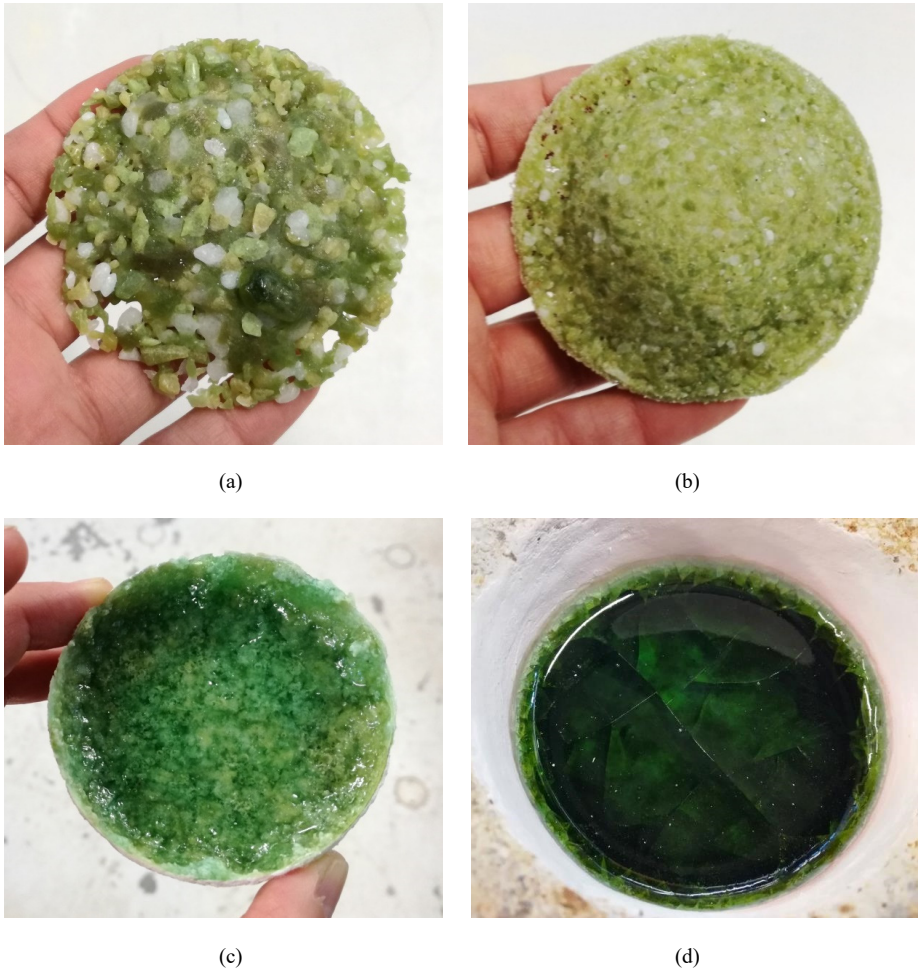

(a) (b)

(c) (d)

Fig. 2.6 Samples of different coloured glass bottles kiln-cast at (a) 970°C (small shards), (b) 970°C (powder), (c) 940°C (powder + flux), (d) 1250°C (powder).

- Soda lime silica/ mouth-blown (artifacts from the glass blowing studio at Southern Illinois University):
  Glass studios, either commercial or academic, produce quite some glass waste during their trial and error explorations. Especially the discarded pieces by the glassblowing hotshop containing colour are not reused for blown objects, as this would imply the contamination of the clear transparent batch in the furnace.

  In contrast to the above glass category, these glasses are meant to be processed according to the power of the human lung, therefore they cannot be as stiff. Also, the artists require a prolonged working time to process their piece, thus a glass that will not set as fast as the container glass. Correspondingly, the content of lime (CaO) in this composition is found around 6.8-7.1 wt% and of sodium oxide (Na_2O) at 14.3-15.4 wt%. The glass samples thus could slowly flow down from the flowerpots to the moulds at 860°C, a temperature considerably lower than the one necessary for the machine-blown glass objects of the same glass family. However, the lack of abrupt quenching can still induce extended crystallization in the samples (Figure 2.7). The differences in the working range between the various colour variations are valid also here. Overall though, these coloured glasses are usually engineered to be compatible and as a result beautiful colour patterns can emerge from their combination. Crystallized samples can lead as well to interesting marble-like smooth components. Since the mechanical properties of these objects are expected to be improved during the devitrification, experimental testing of their strength is required in follow-on research, in order to explore their potential value as building components.

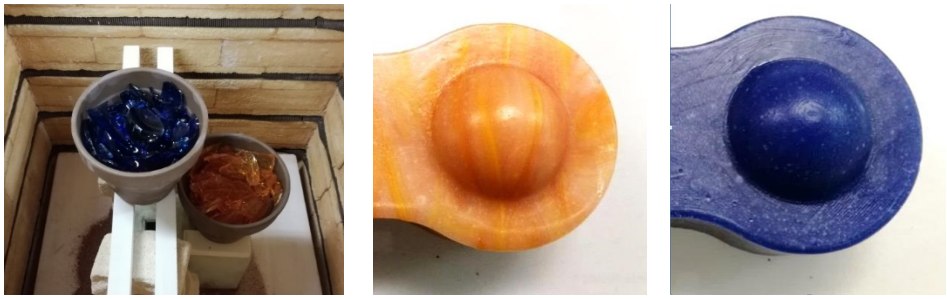

(a) (b) (c)

Fig. 2.7 (a) Set-up of the kiln, (b), (c) glass ceramic samples resulting from the mouth-blown glass waste.

Further investigation on the crystallization issue of these samples showed that a relatively slow cooling rate is not as decisive as the choice of top temperature for kiln-casting (Figure 2.8). Using transparent clear and blue Sprucepine shards, two elements were cast, one at 860°C and one at 950°C, kept at top temperature for 10 hours and then cooled down to annealing point with a rate of 120°C/h. The sample cast at a lower

temperature appeared fully crystallized in comparison to the one cast at a higher temperature, which resulted in a transparent blue glass.

Fig. 2.8 Glass samples cast employing Sprucepine clear and blue glass waste (top and bottom) and lead crystal (middle element). The figure shows the effect of casting temperature to the structure of the glass component. Although the top and bottom sample are cast using the same glass, the one below, cast at 860°C crystallized, in comparison to the clear blue component on top, cast at 950°C.

In order to explain this observation and define the dangerous crystallization zone of this glass, a comprehensive glass thermal analysis (Differential Scanning Calorimetry DSC) was performed to a sample of transparent clear Sprucepine glass, employing a STA 449 F3 Jupiter® apparatus.

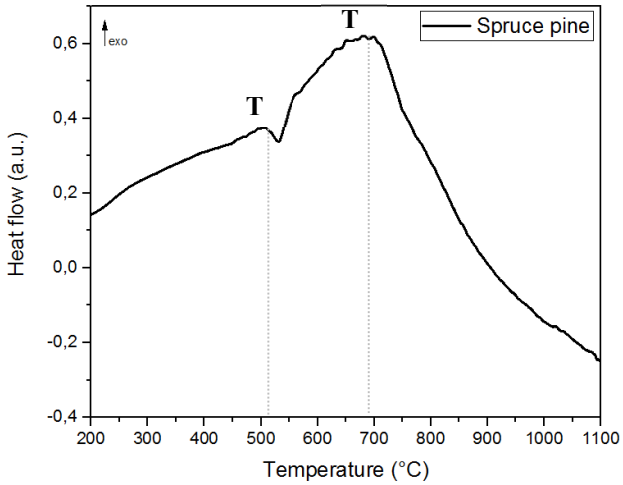

Fig. 2.9 DSC analysis pointing out the glass transition temperature and crystallization peak temperature of Spruce Pine transparent clear glass.

The DSC analysis defines the crystallization peak at around 700ºC (Figure 2.9). Observing the endothermic process after this point, we can notice the drastic fall of the DSC curve. This proves that there is a significant difference between casting this glass at 860ºC and 950ºC.

Regarding the crystallized sample cast at 860ºC, the extent of crystallization was also questioned, especially after observing the remaining glass mass in the flowerpot used for its casting. There, the existence of both crystalline and glassy phases is evident (Figure 2.10). Therefore, an X-Ray diffraction (XRD) test was conducted, employing a Bruker D8 Advance diffractometer Bragg-Brentano geometry and a Lynxeye position sensitive detector.

Fig. 2.10 Glass sample from the flowerpot used during the 860ºC casting experiment, showing the formation of crystals.

Table 2.4: Results of the XRD analyses for samples cast at 950 and 860ºC.The samples are taken from the top surface of the components and not from the remaining glass in the flowerpots.

Spruce pine glass transparent clear and blue						
Sample		Firing	Transparency	Crystalline Phases	Compound	Percentage
1		A) Top temperature: 950°C, Quench ramp: 120°C/hr	Transparent	No	-	0
2a		B) Top temperature: 860°C, Quench ramp: 120°C/hr	Tranparent with opaque zones	Sodium Calcium Silicate (Devitrite)	$Na_2Ca_3Si_6O_{16}$	≈ 3%
2b		B) Top temperature: 860°C, Quench ramp: 120°C/hr	Opaque	Sodium Calcium Silicate (Devitrite)	$Na_2Ca_3Si_6O_{16}$	≈ 10%

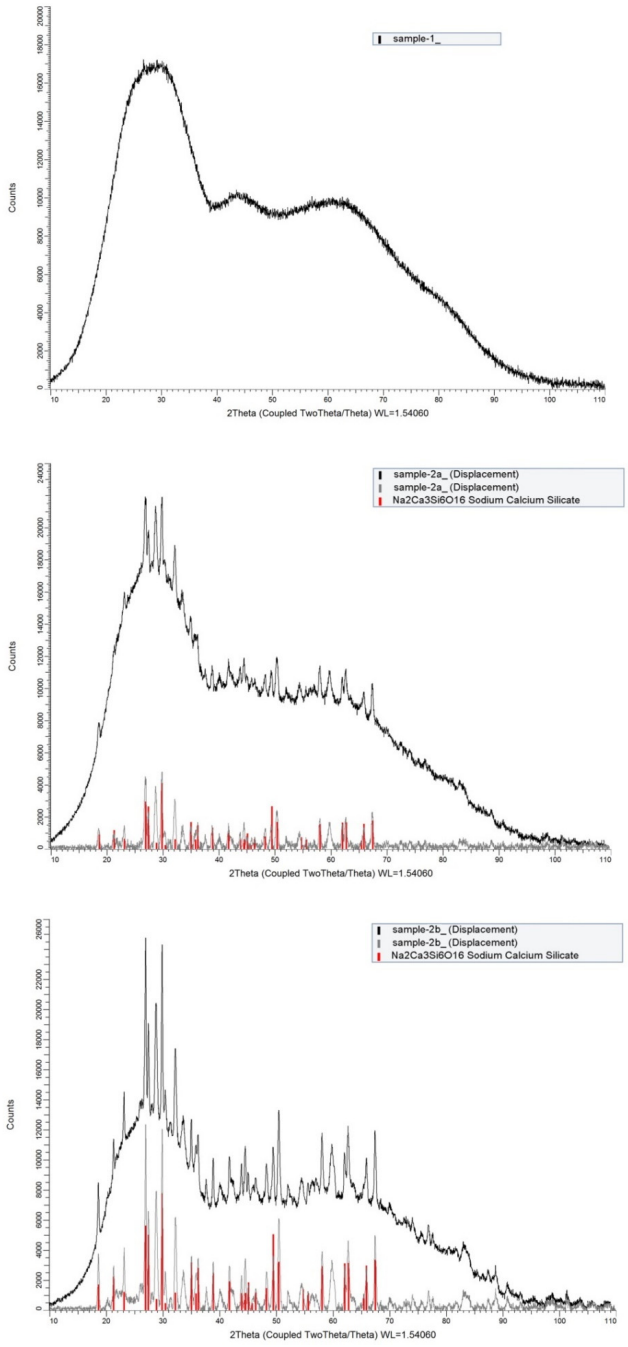

Fig. 2.11 The XRD graph shows the measured patterns in black, after background subtraction. The coloured bars give the peak positions and intensities of the possibly present identified phases, using the ICDD pdf4 database. All samples are amorphous but some have a small fraction of crystalline phases.

The XRD analyses identified the presence of crystalline phases in the sample cast at 860ºC (Table 2.4, Figure 2.11). Specifically, the sodium calcium silicate component $Na_2O.3CaO.6SiO_2$ was found, also known as devitrite. Devitrite is a common crystallization product of soda lime silica glasses (Clark-Monks et al., 1980). Interestingly enough, although the sample appeared as fully crystallized (the exterior surface is completely opaque and clusters of crystal patterns are visible), not more than 10% of its structure was crystalline. The sample taken from the 950ºC specimen, was entirely amorphous. Further experiments need to be conducted to determine how the crystalline percentage can be controlled and what are the effects of these percentages on the structural strength of the components.

- Soda lime silica/ float (window glass, waste glass from furnace clean-up):

The float glass samples present a bit higher weight percentages of SiO_2 74.21-74.56 and Na_2O 12.44-13.32, and lower CaO percentage of 8.91-10.03 in comparison to the automated-blown glass. Magnesium Oxide (MgO) levels are also higher by 1-1.5% wt%. The XRF analysis was conducted at only one surface of the samples which is assumed to be the top surface since no contamination by the tin bed was observed. The glass would be very viscous at 860°C, flowing very slowly. Full crystallization occurred by mechanical quenching at the extra clear sample (PPG Starphire, Figure 2.12a). These glasses could be cast homogeneously at 1120°C (Figure 2.13) and 1200°C and presented only surface crystallization with abrupt cooling (Figure 2.12b, c). Here the difference in the crystallization pattern between the clear and the extra clear float samples should be mentioned. The clear sample presented a subtle translucent finishing at the top surface and a couple of local areas of mild crystal formations. The extra clear (PPG Starphire) glass however, showed a more intense crystallization pattern at the top surface, with visible crystal clusters.

It is not clear- when comparing the two glass compositions- why the extra clear sample is more prone to crystallization, but this could also be related to a possible contamination of the top surface from the tin bath. An XRF analysis of the cast sample should be conducted to further investigate this. To better define the extra clear glass, a comprehensive glass thermal analysis (DSC) was performed. The test showed a stable glass, but with a crystallization peak at around 740°C (Figure 2.14). The glass transition temperature was found at the region of 570°C. With proper cooling- fast enough to avoid the crystallization at the above mentioned peak- this glass can result into very clear and transparent castings.

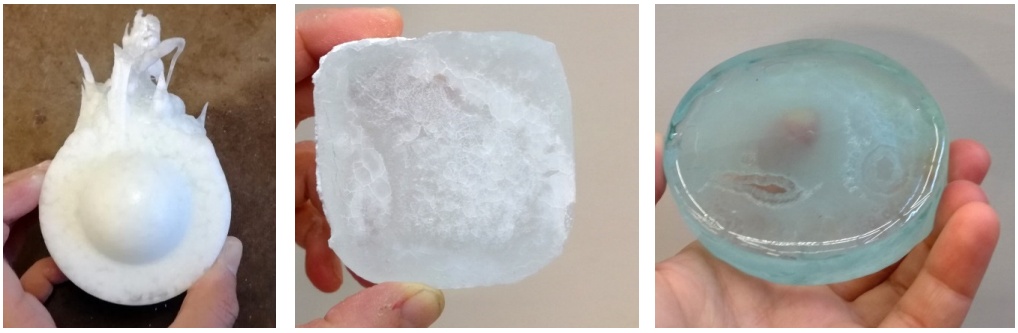

(a) (b) (c)

Fig. 2.12 (a) PPG Starphire kiln-cast at 860°C and mechanically quenched, (b) PPG Starphire sample kiln-cast at 1200°C with top surface crystallization, (c) PPG clear float sample kiln-cast at 1200°C.

Fig. 2.13 PPG furnace waste aquamarine cast at 1120ºC (left) and at 860ºC (middle). PPG Starphire cast at 1120 ºC (right).

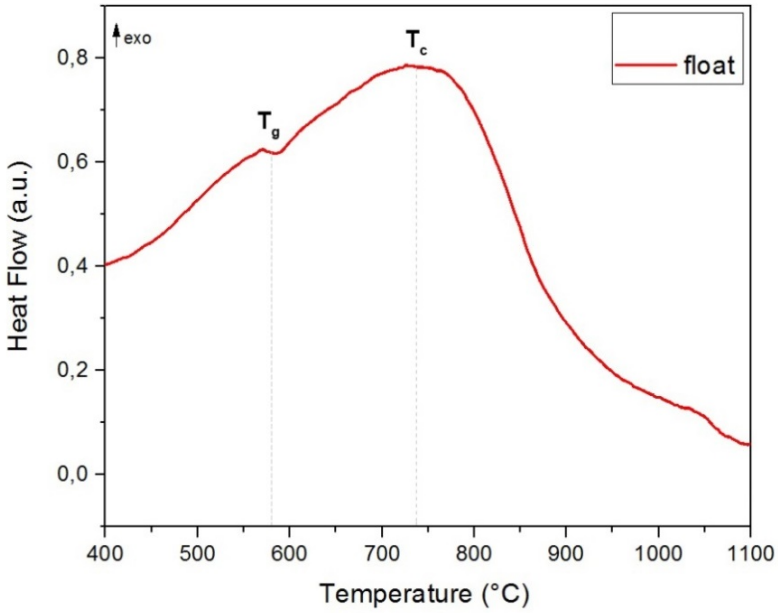

Fig. 2.14 DSC analysis pointing out the glass transition temperature and crystallization peak temperature of PPG Starphire.

Regarding the waste from the float production furnace clean-up, this refers to glass that may be located at the bottom of the furnace for years. The glass slowly decays the refractory materials at the base and absorbs part of their elements in its composition. The resulting glass- although in rough lines similar in composition to the original soda lime silica one, can be quite unpredictable in its exact composition and therefore in its casting behavior. For example, the "PPG light green waste glass" was a very viscous glass (could not flow at 860°C) but was also extremely resistant to crystallization (Figure 2.15a). The increased viscosity can be explained by the high content of alumina (8.8 wt%). According to Zschimmer (2013), although alumina reduces the melting point of soda lime silica glasses when introduced in small amounts, in weight percentages of more than 7% it has the opposite effect. The increased alumina content in combination with the relatively low percentage of lime (5.94 wt%) is what makes this glass so resistant to crystallization. It is also interesting to point out the content of 2.98 wt% of zirconia (ZrO_2) in combination with traces of hafnia (HfO_2). Zirconia is a refractory material found as paving on the furnace bottom (Clark-Monks et al. 1980), especially in cases where very corrosive glasses are melted (Bray et al. 2001). Moreover, Alumina-Zirconia-Silica (AZS) refractories are often used by the glass industry in favour of high-alumina refractories, which tend to more easily corrode and release alumina in the molten glass (Bray et al. 2001). The usage of such refractory products can explain the high content of this glass in alumina and zirconia. Zirconium minerals contain hafnium, in a range of 1.5- 2.5%Hf/Zr+Hf or more (Nielsen 2000), justifying the traces of hafnia

in this glass. Karell et al. (2007) mention that zirconia increases the viscosity of the melt- as observed- but is also used as a substitute to PbO in lead-free crystal glasses, as it increases the refractive index of the glass and thus the light dispersion. The later information can be linked with the high optical quality of the cast sample.

The “PPG furnace waste aquamarine” sample did not exhibit serious contamination from the refractory materials and had a composition very close to that of standard float glass (Figure 2.15b). At 860°C the sample was viscous but could only flow slowly. By inducing mechanical cooling, partial crystallization occurred, with some glassy amorphous regions still preserved within its mass. The same glass could be cast homogeneously at 1120 and 1200°C and presented minor surface crystallization as did sample “PPG clear”. Despite the unpredictable character of this type of glass waste, interesting colours and patterns can emerge from the casting of these- enriched through their prolonged contact with the furnace- glasses.

(a)

(b)

Fig. 2.15 Melting experiments with PPG furnace waste glass. (a) Green glass before (left) and after (right) casting at 860°C. (b) Aquamarine glass cast at 860°C (left) and 1200°C (right).

- Soda potassium lime silica (optical lenses, tableware):

Potassium oxide (K_2O) is often added in soda lime silica systems to achieve extra white clear glass (Zschimmer 2013). K_2O lowers the melting point of the glass yet increases the thermal expansion coefficient. Such alkali-lime silica systems containing considerable amounts of soda and potassium oxide and reduced amounts of lime are preferred for hand- pressing, since these glasses are soft and easy to adapt to the shape of the steel mould while still viscous (Rosenhain 1908). In this category, the optical glass B270 by Schott is used as a reference, since prior experimentation in the lab proved its good optical qualities and workability at 950°C (Bristogianni et al. 2016, 2017). A complete replacement of soda by potassium oxide is found in the pressed historical Bohemian crystal artifacts (Rosenhain 1908). Contemporary Czech (or formerly Czechoslovakian) glass pressed objects however- like the one tested in the scope of this research, may contain considerably lower percentages of K_2O, and more soda and silica. The glass obtained after firing at 950°C was transparent and extra clear, yet presented intense creasing at the top surface (Figure 2.16). Possibly, a small increase in temperature would result in a better quality casting.

Fig.2.16 Czech glass cast at 950°C. Post-processing is required to remove the shrinkage of the top surface and reveal the actual transparent glass.

- Lead crystal (tableware):

Lead silica glass was a glass type commonly used for high quality table and ornamental ware before the use of lead (II) oxide (PbO) was restricted due to its toxicity. This composition was preferred by the manufacturers because of the high refractiveness that the PbO would attribute to the glass, adding brilliancy to the glass artifacts (Rosenhain 1908). Shelby (2005) explains that due to the relatively weakness of the Pb-O bonds caused by the low field strength of the large Pb^{2+} ions, the lead-silicate network can be easily disrupted. This justifies the low glass transformation temperature of this glasses. As these glasses are relatively soft, they are selected by manufacturers, when complicated manipulations during production are required (Rosenhain 1908). Lead glasses also have X-ray protective properties, which increase with the increase of lead content, and are independent from the radiation quality (Singer 1936). Yet, PbO lowers

the Young modulus and the hardness of the glass and significantly increases the density (Zschimmer 2013), factors that should be seriously considered when evaluating the use of such glasses for structural applications.

In this category, Schott LF5 (≈36 wt% PbO) and Gaffer G210 (≈44 wt% PbO) lead crystal are used as a reference in the XRF analyses, as previously conducted castings at 860°C were successful, obtaining extra clear glass without crystallization upon mechanical cooling. In this study, melting experiments were conducted using a pressed crystal bowl of lower lead content (≈24 wt%), which is a typical percentage for such tableware. The glass was successfully cast at 950°C to a clear glass without crystallization (upon abrupt quenching). At this temperature, the sample is expected to have a much lower viscosity in comparison to soda lime silica glass. Yet it is interesting to mention that patterns from the initial design of the bowl were preserved at the bottom of the sample in combination with creasing at the top surface (Figure 2.17). More experiments are required to determine the flowability of this glass at this temperature, but nonetheless this glass can result in very transparent castings.

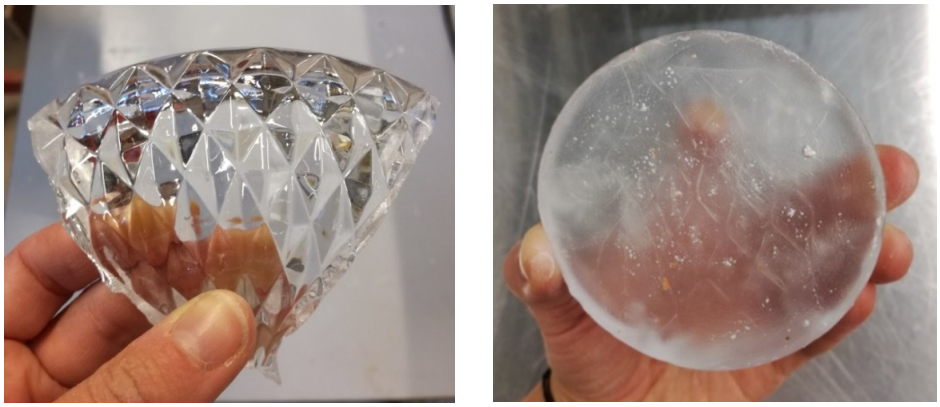

a) b)

Fig. 2.17 Pressed crystal glass before (a) and after casting at 950°C (b). The pattern of the glass remained as a trace at the bottom surface of the sample. Upon post-processing, the glass will be transparent.

- Lead-free crystal (CRT screen/panel):

Due to the health and environmental concerns linked with the toxicity of lead and other heavy metals, various protocols have been issued around the world with the aim to reduce its use. Regarding glass manufacturers, they would chose PbO either to increase the refractive index adding brilliance to the glass, or to provide radiation protection in nuclear plants, hospitals, TV-tubes etc. Currently, lead is replaced with barium, strontium and zirconium, although some of the alternative elements (barium in particular) can be quite toxic themselves, only less than lead (Scoullos et al. 2001). The resulting glasses present good optical quality, lower density than lead crystal, and x-ray

shielding capacity which is however reduced and dependent on the X-ray quality (Singer 1936).

In this section, the casting of the panel of a colour display Cathode Ray Tube (CRT) is attempted. CRT tubes were used in TV and computer screens before the emergence and dominance of Liquid-Crystal Display (LCD) technology. Although currently scarcely in use, CRT glass waste constitutes an accountable percentage of the municipal waste in the European Union (Hreglich et al. 2001; Bernando et al. 2005). Since CRTs are not in production anymore, the route of their recycling into the same product is closed, leaving a question mark on how and where this glass can be used (Edgar et al. 2008). Nonetheless, the glass formulation for the CRTs is of fine quality, employing- among others- expensive barium (Ba) and strontium (Sr) oxides (Compton 2003; Bernando et al. 2005). Specifically, a typical CRT tube consists of three parts: the faceplate (panel), funnel, and neck tubing. The panel is a lead-free barium –strontium glass that protects the viewers from the harmful X-rays (Compton 2003).

A sample of a CRT panel was successfully cast at 950°C, resulting in a clear, homogeneous glass of grey hue that did not crystallize upon abrupt quenching (Figure 2.18). Indeed, this glass composition, rich in Ba and Sr, is expected to be very resistant against crystallization (Kosmal et al. 2017). Of particular interest is however the white dotted pattern that was observed at the sample's top surface, as well as at the top surface of samples cast at higher temperatures (Figure 2.19). The white substance- linked to surface crystallization was easily removed by submerging the sample into water.

(a) (b) (c)

Fig. 2.18 a) CRT panel as retrieved from a computer screen, b) Top surface crystallization of the sample cast at 950°C, c) The sample resulted into a transparent grey glass after being post-processed.

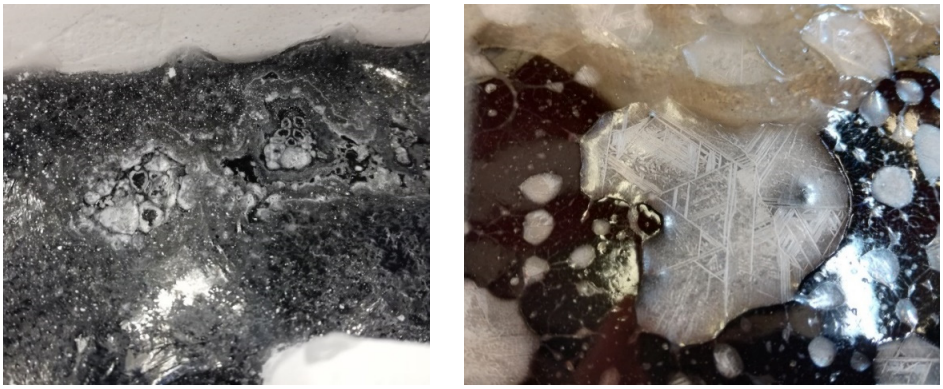

(a) (b)

Fig. 2.19 (a) Surface crystallization on CRT panel glass, kiln-cast at 1120ºC. (b) Surface crystallization pattern on CRT panel glass, kiln-cast at 970ºC.

A DSC analysis was conducted employing a STA 449 F3 Jupiter® apparatus. The test showed a stable glass with a shallow crystallization peak at around 700°C (Figure 2.20). Its glass transition temperature was found at the region of 550°C-580°C. The stability of the glass and its high visual resulting quality prove the potential of this glass for casting glass building components.

The crystal traces on the top surface of the CRT sample kiln-cast at 970°C were isolated and XRF and XRD analyses were conducted (Table 2.5, Figure 2.21). The XRF analysis showed a prevalence of sulphur, followed by alkali. The top surface crystallization can be therefore linked with the precipitation of these compounds during casting, in combination with the temperature occurring around the top surface. This crystallization is mainly considered as a flaw of the kiln-casting technique and is not expected in the melt-quenching casting process that takes place in atmospheric conditions. The XRD analysis showed four different crystalline phases, with barium sulfate and the aphthitalite having the sharpest peaks. Aphthitalite, like other K-salts, is water soluble, explaining the easy removal of the crystallization skin from the sample, when immersed in water.

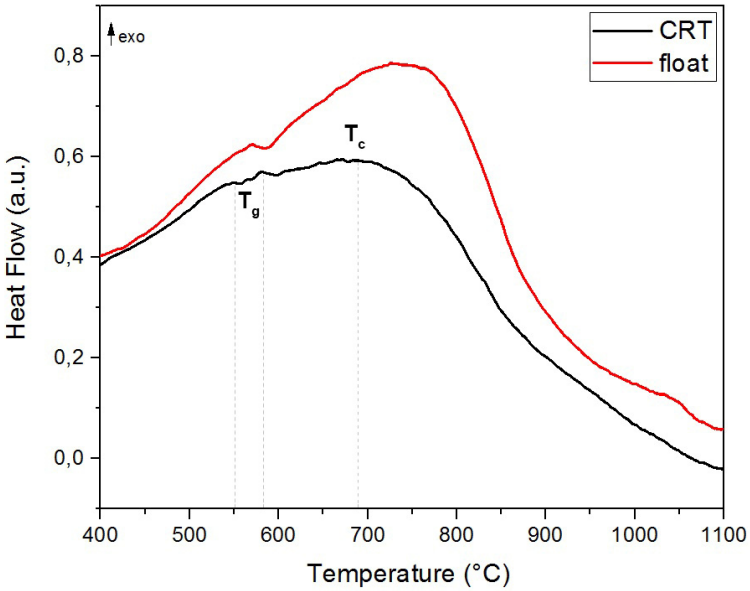

Fig. 2.20 DSC analysis pointing out the glass transition temperature and crystallization peak temperature of the CRT sample. The temperature to heat flow curve of PPG Starphire float glass is included in the diagram as a point of reference.

Table 2.5: XRF analysis of surface crystallization appearing on CRT panel glass sample, kiln-cast at 970ºC (left). The XRF values were normalised to 100%. XRD analysis of the same sample (right).

Surface crystallization CRT panel glass	
Compound name	Content (wt%)
S	52.897
Na_2O	20.051
K_2O	17.43
BaO	4.832
SrO	4.162
SiO_2	0.177
Cl	0.146
CaO	0.11
MgO	0.067
Al_2O_3	0.052
Fe_2O_3	0.044
P_2O_5	0.032

CRT panel glass, surface crystallization		
Firing set-up	Crystalline Phases	Compound
Top temperature: 970°C, Quench ramp: 160°C/hr	Barium sulfate(IV) sulfate(VI)	$Ba(SO_3)_{0.3}(SO_4)_{0.7}$
	Aphthitalite	$KNa(SO_4)$
	Disodium sulfate(VI)	$Na_2(SO_4)$
	Kalistrontite	$K_2Sr(SO_4)_2$

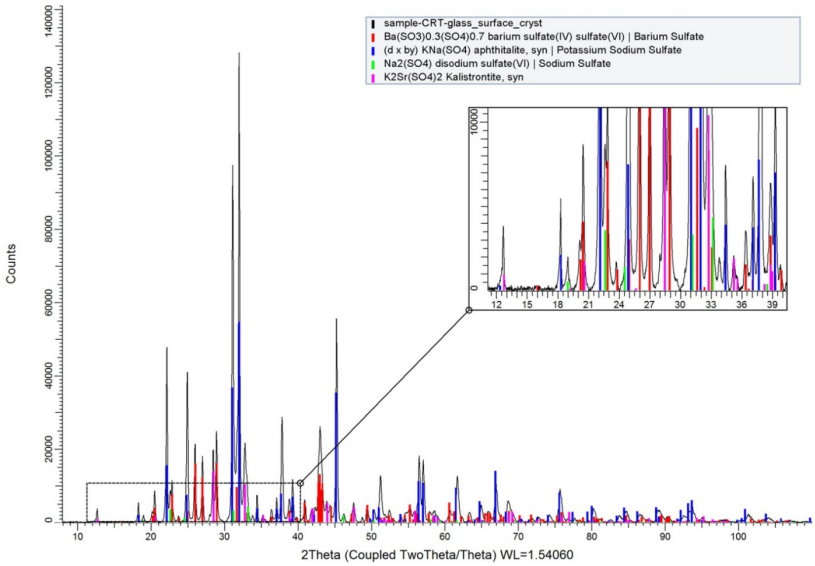

Fig. 2.21 The XRD graph shows the measured patterns in black, after background subtraction. The coloured bars give the peak positions and intensities of the possibly present identified phases, using the ICDD pdf4 database.

- Borosilicate (laboratory tubes):

Borosilicate glass can be attractive for structural applications at demanding environmental conditions, due to its good optical properties and its high thermal and chemical durability (Schott 2014b). It is commonly found in thermal shock resistant cookware and laboratory equipment. Its higher working temperature in comparison to that of soda lime silica adds implications to its processing. Guidelines regarding recycling commonly advise not to discard borosilicate objects together with container glass. Unless chemically contaminated and thus hazardous, this good quality glass often ends up in landfills. Investigations for its downcycling into micro-filler for concrete (Korjakins et al. 2012), glass foams (Chinnam et al. 2014) and other ceramic material applications have been conducted.

A piece of DURAN® laboratory glass produced by Schott was re-cast at 1200°C and resulted into a clear homogeneous glass after being abruptly cooled (Figure 2.22). The top surface was completely flat and showed some local crystallization. DURAN® extruded solid rods by Schott were also successfully re-cast at 1120°C, using Crystalcast moulds within a heat-resistant concrete case (Figure 2.23). Despite the minimum surface crystallization appearing on this sample as well, the result was transparent and contained a minimum amount of bubbles.

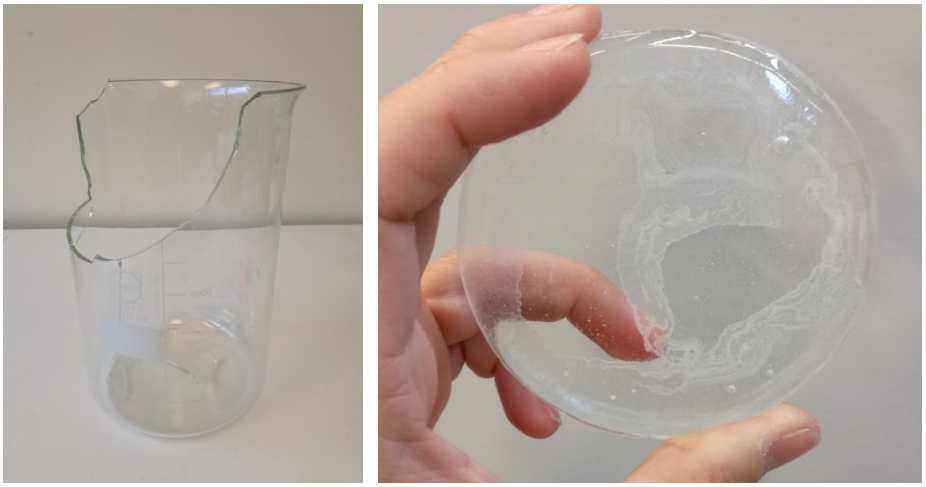

(a) (b)

Fig. 2.22 (a), (b) Borosilicate laboratory tube before and after casting at 1200°C.

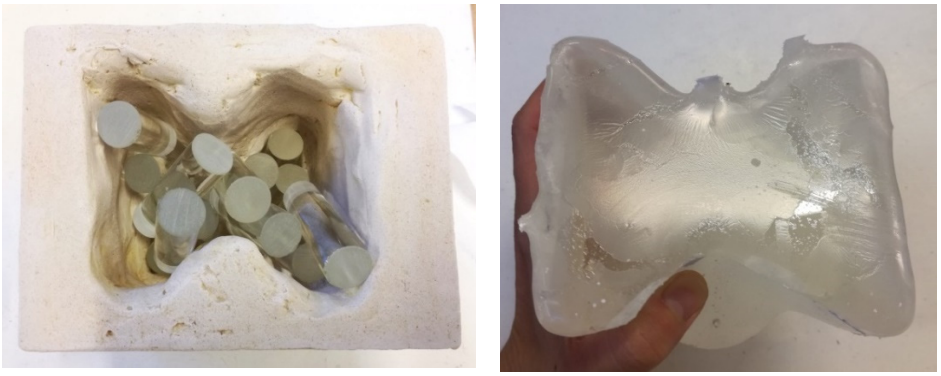

Fig. 2.23 Borosilicate extruded rods successfully re-cast at 1120ºC.

- Alkali-aluminosilicate (mobile phone screen):

Alkali-aluminosilicate glasses are characterized by high glass transition temperatures and excellent mechanical properties such as increased hardness, and scratch and sharp contact damage resistance (Corning 2017; Schott 2014b). Their high alkali content (>10%) enables the ion exchange with bigger alkali ions (ex. potassium bath) that results in a considerably improved surface compressive strength (Schott 2014b). This glass can be drawn via an automated process into very thin sheets of glass (0.4-2mm) that find applications in the screens of smartphones, laptops, tablets and other similar devices (Corning 2015). Due to its outstanding mechanical properties and the fact that touchscreens of that kind are an increasing upcoming source of glass waste, the recycling

of alkali-aluminosilicate glass into building components becomes interesting. Yet, their extremely high working temperatures create challenges for hot-pouring and kiln-casting.

An initial test was conducted by melting a mobile phone screen glass in a high-alumina crucible. At 1500°C the sample still presented a very high viscosity, but some glass drops managed to flow and resulted in a glass of high air-bubble content (Figure 2.24d). The results of the kiln-casting test (Figure 2.24a) at 1250°C were quite unexpected as the glass partially corroded the silica-plaster mould and formed- probably as a reaction to the mould- a three-dimensional sponge structure of opaque white colour (Figure 2.24b). Further testing is required to understand the reasons behind this foam formation. On the contrary, the sample kiln-cast at 970°C successfully formed a glass, although of high air-bubble content (Figure 2.24c). Despite the air-bubbles, the formation of this glass at lower than 1000°C temperatures is very promising.

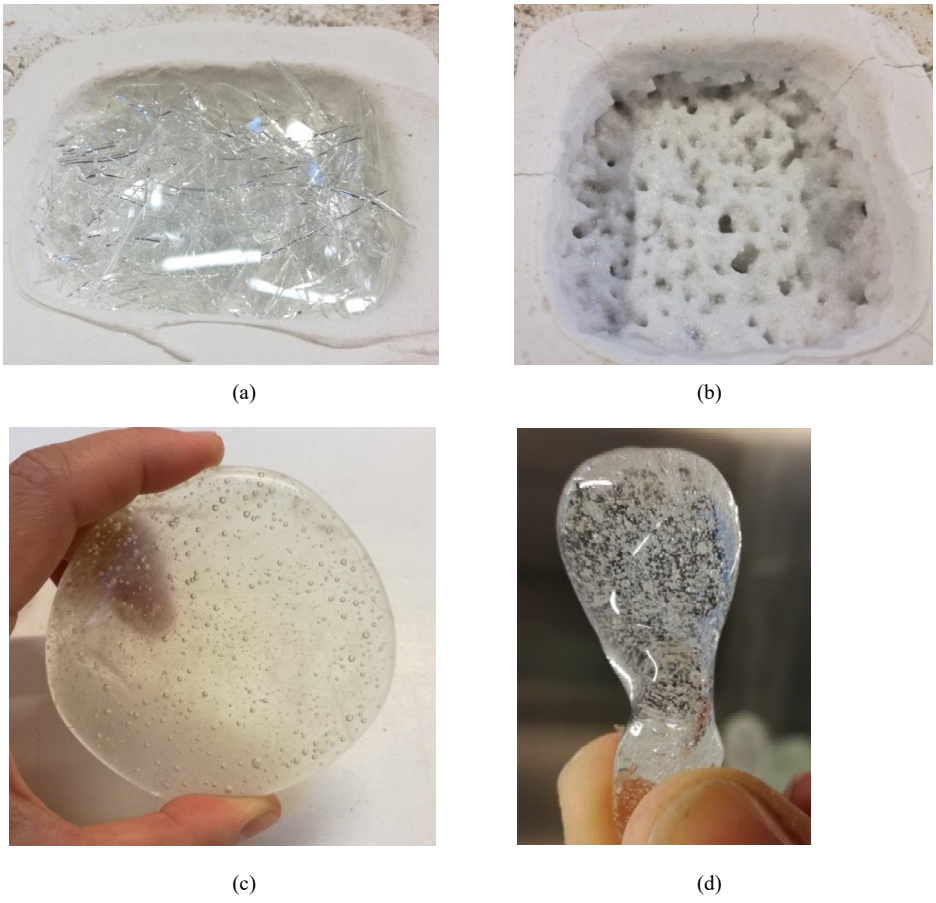

Fig. 2.24 (a), (b) Alkali-aluminosilicate glass retrieved from a mobile phone screen before and after firing at 1250°C, (c) Same type of glass, kiln cast at 970°C. (d) Same glass type melted at 1500°C in a high-alumina crucible and poured into a steel mould.

2.4 Conclusions and further research

The results of this research highlight the vast potential for recycling different types of discarded glass into cast glass building components. Products that are currently almost entirely excluded from the glass-to-glass recycling loop such as CRT panels or crystal tableware- both containing a considerable percentage of heavy metals- proved to be an excellent source of glass that can be kiln-cast at temperatures between 900°C-1000°C. Soda lime silica float, mouth-blown and container glasses, in comparison, needed higher working temperatures (≈1200°C) and faster cooling rates to homogenize into transparent glass samples. Also, glasses from the same family and of similar colours are considered compatible for cast-recycling. The casting of glasses of the above family at temperatures below 1000°C combined with a slow cooling, showed an aesthetically and structurally interesting alternative route, that of glass ceramics. In this case, more investigation is required in order to control the desired percentage of crystalline phases within the material. The recycling of borosilicate laboratory glassware can result into very clear glass, and is worth considering despite of the higher than soda lime silica required working temperatures. More investigation is required for the successful kiln-casting of aluminosilicate glass. Initially, the difficulty to flow even at 1500°C renders this glass unsustainable for recycling through casting. Yet, the ability to form it at 970°C, even with a high content of gas-bubbles, seems promising and requires further testing.

Fig. 2.25 The fundamental differences between various types of glass regarding viscosity, thermal expansion and susceptibility to crystallization, introduce challenges to their mixing. Further research should be conducted to overcome the posed obstacles.

Further research is suggested on the mixing of different glass recipes (Figure 2.25) with the aim of simplifying the initial, meticulous stage of segregation of the cullet in fewer glass categories. Towards this step, a method should be developed for controlling the quality of the segregated cullet and thus the quality of the final product in terms of strength and homogeneity. Future work will be conducted on the mechanical testing of the resulting recycled glass components to define their strength and validate their suitability as building components. Research should also address the recycling of glass contaminated by coatings, laminates, and adhesives, which nowadays constitute a considerable amount of our glass waste. The above steps are necessary for diverting the path of waste glass from landfill to safe and beautiful structures (Figure 2.26).

Fig. 2.26 Successful casting of pieces of (from left to right) float glass, bottle, laboratory tube, computer screen panel, lens, and mouth blown glass, demonstrating the numerous possibilities that arise in creating unique building components.

References

Abrisa Technologies: Specialty Glass Materials Products & Specifications (2014)

ASTM International: Standards & Publications. www.astm.org/products-services/standards-and-publications.html (2022). Accessed 22-08-2022

Bernando, E., Andreola, F., Barbieri, L. and Lancellotti, I.: Sintered Glass–Ceramics and Glass–Ceramic Matrix Composites from CRT Panel Glass. Journal of the American Ceramic Society 88(7) (2005)

Bray, C.: Dictionary of Glass: Materials and Techniques, Second ed. A&C Black, London (2001)

Bristogianni, T., Oikonomopoulou, F., Veer, F.A., Nijsse, R.: Design and production of a structural cast glass element for a transparent dome. In: Zingoni, A. (ed.) Insights and Innovations in Structural Engineering, Mechanics and Computation : Proceedings of the 6th International Conference on Structural Engineering, Mechanics and Computation, SEMC, Cape Town, pp. 1662-1667. CRC Press (2016)

Bristogianni, T., Oikonomopoulou, F., Veer, F.A., Snijder, A.H., and Nijsse, R.: Production and Testing of Kiln-cast Glass Components for an Interlocking, Dry-assembled Transparent Bridge. In: Glass Performance Days, Glaston Finland Oy, Tampere (2017)

Brockway, M.C.: Fluid Bed Chemical Strengthening of Glass Objects. USA Patent 4290793 (1981)

Burch, O.G. and Babcock, C. L.: Effect of Glass Color on Setting Rates in Manufacture of Glass Bottles Journal of the American Ceramic Society 21(10) (1938)

Campbell, D.E. and Hagy, H.E.: Glass and Glass-Ceramics. In: Lynch, C.T. (ed.) CRC Handbook of Materials Science, Volume II: Metals, Composites and Refractory Materials. CRC Press, Florida (1990)

Chinnam, R.K., Molinaro, S., Bernardo, E. and Boccaccini, A.R.: Borosilicate Glass Foams from Glass Packaging Residues. In: Dogan, F., Tritt, T.M., Sekino, T., Katoh, Y., Pyzik, A.J., Belharouak, I., Boccaccini, A.R. and Marra, J. (ed.) Ceramics for Environmental and Energy Applications II. John Wiley & Sons, Inc., New Jersey (2014)

Clark-Monks, and Parker, J.M.: Stones and Cord in Glass. Society of Glass Technology, Sheffield (1980)

Compton, K.: Image Performance in CRT Displays. Spie Press Book (2003)

Cormier, L.: Chapter 1: The classical nucleation theory. In: Neuville, D.R., Cormier, L., Caurant, D., Montagne, L.: From Glass to Crystal: Nucleation, Growth and Phase Separation, from Research to Applications. EDP Sciences, (2017)
CORNING: Corning® Gorilla® Glass 3 (2015)
CORNING: Corning® Gorilla® Glass 5 (2017)
Doremus, R.H.: Glass Science, 2nd ed. Wiley-Interscience (1994)
Dyer, T.D.: Chapter 14 - Glass Recycling. In: Handbook of Recycling. Elsevier, Boston (2014)
Edgar, R., Holcroft, C., Pudner, M. and Hardcastle, G.: UK Glass Manufacture. A Mass Balance Study. CTS (2008)
ELVIROS: Recycled Glass Market Study & Standards Review – 2004 Update (2004)
ESK: EKamold® Boron Nitride Sprays Release Agent and Protective Coating (2013)
Eurostat: Recycling rates for packaging waste (2016)
Gold Star: Gold Star Powders. www.siamcasting.com/download/SCP.pdf.
Heimerl, W.: Chemical Resistance and Corrosion, and Ion Release. In: Bach, H., and Krause, D. (ed.) Analysis of the Composition and Structure of Glass and Glass Ceramics. Springer-Verlag Berlin Heidelberg, New York (1999)
Hestin, M., de Veron, S., Burgos, S.: Economic study on recycling of building glass in Europe. https://glassforeurope.com/wp-content/uploads/2018/04/Economic-study-on-recycling-of-building-glass-in-Europe-Deloitte.pdf. Deloitte, (2016)
Holscher, H.H., Rough, R. R. and Plummer, J. H.: Experimental Studies of the Temperature Gradients in Glasses of Various Colors. Journal of the American Ceramic Society 26(12) (1943)
Hreglich, S., Falcone, R. and Vallotto, M.: The Recycling of End of Life Panel Glass from TV Sets in Glass Fibres and Ceramic Products. In: Recycling and Reuse of Glass Cullet. Thomas Telford Ltd., London (2001)
Karell, R., Kraxner, J., Chroměíková, M. and Liška, M.: Properties of selected zirconia containing silicate glasses II. Ceramics − Silikáty 51 (2007)
Kitaĭgorodskiĭ, I.I. and Solomin, N.W.: Rate of Setting of Glass During Working. Society of Glass Technology Journal 18, 323-335 (1934)
KNIGHT OPTICAL: Technical / Sheet Glasses TSG-B270. http://www.knightoptical.com/technical-library/sheet-and-technical-glasses/.
Korjakins, A., Shakhmenko, G. and Bumanis, G.: Utilisation of Borosilicate Glass Waste as a Micro-Filler for Concrete. Journal of Civil Engineering and Architecture 6 (2012)
Kosmal, M., Reben, M., Pichniarczyk, P., Ziąbka, M. and Skrzypek, S.J.: Surface crystallization and phase evolution of BaO–SrO–TiO2–SiO2–Al2O3-based glass ceramics. Journal of Thermal Analysis and Calorimetry 130 (2017)
Martlew, D.: Viscosity of Molten Glasses. In: Pye, D., Joseph, I. and Montenero, A. (ed.) Properties of Glass-Forming Melts. CRC Press, Taylor & Francis Group, (2005)
Mear, F., Yot, P., Cambon, M. and Ribes, M.: The characterization of waste cathode-ray tube glass. Waste Management 26 (2006)
Müller, R., Zanotto, E.D. and Fokin, V.M.: Surface crystallization of silicate glasses: nucleation sites and kinetics. Journal of Non-Crystalline Solids 274, 208-231 (2000)
Nielsen, R.: Zirconium and Zirconium Compounds. In: Ullmann's Encyclopedia of Industrial Chemistry. Wiley-VCH Verlag GmbH & Co. KGaA, (2000)
Oikonomopoulou, F., Bristogianni, T., Veer, F., & Nijsse, R.: The construction of the Crystal Houses façade: challenges and innovations. Glass Structures & Engineering, 1-22 (2017)
Precision Glass and Optics: PPG-Starphire
Pye, L.D.: Glass-Forming Melts. In: Pye, D., Joseph, I. and Montenero, A. (ed.) Properties of Glass-Forming Melts. CRC Press, Taylor & Francis Group, (2005) Ransom & Randolph: R&R/Dentsply Form
Rosenhain, W.: Glass Manufacture. D. Van Nostrand Company, New York (1908)
SCHOTT: Data Sheet LF5 (2014)
SCHOTT: Technical Glasses, Physical and Technical Properties. Germany, (2014)
SCHOTT: Duran Technical Data (2017)
Scoullos, M., Vonkeman, G.H., Thornton, I., and Makuch, Z.: Mercury – Cadmium - Lead Handbook for Sustainable Heavy Metals Policy and Regulation. Springer Science + Business Media, Dordrecht (2001)
Seward III, T.P. and Varshneya, A.K.: Inorganic Glasses: Commercial Glass Families, Applications, and Manufacturing Methods. In: Harper, C.A. (ed.) Handbook of materials and product design. McGraw-Hill, Inc., USA (2001)
Shelby, J.E.: Introduction to Glass Science and Technology. The Royal Society of Chemistry, Cambridge, UK (2005)
Silva, R.V., Brito, J., Lye, C., and Dhir, R.: The role of glass waste in the production of ceramic-based products and other applications: A review, vol. 167. (2017)
Singer, G.: Absorption of X-rays by Lead Glasses and Lead Barium Glasses. Research of the National Bureau of Standards 16 (1936)
Specialty Glass Products: PPG Starphire Soda Lime Glass. www.sgpinc.com.
Spruce Pine Batch: Cristalica
Vlakglas Recycling Nederland: Vlakglas Recycling Nederland Jaarverslag 2020. Netherlands, (2020)
ZRCI: ZRCI SDS-0018 (2017)
Zschimmer, E.: Chemical Technology of Glass. Society of Glass Technology, Sheffield, UK (2013)

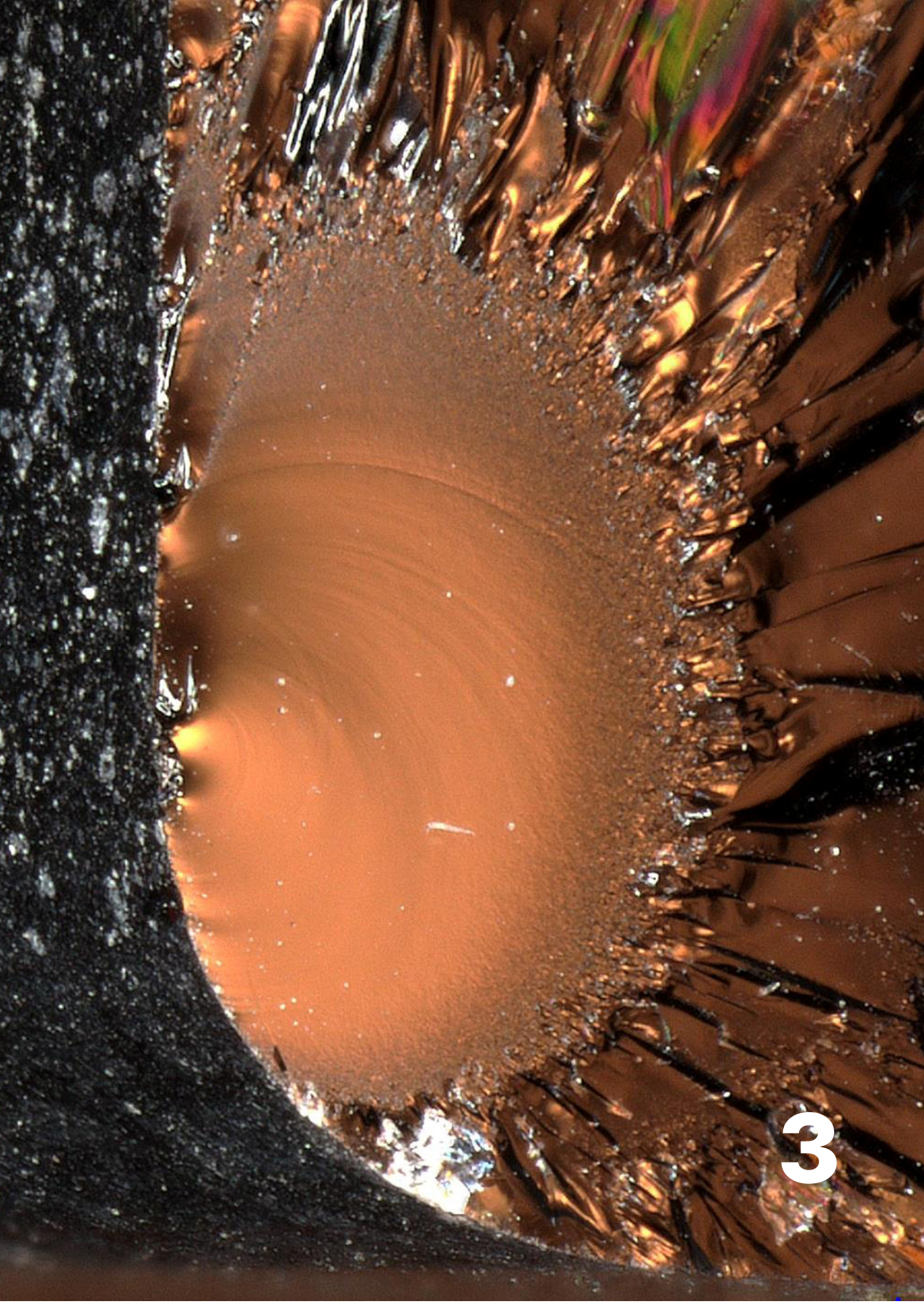
3

Previous page: Fracture mirror observed at a recycled, tinted float glass specimen (kiln-cast at 1120 °C) subjected to 4-point bending.

Chapter 3: Flexural strength and stiffness of cast glass

Based on

Bristogianni, T., Oikonomopoulou, F., Yu, R., Veer, F.A., Nijsse, R.: Investigating the flexural strength of recycled cast glass. Glass Structures & Engineering 5(3), 445-487 (2020). doi:10.1007/s40940-020-00138-2

The aforementioned paper received the "Best Paper 2020" award by the Editors in Chief of Glass Structure & Engineering.

Aim and context

Documentation of defects and meso-level structures in cast glass specimens and correlation to the casting parameters. Investigation by mechanical testing of how the resulting defects affect the flexural strength and stiffness of cast glass. Chapter 3 builds on the knowledge acquired from Chapter 2 for the selection of chemical compositions, cullet characteristics, and firing schedules to be used for the preparation of the flexure tests specimens.

Abstract

Currently, tons of high quality commercial glass are down-cycled or landfilled due to contaminants that prevent closed-loop recycling. Yet, this glass is potentially a valuable resource for casting robust and aesthetically unique building components. Exploring the potential of this idea, different types of non-recyclable silicate glasses are kiln-cast into 30x30x240mm beams, at relatively low temperatures (820ºC -1120ºC). The defects occurring in the glass specimens due to cullet contamination and the high viscosity of the glass melt, are documented and correlated to the casting parameters. Then, the kiln-cast specimens and industrially manufactured reference beams are tested in four-point bending, obtaining a flexural strength range of 9-72MPa. The results are analysed according to the role of the chemical composition, level of contamination and followed casting parameters, in determining the flexural strength, the Young's modulus and the prevailing strength-limiting flaw. Chemical compositions of favourable performance are highlighted, so as critical flaws responsible for a dramatic decrease in strength, up to 75%. The defects situated in the glass bulk, however, are tolerated by the glass network and have minor impact on flexural strength and Young's modulus. The prerequisites for good quality recycled cast glass building components are identified and an outline for future research is provided.

Authors' contribution on the relevant published journal article

Bristogianni, T.: Research concept, organization, sample preparation, conduction of experiments, data analysis, writing of the paper. Oikonomopoulou, F.: Research concept and discussion, paper review. Yu, R.: sample preparation. Veer, F.A.: supervision of research, discussion, paper review. Nijsse, R. : supervision of research.

Acknowledgements

I would like to thank the co-authors of the above mentioned paper for their valuable contribution in this chapter. Moreover, I would like to express my gratitude to Giorgos Stamoulis for his significant contribution in preparing the four-point bending experiment and DIC measurements, as well as Kees van Beek for his guidance. I am particularly grateful to George Quinn and James Varner for their valuable input regarding the experimental procedure and the fracture analysis of the results. The feedback received from Bert Sluijs, Mauro Overend, Christian Louter and Karl-Heinz Wolf is highly appreciated. I would also like to thank Ruud Hendrikx for the XRF and XRD analyses, Mariska van der Velden for assisting in the specimen preparation, Sander van Asperen and Wolfgang Gard for providing access to their labs' Keyence digital microscopes, and Henning Katte and Daniel Schreinert (Ilis) for sponsoring the use of StrainScope Flex. I am also very grateful to Cor Wittekoek (Vlakglasrecycling), Danny Timmers (Maltha Glasrecycling Nederland), Marco Zaccaria and François Boland (AGC Belgium), Brian Wittekoek (Coolrec), Bettina Sommer (Royal Leerdam Crystal), and Klaas Roelfsema (Schott), for the glass cullet contribution, which was of key importance for this work. Finally, I would like to thank Erik Muijsenberg (Glass Service) for the "Glass Defects" (Bartuška 2008) book, and Peter de Haan (AGR Delft) for the "Color Atlas of Container Defects" (Aldinger and de Haan 2019) and "Color Atlas of Stones in Glass" (Aldinger and Collins 2016) books, which were very helpful in the process of defect categorization and identification.

3.1 Introduction

The great potential of glass casting technology for the building industry is so far little explored by structural engineers and architects, but are gradually getting discovered after the success of all cast-glass load bearing structures such as the Crystal Houses façade in Amsterdam (Oikonomopoulou et al. 2018c). The 3D-shaping possibilities provided by casting can offer robust glass components of larger cross-sections and a wider variety of forms and colours than currently available by other glass processing methods. Parallel to the recognition of the structural and aesthetical strengths of cast glass components, questions arise regarding their environmental impact and life-cycle. The use of -currently not recyclable- disposed glass as a raw source for glass casting at lower temperatures, is a promising idea that addresses both the pressing problem of glass waste, and the urgency to lower the carbon footprint of glass building components (Bristogianni et al. 2018, Oikonomopoulou et al. 2018b). To specify the term "currently not recyclable glass", apart from the successful recycling of soda lime silica glass food and beverage

containers, the rest of the discarded -often high quality- commercial glass rarely meets the strict standards of the manufacturers due to contamination from coatings and/or adhesives. The lack of infrastructure for the systematic collection, product disassembly and cullet separation concerning these different types of glass[18], originates from the hesitation of the manufacturers to accept this cullet, and thus limits or prevents its recycling. Therefore, as this glass cannot flow back into the original product system (closed-loop recycling), it gets down-cycled to applications such as aggregate, ceramic-based products, foam insulation, abrasives (Silva et al. 2017), or is disposed of in landfills. As the need of finding alternative routes, markets and end-users for the upcycling of the tons of high-quality discarded glass is imperative, the partial diversion of this waste into the building industry by casting structural glass components is worth exploring.

The above developments reveal a gap in the literature concerning the mechanical properties of cast glass components and the suggestion of a design strength for their structural use. This is linked with the absence of established manufacturing procedures and quality control standards, and thus the great variability in the strength of the cast glass products according to each manufacturer and the corresponding glass composition and casting process applied. The use of waste glass cullet is an added complication to this issue, giving rise to a series of traditional and new types of defects (Bartuška 2008, Bristogianni et al. 2019), which may compromise the strength of the glass product.

This chapter explores the flexural strength of recycled cast glass- a property relevant to the engineering practice. The aim is to give insight into the effect of the casting parameters on the strength, and to assess the plausibility of employing waste glass for the production of safe structural components. Thus, in this work, a variety of commercial glass waste silicates is tested and evaluated for their ability to be kiln-cast into structural components at relatively low temperatures (820^{o}C -1120^{o}C). The occurring defects are documented and correlated with the stage of production during which they are caused. Thereafter, two series of four-point bending experiments are conducted in kiln-cast glass beams of 30x30x240mm dimensions. The results are analysed according to the role of the chemical composition, level of contamination and followed casting parameters, in determining the flexural strength and the origin of fracture. The testing of a limited number of industrially manufactured components serves as a point of reference.

[18] Exceptions apply, at local or national level (e.g. the Saint-Gobain's "Glass Forever" cullet return initiative for post-consumer flat glass recovery and recycling (Saint Gobain) or the energy-saving lamp recycling in the Netherlands by Stichting LightRec and Wecycle (LightRec Nederland 2022)) but are not the norm. Moreover, even if collection and cullet treatment of other than container glass occurs, this does not guarantee the closed-loop recycling of the produced cullet. In the Netherlands, Vlakglas Recycling collects 80% of the construction and demolition glass waste, yet only 7.5% of the collected amount is recycled back to float glass (Vlakglas Recycling Nederland 2020).

3.2 Experimental work

3.2.1 Glass cullet categorization and specimen preparation

This work studies a series of characteristic commercial glasses, used for the production of common glass products such as float glass, glass fibers, cookware and laboratory glassware, cast glass bricks, crystal ware and CRT TV screens[19]. The choice of glasses is made in alignment with the types of waste glass cullet provided by various glass manufacturing and recycling companies, in order to address the recycling of readily available waste glass sources and thus tackle a realistic problem. X-ray fluorescent (XRF) analyses are conducted with a Panalytical Axios Max WDXRF spectrometer to define the chemical composition of the selected glasses. The provided cullet is thoroughly cleaned with isopropanol, and alien material (metal, plastic, cork) is manually removed when possible. The identified contaminants in the given cullet, still present in traces after the cleaning process, are listed in Table 3.1 according to the following categorization:

i. Coatings (soft, hard, mirror, enamel, frit)
ii. Variations in composition of the same glass type (different manufacturer, tints)
iii. External contaminants during sorting: a. Organics (e.g. plastic, textiles), b. Non-glass inorganics (e.g. ceramics, stones, porcelain, glass ceramics), c. Metals, d. Different glass types (e.g. borosilicate, lead glass)

The cullet is then used for kiln-casting the 30x30x240mm glass beams required for the four-point bending tests. This particular beam size is selected as it provides a substantial thickness of cast material so that the influence of the defects in the bulk can be evaluated, while keeping the mass below 1kg, and therefore reducing the annealing time. For each glass cullet, at least 3 samples are produced for statistical purposes[20]. The cullet is positioned inside of disposable silica/plaster investment moulds made from Crystalcast M248[21], in a structured or random manner. The moulds are then placed in a ROHDE ELS 200S or ELS 1000S electric kiln (Figure 3.1) and kiln-cast, meaning that only one kiln is employed for the complete casting process (heating up, forming, annealing and cooling).

[19] Cathode Ray Tube (CRT) screen production has ceased, yet there is still a considerable volume of CRT glass cullet resulting from the separation of disposed screens (Andreola et al. 2005).
[20] In cases where less samples are reported, the cullet available was not sufficient for the production of three samples. These specimens are nonetheless presented in this study to demonstrate the failure mode of the specific type of glass, rather than derive an absolute flexural strength value.
[21] Crystalcast M248 is an investment powder consisting of 73% silica content (cristobalite, quartz), 23% calcium sulphate (gypsum) and 1% organics (Goodwin Refractory Services 2003; Gold Star 2019). The choice of the mould material is related to the kiln-casting technique followed in this work versus the commonly reported casting by melt-quenching. As relatively low forming temperatures are chosen, the corresponding high viscosity of the heated glass does not allow its instant pouring from a melting (platinum or high-alumina) crucible to a preheated (steel or graphite) mould for annealing. Thus, the whole casting process has to take place in one mould that can withstand temperatures up to 1150ºC, does not attach to the glass and does not cause fracture to the specimen during cooling.

Fig. 3.1 Arrangement of the investment moulds inside the ROHDE ELS 1000S kiln.

The glass samples are formed at viscosities between 10^6 - $10^{3.5}$dPa·s and at top temperatures ranging from 820° to 1120°C that are selected according to the chemical composition of each glass. The viscosity (η) range chosen is higher than the 10^4 -$10^{1.5}$dPa·s forming and melting range adopted by the glass industry, taking into account the risk of inhomogeneity of the final product. The approach of glass forming at lower temperatures is chosen on the one hand to reduce the required energy and corresponding CO_2 emissions, and on the other hand to intensify the occurrence of defects and evaluate if their existence is acceptable for a structural glass product. Thus for several samples (e.g. float glass, borosilicate rods), 2-3 different top temperatures are tested, corresponding to viscosity ranges of $10^{5\text{-}6}$dPa·s and $10^{3\text{-}4}$dPa·s, to further study the influence of the defects on the flexural strength. All specimens are kept at top temperature for 10hrs[22], quenched at a -160°C/hr rate down to their annealing point, heat-soaked for 10hrs and cooled down to their strain point with a -4°C/hr ramp, before controllably cooled down to room temperature at a faster rate. This conservative annealing schedule guarantees stress-free specimens, as seen through cross-polarized light.

The specimens are produced at a 40mm component height, and then cut to size with a water-cooled rotary diamond wheel cutter, to remove the top surface that often contains a high amount of flaws (e.g. surface crystallization, bubbles, depletion of alkali in the composition, wrinkling, crazing). Then, the specimens are ground and polished with a Provetro flat grinder and diamond abrasive discs in sequence of 60, 120, 200, 400 and 600[23] grit and their resulting dimensions are

[22] Given the high viscosity at top temperature and the size of the samples, a 10hr dwell is empirically found suitable for the removal of large bubbles (>1mm) and the incorporation of the coatings to the glass network.
[23] The 600 grit finishing is set according to ASTM C1161−13. In addition, Quinn et al. (2005) observe in their study on Machining Cracks in Ground Ceramics that sintered reaction bonded silicon nitride flexural specimens with 600 grit grinding fail due to material flaws rather than machining damage. This observation can be extended to glass specimens.

documented. The inhomogeneities in the glass specimens are observed by naked eye and with the use of a Keyence VHX-5000 or VHX-7000 Digital Microscope. A qualitative assessment of the internal residual stresses in the glass specimens is achieved by using crossed-polarized filters. Lastly, the beams are prepared for the Digital Image Correlation (DIC) measurement by creating a speckle pattern on one of the longitudinal surfaces with elastic white and black spray paints.

The preparation process required for the production of the kiln-cast specimens is described in detail in Table 3.1. Apart from the kiln-cast specimens, the following industrially manufactured specimens are prepared and used as a reference:

- Beams cut out from standard Poesia[24] cast glass bricks, ground and polished to a 30x30x240mm size
- Beams from 8/10mm thick float glass plies, adhesively bonded with Delo Photobond 4468[25], ground and polished to a 30x30x240mm size
- Single 30x240mm float glass panes of a 8/10mm thickness, edges ground and polished

The grinding and polishing procedure followed for the preparation of the above specimens is identical to the one described for the kiln-cast samples. However, the bottom and top surface of the float glass specimens (single and bonded) is kept in its as received condition (optically fine polished) and only the cut edges are processed.

[24] Poesia is the producer of the cast glass bricks for the Crystal Houses façade (Oikonomoulou et al. 2018a).
[25] This UV-curing acrylate is chosen because it forms a strong bond with the glass surfaces that leads to the monolithic behaviour of the glued sample (Oikonomoulou et al. 2018a). Under four-point bending, the bonded glass sample is expected to show cohesive failure in the substrate (glass ply) and not delamination.

Table 3.1 (part a): Specimen preparation, cullet categorization and kiln-casting settings.

Glass type	Specimen description	Source	Composition* (main compounds in wt%)	Cullet contamination**	Cullet size (mm)	Cullet organisation in mould	Forming temperature in ^{o}C (10hr dwell)	Annealing temperature in ^{o}C (10hr dwell)***
Soda Lime Silica (Float Glass)	Fully Tempered float	IFS-SGT	75.4% SiO_2, 12.4% Na_2O, 7.6% CaO, 4% MgO, 0.4% Al_2O_3	Clean	shards ≈30x30x10		1120	560
	Fully Tempered float, fused	IFS-SGT		Clean	shards ≈30x30x10	Same as above	970	560
	Float 10mm, 3 horizontal layers, fused	IFS-SGT		Clean	10x30x240	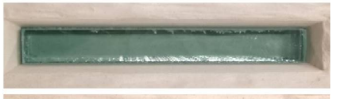	970	560
	Float 10mm, 24 vertical layers, fused	IFS-SGT		Clean	10x30x30		970	560
	Float 10mm, 3 vertical layers, fused	IFS-SGT		Clean	10x30x240	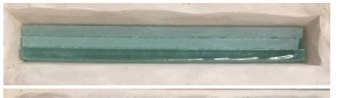	970	560
	Float dark blue	AGC	73.1% SiO_2, 12.8% Na_2O, 8.1% CaO, 4% MgO, 0.9% Al_2O_3, 0.76% Fe_2O_3	Clean	shards thickness ≈3-4, width ≈3-20	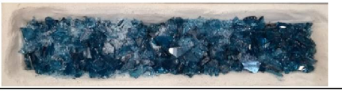	1120	560

*All composition data derived by XRF measurements conducted with a Panalytical Axios Max WD-XRF spectrometer and normalised to 100% by Ruud Hendrikx (TU Delft, 3me), apart from the SiO_2/B_2O_3 ratio in DURAN Schott derived from (Heimerl 1999), the SiO_2/B_2O_3 ratio in Wertheim c-glass adjusted from (Campbell, 1975), the SiO_2/B_2O_3 ratio in Poesia glass derived from personal communication with the company and the characteristic CRT Funnel composition derived from (Mueller 2012).

** The contamination source is organized as:
i. Coatings (soft, hard, mirror, enamel, frit)
ii. Variations in composition of the same glass type (different manufacturer, tints, colour)
iii. External contaminants during sorting, namely: a. Organics (e.g. plastic, textiles), b. Non-glass inorganics (ceramics, stones, porcelain, glass ceramics), c. Metals, d. Different glass types

***All samples have been quenched to the annealing point with a rate of -16C^{o}C/hr

Table 3.1 (part b): Specimen preparation, cullet categorization and kiln-casting settings.

Glass type	Specimen description	Source	Composition* (main compounds in wt%)	Cullet contamination**	Cullet size (mm)	Cullet organisation in mould	Forming temperature in ^{o}C (10hr dwell)	Annealing temperature in ^{o}C (10hr dwell)***
Soda Lime Silica (Float Glass) with contamination	Float combo	Maltha Recycling	Variation of float glass recipes (Tested samples: 71.7-72.8% SiO_2, 12.2-12.5% Na_2O, 8.7-9.3% CaO, 3.5-3.8% MgO, 0.6-2% Fe_2O_3, 0.6-0.9% Al_2O_3)	i) Coatings, ii) Float glass from various manufacturers, tints, iii. b,d) glass ceramics, different glass types	shards thickness ≈6, width ≈20-50		1120	560
	Oven doors	Coolrec	Variation of float glass recipes	i) Ceramic frit, ii) Float glass from various manufacturers, iii.a) Plastic	shards thickness ≈3-4, width ≈3-20	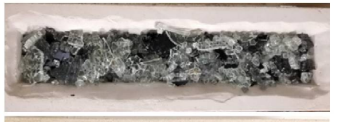	1120	560
	Car windshields	Maltha Recycling	Variation of float glass recipes	i) Coatings, ii) Float glass from various manufacturers, iii. a,b) traces of cardboard, sand, dust, PVB foil	coarse cullet ≈1-5		1120	560
	Float with black enamel, 60 vertical layers	AGC	Standard float glass recipe	i) Black enamel	4x30x30		1120	560
Modified Soda Lime Silica	Poesia standard cast brick	Poesia	72.1% SiO_2, 15.9% Na_2O, 2.5% B_2O_3, 6.1% CaO, 1.9% K_2O, 0.9% Sb_2O_3	Clean	chunks ≈50-100		1070	540
Borosilicate	DURAN tubes	Schott	80% SiO_2, 13% B_2O_3, 3.5% Na_2O, 2.7% Al_2O_3, 0.5% K_2O	Clean	curved shards, thickness ≈6-8, width ≈20-70		1120	560
	DURAN rods x10 vertical, 1120^{o}C	Schott		Clean	radius= 24, height= 50		1120	560
	DURAN rods x10 vertical, 1070^{o}C	Schott		Clean	radius= 24, height= 50	Same as above	1070	560
	DURAN rods x10 vertical, fused 970^{o}C	Schott		Clean	radius= 24, height= 50	Same as above	970	560

Table 3.1 (part c): Specimen preparation, cullet categorization and kiln-casting settings.

Glass type	Specimen description	Source	Composition* (main compounds in wt%)	Cullet contamination**	Cullet size (mm)	Cullet organisation in mould	Forming temperature in °C (10hr dwell)	Annealing temperature in °C (10hr dwell)***
Borosilicate	DURAN rods x2 vertical, fused 970°C	Schott		Clean	radius= 24, length= 240		970	560
	DURAN 24mm rods, honeycomb, fused 970°C	Schott		Clean	radius= 24, width= 30		970	560
	Borosilicate mix	Coolrec	Variation of borosilicate glass recipes, manually sorted	ii) Float glass from various manufacturers, iii. a,c) traces of plastic, cork, metal	thin shards, thickness ≤1, width ≈3-10		1120	560
	Borosilicate mix	Maltha Recycling	Variation of borosilicate glass recipes, mechanically sorted	ii) Float glass from various manufacturers, iii. a,b,c,d) traces of plastic, cork, sand, dust, metal, different glass types	curved shards, thickness ≈1-4, width ≈5-30		1120	560
Wertheim glass (C-glass)	Wertheim pellets	Glasmuseum Wertheim	63.8% SiO_2, 5.5% B_2O_3, 11.8% Na_2O, 6.4% CaO, 5.2% Al_2O_3, 3.7% MgO, 3.2% K_2O	Clean	≈15x10x8		820	540
	Wertheim pellets	Glasmuseum Wertheim		Clean	≈15x10x8	Same as above	900	540
Barium-Strontium silicate	Barium CRT front panel	From Philips CRT monitor	61.5% SiO_2, 8.1% SrO, 8% BaO, 7.2% Na_2O, 6.8% K_2O, 3.6% ZrO_2, 2.3% Al_2O_3, 1.1% CaO	Clean	shards, thickness ≈10, length 50-100		870	430
Potassium-Lead silicate	Lead CRT funnel	Coolrec	Characteristic composition: 52% SiO_2, 22% PbO, 7.8% K_2O, 6.8% Na_2O, 4% Al_2O_3, 3.8% CaO, 1.8% MgO, 1% BaO	ii) Glass from different manufacturers	≈5-15		870	430
	Lead glass	Royal Leerdam	57.7% SiO_2, 28.7% PbO, 9% K_2O, 3% Na_2O, 0.8% Sb_2O_3, 0.6% ZnO	i) Surface colour	shards, thickness ≈5-10, length 50-100		820	430

3.2.2 Four-point bending test set up

1st series of experiments (12 kiln-cast, 6 reference specimens)

The 1st series of experiments is conducted in order to provide a general overview regarding the flexural behavior of the different glass specimens. The specimens are tested using a Zwick Z10 displacement controlled universal testing machine in a laboratory air environment and at a rate of 0.2mm/min. The four-point bending fixtures have a 110mm span for the loading rollers and a 220mm span for the support rollers, with 10mm diameter fixed loading pins, and are loosely connected to the testing machine to allow some hinging (Figure 3.2a).

2nd series of experiments (53 kiln-cast, 5 reference specimens)

The 2nd set of experiments involves the repeated testing of each glass category and provides accurate displacement data. The number of tested specimens per glass category is set to three, which is limited for testing a brittle material whose strength is by default statistical due to the randomness of the occurring flaws in the glass (Quinn et al. 2009). This study, however, aims to cover a broad variety of glass types and compare them according to their flexural behavior, in order to explore which recycled glass products have further potential for structural use. For these tests, a Schenck 100KN displacement controlled hydraulic universal testing machine is employed, and the specimens are tested in a laboratory air environment using a 0.3mm/min displacement rate, which approximately corresponds to a 0.5MPa/s rate [26]. The four-point bending fixtures have a span of 100mm for the loading rollers and 200mm for the support rollers, with 20mm diameter fixed loading pins (Figure 3.2b). To allow for minor adjustments and rotational movements, the support fixture is placed on a semi-circular pin, while the loading fixture is loosely connected to the testing machine. In addition, a 1mm thick silicone rubber strip is placed between each loading pin and the specimen.

To measure the displacement of the beam due to bending, two methods are employed: 1) a Linear Variable Differential Transformer (LVDT) displacement sensor (Solartron AX 2.5 Spring Push Probe calibrated to a 0.5μm accuracy) is placed under the middle point of the lower surface of the beam (measuring the point of maximum displacement), and 2) a 2D-DIC measurement, using a high-resolution (50.6MP) Canon EOS 5Ds camera that takes one picture per second of the speckled surface of the beam. The pictures of the 2D-DIC measurement are analysed using the GOM Correlate software. One image pixel corresponds to 31.5μm, therefore given the software accuracy of 0.05 pixel, any displacement above 1.57μm can be captured.

[26] A slightly faster displacement rate was chosen for the 2nd series, with the aim to reduce the total number of DIC images per experiment and thus confine the size of the files produced by the image processing software GOM Correlate to a maximum of 25 Gigabytes. Both the 1st and 2nd series displacement rates are below the rate of stress increase of 1.1 ± 0.2MPa/s indicated by ASTM C158 − 02. A displacement controlled rate is favoured over force controlled, to avoid the crashing of the specimen upon failure, but also to allow for potential pop-ins (slight crack arrests) at maximum force, when the crack front interacts with an interface encountered in the glass meso-level structure.

a)

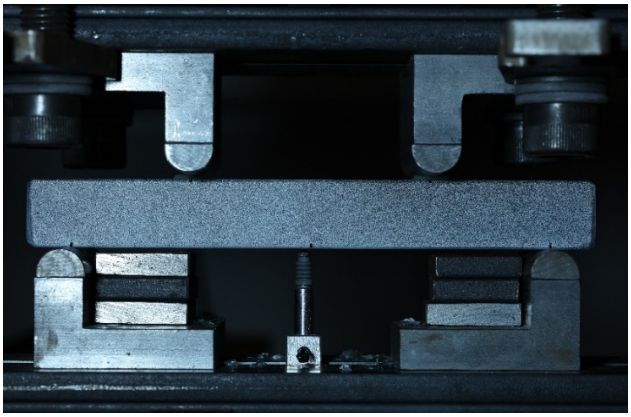

b)

Fig. 3.2 a) Fixture and set-up of 1st series of four-point experiments. b) Fixture and set-up of 2nd series of four-point experiments. An LVDT sensor is placed at the middle of the span. The front surface of the specimen is covered with a speckle pattern for the DIC measurement. The metallic strips placed next to the support pins are cushioning the specimen upon fracture and protect the LVDT sensor from damage. No contact occurs between the specimen and the strips during the bending test.

Flexural strength and Young's modulus calculation

The flexural strength (σ) is computed from the equation below:

$$\sigma = \frac{3 \cdot F \cdot (L - L_i)}{2 \cdot b \cdot d^2} \quad (1)$$

where F the maximum load, L the support span, L_i the load span, b the beam's width and d the beam's height[27].

The calculation of Young's (E) modulus is performed by correlating the force data obtained from the Schenck machine with 1) the maximum displacement from the LVDT sensor and 2) the maximum displacement from the DIC analysis (Figure 3.3).

[27] It should be noted that due to the fixed loading pins, a systematic positive error may occur due to a frictional constraint of μ·F/2 occurring at each pin, with μ being the coefficient of friction (Quinn et al. 2009). This force creates a counteracting moment of μ·F·d/2, thus the above equation should be rewritten as:

$$\sigma = \frac{3 \cdot F \cdot (L - L_i - \mu \cdot d)}{2 \cdot b \cdot d^2} \quad (2)$$

Assuming a moderate μ=0,3, the systematic error could be of magnitude 8,2% for the 1st series of experiments and 9% for the 2nd. However, due to insufficient data regarding the μ value, the flexural strength is not corrected in this study, and the reader should take into account the possibility of an error of approximately the aforementioned magnitude.

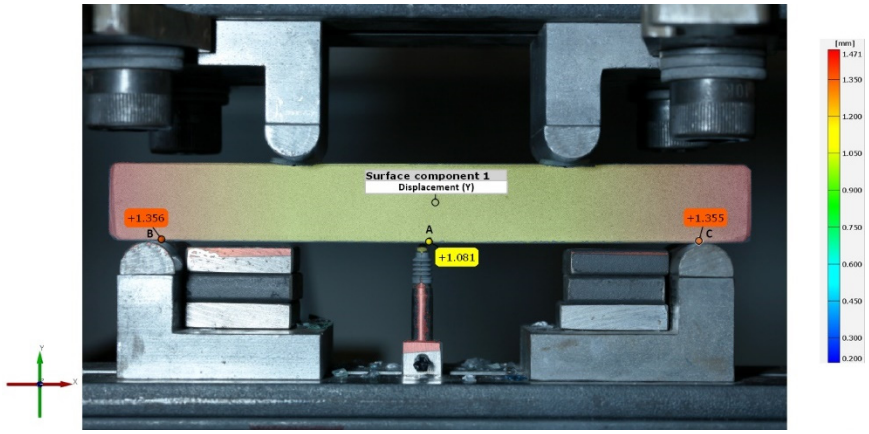

Fig. 3.3 Analysis of the displacement in y axis, using GOM Correlate software. The maximum displacement due to bending at point A is calculated by subtracting the total displacement at point A from the average displacement at point B and C.

Given that the cross section of the beam in relation to the fixture spans results in a relatively stiff structural element, a shear deflection should be accounted to the total vertical deflection. The bending and shear deflection at mid-span with respect to the beam point above the support pins, and for a 1:2 four-point bending fixture ratio, are defined by the formulae below:

$$\Delta l_{Bending\_mid} = \frac{11 \cdot \Delta F \cdot (\frac{L - L_i}{2})^3}{12 \cdot E \cdot b \cdot d^3} \tag{3}$$

$$\Delta l_{shear\_mid} = \frac{\Delta F \cdot \frac{L - L_i}{2}}{2 \cdot G \cdot b \cdot d} \tag{4}$$

where $G = \frac{E}{2 \cdot (1 + v)}$ (5)

Adding the two segments of vertical deflection and solving towards the Young's modulus, it is concluded[28]:

$$E = \frac{\Delta F}{\Delta l_{total\_mid}} \cdot \left(\frac{11 \cdot \left(\frac{L - L_i}{2}\right)^3}{12 \cdot b \cdot d^3} + \frac{(L - L_i) \cdot (1 + v)}{2 \cdot b \cdot d} \right) \tag{6}$$

[28] For the Young's modulus calculation, the Poisson ratio of v=0.22 of soda lime silica glass is used. Although among the tested glasses there may be a +- 0.02 deviation to this value, this has a negligible effect on the results.

3.3 Results

3.3.1 Defect evaluation for kiln-cast specimens

The flaws occurring in the surface and bulk of the produced glass specimens are qualitatively[29] documented according to type and cause. The aim is to correlate the defects found to the glass source used and followed casting and post-processing procedure, and to subsequently assess their contribution to the specimens' flexural strength. The casting related defects are categorized[30] in:

1. Crystalline Inclusions
2. Glassy inhomogeneities (cord/ream)
3. Gaseous inhomogeneities (bubbles)

An overview of the defect categories and their causes is found in Figure 3.4, based on which a documentation of the observed flaws per glass type is presented in Table 3.2.

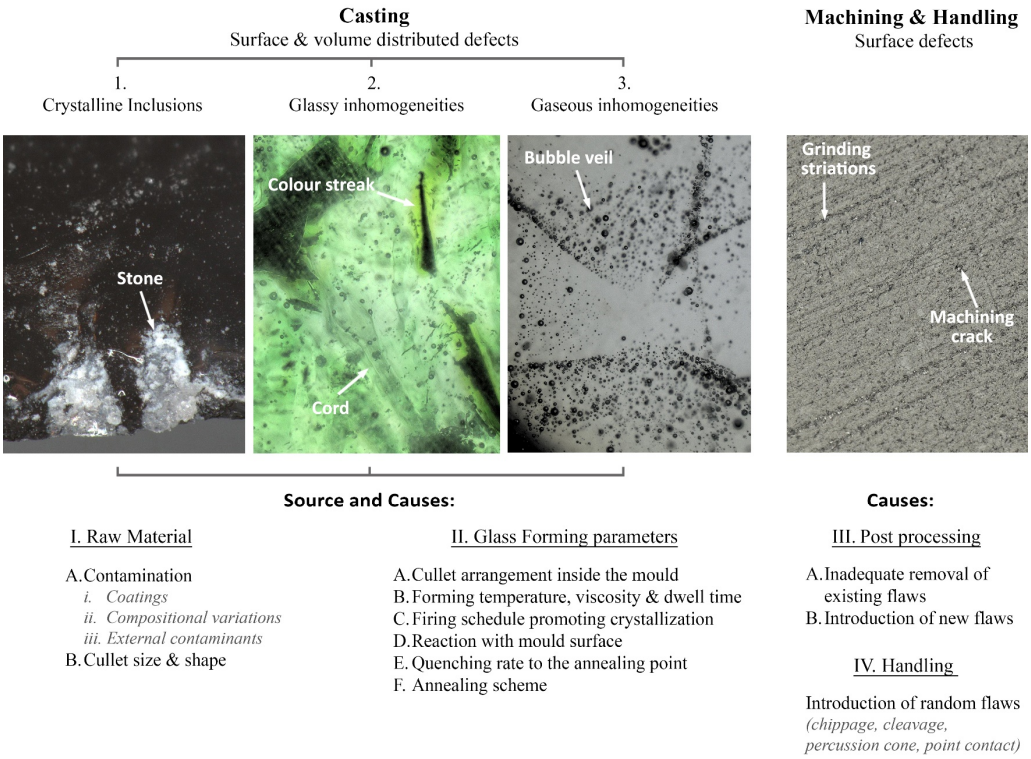

Fig. 3.4 Categorization and causes of the defects encountered in the kiln-cast glass specimens.

[29] The quantitative analysis of the level of inhomogeneities in cast glass specimens of considerable cross section- and thus multiple layers of defects versus a thin-walled glass- is a complex process that involves several different testing methods (e.g. Computed Tomography Scanning to detect and measure density differentials, 3-dimensional Imaging Real-Time Polarimetry to define the location and shape of cord, etc). This analysis is kept out of the scope of this study as the main aim is to firstly identify the type and location of critical flaws that require future attention, and thus quantitative documentation.

[30] Categorization based on Bartuška (2008).

Table 3.2 (part a): Evaluation of kiln-cast specimens.

Glass type	Specimen description	Forming temperature in °C (10hr dwell)	Theoretical viscosity (log10(visc./ poise)) at top temperature*	No. of successfully cast samples out of total castings	Type and cause of observed defects**	Kiln-cast specimen, side view
Soda Lime Silica (Float Glass)	Fully Tempered float	1120	3.5	9/9	1, 3 [II. B, D, III. A] Homogeneous glass of light aquamarine hue with evenly distributed miniscule bubbles. Occasional surface flaws from inadequate fusing of the cullet in combination with embedded material caused by contamination from the mould, challenging to be removed by post-processing.	
	Fully Tempered float, fused	970	5	1/1	1 [II. B, C, D, III. A] Crystallization along the fusion surfaces between the cullet pieces. Intense surface recessions in combination with embedded material caused by contamination from the mould due to inadequate fusing of the cullet at the exterior surfaces, challenging to be removed by post-processing.	
	Float 10mm, 3 horizontal layers, fused	970	5	3/3 (1 sample with surface creazing due to abrupt cooling)	1 [I. B, II. A, B, D] 2 horizontal layers of crystallization in the glass bulk.	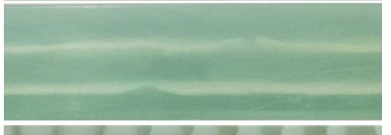
	Float 10mm, 24 vertical layers, fused	970	5	4/4 (1 sample with surface creazing due to abrupt cooling)	1 [I. B, II. A, B, D] 23 vertical layers of crystallization in the glass bulk, also exposed at the longitudinal surfaces of the beam.	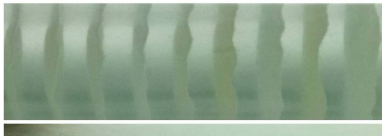
	Float 10mm, 3 vertical layers, fused	970	5	1/1	1 [I. B, II. A, B, D, E, III.A] 2 horizontal layers of crystallization in the glass bulk, also exposed at the top and bottom surfaces of the beam. Surface crazing due to reaction with the mould, challenging to be completely removed by post-processing.	
	Float dark blue	1120	3.5	3/3	3 [II, B] Homogeneous dark blue glass with miniscule bubbles	

*Estimation based on the chemical composition, using the viscosity model by Fluegel (2007).

** The defects are categorized as: 1. Crystalline Inclusions, 2. Glassy inhomogeneities (cord/ream), 3. Gaseous inhomogeneities (bubbles)

The cause of these defects can be associated with the: I. Raw Material (A. Contamination, B. Cullet size and shape), II. Glass forming (A. Cullet arrangement in the mould, B. Forming temperature and corresponding viscosity in relation to dwell time, C. Firing schedule in combination with temperature differentials in the kiln that promote crystallization, D. Reaction with mould surface, E. Quenching rate to the annealing point, F. Annealing scheme), and III. Post processing (A. Inadequate removal of existing flaws).

Table 3.2 (part b): Evaluation of kiln-cast specimens.

Glass type	Specimen description	Forming temperature in °C (10hr dwell)	Theoretical viscosity (log10(visc./ poise)) at top temperature*	No. of successfully cast samples out of total castings	Type and cause of observed defects**	Kiln-cast specimen, side view
Soda Lime Silica (Float Glass) with contamination	Float combo	1120	3.5	1/4	2, 3 [I. A, B, II. B] Heavily corded glass of light blue hue with colour streaks. 3/4 specimens fractured due to glass ceramic content in the cullet.	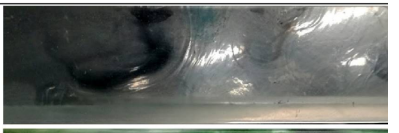
	Oven doors	1120	3.5	4/4	1, 2, 3 [I. A, II. B, III. A] Colour streaks, flat crystalline inclusions (coating residue), occasional surface flaws from inadequate fusing of the cullet in combination with embedded material caused by contamination from the mould that are challenging to be removed by post-processing.	
	Car windshields	1120	3.5	3/3	1, 2, 3 [I. A, B, II. B, III. A] Colour streaks, bubbles, stones and flat crystalline inclusions (coating residue). Occasional surface flaws from inadequate fusing of the cullet in combination with embedded material caused by contamination from the mould, challenging to be removed by post-processing.	
	Float with black enamel, 60 vertical layers	1120	3.5	3/3	1 [I. A, II. A, B] Vertical layers of coating residue, also exposed at the longitudinal surfaces of the beam.	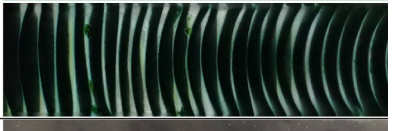
Modified Soda Lime Silica	Poesia standard cast brick	1070	3.5	3/3	3 [II. B] Transparent homogeneous glass with miniscule bubbles.	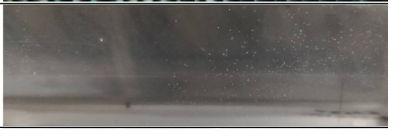

Table 3.2 (part c): Evaluation of kiln-cast specimens.

Glass type	Specimen description	Forming temperature in °C (10hr dwell)	Theoretical viscosity (log10(visc./ poise)) at top temperature*	No. of successfully cast samples out of total castings	Type and cause of observed defects**	Kiln-cast specimen, side view
Borosilicate	DURAN tubes	1120	4.5	6/6	3 [I. B, II. B] Dense veils of bubbles, along the connection surfaces of the glass shards.	
	DURAN rods x10 vertical, 1120°C	1120	4.5	5/5	3 [II. B] Transparent homogeneous glass with miniscule bubbles	
	DURAN rods x10 vertical, 1070°C	1070	5	3/3	3 [I. B, II. A, B] Transparent homogeneous glass with miniscule bubbles organized in vertical veils, also exposed at the longitudinal sides of the beam.	
	DURAN rods x10 vertical, fused 970°C	970	6	4/4	1, 3 [I. B, II. A, B, C] Vertical crystallized layers, also exposed at the longitudinal sides of the beam. Few bubbles in proximity to the fusion layers.	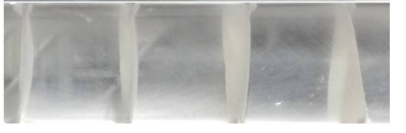
	DURAN rods x2 vertical, fused 970°C	970	6	1/1	1, [I. B, II. A, B, C] One horizontal crystallized layer.	
	DURAN 24mm rods, honeycomb, fused 970°C	970	6	1/1	1, 3 [I. B, II. A, B, C] Crystallized layers in a honeycomb structure, also exposed at the longitudinal sides of the beam. Few bubbles in proximity to the fusion layers.	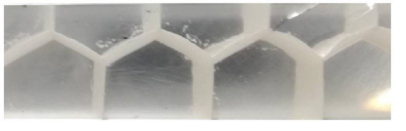

Table 3.2 (part d): Evaluation of kiln-cast specimens.

Glass type	Specimen description	Forming temperature in °C (10hr dwell)	Theoretical viscosity (log10(visc./ poise)) at top temperature*	No. of successfully cast samples out of total castings	Type and cause of observed defects**	Kiln-cast specimen, side view
Borosilicate	Borosilicate mix Coolrec	1120	4.5	1/1	1, 3 [I. A, II. B] Miniscule bubbles and occasional stones in the glass bulk.	
	Borosilicate mix Maltha	1120	4.5	0/3	1, 3 [I. A, II. D] Intense crystallization formed at the top surface, bubbles, heavy reaction with the mould that lead to fracture during cooling due to the different coefficient of thermal expansion of the two materials.	
Wertheim glass (C- glass)	Wertheim pellets	820 / 900	6 / 5	3/3	1, 3 [II, B] Fusion lines and bubbles	
Barium-Strontium silicate	Barium CRT front panel	870	5.5	3/3	3 [II. B] Homogeneous dark black glass	
Potassium-Lead silicate	Lead glass	870	-	1/1	1, 2, 3 [I. A, II. B] Heavily corded glass, bubbles, crystalline inclusions.	
	Lead glass	820	5.5	2/2	2, 3 [I.A, II. B] Colour streaks, bubbles.	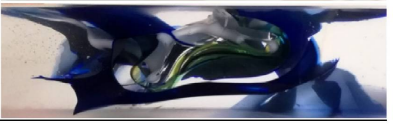

In more detail, the cause of these defects is associated with one or more of the following manufacturing stages[31,32]:

I. Raw Material.

A. Contamination.

i. Coatings.

Several "flat" defects are observed in kiln-cast specimens from float glass cullet covered with enamel paint or ceramic frit, due to the insufficient melting of the coatings (Figure 3.5). The XRF analyses of two characteristic coatings (Table 3.3) show compositions rich in high melting-point metal oxides and in particular in chromium(III) oxide (melting point of Cr_2O_3 is 2435ºC, NIH Database). The X-ray diffraction (XRD)[33] analysis of kiln-cast glass samples (Figure 3.6) shows in these cases the presence of eskolaite (mineral name of chromic oxide).

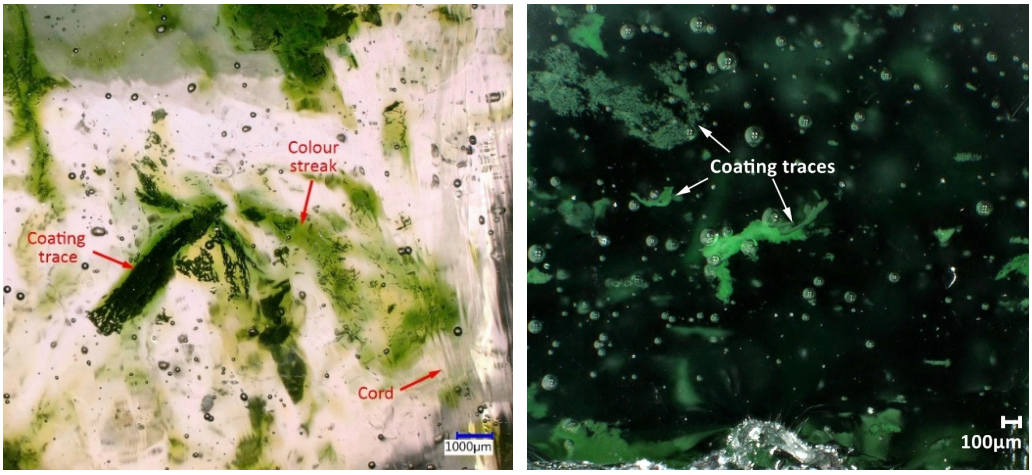

(a) (b)

Fig. 3.5 (a) Microscope image of a "Oven doors, 1120ºC" kiln-cast glass with flat crystalline inclusions, cord, colour streak (due to partially molten coating material) and bubbles. (b) Microscope image of a "Car windshields, 1120ºC" kiln-cast glass with crystalline inclusions and bubbles.

[31] In Table 3.2, flaws caused during stages III.B. and IV (post-processing and handling flaws) are not mentioned as they are not linked to the material and its casting method, but are rather arbitrary and only relevant to the fracture analysis of each specific specimen.

[32] The following microscope images were made using a Keyence VHX-5000 or VHX-7000 Digital Microscope.

[33] All XRD analyses in this work were conducted using a Bruker D8 Advance diffractometer, Bragg-Brentano geometry and Lynxeye position sensitive detector.

Table 3.3: Coating composition.

Coating Type	Glass source	Composition* (wt%)										
		SiO_2	Bi_2O_3	Cr_2O_3	CuO	PbO	Na_2O	TiO_2	Fe_2O_3	Al_2O_3	CdO	ZnO
Black enamel	Enamel float, AGC	30.7	28.6	19.4	10.2		3.3	4.2				1.3
Black frit	Oven door, Coolrec	33.2		22.5	10.6	12.7	7.2	2.2	3.8	3.6	2.9	

*XRF measurements conducted with a Panalytical Axios Max WD-XRF spectrometer by Ruud Hendrikx. The absolute Wt% obtained by the XRF measurements may not be entirely accurate in the case of thin coatings, due to the extremely small thickness of the coating.

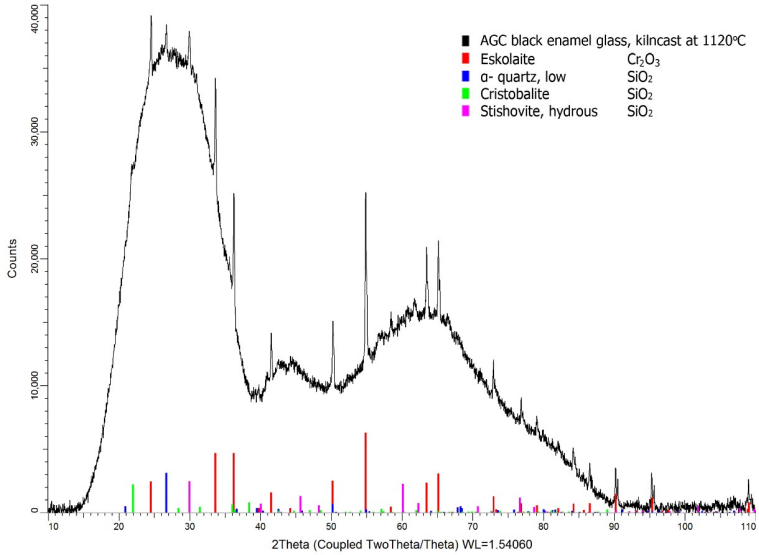

Fig. 3.6 XRD pattern of kiln-cast "AGC Float with black enamel" glass at 1120ºC. The sample is at a large extent amorphous (black curve) yet it presents some sharp crystalline peaks (coloured sticks).

ii. Minor compositional variations.

Minor compositional variations lead to glassy inhomogeneities such as cord and colour streaks. Some examples with heavy striation are identified in the "Float combo" and "Lead CRT" (Figure 3.7) samples.

Fig. 3.7 "Lead CRT, 870ºC" specimen containing intense cord (seen as wavy lines) and bubbles.

iii. External contaminants.

In this category, the presence of glass ceramics or chemically different families of glass in the cullet (not detectable by eye, e.g. aluminosilicate shards in borosilicate or soda lime silica cullet)), is the most critical, leading to specimens which fracture upon cooling, due to strains caused by thermal expansion variations. This is experienced in the "Float combo" (Figure 3.8a) and " Borosilicate mix Maltha" specimens.

Specifically, the "Float combo" specimens were cast by employing a compilation of flat glass shards (of approx. 20-50mm width) provided by Maltha Recycling. This flat glass compilation is rejected from the recycling stream as the erroneous deposition of glass ceramic plates (e.g. cooktops) in the flat glass collection container- an often encountered phenomenon- renders the entire container unsuitable for recycling. The XRF and XRD analyses of characteristic pieces from the flat glass compilation sample (Table 3.4, Figure 3.8b, 3.9) place the contaminants in the commercially applicable lithium aluminosilicate glass ceramics system, which is characterized by the close to zero thermal expansion coefficient (Höland and Beall, 2020). The very low thermal expansion coefficient (CTE) contrasts with the typical $9.5 \cdot 10^{-6}$/K (at 20-300ºC) of float glass (Shelby 2005), leading to unavoidable cracking. However, the reduction of the flat-glass compilation sample's particle size (fine cullet or powder), could minimize the strains in the final cast product, and therefore this strategy requires further investigation.

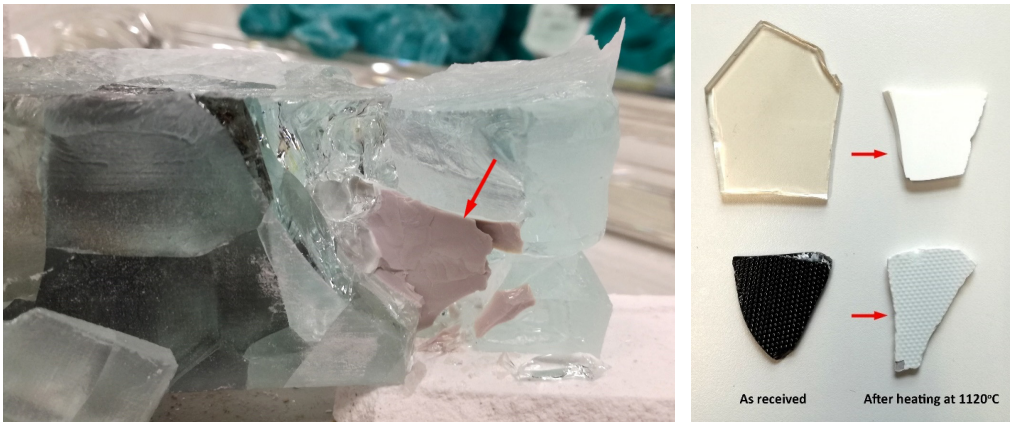

(a) (b)

Fig. 3.8 (a) Fractured "Float combo, 1120ºC" specimen due to glass ceramics contamination. (b) Glass ceramic shards encountered in the flat glass compilation sample. The left column shows the shards in the "as-received" transparent condition, whereas the right column shows their opaque version after heat-treatment at 1120ºC for 10hr. This behavior suggests a lithium aluminosilicate β-quartz solid solution phase in the transparent condition that transforms to β-spodumene during heat-treatment at temperatures above 1000ºC. The larger crystals in the later condition scatter the light and lead to opacity (Shelby 2005).

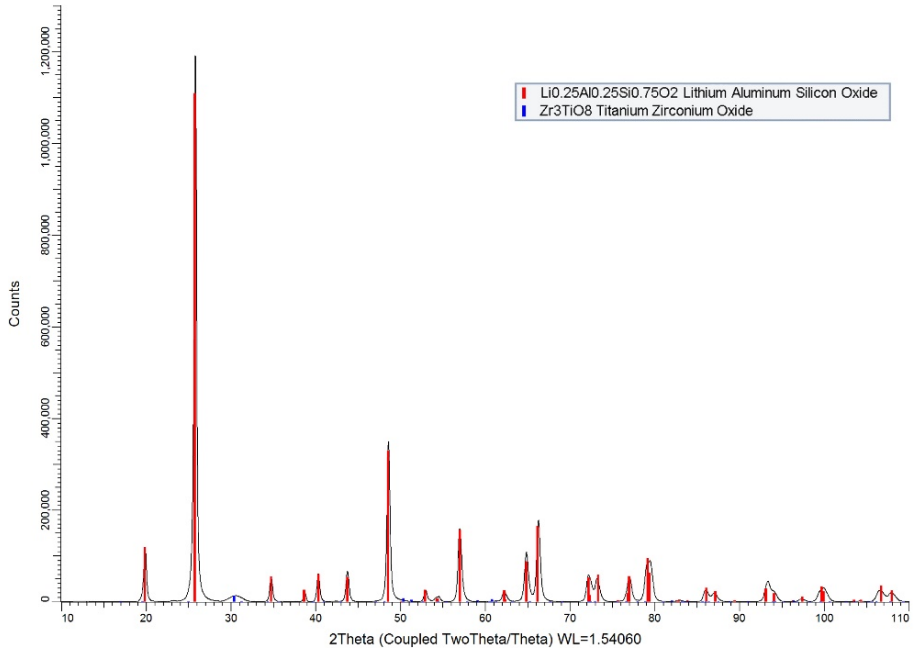

(a)

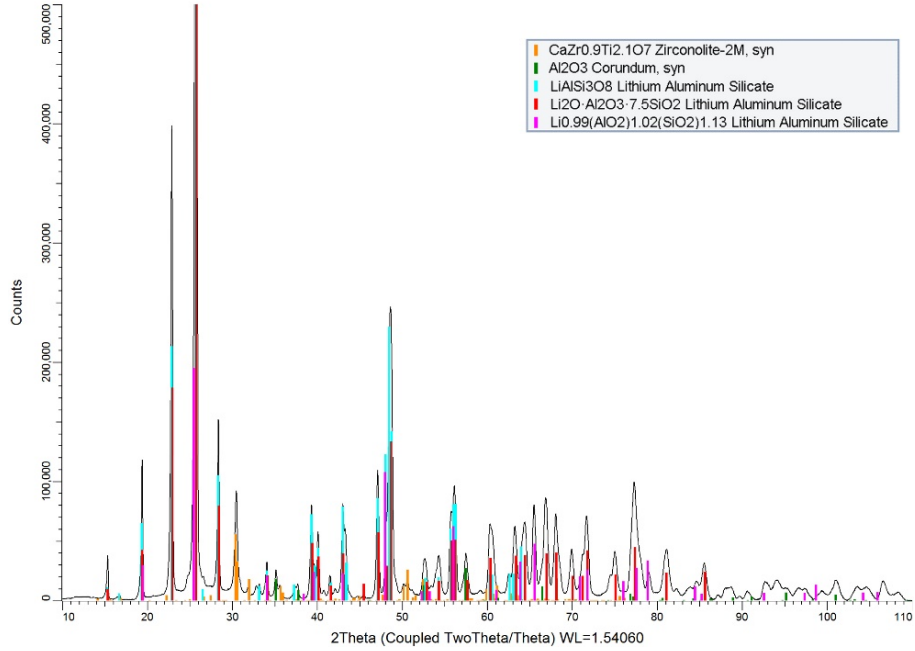

(b)

Fig. 3.9 XRD pattern of the yellow transparent glass ceramic depicted in Figure 3.8b, in the as received condition (a) and after heat-treatment at 1120ºC for 10hr (b). The crystal structure in (b) is similar to β-spodumene, yet the material presents multiple phases.

Table 3.4 (part a, extends to the next page): Chemical composition, crystal phase and CTE of typical Lithium Aluminosilicate Glass Ceramics, compared to the tested glass ceramic samples, the cast "Float Combo Maltha" specimen and a typical window glass.

Type	Stage	Colour/ transparency	Crystal	
			Type	Source
Piece selected from the "Float combo Maltha" sample (Fig. 8b)	As received	Light yellow transparent	Lithium Aluminum Silicon Oxide: $Li_{0.25}Al_{0.25}Si_{0.75}O_2$ Titanium Zirconium Oxide: Zr_3TiO_8	[1]
	After heating at 1120°C for 10hr	White opaque	Lithium Aluminum Silicate: $LiAlSi_3O_8$, $Li_2O{\cdot}Al_2O_3{\cdot}7.5SiO_2$, $Li_{0.99}(AlO_2)_{1.02}(SiO_2)_{1.13}$ Zirconolite-2M: $CaZr_{0.9}Ti_{2.1}O_7$, Corundum: Al_2O_3	[1]
Piece selected from the "Float combo Maltha" sample (Fig. 8b)	As received	Dark brown transparent	*Not verified*	-
"Float combo Maltha" cast sample (containing float glass and glass ceramics)	After heating at 1120°C for 10hr	Transparent with white opaque zones and brown colour streaks	γ- Magnesium Silicate: $Mg_2(SiO_4)$, Quartz: SiO_2, Zirconium Oxide: ZrO_2, Cristobalite low: SiO_2	[1]
Schott Nextrema® 724-3	N/A	Light yellow transparent	Lithium Alumininosilicate	[3]
Schott Nextrema® 712-3		Dark brown transparent		
Schott Ceran®		*Not verified*	β-quartz solid solution	[3]
Corning Vision®		Yellow transparent	β-quartz solid solution	[7]
Corning US4018612A sample no. 2		Light lavender transparent	β-quartz solid solution	[8]
Corning 9617		White opaque	β-spodumene solid solution	[8]
Typical Soda Lime Silica window glass (float)	N/A	Clear transparent	Amorphous	-

* Lithium is a light element that cannot be detected by the XRF analysis and therefore the percentage corresponding to lithium oxide is reflected to a higher content of silica dioxide. According to the bibliography, the presented composition should have a 2-3% lithium oxide content and a lower silica dioxide content by 2-3%.

** A lower than 3% lithium oxide content is expected in the chemical composition.

[1] XRD measurements conducted by Ruud Hendrikx (TU Delft, 3me) using a Bruker D8 Advance diffractometer, Bragg-Brentano geometry and Lynxeye position sensitive detector.

[2] XRF measurements conducted with a Panalytical Axios Max WD-XRF spectrometer by Ruud Hendrikx (TU Delft, 3me).

[3] Montazerian et al., 2015

[4] SonghanPlastic Technology Co., Ltd.

[5] Schott, 2015b

[6] Höland and Beall, 2020

[7] Shelby, 2005

[8] Chyung, 1977

[9] Brennan, 1979

[10] Campbell and Hagy (1975)

Table 3.4 (part b, continues horizontally from previous page): Chemical composition, crystal phase and CTE of typical Lithium Aluminosilicate Glass Ceramics, compared to the tested glass ceramic samples, the cast "Float Combo Maltha" specimen and a typical window glass.

Coefficient of Thermal Expansion (20, 300°C): 10^{-6}/K	Composition* (wt%)																
	SiO_2	Li_2O	Al_2O_3	TiO_2	ZrO_2	ZnO	P_2O_5	BaO	MgO	Na_2O	K_2O	As_2O_3	Sb_2O_3	V_2O_5	Fe_2O_3	CaO	Source
	70.99*	*	20.98	2.06	2.05	0.01	1.37	1.26	-	0.52	0.22	0.4	0.08	-	0.02	0.02	[2]
Not verified																	
	70.62*	*	19.02	2.13	2.29	0.01	1.12	1.29	-	1.515	1.25	0.41	0.08	-	0.04	0.03	[2]
Not verified	72.67*	*	18.46	2.6	1.6	1.48	0.05	0.62	0.78	0.7	0.19	0.45	-	0.19	0.08	0.05	[2]
Multiple CTE values	66.36	**	11.92	1.88	1.16	1.31	0.06	0.35	2.09	10.11	0.26	0.36	-	0.15	0.1	3.28	[2]
-0.28 [4]																	
	50-80	0-5	15-27	0-5	0-5	0-5	-	0-8	0-8	0-2	0-2	-	-	-	-	0-8	[5]
-0.16 [4]																	
±0.15 [6]	64	3.5	21	2.3	1.6	1.5	-	2.5	0.1	0.6	0.5	-	0.85	-	0.23	0.2	[6]
Not verified	68.8	2.7	19.2	2.7	1.8	1	-	0.8	1.8	0.2	0.1	0.8	-	-	0.1	-	[7]
0.78 [8]	68.8	3	19.6	3	1.5	1.2	-	-	2.2	-	-	0.7	-	-	-	-	[8]
3.2 [9]	67.4	3.5	20.4	4.8	-	1.2	-	-	1.6	0.2	0.1	0.4	-	-	-	-	[10]
9.5 [7]	73	-	0.1	-	-	-	-	-	4	14	-	-	-	-	0.1	9	[7]

Traces of metal, clay or stone lead to crystalline inclusions of a maximum of 2mm size, but these are tolerated by the glass network (Figure 3.10, 3.11). However further study is required to identify the crystalline inclusions (employing scanning electron microscopy) and to test if their role remains neutral when the glass is subjected to temperature gradients.

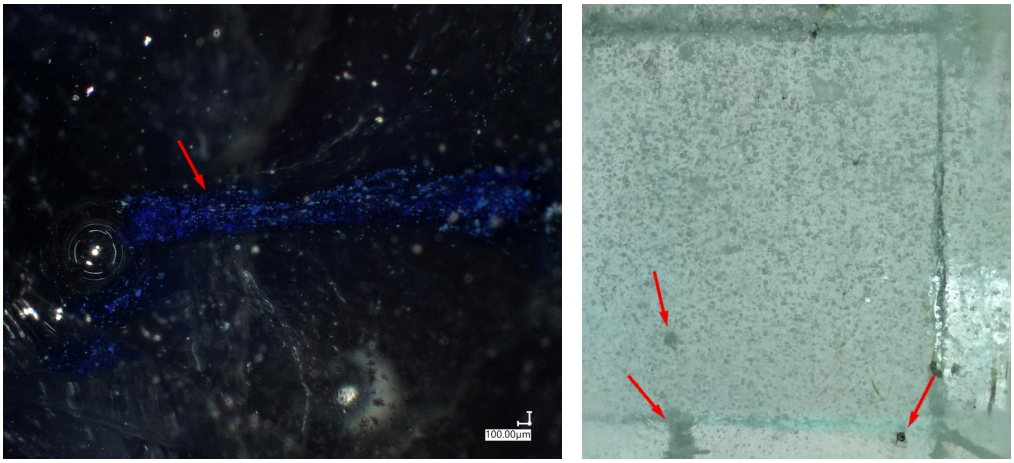

(a) (b)

Fig. 3.10 (a) Microscope image of "Lead CRT, 870ºC" specimen, containing undissolved blue particles of –most probably- cobalt oxide. (b) The variable inclusions in the "Borosilicate mix Coolrec, 1120ºC" specimen are tolerated by the glass network.

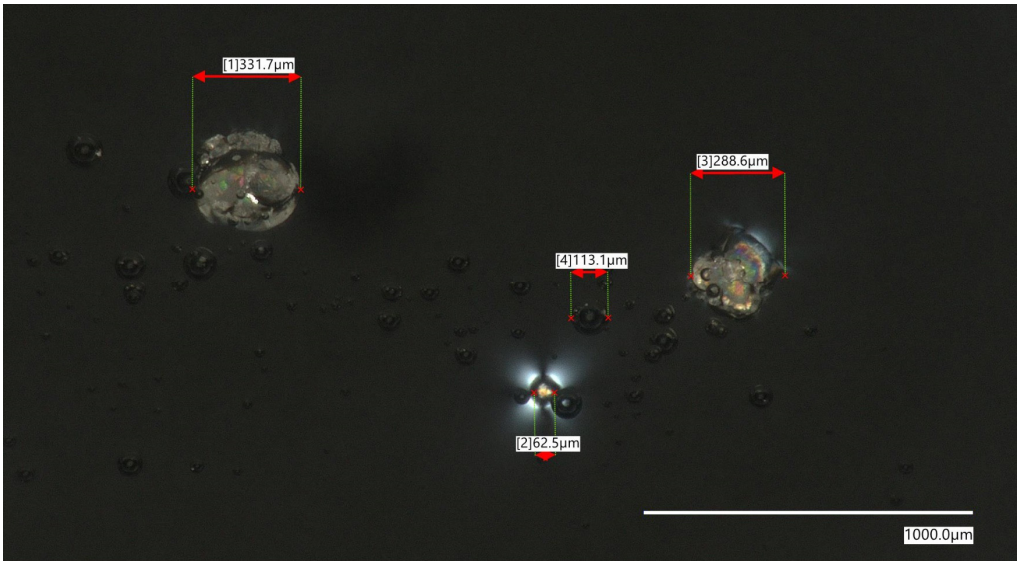

Fig. 3.11 Crystalline inclusions and bubbles detected in the bulk of a "Schott DURAN tubes 1120ºC" specimen, viewed through cross-polarized light. Although some inclusions e.g. the depicted 62.5µm stone, induce stress to the surrounding glass, this is well tolerated within the 30x30mm glass cross section.

B. Cullet size and shape.

In the addressed glass viscosity range, the geometry of the cullet is often reflected in striations and/or three-dimensional bubble veils in the final glass component. In cases of very fine cullet (e.g. “Car Windshields” samples) this geometry is not distinguishable, and a rather high content miniscule bubbles prevails (Figure 3.12).

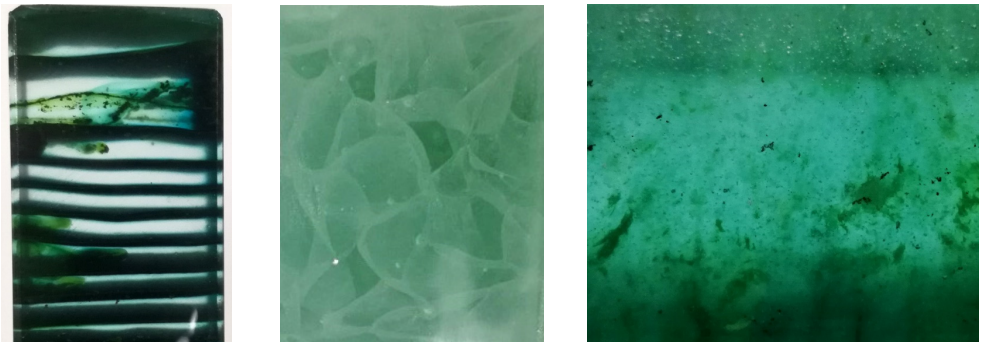

(a) (b) (c)

Fig. 3.12 The size, shape, and arrangement of the cullet, in combination with the forming temperature, lead to organized (a), random visible (b) and random non-traceable (c) meso-level structures in the glass component. (a) “AGC float with black enamel, 1120ºC” (image width ≈ 30mm), (b) “Wertheim, 820ºC” (image height ≈ 30mm), (c) “Car windshields, 1120ºC” (image height ≈ 30mm).

II. Glass forming.

A. Cullet arrangement in the mould.

This is relevant with the geometry of the cullet (I. B) in combination with the firing schedule and corresponding viscosities of the formed glass (II. B, C). A defined cullet shape and high viscosity can lead to organized meso-level structures composed of bubble veils (Figure 3.13b, 3.14), cord or crystallized interfaces which result in a more predictable failure pattern (Figure 3.13). Such organized structures also help in distinguishing the role of these defects when present at the glass surface or in the bulk.

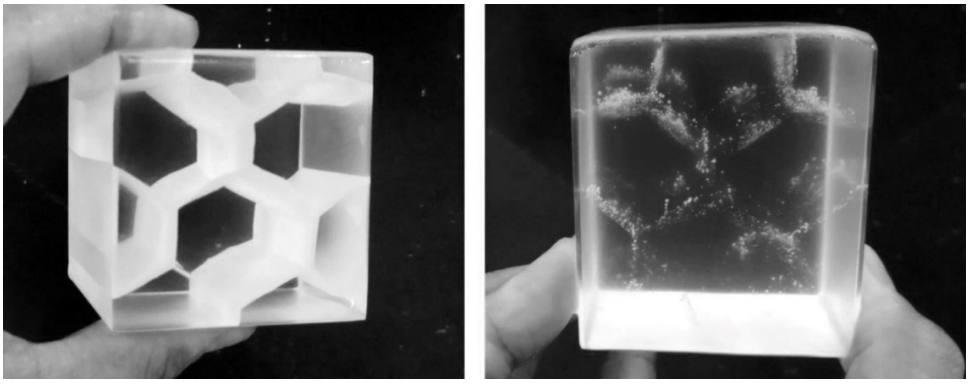

(a) (b)

Fig. 3.13 Kiln-cast experiments with Schott DURAN borosilicate rods of 24mm diameter forming 50mm cubic samples. (a) Crystallized hexagon structure, engineered at 970ºC. (b) Bubble-veil hexagon structure engineered at 1120ºC.

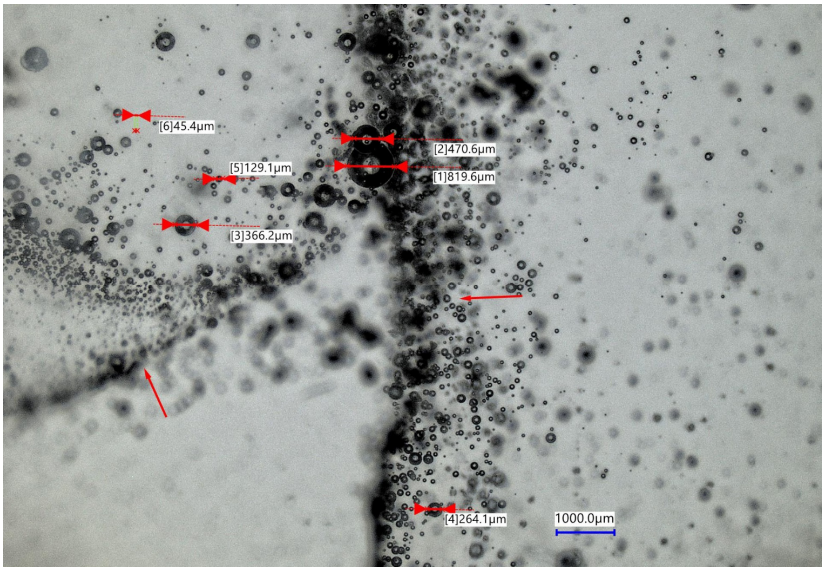

Fig. 3.14 Bubble veil observed in a "Schott DURAN tubes 1120ºC" specimen. The maximum bubble diameter is less than 1mm, while the majority of the bubbles has a diameter below 0.2mm.

B. Forming temperature and corresponding viscosity in relation to dwell time.
The top temperature affects the level of homogenization and the content of air-bubbles. All samples present miniscule bubbles due to the relatively low forming temperatures. In addition, the "cage" principle describing the mixing of dense liquids is applicable in this case, meaning that most of the molecules corresponding to an initial cullet piece will remain in the same position in relation to their neighboring cluster of molecules (cullet piece). The level of diffusion is increased when a viscosity of $10^{3.5}$dPa·s magnitude is reached, but it does not in any case lead to a fully mixed glass in the given dwell time (see Figures 3.12, 3.13).

C. Firing schedule in combination with temperature differentials in the kiln that promote crystallization.
This is particularly applicable for the float and borosilicate glass samples formed at 970ºC. In these samples, the complete interface between each cullet piece is crystallized. According to the XRD analysis (Figure 3.15), the borosilicate samples develop β-cristobalite crystals, while the float glass samples wollastonite 2M, β-cristobalite and devitrite (Figures 3.16, 3.17). Crystallization is favoured because the samples are formed below their liquidus point (T_L is around 1080ºC for the specific float glass, and around 1200ºC for the specific borosilicate[34]) yet reaching a low enough viscosity that kinetically allows nucleation. Nucleation starts at the interfaces, as there, a local compositional variation occurs due to the volatilization of alkali, and boron as well in the case of the

[34] The liquidus point of glasses T_L is found around a viscosity of 10^4 *dPa*·s, and is estimated from the chemical composition of the given glasses according to Fluegel (2007)

borosilicate glass. However, depletion of such elements may lead to unstable local compositions, as observed in the crystallized layer of the borosilicate samples, which proves porous and water-absorbing (Figure 3.17).

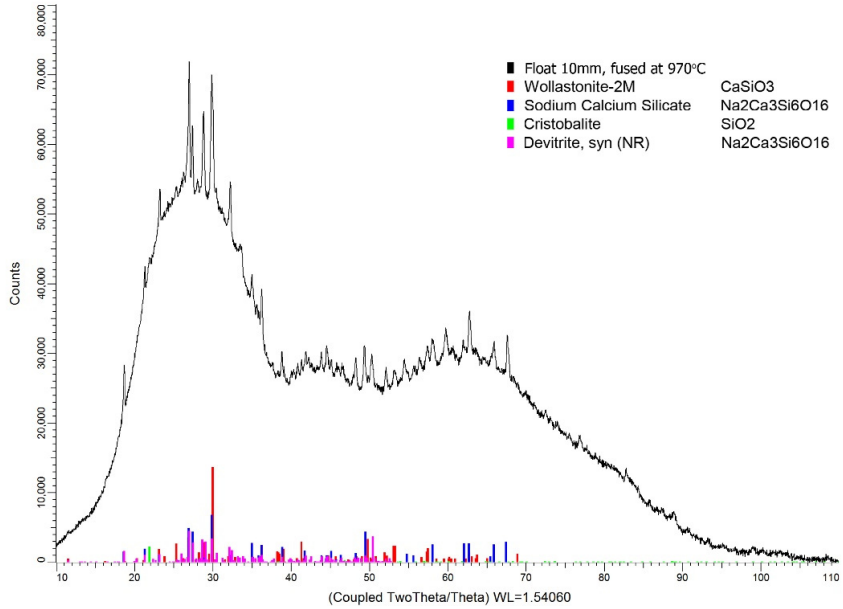

(a)

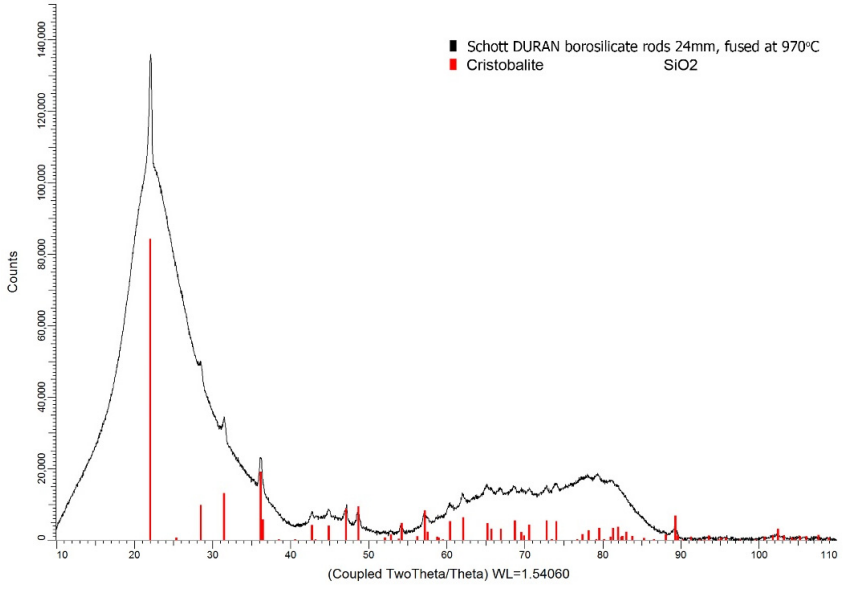

(b)

Fig. 3.15 XRD patterns of float glass (a) and Schott DURAN borosilicate rods (b) fused at 970°C.

Apart from the engineered crystallized structures described above, the temperature conditions and fluctuations within the kiln can also provoke local and random crystallization in the form of stones, at locations of compositional alteration. Local variations in the composition can be caused by contaminants in the raw material, contact with the mould material, volatilization of compounds, and gas bubbles. Therefore, such stones are not only found in specimens produced from evidently contaminated cullet (e.g. "Car windshields" samples), but also in more pure specimens (e.g. "Fully tempered (FT)[35] float" samples).

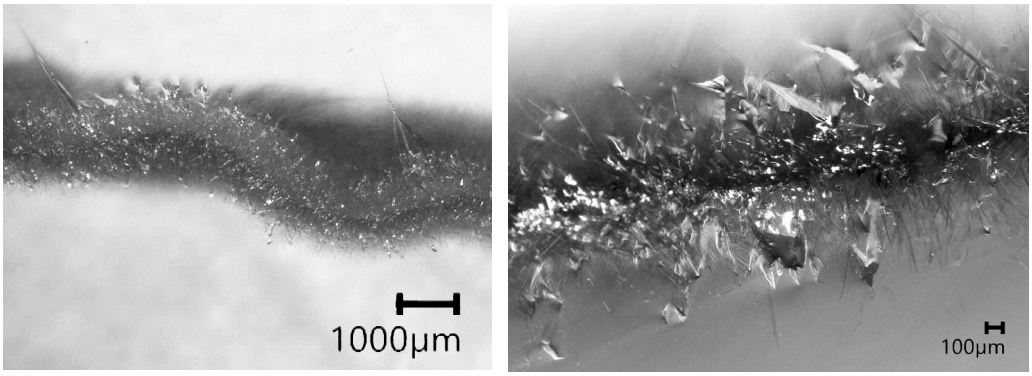

Fig. 3.16 Microscope images of the crystallized interface of the "Float 10mm fused 970ºC" samples (fractured surface). The parallel needle-like form of the crystals refer to devitrite.

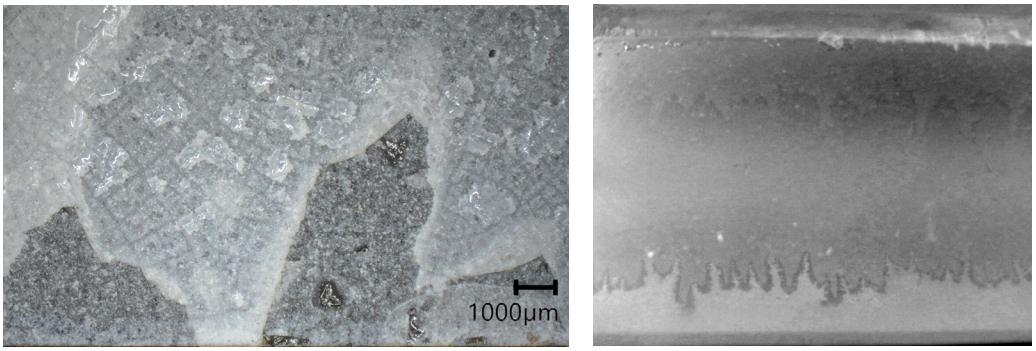

(a) (b)

Fig. 3.17 Crystallized interface of the "Schott DURAN borosilicate rods, fused at 970ºC" samples. (a) Microscope image showing a split interface due to fracture. (b) Water permeability of the crystallized interface (image height ≈ 30mm).

D. Reaction with mould surface.

During the kiln-casting process (at the studied viscosity range), the glass in contact with the silica/plaster investment mould, forms a thin crystallized interface, that can be easily removed by the described post-processing methodology (Figure 3.18). However, of

[35] The designation "Fully tempered" refers to the cullet used for these samples, which originates from shattered fully tempered float glass panels. The final kiln-cast components are annealed and thus not tempered.

particular interest are defects caused by the interaction of the mould with the glass that are deep enough to remain upon grinding (Figure 3.19). These can be, for example, stones of approx. ⌀1-2mm created from loose mould material that accidentally got incorporated in the glass melt. Another characteristic flaw occurs due to the friction of the mould surface that obstructs the complete fusion between the cullet pieces. As a result, localized or networks of infolds appear at the glass surfaces, which can also encapsulate mould material. Upon grinding, the tip of these flaws may remain at the glass surface, and is observed in depths up to 5mm. Lastly, only one case is observed where the glass bonds to the mould surface and breaks during cooling due to thermal expansion variations (sample "Borosilicate mix Maltha").

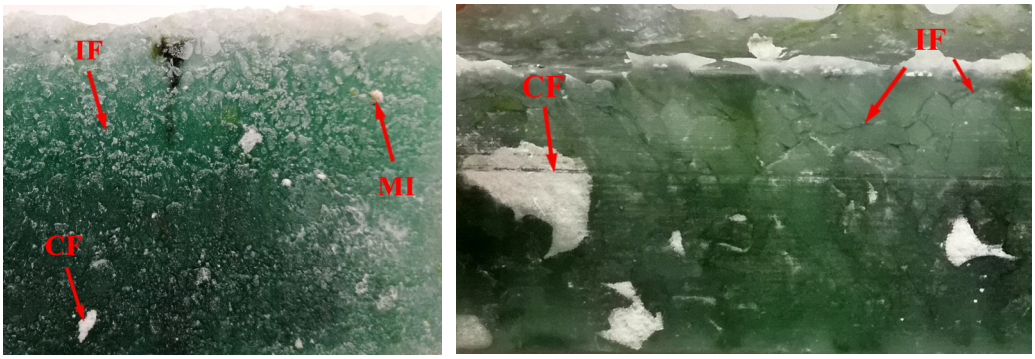

(a) (b)

Fig. 3.18 Surface reaction to the mould material. (a) Side surface of a "Car Windshields, 1120ºC" sample, as released from the mould. Improper fusion (IF) of the cullet, inclusions from the mould material (MI) and stone formations are observed (CF). (b) Side surface of an "Oven doors, 1120ºC" specimen, as released from the mould. The white zones are crystalline formations (CF) from the reaction of the glass coating to the mould material. Improper fusion (IF) of the cullet is also observed, as well as mould material inclusions.

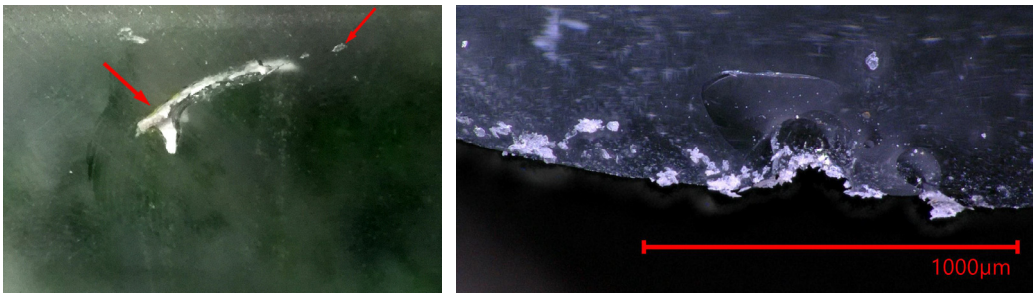

(a) (b)

Fig. 3.19 (a) Infold with stone inclusions from the reaction of the glass to the mould material, in the ground surface of an "Oven doors, 1120ºC" specimen (image height ≈ 30mm). (b) Microscope image of the fracture origin of a "Schott DURAN tubes 1120ºC" specimen. Note that the crystalline inclusion from the reaction to the mould, are not only situated at the bottom surface, but extend to the bulk as well.

E. Quenching rate to the annealing point.

In this study a lower quenching rate of -160ºC/hr is adopted in comparison to the abrupt quenching followed in industrial glass casting[36]. The experimental results show that this rate is sufficient to prevent crystallization. However, attention is raised to the fact that a slower cooling rate may intensify the level of polymerization of the glass network and lead to a denser glass (Ito and Taniguchi, 2004). Although this is not experimentally proven in this study, it remains a possibility to be taken into account.

F. Annealing scheme.

A conservative annealing scheme has been used, thus the residual stresses detected in the samples using cross-polarized filters are negligible and do not seem to compromise the flexural strength. Regarding the samples cut out from the standard Poesia glass bricks, these do have minor residual stresses, which is also seen by the fringe order in the isochromatic pattern obtained by an Ilis StrainScope Flex circular polariscope (Figure 3.20), and also suggested strongly by the tendency of this glass to chip during post-processing.

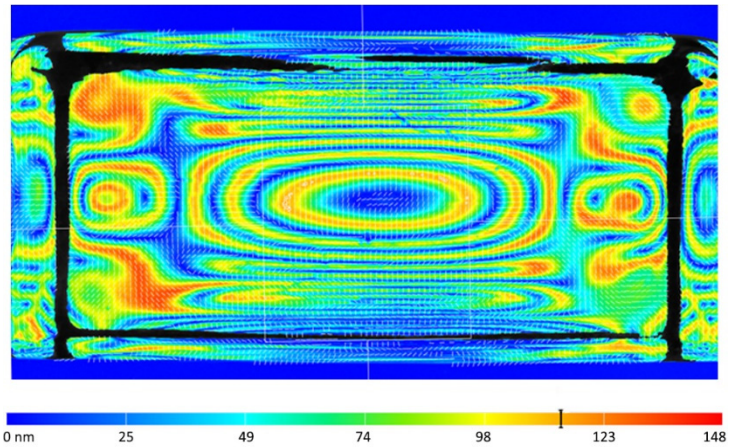

Fig. 3.20 Isochromatic fringes observed via an Ilis StrainScope Flex circular polariscope in a standard Poesia cast glass brick. The depth of the depicted sample is 10cm.

III. Post processing.

A. Inadequate removal of existing flaws.

As also discussed at point II.D, not all surface flaws can be completely removed by post-processing (Figure 3.21a). In this category of defects, the exposure during grinding of bubbles trapped in the glass bulk should be included. This results in stress concentrating semi-circular intrusions of sharp edges at the glass surface that reduce the strength. In addition, since bubbles can offer favourable conditions for the formation of crystals in their interior, the exposure of such gas-pockets at the surface bear the additional risk of stone exposure (see Figure 3.19b, 3.21b).

[36] In this study, quenching may last even 4 hours and takes place within the kiln, which is inherently different from the quenching at atmospheric conditions during hot-pouring of glass that lasts only several minutes.

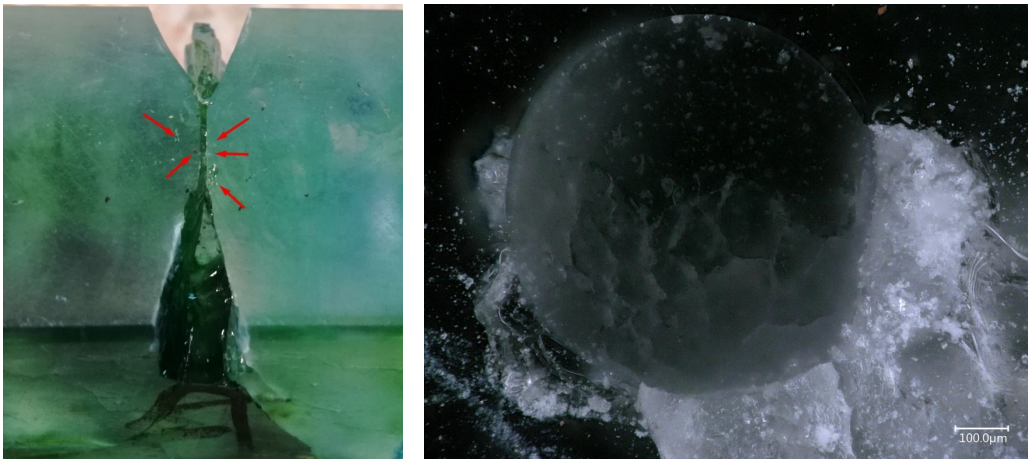

(a) (b)

Fig. 3.21 (a) Clustering of surface bubbles and stone inclusions at the bottom surface of an "Oven doors, 1120ºC" specimen that were not removed after grinding, form the strength limiting flaw. (b) Microscope image of a fractured "Schott DURAN tubes 1120ºC" specimen, showing a bubble in proximity to the surface and stone formations originating from the bubble interior.

B. Introduction of new flaws.

The introduction of new scratches from renegade abrasive grits (Quinn 2016) is mainly observed in glasses with lower hardness, in this study particularly the "Leerdam Lead" samples. Chipping is mainly occurring in the cut-out standard Poesia samples, as discussed in II.F. All samples present the risk of micro-cracking during coarse grinding that is not sufficiently removed in the later stages of grinding and polishing.

IV. Handling.

A series of handling flaws (chippage, cleavage, percussion cone, point contact) randomly occur in some of the specimens. The response of the cast specimens to handling damage versus that of industrially produced glass (e.g. float, extruded rods) requires further investigation, yet the more pure cast specimens are not observed to be more susceptible than standard glass products. However, attention should be drawn to the more contaminated glass samples, as occasional large defects at the surface (>2mm) amplify the effect of an impact.

3.3.2. Four-point bending tests

The results of both series of experiments are presented in Figures 3.22-3.26 and Tables 3.5-3.8. The data from the first series is mainly used for a first general guidance and as a confirmation of the second series, which is the main focus of this study. It should be stressed that the number of tested specimens per category is limited, and thus the presented results are only indicative and not sufficient for deriving statistical conclusions.

Although the first and second series differ in the fixture set-up (span, roller radius, connection detail to universal testing machine) and the sensitivity of the testing machine (10kN max. applied load for the machine used in 1st series versus 100kN for the 2nd), the results of the two tests are aligned. Specifically, the samples of the 1st series that are cast at 1120°C ("FT Float", "Schott DURAN 24mm rods", "Oven doors Coolrec") score within the same flexural strength range (40-50MPa), the fused samples at 970°C are significantly weaker (10-20MPa) while the pure single pane float samples have a slightly better performance (average flexural strength of 55MPa). This performance ranking and value range coincides with the results of the 2nd series apart from the case of the fused float samples at 970°C, where a noticeably low flexural strength is reported (<10MPa). This is attributed to the one-off occurrence of a network of micro-cracks at the surface of these specimens, which could not be easily removed by post-processing.

In Figure 3.24, depicting the flexural strength of the second series of specimens, three main zones can be observed: specimens of a flexural strength below 30MPa, between 30-55MPa- where most samples are located, and between 55-75MPa. In all specimens, crack initiation starts at the bottom surface (or at very close proximity), at the area between the support pins (zone of maximum tensile stress, see Figures 3.27, 3.28). As a general trend, glass specimens produced at lower viscosities and from purer cullet are found at the top zone of the flexural strength graph, while specimens with obvious strength-limiting flaws exposed at the bottom surface fail at low values.

An overview of the main fracture origins is presented in Figure 3.29, summarizing the most critical defect categories: stones, crystalline interfaces, surface bubbles, and machining damage. The size of the fracture mirror is measured in a selection of specimens (Figure 3.30) and plotted against the flexural strength σ (Figure 3.31) based on "Orr's equation" (Quinn 2016):

$$\sigma = \frac{A}{\sqrt{R}} \tag{7}$$

where R corresponds to the mirror radius (in this study the mirror size extending to the mist-hackle boundary at the bottom surface of maximum tension is measured) and A is the characteristic mirror constant per glass composition.

Typically, the larger the failure stress is, the smaller the encountered fracture mirror will be. The increase of the width of the critical flaw is, as expected, responsible for the decrease of the flexural strength (Figure 3.32). The higher strength specimens seem to fail mainly from machining flaws, whereas stones or crystalline interfaces are responsible for the fracture of the lower strength specimens. Yet, the type, size, quantity and location of flaws alone cannot justify why some glass samples score lower than others. The structural performance of each glass type needs to be reviewed as conjointly dependent on the chemical composition of the glass as well as its inherent defects (see Section 4). Also, fracture load uncertainty may be applicable due to environmentally assisted slow crack growth (Quinn et al. 2009), as the applied loading rate is slower (approx. by half) than the suggested rate by the ASTM C158 – 02 guideline. The effect of slow crack growth should be further experimentally investigated in a broader range of testing speeds.

Regarding the Young's modulus, the calculation conducted based on the LVDT data results in values that are approximately 15% lower than those found in literature. This is considered a systematic error and is attributed to the manner the sensor was connected to the support fixture[37]. However, in each triplet of tested glass type, there are matching E values reported. In addition, the stiffness relationship between the different glass families (Figure 3.26) is found in accordance with the literature (Corning 1979; Campbell 1975), and specifically:

$$E_{\text{Potassium Soda Lead-silicate}} \leq E_{\text{Borosilicate}} < E_{\text{BaO/SrO-Silicate}} < E_{\text{Soda Lime Silica}}$$

Therefore, although the LVDT calculation does not provide exact values, it can be reliably used for a comparative analysis between the different glass types. The DIC measurement is utilized to provide more accurate data regarding the maximum deformation, and for performing more precise calculations of the E moduli for a selection of glass samples (see Section 3.4 (a) for further analysis). Nonetheless, the coupling of the DIC measurement during 4-point bending with a non-destructive testing method for determining the E modulus, such as the Impulse Excitation Technique, is advised in future testing, to verify the reliability of the results.

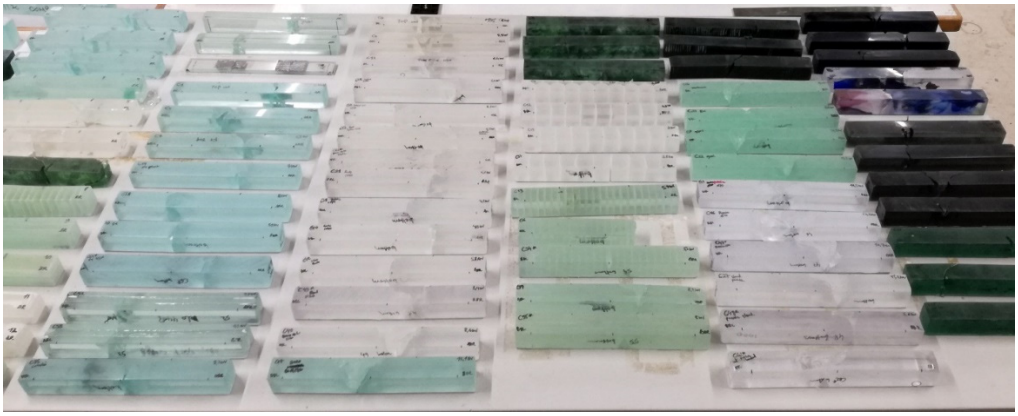

Fig. 3.22 Overview of tested specimens.

[37] The body of the sensor would pass through a metal casing glued on the support fixture (the base of the fixture was drilled at this location), and would be secured into position by a pressing bolt (see Figure 3.2b). This connecting method (versus for example an adhesive solution) was used to ensure the reusability of the sensor after the completion of the experiments. It is speculated that during the bending of the specimens, minor downward movements could occur at the connection point of the sensor, causing a systematic error in the displacement measurements. This hypothesis could not be confirmed nor the downward movement could be quantified, as upon the fracture of each specimen, the fractured glass pieces would push the sensor down and out of position. The sensor was readjusted each time before the next test would start.

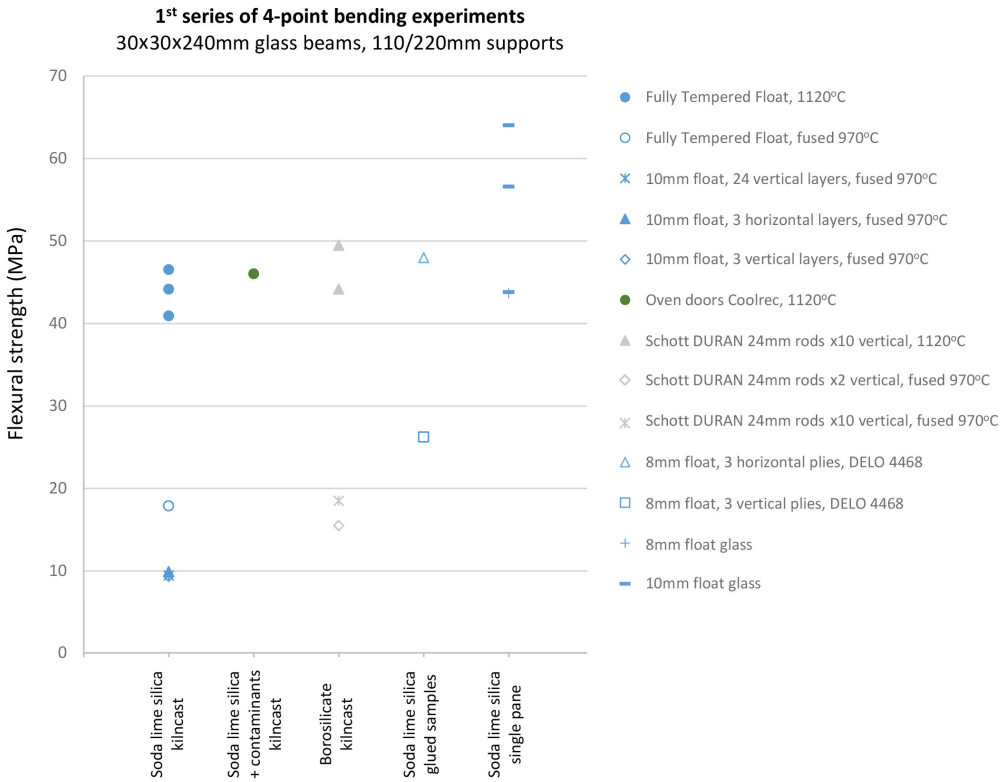

Fig. 3.23 Flexural strength results of 1st series of four-point bending experiments.

Table 3.5: Results of 1st series of four-point bending experiments concerning the kiln-cast beams.

1st four-point bending experiment: Kilncast glass beams 30x30x240mm, 110/220mm supports						
Glass type	Specimen description	Forming temperature (°C)	No. of tested specimens	Flexural strength (MPa) Minimum	Maximum	Average flexural strength (MPa)
Soda Lime Silica (Float Glass)	Fully Tempered float	1120	3	40.9	46.5	43.9
	Fully Tempered float	970	1	17.9		-
	Float 10mm x3 horizontal layers	970	1	9.5		-
	Float 10mm x24 vertical layers	970	1	9.9		-
	Float 10mm x3 vertical layers	970	1	9.4		-
	Oven doors	1120	1	46.1		-
Borosilicate	DURAN rods x10 vertical	1120	2	44.2	49.5	46.8
	DURAN rods x10 vertical	970	1	15.5		-
	DURAN rods x2 vertical	970	1	18.5		-

Table 3.6: Results of 1st series of four-point bending experiments concerning the reference beams.

1st four-point bending experiment: reference beams (240mm length), 110/220mm supports						
Glass type	Specimen description	Width	No. of tested specimens	Flexural strength (MPa) Minimum	Maximum	Average flexural strength (MPa)
	Float 8mm, 3 horizontal layers glued with DELO 4468	30	1	48		-
Soda Lime Silica	Float 8mm. single pane	30	1	43.7		-
	Float 10mm. single pane	50	3	43.8	64	54.8

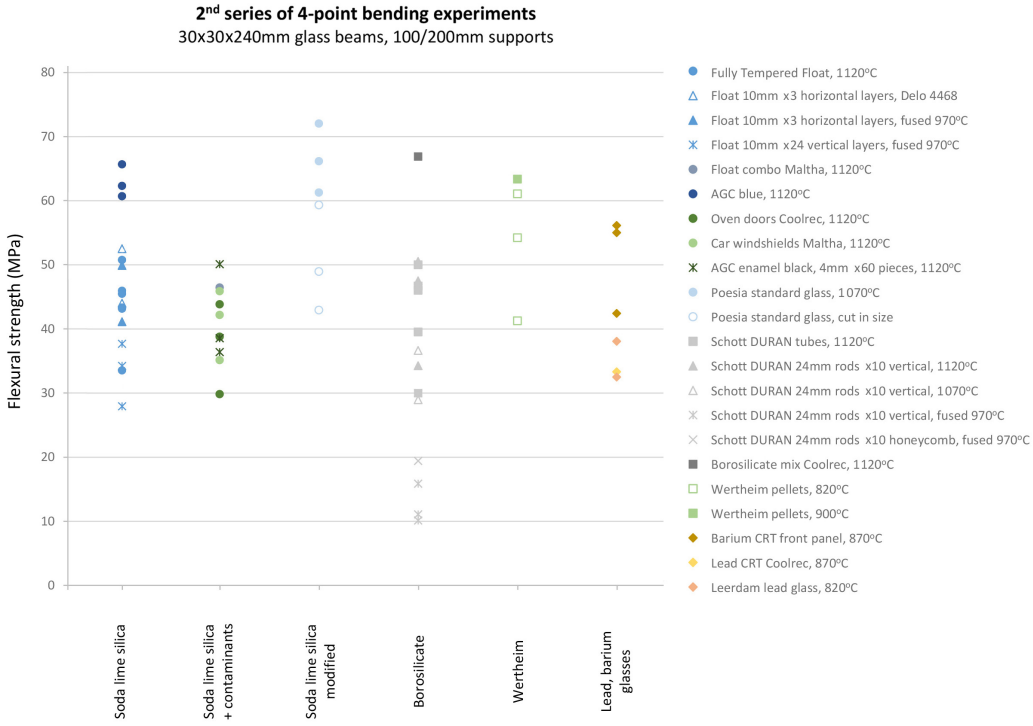

Fig. 3.24 Flexural strength results of 2nd series of four-point bending experiments.

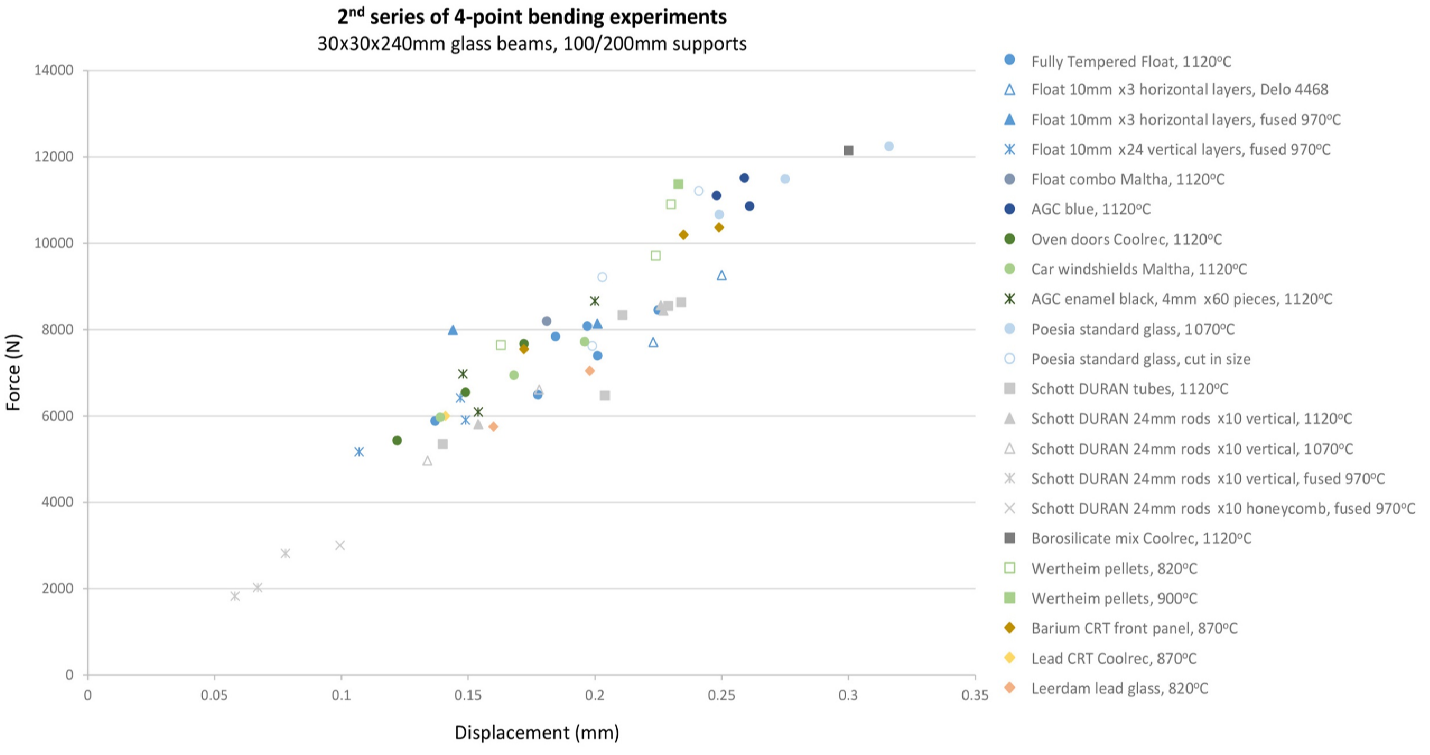

Fig. 3.25 Force vs. Displacement graph. The displacement is measured from the DIC analysis.

Table 3.7: Results of 2nd series of four-point bending experiments concerning the kiln-cast beams.

2nd four-point bending experiment: Kilncast glass beams 30x30x240mm, 100/200mm supports							
Glass type	Specimen description	Forming temperature (°C)	No. of tested specimens	Flexural strength (MPa) Minimum	Maximum	Average flexural strength (MPa)	Average E modulus (GPa), LVDT calculation*
Soda Lime Silica (Float Glass)	Fully Tempered float	1120	6	33.5	50.8	43.7	59.3
	Float 10mm x3 horizontal layers	970	2	41.1	49.9	45.5	59.7
	Float 10mm x24 vertical layers	970	3	27.9	37.7	33.3	58.6
	Float dark blue	1120	3	60.7	65.7	62.9	62.3
Soda Lime Silica (Float Glass) with contamination	Float combo	1120	1		46.5	-	61.8
	Oven doors	1120	3	29.9	43.8	37.5	58.3
	Car windshields	1120	3	35.2	45.9	41.1	59.8
	Float with black enamel x60 layers	1120	3	36.4	50.1	41.7	60.7
Modified Soda Lime Silica	Poesia standard cast brick	1070	3	61.3	72.1	66.5	61.1
Borosilicate	DURAN tubes	1120	5	30	50	42.5	52.4
	DURAN rods x10 vertical	1120	3	34.3	50.6	44.1	53
	DURAN rods x10 vertical	1070	3	24.5	36.7	30	50.9
	DURAN rods x10 vertical	970	3	10.1	15.9	12.4	36.9
	DURAN x24mm rods, honeycomb	970	1		19.4	-	41
	Borosilicate mix Coolrec	1120	1		66.9	-	59.2
Wertheim (C-glass)	Wertheim pellets	820	3	41.3	61.1	52.2	62.6
	Wertheim pellets	900	1		63.4	-	64.6
Barium-Strontium silicate	Barium CRT front panel	870	3	42.4	56.1	51.2	58
Potassium-Lead silicate	Lead CRT funnel	870	1		33.3	-	56.1
	Lead glass	820	2	32.5	38.1	35.3	49.8

* The LVDT calculation results in a lower than expected Young's modulus by approximately 15%, due to sensor errors.
The provided data are only for comparison between the different glass types.

Table 3.8: Results of 2nd series of four-point bending experiments concerning the reference beams.

2nd four-point bending experiment: reference beams 30*30*240mm, 100/200mm supports						
Glass type	Specimen description	No. of tested specimens	Flexural strength (MPa) Minimum	Maximum	Average flexural strength (MPa)	Average E modulus (GPa), LVDT calculation*
Soda Lime Silica	Float 10mm, 3 horizontal layers glued with Delo 4468	2	44	52.5	48.3	49.7
Soda Lime Potash Borosilicate	Poesia standard cast glass brick, cut & polished	3	42.9	59.3	50.4	59

* The LVDT calculation results in a lower than expected Young's modulus by approximately 15%, due to sensor errors.
The provided Young's modulus data are only for comparison between the different glass types.

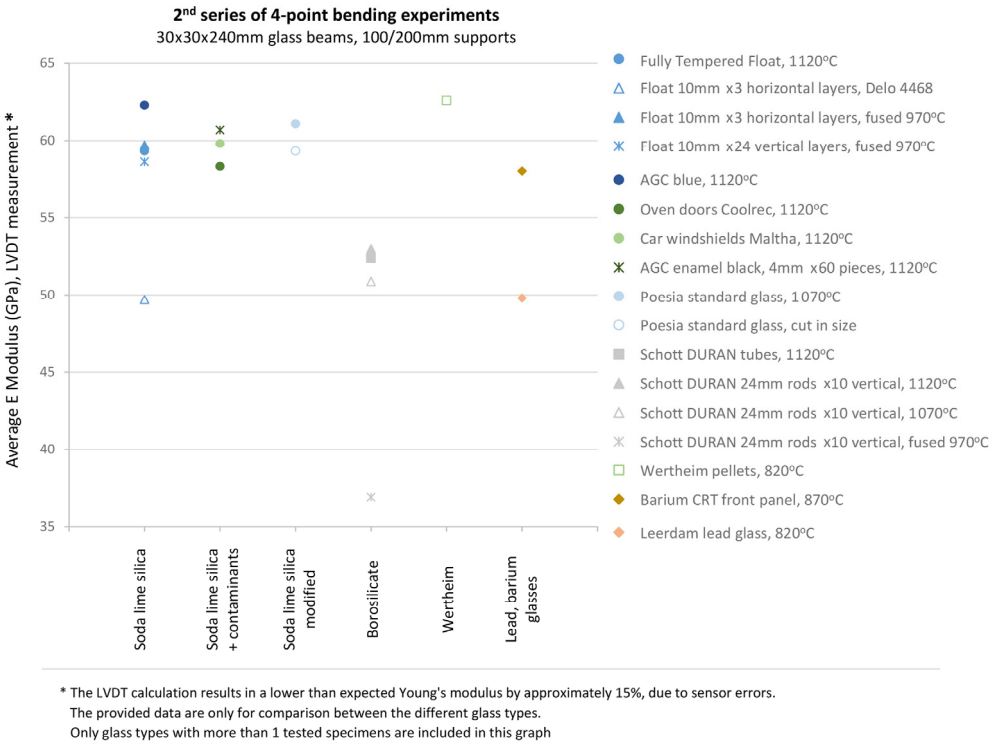

Fig. 3.26 Comparative graph of the Young's modulus measured by the LVDT sensor during the 2nd series of four-point bending experiments.

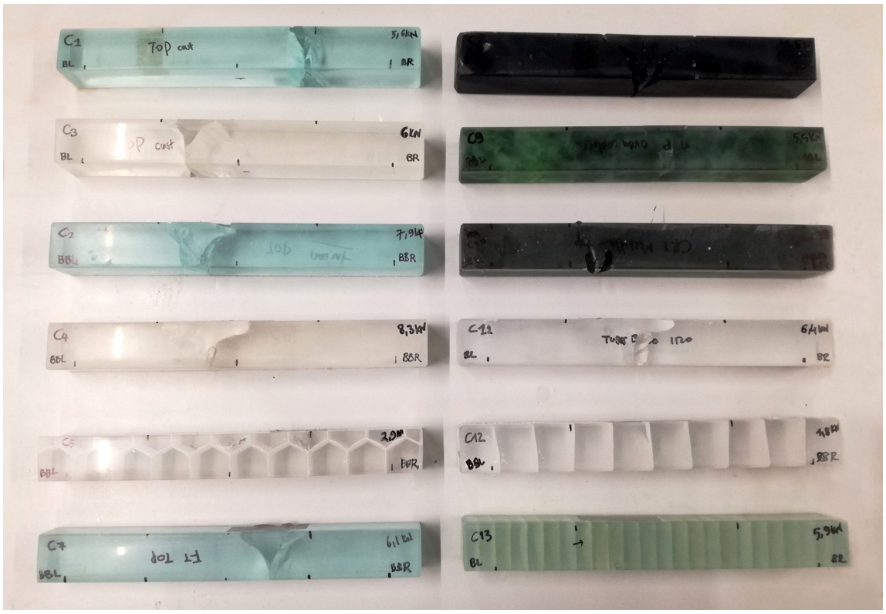

Fig. 3.27 Side view of kiln-cast specimens fractured during the 2nd series of four-point bending tests. Note that the primary crack starts perpendicular to the beam's long axis and then splits in the case of medium/large accumulated elastic energy (prior to cracking), or propagates as one crack in the case of low energy (e.g. crystallized specimens). At the top (compressive zone), the crack forms compression curls.

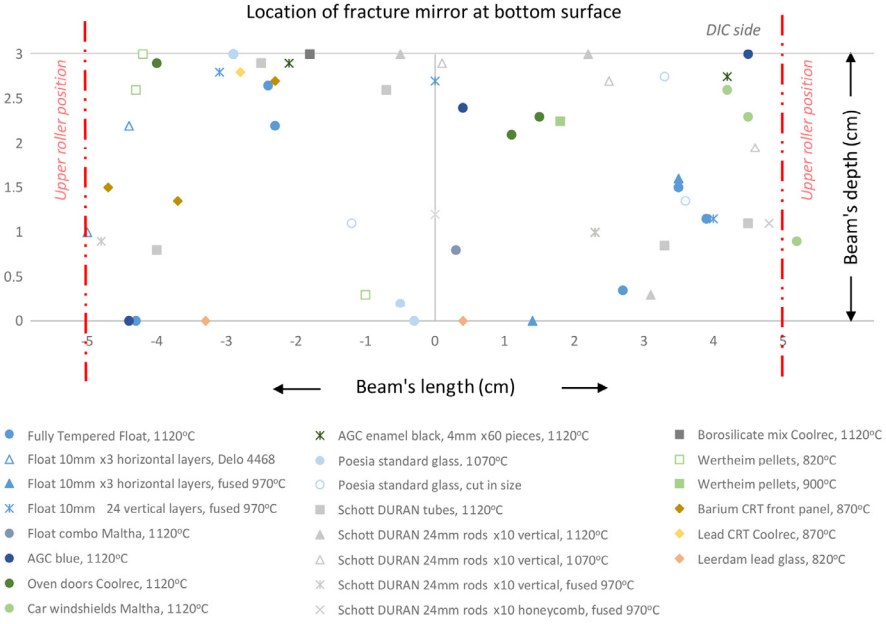

Fig. 3.28 Graph depicting the location of the fracture origin of the 2nd series specimens at the bottom surface. Note that fracture origins found at the two long edges are usually related to machining flaws.

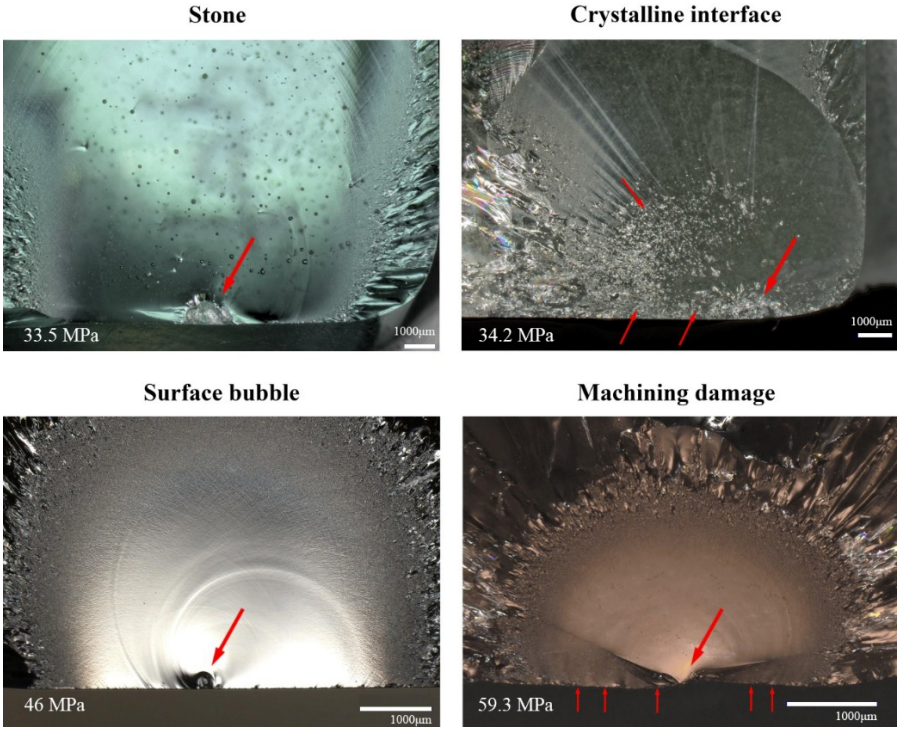

Fig. 3.29 Mirror surfaces of fractured specimens (2nd series of experiments) depicting the main defect categories responsible for catastrophic failure. The reported flexural strength is linked to the type of defect but also to its size.

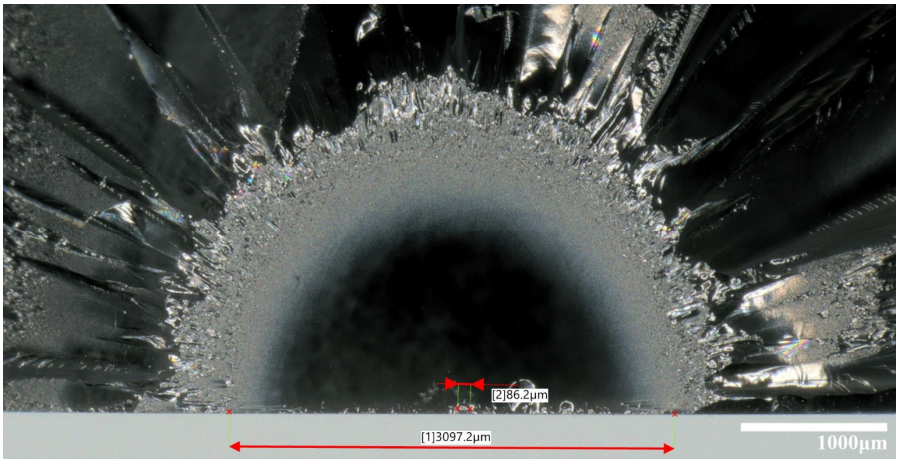

Fig. 3.30 Measuring example of the fracture mirror and defect size at origin. All measurements are conducted employing a Keyence VHX-7000 Digital Microscope and with the fractured surface positioned perpendicularly to the microscope's optical path. To obtain the mirror radius, the diameter of the mist-hackle boundary at the bottom surface line (maximum tensile stress) is measured and then divided by half. This method is chosen as not all mirrors are found to be semi-circular. Specifically, due to the stress gradient along the height of the sample (due to loading in bending), the mirrors appear elongated in this direction, or may even be incomplete. Therefore a measurement along the bottom surface is preferred. Moreover, extended flaws at the surface or machining damage can cause the one-sided elongation of the mirror, and thus the measurement of the diameter instead of the radius is opted.

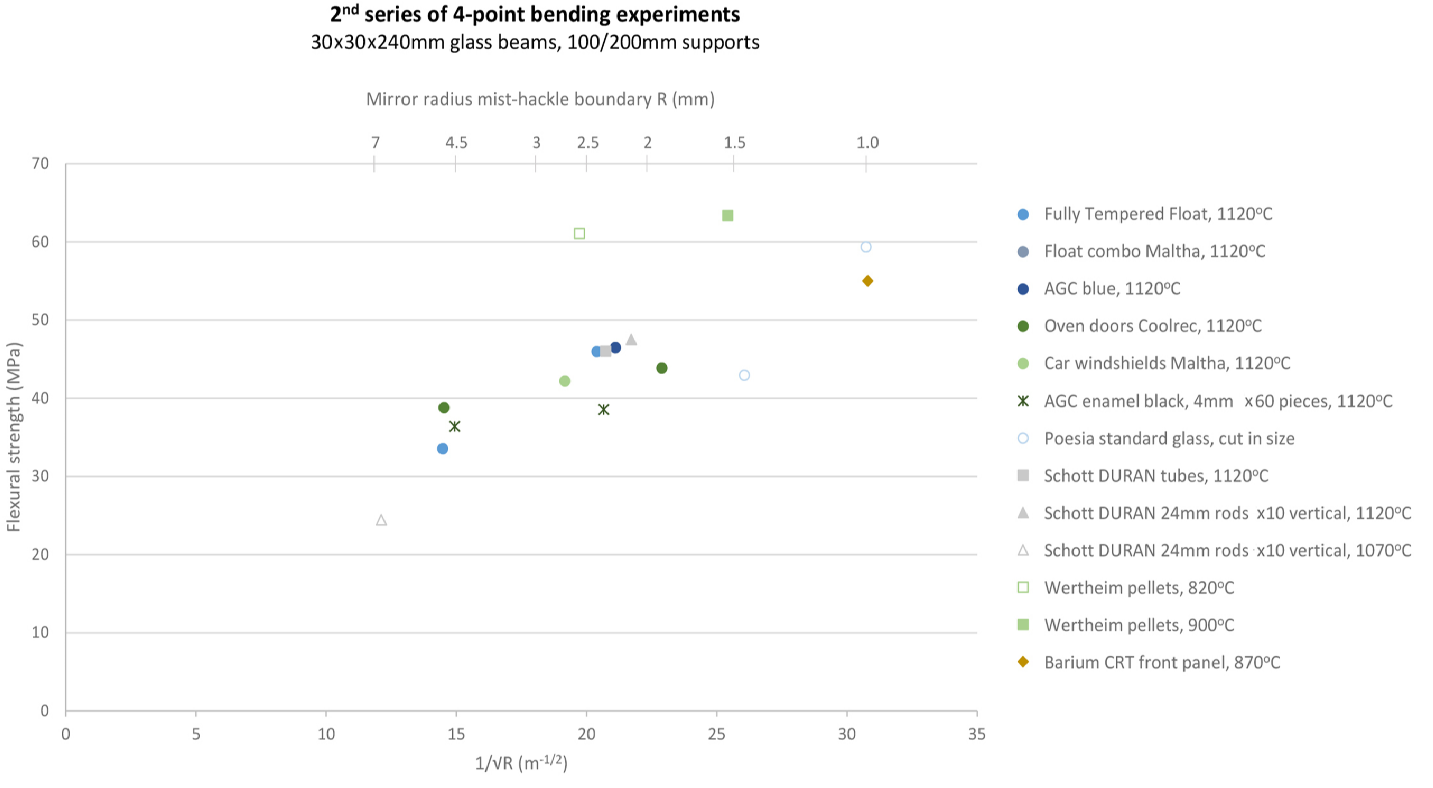

Fig. 3.31 Flexural strength versus 1/√R graph for a selection of glass specimens. In general, the higher the strength, the smaller the mirror size. However, since the mirror size to strength relationship of different glass compositions is reported, more than one mirror constants A are applicable, and thus the data are not all corresponding in one line (e.g. “Wertheim pellets” samples).

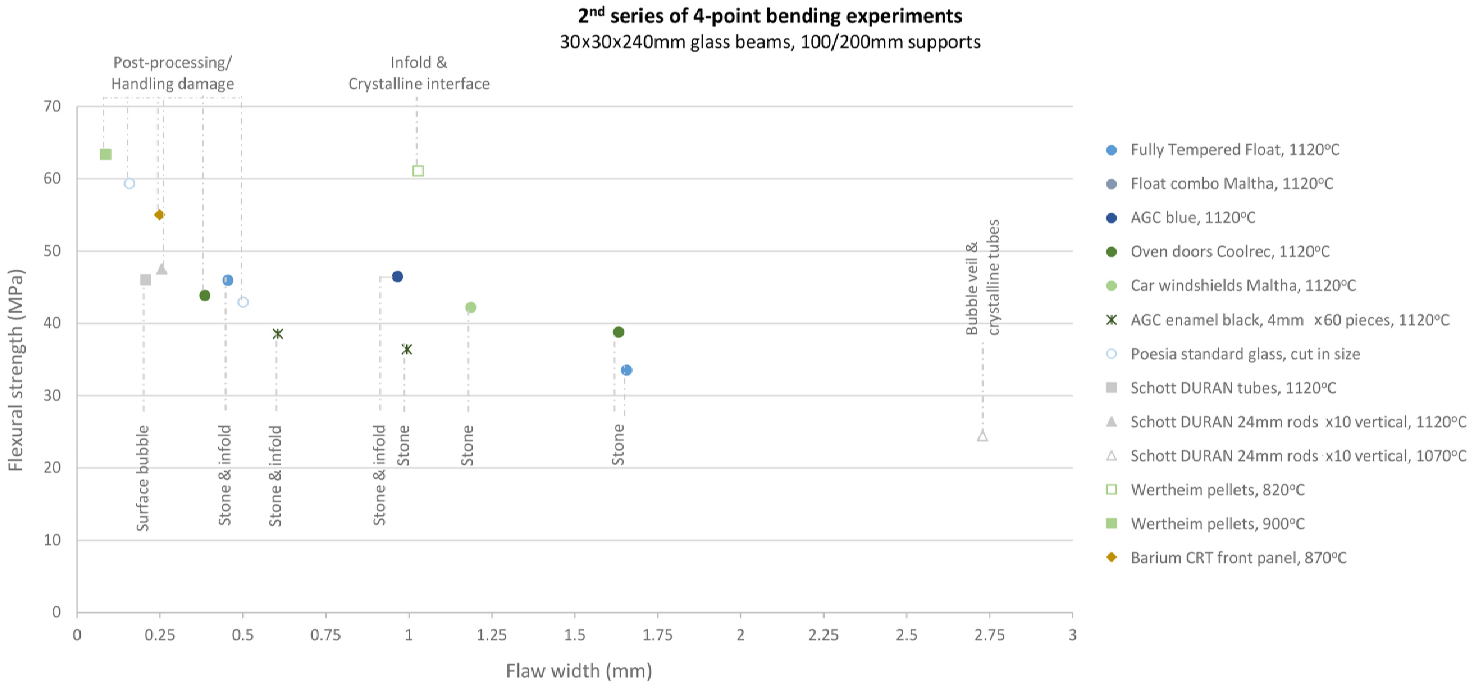

Fig. 3.32 Flexural strength versus critical flaw size (at fracture origin) for a selection of glass specimens. The strength reduces with the increase of the flaw size, and specimens with surface stones tend to fail at lower strength values than the purer samples that fail from post-processing and handling flaws.

3.4 Discussion

The flexural strength of the cast glass specimens is conjointly related to their chemical composition and inherent defects. To comprehend in which cases the flaws are the strength limiting factor and when the mechanical properties related to the composition have a determining role, the interpretation of the results is structured in the following categories: a. Non-contaminated glass specimens, b. Contaminated vs. non-contaminated glass, c. Non-contaminated homogeneous glass specimens vs. with crystallized interfaces, and d. Reference specimens. In this manner, the defects are categorized and isolated so their effect can be studied with more clarity, while the absence of overruling flaws (in the case of the pure samples) highlights the effect of the chemical composition.

a) Non-contaminated glass specimens

The purest, most homogeneous samples of each glass family included in this work are selected for comparison (Figure 3.33, 3.34). As these examples contain less imperfections, the effect of their chemical composition on their flexural strength is highlighted. Table 3.9 lists relevant calculated and/or measured physical and mechanical properties of these glasses, along with data found in literature for similar compositions.

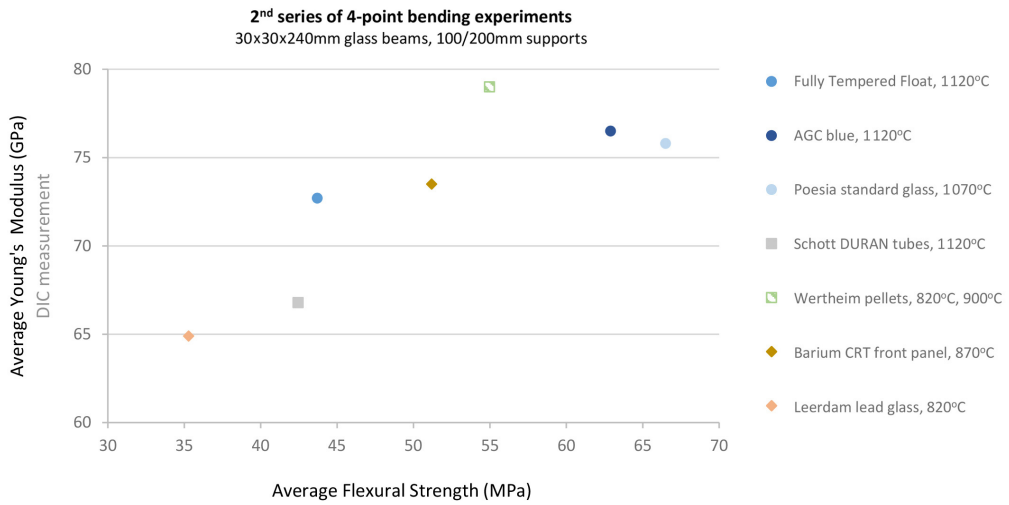

Fig. 3.33 Average flexural strength to Young's modulus graph concerning the non-contaminated kiln-cast specimens of the 2nd series.

Table 3.9 (part a, extends horizontally to the next page): Measured and calculated properties of the selected (pure) glasses (in bold), and reference glasses of similar composition.

Glass Type	Name	Composition (wt%)														Annealing Point 10^{13} dPa · s (°C)	Density (g/cm^3)
		SiO_2	B_2O_3	Na_2O	K_2O	CaO	MgO	Al_2O_3	PbO	Fe_2O_3	Sb_2O_3	ZnO	BaO	SrO	Source		
Soda Lime Silica	Standard float	70-74		12-16	0-0.5	8-13	0-5	0-2		0.01-1.5					[1]	525-545 [3]	2.48-2.52 [1]
	PPG Starphire (low iron)	74.6		13.3		8.9	3	0.04							[5]	547 [4]	2.51 [4]
	FT Float	75.4		12.4		7.6	4	0.4		0.09					[5]	553 [6]	2.466 [7]
	AGC blue	73.1		12.8		8.1	4	0.9		0.76					[5]	550 [6]	2.492 [7]
Modified Soda Lime Silica	**Poesia glass**	72.1	2.5	15.9	1.9	6.1	0.06	0.3			0.9				[5, 8]	≈520 [6]	2.486 [7]
Borosilicate	Corning 7740 Pyrex	80.6	13	4				2.3							[9]	560 [10]	2.23 [10]
	Schott DURAN	81	13	4				2							[11]	560 [12]	2.23 [11]
C-Glass	Johns Manville 753 C-glass fibers	63.5	5.5	14.6	1	6	3	5.5		0.1					[14]	527 [14]	2.52 [16]
	Wertheim glass	63.8	5.5	11.8	3.2	6.4	3.7	5.2		0.06			0.08		[5, 14]	550 [6]	2.502 [7]
SrO/BaO Silicate	Corning 9068	63.2		7.1	8.8	1.8	0.9	2	2.3		0.4		2.4	10	[17]	503 [17]	2.696 [16]
	Philips CRT panel	61.6		7.2	6.8	1.1	0.3	2.3		0.1			8	8	[5]	530 [6]	2.766 [7]
Potassium-Lead-Silicate	Corning 0120	55	3	4	9			2	27						[18]	435 [10]	3.050 [10]
	Leerdam glass	57.7		3	9				28.7		0.8	0.6			[5]	465 [6]	3.031 [7]

Sources

[1] Quinn et al. (2017)
[2] Shelby (2005)
[3] Martienssen and Warlimont (2005)
[4] Specialty Glass Products
[5] XRF measurements conducted by Ruud Hendrikx
[6] Calculated using viscosity model by Fluegel (2007a)
[7] Calculated using density model by Fluegel (2007b)
[8] Personal correspondance with Poesia
[9] Friedrich & Dimmock Inc.
[10] Corning (1979)
[11] Schott (2015)
[12] Schott (2017)

* Properties corresponding to a generic c-glass fiber

** Calculated based on data from Inaba et al. (1999)

*** (III) Corresponds to B_2O_3 with coordination number= 3, (IV) to B_2O_3 with coordination number= 4. The coordination number ratio for the Schott DURAN glass is calculated using the formulas proposed by Yun and Bray (1978). For the Poesia, Wertheim and Corning 0120 glass, a 100% four-fold coordination is assumed given the high alkali/boron ratio (Priven 2000; Zhdanov 1975).

Table 3.9 (part b, extends horizontally from the previous page): Measured and calculated properties of the selected (pure) glasses (in bold), and reference glasses of similar composition.

Poisson's ratio	Knoop Hardness KHN100	Molar volume V_m (cm^3/mol), calculated	APF Calculated based on Pauling's ionic radii	G_t Total Dissociation energy (kJ/cm^3), calculated**	E (GPa), calculated^	E (GPa) from literature	E (GPa) from LVDT data	E (GPa) from DIC data	Average Flexural Strength (MPa) 2nd four-point bending tests
0.22-0.23 [1]	550 [4]					70-75 [2]			
0.22 [4]	448 [4]	23.55	0.5492	64.03	70.33	73.1 [4]			
		23.92	0.5413	64.84	70.19		59.3	72.7	43.71
		23.81	0.5436	64.87	70.52		62.3	76.5	62.9
		24.65	0.5471	61.84 (IV)***	67.67 (IV)***		61.1	75.8	66.5
0.20 [10]	418 [10]					64 [10]			
0.20 [11]	480 [13]	27.53	0.5383	64.13 (B_2O_3 66% III, 34% IV)***	69.04 (B_2O_3 66% III, 34% IV)***	63 [11]	52.4	66.8	42.45
0.27* [15]			0.5586	66.01 (IV)***	73.74 (IV)***	68.9* [15]			
		24.56	0.5555	66.38 (IV)***	73.75 (IV)***		63.6	79	54.98
			0.5456	61.00	66.56	69.6 [14]			
		25.24	0.55	62.22	68.20		58	73.5	51.19
0.22 [10]	382 [10]		0.5484	60.17 (IV)***	65.99 (IV)***	60 [10]			
		26.5	0.5288	58.35	61.71		49.8	64.9	35.29

[13] Abrisa Technologies, 2014

[14] Campbell and Hagy (1975)

[15] Matweb

[16] ASM International, 1995

[17] Thompson (1980)

[18] Gregory (1998)

^ Calculated using V_i values from Makishima & Mackenzie (1972), and G_i values from Inaba et al. (1999)

^^ The LVDT calculation results in a lower than expected Young's modulus by approximately 15%, due to sensor errors. The provided data are only for comparison between the different glass types.

^^^ The reported E modulus is approximately 5% higher than in literature, partly due to testing errors and partly due to the material itself and its casting procedure.

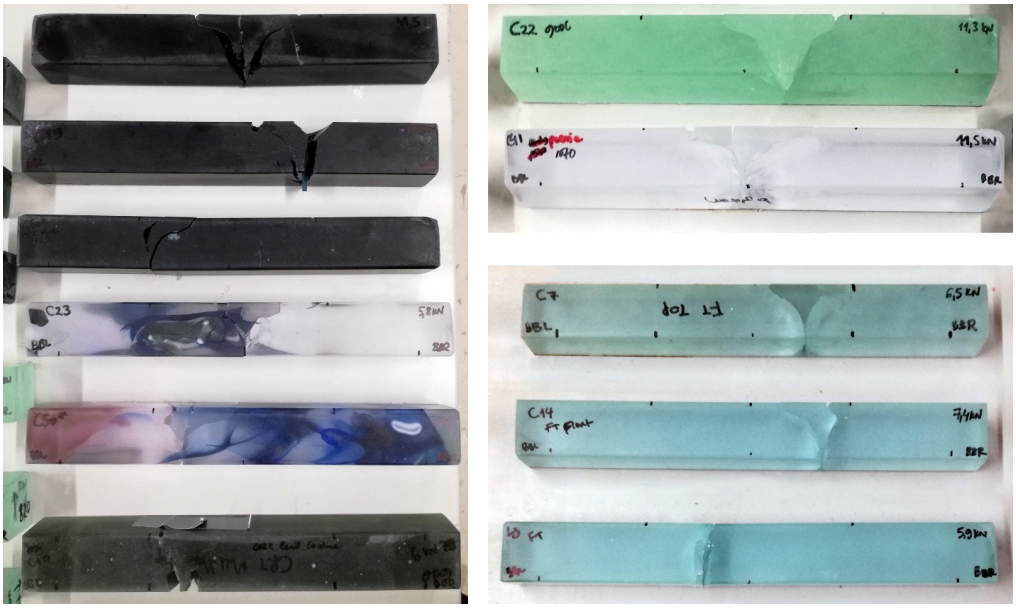

(a) (b)

Fig. 3.34 Side surface of fractured specimens. (a) First three specimen correspond to "AGC dark blue float 1120ºC" glass, then the next two are "Leerdam 820ºC", followed by a "Barium CRT 870ºC" glass. (b) From top to bottom: "Wertheim 900ºC", "Poesia 1070ºC" and three "FT Float 1120ºC" specimens.

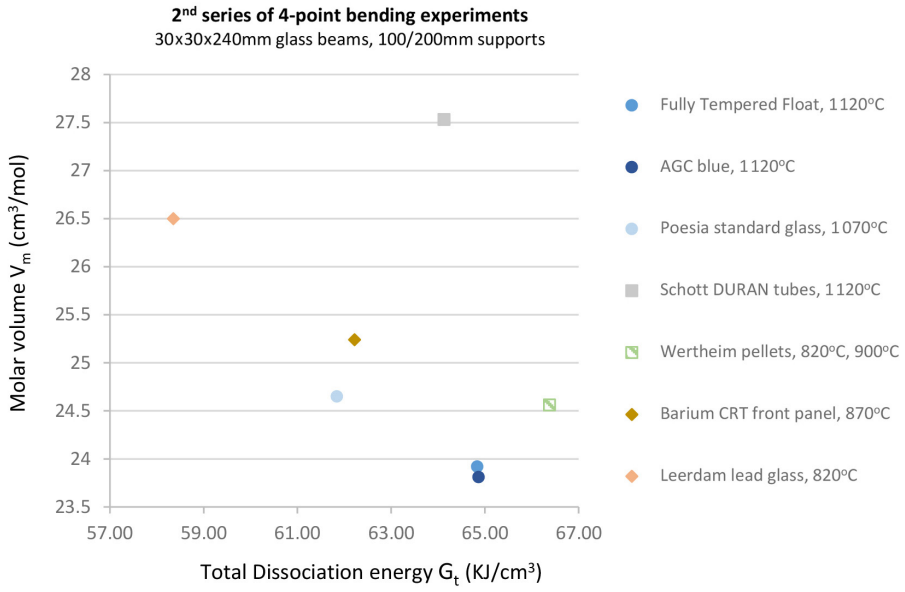

Fig. 3.35 Graph of total dissociation energy vs. the molar volume.

As seen in Figure 3.35, there is an increase in the flexural strength with increasing Young's modulus[38], in the lead silicate, borosilicate, barium silicate and AGC dark blue float glass samples. The increase in strength is attributed to the increase of the average bond strength and atomic packing density of the glass network. This is related to the Young's modulus by the equation below (Makishima and Mackenzie 1973):

$$E = 2 \cdot C_g \cdot G_t \quad (8)$$

where C_g is the atomic packing density (also mentioned as Atomic Packing Factor, APF), and G_t the total dissociation energy per unit volume. Based on the chemical compositions derived by the XRF analyses, the APF[39] and G_t[40] are calculated and listed in Table 3.9.

Therefore, by reviewing Table 3.9, it is anticipated that the lead silicate glass samples, which present the lowest dissociation energy and packing density, will have the lowest strength as well[41], while the soda lime silica (SLS) glasses will have the highest strength. Also in accordance with the literature, the BaO containing silicate glass has a lower flexural strength and Young's modulus than the CaO silicates but higher than the lead silicates (Volf, 1984; Corning 1979). However, the Young's modulus alone cannot justify the deviation from the linear E/strength relationship that the Poesia, Wertheim, and FT float glass samples present, and further explanation is required per glass type.

The Poesia glass is a modified soda lime silica glass with a decreased forming temperature compared to conventional float glass (T_L is at around 980°C, therefore 80-100°C lower than for SLS). It contains K_2O and B_2O_3 in small amounts (<3 wt%), and has a higher Na_2O/CaO ratio than typical SLS recipes. Despite the slightly lower E modulus[42] than the one of AGC dark blue

---

[38] The graph in Figure 3.33 is based on the Young's modulus calculated from the DIC measurements. The reported E modulus is approximately 5% higher than in literature, which could be partly related to testing errors and partly to the material itself and its casting procedure.

[39] The atomic packing density is calculated using the following formulae:

$$APF = \frac{\sum x_i \cdot V_i}{V_m} \quad (9)$$

Where x_i is the molar fraction, V_i the ionic volume of the i^{th} oxide and V_m is the molar volume of glass, and specifically:

$$V_i = \frac{4}{3} \cdot \pi \cdot N_A \cdot (x \cdot r_A^3 + y \cdot r_B^3) \quad (10) \qquad \text{and} \qquad V_m = \frac{M}{\rho} \quad (11)$$

Where N_A is the Avogadro's number, $r_{A,B}$= ionic radii of M_xO_y oxide, M is the molecular mass and ρ is the density of the glass. The V_i is derived from Makishima and Mackenzie (1973) and Inaba et al. (1999) based on Pauling's ionic radii. The density is calculated from the chemical composition using the model developed by Fluegel (2007).

[40] The total dissociation energy is calculated from the dissociation energy of the oxide constituents listed in the work of Inaba et al. (1999).

[41] PbO has one of the lowest G_i values as reported by Makishima and Mackenzie (1973), and a relatively high molar atomic mass. The increased mass of the lead ion slows down the chemical reactions during quenching, and results in a less organized/packed network.

[42] It should be noted that the calculated E_{Poesia} using the APF and G_t corresponding to the chemical composition is found much lower than the $E_{AGC\ blue}$. This could be related to an incorrect estimate of the B_2O_3 content, which cannot be determined by the XRF analysis, and/or a higher packing density attributable

glass, it presented the highest flexural strength among all tested specimens. This is attributed to a lower brittleness of this particular glass. Sehgal and Ito (1998) state that a higher molar volume (V_m) plays a key role in the reduction of the brittleness, as a more open structure allows more deformation prior to crack initiation. Specifically, an increasing soda/calcia ratio would decrease the brittleness, as well as the partial substitution of soda for potassium oxide. This is in accordance with the compositional variations of Poesia glass to the typical SLS recipe, which contribute to a more open structure (Figure 3.35) that allows for a slightly increased accommodation of the stresses around the point/flaw where the crack will initiate. The "Poesia 1070ºC" specimens failed due to machining damage (Figure 3.36).

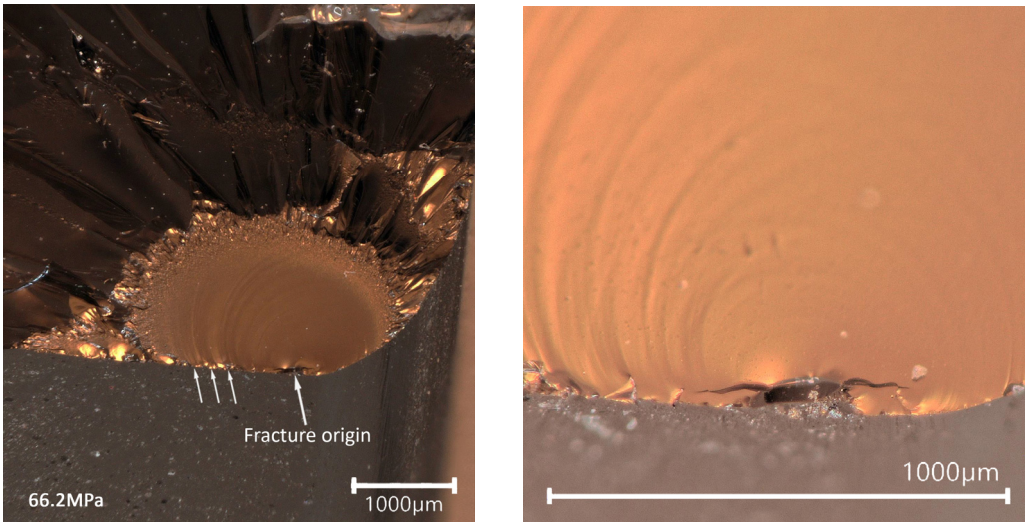

(a) (b)

Fig. 3.36 (a) Microscope image of the bottom surface and corner, and the fracture surface of a "Poesia 1070ºC" specimen. The cause of failure is grinding damage, which is demonstrated by the fracture mirror elongation to the left and the consecutive machining crack hackles along the fractured edge. (b) close-up of the fracture origin.

The Wertheim glass has the highest measured Young's modulus and the highest calculated total dissociation energy, while it's calculated molar volume is similar to the Poesia glass. The higher stiffness (in comparison to an SLS glass) can be attributed to the partial substitution of silica with alumina (≈5%), that reduces the openness of the network (Seghal and Ito 1998). Similar to the Poesia glass, it has a lower forming temperature than SLS glasses (T_L at around 1015ºC), which can be linked to the mixed alkali effect[43] and the presence of boron trioxide in a small quantity (Morey 1932). According to the E/V_m properties of this glass, a much higher flexural strength should have been expected. The reason this glass failed at a lower stress is linked to its kiln-

to the thermal history of the kiln-cast components. The E_{Poesia} derived from the LVDT data is thus considered more reliable for further analysis.

[43] The term describes anomalies observed in glasses and melts containing a mixture of two or more alkali oxides. According to Shelby (2005), the viscosities of such melts are lower than those containing the same amount of a single alkali oxide.

casting at temperatures (820ºC, 900ºC) well below its liquidus point, which resulted in evident inhomogeneities. These inhomogeneities are concentrated in the interface created between each pellet of glass, and compose a 3-dimensional network of planar zones consisting of bubbles and loose crystal formations. In addition, the forming temperature favours the occurrence of stones, due to the reaction of the hot glass with the mould, which are sufficiently sub-surface that they cannot be entirely removed during standard post-processing. These stones seem to weaken the glass surface and contribute to the formation of deeper striations during grinding, which are the sources of failure. The above described 3D network may not be responsible for the crack origin, but given that the specimens fail from a flaw in close proximity to the network, it may contribute to zones of concentrated stress along the surface (Figure 3.37).

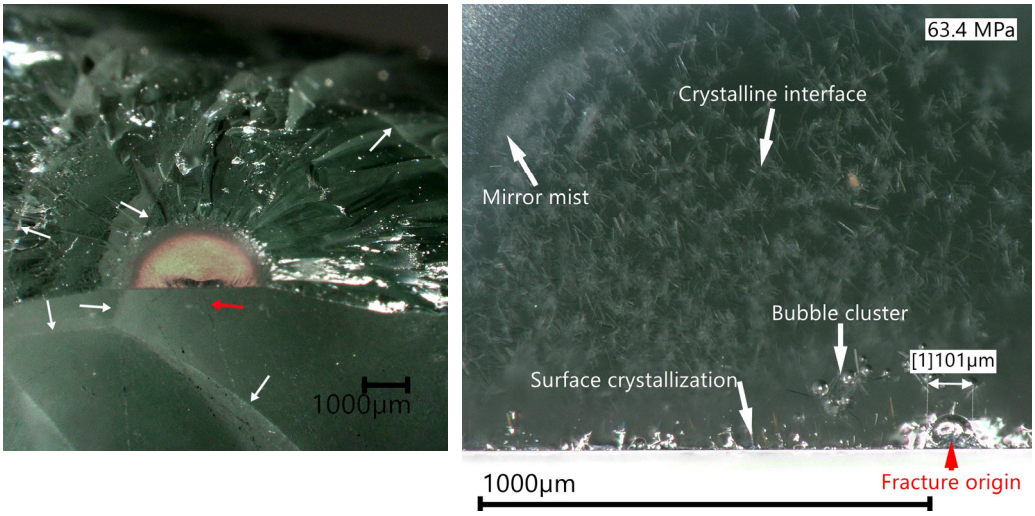

Fig. 3.37 Fracture surface of the "Wertheim 900ºC" specimen. (a) Microscope image showing the bottom surface and fracture mirror. The specimen failed from a grinding scratch (red arrow) next to the fusion interface (white arrows). (b) Close-up of the mirror and the crystalline interface located just below the fractured surface (only the crystal formations along the bottom surface are fractured).

It is also interesting to compare the "AGC dark blue float" to the "FT float" specimens. These two glasses have very similar compositions and are almost identical in calculated atomic packing density and total dissociation energy. However, the measured Young's modulus of the "FT float" glass specimens is lower, and so is the flexural strength. This is probably linked to the thermal history of these two glasses. On the one hand, the "AGC dark blue" glass has a slightly lower liquidus point (T_L is around 1046ºC, while for the "FT Float" is 1063ºC). On the other hand, the dark colour of the AGC glass seems to contribute to the quality of the casting. The dense dark blue colour absorbs more infra-red light during heating than the transparent light blue, thus the body will heat up faster. In a similar manner, the dark glass will set faster during cooling due to the greater heat loss by radiation (Kitaĭgorodskiĭ et al. 1934; Burch et al. 1938). The faster setting rate can influence the coordination state of the transition metal oxides included in the

composition[44] and thus affect the total dissociation energy of the network bonds- something not accounted for in the calculations. In addition, the lower liquidus point and increased heat absorption promote the full fusion of the cullet pieces and the elimination of stone formation, thus leading to the diminishing of flaws at the glass surface, and to a higher flexural strength. In antithesis, infolds at the glass surface of the "FT float" specimens are created by insufficient fusion of the cullet positioned next to the mould walls, and crystalline inclusions due to contamination from the mould, are the main cause of failure of the "FT float" samples, according to the analysis of the fracture mirrors (Figure 3.38). Due to these flaws, the "FT float" glass specimens fail at values lower than expected in comparison to the rest of the samples.

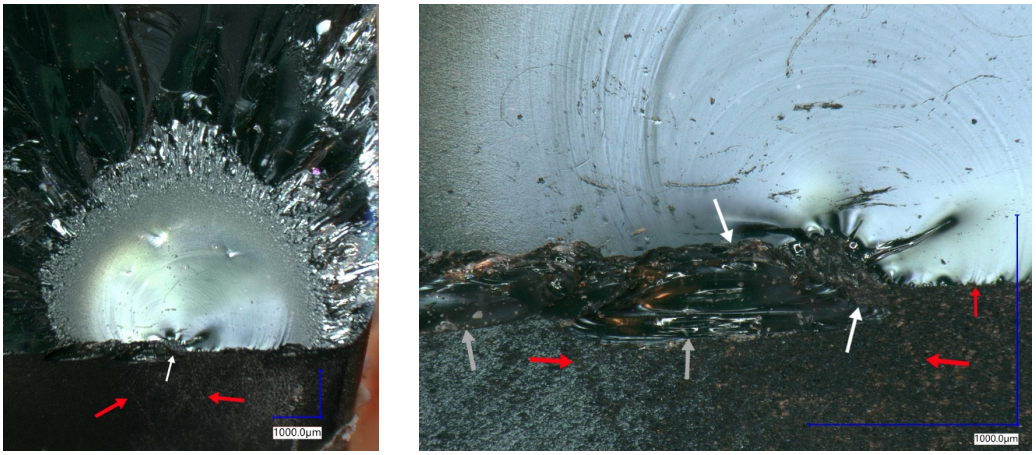

(a) (b)

Fig. 3.38 Microscope images of the bottom and fracture surface of a "FT Float 1120ºC" specimen, showing the fracture origin (Fig. 3.38b is a magnification of the fracture origin). The cause of failure is a combination of grinding scratches (red arrows) acting upon a surface infold with crystalline inclusions (white arrows). The hertzian cones (grey arrows) that refer to impact damage have an opposite to the crack front direction and are considered secondary breaks. Looking through the hertzian cones, traces of crystalline inclusions can be observed.

Regarding the fracture analysis of the glasses studied in this category, the most prevailing causes of failure are found to be machining damage and handling flaws (see also Figure 3.28, most "pure" specimens fail at an edge flaw), justifying that the purity of the cullet and the relatively high forming temperatures (in comparison with other glass samples in this work) eliminate the quantity of strength limiting flaws. Exceptions are found in the "FT float" series, as described above, and the "Schott DURAN tubes" specimens. These borosilicate glass samples are in fact formed at a high viscosity ($\approx 10^{4.5}$ dPa·s < T_L) and are characterized by an increased amount of bubbles (mainly concentrated at the interfaces created between each cullet piece during forming). These bubbles form clusters for crystal growth and if located at the glass surface or at close proximity, they become the strength limiting flaw that leads to fracture (Figure 3.39). The flexural

[44] The XRF identifies a series of transition metals in this glass that act as colorants: 0.76% Fe_2O_3, 0.065% TiO_2, 0.029% MnO, 0.023% Cr_2O_3)

data obtained for these two glasses from the 1st series of four-point bending experiments match with the results of the second test.

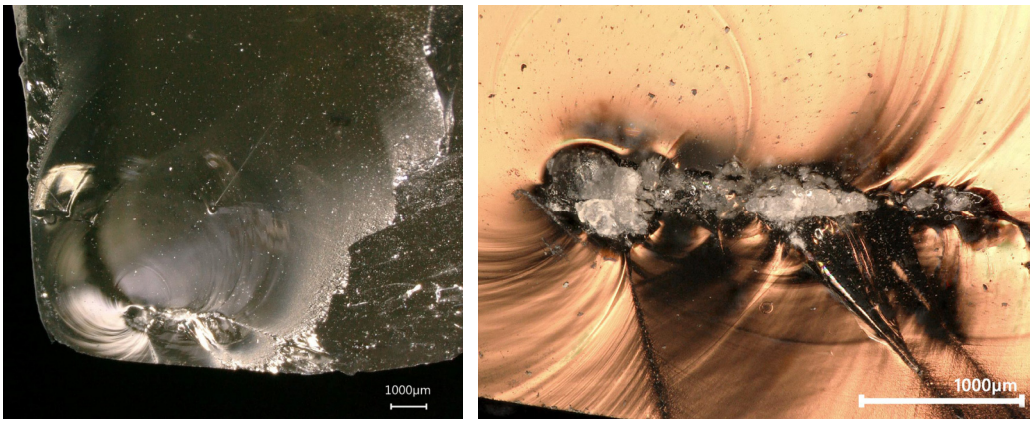

(a) (b)

Fig.3.39 Microscope images of the fracture origin of a "Schott DURAN tubes 1120ºC" specimen. (a) Incomplete fracture mirror around the origin flaw, which is a crystalline inclusion at 1mm inside from the bottom surface. This is the only specimen that did not break at a flaw exactly at the surface. (b) Magnification of the crystalline inclusion, which is clustered together with air bubbles. Early mist and hackle appear within the mirror as a result of interaction of the elastic wave with the defect.

b) Contaminated vs. non-contaminated glass specimens

This category studies glass specimens kiln-cast from contaminated cullet, and compares them to the purer specimens described above. All of the studied specimens, "Float combo", "Oven doors", "Car windshields", and "AGC enamel black" are typical soda lime silicates and have a large amount of distinct crystalline inclusions, and/or heavy cord. Their flexural strength is slightly lower than the one observed for the FT Float specimens and their Young's moduli are comparable. The "AGC enamel black" series seems to have the highest flexural strength in this category, which is attributed to the fact that only one type of glass is used for the casting of these samples (thus no cord is observed due to minor compositional variations). In addition, the substantial size of the glass pieces allows their thorough cleaning, which is not the case in the smaller sized cullet of the "Oven door" and "Car windshield" samples. All specimens fail at lower values than most of the purer glasses studied above, mainly due to crystalline formations at the surface (Figure 3.40). These stones are created either from inherent contamination, or from further reaction of the contaminants with the mould material. The multiple defects located in the bulk of these specimens are not activated during the 4-point bending nor do they seem to reduce the Young's modulus. On the contrary these defects are tolerated within the glass network. However, the more the defects in the bulk, the more the chances of such flaws to be exposed at the surface, and consequently the higher the risk of failure.

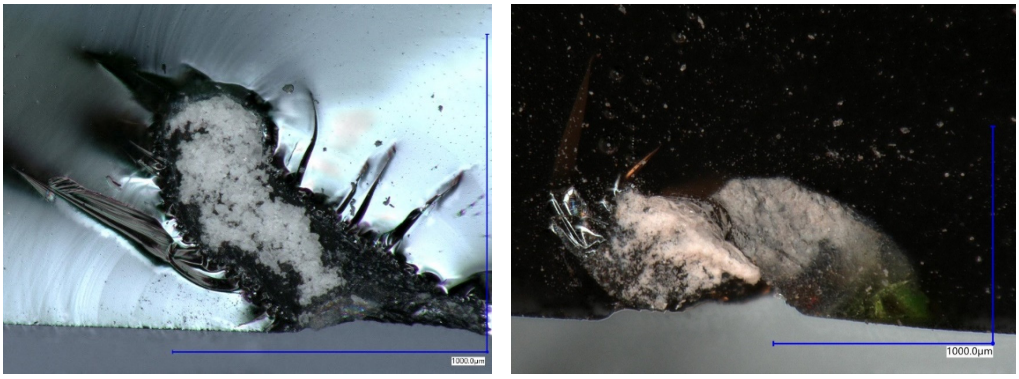

(a) (b)

Fig. 3.40 Microscope images of crystalline formations that function as the origin of fracture in contaminated kiln-cast specimens. The reaction of cullet contaminants (e.g. coatings) with the mould seem to promote such formations. (a) The stone in the "AGC Float with black enamel, 1120ºC" specimen is adjacent to the enamel interface. (b) Stone in a "Oven doors 1120ºC" specimen.

c) Non-contaminated homogeneous glass specimens vs. with crystallized interfaces

In this category, the soda lime silica and borosilicate glass samples that are kiln-formed at 970ºC and contain structured crystallized interfaces ("Float 1cm, 3 horizontal layers", "Float 1cm, 24 vertical layers", "Schott DURAN 10 vertical layers"), are studied in comparison to their more homogeneous versions, kiln-formed at 1070ºC and/or 1120ºC ("FT Float 1120ºC", "Schott DURAN 10 vertical layers 1070ºC, 1120ºC"). The particular aspect with this category is that the "defects" or zones of compositional/structural variation, are deliberately engineered at specified locations and geometrical patterns. Thus, in antithesis with the random occurrence of stones described in the category above, in this section, the size and distribution of the crystalline formations can be anticipated. As a consequence, their effect on the structural performance can be directly correlated.

Therefore, it can be observed that the fused "Float 1cm, 3 horizontal layers" specimens present very similar flexural strength and Young's modulus with the more homogeneous "FT Float" specimens (Figure 3.41). This is because the crystalline interfaces are located in the bulk, in parallel layers to the bottom surface, and thus are not exposed to the maximum tensile stress zone. They behave therefore in a similar manner to the homogeneous specimens. This is not the case however with the "Float 1cm, 24 vertical layers" specimens, where the crystalline interfaces are exposed at the bottom surface, and in fact aligned perpendicularly to the tensile forces. Although the Young's modulus remains similar, the flexural strength is reduced by more than 20%. The fracture origin of these samples is always located at these crystal-glass interfaces and initiates from the glass zone in immediate proximity. The crystalline formations thus seem to act as stress inducing elements, of perhaps higher fracture toughness than the surrounding glass matrix, which weaken the glass specimen.

The type and thickness of the crystalline interface also plays a significant role. The thin β-cristobalite layer created in "Schott DURAN 10 vertical layers 970ºC" results in a dramatic drop of 75% of the strength, and a decrease of the Young's modulus. The fracture origin is, in a similar manner to the float examples, always located at the crystalline-glass interface.

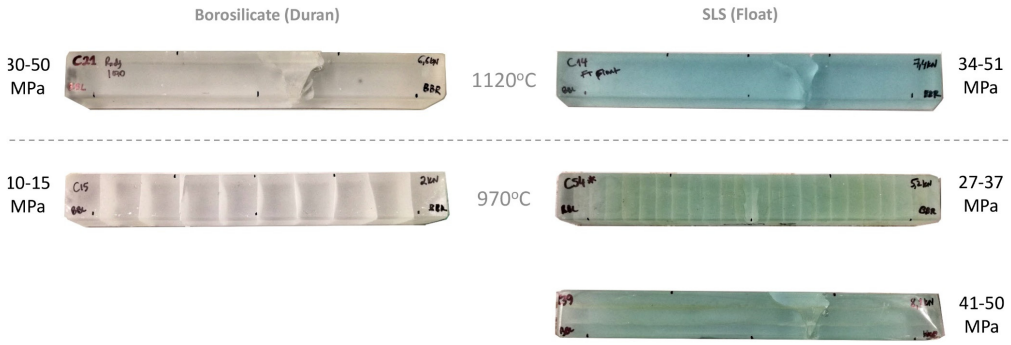

Fig. 3.41 Fracture pattern and flexural strength range (MPa) of homogeneous (top) and with crystallized interfaces (bottom) specimens. Note that if the crystallized interface is situated only in the bulk (bottom right), the bending strength of the specimen is similar to a homogeneous one (top right). When the crystallized interface is exposed at the bottom surface, the specimens fail at a lower force, from a flaw originating at the glass-crystal interface. Especially in the case of the borosilicate crystallized specimens, the low elastic energy stored results in a single crack without forking.

At this point, knowing the effect of these crystalline formations and their geometrical arrangement, attention should be raised to the intermediate states between a fused glass specimen produced at viscosities around 10^6 dPa·s and a homogeneous specimen cast at temperatures well above the liquidus point (where the rate of diffusion is much higher). Specimens produced at a 10^5 or even a 10^4 dPa·s viscosity seem to retain traces of the interface created between each cullet piece during heating up, in the form of subtle bubble veils, cord and spots of crystalline formation. This is evident for example in the "Schott DURAN 10 vertical layers 1070ºC", kiln-cast at a 10^5 dPa·s viscosity (Figure 3.42). These samples contained the above described bubble veils and stones in the same geometrical arrangement as the "Schott DURAN 10 vertical layers 970ºC". These specimens, although stronger than the fused version, had a 30% lower flexural strength than the specimens kiln-cast at a 50ºC higher temperature. They all failed from either a crystalline flaw or a bubble located in one of these veils (Figure 3.43). This is a very crucial issue, given the fact that both the 1070ºC and 1120ºC produced specimens look the same and are transparent and not comparable to the contaminated samples described in the category above. This highlights how critical a 50ºC temperature difference can be when casting at viscosities just around and below the liquidus point.

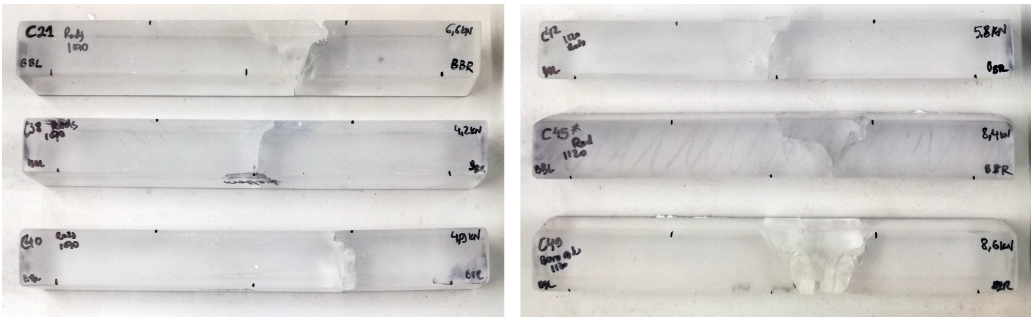

Fig. 3.42 “Schott DURAN 10 vertical layers” specimens produced at 1070ºC (left column) and 1120ºC (right column). The remnant bubble veils in the specimens produced at a lower temperature result in a lower flexural strength. The origin of fracture in these specimens can be found in one of these bubble veils.

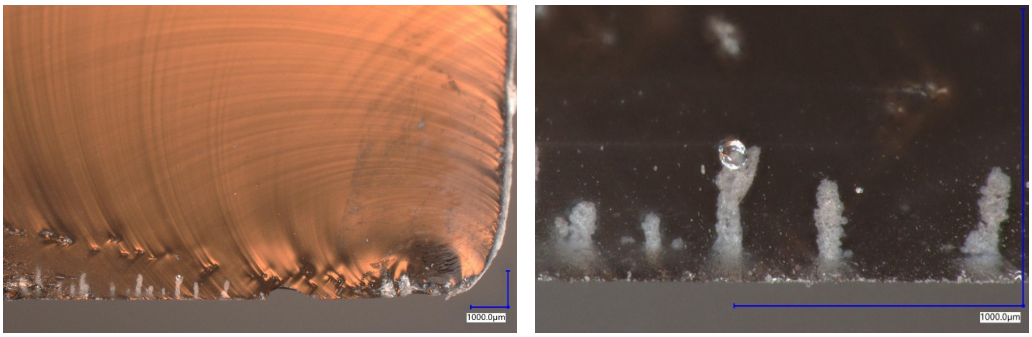

(a) (b)

Fig. 3.43 Microscope images of the fracture mirror of a “Schott DURAN 10 vertical layers, 1070ºC” specimen. (a) Succession of air bubbles close to the bottom surface, interacting with the elastic wave. The cause of fracture is a stone formation (right end of the picture) in proximity to the bubble clustering. (b) Magnification of stone formations extending from the surface to the bulk. Their perpendicular to the surface direction and the presence of a bubble, suggest that these stones are formed from the interaction of the mould material with the bubbles created at the fusion interface between the glass rods during forming at a -favourable for crystallization- temperature.

d) Reference specimens

The industrially manufactured glass specimens are tested in order to provide a point of reference and comparison with the kiln-cast glass samples. Their structural performance is described below per type.

The beams cut out from standard Poesia cast glass bricks (originally hot poured at around 1200ºC) are more homogeneous than the kiln-cast specimens produced in the lab. Apart from some minor striae and few bubbles, they do not contain critical defects such as stones, since the purity of the raw source, the above liquidus point forming temperature, the abrupt quenching at atmospheric conditions, and the stainless steel moulds used for their casting, prevent their formation. Nonetheless, these specimens present a 10% lower flexural strength than the less homogeneous,

re-cast specimens at 1070°C. This is attributed to the faster annealing scheme followed for these components, which causes residual stresses frozen in the glass, and makes it more susceptible to damage. As a consequence, during the cutting and grinding of the component in size, multiple chips and resulting cleavage damage are caused due to insufficient annealing, which are not entirely removed during polishing. The added stress and machining defects are the cause of fracture, at a lower strength.

Considering the single float glass pane specimens, these are the most homogeneous of all studied samples, with a pristine polished bottom and top surface. Since these specimens are cut out from larger float panels, their edges are ground and polished as described in section 3.2.1. All single pane samples from the first series of four-point bending experiments failed from a machining flaw at the edge, within the bottom zone of maximum tensile stress. The average flexural strength for the 10mm panes is 55MPa, which is 20% higher than the "FT Float 1120°C" specimens but 20% lower than the highest scoring specimens "AGC dark blue 1120°C" and the "Poesia 1070°C". Undoubtedly, the quality of the bottom edges can dramatically affect the flexural strength of the float glass sample in bending. According to the size and the polishing quality of the samples, and the test settings, a wide range of flexural strengths in 4 point-bending are reported in literature, from 35-170MPa (Veer and Rodichev 2011), 51-71.5MPa (Veer 2007), 53-129 MPa (Yankelevsky et al. 2016), 28-127MPa (Vandebroek et al. 2012), 40.9-56.2MPa (Vandebroek et al. 2014), 50.5-79.5MPs (Chmykhova et al. 2013), 51.7-71MPa (Pankhardt 2008), 48.9-59.2MPa (Bouška et al. 2014), 14-74MPa (Sable and Kalnins 2017) and 35-103.8MPa (Bukieda et al. 2020) to name a few. Although a direct comparison cannot be made between the obtained average strength of the reference float glass specimens and the values found in the literature (distinct experimental parameters apply), it can still be safely concluded that the obtained 55MPa strength of the tested samples in this study lies within the range found in the literature, and specifically within the lower end of this range. This is logical given the relatively rough edge finishing of the tested specimens, and a much higher strength is expected with finer polishing. In that sense and taking into account that the kiln-cast specimens exhibiting higher tensile strengths failed as well from machining flaws, it can be derived that a much higher strength is possible with the industrial fine polishing of the kiln-cast specimens.

The beams produced from adhesively bonded (Delo Photobond 4468) 8/10mm thick float glass plies, and tested with their plies parallel to the bottom surface, have an average flexural strength of 48MPa (1st and 2nd four point bending series), which is 10% higher than the kiln-formed "FT Float 1120°C" specimens. None of the specimens failed from an edge flaw; the cause of fracture is attributed to minor handling damage at the bottom surface. The Young's modulus of the adhesively bonded beams is lower than that of the monolithic, kiln-cast SLS specimens, due to the adhesive layers.

Overall, the flexural strength values obtained from the industrially produced reference samples are at the top end of the 30-55MPa (second) zone, and do not exceed the performance of the purest kiln-cast samples (found in the first zone). This is an encouraging result, given the fact that all the kiln-cast specimens produced for this study have some level of inhomogeneities.

3.5 Conclusions

A variety of commercial glass waste types is tested for the ability to be kiln-cast into structural components at relatively low temperatures (820°-1120°C), and the flexural strength of the kiln-cast specimens is evaluated.

The kiln-casting experiments show that meticulous separation of cullet at the recycling facilities guarantees a successful casting. Coatings and traces of external contaminants such as organics and metals are tolerated by the glass network yet lead to defects and low flexural strength, while contamination by glass ceramics and glasses with significant compositional variations causes the fracture of the specimens during cooling. Glass compositions with a lower liquidus point facilitate low temperature kiln-casting which leads to more homogeneous glass surfaces, as the lower viscosity during forming minimizes the occurrence of sintering flaws, surfaces bubbles and stone formation from mould contamination.

Regarding the four-point bending experiments, although the number of tested specimens per glass type is not sufficient for deriving statistical data, they do provide a good overview and reasonable estimate of the structural performance of each specimen type, according to the chemical composition, level of contamination, and followed casting parameters.

The effect of the chemical composition on the strength is distinctly observed in the specimens produced from purer cullet and at higher forming temperatures. Among these samples, a clear increase in the strength and Young's modulus is observed, consecutively from the lead silicate, to the borosilicate, barium silicate and up to the soda lime silica family. The purer, more homogeneous samples predominantly fail from external defects induced by machining and handling damage. The effect of the composition is however blurred in the more contaminated samples, where crystalline formations formed at the bottom surface within the zone of maximum tensile stress, are the prevailing cause of fracture leading to a significantly lower strength.

Within the soda lime silica family, particularly promising are the slightly modified recipes containing small amounts of K_2O and B_2O_3 and a higher Na_2O to CaO ratio. The lower viscosity of these glass melts facilitates the casting process, while their more open structure (higher molar volume) presents a less brittle alternative for a similar Young's modulus to that of SLS glasses, leading eventually to a higher flexural strength.

Glass families of an even lower liquidus point, such as the studied lead silicate and barium silicate samples, are attractive for lower energy manufacturing. However, for structural applications demanding higher strength, the barium silicate option is much more promising due to the higher E modulus and less susceptibility to scratching[45].

[45] Yamane and Mackenzie (1974) prove in their model the proportional relationship of Vicker's hardness to the Young's modulus and bond strength. As a point of reference, Ainsworth's (1954) measurement of Vicker's hardness for a $18Na_20 \cdot 10BaO \cdot 72SiO_2$ (mol %) glass is 522 kg/mm^2 and for a $18Na_20 \cdot 10PbO \cdot 72SiO_2$ (mol %) glass 445 kg/mm^2.

Regarding the more inhomogeneous specimens, produced from contaminated cullet at temperatures around the liquidus point, they still present a good flexural strength and are suitable for structural applications demanding lower tensile strength, such as bricks. The flaws occurring in the bulk are not activated during the four-point bending test and have a minor or even negligible contribution to the strength and E modulus. However, an increased density of defects in the bulk should imply a higher density of flaws at the surface as well, which should lead to an average strength reduction. A higher forming temperature (above the liquidus point) would significantly help in diminishing the amount of flaws, but considering the economic and environmental advantages of lower temperature processing, such an act would be only meaningful if higher design strengths were required per specific case.

Crystallized geometrical structures are induced within soda lime silica and borosilicate specimens produced at higher viscosities (10^6 -10^5dPa·s). If these structures are located in the bulk, the flexural strength of the specimen is equal to that of a more homogeneous casting at a higher temperature (close to the liquidus point). However, the exposure of such structures at the surface subjected in tension can lead to a dramatic decrease of strength of even 75% according to the nature of the produced crystalline formations. In this case, the origin of fracture always occurs in the glass/crystal interface. Specific attention should be given to castings formed at between 10^5 - 10^4dPa·s viscosities, as the glass products may appear homogeneous but retain significant inhomogeneous zones of miniscule bubbles and stones at the former interface created between each cullet pieces during heating up. Such formations exposed at the tensile surface are critical for the specimen's strength.

Industrially SLS manufactured glass samples, post-processed in the lab facilities to match the studied specimen size, present similar flexural strength to that of the float glass kiln-cast specimens (at 1120^{o}C), yet score at the lower end of strength values reported in the literature. Machining flaws from the processing to size, and insufficient annealing in the case of the cast bricks, are the factors responsible for the lower strength. A finer polishing would significantly increase the strength, not only of these samples, but also of the purer kiln-cast specimens. However, given that the lowest strength specimens would be less affected by a finer polishing quality, the statistical strength would not be increased that much, as it is dominated by these lower outliers.

3.6 Recommendations

The results of this study show the potential of recycling waste glass into cast structural building components. However, for the safe application of such products, further validation is required and an increased number of specimens per category (≥30, Quinn et al. 2009) is needed to derive statistical predictions. In particular, the repetition of testing is of crucial importance in the case of the contaminated samples, where a higher degree of variability is expected in the mechanical properties. The systematic testing of such samples should be linked with a quantified documentation of the type and level of inhomogeneities in the glass prior to testing. Careful and extensive fracture analysis of the tested specimens is also necessary to identify the most critical defects, and the relationship of the flaw size to the flexural strength. The physiochemical

identification of the crystalline formations at the glass surface by scanning electron microscopy is required for categorizing such critical flaws. Further testing is necessary, as well, to determine the influence of scale factor, and of static fatigue in moist environments (effect of slow crack growth). In addition, the studying of the behaviour of crystalline inclusions in the bulk glass under thermal gradients relevant to building applications is important to eliminate the risk of thermal cracking. Additional, non-destructive testing for determining the Young's modulus and the level of inhomogeneities in the cast glass is also suggested, implementing the Impulse Excitation Technique. Investigation of whether such a fast and inexpensive non-destructive technique could serve as a quality control method for cast glass products is worth exploring.

Regarding the more contaminated components, attention should be given in improving the quality of the stone-containing surface of the recycled glass. Chemical strengthening of the surface by ion exchange could be a -high cost- solution although this is not likely to help with deep defects. Another simpler solution applicable for high viscosity castings (where the diffusion rate is low), is the structuring of two (compatible) cullet qualities inside the mould: a purer along the demanding zones, and a lower more contaminated quality in the bulk (Figure 3.44). Such a composite glass would enable the use of contaminated, unwanted cullet without necessarily compromising the strength of the final product.

Lastly, the engineering of crystalline or bubble veil geometrical structures within the glass is worth further exploration, as they can lead to fractures within a predictable strength range and location. They also can lead to building components with non-standard appearance and thus higher architectural appeal.

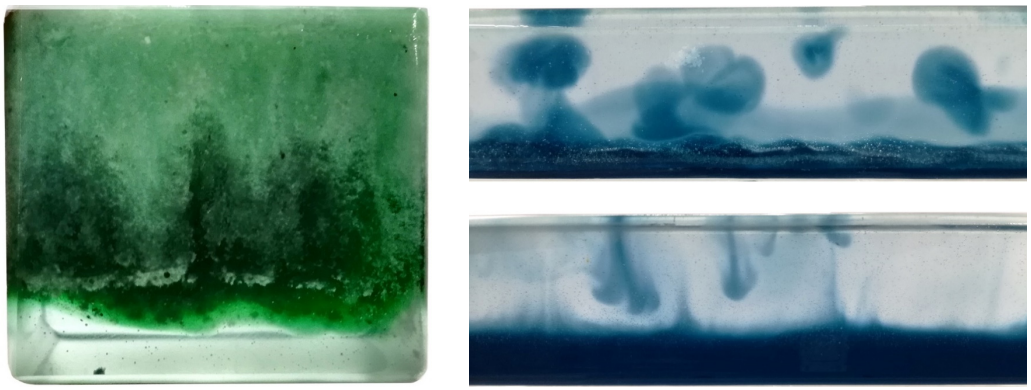

(a) (b)

Fig. 3.44 Prototypes of composite kiln-cast glass components, containing a purer glass at the bottom and a weaker, more contaminated glass at the bulk and top zone. (a) Gradient from a pure transparent soda lime silica glass (bottom) to a partially crystallized zone produced from waste glass powder (residue from the glass container recycling process). (b) Reinforcement of a "FT Float" glass beam by a bottom layer comprising the stronger "ACG blue" glass.

References

Abrisa Technologies: SCHOTT Duran® Lab Glass (Tubed). (2014)

Ainsworth, L.: The diamond pyramid hardness of glass in relation to the strength and structure of glass. Society of Glass Technology(38), 501-547 (1954)

Aldinger, B.S., Collins, B.K.: Color Atlas of Stones in Glass. American Glass Research, Butler, PA (2016)

Aldinger, B.S., de Haan, P.W.: Color Atlas of Glass Container Defects. American Glass Research, Butler, PA (2019)

Andreola, F., Barbieri, L., Corradi, A. Lancellotti, I., Falcone, R., Hreglich, S.: Glass-ceramics obtained by the recycling of end of life cathode ray tubes glasses. Waste management (New York, N.Y.) 25, 183-189 (2005). doi:10.1016/j.wasman.2004.12.007

ASM International: Applications for Glasses Engineered Materials Handbook Desk Edition. ASM International, (1995)

Bartuška, M.: Glass defects. Glass Service Inc. and Práh, Prague (2008)

Bouška, P., Bittner, T., Eliášová, M., Špaček, M., Vokáč, M., Mandlík, T.: Estimating the Flexural Strength of Float Glass. In: 52nd International Scientific Conference on Experimental Stress Analysis (EAN 2014), Marianske Lazne, Czech Republic 2014. Czech Society for Mechanics (CSM)

Brennan, J.J.: Program to Study SiC Fiber Reinforced Glass Matrix Composites. United Technologies Research Center, Connecticut, USA, (1979)

Bristogianni, T., Oikonomopoulou, F., Justino de Lima, C.L., Veer, F.A., Nijsse, R. : Structural cast glass components manufactured from waste glass: Diverting everyday discarded glass from the landfill to the building industry. Heron 63 (1/2 Special issue: Structural Glass) (2018)

Bristogianni, T., Oikonomopoulou, F., Veer, F.A., Nijsse, R.: The effect of manufacturing flaws in the meso-level structure of cast glass on the structural performance. In: Zingoni, A. (ed.) Advances in Engineering Materials, Structures and Systems: Innovations, Mechanics and Applications. pp. 1703-1708. CRC Press, Leiden (2019)

Bukieda, P., Lohr, K, Meiberg, J., Weller, B.: Study on the optical quality and strength of glass edges after the grinding and polishing process. Glass Structures & Engineering 5(3), 411-428 (2020). doi:10.1007/s40940-020-00121-x

Burch, O.G., Babcock, C. L.: Effect of Glass Color on Setting Rates in Manufacture of Glass Bottles. Journal of the American Ceramic Society 21(10), 345-351 (1938)

Campbell, D.E., Hagy, H. E.: Glasses and Glass-Ceramics. In: Lynch, C.T. (ed.) CRC Handbook of Materials Science, vol. Volume II: Material Composites and Refractory Materials. CRC Press US (1975)

Chmykhova, A.N., Chesnokov, G. A., Chesnokov, A. S.: Strength properties study for flat glass with various thicknesses, sizes and test methods. In: GPD Glass Performance Days Tampere, Finland 2013

Chyung, K.: Transparent Beta-Quartz Glass Ceramics. Corning Glass Works, United States Patent US4018612A (1977)

Corning: Properties of Corning's Glass and Glass Ceramic Families. In: Materials for the Design Engineer. USA, (1979)

Fluegel, A.: Glass Viscosity Calculation Based on a Global Statistical Modeling Approach. Glass Technology - European Journal of Glass Science and Technology Part A 48, 13-30 (2007)

Fluegel, A.: Global Model for Calculating Room-Temperature Glass Density From the Composition. Journal of The American Ceramic Society 90, 2622-2625 (2007). doi:10.1111/j.1551-2916.2007.01751.x

Friedrich & Dimmock Inc.: Comparative Values of Borosilicate Glasses. In: Simax Glass Properties.

Gold Star: Investment Casting Powder Safety Data Sheet, www.goldstarpowders.com (2019)

Goodwin Refractory Services Ltd: Crystalcast (M248), www.grscastingpowders.com (2003)

Gregory, C.: Hollow Fibers. In: Sanghera, J.S.A., I.D. (ed.) Infrared Fiber Optics. CRC Press LLC, USA (1998)

Heimerl, W.: Chemical Resistance and Corrosion, and Ion Release. In: Bach, H., and Krause, D. (ed.) Analysis of the Composition and Structure of Glass and Glass Ceramics. Springer-Verlag Berlin Heidelberg, New York (1999)

Höland, W., Beall, G.H.: Glass-Ceramic Technology, Third ed. John Wiley & Sons, Inc., Hoboken, New Jersey (2020)

Inaba, S., Fujino, S., Morinaga, K. : Young's modulus and compositional parameters of oxide glasses. Journal of the American Ceramic Society 82, 3501-3507 (1999). doi:10.1111/j.1151-2916.1999.tb02272.x

Ito, S., Taniguchi, T.: Effect of cooling rate on structure and mechanical behavior of glass by MD simulation. Journal of Non-Crystalline Solids 349, 173-179 (2004). doi:https://doi.org/10.1016/j.jnoncrysol.2004.08.180

Kitaĭgorodskiĭ, I.I., Solomin, N.W.: Rate of Setting of Glass During Working. Society of Glass Technology Journal (18), 323-335 (1934)

LightRec Nederland: Recycling lampen en armaturen. https://www.lightrec.nl/producenten-/-importeurs/recycling-lampen-en-armaturen/ (2022). Accessed 28-08-2022

Makishima, A., Mackenzie, J. D.: Direct calculation of Young's moidulus of glass. Journal of Non-Crystalline Solids 12(1), 35-45 (1973). doi:https://doi.org/10.1016/0022-3093(73)90053-7

Martienssen, W., Warlimont, H.: Springer Handbook of Condensed Matter and Materials Data. (2005)

MatWeb: C-Glass Fiber, www.matweb.com

Montazerian, M., Singh, S.P., Zanotto, E.: An analysis of glass–ceramic research and commercialization. American Ceramic Society Bulletin 94, 30-35 (2015)

Morey, G.W.: The Effect of Boric Oxide on the Devitrification of the Soda-Lime-Silica Glass. The Quaternary System, Na2O-CaO-B2O3-SiO21. 15(9), 457-475 (1932). doi:10.1111/j.1151-2916.1932.tb13959.x

Mueller, J., Boehm, M., Drummond, C.: Direction of CRT waste glass processing: Electronics recycling industry communication. Waste management (New York, N.Y.) 32, 1560-1565 (2012). doi:10.1016/j.wasman.2012.03.004

National Institutes of Health (NIH): PubChem database, https://pubchem.ncbi.nlm.nih.gov/
Oikonomopoulou, F., Bristogianni, T., Veer, F.A., Nijsse, R.: The construction of the Crystal Houses façade: challenges and innovations. Glass Structures & Engineering 3(1), 87-108 (2018). doi:10.1007/s40940-017-0039-4
Oikonomopoulou, F., Bristogianni, T., Barou, L., Jacobs, E., Frigo, G., Veer, F.A., Nijsse, R.: Interlocking cast glass components, Exploring a demountable dry-assembly structural glass system. Heron 63, 103-138 (2018)
Oikonomopoulou, F., Bristogianni, T., Barou, L., Veer, F.A., Nijsse, R.: The potential of cast glass in structural applications. Lessons learned from large-scale castings and state-of-the art load-bearing cast glass in architecture. Journal of Building Engineering 20, 213-234 (2018). doi:https://doi.org/10.1016/j.jobe.2018.07.014
Pankhardt, K.: Investigation on load bearing capacity of glass panes. Periodica Polytechnica Civil Engineering 52(2), 73-82 (2008). doi:doi.org/10.3311/pp.ci.2008-2.03
Priven, A.I.: Evaluation of the fraction of fourfold-coordinated boron in oxide glasses from their composition. Glass Physics and Chemistry 26(5), 441-454 (2000). doi:10.1007/BF02732065
Quinn, G.D., Ives, L.K., Jahanmir, S.: On the Nature of Machining Cracks in Ground Ceramics: Part II, Comparison to Other Silicon Nitrides and Damage Maps. Machining Science and Technology - MACH SCI TECHNOL 9, 211-237 (2005). doi:10.1081/MST-200059051
Quinn, G.D., Sparenberg, B.T., Koshy, P., Ives, L.K., Jahanmir, S., Arola, D.D.: Flexural Strength of Ceramic and Glass Rods. Journal of Testing and Evaluation 37, 222-244 (2009). doi:10.1520/JTE101649
Quinn, G.D.: NIST Recommended Practice Guide: Fractography of Ceramics and Glasses, 2nd edition. (2016)
Quinn, G.D., Swab, J.J.: Fracture toughness of glasses as measured by the SCF and SEPB methods. Journal of the European Ceramic Society 37(14), 4243-4257 (2017). doi:https://doi.org/10.1016/j.jeurceramsoc.2017.05.012
Sable, L., Kalnins, K.: Verification of available glass mechanical properties against recommendation by the draft Eurocode design practice. Technology of Inorganic Materials 68(1) (2017). doi:doi.org/10.5755/j01.ct.68.1.18872
Saint-Gobain: Glass Forever, a commitment to a circular economy for flat glass. https://techhub.uk.saint-gobain-building-glass.com/glass-forever. Accessed 28-08-2022
Schott: Tubular Glass Photobioreactors. (2015)
Schott: NEXTREMA®. (2015)
Schott: DURAN Technical Data. (2017)
Sehgal, J., Ito, S.: A New Low-Brittleness Glass in the Soda-Lime-Silica Glass Family. 81(9), 2485-2488 (1998). doi:10.1111/j.1151-2916.1998.tb02649.x
Shelby, J.E.: Introduction to Glass Science and Technology. The Royal Society of Chemistry, UK (2005)
Silva, R.V., de Brito, J., Lye, C.Q., Dhir, R.K.: The role of glass waste in the production of ceramic-based products and other applications: A review. Journal of Cleaner Production 167, 346-364 (2017). doi:https://doi.org/10.1016/j.jclepro.2017.08.185
Songhan Plastic Technology Co., L.: Schott Nextrema® 724-3, 712-3 Glass Ceramic.
Specialty Glass Products: STARPHIRE Ultra-Clear™ Soda Lime Glass.
Thompson, D.A.: Low liquidus glasses for television tube faceplates. US Patent, US4331770A (1980)
Vandebroek, M., Belis, J., Louter, C., Van Tendeloo, G.: Experimental validation of edge strength model for glass with polished and cut edge finishing. Engineering Fracture Mechanics 96, 480-489 (2012). doi:https://doi.org/10.1016/j.engfracmech.2012.08.019
Vandebroek, M., Louter, C., Caspeele, R., Ensslen, F., Belis, J.: Size effect model for the edge strength of glass with cut and ground edge finishing. Engineering Structures 79, 96-105 (2014). doi:https://doi.org/10.1016/j.engstruct.2014.08.004
Veer, F.A.: The strength of glass, a nontransparent value. Heron 52, 87-104 (2007)
Veer, F.A., Rodichev, Y.: The structural strength of glass: Hidden damage. Strength of Materials 43, 302-315 (2011). doi:10.1007/s11223-011-9298-5
Vlakglas Recycling Nederland: Vlakglas Recycling Nederland Jaarverslag 2020. Netherlands, (2020)
Volf, M.B.: Chemical Approach to Glass. Elsevier, (1984)
Yamane, M., Mackenzie, J.D.: Vicker's Hardness of glass. Journal of Non-Crystalline Solids 15(2), 153-164 (1974). doi:https://doi.org/10.1016/0022-3093(74)90044-1
Yankelevsky, D., Spiller, K., Packer, J., Seica, M.: Fracture Characteristics of Laboratory-Tested Soda Lime Glass Specimens. Canadian Journal of Civil Engineering 44 (2016). doi:10.1139/cjce-2016-0374
Yun, Y.H., Bray, P.J.: Nuclear magnetic resonance studies of the glasses in the system Na_2O-B_2O_3-SiO_2. Journal of Non-Crystalline Solids 27(3), 363-380 (1978). doi:https://doi.org/10.1016/0022-3093(78)90020-0
Zhdanov, S.P., Shmidel', G.: Coordination State of Boron in Sodium Borosilicate Glasses from NMR Data. Fiz. Khim. Stekla vol. 1(no. 5), pp. 452–456 (1975)


4

Previous page: Mixing interface between a blue-tinted and a clear float glass, kiln-cast at 1120ºC.

Chapter 4: Revisiting the flexural strength and stiffness of cast glass

Based on

Bristogianni, T., Oikonomopoulou, F., Veer, F.A.: On the flexural strength and stiffness of cast glass. Glass Structures & Engineering 6(2), 147-194 (2021).

Aim and context

Further investigation on the flexural strength and stiffness of cast glass, in relation to the size effect. Chapter 4 builds on the knowledge acquired in Chapter 3, to confirm prior conclusions, improve the experimental procedures, and study in more depth the role of defects and thermal history in determining the flexural strength of cast glass.

Abstract

Cast glass has great potential for diverse load-bearing, architectural applications; through casting, volumetric glass components can be made that take full advantage of glass's stated compressive strength. However, the lack of engineering, production and quality control standards for cast glass and the intertwined ambiguities over its mechanical properties -particularly due to the variety in chemical compositions and the lack of understanding of the influence of flaws occurring in the glass bulk- act as an impediment to its wide-spread application. Addressing the above uncertainties, this work studies a total of 64 silicate-based glass specimens, prepared in 20x30x350mm beam size, either by kiln-casting at relatively low forming temperatures (970-1120^{o}C), or by modification of industrially produced glass. For the kiln-casting of the specimens, pure and contaminated recycled cullet are used, either individually or in combination (composite glasses). The defects introduced in the glass specimens during the casting process are identified with digital microscopy and qualitative stress analysis using cross polarized light, and are categorized as stress-inducing, strength- reducing or harmless. The Impulse Excitation Technique is employed to measure the Young's modulus and internal friction of the different glasses. Differential Scanning Calorimetry is used on a selection of glasses, to investigate changes in the glass transition range and fictive temperature of the kiln-cast glasses due to the slower cooling and prolonged annealing. The four-point bending experiments shed light upon the flexural strength and stiffness of the different glasses, while the fractographic analysis pinpoints the most critical defects per glass category. The experiments show the flexural strength of cast glass ranging between 30-73MPa, according to the level of contamination and the chemical composition. The measured E moduli by both methods are in close agreement, ranging between 60-79GPa. The comparison of the flexural strength with prior testing of cast glass involving

shorter span fixtures showed a decreasing strength with increasing size for the contaminated specimens, but similar strengths for pure compositions. The results highlight the versatile role of defects in determining the glass strength and the complexity that arises in creating statistical prediction models and performing quality control.

Authors' contribution on the relevant published journal article

Bristogianni, T.: Research concept, organization, sample preparation, conduction of experiments, data analysis, writing of the paper. Oikonomopoulou, F.: Discussion and paper review. Veer, F.A.: supervision of research, discussion, paper review.

Acknowledgements

I would like to thank the co-authors of the above mentioned paper for their valuable contribution in this chapter. I am also very grateful to Georgos Stamoulis and Fred Schilperoort for their dedicated support in setting up the four-point bending experiment, and to Rong Yu and Mariska van der Velden for their valuable assistance with the preparation of the glass specimens. This research has been greatly supported by Professor Rob Nijsse, to whom I express my sincere gratitude. I would also like to acknowledge Nicky Slootmans and Theo Bollen (IMCE NV) for conducting the IET measurements and providing insights into the relevant theory, John van den Berg for his guidance with the DSC tests, and Ruud Hendrikx for his important contribution with the XRF characterization. I am very thankful to George Quinn (NIST), Mauro Overend, Bert Sluijs and Clarissa Justino de Lima (AGR Delft) for their scientific advice and insightful suggestions. Finally, I am very grateful to Danny Timmers (Maltha Glasrecycling Nederland), Marco Zaccaria and François Boland (AGC Belgium), and Klaas Roelfsema (Schott), for their important contribution in glass cullet.

4.1 Introduction

Only within the last two decades, have we seen architectural projects exploring the structural potential of cast glass components, such as the Atocha Memorial (Paech and Göppert, 2008) and the Crystal Houses (Oikonomopoulou et al. 2018a, b). Recent research by the authors has further shown that casting glass components for architectural applications can be a promising upcycling approach for currently discarded glass of a variety of chemical compositions (Oikonomopoulou et al. 2018c, Bristogianni et al. 2018, 2019). Volumetric glass components are anticipated to tolerate a far higher contamination rate than thin-walled glass, allowing for the closed-loop recycling of different glass types in their as-received condition (e.g. coated glass), reducing in this manner the need for treatment & purification.

Yet, despite the rising interest on cast glass from architects, designers and engineers, the lack of a standardized production method, quality control process and relevant engineering data and thus,

the intertwined knowledge gaps on the strength of such components, hinder the upscaling of its application. Added complexity is introduced in the case of the aforementioned environmental aspirations, where recycled glass cullet and lower casting temperatures are employed to reduce the carbon footprint of cast glass components. The presence of impurities in the batch and the high forming viscosities introduce inhomogeneities in the cast glass, creating unique identities of mechanical and aesthetical properties, closely related to glass composition and inherent defects.

This study addresses the uncertainties surrounding the design strength and stiffness of cast silicate-based glasses, and the quality control procedure to be followed, as a continuation of previously published research by Bristogianni et al. (2020)[46]. For this purpose, 20x30x350 mm glass beams are kiln-cast at relatively low forming temperatures (970-1120ºC), using pure and contaminated silicate-based cullet, either individually or in combination. Reference specimens made from industrially produced glass are employed for comparison. The beams are tested by Impulse Excitation and in four-point bending (4PB), to derive their stiffness and flexural strength. The purposes of this work are to i) verify the previously obtained stiffness and flexural strength data while improving the accuracy of the four-point bending experiments, ii) investigate if a longer fixture span affects the flexural strength, iii) cross-check the E moduli resulting from the 4PB measurements with values obtained from non-destructive testing methodologies such as Impulse Excitation, iv) examine changes in the glass nano-structure due to a longer cooling and annealing scheme, and how this thermal history affects the macro-properties, v) further analyse the profile of the different casting defects and investigate how critical they are, and vi) experiment with the concept of improving the glass strength by engineering composite glasses.

4.2 Experimental work

4.2.1 Specimen preparation and analysis

For the purposes of the four-point bending experiments, beams of 20x30x350 mm size are kiln-cast from different pure or contaminated silicate-based glasses, in triplets per glass type. To achieve comparable data to preceding research (Bristogianni et al. 2020), the study focuses on the same characteristic commercial silicate glasses as the ones used before, and adopts the same casting process and thermal history for the majority of the samples (unless otherwise stated). The chemical composition of the glass cullet types is defined by X-ray fluorescence (XRF) analyses conducted with a Panalytical Axios Max WDXRF spectrometer. The beams are kiln-cast in silica-plaster investment moulds (Crystalcast M248[47]) using an ROHDE ELS 200S or ELS 1000S

[46] This work explores the flexural strength and stiffness of 30x30x240mm recycled glass beams. The specimens are kiln-cast at 820–1120◦C using different types of pure and contaminated silicate-based glasses. The occurring glass defects are documented and correlated to the used casting parameters. The four-point bending experiments on the pure and contaminated specimens show a flexural strength range of 9–72MPa. The Young's modulus of the more homogeneous glass beams ranges between 65-79GPa. The test results are analysed according to the role of the chemical composition, level of contamination and followed casting parameters, in determining the flexural strength, the Young's modulus and the prevailing strength-limiting flaw.

[47] Crystalcast M248 is an investment powder made of 73% silica powder (cristobalite, quartz), 23% calcium sulphate (gypsum) and 1% organics (Goodwin Refractory Services 2003; Gold Star 2019).

electric kiln (Figure 4.1). The forming temperatures range from 970 ºC to 1120ºC, corresponding to viscosities between 10^6–$10^{3.5}$ dPa·s. The moulds containing the glass cullet are heated up to the selected forming temperature per glass type with a rate of 50ºC/hr, kept at that temperature for 10hr, and then cooled in the same kiln with a rate of -160ºC/hr to a temperature 20ºC above the annealing point. There a dwell of 5hrs takes place before cooling down to the annealing point with a rate of -3ºC/hr, annealing there for 10 hr, and then controllably going down to the strain point with the same rate before cooling down to room temperature in a faster pace. Information on the chemical composition of the selected glasses, and on the forming and annealing temperatures used per glass type can be found in Table 4.1. The only exception to the above described firing schedule is the sample type "FT[48] Float 1120ºC, 2hr, -50ºC/hr". In this case, a shorter dwell time of 2hr is kept at forming temperature, and a slower cooling rate of -50ºC/hr instead of -160ºC/hr is used for the cooling segment to the 20ºC above annealing point temperature. The different firing schedule is selected, in this case, to investigate the effect of the thermal history to the mechanical properties of the glass sample. For the same reason, several glass types are kiln-cast at several top temperatures (e.g. Poesia kiln-cast 970ºC vs 1070ºC).

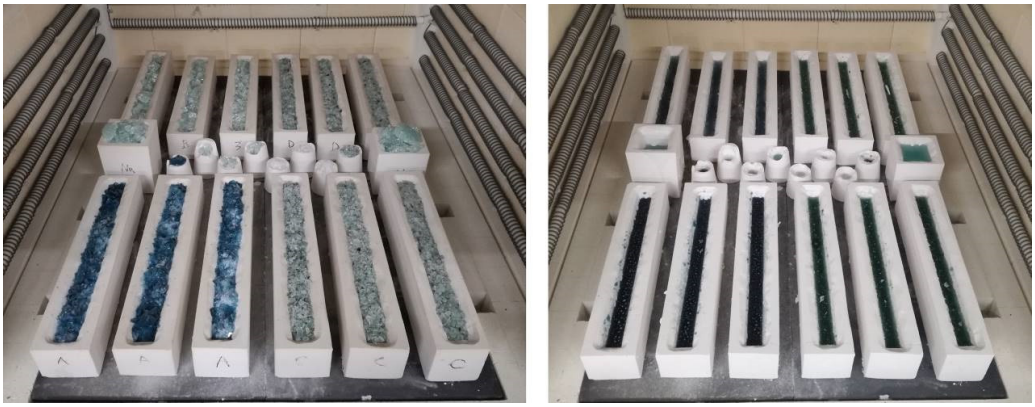

Fig. 4.1 Arrangement of the investment moulds and glass cullet inside the ROHDE ELS 1000S kiln (left) and final kiln-cast components after a complete heating and cooling cycle.

Apart from the beams produced by a single cullet type, two different composite glasses are engineered. The selection of the glasses to be mixed is based on the purity of the cullet, and the stiffness and flexural strength of the individual cast glasses (as defined by Bristogianni et. al 2020). The goal of this mixing is to either locally (e.g. bottom beam surface subjected to maximum tension during bending) or globally reinforce a beam made from a weak/contaminated glass with a small percentage of stronger/purer compatible glass. The ratio of pure to contaminated/weak glass used is 1:3. The two produced combinations involve float glass of:

i) AGC Blue cullet (pure, E modulus= 76.5GPa, Flexural strength= 63MPa, density[49]≈ 2.548g/cm^3) mixed with FT Float (pure but prone to crystallization, E modulus=

[48] FT refers to glass shards collected from Fully Tempered float glass panes. The heat-treatment history of the shards is erased during casting and the final kiln-cast components are simply annealed.
[49] Density measured with the Archimedes' Principle.

72.7GPa, Flexural strength= 44MPa, density≈ 2.508g/cm^3). In this combination, a localized reinforcement at the beam's bottom surface is achieved. Additional specimens are produced with localized reinforcement at the beam's side surface, exposing in this manner both the pure and weak glass qualities to the zone of maximum tensile stress. These additional specimens serve to investigate if the pure/weak glass interface is a stress inducing factor that can lead to component failure.

ii) AGC Clear pure cullet mixed with contaminated Maltha Car windshields cullet (Flexural strength= 41MPa). The clear glass in this case diffuses throughout the beam's mass, leading to a global improvement of the properties.

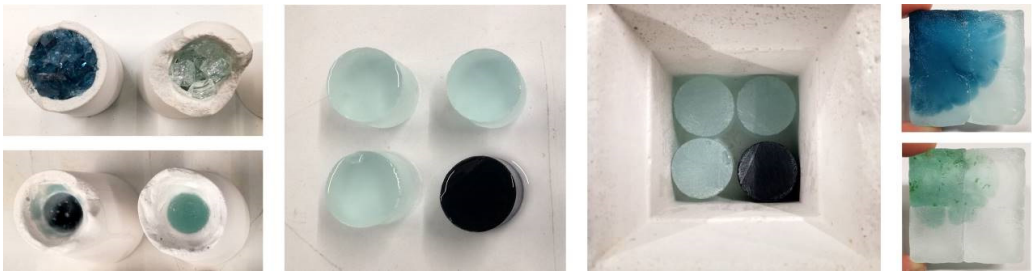

Fig. 4.2 Two-step viscosity test from left to right: kiln-casting of ø24mm rods out of FT Float and AGC Blue cullet at 1120ºC, polishing of the rods, kiln-casting of the rods in 50x50mm area investment moulds at 1120ºC, and studying of the compatibility and mixing gradient of the two glasses. In the images on the right, a comparison can be seen between the FT Float-AGC Blue combination (top) and the Car glass-AGC Clear mix (bottom). These relationships help determine the positioning of the different cullet types in the mould in order to achieve the desired composite glass.

Prior to arranging the different cullet types inside the mould, a simple two step test showing the viscosity and density differential between the mixed glasses is made at the selected top temperature, as seen in Figure 4.2. The information derived from this test is used in combination with the selection of cullet size, in order to engineer the desired composite glasses. Specifically, in the first scenario (i), the AGC blue glass will soften faster at the selected top temperature, and flow to the bottom of the mould due to its higher density. A localized reinforced surface out of AGC blue glass can be produced, either by placing the coarse (as received) blue shards at the bottom of the mould and then placing on top the FT shards, or by arranging the blue cullet sideways, parallel to an FT float part precast into one piece, which due to its size will take longer to melt (confining thus the blue glass in its specified region). For the second scenario (ii), given that the two glasses have very similar melting behavior -with the contaminated one being slightly heavier and the pure one less viscous- an arrangement of the pure cullet at the bottom of the mould in combination with a long dwell time of 10hr at top temperature, will promote the diffusion and intermixing of the two glasses leading to a more global reinforcement (Figures 4.3, 4.4).

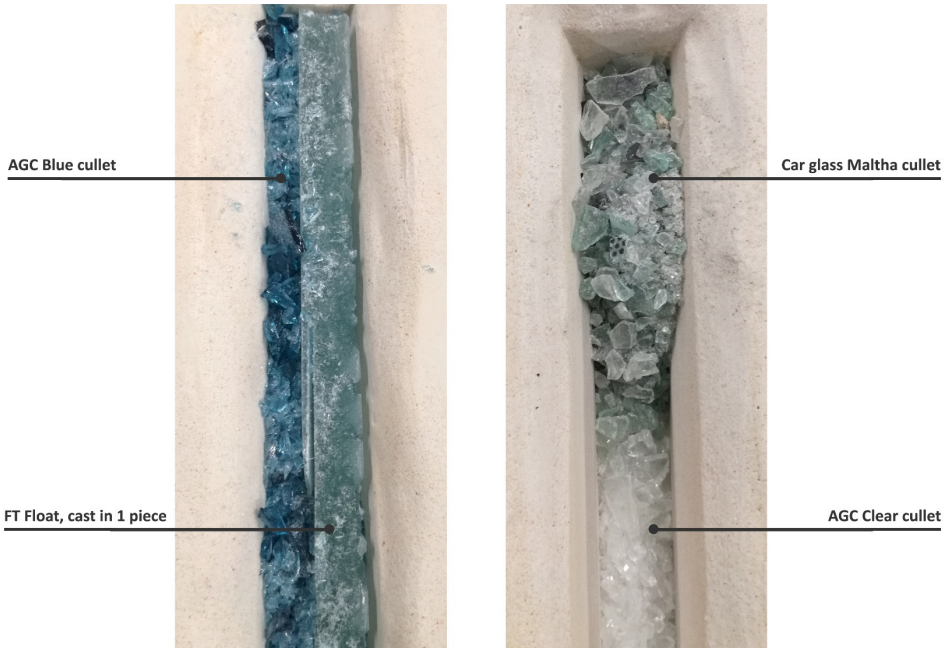

Fig. 4.3 Positioning of the cullet in a vertical layering (left, AGC Blue shards and FT Float precast in a single slab) or horizontal (right, AGC clear shards at the bottom of the mould and Car glass shards on top).

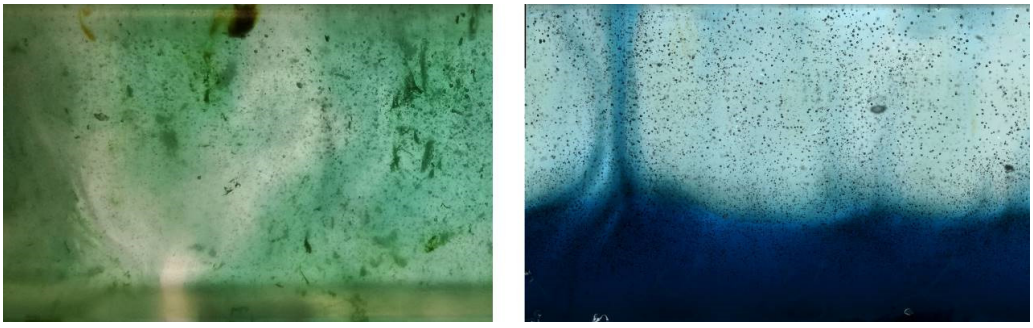

Fig. 4.4 Global (left, AGC Clear and Car glass) versus local (right, AGC Blue and FT Float) reinforcement. Both specimens were produced by adding the purer cullet at the bottom of the mould, so AGC clear and AGC Blue respectively. Considering however the viscosity differential between the chosen pure and contaminated glasses (Figure 4.2), the car glass flowed to the bottom, evoking the diffusion between the two glasses, while the AGC glass remained to its position promoting a functional layering.

All kiln-cast specimens are cast with their side surfaces (20x350mm) oriented at the bottom and top of the mould. The beams are produced at a 40mm height, and then cut to size (30mm) with a water-cooled rotary diamond wheel cutter. This step is necessary to remove compositional inhomogeneities, seeds, stones and crazing often occurring at the top cast surface. Then, the specimens are ground and polished using a Provetro flat grinder and diamond abrasive discs in sequence of 60, 120, 200, 400 and 600 grit.

Moreover, a series of tack-fused float glass specimens is produced. Two 10mm float plies are placed on thin kiln paper above the kiln's base and heated up to 650°C for 1 hr. Upon annealing and cooling, the fused plate is cut and polished to beam size. As the fusing temperature and dwell are not sufficient for a complete bonding between the two panes, a dominant weak zone is introduced at the longitudinal middle of these beams.

In addition to the kiln-cast and tack-fused specimens, industrially produced specimens are prepared to serve as a reference. The specimens are cut to size and the damaged cut surfaces are polished in the same procedure as previously described, while the rest of the surfaces are left in the as received condition (fine glossy polishing, occasional scratches). The reference specimens are divided in the categories below:

- Beams of 20x30x350mm size, cut out from Poesia cast glass frames[50]
- Single float glass panes of 10x30x350mm size
- Double float glass panes of 8x30x350mm size, laminated (thickness of interlayer ≈700μm). Total beam height approx. 16.6mm
- Double float glass panes of 10x30x350mm size, glued with UV-curing acrylate DELO 4468 (adhesive thickness varies from 30-235μm). Total beam height approx. 19.9mm

The dimensions of all the produced samples are measured with a digital caliper, and the density of a selection of samples is defined using the Archimedes' Principle. A Keyence VHX-7000 digital microscope with a 20-200x zoom lens is used for analyzing characteristic defects in the cast samples under standard and polarized illumination. The cross-polarization of the filters allows for the qualitative detection of internal stresses in the glass induced by the defects. Upon inspection of the samples, a white/black speckle pattern is sprayed on one side of the beams, to be used for the Digital Image Correlation (DIC) measurement.

4.2.2 Impulse excitation test set-up and Differential Scanning Calorimetry test

Measurements employing the Impulse Excitation Technique (IET) are performed at room temperature according to the ASTM E1876-15 standards. The goal is to measure the elastic properties and internal friction of the glasses -using a non-destructive method- prior to the four point bending experiment, and compare the resulting E moduli from both tests. For this measurement, a Resonant Frequency and Damping Analyser (RFDA) Professional system developed by IMCE NV is used (Figure 4.5). One cast specimen per cast glass triplet is selected, as well as one float glass pane to be used as reference. The samples are placed on a wire support frame and are gently tapped with a manual excitation tool at the middle of the top surface (flexural vibration mode). The induced vibration signal is detected by a microphone placed above the

[50] The specific cast glass frames were produced as test pieces for the Crystal Houses façade (Oikonomopoulou et al. 2018), in a 65x150x790mm size.

middle of the beam, and is amplified and sent to a computer for analysis. The test is repeated ten times per specimen.

The captured resonant frequency of each beam is related to its mass, dimensions and elastic properties. For rectangular beam sections[51] of a homogeneous, isotropic material, the E modulus can be calculated from the following equation (ASTM 2001):

$$E = 0.9465 \left(\frac{m \cdot {f_f}^2}{w}\right)\left(\frac{L^3}{h^3}\right)T \quad (1)$$

Where m is mass, f_f is flexural frequency, L, h, w the length, height and width of the beam, and T is a correction factor[52]. Based on the amplitude decay of the free vibration, the internal friction Q^{-1} is also calculated by the IMCE software.

To identify possible alterations in the glass transition region of float glass after casting, a Differential Scanning Calorimetry (DSC) analysis is conducted for a selection of glasses before and after forming[53], using a Netzsch STA 449 F3 Jupiter® apparatus. The measurements are performed in inert atmosphere (Argon) together with a correction blank sample. Pure (99.99%) alumina crucibles are used, closed with a lid that allows for gas release, and the used glass sample mass is approximately 60mg. A heating rate of 10K/min is used until the samples reach 1120ºC. The obtained data are analysed via the Proteus Software.

[51] ASTM advises rectangular beams without chamfered or round edges to avoid calculation errors. In this study the edges are rounded to eliminate post-processing damage, so a minor error is to be expected in the calculations.

[52] The correction factor T accounts for the finite thickness of the beam and the Poisson's ratio. For beams of L/h≥20 ratio, then:

$$T = 1 + 6.858\left(\frac{h}{L}\right)^2 \quad (2)$$

While for L/h<20 the following formula can be used, with ν being the Poisson's ratio: (3)

$$T = 1 + 6.585(1 + 0.0752\nu + 0.8109\nu^2)\left(\frac{h}{L}\right)^2 - 0.868\left(\frac{h}{L}\right)^4 - \left[\frac{8.340(1 + 0.2023\nu + 2.173\nu^2)\left(\frac{h}{L}\right)^4}{1 + 6.338(1 + 0.1408\nu + 1.536\nu^2)\left(\frac{h}{L}\right)^2}\right]$$

In this study, the L/h ratio for the float panes is 35 so the simplified formula can be used, while for the cast beams this ratio is approximately 17.5 and requires the second equation for the E modulus calculation. However, it is found that for the given beam dimensions and a hypothetical ν=0.22 that corresponds to typical float soda lime silica compositions, the difference in the E modulus deriving from the use of the simple and the elaborate formula is in the order of 0.015GPa, thus for simplification purposes, the shorter equation can be used.

[53] The samples referring to the cast specimens are collected after the 4-point bending test.

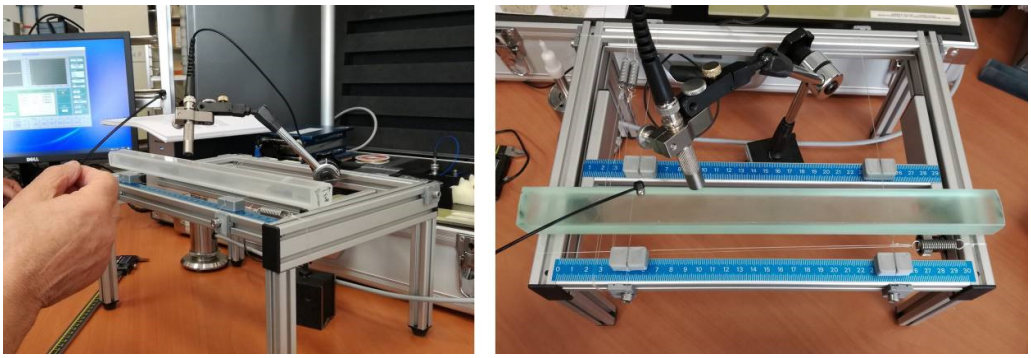

Fig. 4.5 Impulse Excitation experiments at IMCE NV, employing a Resonant Frequency and Damping Analyser (RFDA) Professional system.

4.2.3 Four-point bending experiment set-up

A total of 64 beam specimens of 350mm length, 30mm width and 20mm height (with the reference beams varying from 8-20mm height) are tested in four point bending, in room temperature conditions. An Instron 1251 (100kN) Universal Testing hydraulic machine is used, set to a displacement controlled loading rate of 0.6mm/min[54]. The four-point bending fixtures have a span of 140mm for the loading rollers and 280mm[55] for the support rollers, and articulate in pairs. To allow for minor adjustments and rotational movements, a semi-circular pin is placed below the support fixture, while the loading fixture has a loose connection to the machine's head. The rollers are made from S355J2 (St52-3) steel, have a 14mm diameter[56] and are free to roll sideways to relieve frictional constraints (free movement outwards for the support rollers, and inwards for the loading rollers). Silicone rubber strips of 1mm thickness are placed between the beam and the loading cylinders to correct minor deviations in the beam's height (Figure 4.6).

The displacement during loading is measured[57] with the 2D-DIC technique, using a high-resolution (50.6MP) Canon EOS 5Ds camera that captures a picture per second of the deformed speckled surface of the beam. The pictures are consequently analysed using the GOM Correlate software[58] (Figure 4.7).

[54] According to the glass stiffness, the loading rate corresponds to a stress increase of 0.4-0.7MPa/s, which is below the 1.1±0.2MPa/s rate indicated by ASTM C158-02 (2012).
[55] The beam size and fixture spans are adapted from the suggested ASTM C1161 – 13 dimensioning. As a basis the 1.5x2x25mm specimen size is used that corresponds to a 10:20mm load span to support span.
[56] The bearing's diameter is adjusted from the ASTM C158 − 02 (2012) suggestion for testing glass plates. For a 250mm long glass beam, a 3mm radius is advised.
[57] A Linear Variable Differential Transformer (LVDT) displacement sensor (Solartron AX 2.5 Spring Push Probe calibrated to a 0.5µm accuracy) that reports the displacement under the middle of the beam was also used. However, since the sensor was fixed with a bolt, the full body (thus not only the spring), would move downwards during bending, resulting in a slightly higher deformation. The results of the LVDT were therefore not used in this work.
[58] One image pixel equals to 31.5µm, therefore given the software accuracy of 0.05 pixel, displacements larger than 1.57µm are detected.

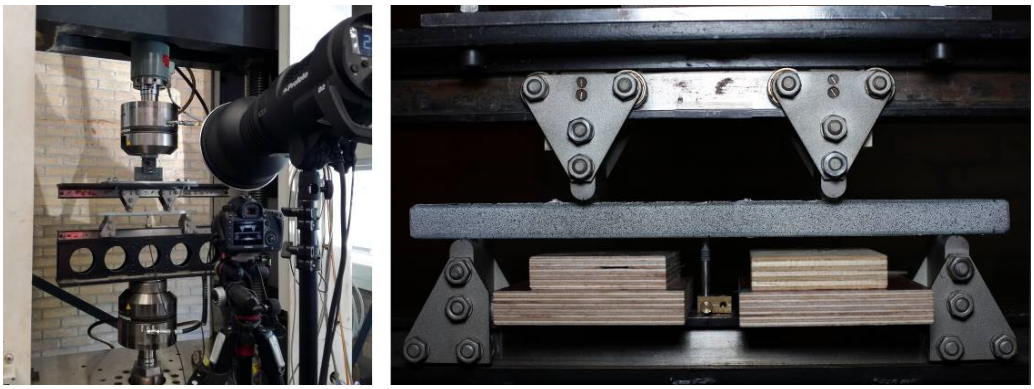

Fig. 4.6 Four-point bending set-up (left) and image of the beam's side surface containing the speckle pattern to be used for the DIC analysis (right).

Fig. 4.7 Measurement of displacement in y direction, by analyzing the captured images using the GOM Correlate software. The maximum displacement due to bending at the middle, is calculated by subtracting the total displacement at the middle from the average displacement at the beam points above the supports (displacement marked in dark yellow).

For the flexural strength (σ) calculation, the following formula is applied:

$$\sigma = \frac{3 \cdot F \cdot (L_s - L_l)}{2 \cdot w \cdot h^2} \tag{4}$$

where F the maximum load, L_s the support span, L_l the load span, w the beam's width and h the beam's height. The calculation of Young's (E) modulus is performed by correlating the force data obtained from the Instron machine with the maximum displacement at the bottom middle of the beam as reported by the DIC analysis. Equation 5 is applied for calculating the E modulus:

$$E = \frac{\Delta F}{\Delta l_{max}} \cdot \frac{\left(\frac{L_s - L_l}{2}\right)\left(3L_s^2 - 4\left(\frac{L_s - L_l}{2}\right)^2\right)}{4 \cdot w \cdot h^3} \quad (5)$$

Considering the beam proportion, the shear contribution to the maximum deformation is negligible and thus excluded from the E modulus calculation.

4.3 Results

4.3.1 Glass casting defect evaluation

A variety of defects are encountered in the kiln-cast glass specimens, which are formed during:

a. Casting: these flaws (e.g. stones, bubbles) are linked to the chosen casting parameters and can be situated both in the bulk and at the surface of the glass beams

b. Post-processing and handling: these are surface flaws (e.g. scratches, chippage) that are caused during the grinding, polishing and handling of the glass beams. In this case, the quality of the diamond discs, machinery, and polishing work, act together with the predisposition of each glass type to get easily damaged (for example due to low hardness or the presence of surface stones)

In this chapter, first the casting related defects (a) will be discussed, linking them to the casting parameters responsible for their formation. Thereafter, both casting (a) and post processing (b) defects will be evaluated, according to the effect they have on the glass, based on the characterization proposed by Aldinger and de Haan (2019) in:

- Stress increasing: these are defects that introduce stress in the glass that adds to a stress created by an applied load. Such defects can be situated in the bulk or/and at the surface of the glass

- Strength reducing: these defects reduce the strength of glass and are mainly surface flaws in this research work

The effect of the different flaws will be further evaluated by analyzing the results of the four-point bending experiments. Understanding the cause and the effect of the different encountered

flaws will contribute to distinguishing the tolerable from the critical defects, and will indicate how the occurrence of the later can be avoided.

Defects due to the casting process

Table 4.1 presents an overview of the defects found in the kiln-cast beams which form during the casting process at the chosen high viscosities. The documentation of and the reasoning behind the occurring defects are required to understand the structural performance of the specimens in the succeeding sections.

The majority of the specimens are made from pure cullet of a single glass composition, either manually selected and cleaned in the laboratory (e.g. FT float shards, Poesia glass), or gathered at the rejection point of float line production[59] (e.g. ACG blue, AGC clear). In this category of more pure samples, the defects occurring due to the casting process (e.g. cullet shape and size, mould material) and thermal history (forming temperature, dwell times, cooling scheme) are highlighted. In comparison, two series of samples are made from contaminated "Car glass Matlha" cullet, highlighting the contribution of contaminants in the formation of defects during casting. Specifically, the cullet is characterized by minor compositional variations (float glass from various producers), the presence of various anti-glare and sun-blocking coatings, and of several external contaminants such as lamination foil, traces of metal and ceramic-stone-porcelain (CSP). Lastly, the defects occurring in the composite glass series are addressed.

[59] In this case, minor traces of metal contaminants may appear in the cullet.

The glass defects occurring from the selected casting parameters- from the quality and characteristics of the cullet and the type of mould to the imposed thermal history- can be categorized in three groups (Figure 4.8): (i) Crystalline inclusions, (ii) Glassy inhomogeneities and (iii) Gaseous inhomogeneities (characterization according to Bartuška 2008).

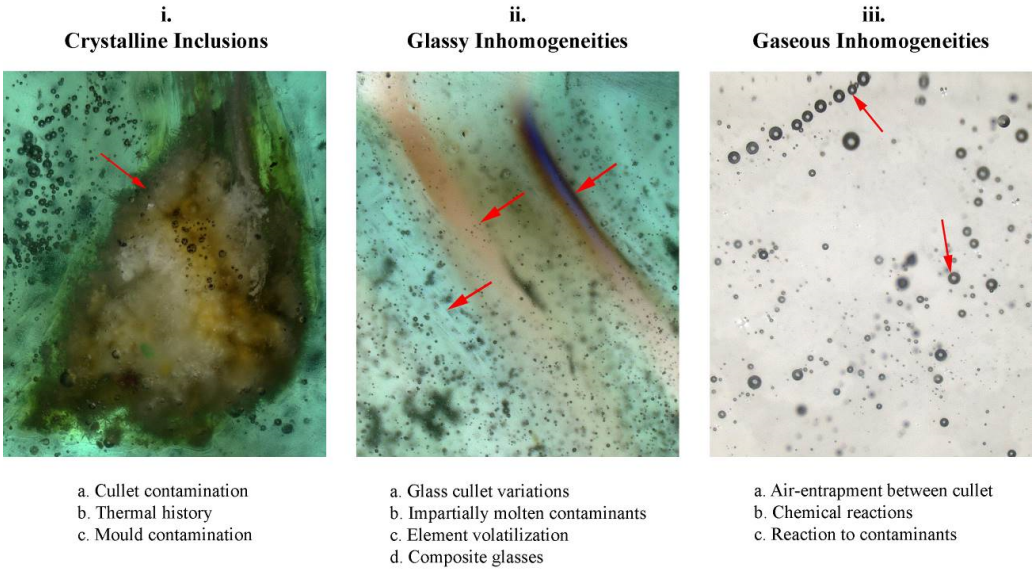

Fig. 4.8 Overview of the three categories of casting defects (i-iii), and the main causes of their formation.

Table 4.1 (part a, extends horizontally to the next page): Chemical composition, thermal profile, casting defects and internal stresses of the kiln-cast specimens.

Glass type	Specimen description	Source	Composition* (main compounds in wt%)	Forming temperature in °C (10hr dwell unless other specified)	Theoretical viscosity (log10(visc. in poise)) at top temperature**	Annealing temperature in °C (10hr dwell)***
Soda Lime Silica (Float Glass)	FT^ float			1120	3.5	560
	FT float, slow cooling		75.4% SiO_2, 12.4% Na_2O, 7.6% CaO, 4% MgO, 0.4% Al_2O_3	1120 (2hr dwell)	3.5	560 (50°C/hr cooling rate)
	Float 10mm, 35 vertical layers, fused	IFS-SGT		970	4.5	560
	Float 10mm, 2 horizontal layers, fused		72.4% SiO_2, 12.3% Na_2O, 9.9% CaO, 4.1% MgO, 0.6% Al_2O_3	970	4.5	560
	Float 10mm, 2 horizontal layers, tack-fused			650 (1hr dwell)	9.5	560
	Float Dark Blue	AGC	73.1% SiO_2, 12.8% Na_2O, 8.1% CaO, 4% MgO, 0.9% Al_2O_3, 0.76% Fe_2O_3	1120	3.5	560
	Composite Float dark blue and FT Float (blue glass on beam's DIC side)	AGC & IFS-SGT	75% FT Float & 25% Float dark blue	1120	3.5	560
	Composite Float dark blue and FT Float (blue glass on beam's bottom surface)	AGC & IFS-SGT	75% FT Float & 25% Float dark blue	1120	3.5	560

*All composition data derived by XRF measurements conducted with a Panalytical Axios Max WD-XRF spectrometer by Ruud Hendrikx (TU Delft, 3mE), apart from the SiO_2/B_2O_3 ratio in DURAN Schott derived from (Heimerl 1999), the SiO_2/B_2O_3 ratio in Wertheim c-glass adjusted from (Campbell, 1975), and the SiO_2/B_2O_3 ratio in Poesia glass derived from personal communication with the company.

**Estimation based on the chemical composition, using the viscosity model by Fluegel (2007).

***All samples have been quenched to the annealing point with a rate of -160 °C/hr unless differently stated.

^ The labelling "FT Float" refers to the use of Fully Tempered float glass shards as cullet. The final kiln-cast components are annealed and the thermal history of the shards is erased.

Table 4.1 (part b, extends horizontally from the previous page): Chemical composition, thermal profile, casting defects and internal stresses of the kiln-cast specimens.

Type of observed defects (1. Crystalline Inclusions, 2. Glassy inhomogeneities, 3. Gaseous inhomogeneities) & internal stresses	Kiln-cast specimen	Internal stresses (polariscope image where applicable)
1, 3: Homogeneous glass with evenly distributed miniscule bubbles. Occasional surface flaws from inadequate fusing of the cullet in combination with embedded material caused by contamination from the mould, challenging to be removed by post-processing.		Not observed
1, 3: Increased content of miniscule bubbles (often grouped in zones vertical to the top casting surface) due to insufficient dwell at top temperature and fast cooling. Occasional surface flaws from inadequate fusing of the cullet in combination with embedded material caused by contamination from the mould, challenging to be removed by post-processing.		Not observed
1: 34 vertical layers of crystallization. Traces of crystals observed at the surfaces, challenging to be removed by post-processing. Stresses: observed along the crystalline layers and at the crystal traces at the surfaces.		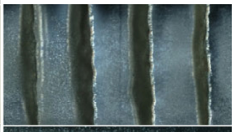
1: 1 horizontal layer of crystallization parallel to the bottom surface. Traces of crystals observed at the surfaces as well, challenging to be removed by post-processing. Stresses: observed along the crystalline layer and at the crystal traces at the surfaces.		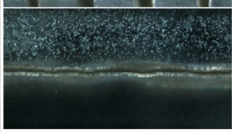
3: Improper fusion zones in the form of contouring (trapped air).	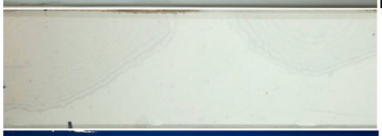	Not observed
3: Homogeneous dark blue glass with miniscule bubbles		Not observed
1, 2, 3: AGC Blue side is smoother than the FT Float side where long infolds are observed. Colour streaks are present in the diffusion interfaces between the two glasses. Miniscules bubbles present in the material, with an intensified content at the hard barrier of the two glasses. Minor metal inclusions. Stresses: minor at the blue glass/FT glass transition, no stress around the metal inclusions.	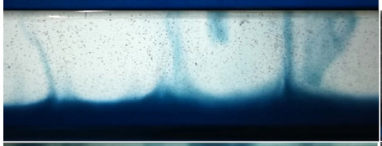	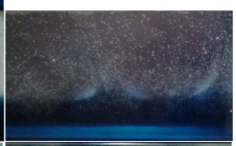
1, 2, 3: Bottom beam surface (AGC Blue side) is smoother than the top surface (FT Float side) where evident, long infolds are observed. Colour streaks are present in the diffusion interfaces between the two glasses. Miniscules bubbles present in the material, with an intensified content at the hard barrier of the two glasses. Minor metal inclusions. Stresses: around the blue colour streaks.	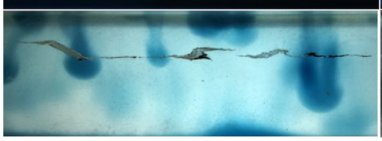	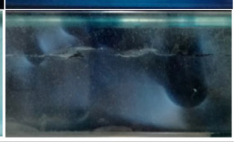

Table 4.1 (part c, extends horizontally to the next page): Chemical composition, thermal profile, casting defects and internal stresses of the kiln-cast specimens.

Glass type	Specimen description	Source	Composition* (main compounds in wt%)	Forming temperature in °C (10hr dwell unless other specified)	Theoretical viscosity (log10(visc. in poise)) at top temperature**	Annealing temperature in °C (10hr dwell)***
Soda Lime Silica (Float Glass) with contamination	Car windshields	Maltha Recycling	Variation of float glass recipes	1120	3.5	560
	Composite Car windshield and AGC Clear		70% Car windshields & 30% AGC Clear: 73.8% SiO_2, 12.6% Na_2O, 7.7% CaO, 4.5% MgO, 1.3% Al_2O_3	1120	3.5	560
Modified Soda Lime Silica	Poesia cast glass frame, 1070°C	Poesia	72.1% SiO_2, 15.9% Na_2O, 2.5% B_2O_3, 6.1% CaO, 1.9% K_2O, 0.9% Sb_2O_3	1070	3.5	540
	Poesia cast glass frame, 970°C			970	4	540
Wertheim glass (C-glass)	Wertheim pellets	Glasmuseum Wertheim	63,8% SiO_2, 5,5% B_2O_3, 11,8% Na_2O, 6,4% CaO, 5,2% Al_2O_3, 3,7% MgO, 3,2% K_2O	1020	4	540
Borosilicate	DURAN tubes	Schott	80% SiO_2, 13% B_2O_3, 3.5% Na_2O, 2.7% Al_2O_3, 0.5% K_2O	1120	5	560
	DURAN 20mm rods, 17 vertical, fused			970	6	560

*All composition data derived by XRF measurements conducted with a Panalytical Axios Max WD-XRF spectrometer by Ruud Hendrikx (TU Delft, 3mE), apart from the SiO_2/B_2O_3 ratio in DURAN Schott derived from (Heimerl 1999), the SiO_2/B_2O_3 ratio in Wertheim c-glass adjusted from (Campbell, 1975), and the SiO_2/B_2O_3 ratio in Poesia glass derived from personal communication with the company.

**Estimation based on the chemical composition, using the viscosity model by Fluegel (2007).

***All samples have been quenched to the annealing point with a rate of -160 °C/hr unless differently stated.

^ The labelling "FT Float" refers to the use of Fully Tempered float glass shards as cullet. The final kiln-cast components are annealed and the thermal history of the shards is erased.

Table 4.1 (part d, extends horizontally from the previous page): Chemical composition, thermal profile, casting defects and internal stresses of the kiln-cast specimens.

Type of observed defects (1. Crystalline Inclusions, 2. Glassy inhomogeneities, 3. Gaseous inhomogeneities) & internal stresses	Kiln-cast specimen	Internal stresses (polariscope image where applicable)
1, 2, 3: Colour streaks, bubbles, big stones and flat crystalline inclusions (coating residue), metal inclusions. Occasional surface flaws from inadequate fusing of the cullet in combination with embedded material caused by contamination from the mould, challenging to be removed by post-processing. Stresses: around some stones in the bulk.	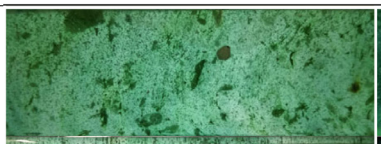	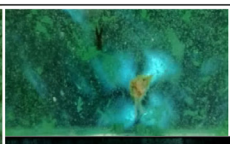
1, 2, 3: Colour streaks, intense cord, bubbles, metal inclusions, minor stones and flat crystalline inclusions (coating residue). Occasional surface flaws from inadequate fusing of the cullet in combination with embedded material caused by contamination from the mould, challenging to be removed by post-processing. Stresses: between the two different glasses.		
2, 3: Transparent homogeneous glass with miniscule bubbles and occasional cord. Stresses: along the cord lines.		
1, 2, 3: Transparent glass with bubble veils and miniscule bubbles. Extended cord. Minor surface infolds. Stresses: along the cord lines.		
2, 3: Very few miniscule bubbles, cord at the top casting surface. Stresses: intense along the top casting surface.		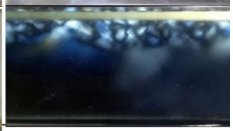
3: Dense veils of bubbles, along the connection surfaces of the glass shards.		Not observed
1: 17 vertical crystallized layers. Isolated crystals at the center of each glass division. Stresses: minor along the crystallized surfaces and isolated crystals.	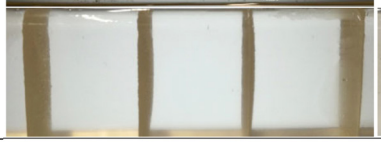	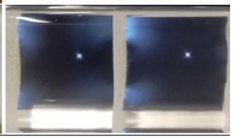

The different casting defects and their causes are described below in more detail:

i. Crystalline Inclusions

Three main causes for the formation of stones (crystalline inclusions) are observed in the specimens: (a) cullet contamination (coatings, metal/CSP traces), (b) thermal history (top forming temperature falls into the crystallization temperature range) and (c) mould contamination (Figure 4.9).

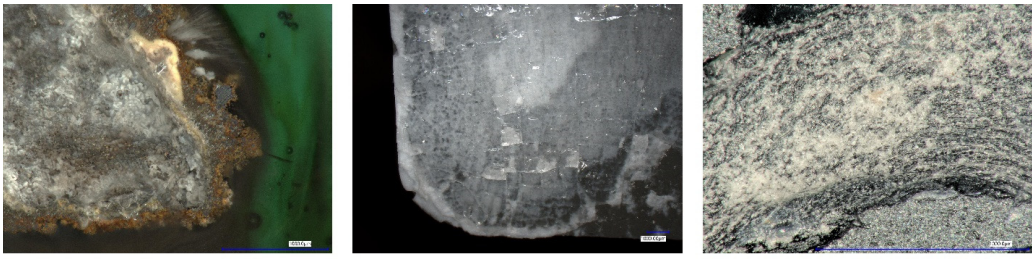

(a) Stones due to contamination (b) Crystalline fusion interface (c) Stones due to mould reaction

Fig. 4.9 Different causes for the formation of crystalline inclusions in the kiln-cast specimens.

Type (a) will occur both in the glass bulk and at the surface, in relation to the presence of a contaminant, (b) will occur in the fusion interfaces between the cullet pieces and can be either exposed to the surface ("Float 10mm x35 vertical layers, 970ºC" sample) or mainly situated in the bulk ("Float 10mm x2 horizontal layers, 970ºC" sample), and (c) will be formed at the surface and the adjacent interior zone. Figures 4.10-4.11 provide an overview of the occurred crystalline formations.

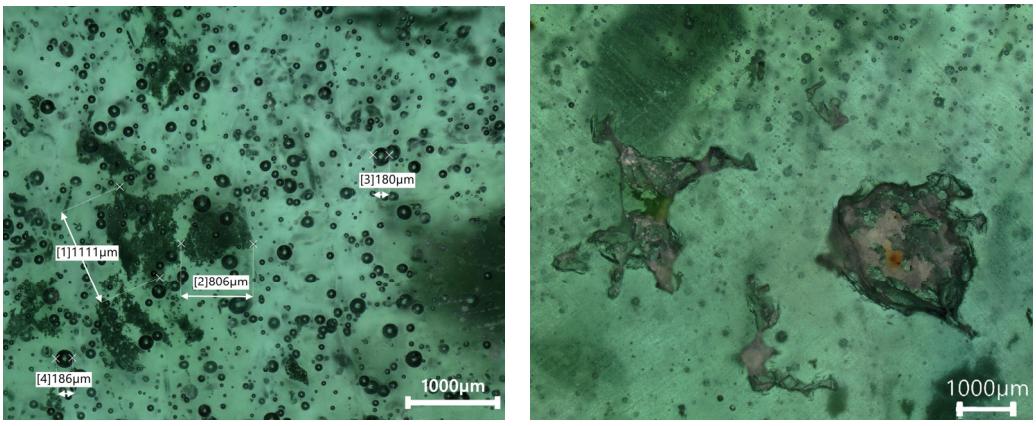

(a) (b)

Fig. 4.10 Crystalline inclusions in a "Car Glass Maltha 1120ºC" specimen. (a) Traces of non-molten coating in the glass bulk. These are flat inclusions of typically 0.5-1mm width. (b) Infolds with encapsulated crystalline material, resulting from contamination from the mould. The alien material could be silica, while the yellow singularity could be associated with clay contamination.

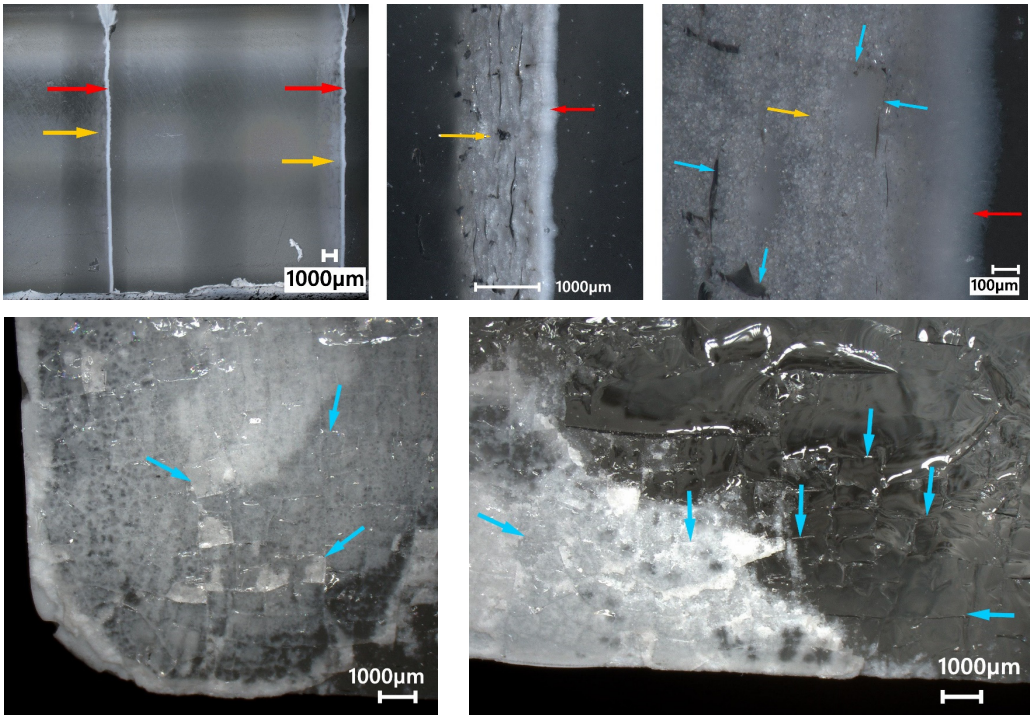

Fig. 4.11 Crystalline interfaces in the "Borosilicate DURAN rods, 970ºC specimen. The top row images show the beam's side surface (focusing at different depths). The red arrows point out the interface at the surface (ground and polished) while the orange arrows show part of the interface in the bulk, as seen through the glass. The interior view of the interface reveals parcellation (blue arrows) and miniscule round particles. Previous X-Ray Diffraction analysis (Bristogianni et al. 2020) identified this crystal as β-cristobalite. β-cristobalite is a typical crystallization product of low-alkali silicate glasses such as the studied borosilicate glass, and form dendrites that are structured at 90º angles (Bartuška 2008), leading to the depicted parcellation. This structure (blue arrows) can be seen more clearly in the images at the bottom row, which show a fractured glass-crystalline interface (beam's cross section view). The imprint of this geometry passes also to the glassy part of the fractured interface (bottom right image).

ii. Glassy inhomogeneities

Glassy inclusions in the form of cord, coloured cord ("colour streak") or parallel wavy cord ("cat scratch cord") are occasionally observed in the specimens. Cords, although potential miscible to the surrounding glass, differ either in composition, thermal history or structural arrangement (Hulínský 2008). In this study, the main causes for the occurrence of cord involve: (a) glass compositional variations in the cullet (e.g. Car glass Maltha, see Figure 4.12a), (b) partially molten coatings or metal traces (e.g. iron, see Figure 4.13) resulting in colour streaks, (c) volatilization of alkali and/or boron starting from the outer surface of each cullet piece (Figure 4.14), and (d) intentional mixing of two compatible glass recipes for achieving composite samples (Figure 4.12b). Type (a) and (b) are mainly observed in the contaminated car glass cullet, and in the case of minor metal inclusions in the AGC blue cullet (sorted from the float line rejection

point[60]). Type (c) is observed in the Wertheim and Poesia samples, both of which contain a small amount of B_2O_3 (5.5 and 2.5 in wt% respectively) and a higher content of alkali than typical soda lime silica (SLS) glasses (combined Na_2O and K_2O content = 15 and 17.8 in wt% respectively). The evaporation of boron, sodium and potassium from the melt is common in borosilicate furnaces (van Limpt 2007), and can lead to cord and layering in the glass structure (Hulínský 2008). In the case of the Poesia glass, the cord occurred in half of the samples, in long, often parallel waves, as a result of the chemical reactions and evaporation occurring between the glass shard interfaces during kiln-casting. Therefore this cord may potentially appear in all areas of the bulk, in relation to the initial position of the shards in the mould. On the contrary, a more heavily corded zone appeared in all Wertheim specimens, concentrated along their top casting surface. This cord is associated with the intense volatilization of boron and alkali at the top of the samples. Nonetheless, the Borosilicate DURAN specimens (13% B_2O_3, 4% alkali oxides in wt%) did not present any cord. This could be related to the lower content of alkali of the later, in combination with the higher casting viscosity used (10^5 dPa·s). Lastly, type (d) cause of cord mainly appears in the form of colour streaks and parallel cord, and will have a direction relevant to the manner the cullet was structured in the mould prior to kiln-casting.

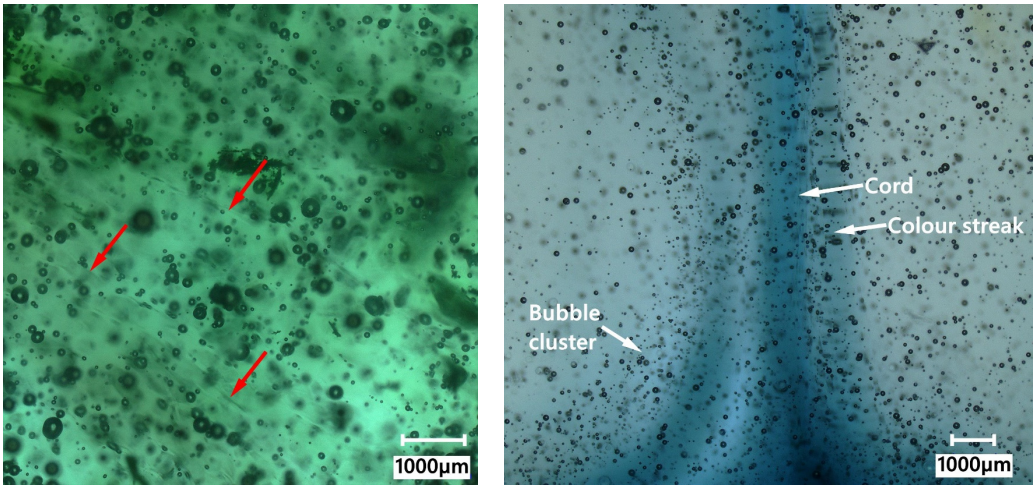

(a) (b)

Fig. 4.12 (a) Cord in a Car Glass Maltha specimen due to compositional variations in the cullet, (b) cord and colour streaks in an composite AGC Blue & FT Float specimen at the mixing interface of the two glasses.

[60] In-plant iron contamination is a common phenomenon from hardware and fasteners accidentally entering the cullet stream (Aldinger and Collins, 2016)

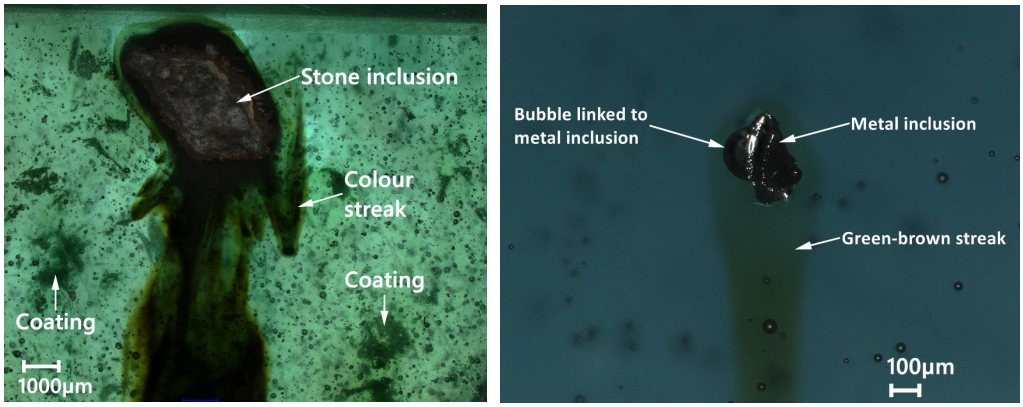

(a) (b)

Fig. 4.13 Brown-green colour streaks associated with the partial melting of a stone or metal inclusion in a (a) Car Glass Maltha and (b) AGC Blue specimen. The lack of high stress in the cross-polarized image on the right, and the colour of the streak suggest iron contamination (Aldinger and Collins, 2016).

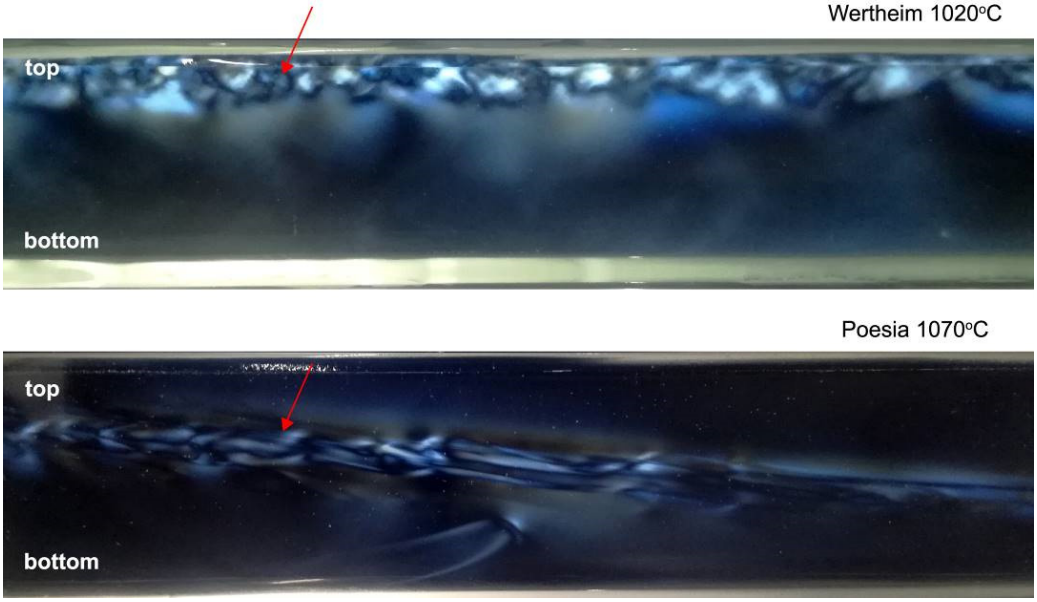

Fig. 4.14 Cross-polarized images of a Wertheim 1020°C and a Poesia 1070°C specimen, showing concentrated cord at the top casting surface in the first case, and a diagonal cord across the beam's height in the later. The first example is associated with the volatilization of alkali and boron compounds from the melt, while in the Poesia example, the cord is formed at the meeting point between two large glass shards.

iii. Gaseous inhomogeneities

Bubbles are present in all of the produced kiln-cast specimens, due to a number of causes, such as: (a) air-entrapment between the cullet pieces/granules, (b) chemical reactions during the

bonding of the cullet pieces and evaporation of volatile components, and (c) reactions and partial melting of CSP and metal inclusions. Overall, the maximum bubble size measured, was 805μm in a Borosilicate DURAN tubes 1120ºC specimen. The high forming viscosities used in this study do not facilitate the removal of such bubbles. As a result, glass made from fine-sized cullet (e.g. Car glass Maltha) or random shaped small shards (e.g. FT Float) at a $10^{3.5}$ dPa·s viscosity, will contain numerous, evenly distributed bubbles in the first case, or a network of bubbles that starts along the cullet bonding surfaces and slowly moves upwards with prolonged dwell times in the latter case. The increase of dwell time at top temperature will promote the connection of bubbles into larger air-pockets that can rise more easily out of the melt (see FT Float 2hr vs 10hr, Figure 4.15). On the other hand, specimens produced from larger orthogonal or cylindrical glass pieces, vertically organized inside the mould (e.g. Borosilicate DURAN rods 970ºC, Float 10mm x35 970ºC) would have the least occurrence of bubbles, despite their forming at lower temperatures (corresponding viscosity $10^{4.5 \text{ to } 6}$ dPa·s), as the air could easily chimney up. The use of large irregular shaped cullet horizontally structured inside the mould will promote the formation of bubble veils in the bulk but also along the vertical surfaces of the mould (Figure 4.16a). In practice, small clusters of bubbles in the bulk are negligible in terms of final component strength, but can deteriorate the strength if exposed at the surface of the cast object. Yet, despite their negative function as defects in the final product, bubbles, according to Němec 2008, can be beneficial to the molten glass, as their movement promotes convection and homogenization. This is particularly observed in the "AGC blue & FT float- blue glass on beam's side" composite samples, where the upward movement of the bubbles assists in the mixing of the AGC blue glass (positioned at the bottom of the mould) with the FT glass (located on top), as seen in Figure 4.16b.

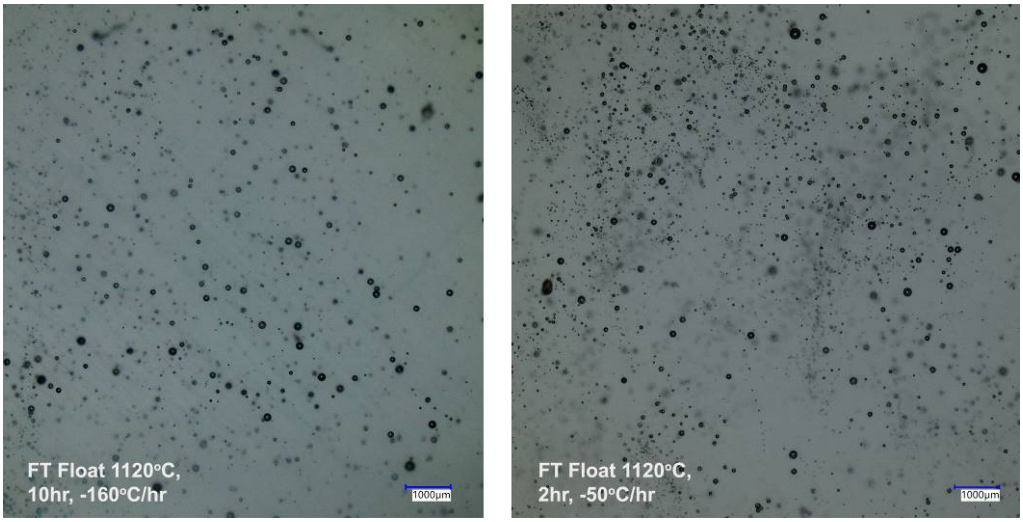

Fig. 4.15 Differences in the size and population of bubbles due to variations in the imposed thermal history of FT Float specimens. The specimen at the right, due to the shorter dwell at top temperature (2hr at 1120ºC) has an increased number of miniscule bubbles, which given more time, would have grouped into larger bubbles, risen to the top surface and escaped.

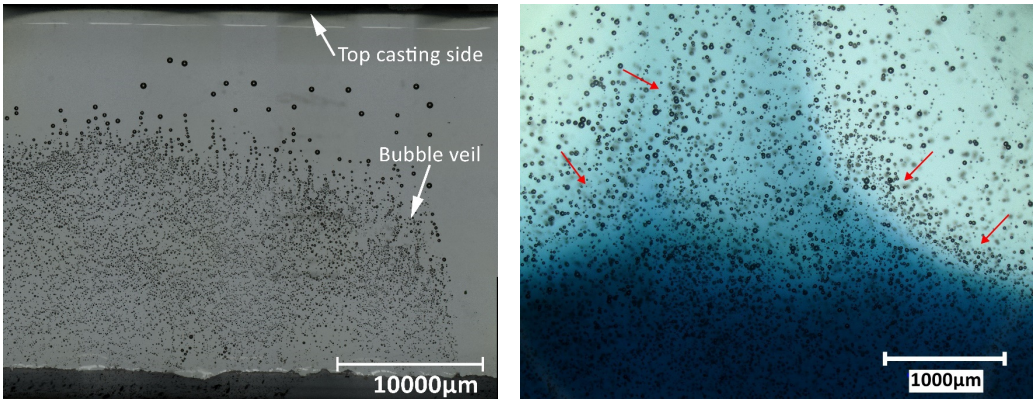

(a) (b)

Fig. 4.16 Clustering of bubbles (a) in a bubble veil travelling upwards along the side wall of the mould, in a Poesia 970ºC specimen, (b) along the interface of the two glasses, in a AGC Blue & FT Float composite specimen.

A special category of gaseous inhomogeneity is observed in the tack fused "Float 10mm x2 horizontal layers, 650ºC" (Figure 4.17), in the interface of the two float plies. Due to the low fusing temperature (650ºC) and the insufficient dwell time (1hr), extended zones of entrapped air and inadequate fusion appear along the interface.

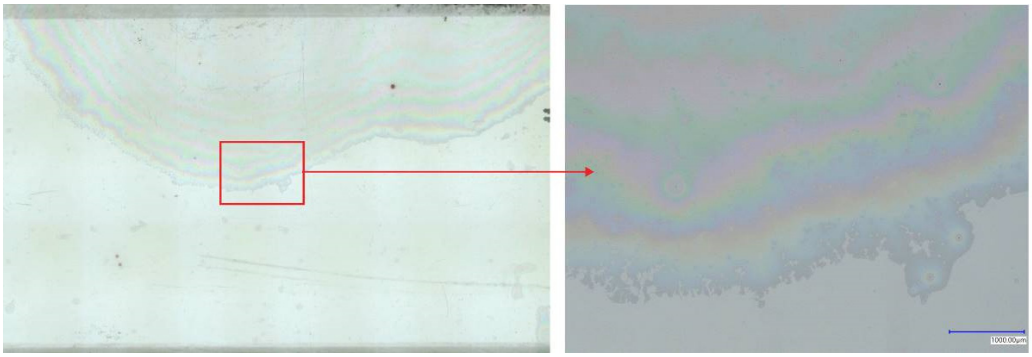

Fig. 4.17 Interference fringes in tack-fused (650ºC) float glass specimens suggest that the two glass plies are partially separated by a thin film of air.

Stress inducing defects

This category includes only casting related defects (in the bulk and/or surface of the glass beams), as post-processing and handling defects were not found to be stress increasing in this study. Assessing the above mentioned casting related flaws, four defect types seem to be occasionally inducing stress in the specimens, according to the analysis under cross-polarized light: (a) cord in boron/alkali silicate glasses (Poesia, Wertheim), (b) interface and cord between different glasses in the composite specimens, (c) presence of CSP stones in the contaminated glasses, and (d) crystalline interlayer in fused glasses (Figures 4.18-4.19). In all cases, the induced stress is not sufficient for leading to local/global cracking of the component. Regarding the impact of cord,

a range of stress intensities were observed. The intensity of this stress is linked with the mismatch of the thermal expansion coefficient between the cord and the surrounding glass, and although cord on its own may not damage the glass, it can lead to failure when acting together with other stresses (Aldinger and de Haan, 2019). On the contrary, the encountered metal inclusions, coatings and bubbles did not introduce stresses in the samples.

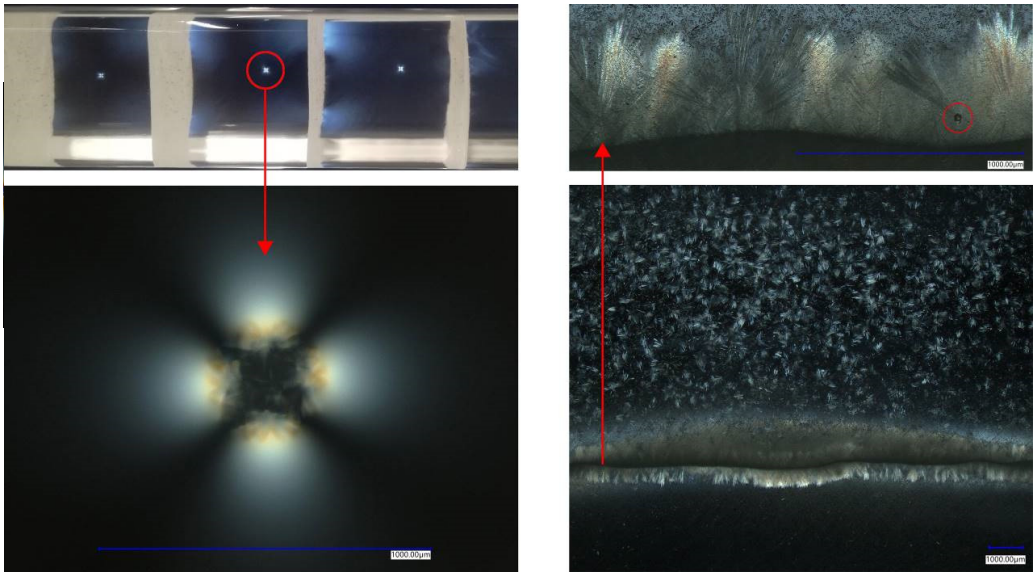

(a) (b)

Fig. 4.19 Cross-polarized images of a "Borosilicate DURAN rods 970ºC" specimen (left) and a "Float 10mm x2 layers 970ºC" specimen (right). Minor stress (in the form of while light) is observed at the crystalline interfaces as well as around isolated crystal formations in the middle of the glass region (a) or at the surface (b). According to prior X-Ray Diffraction analyses (Bristogianni et al. 2020), the crystal in (a) is β-cristobalite while in (b) is devitrite.

Strength-reducing defects (surface defects)

A combination of casting defects acts together with machining (e.g. sawing damage, grinding scratches) and handling damage (e.g. impact, scratch, frictive damage) towards the deterioration of the surface of the specimens (Figure 4.20). Bubble veils, stones and crystalline interlayers may be tolerable when situated in the bulk, but will reduce the flexural strength when exposed at the surface of maximum tensile stress (Bristogianni et al. 2020) (Figure 4.21a). Another encountered defect that is difficult to remove by polishing, is the formation of infolds/recesses at the surface due to insufficient fusion between the cullet pieces (Figure 21b). These cavities often promote the creation of a crystalline layer, due to the incorporation of loose mould material. The quality of glasses that are prone to such defects (e.g. FT float) can be improved by locally reinforcing the surface with a less prone, smoother compatible glass (e.g. AGC blue). However, to achieve such a distinct layering, careful selection of the forming temperature and dwell time is required to

avoid the transferring of faulty material to the good glass region- a problem identified in the composite beams of this study.

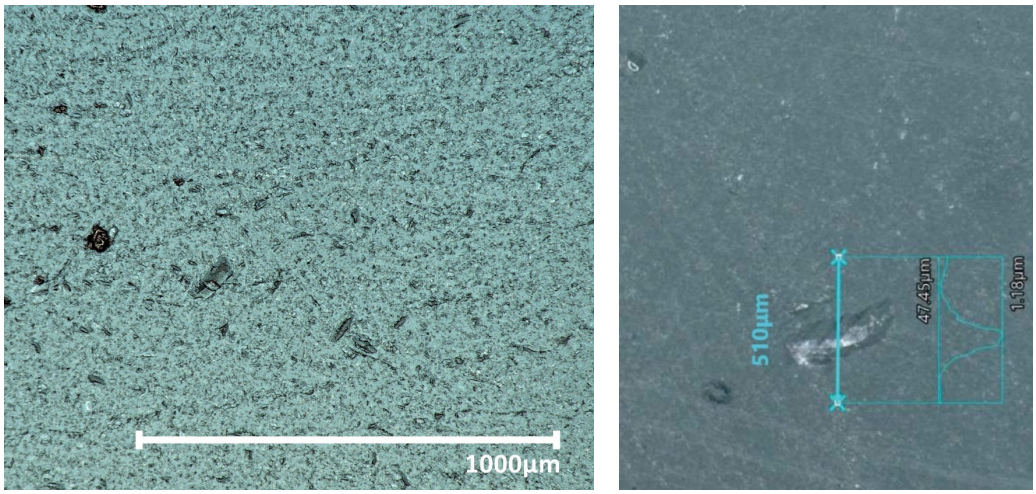

(a) (b)

Fig. 4.20 (a) Micro-damage at an AGC blue surface due to machining, (b) shows a 46µm deep surface chipping damage evoked during grinding around a crystalline inclusion.

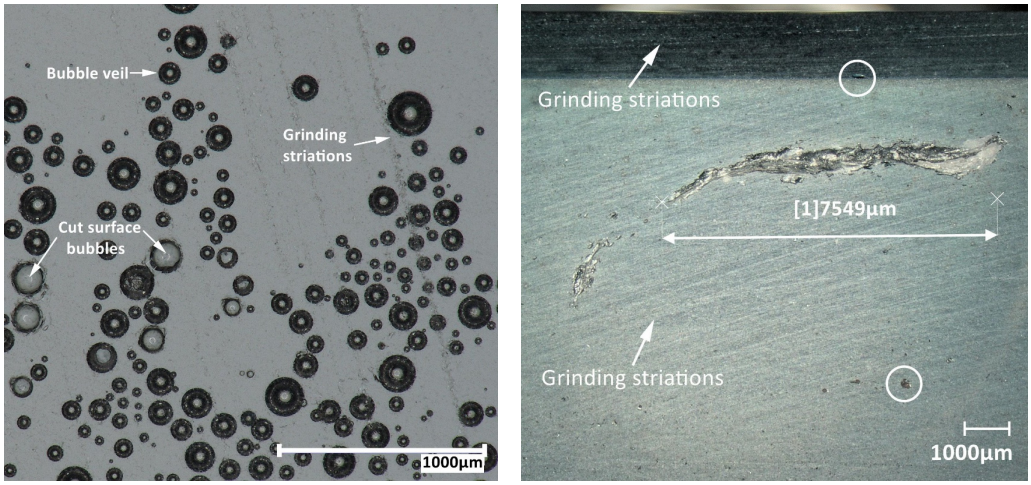

(a) (b)

Fig. 4.21 (a) Bubble veil at the bottom surface of a Poesia 970ºC specimen. During grinding, several bubbles are exposed, becoming craters of stress concentration during loading. Deep grinding striations from a renegade-grit also act upon the exposed bubble veil to deteriorate the surface quality (Quinn et al. 2005). (b) Surface damage at an AGC blue specimen. Extended infolds are present (7.5mm length) together with grinding striations and small machining cracks (in circle).

Although all specimens were ground and polished down to a 600grit level, following the same procedure, the final surface quality of the different glass beams is not equal. Some glasses were easier/softer to post-process (Borosilicate, Poesia) than others (FT Float, AGC Blue, Car Glass). In addition, some glasses were more prone to scratches (softer glasses) or chipping (Figures 4.20b, 4.21b). As seen in Figure 4.22, the Borosilicate and Poesia surfaces look smoother than the rougher AGC Blue or Car Glass surfaces. However, by studying the 3-dimensional (3D) profile of a transverse section at the bottom surface of the beams (Figure 4.23), it can be seen that less variations occur in the AGC Blue or Car glass profile than in the FT Float or Borosilicate sample. These deviations are associated with the occurrence of deeper scratches in the later samples. Lastly, Figure 4.24 shows the differences at the bottom surface between the cut-to-size Poesia frame glass and its kiln-cast version at 1070ºC, which appears to be smoother. The observed differences in the final surface quality are expected to affect the flexural strength of the different glasses.

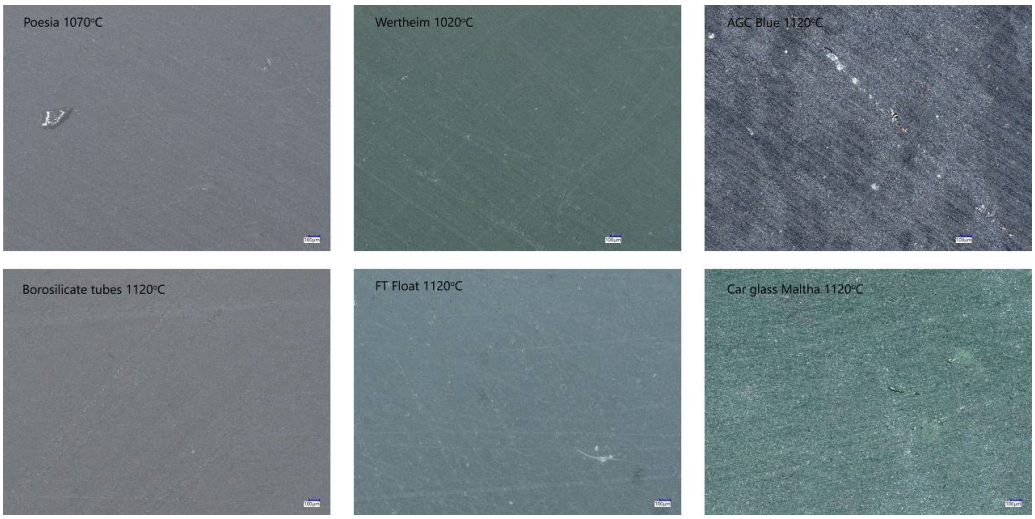

Fig. 4.22 Microscope images of the bottom surfaces of different glass samples. The left-right orientation of the images is aligned with the field of tensile stress.

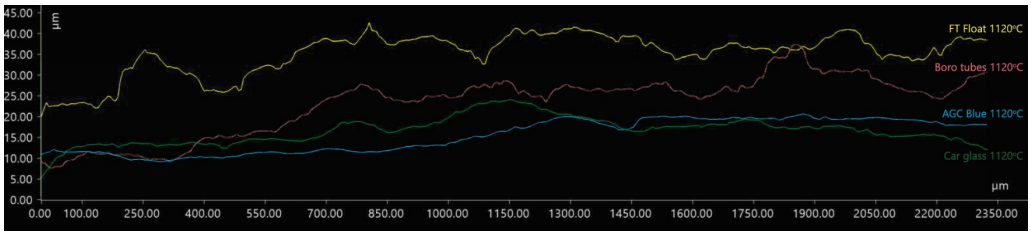

Fig. 4.23 3D profile of a transverse section (perpendicular to the tensile stress) at the bottom surface of different glass specimens.

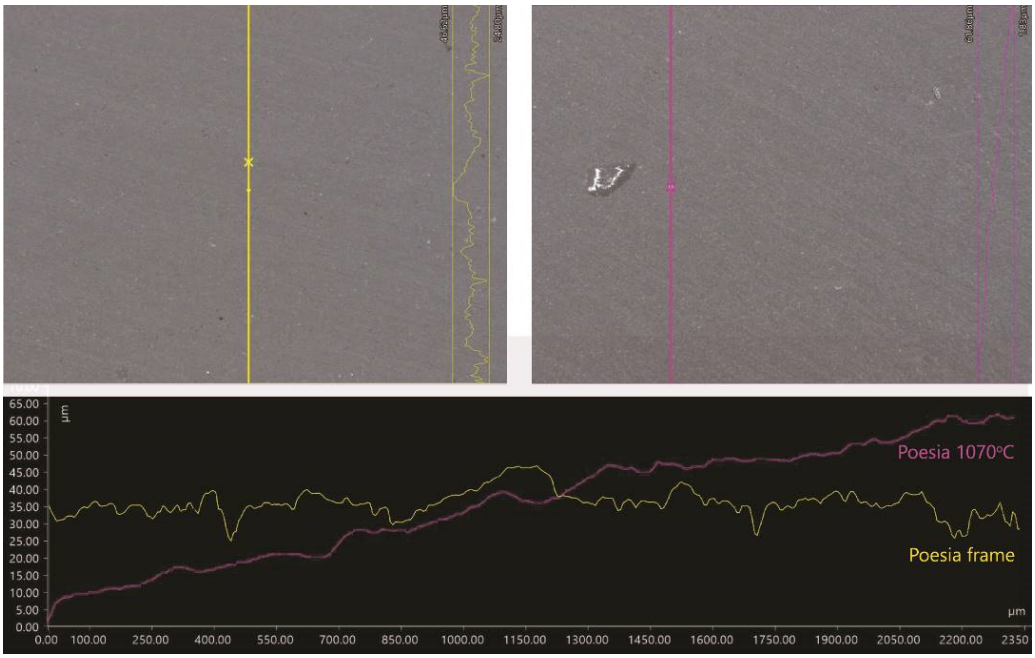

Fig. 4.24 3D profile of a transverse section at the bottom surface of a standard Poesia (yellow) and a kiln-cast Poesia 1070ºC specimen.

4.3.2 Impulse excitation test

From the obtained flexural vibration frequencies during the impulse excitation experiment, the Young's modulus of the tested specimen is calculated (Table 4.2). The resulting E values are in accordance with the literature and prior testing (Bristogianni et al. 2020): 62GPa for DURAN borosilicate glass, 70-76GPa for soda lime silica float and 79GPa for Wertheim C-glass, and only the stiffness of the Poesia glass is found lower than previously reported. In addition, the IET shows changes in the E modulus of the same glass composition by 1-3GPa, when a different thermal history is applied (e.g. FT Float, Poesia). Specifically, in the case of the FT Float, the shorter homogenization time at 1120ºC (2hr) seems to have a negative effect to the stiffness. Regarding the Poesia glass, the increase in E modulus (standard[61] < kiln-cast at 1070ºC < kiln-cast at 970ºC) is aligned with the increase in density, and the maximum stiffness is achieved at the lowest casting temperature (970ºC).

[61] Regarding the melt-quenching production of standard Poesia bricks and frames, molten glass at around 1200ºC temperature is poured in a preheated mould and rapidly cooled down to approx. 700ºC at atmospheric conditions, before the glass components are inserted in the annealing lehr (Oikonomopoulou et al. 2018a)

Table 4.2: Results of the Impulse Excitation experiment.

Glass Type	Temperature (°C)	Mass (g)	Density (Kg/m^3)	Length (mm)	Height (mm)	Width (mm)	Flexural Frequency (Hz) *Shape/Size related*	E modulus (GPa) by IET	Damping
Float 10mm	Industrial product	241.54	2504	349.33	9.88	28.66	448.82	71.43	0.001007
FT Float	1120	438.15	2508	345.78	20.21	25.19	942.42	75.01	0.000733
FT Float, 2hr, -50°C/hr	1120	519.40	2515	347.08	20.24	29.96	932.48	73.68	0.000744
Float 10mm x35 vertical layers, fused	970	539.00	2509	347.80	19.97	32.08	903.83	70.23	0.000732
AGC Blue	1120	498.20	2548	347.33	19.79	29.01	919.77	76.05	0.000736
AGC Blue + FT (blue on beam's bottom)	1120	512.60	2510	348.32	20.05	29.67	918.14	73.97	0.000739
Car glass Maltha	1120	468.90	2561	347.91	19.58	27.77	899.88	74.23	0.000719
Car glass Maltha + AGC clear	1120	472.80	2542	347.42	19.39	28.26	897.21	74.94	0.000750
Poesia	1070	471.85	2490	343.19	19.82	28.09	912.55	70.36	0.000636
Poesia	970	512.20	2525	345.12	19.82	28.09	915.98	72.07	0.000627
Poesia frame	Industrial product	473.35	2477	347.23	19.47	28.49	871.38	69.24	0.000615
Wertheim	1020	536.90	2511	347.50	20.49	30.25	971.60	79.26	0.000334
Borosilicate DURAN tubes	1120	460.73	2224	347.30	20.45	29.55	916.34	62.19	0.000256

The results of the internal friction[62] Q^{-1} measurement at room temperature by IET can be found in Table 4.2, Figure 4.25. The internal friction in a material is the dissipation of energy after an applied elastic strain or stress. Mechanical losses in alkali containing glasses are related to the relaxation of the alkali ions in the network as a result of the applied deformation (Stevels 1962). In addition, large structural defects such as cracks can lead to energy losses though friction (Roebben et al. 1997), and Q^{-1} is closely related to the micro-mobility of defects in the

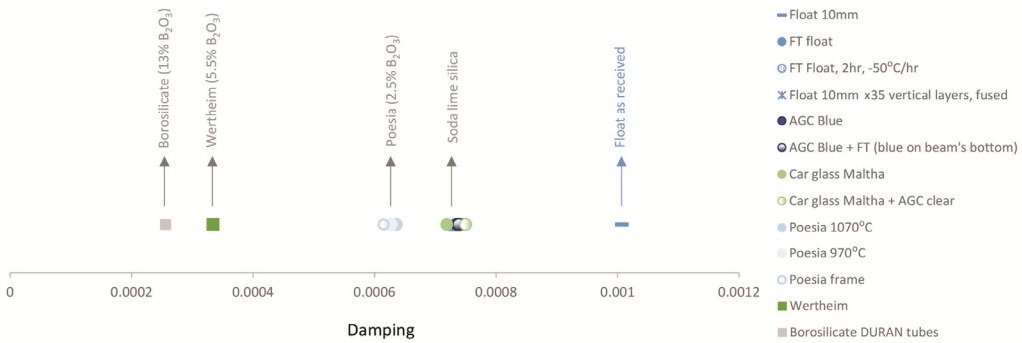

Fig. 4.25 Internal friction measurement by IET. For glass compositions containing boron trioxide, this content is noted in the parenthesis.

microstructure (Duan et al. 2001, Roebben et al. 1998). The internal friction measurement can provide therefore information about the connectivity of the glass network.

[62] The internal friction Q^{-1} is calculated from the amplitude decay of the free vibration:

$$Q^{-1} = \frac{k}{\pi \cdot f_r} \quad (6)$$

Where k is the exponential decay parameter of the vibration and f_r the resonant frequency of the tested material (Roebben et al. 1997).

Minor thermal history variations per glass category (e.g. Poesia 970ºC to Poesia 1070ºC) and contamination variations (e.g. pure "FT Float" to contaminated "Car glass") do not seem to have a major impact on the internal friction of the cast glass samples[63] (Float reference glass is excluded). The chemical composition is dominant as portrayed by the "clustering" of the glasses per category in Figure 4.25. Analyzing the internal damping results, a reduction in the damping is observed with an increase in the B_2O_3 content, with the "Borosilicate Tubes" glass (4% alkali oxides, 13% B_2O_3, 81% SiO_2) presenting the lowest internal friction. A lower internal friction of such borosilicate composition in comparison to SLS is also reported in the literature (Duan et al. 2003). In the case of the "Borosilicate Tubes" glass, the low alkali to boron ratio, favours the association of the alkali to the boron, converting the oxygen coordination of boron from 3 (triangle) to 4 (tetrahedra), and thus increasing the degree of connectivity of the network, without creating Non-Bridging Oxygen (NBO) ions (Biscoe and Warren 1938; Bray and O'Keefe 1963; Milberg et al. 1972). However, an increase of the alkali content above a threshold[64] will lead to the creation of NBOs and therefore a looser structure, which is the case in the Wertheim and Poesia glass. The float glass samples, as typical soda lime silica compositions, are expected to have ≈0.75 NBO per tetrahedron (T)[65] (Glass for Europe 2015). The difference though between the SLS glasses and Poesia and Wertheim glasses, is that the latter two are falling under the "mixed-alkali" category. A densification is reported in silica glasses containing more than one alkali type, due to the packing efficiency in the interstices of the glass network resulting from the different ion sizes (Sheybany 1948). Shelby and Day (1969) report changes in the internal friction of soda-silicates when there is a partial substitution of the Na_2O with a second alkali oxide, and in particular a shift in the internal friction peak to a higher temperature.

Given that a more open network will absorb more energy during mechanical excitation thus reporting a higher damping, information on the internal friction can suggest the level of connectivity of the glass network. However to reach meaningful comparisons between the different glasses, an internal friction measurement over a temperature range of ≈0 - 400ºC is required. In this manner, misinterpretations resulting from isolated data with no indication of the corresponding temperature peak can be avoided. Such a measurement would also shed light to structural variations occurring in the cast glass due to differences in the thermal history.

Attention should be also given to the network structural changes that can occur from the thermal history of the glass at and below the glass transition region, and during the cooling process down to room temperature. This is of relevance given that the glasses in this study are characterized by longer annealing times and slower cooling rates than the ones followed in the industry.

[63] All cast samples tested via the IET have a similar annealing history but may differ in the selection of top forming temperature, dwell at top temperature or cooling rate down to the annealing point, as explained in section 4.2.1.

[64] In an alkali borosilicate $RM_2O{\cdot}KSiO_2{\cdot}B_2O_3$ glass, an alkali content of R>0.5 will create NBOs according to the K value (Milberg et al. 1972).

[65] The float glass network is considered fairly polymerized. As a reference, the NBO/T ratio for amorphous silica is 0 (all oxygen ions are bridging) and of pure $Na_2O{\cdot}SiO_2$ is 2 (2 BO and 2 NBO per tetrahedra) (Glass for Europe 2015).

Varshneya (2013) indicates that glass properties are linked with the imposed thermal history. Specifically, the temperature scheme followed around the glass transition range T_g is the most crucial for structural rearrangements and for a consequent change in properties to occur. A slower cooling rate will lead to a smaller final volume (higher density) and a lower fictive temperature T_f[66]. Standard SLS glasses (Gross and Tomozawa 2008) and E-fiber glasses (Smedskjaer et al. 2010) will exhibit an increasing hardness with decreasing T_f, imposed by a longer heat-treatment. A prolonged annealing will increase the structural density (APF) without affecting the macroscopic glass density (Smedskaer et al. 2010). Ito and Taniguchi (2004) prove using molecular dynamics (MD) simulations that a fast cooling rate will reduce the polymerization of a typical SLS glass network leading to a smaller E modulus and lower brittleness. Varughese et al. (1998) heat-treated SLS glasses at and below T_g, reporting higher strength with higher T_f, while and Li et al. (1995) show an increase in fatigue resistance. Striepe et. al (2013) report similar behavior in alkaline earth aluminosilicate glass after prolonged annealing; the Young's modulus, hardness[67] and brittleness increases with decreasing fictive temperature. Overall, the more open, unstable structure of a quenched glass will change more easily upon mechanical stress, thus the higher strength and lower brittleness reported in the literature.

In addition, Duan et al. (2001) shows that the heating of $15Na_2O$-$20CaO$-$65SiO_2$ glass up to 500ºC (so below their glass transition temperature) leads to the rearrangement of the SiO_4 structure, inducing irreversible changes to the stiffness of glass once cooled down, while even at lower temperatures (in this case 230 ºC), the Na^+ and Ca^{2+} ions will diffuse into the silica network holes. Specifically, a reduced internal friction and a higher frequency (so higher E modulus) is reported after the heat treatment of the glass below the glass transition point.

It is therefore speculated that the cast glass specimens created in this study, which are characterized by a longer dwell time at the forming temperature, a slower cooling rate and a more conservative annealing and cooling schedule, will have a more compact network, as the prolonged processing time favors the rearrangement of the alkali ions and the polymerization of the network. The above is supported by the much higher damping, lower E modulus and lower density reported for the industrially produced float glass specimen ("Float 10mm", see Table 4.2, Figure 4.25) in comparison to the rest of the specimens.

4.3.3 Differential Scanning Calorimetry experiment

The DSC technique has been used to study the glass transition and fictive temperature of a selection of glasses, and specifically to identify changes in glasses of same composition due to different thermal history. The results of the DSC measurements can be found in Figures 4.26-4.27 and Table 4.3.

---

[66] Considering the typical free volume- temperature graph for a glass-forming liquid, the Fictive Temperature T_f is found in the intersection of the extrapolated lines of the glass and supercooled liquid.

[67] For a glass of 25x25x0.7mm size, 18300min (≈12.7 days) of annealing versus 15min would lead to an increase of E modulus by 2GPa, while the crack resistance would drop from 6N to 2.8N.

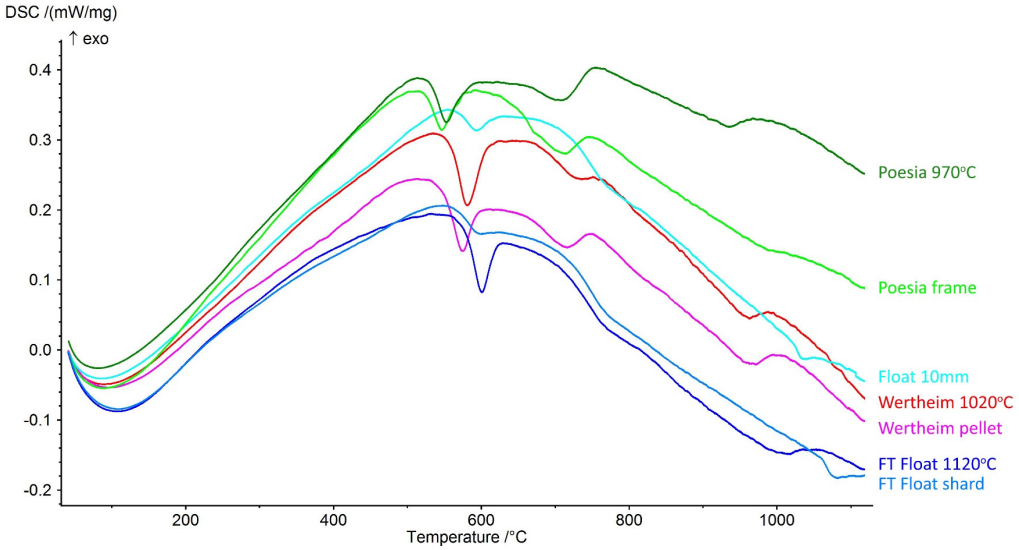

Fig. 4.26 Heat Flow versus Temperature graph for a selection of glasses, prior and after kiln-casting. The DSC curves show the required heat to change the temperature of the samples. The first endotherm peak around 500-600°C corresponds to the glass transition range.

Table 4.3: Results of the DSC experiments.

Glass Type	Process/Temperature (°C)	Glass Transition T_g (°C)	Configurational heat capacity at T_g: $C_{p,\,conf} \approx \Delta C_{p,\,glass\ to\ liquid}$ (J/(g·K))	Enthalpy of T_g Overshoot (J/g)
Float 10mm	Float line	557	0.059	-4.382
FT Float shard	Float line & tempering	554	0.232	-2.982
FT Float 1120°C	Kiln-cast at 1120°C	568	0.232	-13.19
Poesia frame	Hot-pour casting	516	0.007	-8.926
Poesia 970°C	Kiln-cast at 970°C	523	0.036	-10.78
Wertheim pellet	Drawn glass, hot-cut	533	0.256	-13.18
Wertheim 1020°C	Kiln-cast at 1020°C	550	0.056	-17.39

The comparison between the DSC curves of the "as received" and upon kiln-casting glasses shows an increase in the T_g and decrease in the T_f of the longer annealed and slower cooled kiln-cast glasses. Characteristic of the kiln-cast glasses is the deeper endothermic drop or "C_p[68] overshoot" after T_g. Shelby (2005) explains, based on the method for the determination of the fictive temperature suggested by Moynihan et al. (1976), that such a deep endotherm between the glass and liquid DSC curve shows a lower fictive temperature than a shallow endotherm for the same glass composition. The magnitude of the overshoot reflects the enthalpy loss occurring

[68] C_p refers to the isobaric hear capacity

during the annealing (Hodge 1994, Zheng et al. 2019), and specifically, the slower the cooling rate and the longer the annealing around T_g, the higher the extent of the overshoot (Boehm et al. 1981). Boehm also reports the increase of T_g with decreasing T_f, arguing that a better annealing lowers the intrinsic mobility of the system's particles, increasing thus the required energy to initiate their rearrangement.

The largest difference in the endothermic peak is observed between the "FT float" shards (and of the standard Float) and the "FT float" 1120ºC, and the smallest between the hot-poured and kiln-cast "Poesia" samples. This is attributed to the distinct differences between the float and kiln-casting production methods, especially regarding the annealing process. In a standard float line, the glass strip enters the annealing lehr at around 600ºC and exits at 60ºC is a matter of less than an hour[69], which forms a great contrast to the prolonged scheme used in this study for the cooling of the 20mm thick beams. It should be mentioned that despite the different thermal history between the two samples- as reflected in the deep overshoot and higher T_g for the kiln-cast glass- no significant changes in the chemical composition are observed in the XRF analyses (Table 4.4), apart from a minor alkali (Na_2O) volatilization. This is also confirmed by the fact that the configurational heat capacity $C_{p,conf}$ at T_g is the same for the two samples (Figure 4.27, Table 4.3).

Table 4.4: Determination of the chemical composition of FT Float glass (as received and after kiln-casting) by X-Ray Fluorescence. The presented values are normalised to 100%.

Name	State	Sample	Side	Composition* (wt%)								
				SiO_2	Na_2O	CaO	MgO	Al_2O_3	SnO_2	K_2O	Fe_2O_3	S
FT Float	As received	a	**non-Sn**	**75.4**	**12.4**	**7.6**	**4**	**0.38**	**-**	**0.1**	**0.09**	**0.07**
			Sn	74.2	12.5	7.6	4	0.36	1	0.1	0.09	0.06
		b	**non-Sn**	**75.9**	**11.8**	**7.6**	**4**	**0.36**	**-**	**0.1**	**0.08**	**0.1**
			Sn	74.8	12.5	7.9	4.1	0.34	0.03	0.1	0.14	0.05
	Kiln-cast at 1120°C	c	-	**75.3**	**11.5**	**8.1**	**3.9**	**0.43**	**-**	**0.1**	**0.09**	**0.36**

*All composition data derived by XRF measurements conducted with a Panalytical Axios Max WD-XRF spectrometer by Ruud Hendrikx (TU Delft, 3mE).

[69] Cooling rates used by the float industry are based on the work of Narayanaswamy (1981) and Gardon (1982). As an indication, Narayanaswamy suggests a 5min long cooling schedule from 600ºC down to 380ºC for a float glass of 6.9mm thickness. Rough calculations considering the daily production of 800tn in a typical float glass factory such as the Euroglas plant in Osterweddingen (DE), which is equipped with a 140m long annealing lehr (EUROGLAS 2016), shows that a 10mm thick and 3210mm wide glass would need approximately 20min to travel through the annealing lehr and cool down from 600ºC to 60ºC. This implies that for the same production volume, the much more common 4mm glass pane is cooled 2.5 times faster.

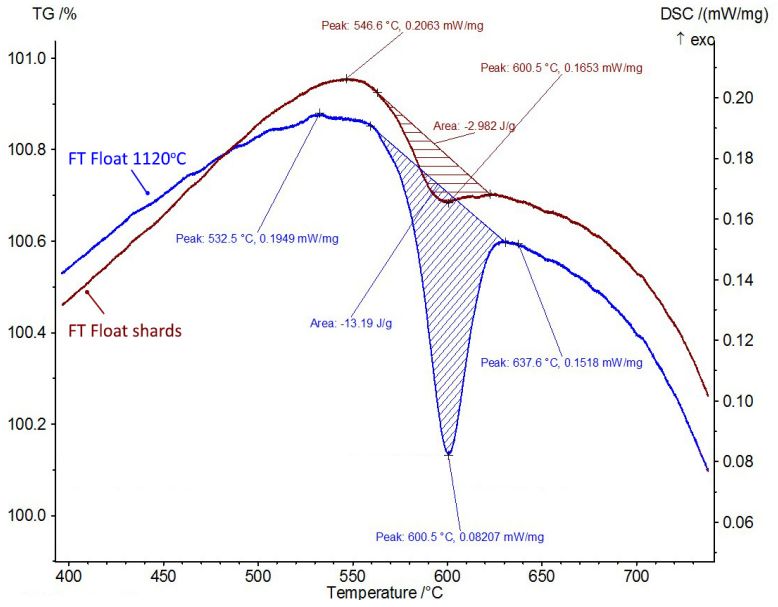

(a)

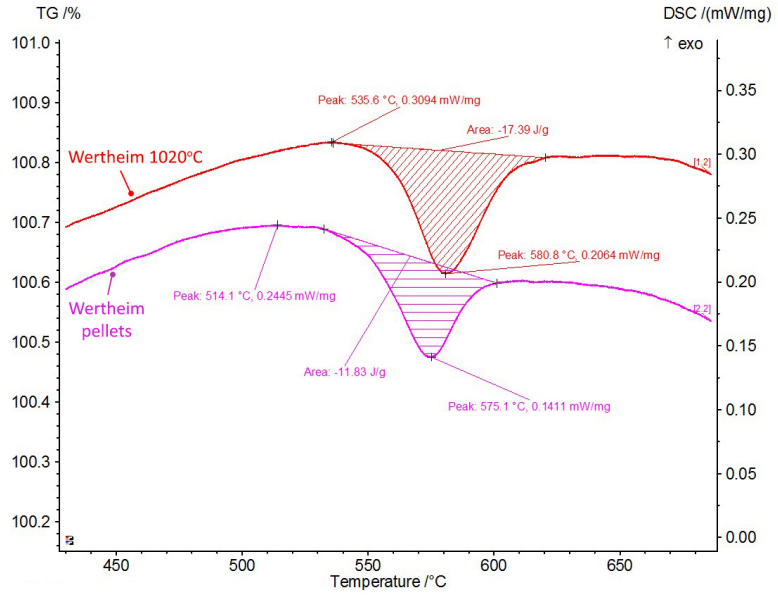

(b)

Fig. 4.27 DSC curve showing the enthalpy overshoot after the Tg of a selection of glasses, before and after kiln-casting. In the case of FT Float (a), the enthalpy change between the original and the kiln-cast glass is larger than in the case of the Wertheim glass (b). The graph on the left also shows the ΔCp at Tg (equal to the configurational heat capacity Cp,conf at Tg), which characterizes the glass-liquid transition. The Cp,conf at Tg value is the same for the two FT glasses.

4.3.4 Four-point bending experiment

The results of the four-point bending experiments can be found in Table 4.5 and Figures 4.28-4.29. The reader should take into account that only a low number (1-5) of specimens could be tested per category, and thus the results are indicative, and not statistically conclusive.

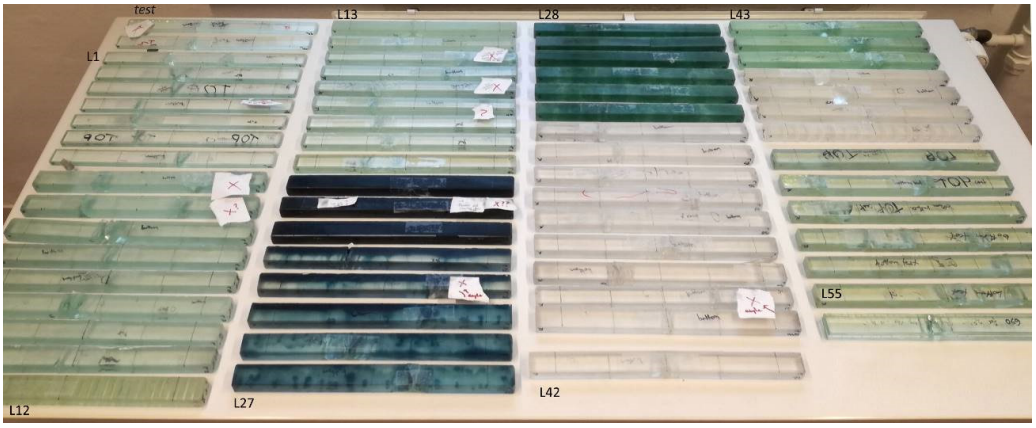

Fig. 4.28 Overview of tested glass specimens. The specimens in this figure are organized according to the L1-55 order seen in Table 4.5. Specifically, the row to the left contains specimens L1-L12, the row to the middle-left L13-L27, the row to the middle-right L28-L42 and finally the row to the right specimens L43-L55.

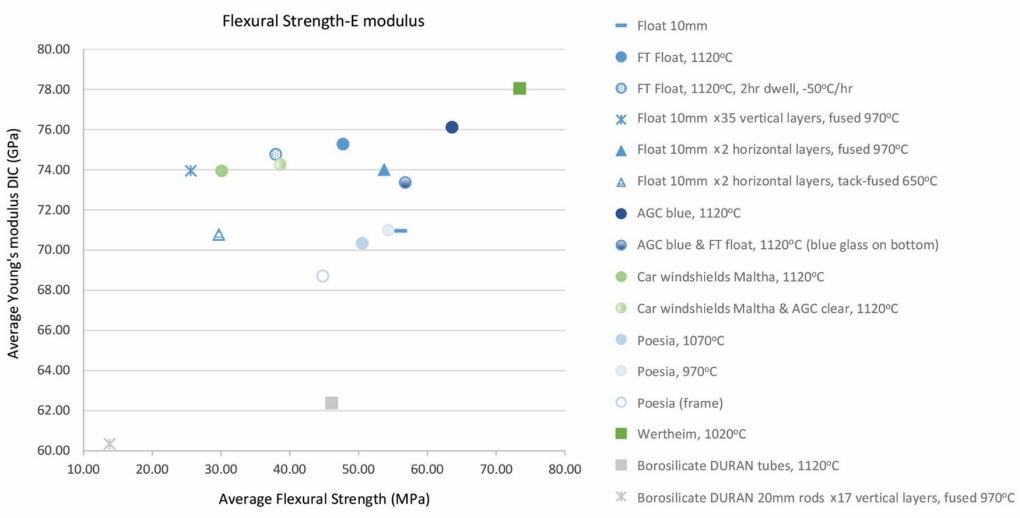

Fig. 4.29 Average E modulus versus Flexural strength.

Table 4.5 (part a): Results of four-point bending test and fractographic analysis

4-point bending experiments with 20x30x350mm glass specimens. Rollers loading/support span: 140/280mm, loading rate: 0.01 mm/s (0.6mm/min)									
Specimen no.	Glass Type	Flexural strength (MPa)	Flexural strength average (MPa) (ex. grey values in italic)*	Young's modulus (GPa) DIC	Young's modulus (GPa) DIC average (ex. grey values in italic)	Young's modulus (GPa) IET	Fracture origin length (cm) from middle	Fracture origin depth (cm) from non-DIC side (top cast side)	Flaw type
1		59.03		71.48			-6.65, 3.7	2.9, 3	Machining
2		75.36		71.49			-3.6	0	Side surface: machining
3 (IET)		*59.60*		*70.48*			-7.4	0.7	Scratch
2b	Float 10mm	46.46	56.10	71.09	70.96	71.43	-2.95	0.25	Machining
2c		*30.61*		*68.05*			-8.3	0.35	Scratch
3b		49.65		71.36			-5.55	0.85	Scratch
3c		49.98		69.37			2.8	0.3	Machining
4		53.99		75.26			-7.9	1.85	Big inclusion
5		52.22		75.78			-8.35 (shear lines), 6.25	0.95, 0.7	Inclusion
6	FT float 1120°C	56.83	47.69	75.48	75.28	75.01	-2.65	0.7	Infold/inclusion
7		37.77		75.17			-1.9	0.45	Semi-internal flaw
8 (IET)		37.62		74.71			-0.1	0.35	Internal: inclusion
9		49.49		74.94			-3.65	0.55	Inclusion
10	FT float 1120°C, 2hr dwell, -50°C/hr	36.30	37.91	76.44	74.77	73.68	0.1	1.45	Big inclusion
11 (IET)		27.93		72.95			-1.9	2	Big inclusion
12 (IET)	Float 10mm x35 vertical layers, fused at 970°C	25.59	25.59	73.95	73.95	70.23	-3.5	0.2	Crystalline interface
13	Float 10mm x2 horizontal layers, fused at 970°C	53.69	53.69	74.00	74.00	-	-2.2	0.2	Machining
14		44.05		52.91			-4.2	1.1	Scratch
15	Float 10mm x2 horizontal layers, glued with Delo 4468 (≈30-50µm adhesive layer thickness)	53.60	52.99	52.70	62.31	-	8	0.3	Scratch
16		61.30		51.32			-7.6	0.25	Machining
15b	Float 10mm x2 horizontal layers, glued with Delo 4468 (≈90-230µm adhesive layer thickness)	33.48	32.97	44.99	48.23	-	4.5	0.95	Scratch/impact
16b		32.46		51.47			-7.4	0.3	Machining
17	Float 8mm x2 horizontal layers, laminated (≈700µm interlayer thickness)	18.54	18.01	17.67	16.98	-	-5.3	0.45	Machining
18		18.91		16.62			-3.1	1.4	Scratch
19		16.57		16.66			-6.4	0.3	-
20		67.37		-			1.7	1.8	Gap/infold
21	AGC blue, 1120°C	68.63	63.54	76.13	76.13	76.05	7.5	0.55	Scratch
22 (IET)		54.62		76.14			6.4	0.25	Machining
23	AGC blue +FT float, 1120°C, blue glass located on DIC side	41.38	-	70.06	-	-	-5.8	0.6	Deep inclusion, FT glass zone
24		56.63		76.15			7.85	2.2	Infold at blue/FT glass interface
25	AGC blue +FT float, 1120°C, blue glass located on the beam's bottom surface	53.56	56.76	59.55	73.37	73.97	6.75	1.4	Internal: metal inclusion
26		58.09		73.47			-3.55	0.25	Internal: inclusion
27 (IET)		58.64		73.28			5.1	0.3	Big infold

Table 4.5 (part b): Results of four-point bending test and fractographic analysis.

4-point bending experiments with 20x30x350mm glass specimens. Rollers loading/support span: 140/280mm, loading rate: 0.01 mm/s (0.6mm/min)									
Specimen no.	Glass Type	Flexural strength (MPa)	Flexural strength average (MPa) (ex. grey values in italic)*	Young's modulus (GPa) DIC	Young's modulus (GPa) DIC average (ex. grey values in italic)	Young's modulus (GPa) IET	Fracture origin length (cm) from middle	Fracture origin depth (cm) from non-DIC side (top cast side)	Flaw type
28		30.78		73.97			-4.7	0.25	Big infold/stone (coating)
29	Car glass Maltha 1120°C	37.11	30.08	74.67	73.95	74.20	4	2.4	Inclusion
30 (IET)		22.36		73.22			7.1	0.75	Internal: big inclusion
31		44.04		74.52			0.85	0.4	Infold/inclusion
32	Car glass Matlha +AGC clear, 1120°C	35.91	38.61	73.14	74.27	74.94	6.2	1	Infold/inclusion
33 (IET)		35.88		75.15			-5.25, 5.5	2.55, 1	Infold/inclusion
34		57.27		70.89			-7	0	Sice surface: machining
35	Poesia 1070°C	39.64	50.51	70.04	70.35	70.36	-3.8	1.45	Infold+machining
36 (IET)		54.63		70.11			-6.9	0	Sice surface: machining
37		52.97		71.56			7	2.6	Bubble veil/bubble above surface
38	Poesia 970°C	42.69	54.27	69.95	71.00	72.07	-7	0.95	Impact/machining
39 (IET)		67.14		71.50			2	2.3	Impact/machining
40		49.16		66.93			-5.4	1.1	Machining damage
41	Poesia frame	*33.81*	44.76	*70.87*	68.71	69.24	7.5	1.1	Machining/impact
41b		40.11		69.45			0.4	1.1	Machining
42 (IET)		45.00		69.75			-0.1	1.5	Impact
43		73.31		77.48			0.8	0	Machining, cord zone
44	Wertheim 1020°C	77.37	73.39	77.79	78.06	79.26	5	0.2	Machining, cord zone
45 (IET)		69.49		78.90			5.1	2.9	Machining
46		47.84		62.96			-3.15	0.95	Machining
47	Borosilicate DURAN Tubes, 1120°C	49.00	46.07	62.27	62.39	62.19	-0.75	0.5	Machining+bubble veil
48 (IET)		41.37		61.92			1.2	1.4	Impact
49	Borosilicate DURAN 20mm rods x17 vertical layers, fused at 970°C	13.74	13.78	60.35	60.35	-	-6.15	0.65? 1.15?	Crystalline interface
50		22.54		72.56			+8/8.7	1.5/2	Internal: improper fused interface
51		48.78		72.72			-11.8, +4.1 (bend)	1.3, 0.95 (bend)	Bending crack + internal interface failure
52	Float 10mm x2 horizontal layers, tack-fused for 1hr at 650°C	23.56	29.70	70.16	70.77	-	-11.25	1.6	Internal: improper fused interface
53		36.36		70.03			-7.25, -2.7, +8.35/9.3	2.9, 3, 1.7/1.5	Internal: improper fused interface
54		10.43		68.16			+10.35/10.55	2.15/2.25	Internal: improper fused interface
55		36.54		70.97			+1.4/5.3,+10.6	0.2/1.25, 1	Internal: improper fused interface

* Test samples in grey italic have been excluded due to failure outside of the maximum tensile stress zone (outside the -7 to 7 cm length zone counting from the beam's middle). However, samples that failed outside this zone due to big flaws, were included in the average calculations.

Regarding the performance of the soda lime silica kiln-cast glasses (Specimens 4-13 and 20-33, produced from float glass), AGC Blue has the highest stiffness and flexural strength (64MPa) while the FT Float 1120ºC has a lower strength (≈48MPa) and stiffness. The "FT Float 1120ºC, 2hr, -50C/h" has even lower strength (38MPa) due to the increased population of defects resulting from the poor homogenization of the glass at the top temperature. The fused float sample with exposed crystalline layers at the bottom surface ("35 layers fused at 970ºC) has a significantly reduced strength as well (26MPa), whereas the fused sample with one crystalline interface in the bulk, has double the strength (54MPa). The crystalline interface will be a certain cause of early failure when exposed to the zone of maximum stress, but will have a negligible effect when located at the middle horizontal zone of the beam. Lastly, the heavily contaminated Car glass Maltha series has a rather low average strength (30MPa).

The concept of improving a lower strength glass (FT Float, Car glass Maltha) with a purer compatible glass (AGC Blue, AGC clear respectively) seems to be effective. Both composite versions showed an improvement in strength in relation to the poorer glass quality (FT float improved by 19%, Car glass improved by 29%) regardless of the occurrence of stress zones in the interface between the two glasses.

Regarding the boron containing glasses, "Borosilicate DURAN tubes 1120ºC" samples have a similar flexural strength (46MPa) to "FT Float 1120ºC" samples, but a lower E modulus (62GPa), which matches the stiffness of the original cullet (63GPa, Schott 2017). The fused Borosilicate sample (970ºC) has a 70% reduced strength due to the crystalline interfaces exposed to the bottom beam surface. Poesia glass showed a better performance, with the samples kiln-cast at 970ºC having a slightly higher strength and E modulus than the samples prepared at a 100ºC higher temperature. The highest flexural strength and E modulus were measured for the Wertheim 1020ºC specimens. The high E modulus of this glass was previously associated (Bristogianni et al. 2020) with the small (≈5%) addition of B_2O_3 and Al_2O_3 to the standard SLS composition.

Comparing the performance of the kiln-cast specimens to the reference samples, the "FT Float 1120ºC" samples have a lower average flexural strength (σ_f= 48MPa) than the single 10mm float panes (56MPa) or the adhesively bonded DELO 4468 samples[70], in the case where the adhesive thickness was between 30-50μm (53MPa). Nonetheless, the DELO bonded specimens show a reduced strength with the increase of the adhesive layer up to 230μm (33MPa). The FT Float kiln-cast samples have a higher E modulus (75GPa) than the single float (71GPa) or DELO bonded samples (62GPa for the 30-50μm series, 48GPa for larger adhesive thicknesses). The best performing kiln-cast samples on the other hand (e.g. AGC Blue, Wertheim) present both a higher strength (64MPa and 73MPa respectively) and E modulus (76GPa and 78GPa respectively) in comparison to the industrially produced reference beams. The case of the laminated float glass

[70] DELO Photobond 4468 adhesive has been chosen due to the strong bonding to glass, which leads to monolithic behaviour of the bonded glass, as proven by Oikonomopoulou et al. 2018a. When the applied adhesive layer is thin enough, during the bending of the horizontally bonded glass sample, any shear gradient in the adhesive layer is eliminated, and thus the stress/strain is directly transferred from the bottom glass layer to the top, contributing to the successful cooperation of the two layers.

samples is somewhat different, as in this case, due to the very low shear modulus[71] and increased thickness of the interlayer (700μm), the float glass plies act separately (the bottom ply will fail at a similar load to a single ply). As a result, both the strength and E modulus are low in comparison to the cast samples (σ_f=18MPa, E=17GPa).

The tack-fused (650ºC) float samples, due to the insufficient bonding at the interface, fail at low average strength values (30MPa), from a flaw originating at the interface and not the bottom surface, and specifically at the shear zone (area between the loading and the support rollers). After failure, the separated glass panes have often clear delaminated surfaces, which is a proof of non-fusion. Nonetheless, despite the prolonged zones of non-bonding in the interface, the modulus of the tack-fused components is the same (71GPa) as of the original float glass used for its making.

The industrially produced Poesia glass beams were 15% less strong than the kiln-cast beams at 970ºC, accompanied by a decrease in E modulus of 2GPa.

The E Moduli measured by the Impulse Excitation technique were to a great extent coinciding with the values calculated from the four-point bending experiment and DIC measurement. Radovic et al. (2004) have already reported the great precision of dynamic measurements, such as impulse excitation, for determining the elastic properties of solids, in comparison to the higher percentage of uncertainty of the four-point bending test due to strain gauge associated errors[72]. The proximity of the results of this study between the two tests is associated with the high accuracy of the DIC measuring method[73].

4.3.5 Fractographic analysis

The majority of the kiln-cast specimens (excluding the tack-fused samples), failed from a defect or combination of defects situated at the bottom surface, predominantly at the maximum tensile stress zone (bottom beam surface situated between the loading rollers), or in close proximity in the case of a wide flaw (0.5-1mm size) (Figure 4.30). Only four specimens failed from an entirely interior flaw, situated just above the bottom surface (75-100μm above the surface for flaw width around 160-380μm) or 1mm above for bigger flaw size (width ≈ 3.6mm) (Figure 4.31). Defects

[71] As an indication, the shear modulus of a standard PVB interlayer ranges between 10-20MPa in comparison to the shear modulus of SLS glass that is ≈29GPa (van Dam 2017).

[72] The comparative study by Radovic and co-workers included specimens of Pyrex glass, 4140 steel, pure alumina and 7075 aluminum, of various shapes and sizes. The Young's and Shear moduli of the materials were measured using static (Four-point bending, Nanoindentation) and dynamic (impulse excitation, resonant ultrasound spectroscopy) techniques. The dynamic techniques presented the lowest variability of results, below 0.5%. For the pyrex glass samples, the four-point bending technique showed the highest coefficient of variation (1.4%) and typically higher E modulus values than the other techniques. The lower confidence level of the four-point bending test (95%) is attributed to inaccuracies from the strain gauge readings. Such inaccuracies have also been observed by the authors in several studies.

[73] A Linear Variable Differential Transformer (LVDT) displacement sensor was also employed during the four-point bending tests but the reported displacement was higher than the actual movement, due to micro-movements of the sensor during bending. The values obtained were therefore not used.

situated in the meso-level structure, typically from miniscule in size up to 4mm wide (different defect types and sizes as described in section 4.2.1), were not activated.

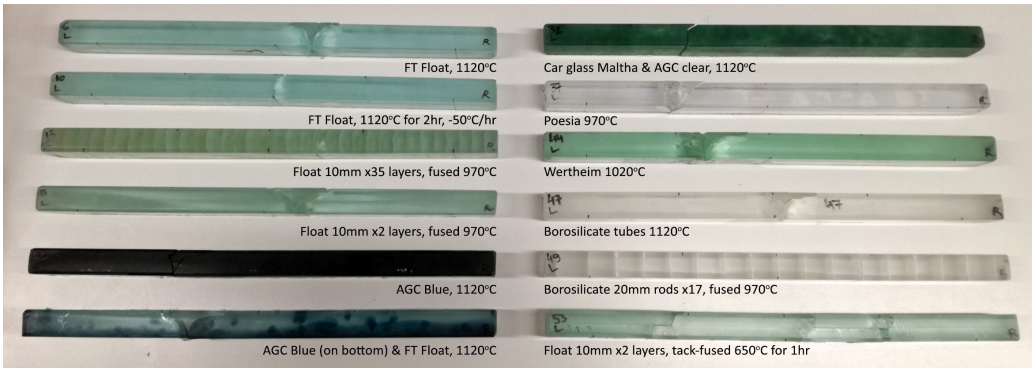

Fig. 4.30 Side view of a selection of tested specimens. All beams apart from the tack-fused specimen (L53: bottom right) failed from a defect situated at the bottom surface, within the maximum tensile stress zone. Low energy failures are manifested with a single fracture surface (e.g. L10: FT Float 2hr, L49: Borosilicate 970ºC) while branching will occur when higher failure loads are achieved (e.g. L44: Wertheim). Note the characteristic for flexural fractures compression curl at the top of the beams.

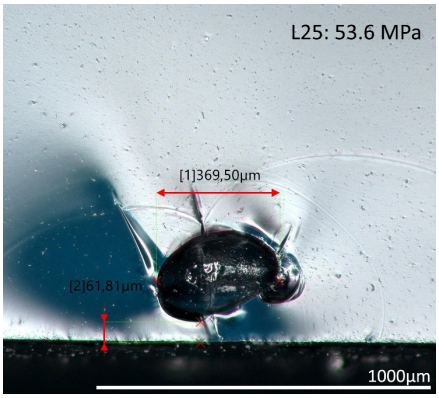

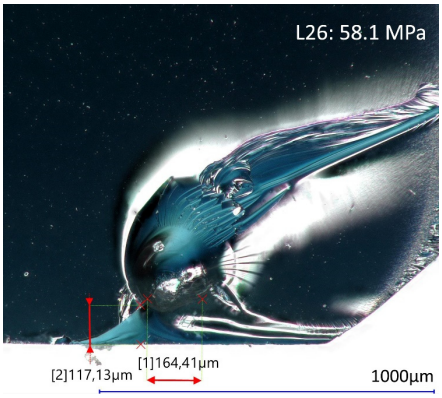

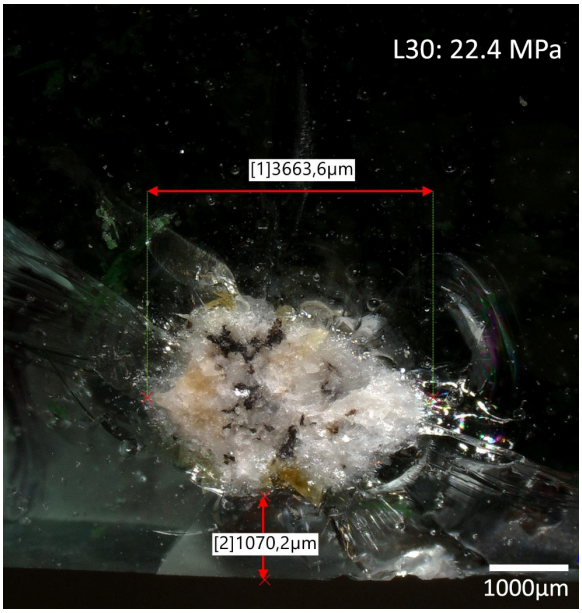

Fig. 4.31 Fracture mirror surfaces of AGC Blue & FT Float composite specimens (left) and a Car glass maltha specimen (right). In all of the above cases, the fracture initiated from a crystalline inclusion above the bottom surface.

Figures 4.32-4.34 show the cause of failure in relation to the flexural strength and mirror size. The type of flaw (machining/handling, infold, stone or bubble), and its location act upon the glass composition and correlated mechanical properties. In general, the purer specimens fail from machining/handling flaws at a higher strength (Figure 4.35), while the stone containing specimens will have a reduced strength according to the width and location (at or above the bottom surface) of the stone. For pure specimens with machining flaws of similar size as the fracture cause (e.g. Wertheim, AGC Blue, FT Float), a higher E modulus will correspond with a higher flexural strength. Only in two cases is the fracture origin associated with a surface bubble or bubble veil (Figure 4.36a). None of the specimens failed due to the presence of cord. The presence of cord does not seem to be decisive for a specimen's fracture, as failure from flaws outside the cord zone was equally possible. The fused (970ºC) specimens failed from the crystalline-glass interface at low strength values, when this interface was exposed at the bottom surface of maximum stress (Figure 4.36b).

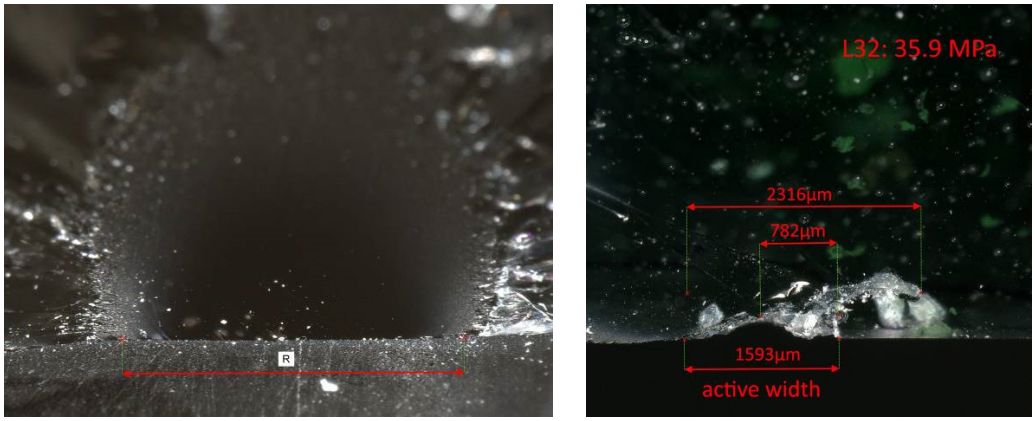

Fig. 4.32 Example of how the mirror radius (left) and flaw width (right) are measured in this study. Regarding the mirror radius, the diameter between the mist/hackle boundaries at the level of the bottom surface is measured, and divided by two. Often in elongated defects that extend towards the interior of the glass (right image), only the width exposed at the bottom surface is measured as active.

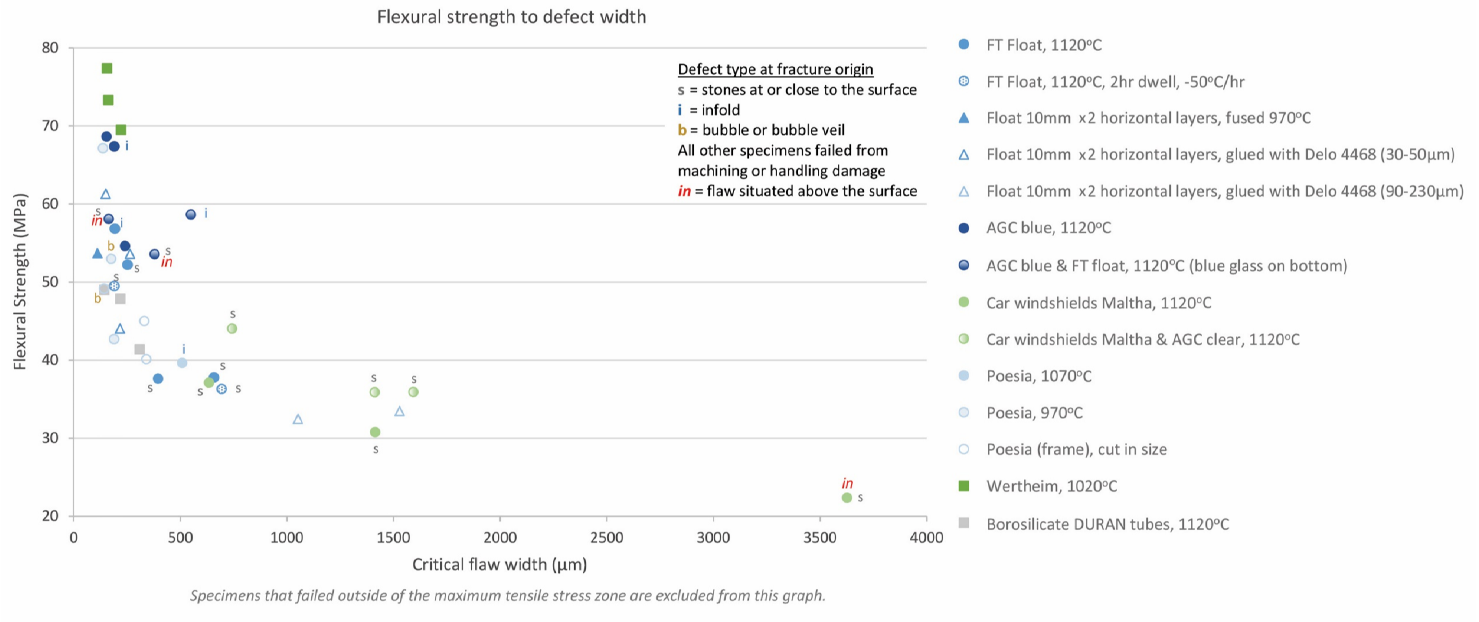

Fig. 4.33 Flexural strength as a function of critical flaw width. The cause of failure is noted for each specimen.

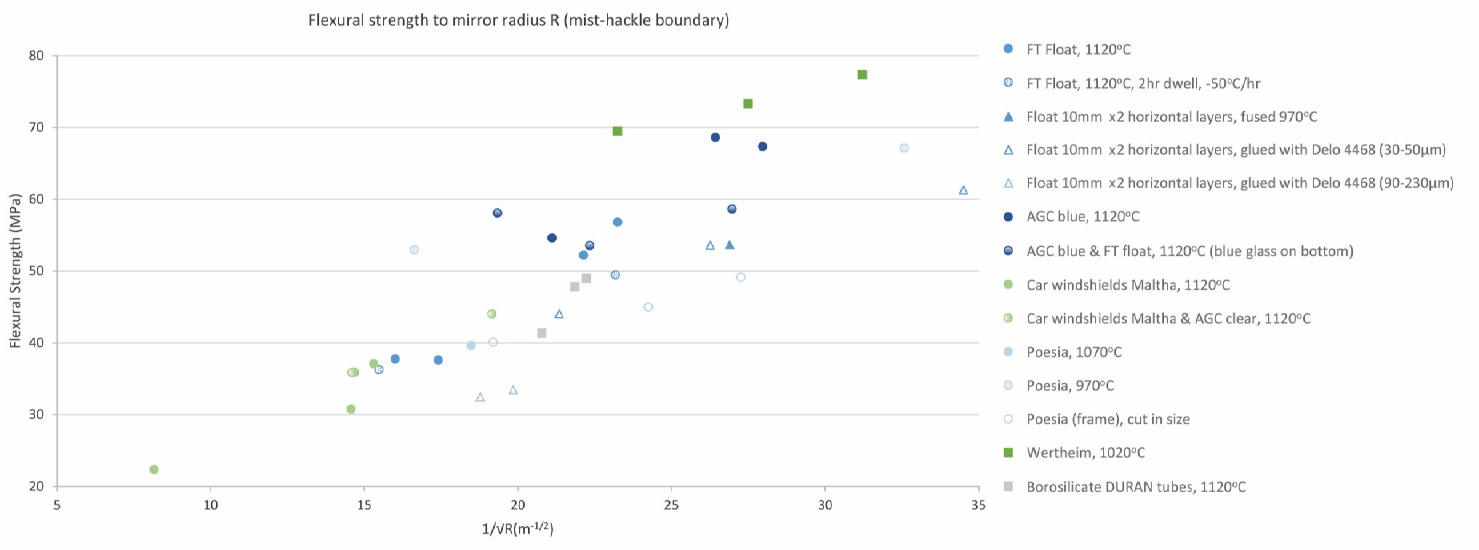

Fig. 4.34 Flexural strength to 1/√R graph. As a general trend, the higher the strength, the smaller the mirror size.

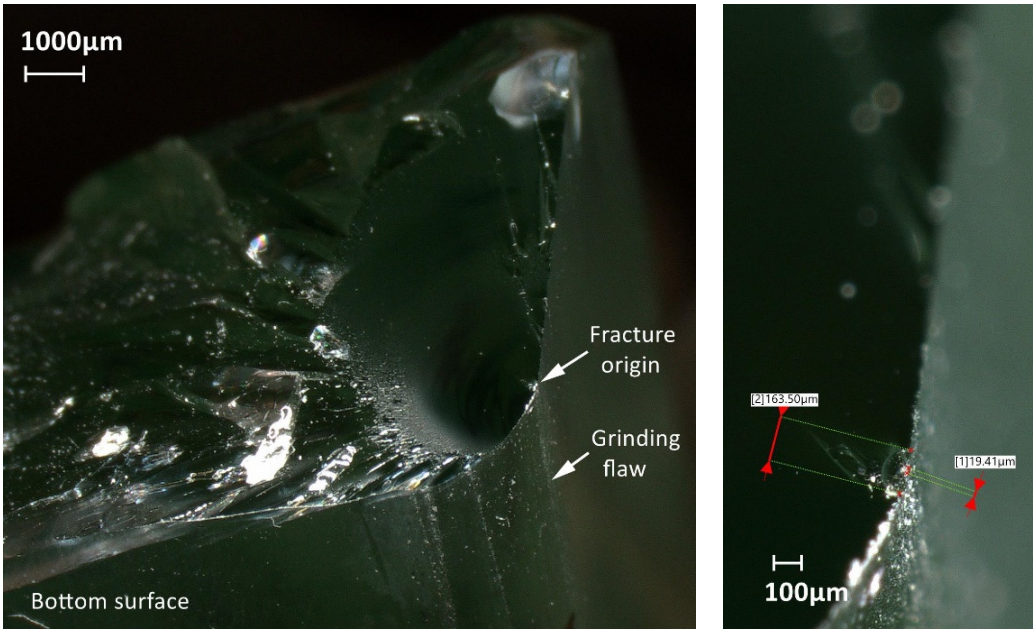

Fig. 4.35 The rough edge polishing/filleting of a Wertheim 1020ºC specimen acts as the fracture origin. The magnification of the critical flaw shows multiple striations arriving to that point, together with a semi-elliptical fracture within the glass. This defect, observed in several samples that failed from machining damage, is believed to be created during grinding.

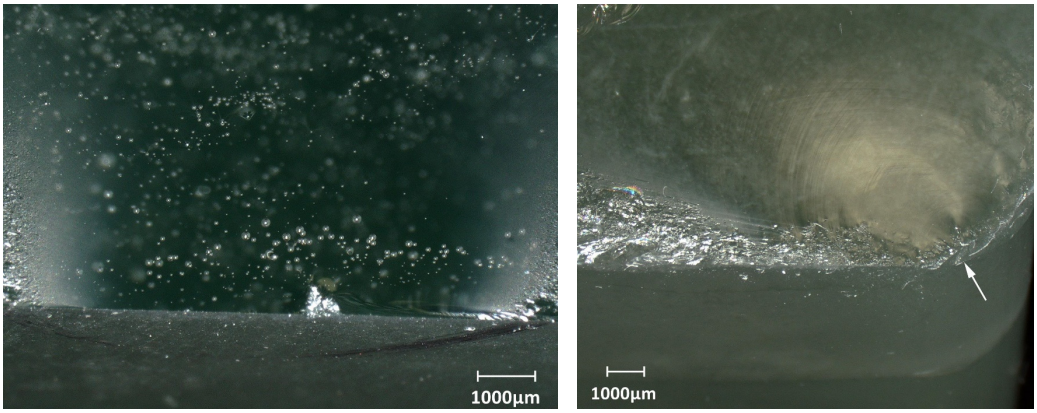

(a) (b)

Fig. 4.36 (a) The fracture surface of an "FT Float 1120ºC, 2hr -50ºC/hr" specimen forms a characteristic example of multiple flaws acting around a location, such as grinding damage, bubble veils, and stone inclusion. (b) Fracture mirror of a "Float 10mm x35 970ºC" specimen, which failed at the crystalline-glass interface.

The reference float glass specimens (single, laminated, adhesively bonded) and the standard Poesia specimens all failed from a machining or handling flaw. For the float specimens with "as received" polished bottom surface, the critical flaw would be either situated at the fillet edge line

(cut, ground and polished at the laboratory down to 600grit) or would start from a deep scratch at the surface.

The tack fused specimens are the only cases where failure originated from the bulk, and more precisely at the horizontal interface at the middle of the beam (Figure 4.37a). The extended zones of improper fusion along this interface lead to local stress concentrations at the connection zones that exceed the tensile strength of the material during loading. All specimens had a low flexural strength, between 10-37MPa, apart from a single specimen that failed from a flaw at the maximum tensile stress zone at the bottom surface (Figure 4.37b). This sample had a comparable strength (49MPa) to the kiln-cast float components (FT Float 1120ºC ≈ 48MPa).

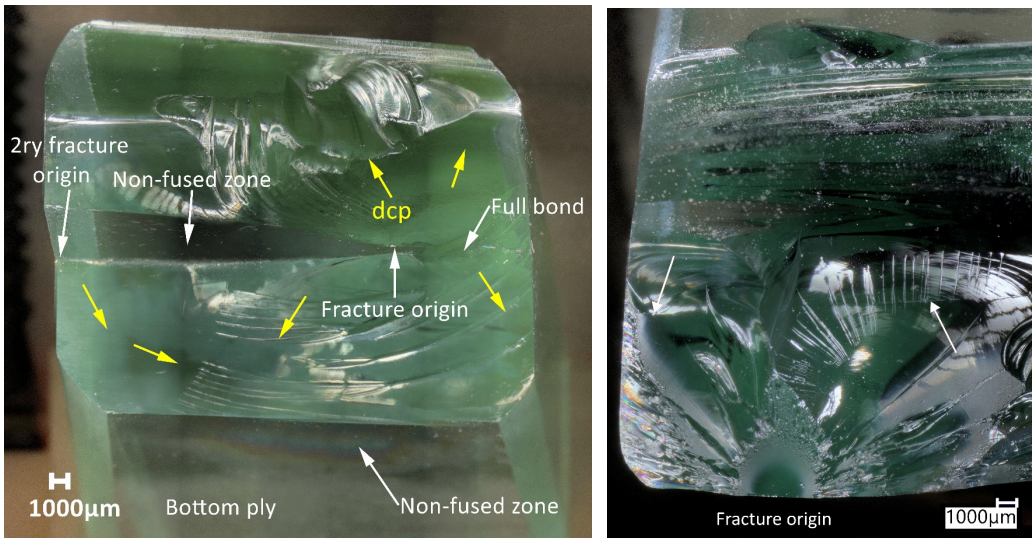

(a) (b)

Fig. 4.37 Fracture surfaces of tack-fused Float glass beams (650ºC, 1hr). (a) Typical failure observed in this series, with the fracture origin originating at the middle of the beam's height, at the interface between the two float glass planes. The yellow arrows show the direction of crack propagation (dcp). Zones of insufficient fusion are also marked at the image. (b) Single example of a standard flexural fracture, originating from the bottom surface. Despite the visible traces of the fusion interface (red arrows), the bonding of the two float layers was sufficient at this location, leading to the monolithic behaviour of the beam and to a higher flexural strength.

4.4 Discussion

4.4.1 Flexural strength comparison to shorter-span cast glass beams

A comparison between the flexural strength and E modulus of the currently tested cast glass specimens (20x30x350mm, 140/280mm span) with values for shorter testing span specimens (30x30x240mm, 100/200mm span) previously reported by Bristogianni et al. (2020) is made (see Figure 4.38, Table 4.6). It should be stressed that differences in the mechanical properties are not directly related to the "size factor", but are also at least partially linked to the differences between

the bending fixtures (e.g. roller radius, free rollers vs. fixed[74]), stiffness of the beam shape (actively contributing to shear displacement or not[75]), the post-processing quality of the specimens and even to minor variations in composition and contamination of the cullet (e.g. for Poesia or Car glass cullet).

Fig. 4.38 Comparison of flexural strength between current and prior four point bending experiments.

[74] Fixtures that do not allow sideway rolling of the pins lead to a frictional constraint that positively influences the reported strength (Quinn et al. 2009).

[75] The geometry of the specimens used in the experimental work of Chapter 3 (30x30x240mm beams) increases the stiffness of the beams, in comparison to the stiffness encountered when testing more slender beam elements. As a result, during the 4-point bending of these specific specimens, a shear displacement should be accounted at the middle of the span, in addition to the flexural displacement.

Table 4.6: Comparison of the average Flexural strength and E modulus between current and prior four point bending experiments.

Glass Type	FT float 1120°C		AGC blue 1120°C		Car glass Maltha 1120°C		Poesia 1070°C		Poesia standard		Borosilicate DURAN Tubes 1120°C	
Experiment	L	S	L	S	L	S	L	S	L	S	L	S
Average Flexural Strength (MPa)	47.7	43.7	63.6	62.9	30.1	41.1	50.5	66.5	44.8	50.4	46.1	42.5
Average Young's Modulus (GPa) by DIC	75.3	72.7	76.1	76.5	74	-	70.4	75.8	68.7	-	62.4	66.8

* L refers to the current 4-point bending experiments (20x30x350mm beam size, 140/280mm load/support spans) while S to prior testing (30x30x240mm beam size, 100/200mm load/support spans, see Bristogianni et al. 2020)

** The Poesia reference beams in this study (L) are cut out from larger cast glass pieces (65x150x790mm), than in the previous study (S), where 65x105x210mm cast glass bricks were used. Although the compositional differences should be neglegible, the thermal history of the components could to differ.

In general, the measured stiffness by the DIC and IET methods is found in agreement with the DIC measurements of the prior study, apart from the case of the Poesia glass, where a lower E modulus by 5GPa is found (this corresponds to a reduction of ≈6.6%). This change is more likely to be associated with an alteration in the cullet used[76]. In terms of flexural strength, two trends were identified: the Poesia (standard and cast at 1070ºC) and the contaminated Car glass specimens showed a reduced flexural strength by 11-24% and 27% respectively, while the cast at 1120ºC AGC Blue, Borosilicate Tubes and FT Float specimens showed a slight improvement in the flexural strength in the order of 1, 8 and 9% accordingly. The increased improvement in the flexural strength (+41%) of the Wertheim glass is linked to the by 200ºC increased forming temperature, which led to the dissolution of crystalline interfaces and thus the creation of a more homogeneous glass.

Considering the larger area where a maximum tensile stress applies in the case of the longer span beams (4200mm^2 for the 20x30x350mm beams vs 3000mm^2 for the 30x30x240mm beams[77]), lower strength values would have been expected for all specimens. This is because in general larger specimens have a higher chance of a larger, more critical flaw (Quinn 2003). However, in cases of concurrent flaw populations- such as the studied cast glasses- changing the specimen size may alter the significance of one type of flaw over another (Quinn and Morell 1991).

The explanation between the two observed trends is that the purer specimens seem to predominantly fail from machining flaws, which are of the same character and magnitude in both series of experiments. Therefore, similar strengths can be expected. On the other hand, in the case of the more contaminated samples (Car glass Maltha), indeed larger stones are traced in the larger

[76] Possible compositional changes/improvements in the batch may occur during the years in medium-sized foundries such as Poesia. Given the uncertainty of the XRF analysis which cannot detect Boron, such minor changes cannot be easily detected in this study. Determination of the B_2O_3 content in the Poesia cullet resulting from different production periods should be conducted employing Electron Probe Micro Analysis (EPMA).

[77] The area of maximum tensile stress (situated at the bottom of the beam) is calculated by multiplying the distance between the loading rollers to the width of the beams. Therefore, the area for the 20x30x350mm specimens can be calculated by multiplying 140mm to 30mm, while the area for the 30x30x240mm specimens can be found by multiplying 100mm to 30mm.

specimens, leading to a significant reduction of the strength (as anticipated), when such stones are exposed at the area of maximum stress.

Also, when comparing the two tests, it is important to take into account the change in the tested cross section (30x20mm vs 30x30mm). In the current study where the beam height is shorter, proportionally a higher zone above the surface is subjected to high tensile stresses. As a result, 4 out 57 (tack-fused excluded) specimens failed from an inclusion above the bottom surface in comparison to 1 out of 58 in the smaller span testing.

Lastly, it should be noted that the casting itself of two different shapes can lead to small variations between specimens of the same glass (due to different heat-flow for example), apart from the alterations that can occur due to randomness in the consistency of the cullet (e.g. Car glass) or unexpected changes in the ratio of the batch materials (e.g. Poesia glass).

The limited number of samples per glass type in both four-point bending tests does not allow for deriving strength scaling ratios using the Weibull size scaling approach. It pinpoints however the complexity arising in strength prediction, when failure is governed by more than one flaw type, and the glass quality is affected both by changes in the geometry and minor variations in composition as well as in the casting parameters.

4.4.2 Role of the different flaw types and uncertainties in predicting the critical flaw

The previously identified defect categories are crystalline inclusions (and interfaces), infolds, bubbles, cord and machining damage. Considering the prevailing failure due to inclusions and infolds in the case of Car glass Maltha or FT Float glass, compared to the failures from machining damage in more pure specimens, in theory predictions could be made based on the most critical from a pool of flaws at the bottom beam surface. In addition, when studying the relationship of flexural strength to flaw width in each glass series, usually a direct inverse relationship exists between the two values (see fracture mirror surfaces in Figures 4.39-4.42). However, by studying the bottom surface of the specimens upon fracture, it is often observed that failure occurred at a much less prominent flaw, than the ones situated in its surrounding (see Figure 4.43a). Such phenomena rank on the one hand the criticality of each different type of flaw, but on the other hand draw the attention to three facts (i) stress gradients due to the loading conditions (flaw location in/outside of maximum stress zone, unevenness in the sample leading to asymmetric loading) will expose some flaws more than others, (ii) more than one type of flaw may be acting in combination (e.g. machining damage together with bubble veil), weakening a specific spot, and (iii) the criticalness of a flaw depends on its orientation in respect to the stress field.

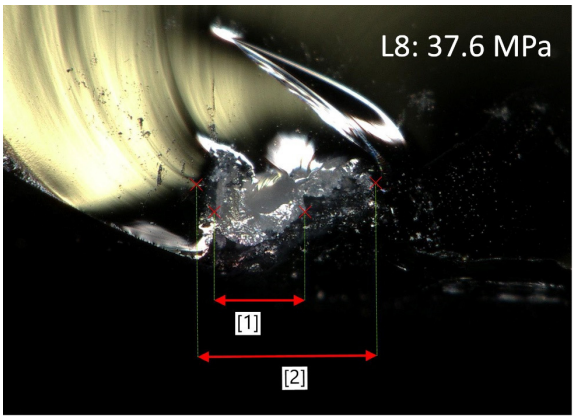

396-783µm
Interior inclusion

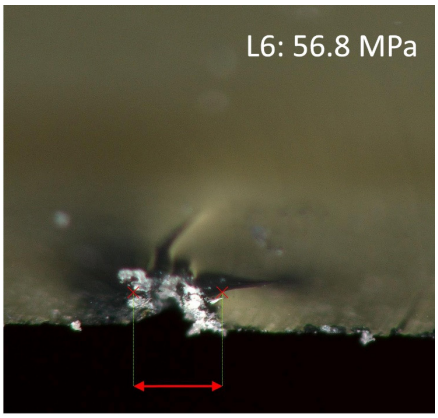

195µm
Infold/inclusion

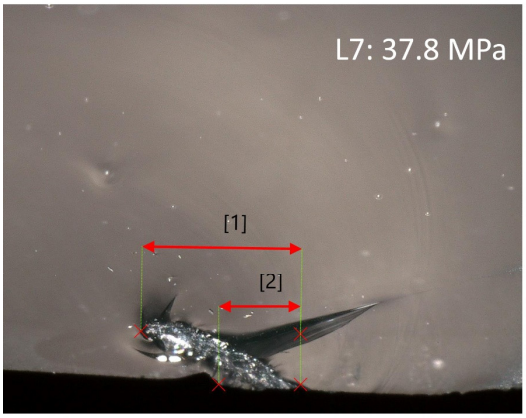

658-1250µm
Semi-interior inclusion

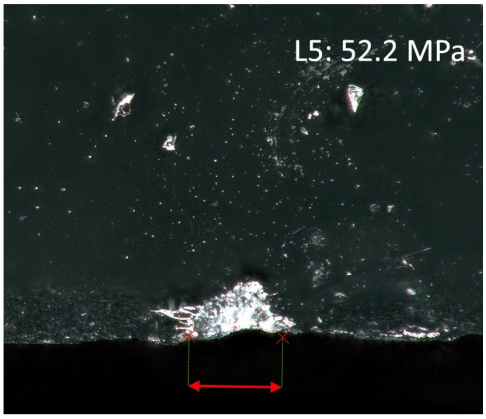

253µm
Infold/inclusion

Fig. 4.39 Critical flaw type (crystalline inclusion) and width leading to failure in the "FT Float 1120ºC series. The flexural strength increases with the decrease of the flaw width.

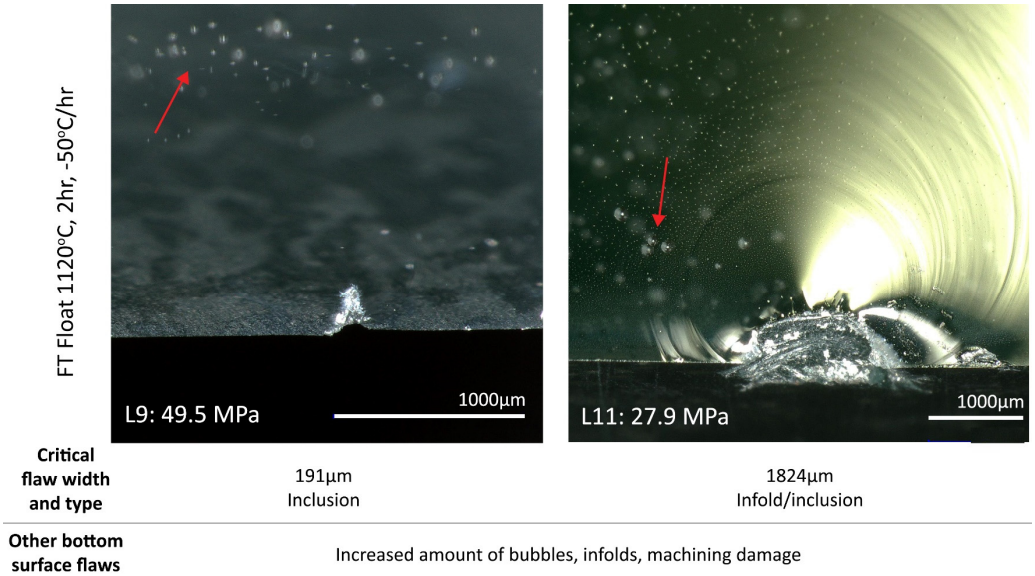

Fig. 4.40 Critical flaw at the mirror surface of "FT Float 1120°C, 2hr, -50°C/hr" specimens. The increased width of the inclusion in L11 is responsible for the reduction of flexural strength by more than 20MPa. The surface quality is further weakened by the proximity of bubble clusters.

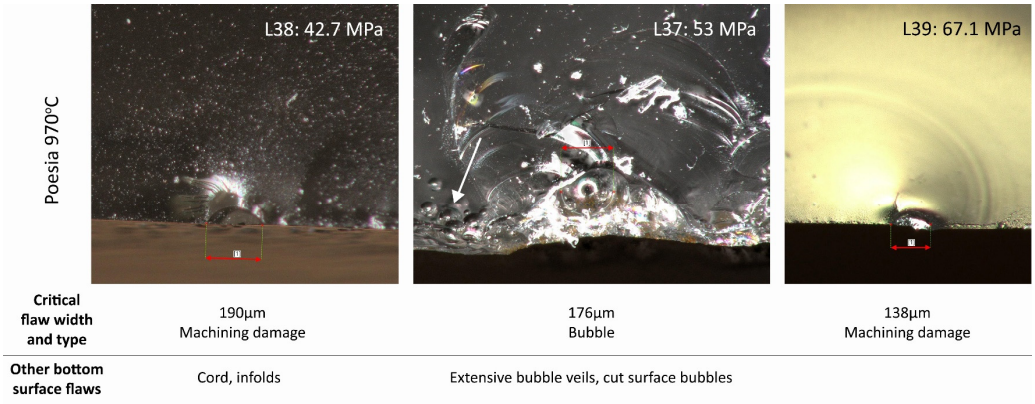

Fig. 4.41 Critical flaw at the "Poesia 970°C" series. Several defects (e.g. cord, bubble veils) act upon the grinding surface damage, leading to a 15MPa range in the flexural strength.

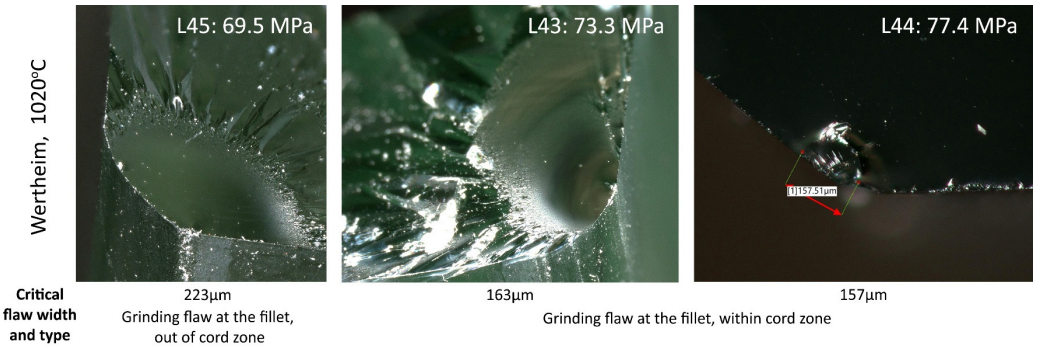

Fig. 4.42 Mirror surface of Wertheim series. All specimens failed due to grinding damage (rough fillet edge). Despite the presence of cord, the variations in the flexural strength (8MPa) are less than in prior presented examples (e.g. Fig. 4.40-4.41). In fact the specimens that failed from a flaw situated in the cord zone reached a higher strength.

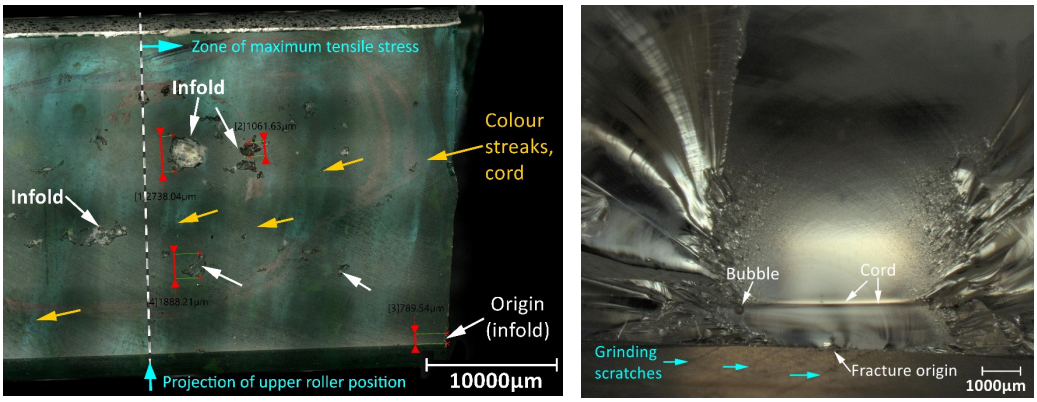

(a) (b)

Fig. 4.43 (a) Bottom surface of an "AGC Clear & Car glass" composite specimen, depicting the population of defects surrounding the fracture origin. The cord originating from the mixing of the two glasses is shown with yellow arrows. The specimen failed from a much smaller flaw than its surrounding, either due to accidental asymmetrical loading, or due to the influence of the repeated transverse cord. (b) Mirror surface of a "Poesia 970°C" specimen that failed due to grinding damage. It is uncertain if the presence of cord influenced the strength.

In that sense, although in several cord-containing specimens failure does not occur at the cord (Figures 4.42, 4.43b, 4.44), the presence of cord could intensify a flaw that by first sight looked less critical than its adjacent (Figure 4.43a). The presence of such a glass inhomogeneity implies a minor local change in the mechanical properties of the beam (e.g. change hardness or fracture toughness) that could alter the way the glass beam responds to a flaw situated in this specific location. Similarly, although bubbles in the bulk will not have a serious impact on the strength, a bubble or bubble veil just above the bottom surface will weaken this part of the surface. Figure 43a also suggests that infolds, despite their size, remain cavities that cause stress concentrations around them during loading, but will not induce stress themselves, as stone inclusions would do.

In the occasion of the simultaneous presence of similar size infolds and stones at a surface, failure from a stone is more probable.

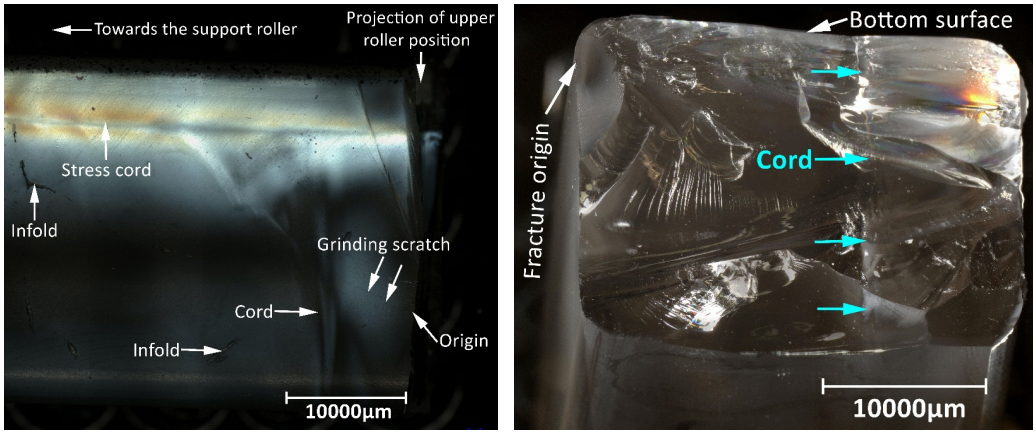

(a) (b)

Fig. 4.44 Fracture origin in a (a) Poesia 970ºC and (b) Poesia 1070ºC specimen, showing that the occurring cord was not the cause of failure.

Although grinding damage occurs in all specimens, some glasses with lower hardness will develop deeper scratches (as seen in Section 4.3.1). Moreover, specific locations will be more prone to parallel transverse grinding scratches due to the grinding process in relation to the beam geometry. This is particularly the case with the fillet edges of the beams, which proved to be a critical failure zone (Figure 4.45).

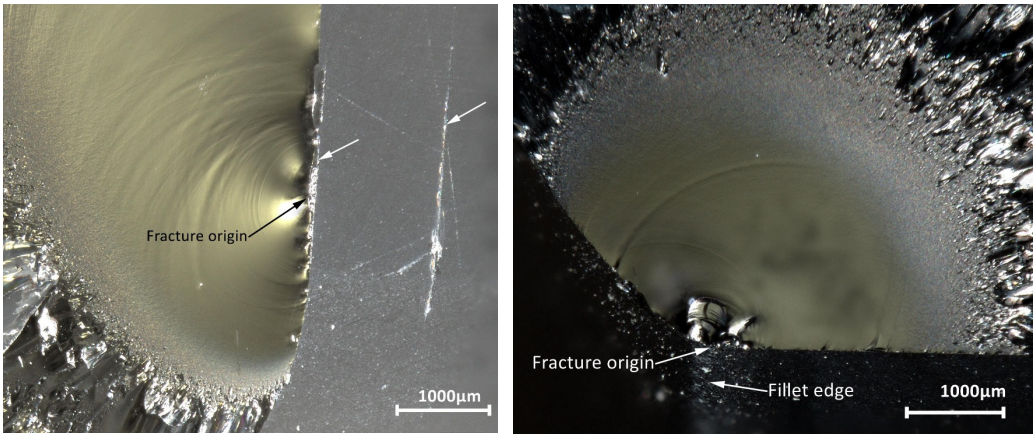

(a) (b)

Fig. 4.45 Examples of transverse surface damage such as repetitive scratches in a Poesia 1070ºC specimen (a) or continuous parallel grinding scratches during the filleting of an AGC Blue 1120 ºC specimen (b). In both cases, fracture originated from such a machining defect. Transverse flaws have a bigger impact in the strength than longitudinal flaws of the same sort, as in the first case, a wider flaw zone is exposed to tensile stress.

Apart from large (>1mm) CSP inclusions located at the maximum stress zone (in the case of Car glass- see Figure 4.46), or exposed crystalline interfaces (in the case of the fused samples at 970ºC) that can be characterized as high risk, all the rest of the flaws seem to have a versatile role that depends on the population of surrounding flaws and the exact loading condition (e.g. uneven load introduction). This complex interaction highlights the complexity of failure predictions and quality control for real-world applications of cast glass components. The subjection of such components to dynamic loading and thus a variable stress field, leads to a continuous shift of flaw activation, rendering a higher percentage of flaws as dangerous than expected in an evaluation with a static stress field in mind.

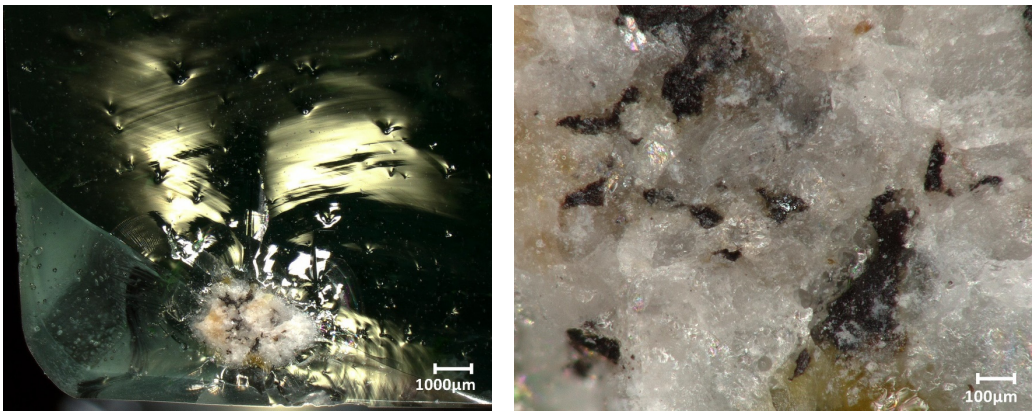

Fig. 4.46 Large crystalline inclusion (3.6mm wide) in a Car Glass Maltha specimen, possibly originating from CSP contamination in the cullet. Traces of metal and colour streak can be found in the stone. The fracture originated from the stone and not from the bottom surface.

4.4.3 Observations on the stiffness and structure of cast glass

The study showed that even in cases with an increased density of flaws in the bulk (e.g. Car glass Matlha) such as bubbles, coating residues and cord, the global stiffness of the specimen will not be affected. On the contrary, higher values were reported for kiln-cast SLS glass specimens than for the original float glass cullet. Even in the case of extended discontinuations, such as in the tack fused (650ºC) specimens, the E modulus was not reduced but stayed constant. This fact combined with the results of the IET damping values and the DSC tests suggests that the complete kiln-casting process- including the prolonged homogenization dwell at top temperature, the slower cooling rate down to the glass transition range and the prolonged annealing until below the strain point- contribute to a structural change in the glass network. This densification seems to be increasing the E-modulus, but could also simultaneously be increasing the hardness of kiln-cast components- an hypothesis that requires further investigation, as the thermal history could thus be increasing the brittleness. This information will shed light to how the glass network around a flaw will respond once a tensile stress is applied. The thermal history thus can counteract

upon the chemical composition[78]. Given the multiple casting parameters and variables applicable from one casting foundry to another, once more the issue of quality control of cast glass is raised, including the impact of the imposed thermal history (beyond the study of internal stress) to other obvious variations such as the chemical composition.

Nonetheless, the thermal history will affect both the microscopic and the macroscopic properties of the cast glass. At a macroscopic level, different types or more flaws may appear due to alterations in the firing schedule. As a direct example, the faster homogenization at top temperature and the slower cooling imposed on the FT Float glass, led to an increased amount of miniscule bubbles in the material. The fractographic analysis suggests that the occurring flaws contributed to a lower strength (by 20%) in a more significant manner than any changes in the nanostructure of the network did.

4.5 Conclusions

A total of 64 silicate based glass specimens were prepared by kiln-casting at relatively high viscosities (10^6–$10^{3.5}$ dPa·s) or by modifying industrial glass products into 20x30x350mm beam size, to be tested in four-point bending (140-280mm roller spans). Prior to testing, the defects of the kiln-cast samples were documented. These are grouped in casting-related defects that occur both in the bulk and surfaces (crystalline inclusions, glassy inhomogeneities and air bubbles) and post-processing defects (e.g. machining, impact). From the occurring defects, the CSP stones and cord were identified as stress inducing.

A low number of specimens (1-5) was tested per glass category, providing an indication on the flexural strength and stiffness of each glass type, but not sufficient data for deriving to statistical predictions. The four-point bending experiments of kiln-cast glass specimens showed a flexural strength range of 30-73MPa, according to the level of contamination and the chemical composition of the glass. The measured E moduli by the IET and DIC/4PB were in close agreement, and ranged from 60-62GPa for Borosilicate samples, 69-72GPa for Poesia, 70-76GPa for SLS glasses, to 79GPa for the Wertheim glass. The “Wertheim 1020ºC” specimens, had the highest flexural strength as, in terms of structure, the small addition of Al_2O_3 and B_2O_3 and the higher Na_2O/CaO ratio contribute to a higher bond strength yet more flexibility in comparison to a conventional SLS glass, while its fluidity at the forming temperatures contributed to a smooth surface without infolds or stones. The heavily contaminated Car glass Maltha cullet rendered the lowest strength results, when cast at 1120ºC, due to the presence of even 3mm wide CSP stones. However, by adding ≈ 30% of a pure compatible SLS cullet to the original car glass cullet, the strength improved by 29%. Improvement by 19% in the flexural strength was also observed in the FT Float composite beams, which showed an equivalent strength to the industrially produced single float glass panes (≈56MPa). Thus the engineering of composite glasses can lead to the

[78] The previous study (Bristogianni et al. 2020) suggests that some compositions are more favorable (e.g. Poesia, Wertheim) than others, as they tend to deform more around a flaw due to a higher ratio of alkali oxides over calcium oxide and small percentage of boron. This ability of micro-deformation leads to the relaxation of the stress field and to a higher flexural strength.

improvement of contaminated cullet, provided that no significant stress is developed between the mixed glasses.

The fused (970ºC) and tack-fused (650ºC) specimens had a reduced failure stress, either due to the exposure of the crystalline interface at the bottom surface or due to the insufficient bonding at the tack-fused interface respectively. In the first case however, if the crystalline interface was situated in the bulk (parallel to the bottom surface), the strength was unaffected. On the contrary, the majority of the tack-fused samples failed at the interface due to high stress concentration developing due to the improper bonding. Regarding the kiln-cast specimens produced at higher temperatures and the industrially produced glass specimens, the majority failed from a flaw situated at the bottom surface, at the zone of maximum tensile stress. Only four cases showed failure from a flaw just above the surface, at a maximum distance of 1mm. Other flaws situated in the bulk were not activated, showing the increased capacity of voluminous cast glass specimens to tolerate defects situated in the bulk, as long as the inclusions' thermal expansion coefficient and size do not introduce stresses to the parent glass.

The main causes of failure identified were crystalline inclusions (and interfaces), infolds, bubbles, and machining damage. Machining damage was the prevailing cause of failure in the case of more pure specimens and industrially produced reference specimens, while contaminated or fused specimens failed from crystalline inclusions. This pattern explains the double trend observed when comparing the previously tested kiln-cast specimens (30x30x240mm) of smaller fixture span (100-200mm) with the current tested specimens. Despite the expectation that scaling up the specimens would lead to a general reduction in strength, this effect was only occurring in the case of the contaminated samples. Given that the purer samples would fail in both cases from similar grinding or impact flaws, no significant differences would appear in the flexural strength.

Regarding the degree of criticality of the different flaws, it was observed that fracture will not always initiate from the most defect populated zone or from the most suspicious singularity. This is linked either to the presence of a stress gradient (e.g. asymmetric loading due to surface unevenness of the beam at the rollers) or to the simultaneous acting of more than one flaw on the same spot. This fact reflects an engineering challenge for real-world applications of cast glass, as the subjection of the components to dynamic loading can turn an initially negligible defect (including defects in the bulk) to the weakest link. Quality control and defect inspection therefore becomes a multi-dimensional (6D) problem, where the defect profile is determined by the type, size, shape, location, orientation and the strength of the glass. Upon this matrix, two parameters are imposed: the local stress field (combination of loading scheme, component geometry and internal stresses) and the general population of flaws. This highlights the complications involved in any attempt to do size scaling and develop statistical predictions.

Adding to the above complexity due to the macroscopic defects originating from the casting and post-processing of glass, microscopic alterations take place in the glass structure as well, in relation to the imposed thermal history. Both DIC/4PB and the IET measurements showed an increase of the E modulus upon kiln-casting, in the order of 2-3GPa. In addition, the DSC curves

of selected samples showed an increase of the T_g by 7-17°C and a lower fictive temperature for the kiln-cast glass. Moreover, a lower damping was reported for kiln-cast SLS glasses in comparison to the industrialized float glass. All the above information suggests increased compacting of the glass network due to the imposed slower cooling rates and the prolonged annealing schedule. This slower cooling could also be associated with an increase in hardness and thus with more brittle behavior of the glass. Further research is required to verify these microscopic changes and to identify the extent to which each individual factor (stiffness, hardness) affects the overall structural performance. Still, the effect the thermal history may have on the creation of macroscopic defects (e.g. larger or higher content of bubbles, extended crystallization) will have a greater impact on the flexural strength than the changes that the thermal history will impose to the glass network.

4.6 Recommendations

Several recommendations arise from this study concerning the engineering, production, testing, and quality control of cast glass components for building applications. Regarding the glass selection and engineering, the design of composite glasses is a promising idea worth exploring. Further experimentation with a broader range of glass combinations of different qualities is required, together with trials on the transition interface between the two glasses (abrupt vs. diffuse). Better grinding and polishing of the component surface is advised to improve the strength of the specimens.

Regarding the mechanical testing, in general a larger number of specimens (≈30 per category) is required to derive statistically valid conclusions and safe engineering data. Particularly meaningful would be the testing in large numbers of not only laboratory-produced, but also industrially cast specimens by different manufacturers. In this manner, the effect of the casting process (and thus of the thermal history and occurring defects) on the strength of the components can be properly studied. The reliability of the four-point bending test can be increased by introducing soft aluminum strips between the fixture pins and the glass specimens, to reassure complete contact of the beam and the rollers, and thus increased symmetry in the load distribution. Moreover, the use of a universal testing machine of smaller load capacity, closer to the expected failure load, can increase the accuracy of the results. In addition, it is advised to perform four-point bending experiments at different loading speeds, to investigate the influence of the sub-critical crack growth on the failure stress. Higher accuracy in the IET measurements can be achieved if completely rectangular beams with sharp edges (no filleting) are used. Measurement of the internal friction of the kiln-cast glasses should be performed in a temperature range from room temperature to annealing point in order to reveal structural modifications occurring due to thermal history. This information should be linked with repeated DSC testing to investigate possible transitions in the T_g and fictive temperatures, and Knoop hardness experiments to see to what extent densification takes place. The investigation of hardness variations along the glass specimens is important for understanding the gradient of critical stress levels per flaw type and location along an inhomogeneous glass component.

In addition, the physio-chemical characterization of the most common casting-related defects by Scanning Electron Microscopy (SEM) is required, together with the development of automated defect mapping methodologies for the produced components. The development of a digital scanning system that documents the type, shape and orientation of surface and bulk flaws should be combined with repeated mechanical testing and fracture analysis, to lead to a reliable mathematical prediction model. For more pure cast glass components, the relationship between flaws and strength may be straight-forward and quality control will be a more simple process to follow. However, in the case of more contaminated components, produced from recycled cullet, defining the defect-strength relationship is a complex, multidimensional problem. Machine learning techniques could potentially be employed to reach safe strength predictions and aid the quality control process.

References

Aldinger, B.S., Collins, B.K.: Color Atlas of Stones in Glass. American Glass Research, Butler, PA (2016)

Aldinger, B.S., de Haan, P.W.: Color Atlas of Glass Container Defects. American Glass Research, Butler, PA (2019)

ASTM: E 1876 – 01: Standard Test Method for Dynamic Young's Modulus, Shear Modulus, and Poisson's Ratio by Impulse Excitation of Vibration. In. United States, (2002)

Bartuška, M.: Glass defects. Glass Service Inc. and Práh, Prague (2008)

Biscoe, J., Warren, B.E.: X-Ray diffraction study of soda-boric oxide glass. Journal of the American Ceramic Society 21(8), 287-293 (1938). doi:doi:10.1111/j.1151-2916.1938.tb15777.x

Boehm, L., Ingram, M.D., Angell, C.A.: Test of a year-annealed glass for the cohen-grest percolation transition. Journal of Non-Crystalline Solids 44(2), 305-313 (1981). doi:https://doi.org/10.1016/0022-3093(81)90033-8

Bray P.J., O.K.J.G.: Nuclear magnetic resonance investigations of the structure of alkali borate glasses. Physics and Chemistry of Glasses 4, 37-47 (1963)

Bristogianni, T., Oikonomopoulou, F., Justino de Lima, C.L., Veer, F.A., Nijsse, R.: Structural Cast Glass Components Manufactured from Waste Glass: Diverting Everyday Discarded Glass from the Landfill to the Building Industry. Heron 63 (1/2 Special issue: Structural Glass) (2018)

Bristogianni, T., Oikonomopoulou, F., Veer, F.A., Nijsse, R.: The effect of manufacturing flaws in the meso-level structure of cast glass on the structural performance. In: Zingoni, A. (ed.) Advances in Engineering Materials, Structures and Systems: Innovations, Mechanics and Applications, pp. 1703–1708. CRC Press, Leiden (2019)

Bristogianni, T., Oikonomopoulou, F., Yu, R., Veer, F.A., Nijsse, R.: Investigating the flexural strength of recycled cast glass. Glass Structures & Engineering (2020). doi:10.1007/s40940-020-00138-2

Campbell, D.E., Hagy, H.E.: Glasses and Glass-Ceramics. In: Lynch, C.T. (ed.) CRC Handbook of Materials Science, vol. Volume II: Material Composites and Refractory Materials. CRC Press US (1975)

Duan, R.G., Roebben, G., Van der Biest, O., Liang, K.M., Gu, S.R.: Microstructure research of glasses by impulse excitation technique (IET). Journal of Non-Crystalline Solids 281(1), 213-220 (2001). doi:https://doi.org/10.1016/S0022-3093(00)00397-5

Duan, R.G., Roebben, G., Van der Biest, O.: Glass microstructure evaluations using high temperature mechanical spectroscopy measurements. Journal of Non-Crystalline Solids 316(1), 138-145 (2003). doi:https://doi.org/10.1016/S0022-3093(02)01946-4

EUROGLAS: Products and data. In: 4th edition. Haldensleben, (2016)

Glass For Europe.: The status of Flat Soda Lime Silicate Glass and its raw materials under REACH (Regulation (EC) No 1907 /2006). In. (2015)

Gold Star: Investment Casting Powder Safety Data Sheet, www.goldstarpowders.com (2019)

Goodwin Refractory Services Ltd: Crystalcast (M248). www.grscastingpowders.com (2003)

Gross, T.M. and Tomozawa, M.: Fictive temperature-independent density and minimum indentation size effect in calcium aluminosilicate glass. 104(6), 063529 (2008). doi:10.1063/1.2985907

Fluegel, A.: Glass Viscosity Calculation Based on a Global Statistical Modeling Approach. Glass Technology - European Journal of Glass Science and Technology Part A 48, 13-30 (2007)

Gardon, R.: Modelling Annealing Lehrs for Flat Glass. 65(8), 372-379 (1982). doi:https://doi.org/10.1111/j.1151-2916.1982.tb10487.x

Heimerl, W.: Chemical Resistance and Corrosion, and Ion Release. In: Bach, H., and Krause, D. (ed.) Analysis of the Composition and Structure of Glass and Glass Ceramics. Springer-Verlag Berlin Heidelberg, New York (1999)

Hodge, I.M.: Enthalpy relaxation and recovery in amorphous materials. Journal of Non-Crystalline Solids 169(3), 211-266 (1994). doi:https://doi.org/10.1016/0022-3093(94)90321-2
Hulínský, V.: Glassy inhomogeneities- cords and layers. In: Bartuška, M. (ed.) Glass Defects. Práh, Prague (2008)
Ito, S., Taniguchi, T.: Effect of cooling rate on structure and mechanical behavior of glass by MD simulation. Journal of Non-Crystalline Solids 349, 173-179 (2004). doi:https://doi.org/10.1016/j.jnoncrysol.2004.08.180
Li, H., Agarwal, A., Tomozawa, M.: Effect of Fictive Temperature on Dynamic Fatigue Behavior of Silica and Soda-Lime Glasses. 78(5), 1393-1396 (1995). doi:10.1111/j.1151-2916.1995.tb08502.x
Lord, J.D., Morrell, R.: Elastic Modulus Measurement. In: A National Measurement Good Practice Guide. vol. 98. NMS, (2006)
Milberg, M.E., O'Keefe, J.G., Verhelst, R.A., Hooper, H.O.: Boron Coordination in Sodium Borosilicate Glasses. Physics and Chemistry of Glasses 13(3), 79-84 (1972)
Moynihan, C.T., Easteal, A.J., De Bolt, M.A., Tucker, J.: Dependence of the Fictive Temperature of Glass on Cooling Rate. 59(1-2), 12-16 (1976). doi:10.1111/j.1151-2916.1976.tb09376.x
Narayanaswamy, O.S.: Optimum Schedule for Annealing Flat Glass. 64(2), 109-114 (1981). doi:https://doi.org/10.1111/j.1151-2916.1981.tb09586.x
Němec, L.: Gaseous inhomogeneities in the glass- bubbles. In: Bartuška, M. (ed.) Glass Defects. Práh, Prague (2008)
Oikonomopoulou, F., Bristogianni, T., Veer, F.A., Nijsse, R.: The construction of the Crystal Houses façade: challenges and innovations. Glass Structures & Engineering 3(1), 87-108 (2018a). doi:10.1007/s40940-017-0039-4
Oikonomopoulou, F., Bristogianni, T., Barou, L., Veer, F.A., Nijsse, R.: The potential of cast glass in structural applications. Lessons learned from large-scale castings and state-of-the art load-bearing cast glass in architecture. J. Build. Eng. 20, 213–234 (2018b). https://doi.org/10.1016/j.jobe.2018.07.014
Oikonomopoulou, F., Bristogianni, T., Barou, L., Jacobs, E., Frigo, G.,Veer, F.A., Nijsse,R.: Interlocking cast glass components, exploring a demountable dry-assembly structural glass system. Heron 63, 103–138 (2018c)
Paech, C., Göppert, K.: Innovative Glass Joints – The 11 March Memorial in Madrid. Paper presented at the Challenging Glass, Conference on Architectural and Structural Applications of Glass, Delft (2008)
Quinn, G., Morrell, R.: Design Data for Engineering Ceramics: A Review of the Flexure Test. Journal of the American Ceramic Society 74, 2037-2066 (1991). doi:10.1111/j.1151-2916.1991.tb08259.x
Quinn, G.D.: Weibull Strength Scaling for Standardized Rectangular Flexure Specimens. 86(3), 508-510 (2003). doi:https://doi.org/10.1111/j.1151-2916.2003.tb03329.x
Quinn, G.D., Ives, L.K., Jahanmir, S.: On the nature of machining cracks in ground ceramics: part II—comparison to other silicon nitrides and damage maps. Mach. Sci. Technol. 9, 211–237 (2005). https://doi.org/10.1081/MST-200059051
Quinn, G.D., Sparenberg, B.T., Koshy, P., Ives, L.K., Jahanmir, S., Arola, D.D.: Flexural Strength of Ceramic and Glass Rods. Journal of Testing and Evaluation 37, 222-244 (2009). doi:10.1520/JTE101649
Radovic, M., Lara-Curzio, E. and Riester, L.: Comparison of different experimental techniques for determination of elastic properties of solids. Materials Science and Engineering: A 368(1), 56-70 (2004). doi:https://doi.org/10.1016/j.msea.2003.09.080
Roebben, G., Bollen, B., Brebels, A., Humbeeck, J., Van der Biest, O.: Impulse Excitation Apparatus to Measure Resonant Frequencies, Elastic Moduli, and Internal Friction at Room and High Temperature. Review of Scientific Instruments 68, 4511-4515 (1997). doi:10.1063/1.1148422
Roebben, G., Donzel, L., Stemmer, S., Steen, M., Schaller, R., Van der Biest, O.: Viscous energy dissipation at high temperatures in silicon nitride. Acta Materialia 46(13), 4711-4723 (1998). doi:https://doi.org/10.1016/S1359-6454(98)00131-1
Schott: DURAN Technical Data (2017)
Shelby, J.E.: Introduction to Glass Science and Technology. The Royal Society of Chemistry, UK (2005)
Shelby, J.E.J., Day, D.E.: Mechanical Relaxations in Mixed-Alkali Silicate Glasses: I, Results. 52(4), 169-173 (1969). doi:10.1111/j.1151-2916.1969.tb13358.x
Sheybany, H.A.: De La Structure Des Verres Alkalinosilicates Mixtes. Verres et Refractaires 2, 127-145 (1948)
Smedskjaer, M.M., Jensen, M. and Yue, Y.: Effect of thermal history and chemical composition on hardness of silicate glasses. Journal of Non-Crystalline Solids 356(18), 893-897 (2010). doi:https://doi.org/10.1016/j.jnoncrysol.2009.12.030
Stevels, J.M.: The structure and physical properties of glass. In: Flügge, S. (ed.) Handbuch der Physik, vol. 13. vol. Thermodynamics of Liquids and Solids, pp. 511-643. Springer-Verlag, Berlin (1962)
Striepe, S., Potuzak, M., Smedskjaer, M.M., Deubener, J.: Relaxation kinetics of the mechanical properties of an aluminosilicate glass. Journal of Non-Crystalline Solids 362, 40-46 (2013). doi:https://doi.org/10.1016/j.jnoncrysol.2012.11.017
van Dam, S.: Experimental Analysis of the Post-Fracture Response of Laminated Glass under Impact and Blast Loading. Ghent University (2017)
van Limpt, J.A.C.: Modeling of evaporation processes in glass melting furnaces. Technische Universiteit Eindhoven (2007)
Varshneya, A.K.: Fundamentals of inorganic glasses, 2nd ed. Society of Glass Technology, Sheffield , UK (2013)

Varughese, B., Lee, Y.K., Tomozawa, M.: Effect of fictive temperature on mechanical strength of soda-lime glasses. Journal of Non-Crystalline Solids 241(2), 134-139 (1998). doi:https://doi.org/10.1016/S0022-3093(98)00762-5
Zheng, Q., Zhang, Y., Montazerian, M., Gulbiten, O., Mauro, J. C., Zanotto, E. D., Yue, Y.: Understanding Glass through Differential Scanning Calorimetry. Chemical Reviews 119(13), 7848-7939 (2019). doi:10.1021/acs.chemrev.8b00510


5

Previous page: Fractured surface of a recycled container glass specimen (kiln-cast at 1120ºC) subjected to splitting, as seen through polarized light.

Chapter 5: Fracture resistance of cast glass

Based on

Bristogianni, T., Oikonomopoulou, F., Veer, F., Nijsse, R.: Exploratory Study on the Fracture Resistance of Cast Glass. International Journal of Structural Glass and Advanced Materials Research 5, 195-225 (2021). doi:10.3844/sgamrsp.2021.195.225

For this paper, the main author received the "Young Researcher Award SGAMR-YRA-2021" by the Editorial Board.

Aim and context

Investigation of the fracture resistance of cast glass and how this is affected by the chemical composition and the meso-level structure of the glass. Chapter 5 employs a selection of cast glasses and distinct meso-level structures, based on the characteristics of previously tested specimens (Chapters 3-4), and studies the role of composition, thermal history and defects in determining the fracture resistance of cast glass.

Abstract

The emerging interest in the architectural applications of cast glass components reveals a knowledge gap on the mechanical properties of cast glass. Apart from its chemical composition, cast glass is characterized by its manufacturing history and thermal profile, often inheriting a set of defects that define its properties. The role that inhomogeneities in the bulk of voluminous glass components have on the strength of the final product is also uncertain. Systematic testing is therefore necessary for the safe structural application of cast glass. Towards this direction, the presented research aims to experimentally investigate the fracture resistance of cast glass under sharp contact loading, by means of a customized splitting test using a sharp linear indenter. Cubic specimens with 50mm sides are kiln-cast at low forming temperatures, employing a variety of silicate-based cullet and firing schedules, and their inherent defects are documented. The results of the splitting tests show that the borosilicate specimens fail at the highest splitting force, followed by the soda lime silica float specimens, while the fused or porous specimens have a significantly lower resistance to fracture. The strength order of the various glasses- as this results from the splitting tests- is opposite to that found earlier in four-point bending tests, due to the different fracture mechanisms activated. The fracture resistance of a glass specimen is governed, first by its ability to deform around the indenter to relief the developing stresses, and then by its bond strength to resist crack propagation. Thus, a good balance between glass network flexibility and high bond dissociation energy is required, explaining why the tested homogeneous borosilicate and soda lime silica glasses are more resistant than the modified soda lime silica

compositions with high alkali content. In addition, the fractographic analysis indicates that the non-stress inducing flaws in the bulk have a negligible contribution to the fracture resistance of the specimens.

Authors' contribution on the relevant published journal article

Bristogianni, T.: Research concept, organization, sample preparation, conduction of experiments, data analysis, writing of the paper. Oikonomopoulou, F.: Discussion and paper review. Veer, F.A.: Design of splitting test, supervision of research, discussion, paper review. Nijsse, R. : supervision of research.

Acknowledgements

I would like to thank the co-authors of the above mentioned paper for their valuable contribution in this chapter. I would like to express my gratitude to Rong Yu and Tommaso Venturini for assisting with the preparation of the glass specimens, and Ruud Hendrikx and his team for conducting the XRF and XRD analyses. I am also very grateful to George Quinn and James Varner for the meaningful discussions regarding the interpretation of the splitting test and the fractured surfaces, and to Bert Sluijs for his guidance and suggestions in this study. In addition, I am very thankful to Henning Katte and Daniel Schreinert for sponsoring the use of the Ilis StrainScope Flex Polariscope. Lastly, I would like to express my gratitude to Ewald Jooste (Cricursa), Hans van Limpt & Bart Wilms (Sibelco), Bianca Lambrechts & Danny Timmers (Maltha), and Martijn Rietveld (NSG Pilkington) for providing cullet material for the experiments.

5.1 Introduction

The use of cast glass as a structural material has been explored in several architectural projects such as the Atocha Memorial in Madrid (Paech and Göppert, 2008), the Optical Glass House in Hiroshima (Nakamura & NAP 2012), the Crystal Houses in Amsterdam (Oikonomopoulou et al. 2018a, b) and the Robotic Glass Vault in London (Parascho et. al 2020). The success of these projects showcases the aesthetical and structural potential of cast glass, intriguing the architectural and engineering community to consider cast glass as a promising building material.

Yet, as the interest in the structural application of cast glass, made either out of pure batch materials or recycled waste cullet, increases, the need of establishing suitable testing methods for voluminous glass components becomes imperative. Widely used experimental procedures such as the four-point bending test give valuable indications about the strength of cast glass (Bristogianni et. al 2020), but are mainly linked to the quality of the glass surface and ignore the bulk properties. In addition, the subjection of a glass element to a far-field stress involves different fracture mechanisms than those involved in contact loading. Cast glass components, however, are

more often employed in compressive load-bearing structures (e.g. walls, arches), being thus subjected to contact peak stresses rather than bending stresses. In this case, the fracture resistance of cast glass is influenced by two processes: stage a, the ability of the loaded glass surface zone to resist crack initiation by deformation and stage b, the ability of the glass matrix surrounding the eventually initiated crack to resist unstable crack propagation. Understanding the fracture resistance of ceramics to contact loading is commonly approached by testing two distinct material properties; Hardness (stage a, resistance to deformation) and Fracture Toughness[79] (stage b, resistance to catastrophic crack propagation).

In this study, a new experimental approach is developed that tests the combined fracture resistance of cast glass, from crack initiation to total component failure, with the aim of providing direct indications about the brittleness of cast glass. Specifically, a splitting test is proposed, by introducing increasing pressure on a cast glass cubic specimen with a longitudinal sharp indenter, until complete fracture. The experiment borrows elements from the Diametral Compression experiment (Brazilian Disk), which is commonly used for the evaluation of the tensile strength of concrete (ASTM C 496). Diametral compression testing in glass is not common practice, yet several examples concerning the testing of glass spheres (Kschinka 1986), or glass discs (Nyounguè 2016, Sheikh 2019) are reported in literature. Although the Brazilian Disk test aims to subject the core of the tested cylinder in uniform tension, Mellor and Hawkes (1971) report regarding their experiments on glass that fracture started from the surface, due to machining flaws that were more severe than the defects in the bulk.

The splitting test proposed in this study, simplifies the specimen's casting and post-processing and increases its dimensional accuracy, by changing the cylindrical shape into a cube. Further on, it simplifies the support conditions at the universal testing machine, by introducing the concentrated linear force at only one side (bottom) of the specimen. Crack initiation starts from this contact zone and leads to the splitting of the specimen into two fragments once the load reaches a critical value. The two fragmented surfaces allow studying the interaction of the crack front with singularities present in the cast glass meso-level structure. Although such defects in the bulk are not directly activated by the splitting test, their interaction with the crack path can expose information about their contribution to the fracture behaviour of cast glass (e.g. formation of weak zones, arrest of crack propagation). Such information is particularly relevant for the testing of voluminous cast glass components made out of waste glass at high casting viscosities, where a high population of defects are expected to be present in the meso-level structure.

[79]Typical fracture toughness test methods such as the single-edged precracked beam (SEPB) assume a given starting crack size upon which stable crack growth and catastrophic propagation build upon. Yet, regarding the chance of a crack to initiate, some glasses will show more susceptibility to external damage due to their chemical composition, insufficient annealing, intrinsic flaws or machining and handling damage. Such glasses in real-world applications will have higher chances to failure, thus the need to review the resistance to crack initiation together with the fracture toughness.

5.2 Materials and Methods

5.2.1 Specimen Preparation and Analysis

Cast glass specimens with different degrees of inhomogeneity, are produced for the purposes of the splitting test, using recycled glass cullet. The 50mm cubic glass specimens are kiln-cast in triplets per glass type and firing schedule. Relatively low forming temperatures (870º-1120ºC) and corresponding high viscosities (10^6–$10^{3.5}$ dPa·s) are employed, intensifying the occurrence of defects in the glass surface and meso-level structure. The glass cullet employed involves common silicate based glasses such as Soda Lime Silica "SLS" (Float with/without coatings, container glass, modified) and Borosilicate. X-ray fluorescent (XRF) analyses are conducted with a Panalytical Axios Max WDXRF spectrometer, in order to determine the chemical composition of the used glass cullet and of possible present contaminants (e.g. mirror coating).

Various different cullet sizes/shapes are used in this study, which are either deposited directly (Figure 5.1) in silica-plaster investment moulds (Crystalcast M248) or fed in terracotta flowerpots placed above the moulds. The moulds and terracotta pots are placed inside a ROHDE ELS 200S electric kiln, heated up to the forming temperature and controllably cooled down to room temperature according to the selected firing schedule.

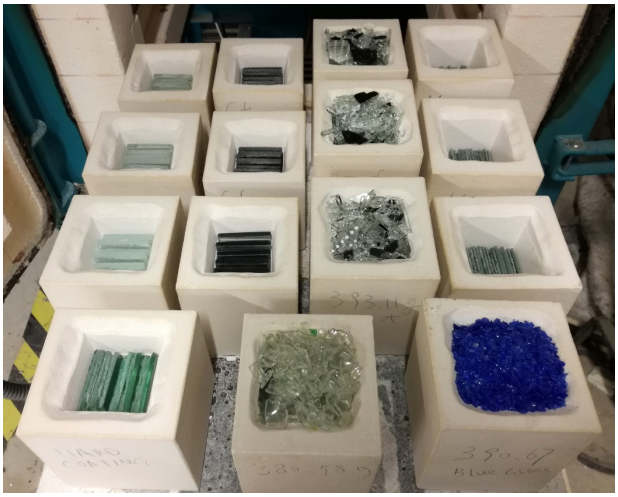

Fig. 5.1 Arrangement of glass cullet in disposable silica plaster moulds.

Below the list of different firing schedules used for the kiln-casting of the samples can be found (Table 5.1):

- 10hr dwell time at 1120 ºC top temperature (870ºC for B270 glass), -160ºC/hr cooling rate down to annealing point (referred to as "fast-cooling" in this article)
- 2hr dwell time at 1120ºC top temperature, with a cooling rate of -50ºC/hr down to annealing point (referred to as "slow-cooling")

- 10hr dwell time at 970ºC top temperature, with a cooling rate of -160ºC/hr down to annealing point (referred to as “fused”)
- 3hr dwell time at 1050/1070ºC top temperature, with a cooling rate of -160ºC/hr down to the heat treatment point between 760-890ºC, (referred to as “heat-treated”)

All samples are annealed for 10hr at their corresponding annealing temperature. Upon cooling, the top and bottom surface of the specimens are ground and polished using a Provetro flat grinder and diamond abrasive discs in sequence of 60, 120, 200, 400 and 600 grit.

In order to provide a reference, a series of 50mm cubic specimens are prepared using industrially produced glass in the following manner:

- 10x50x50mm float glass panes glued with UV-curing acrylate DELO 4468. The cut edges are polished as described above, while the longitudinal glossy surface is left in its as received condition (fine polishing, occasional scratches).
- 50mm cubes cut out of Poesia[80] cast glass bricks. Clear and hazy cast glass brick variants are used. The cubes are either left to their as received glossy condition, or polished at 600 grit, as described above.

A Keyence VHX-7000 digital microscope with a 20-200x zoom lens is used to photograph defects on and in the cast samples. A selection of specimens is also inspected using an Ilis StrainScope Flex polariscope to determine potential residual stresses.

[80] Poesia is the producer of the cast glass bricks employed for the building of the Crystal Houses Façade (Oikonomopoulou et. al 2018).

Table 5.1 (part a): Casting parameters implemented for the preparation of the glass specimens.

Glass type	Specimen description	Source	Chemical composition of glass and contaminants^ (main compounds in wt%)	Forming temperature in °C (10hr dwell unless differently specified)	Cooling rate (°C/hr), heat treatment if applicable	Annealing temperature in °C (10hr dwell)	Cullet size, shape and array
Soda Lime Silica (Float Glass)	FT float*	IFS-SGT	75.4% SiO_2, 12.4% Na_2O, 7.6% CaO, 4% MgO, 0.4% Al_2O_3	1120	-160	560	
	Float 10mm x5 layers		72.4% SiO_2, 12.3% Na_2O, 9.9% CaO, 4.1% MgO, 0.6% Al_2O_3	1120 (2hr)	-50	560	
	Float 10mm x5 layers, fused			970	-160		
	Low-iron float			1120	-160	560	
	Low-iron float, heat-treated**	Cricursa	74% SiO_2, 12.7% Na_2O, 8.4% CaO, 4.2% MgO, 0.55% Al_2O_3	1050 (3hr)	-30 Heat treatment, 1: 10hr 860°C 2: 10hr 840°C		
	Low-iron float powdered, fused***			970	-160		

^All composition data derived by XRF measurements conducted with a Panalytical Axios Max WD-XRF spectrometer by Ruud Hendrikx (TU Delft, 3mE), apart from the SiO_2/B_2O_3 ratio in DURAN Schott derived from (Heimerl 1999), and the SiO_2/B_2O_3 ratio in Poesia glass derived from personal communication with the company.

* The labelling "FT Float" refers to the use of Fully Tempered float glass shards as cullet. The final kiln-cast components are annealed and the thermal history of the shards is erased.

** Sample prepared by Shan Cindy Lei (2019) as part of her MSc work.

*** Sample prepared by Guilia Maria Anagni, as part of her MSc work (Anagni et al. 2020).

Table 5.1 (part b): Casting parameters implemented for the preparation of the glass specimens.

Glass type	Specimen description	Source	Chemical composition of glass and contaminants^ (main compounds in wt%)	Forming temperature in °C (10hr dwell unless differently specified)	Cooling rate (°C/hr), heat treatment if applicable	Annealing temperature in °C (10hr dwell)	Cullet size, shape and array
Soda Lime Silica (Float Glass, coated)	Soft coating, 6mm x8 layers	Pilkington	74.4% SiO_2, 12.5% Na_2O, 8.2% CaO, 3.9% MgO, 0.55% Al_2O_3 Coating: ZnO based	1120 1120 (2hr)	-160 -50	560	
	Soft coating, 6mm x8 layers, fused			970	-160		
	Mirror, 5mm x10 layers		73.5% SiO_2, 12.8% Na_2O, 8% CaO, 4.3% MgO, 0.9% Al_2O_3 Coatings contain ZnO, BaO, TiO_2, Fe_2O_3	1120 (2hr)	-50	560	
Soda Lime Silica (Container Glass)	Clear cullet	Sibelco	Mix of typical container glass, traces of metal contamination	1120	-160	560	
	Clear and light-tinted cullet	Maltha	Mix of typical container glass	1120	-160	560	
	Clear bottle cullet, fused**	Clear bottle	72.7% SiO_2, 12% Na_2O, 10% CaO, 3% MgO, 1.3% Al_2O_3, 0.5% K_2O	1070 (3hr)	-30 Heat treatment: 5hr 780°C, 10hr 860°C	560	

Table 5.1 (part c): Casting parameters implemented for the preparation of the glass specimens.

Glass type	Specimen description	Source	Chemical composition of glass and contaminants^ (main compounds in wt%)	Forming temperature in °C (10hr dwell unless differently specified)	Cooling rate (°C/hr), heat treatment if applicable	Annealing temperature in °C (10hr dwell)	Cullet size, shape and array
Soda Lime Silica (Container Glass)	Clear bottle shards, fused**	Clear bottle	72.7% SiO_2, 12% Na_2O, 10% CaO, 3% MgO, 1.3% Al_2O_3, 0.5% K_2O	1050 (3hr)	-120 Heat treatment: 5hr 760°C, 10hr 890°C	560	
Modified Soda Lime Silica	Poesia standard brick	Poesia	72.1% SiO_2, 15.9% Na_2O, 2.5% B_2O_3, 6.1% CaO, 1.9% K_2O, 0.9% Sb_2O_3	1120 1120 (2hr)	-160 -50	540	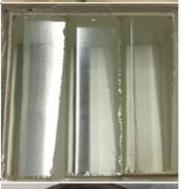
	B270	Schott	71.8% SiO_2, 10.1% Na_2O, 6.3% K_2O, 5.2% CaO, 2.2% ZnO, 2% Al_2O_3, 1.8% TiO_2	870	-160	540	
Borosilicate	DURAN 24mm rods	Schott	80% SiO_2, 13% B_2O_3, 3.5% Na_2O, 2.7% Al_2O_3, 0.5% K_2O	1120	-160	560	
	DURAN 24mm rods fused			970	-160		
	DURAN powder***			1120	-160		

5.2.2 Splitting test design and experimental set-up

A destructive splitting test is designed for the testing of 50mm cubic cast glass specimens. The set-up comprises a High-Speed Steel 10% Cobalt (HSS Co 10) toolbit of 25mm square cross section, rotated by 45° and positioned on a milled 52.4 hardened steel base, which is fixed on the base of a Zwick Z100 displacement controlled universal testing machine (Figure 5.2). The cubic glass specimens are centrally positioned above the toolbit edge, and locally taped under a ø150mm steel compression fixture that is fixed[81] to the top part of the testing machine. The toolbit edge, only slightly filleted to a radius of 233μm, acts as a longitudinal sharp indenter on the bottom glass cube surface, as the compression fixture starts to move downwards with a 0.2mm/min rate[82], putting pressure to the bottom glass surface. With the increasing force, the indenter tip creates initial glass densification and crushing around it, accompanied by stable radial cracks, both at the direction of the force and perpendicular to it. When the force reaches a critical level, the glass cube is split in two pieces. The fractured surfaces are then studied with the Keyence VHX-7000 microscope. The splitting test provides quantitative information about the resistance of the tested glasses to deformation (hardness) and the resistance to fracture (toughness). Also qualitative information are extracted from the fracture analysis of the fractured surfaces regarding the role of inhomogeneities in the meso-level structure to the glass network.

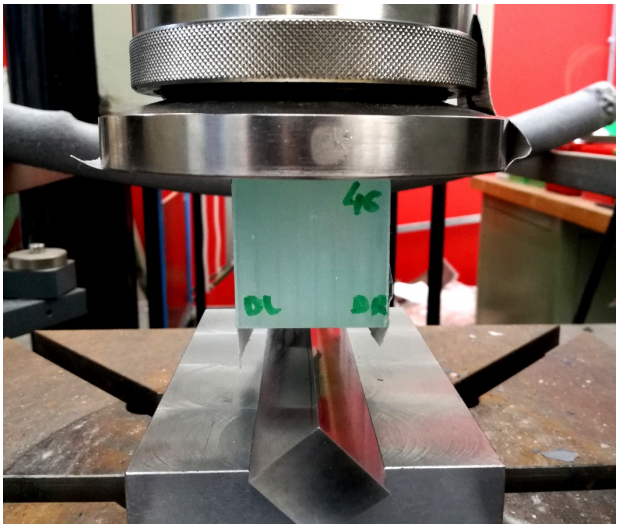

Fig. 5.2 Splitting test experimental set-up. The toolbit at the base acts as a longitudinal sharp indenter at the bottom surface of the glass specimen.

[81] Trial experiments using a pinned compression fixture often led to uncertain results. Due to the manual polishing of the specimens, the top and bottom side of the cubes may not have been precisely parallel to each other. During loading, small deviations between the top and bottom surface would cause the pinned fixture to tilt (to establish good contact with the top surface), and as a consequence, the specimen would also tilt around the toolbit edge (in the perpendicular plane to the edge), failing to be loaded as designed in the experiment. For this reason, a fixed connection was preferred.

[82] A relatively low displacement rate is chosen to allow for possible crack arrests when singularities are encountered along the crack front.

5.3 Results

5.3.1 Cast Glass Specimens evaluation

The selected forming temperatures correspond to high glass viscosities, resulting to inhomogeneous glass specimens. The degree of inhomogeneity relates to the purity and shape of the cullet, in combination with the firing schedule (e.g. slow cooling, heat-treatment). Therefore, a variety of meso-level structures are observed in the specimens, grouped in the following categories, as also seen in Figure 5.3:

a. Fairly homogeneous: these specimens may contain miniscule air-bubbles. The lack of other defects and inhomogeneities results from the purity of the initial cullet, the high forming temperature and long dwell time used (e.g. at 1120^{o}C for 10hr), and the fast cooling scheme.

b. Structured bubble veils: these concern parallel layers composed by multiple bubbles and occasionally cord, which are found within the glass specimen. Such layers are observed in coated float samples with a short dwell time at top temperature (2hr) that did not allow for the complete melting of the coating and its incorporation to the glass network (Figure 5.4 right). The parallel appearance of these veils in the glass specimens is a result of the insertion of the cullet inside the mould in parallel orthogonal pieces.

c. Random glassy/gaseous inhomogeneities: such random structures may occur due to glass compositional variations in the cullet (e.g. Maltha clear glass consists of container glass produced by various manufacturers, see Figure 5.5 left) in combination to its random shape (e.g. shards). In addition, the slow pouring of the glass inside the mould (at high viscosity) can create swirling patterns of bubbles and cord which are reminiscent of the coiling of the glass pouring thread (Figure 5.4 left).

d. Structured crystalline interlayers: These are thin crystallized layers within the glass network, situated at the contact surfaces of the cullet pieces (Figure 5.6 right). They are formed during fusing at low temperatures (e.g. 970^{o}C) and prolonged dwell times (e.g. 10hr) at a temperature range that promotes crystallization. The crystalline types identified by X-Ray Fluorescent (XRD) analyses are wollastonite 2M, β-cristobalite and devitrite for the Float 970^{o}C glass and β-cristobalite for the Borosilicate 970^{o}C glass (Bristogianni et al. 2020). The structured geometry is linked to the defined shape of the original cullet.

e. Random crystalline elements: these consist of acicular or linear crystalline formations of larger thickness than in the category above. These crystals form due to the kiln-casting of the specimens at temperatures below the liquidus point and the heat-treatment at the crystallization peak zone thereafter. XRD analyses characterize these crystals as Wollastonite-2M and α-cristobalite (Lei, 2019, Figure 5.6 left) in the case of container glass. The shape of these crystals is directly linked to the initial cullet shape (round cullet leads to singular acicular formations while shards lead to the grouping of the crystals into linear arrangements).

f. Fused, porous: the specimens are produced by the sintering of powdered cullet at relatively low temperatures (e.g. 970ºC for soda lime silica glass) which may coincide with the peak-crystallization temperature range (Anagni et. al 2020). A crystallized, porous structure is therefore achieved. At higher temperatures (e.g. 1120ºC), a glassy porous structure is obtained (Figure 5.5 right).

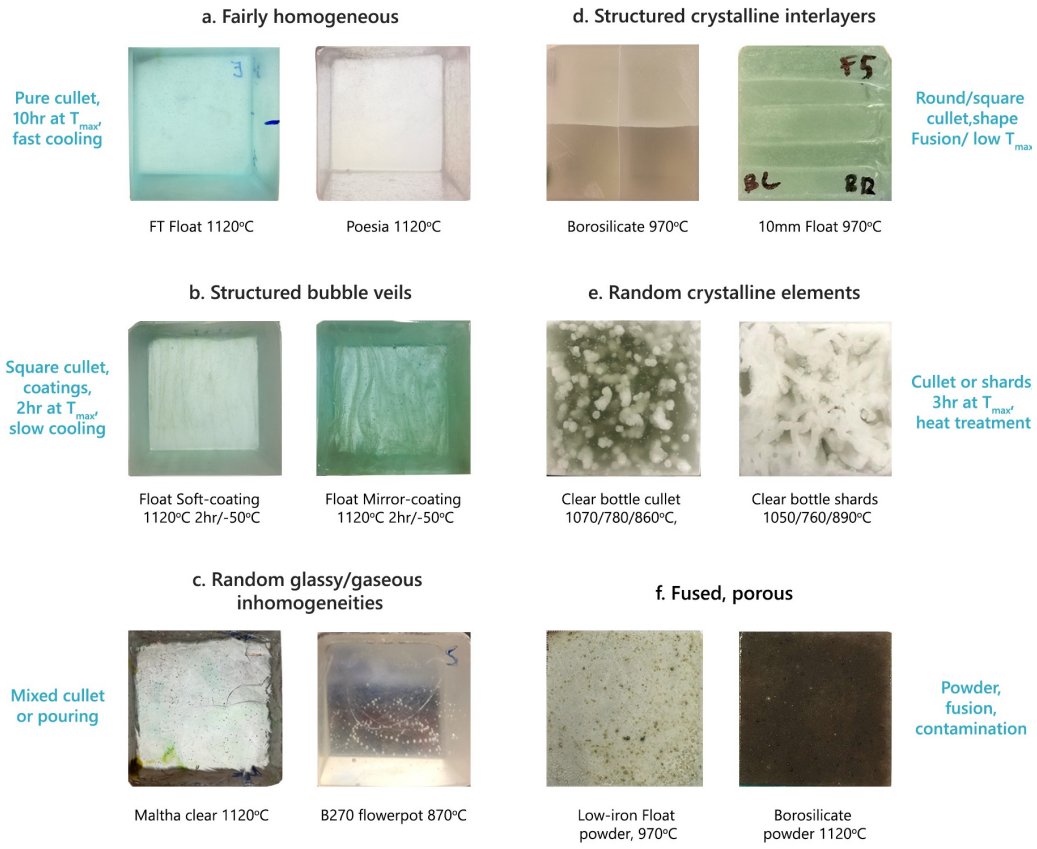

Fig. 5.3 Categories of encountered meso-level structures, as a result of the casting parameters followed. The defects creating these meso-level structures are crystalline formations, glassy inhomogeneities or gaseous inclusions, either acting alone or in combination.

In cases where the geometry of the meso-level structure is prominent, such as in categories b and d, then the orientation of the interfaces -either in the form of bubble veils or crystalline layers- in relation to the toolbit and force direction is marked during testing. In this manner, the effect of such interlayers to the structural performance of the glass cubes can be studied (Figure 5.7).

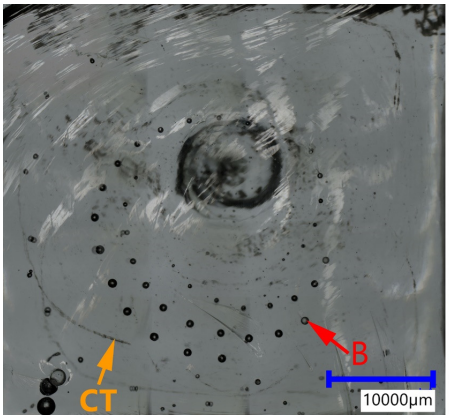

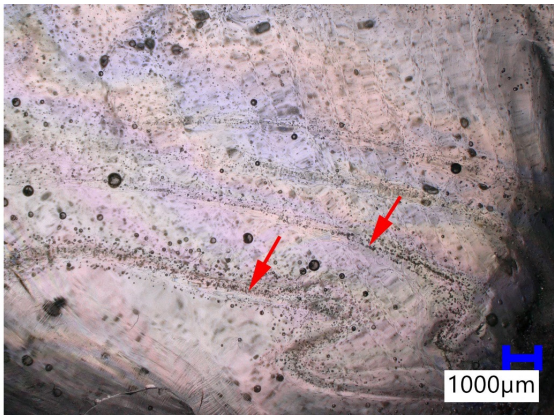

Fig. 5.4 Bubble formation (“B”), cord and crystalline traces (“CT”) in a spiral arrangement in a “B270 870ºC” specimen (left); a reminisce of the coiling of the molten glass as it was slowly poured inside the mould from the flowerpot. Parallel bubble veils in a “Mirror 1120ºC, -50ºC/hr specimen (right). The presence of the specific hard-to-melt metallic coating in combination with the shorter dwell time (2hr instead of 10hr) at top temperature, results in bubble veils at the fusion area between the glass pieces.

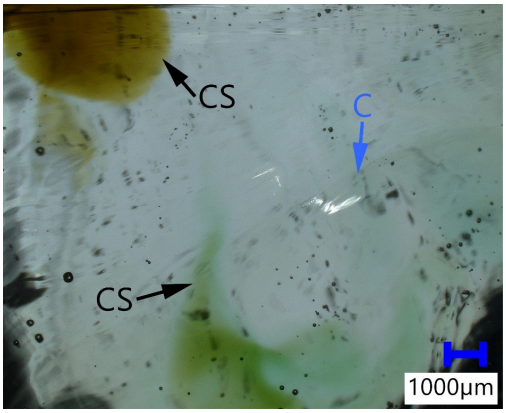

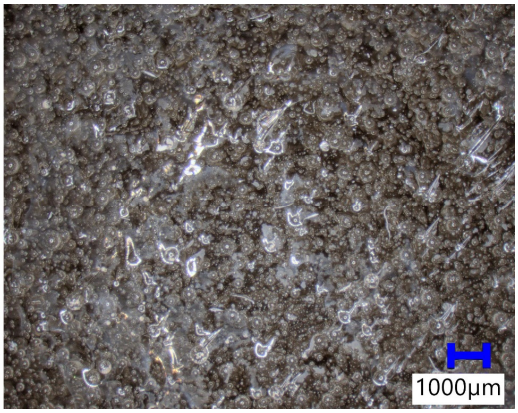

Fig. 5.5 Glassy inhomogeneities in the form of transparent cord (“C”) and colour streak (“CS”) in a “Maltha Clear 1120ºC bottle” (left) and high population of bubbles in a “Borosilicate powder 1120ºC” specimen (right).

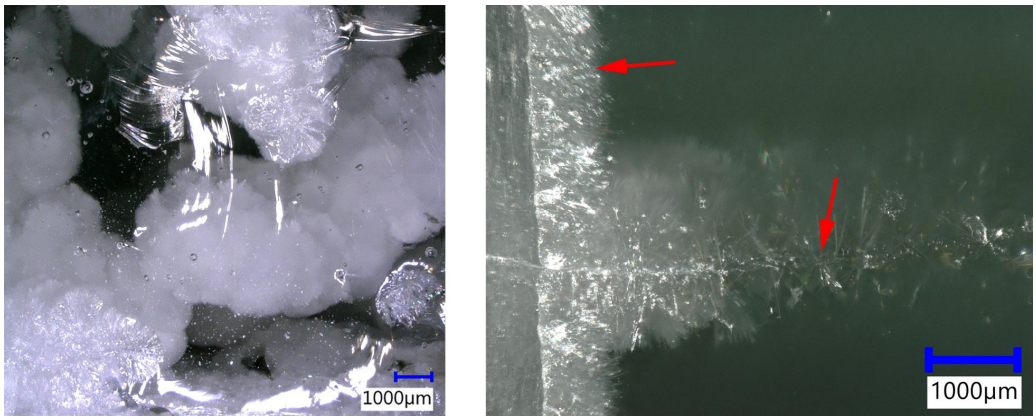

Fig. 5.6 Crystalline inhomogeneities encountered in a heat-treated “Clear bottle cullet 1070ºC” specimen (left) and a fused “Soft Coated float 970ºC” specimen (right). The forming or heat-treating of these soda lime silica glasses below the liquidus point and at temperatures that favour crystallization, is responsible for the encountered crystalline inclusions.

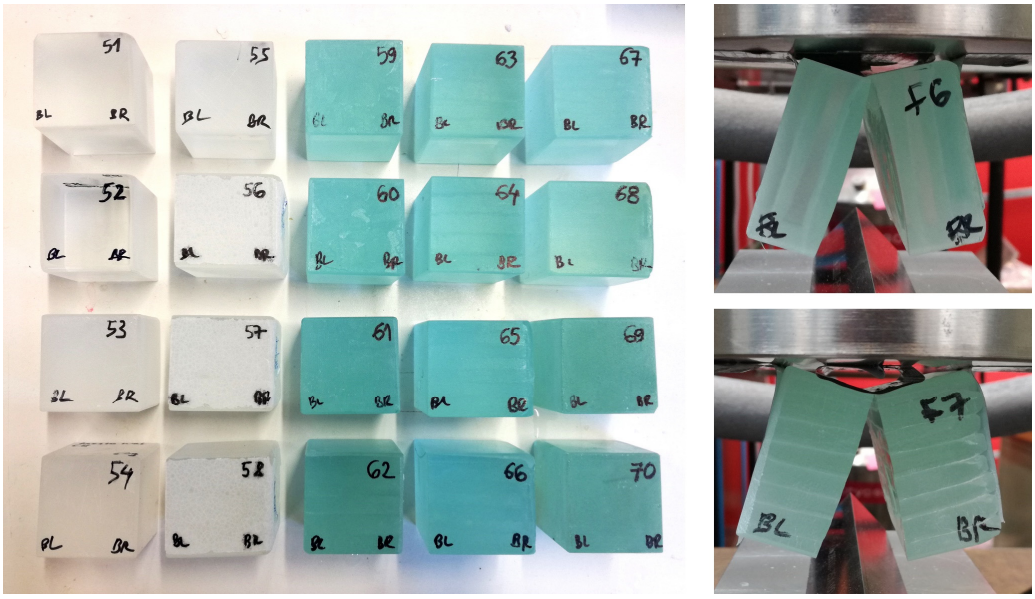

Fig. 5.7 Cast Poesia and Float glass cubic specimens (left) and orientation of the crystalline interlayer meso-level structure of two fused float specimens to the direction of the force (right). Only the bottom and top surface of the specimens are polished up to 600grit, while the side surfaces are left unprocessed.

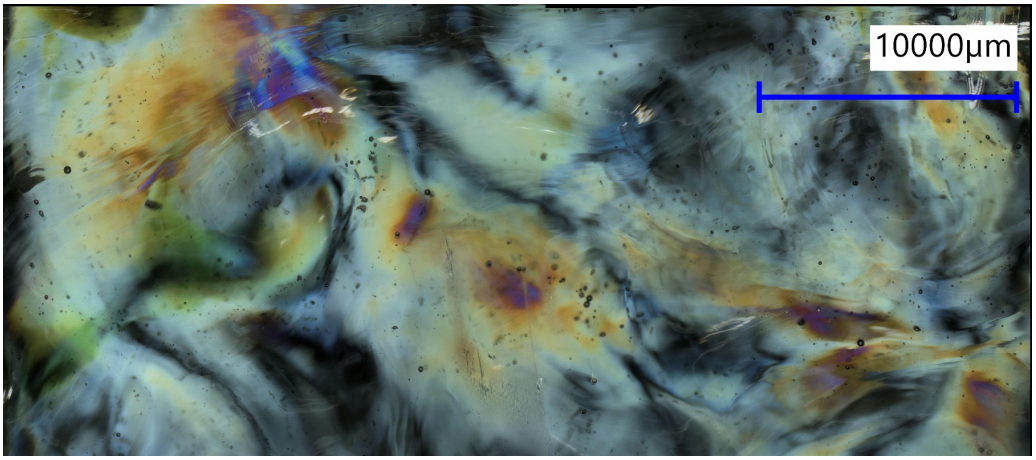

Fig. 5.8 “Maltha Clear 1120ºC bottle” specimen, as seen through crossed-polarized light. The localized stress zones are the result of compositional variations in the initial cullet shards.

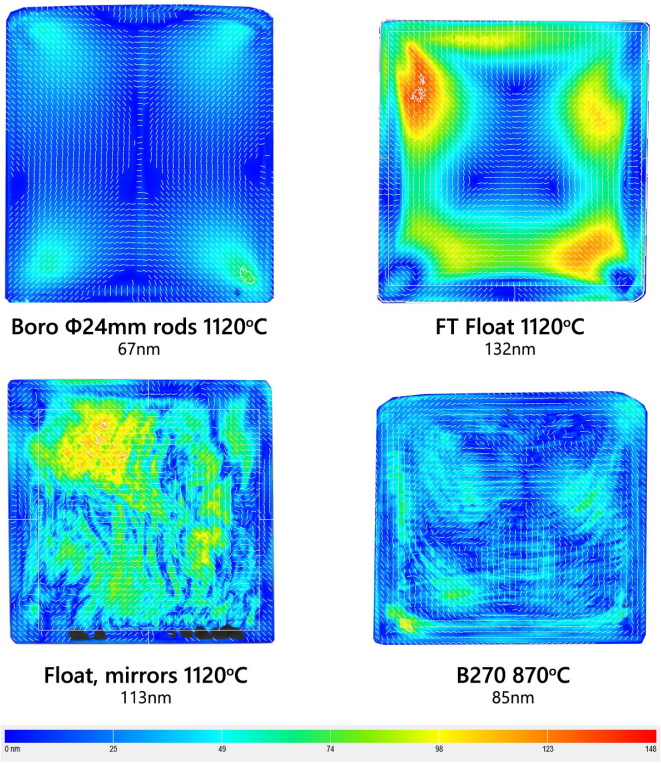

Fig. 5.9 Internal stresses in a selection of cast glass specimens, as captured with an Ilis polariscope. The colour gradient refers to the relative phase retardation between the two component waves of the polarized light.

The above described inhomogeneities become prominent once the specimens are observed through cross-polarized light (Figure 5.8). The optical path traveling through the glass matrix will propagate at a different speed when encountering a compositional variation or a zone experiencing mechanical stress. The optical retardation (optical path difference) due to these inhomogeneities is measured via an Ilis StrainScope Flex circular polariscope (Figure 5.9). Subtle bubble veils such as in the case of the pure Borosilicate 1120ºC or the spiral coiling structure of the B270 samples, barely cause any optical retardation, whereas the bubble veils created from non-incorporated coatings (e.g. mirrors) will have a more significant impact on the direction of the light path. Nonetheless, higher optical retardation was occasionally observed in pure specimens such as the FT Float 1120ºC or Poesia 1120ºC than in the inhomogeneous ones (Figure 5.9). These zones are located at the corners of the cubes, where –due to the shape of the glass- tensile stresses are more likely to appear during cooling. This suggests that incomplete relief of the internal stresses due to random alterations to the thermal history (e.g. location of the specimen in the kiln may affect its thermal profile) may be more significant than the stresses induced by glassy or gaseous inhomogeneities.

Apart from the observed inhomogeneities originating by the followed casting process, the specimens may also bear surface flaws due to machining and handling damage (Figure 5.10). These are mainly striations, small inclusions caused by mould contamination, and chipping.

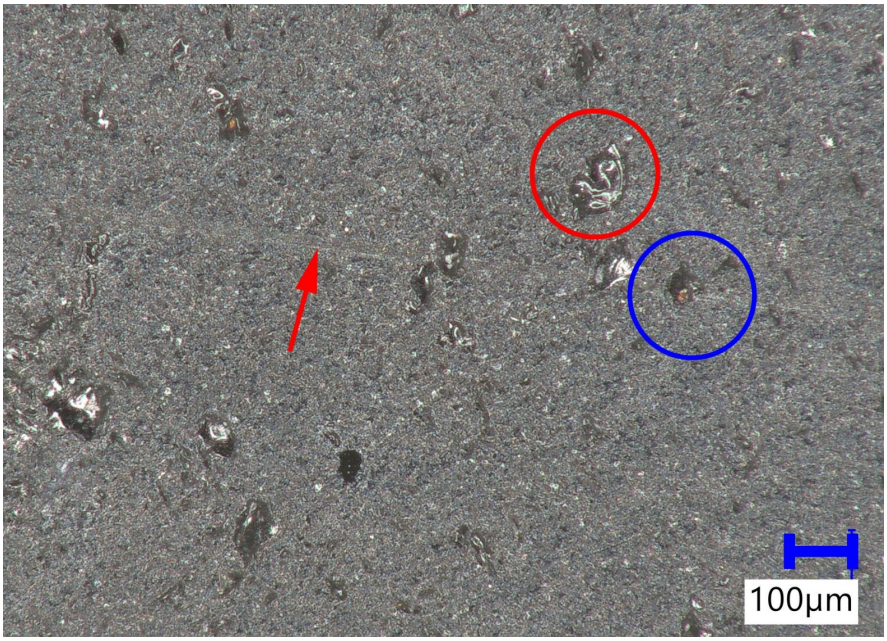

Fig. 5.10 Bottom surface of an “FT Float 1120ºC” specimen that has been ground and polished up to a 600grit. Common defects include striations (arrow) and chipping (red circle) caused during grinding, and inclusions originating from mould contact (blue circle).

5.3.2 Splitting tests

Figures 5.11-5.12 and Table 5.2 show the force at failure of the 50mm cubic specimens subjected to the splitting test. From the 64 tested specimens, 33 had established full contact with the toolbit and thus an even distribution of the force. These results are considered accurate for evaluating the force in relation to the glass composition and meso-level structure characteristics. They also allow a reliable correlation between the force and the extent of lateral damage at the bottom surface. The rest of the specimens tilted during the building up of the force while testing, having as a result an uneven stress distribution along the toolbit that exposed one side of the cube to a maximum stress while the opposite side was not in contact with the toolbit[83]. This would lead to an obvious failure of the specimens at lower force values. Nonetheless, seven from these specimens, making at least 85% contact with the toolbit, where used together with the 100% contact specimens for calculating the average force per glass type. This distribution (Figure 5.12), although depicting lower force values, still serves as a good comparison between the glass types. Specimens with less than 85% contact were discarded as inaccurate.

Relative to the fully supported specimens (Figure 5.11), the data for each glass type is consistent within a range of 5kN. The highest force values are seen in the homogeneous (1120^{o}C) and the fused (970^{o}C) borosilicate specimens (42kN and 38.6kN respectively), followed by the FT Float (36.5kN), Float (32.9kN) and Soft-coating (33.9kN) samples produced at high temperature and quenched either at a -160^{o}C/hr or -50^{o}C/hr rate. The fused variants of these SLS glasses resist much lower forces (in average 16.9-19.3kN), presenting similar results regardless of the orientation of the crystallized interfaces. Significant differences are found in the Poesia glasses (12-28.9kN), in regard to the firing schedule (fast vs. slow cooling, kiln-cast vs. hot poured) and the finishing surface (glossy vs. mat). The samples produced by powdered glass (porous and crystallized) are significantly weaker (as low as 11.1kN in the case of Low-iron float, powdered and fused) from the homogeneous or even fused variants of the same glass composition. Specifically, both Borosilicate and Low-iron float powdered specimens (cast at 970^{o}C) are found to be ≈43% weaker than their homogeneous variants (cast at 1120^{o}C using cullet).

[83] This tilting along the edge of the toolbit was encountered in cases where the top and bottom surfaces of the cubes were not precisely parallel to each other, due to the manual post processing of the specimens. This error occurred due to the fixed top fixture (see 5.2.2). Despite this risk associated with the fixed fixture, the fixed connection was much more reliable than a pinned one, and therefore preferred.

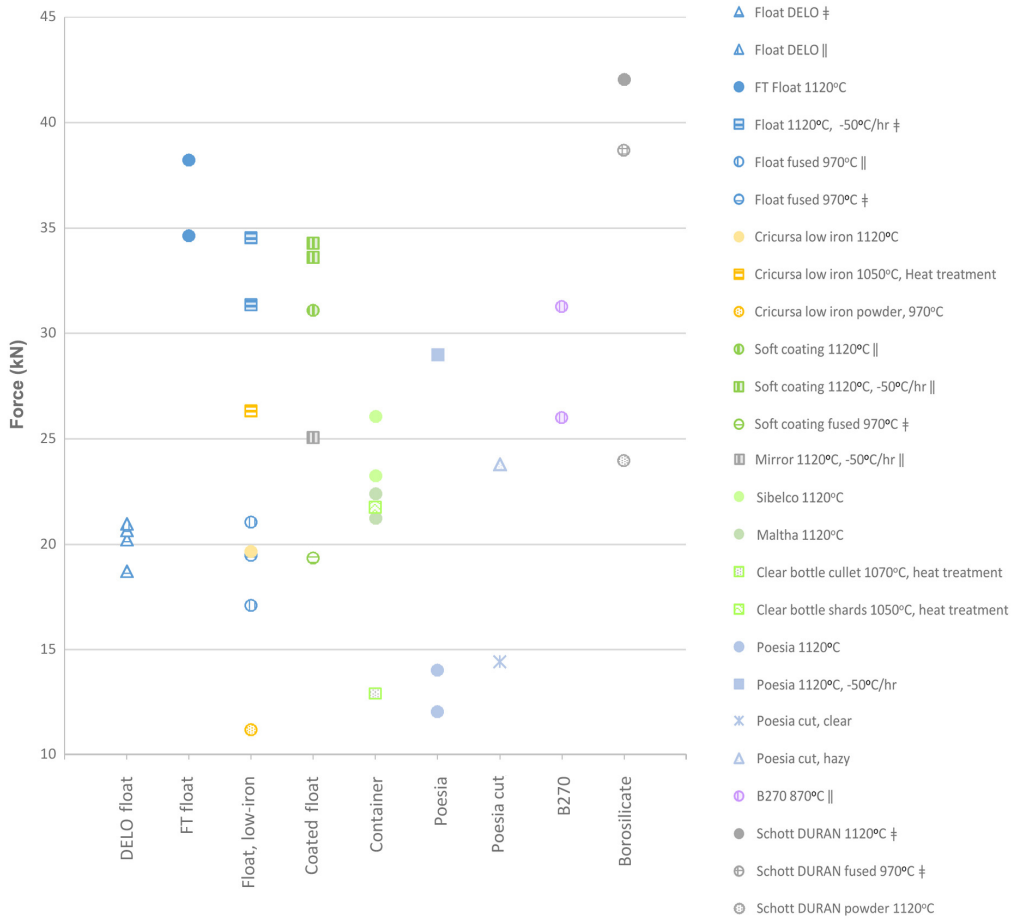

Fig. 5.11 Force at failure, as reported during the splitting test. Only fully supported specimens are included in the graph.

Container glass specimens, either homogeneous or with crystalline inclusions, are found to be weaker (21.8-24.6kN in average) than the homogeneous float glass variants. The obtained data is nonetheless only an indication of the fracture resistance of the different glasses, and due to the limited number of test repetition, they cannot be statistically conclusive.

The reference adhesively bonded float glass specimens have almost identical results regardless of the orientation of the float glass plies (18.7-20.9kN), and are comparable to the fused float samples, but 40% less resistant than the homogeneous kiln-cast float samples (1120°C, -50°C/hr).

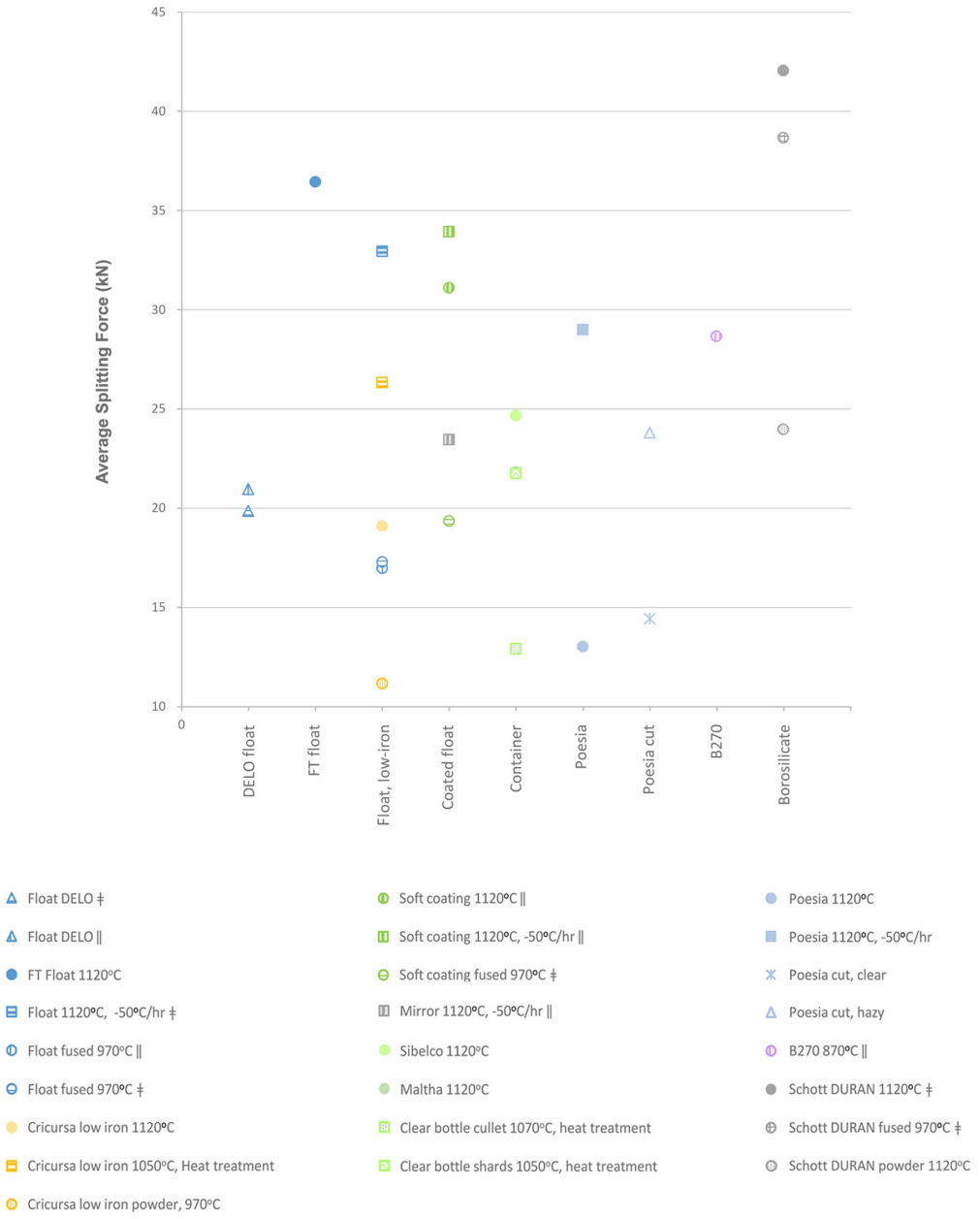

Fig. 5.12 Average force at failure of glass specimens establishing 85-100% contact with the toolbit.

Table 5.2 (part a): Results of the splitting test.

Glass type	Specimen description	Source	Forming temperature in °C (10hr dwell unless differently specified)	Cooling rate (°C/hr), heat treatment if applicable	Meso-level structure orientation in respect to the force direction (if applicable)	Number of valid specimens	Splitting force (kN)		
							Minimum	Maximum	Average
						85-100% support	85-100% support	100% support	85-100% support
Soda lime silica (Float glass), glued	Float Delo 4468, 10mm x5 layers	IFS-SGT	Industrially produced		Adhesive interlayers perpendicular to F	3	18.72	20.64	19.86
					Adhesive interlayers parallel to F	1	-	20.96	-
Soda lime silica (Float glass)	FT float^	IFS-SGT	1120	-160	-	2	34.63	38.22	36.42
	Float 10mm x5 layers		1120 (2hr)	-50	Subtle bubble veils perpendicular to F	2	31.34	34.51	32.93
	Float 10mm x5 layers, fused		970	-160	Crystalline interfaces parallel to F	3	12.65	21.05	16.97
					Crystalline interfaces perpendicular to F	2	15.07	19.46	17.27
	Low-iron float		1120	-160	-	2	18.53	19.65	19.09
	Low-iron float, heat-treated**	Cricursa	1050 (3hr)	-30 Heat treat.	-	1	-	26.32	-
	Low-iron float powdered, fused***		970	-160	-	1	-	11.15	-

^ The labelling "FT Float" refers to the use of Fully Tempered float glass shards as cullet. The final kiln-cast components are annealed and the thermal history of the shards is erased.

** Sample prepared by Shan Cindy Lei (2019) as part of her MSc work.

*** Sample prepared by Guilia Maria Anagni, as part of her MSc work (Anagni et al. 2020).

Table 5.2 (part b): Results of the splitting test.

Glass type	Specimen description	Source	Forming temperature in ºC (10hr dwell unless differently specified)	Cooling rate (ºC/hr), heat treatment if applicable	Meso-level structure orientation in respect to the force direction (if applicable)	Number of valid specimens	Splitting force (kN)		
							Minimum	Maximum	Average
						85-100% support	85-100% support	100% support	85-100% support
Soda lime silica (Float glass, coated)	Soft coating, 6mm x8 layers	Pilkington	1120	-160	Subtle bubble veils parallel to F	1	-	31.09	-
			1120 (2hr)	-50	Bubble veils parallel to F	2	33.59	34.27	33.93
	Soft coating, 6mm x8 layers, fused		970	-160	Crystalline interfaces perpendicular to F	1	-	19.33	-
	Mirror, 5mm x10 layers		1120 (2hr)	-50	Prominent bubble veils parallel to F	2	21.84	25.04	23.44
Soda lime silica (Container glass)	Clear cullet	Sibelco	1120	-160	-	2	23.25	26.06	24.66
	Clear and light-tinted cullet	Maltha	1120	-160	-	2	21.22	22.39	21.80
	Clear bottle cullet, fused**	Clear bottle	1070 (3hr)	-30 Heat treat.	-	1	-	12.89	-
	Clear bottle shards, fused**		1050 (3hr)	-120 Heat treat.	-	1	-	21.74	-

^ The labelling "FT Float" refers to the use of Fully Tempered float glass shards as cullet. The final kiln-cast components are annealed and the thermal history of the shards is erased.

** Sample prepared by Shan Cindy Lei (2019) as part of her MSc work.

*** Sample prepared by Guilia Maria Anagni, as part of her MSc work (Anagni et al. 2020).

Table 5.2 (part c): Results of the splitting test.

Glass type	Specimen description	Source	Forming temperature in ºC (10hr dwell unless differently specified)	Cooling rate (ºC/hr), heat treatment if applicable	Meso-level structure orientation in respect to the force direction (if applicable)	Number of valid specimens	Splitting force (kN)		
							Minimum	Maximum	Average
						85-100% support	85-100% support	100% support	85-100% support
Modified soda lime silica	Poesia standard brick	Poesia	1120	-160	-	3	12.00	14.02	13.00
			1120 (2hr)	-50	-	1	-	28.98	-
			Industrially produced (clear)		-	1	-	14.42	-
			Industrially produced (hazy)		-	1	-	23.79	-
	B270	Schott	870	-160	Coiling bubble veils parallel to F	2	26.01	31.28	28.64
Borosilicate	DURAN 24mm rods	Schott	1120	-160	2 Crossed subtle bubble veils, perpendicular to F	1	-	42.04	-
	DURAN 24mm rods fused		970	-160	2 Crossed crystalline interfaces, perpendicular to F	1	-	38.66	-
	DURAN powder***		1120	-160	-	1	-	23.97	-

^ The labelling "FT Float" refers to the use of Fully Tempered float glass shards as cullet. The final kiln-cast components are annealed and the thermal history of the shards is erased.

** Sample prepared by Shan Cindy Lei (2019) as part of her MSc work.

*** Sample prepared by Guilia Maria Anagni, as part of her MSc work (Anagni et al. 2020).

5.3.3 Fracture analysis

A repeating fracture pattern is found among the majority of the tested samples. Looking at the crack-front surface, an initial, crushed zone of maximum 500μm thickness appears along the area directly exposed to the sharp toolbit (Figures 5.13-5.14). This zone is followed by a second zone that involves the formation of stable median-radial cracks of maximum 4000μm radius. The extent of the crushed zone and radius of the stable cracks is linked to the applied force.

Building upon the created damage by the sharp indenter tip, unstable crack propagation will start once the critical fracture toughness is reached, at 1 or 2 damaged points simultaneously. The crack origin is not associated with a specific inherent material flaw, but with the stress intensity and the damage caused by the toolbit, which is overruling the presence of any other defect. The fracture origin is usually located close to one of the cube sides, possibly due to minor tilting of the specimen during testing. From the origin site and following the direction of crack propagation, secondary Wallner lines start, created from the interaction with singularities at the cube's bottom and side surfaces (Figures 5.15-5.16). The Wallner lines reveal the direction of crack propagation (dcp) in each specimen. Intense shear hackle lines appear around the fracture origin, while they are also present at secondary damage sites to a smaller extent (Figure 5.15).

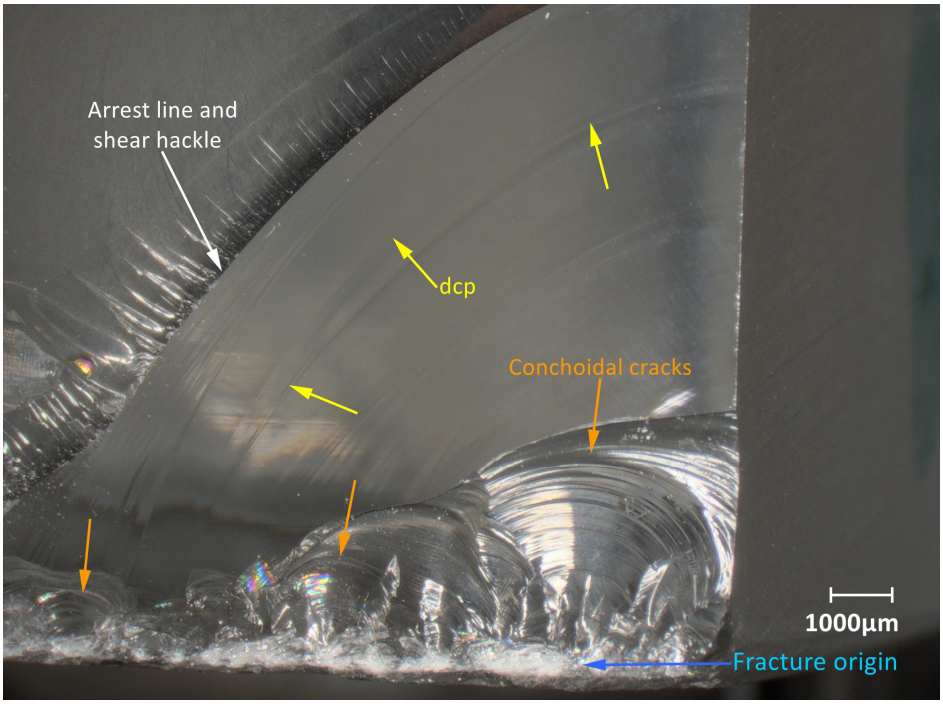

Fig. 5.13 Crack front showing the fracture origin in a "Poesia cut, clear" specimen, the crushed zone in contact with the toolbit, the formation of multiple conchoidal cracks, the direction of crack propagation (dcp), and the momentary arrest of the crack.

The fracture origin is in most cases mist-free, which according to Gopalakrishnan and Mecholsky (2014) is characteristic for mixed loading conditions (mode I: tension, combined with mode II: shear). Arrest lines often accompanied by perpendicular shear marks. The intensity in the morphology of the Wallner lines is proportional to the amount of stored elastic strain energy prior to cracking (Figure 5.16).

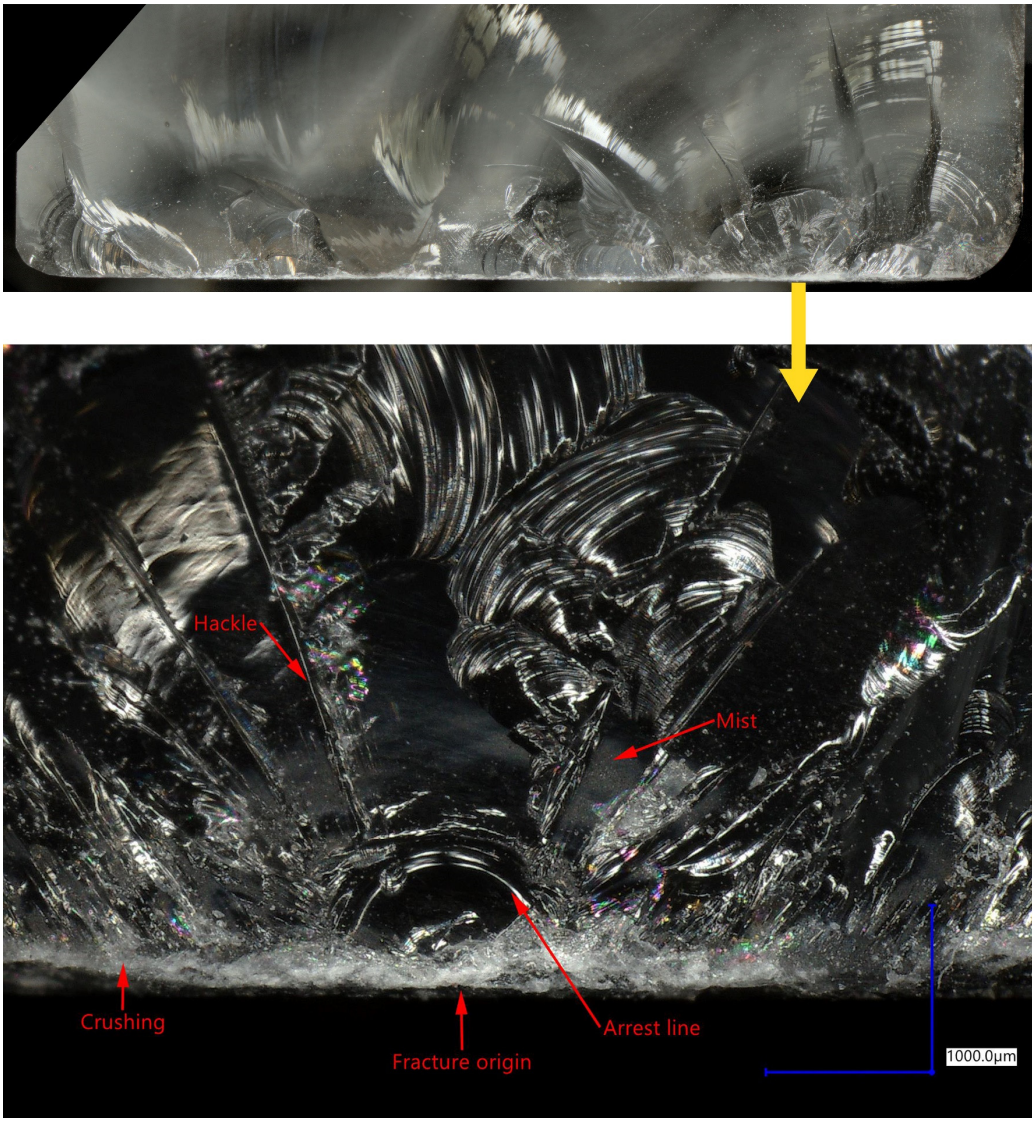

Fig. 5.14 Crack front in a "Poesia cut, clear" specimen. The fracture origin is located at the position with the most prominent hackle lines. The arrest line at the fracture origin site could suggest a slow crack growth. In addition, this is one of the very few specimens in this study that showed mist around the fracture origin.

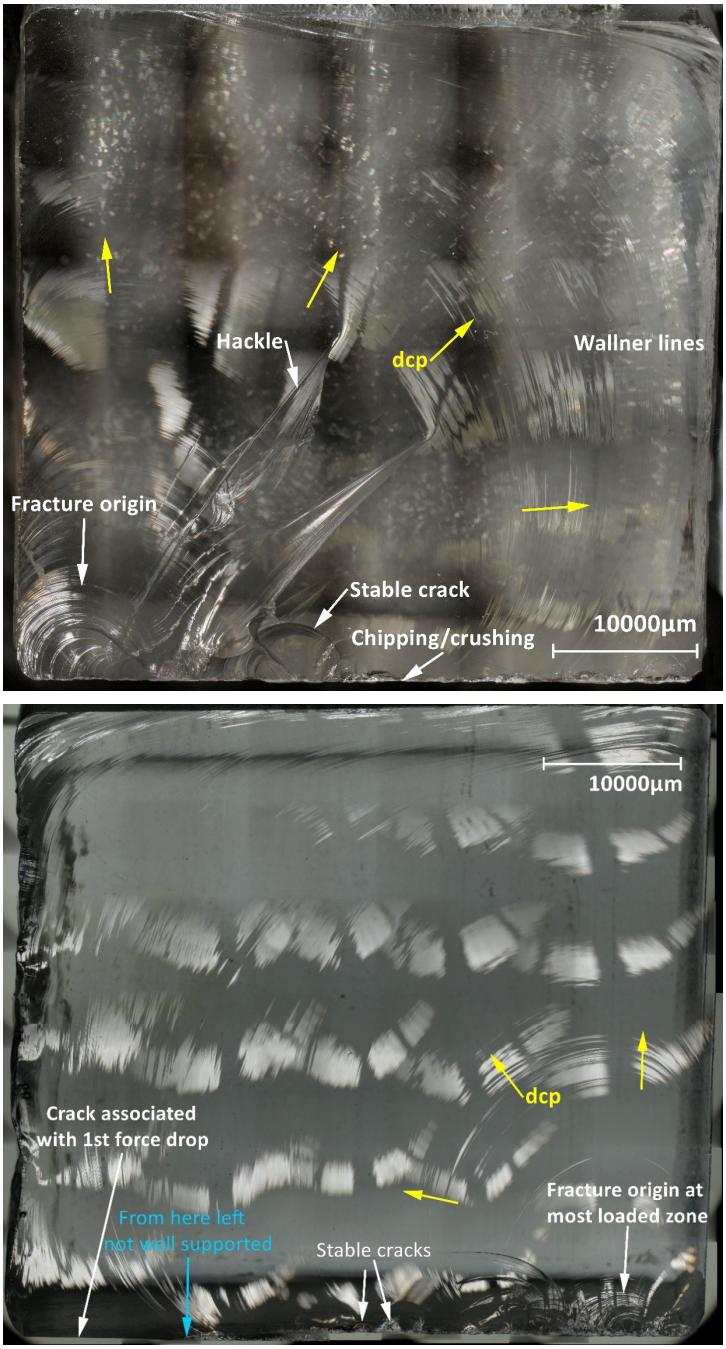

Fig. 5.15 Crack front surface of a fully supported "Poesia 1120ºC" specimen that failed at 14kN (top) and a partially supported "Cricursa Low-iron Float 1120ºC" specimen that failed at 13.5kN (bottom). The Wallner lines show the direction of crack propagation.

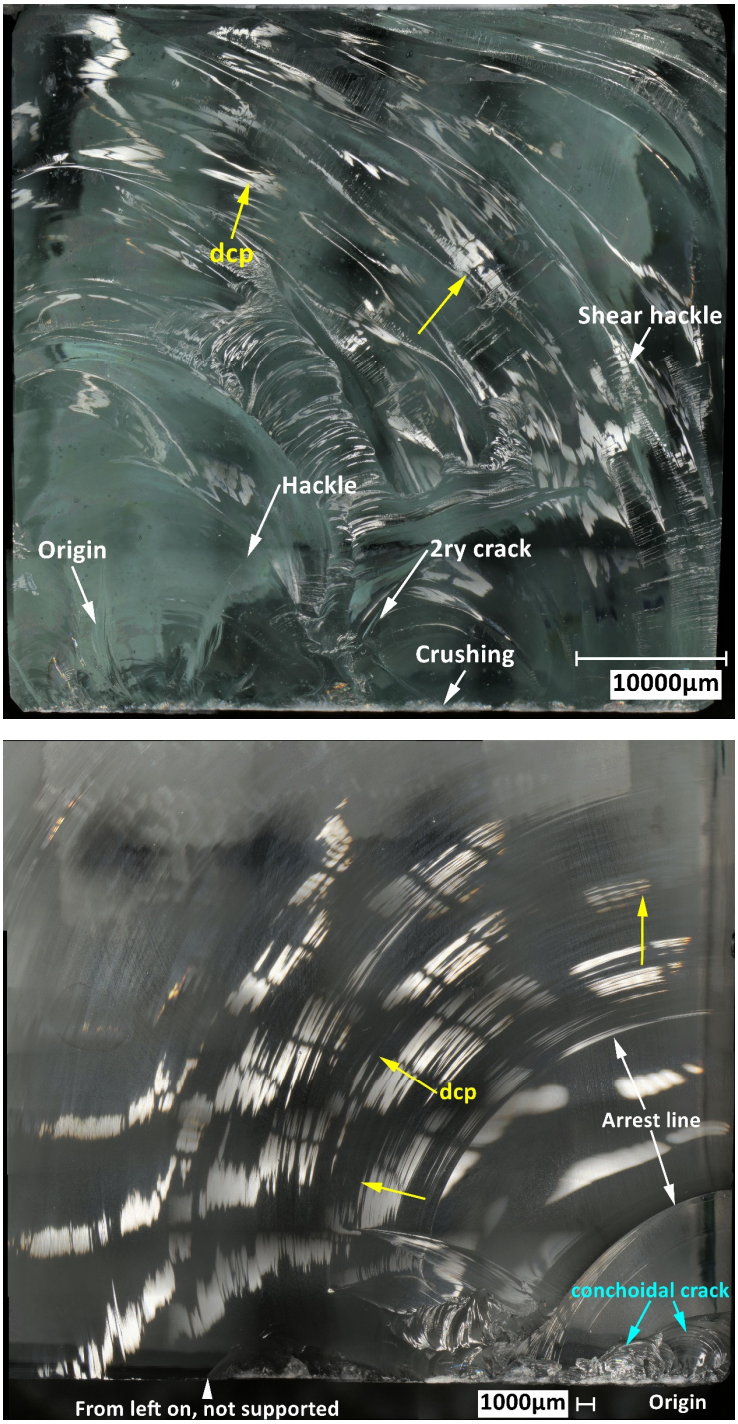

Fig. 5.16 Crack front surface of a fully supported "FT Float 1120ºC" specimen that failed at 38.2kN (top) and a partially supported "Poesia cut, clear" specimen that failed at 5.8kN (bottom).

The crack front will interact with singularities in the meso-level structure of the kiln-cast specimens in the form of gull wings, arrest lines, or shear hackle lines (Figures 5.17-5.19). However, a significant crack path deviation due to the presence of a zone of gaseous or glassy inhomogeneity in the glass- for example a bubble veil or extended cord close to and parallel to the crack front- is not observed.

Such zones, although in theory weaker, are not considered disruptive enough to the glass network (as long as they are not stress inducing), so that a fast propagating crack will alter its path. Such path alteration is only observed in the (parallel to the force) glued specimens, where partial delamination will occur (Figure 5.20).

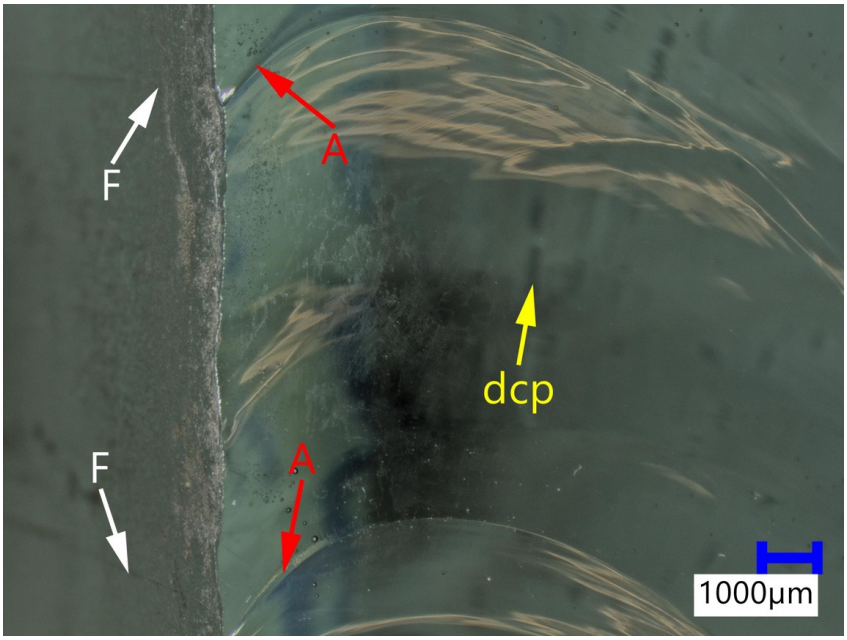

Fig. 5.17 Crack front surface and side view of a "Float 10mm x5, 1120ºC, -50ºC/hr" specimen. The insufficient homogenization between the float plies due to a short dwell time at top temperature (2hr) results in subtle bubble veils at the fusion zones and linear marks at the side surface ("F"). The crack will show a momentary arrest ("A") at these lines.

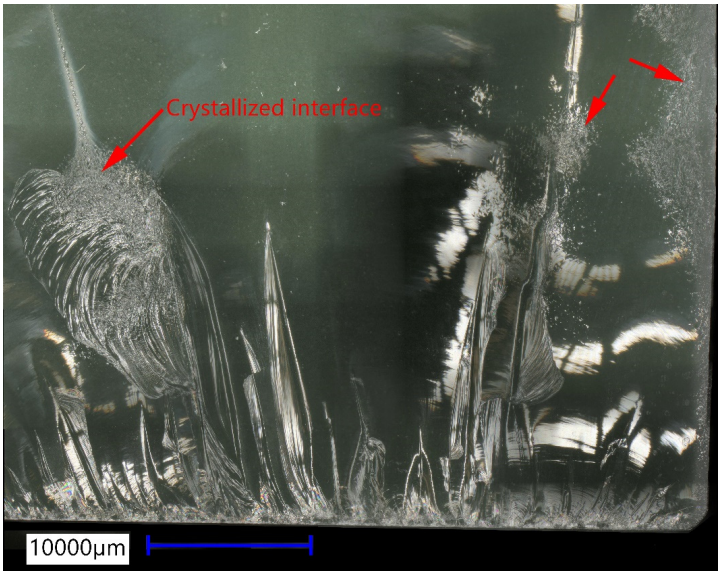

Fig. 5.18 Crack front of a fused “Float 10mm x5, 970ºC” specimen, with the crystalline interfaces oriented in parallel to the force direction during testing. The crack front will interact with the crystalline interface if encountered during its propagation, but will not change its direction of growth

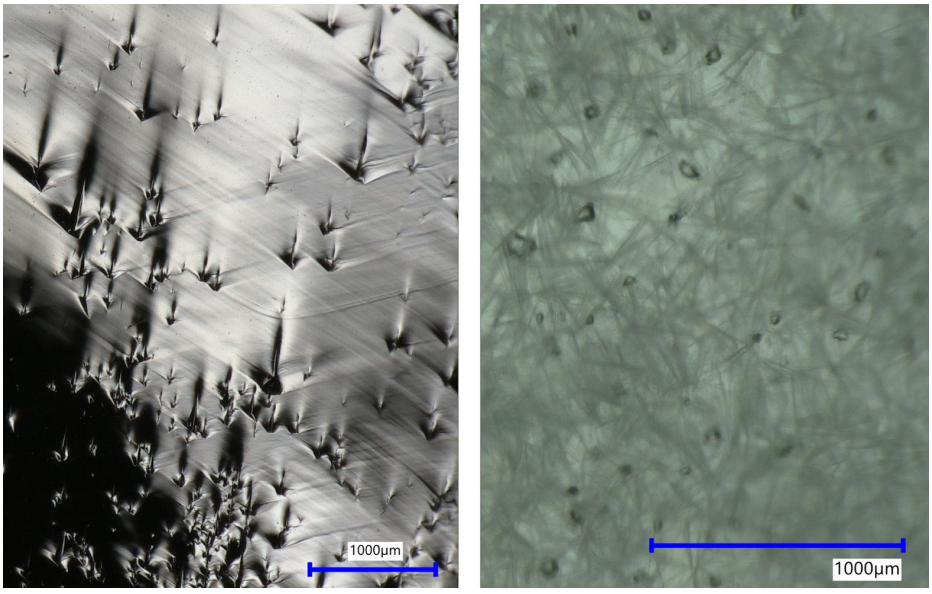

Fig. 5.19 Detail from specimen in Figure 5.18 (right red arrows) showing the formation of gull wings when the crack front encounters the crystalline interface (left). On the right, an image of the crystalline interface, showing the existence of acicular crystals.

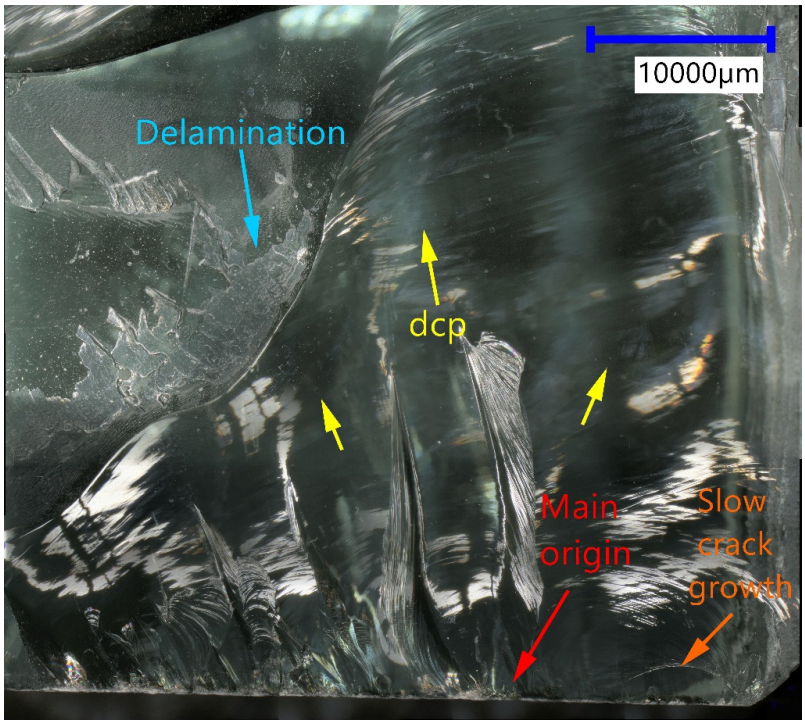

Fig. 5.20 Crack front surface of a glued "Float 10mm x5 Delo" specimen, with its adhesively bonded interfaces being in parallel to the force direction during testing. Once the adhesive interface is encountered, delamination will occur and the crack will move along the glued surface of lower stiffness.

A higher degree of interaction is observed when crystalline zones are incorporated in the glass (Figure 5.21). Most characteristic is the example of the fused Borosilicate (970ºC), which contains two crossed 50x50mm crystalline interfaces, one perpendicular to the toolbit and the second one in parallel to the bottom surface (Figure 5.21 right). The perpendicular to the toolbit crystalline interface -due to its expected higher hardness than the surrounding glass- seems to divide the glass sample in two distinct parts. This can be observed at the bottom surface, where around the interface, only minimum lateral damage occurs, in contrast to the middle zone of the two glass parts (Figure 5.23). At the crack front surface, two distinct fracture origins and intense shear hackle lines are observed at the middle of each glass part.

The crack eventually propagates across the crystalline borders, yet intense median-cracking and shear lines are observed along the interface. The crystalline interface, at least in this thickness (≈70-85μm) and for this specimen size (50mm), is not sufficient to completely arrest the crack propagation, as in the example of the (perpendicular to the force) glued specimens (Figure 5.22).

Examples of specimens having an alternating structure of glassy and crystalline material exposed to the toolbit line (e.g. Clear bottle cullet/shards, heat-treated, Figure 5.24) or a high porosity (Figure 5.25) show a fluctuating response (e.g. densification, stable cracking) during loading. The uneven processing of the load due to material property differences of the two structures is stress-inducing, and accelerates failure.

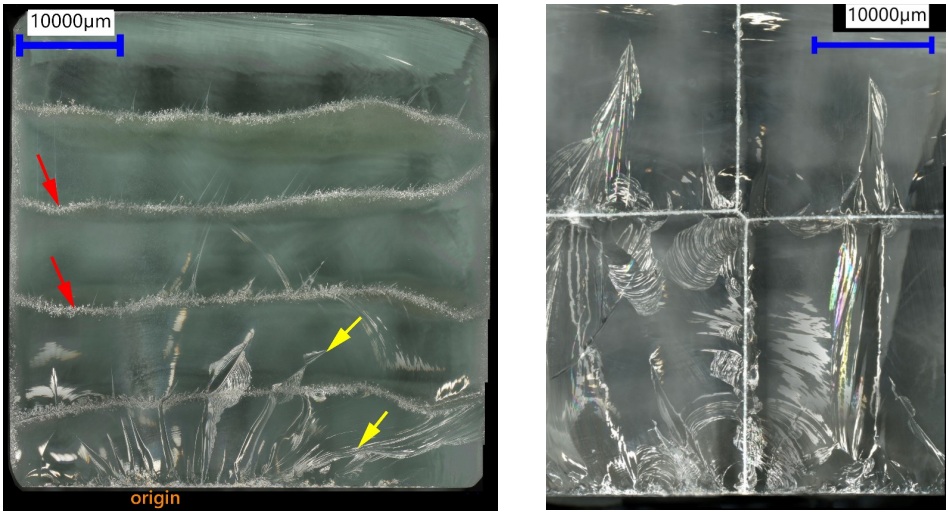

Fig. 5.21 Crack propagation in a fused "Float 970ºC" specimen with crystalline interlayers (red arrows) oriented perpendicularly to the force direction (left) and in a fused "Borosilicate 970ºC" specimen (right). The crack may momentarily slow down or arrest when encountering a crystalline interface, but it will not stop from propagating. Hackle lines (for indication see yellow arrows, left figure) may turn into twist hackle upon encountering a crystalline interface.

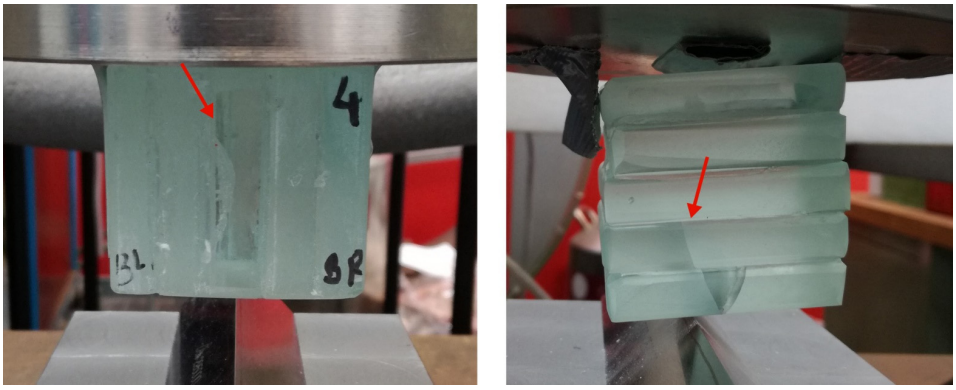

Fig. 5.22 Float specimens glued with DELO and tested in parallel (left) or perpendicular (right) orientation. In the left case, the crack will propagate throughout the specimen, and move along the adhesive layer once it reaches it, while in the right case, the propagation will be completely arrested by the adhesive interface.

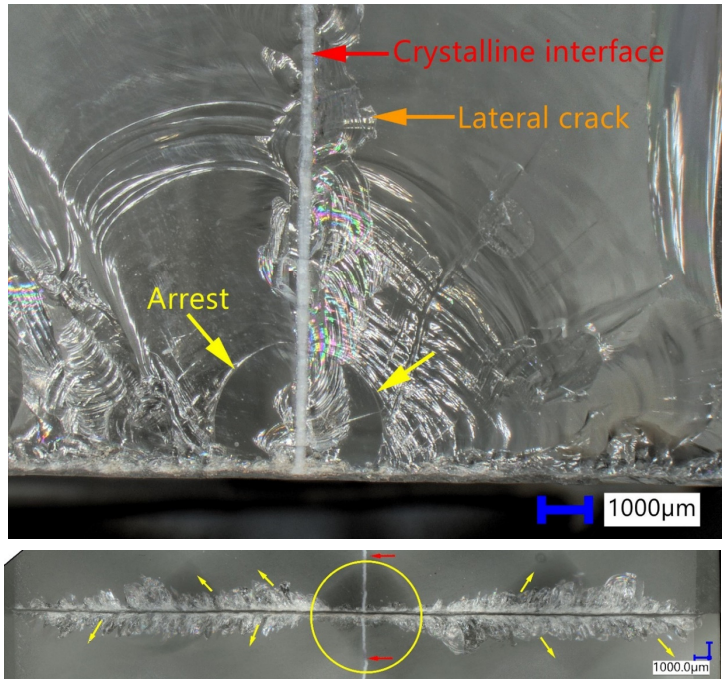

Fig. 5.23 Crack front (top) and bottom surface (bottom) of a fused “Borosilicate 970ºC” specimen. The perpendicular to the toolbit crystalline interface is separating the component in two parts.

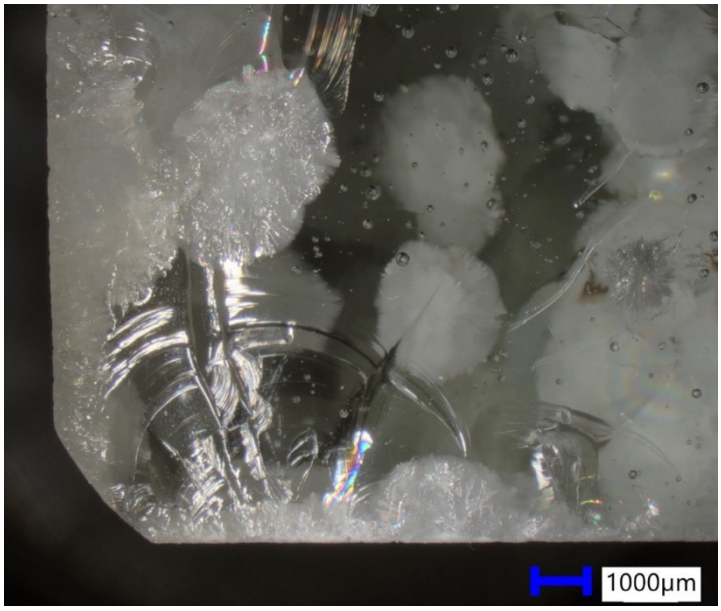

Fig. 5.24 Fracture origin of a heat-treated “Clear bottle cullet” specimen, showing the interchange between glassy and crystalline material at the process zone of the crack.

Fig. 5.25 Crack front of a fused "Low-iron float powder 970ºC specimen. The intense porosity at the process zone of the crack is weakening the specimen.

Regarding the bottom surface and likewise to the crack front surface, a crushed zone of maximum 500µm thickness is observed followed by an array of median-radial cracks of maximum 5mm (either at the surface in the form of chips, or in the sub-surface, see Figure 5.26). The extent of the lateral damage (both crushing and chipping) is directly related to the force (Figures 5.28-5.29). However, specimens that have been heat-treated or slowly cooled, show relatively less damage. On the other hand, the heat-treated "Clear bottle cullet" specimen, due to the inherent intermix between crystalline and glassy structure, is more prone to lateral damage. The presence of scratches (due to post-processing damage) or pores (e.g. crystalline material from mould contamination, cut bubbles) at the bottom surface often seems to intensify the occurrence of chipping (Figure 5.27). Significant unevenness in the thickness of the crushed layer along the contact line, is a telltale sign of specimen tilting during testing. These specimens are discarded from the surface damage analysis, since they are not comparable to the fully supported specimens.

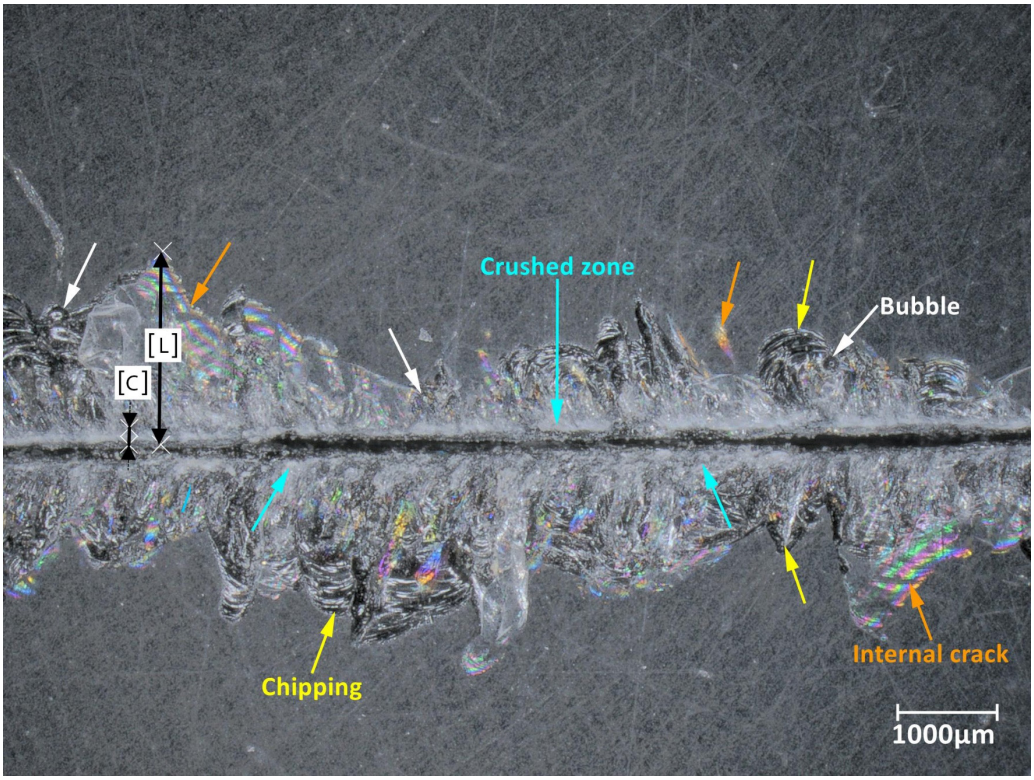

Fig. 5.26 Bottom surface of a "Sibelco Clear bottle" specimen, showing the zone in contact with the toolbit, and subsequently the zone of crushed glass and the lateral damage caused by the increasing pressure. The extent of crushing (C) and lateral damage (L) are measured in each sample as indicated in the image above.

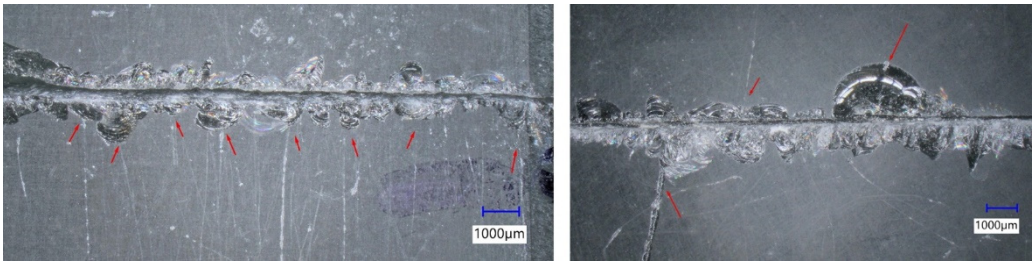

Fig. 5.27 Bottom surface of "Sibelco Clear bottle" specimen showing the link of lateral damage to surface defects such as scratches or bubbles.

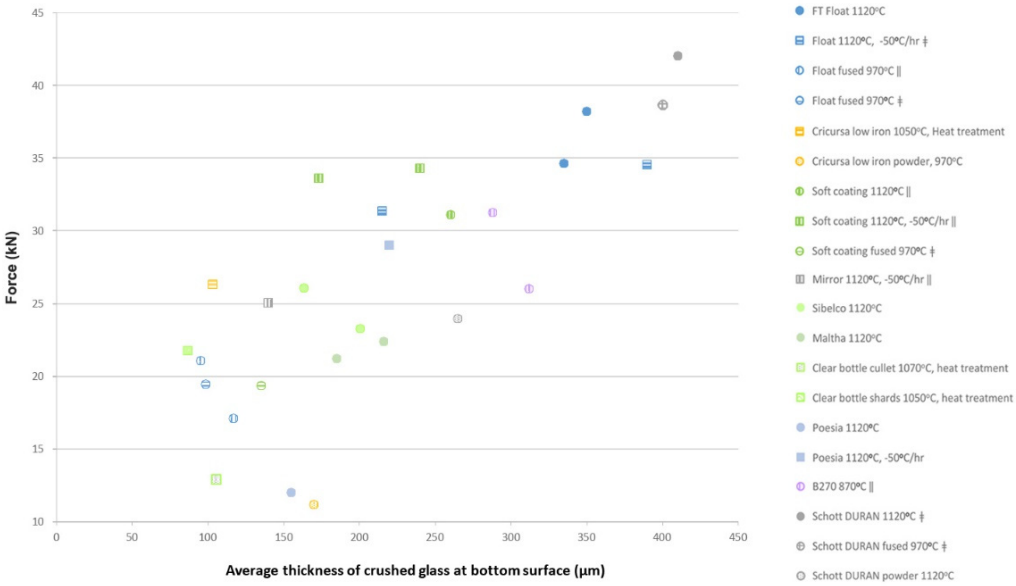

Fig. 5.28 Extent of crushing in relation to the splitting force at failure. Only fully supported specimens are included in the graph.

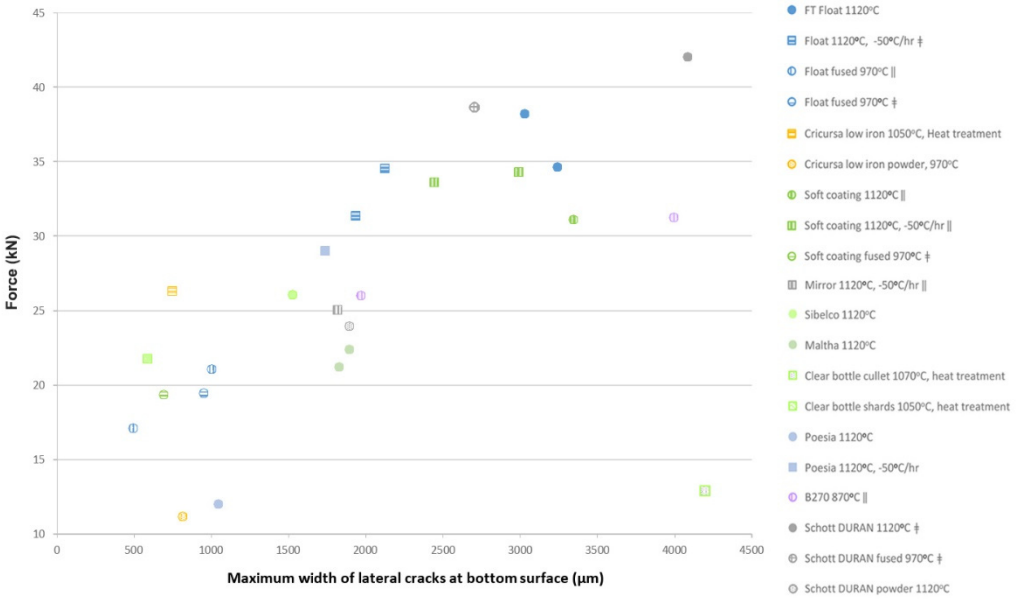

Fig. 5.29 Maximum width of lateral damage in relation to the splitting force at failure. Only fully supported specimens are included in the graph.

5.4 Discussion

5.4.1 Comparison between splitting and four-point bending experiments

A comparison between the resistance of cast glass to catastrophic fracture due to a pressing sharp indenter, to its strength in flexure due to bending is made. For this comparison, current data from the splitting experiment and previously obtained data from four-point bending experiments (Bristogianni et. al 2020, Bristogianni et al 2021), are used.

Reversed results can be seen, by comparing the obtained data of homogeneous Borosilicate, FT Float and Poesia glass. Specifically, the flexural strength increases in the order of Borosilicate 1120ºC (44MPa) < FT Float 1120ºC (45MPa) < Poesia 1070ºC (58MPa), while the fracture resistance decreases respectively to 42kN> 36.4kN> 28.3kN. Similarly for the fused specimens, the Borosilicate 970ºC showed an average flexural strength of 13.9MPa, which was the lowest value from all tested glass types, and the 2nd highest fracture resistance force, 38.7kN. On the contrary, although the Fused Float 970ºC had a higher flexural strength (33.3MPa), its fracture resistance in the cube splitting test was reduced to 16.6kN. The above reverse results do not imply a straightforward relationship however; the fused float versus the homogeneous float specimen remains weaker in both tests, and so does the industrially cast Poesia glass versus the kiln-cast version.

The distinct differences between the two tests in the performance of the different glass types highlight the different mechanisms involved in the failure of the specimens. In the four-point bending experiment, a far-field tensile stress is developed at the bottom zone of the beam, reaching a maximum level at the bottom surface area between the loading rollers. Any flaws located in this zone, either inherent (e.g. stones, cord, bubbles) or external (e.g. post-processing damage, impact, scratches), will be activated inducing stress concentration to the surrounding glass, and with the most critical flaw leading to catastrophic failure. The strength of glass in this case is highly dependent on the set of flaws that each glass type is prone to have, in combination to its material properties resulting from the chemical composition and thermal history. The stiffness[84] of glass plays a prominent role in this process. However, although a high bond strength is desired to resist fracture, a slightly more open structure is beneficial as it allows for minor deformations around the flaws and thus stress relief during loading. In that sense, the borosilicate glass that has a much lower stiffness (E= 62GPa) than FT Float (E= 75GPa) will have as well lower flexural strength, yet the Poesia glass with E= 70-72GPa but also a higher molar volume than FT Float due to the increased Na_2O/CaO ratio, will be stronger (Bristogianni et al 2021). Nonetheless, given that each glass is characterized by a unique set of flaws- whose distribution,

[84] The Young's modulus, according to Makishima and Mackenzie (1973) is related to the atomic packing density (APF), and the total dissociation energy (G_t) that reflects the bond strength:

$$E = 2 \cdot APF \cdot G_t \quad (1)$$

shape and quantity are to a great extent random- the exact interaction between chemical composition and glass structure cannot be elucidated at this stage[85].

In the case of the splitting test, given the prominent role of the indenter as the cause of failure, the uncertainty created by the incidental population and type of flaws is to some extent reduced. As the sharp toolbit gradually gets inserted deeper in the material and lateral tension builds up, the glass will initially respond by permanently deforming. According to Rouxel (2008), this deformation is mainly in the form of densification rather than shear flow for silicate-based glasses, due to low Poisson's ratio (ν). Specifically, the lower the ν in silicate glasses, the higher the displacement of matter and thus the relaxation of stress, leading to a higher crack resistance (CR, resistance to crack initiation). A higher crack resistance delays the formation of median-radial cracks that will gradually weaken the glass cubes to a more decisive extent than the inherent flaws they may have. Once such cracks are formed and the pressure from the toolbit continues to increase, then the fracture surface energy[86] (γ) and consequently the fracture toughness (K_{Ic}, resistance to crack growth) of glass become dominant in resisting the unstable propagation of the growing crack. Yet, although singular defects in the glass structure will have a much less prominent role in the splitting test, once the defects start to significantly degrade the glass zone in contact with the toolbit (e.g. in the case of the porous and crystallized glass specimens, or the heavily crystallized "Clear bottle cullet, heat-treated" specimen), then a significant reduction in the fracture resistance will be observed.

The splitting test therefore measures the complete process from crack initiation due to sharp contact loading, to fracture propagation and catastrophic failure:

$$Fracture\ resistance = Crack\ initiation\ resistance \cdot\ Crack\ propagation\ resistance \qquad (3)$$

To better comprehend the splitting test results, a deeper look at the relationship of the glass composition and structure to the crack resistance and fracture surface energy is required.

[85] Distinguishing these roles may not be appear directly relevant in the engineering practice for calculating a cast glass structure. However, this deeper understanding is important for engineering stronger cast glass components, improving the casting production process and conducting responsible quality control.

[86] Fracture surface energy is the energy linked to the formation of new surfaces during fracture. When the introduced mechanical energy cannot be further accommodated by stress relaxation, it is energetically preferable for a brittle material to fracture, converting this energy into surface energy. According to Griffith (1920), crack propagation will occur when:

$$S = \sqrt{\frac{2 \cdot E \cdot \gamma}{\pi \cdot c}} \qquad (2)$$

With S being the applied stress and c the half-length of an elliptical flaw. The formula shows that a higher fracture surface energy leads to a higher amount of stress that can be accommodated prior to fracture.

5.4.2 The effect of chemical composition, thermal history and meso-level structure to the fracture resistance of cast glass

There is no systematic correlation between crack resistance and fracture toughness, according to research conducted by To et al. (2020), yet both parameters depend on the glass composition and thermal history (e.g. cooling rate). Glasses with simultaneously high CR[87] and K_{Ic} values, would then exhibit low-brittleness behaviour.

Specifically, the crack initiation resistance is controlled by the extent to which the glass can densify or shear in the process zone under the indenter, with densification being favoured in glasses with small Poisson's ratio (Sellappan et al. 2013). A more open glass structure, reflected by a lower Atomic Packing Factor (APF) and higher molar volume (V_m), will allow for more deformation, leading to a higher crack initiation load and less brittleness (Seghal and Ito 1998, Hasdemir et al 2015). Table 5.3 shows the calculated APF and V_m of the tested glasses based on the chemical composition. As it can be seen, the Schott DURAN borosilicate presents the lowest APF and highest V_m that suggests a more open structure[88]. The SLS glasses show on the other hand the lowest V_m from the tested glasses. The B270 and the Poesia glass have a higher molar volume than the SLS glasses, due to their K_2O content and the higher alkali to calcia ratio (Seghal and Ito 1998).

The ability of the borosilicate glass to densify more under a sharp load, is also seen by the lower Poisson's ratio (0.2 versus 0.22 of SLS glass, Table 5.3), which according to Makishima and Mackenzie (1975) is directly related to the APF through the formula:

$$v = 0.5 - \frac{1}{7.2 \cdot APF} \quad (4)$$

[87] Crack Resistance CR is often measured using the method suggested by Wada et al. (1974): a Vicker's indenter creates imprints at various loads, and the number of corners presenting radial cracks is evaluated. Januchta and Smedskjaer (2019) stress however that CR refers to the critical load for radial crack initiation, and not for all types of cracks under a sharp indenter (e.g. lateral cracks). The value is also influenced by the testing and atmospheric conditions. In this study, CR is used to compare different silicate-based glass compositions in a quantitative manner, and less attention is given to the actual value.

[88] The less rigid glass structure is attributed to the higher content of silica and the portion of threefold-coordinated boron in the network (66% as calculated using the formulae by Yin and Bray (1978)). Kato (2010 a, b) showed that, as the tetrahedral boron is responsible for a rigid 3D glass structure that prohibits densification and therefore increases the residual stress, a reduction in its percentage will increase the CR.

Table 5.3 (part a): Chemical composition and mechanical properties of the studied and relevant reference glasses.

Glass Type	Name*	Composition (wt%)												
		SiO_2	B_2O_3	Na_2O	K_2O	CaO	MgO	Al_2O_3	TiO_2	Fe_2O_3	Sb_2O_3	ZnO	BaO	Source
Soda lime silica	**FT float**	75.4		12.4		7.6	4	0.4	0.02	0.09				[1]
	Float IFS-SGT	72.4		12.3	0.1	9.9	4.1	0.6	0.06	0.07				[1]
	Cricursa low iron	74		12.7		8.4	4.2	0.55		0.02				[1]
	Starphire PPG	74.6		13.3		8.9	3	0.04						[1]
	Pilkington soft coating	74.4		12.5	0.15	8.2	3.9	0.55	0.03	0.06				[1]
	Clear bottle	72.7		12	0.5	10	3	1.3	0.045	0.17				[1]
Modified soda lime silica	**Poesia**	72.1	2.5	15.9	1.9	6.1	0.06	0.3			0.9			[1, 9]
	B270	71.8		10.1	6.3	5.2		2	1.8		0.4	2.2	0.03	[1]
Borosilicate	**Schott DURAN**	80	13	3.5	0.5			2.7						[1, 11]
Amorphous silica	a-SiO_2	100												[14]

* Only the glasses in bold characters are experimentally tested in this study. The Starphire and Amorphous silica glasses are included in this table as a reference.

[1] XRF measurements conducted by Ruud Hendrikx

[2] Calculated using viscosity model by Fluegel (2007a)

[3] Calculated using density model by Fluegel (2007b)

[4] Yet unpublished prior work by the authors

[5] Vitro Architectural Glass (2020)

[6] Quinn and Swab (2017)

[7] Calculated as G= E/[2(1+v)]

[8] Calculated as K= E/[3(1-2v)]

Table 5.3 (part b): Chemical composition and mechanical properties of the studied and relevant reference glasses.

Name*	Annealing Point 10^{13} dPa · s (°C)	Density (g/cm^3)	Knoop micro hardness (kgf/mm^2)	Molar volume V_m (cm^3/mol), calculated	APF Calculated based on Shannon's ionic radii	G_t Total Dissociation energy (kJ/cm^3), calculated using Inaba et al.	E (GPa) from literature	Shear modulus G (GPa), literature	Bulk modulus K (GPa), literature	Poisson's ratio v calculated using Makishima and Mackenzie formula and Shannon's APF	Poisson's ratio v (literature)	Vicker's hardness calculated using Yamane and Mackenzie formula
FT float	553 [2]	2.47 [3]		23.92	0.4920	64.83				0.218		
Float IFS-SGT	562 [2]	2.5 [4]		23.8	0.4907	64.87	71 [4]			0.217		6.9
Cricursa low iron	554 [2]	2.48 [3]		23.73	0.4937	64.85				0.219		
Starphire PPG	545 [5]	2.48 [3] 2.51 [5]	470 (Force: 500gf) [5]	23.55	0.4997	64.03	73.1 [5]	30.4± 0.3 [6] 29.9 [7]	42.2 ± 0.9 [6] 43.5 [8]	0.222	0.22 [5]	7.1
Pilkington soft coating	554 [2]	2.48 [3]		23.85	0.4930	64.76				0.218		
Clear bottle	564 [2]	2.49 [3]		23.88	0.4943	64.72				0.219		
Poesia	≈520 [2]	2.49 [3]		24.65	0.4997	61.83	69 [4]			0.222		6.6
B270	535 [10]	2.49 [3]	500 (Force: 100gf) [10]	25.26	0.4939	62.91	71.1 [10]	29 [10]	42.4 [8]	0.219	0.22 [10]	6.8
Schott DURAN	560 [12]	2.23 [11]	480 (Force 100gf) [13]	27.54	0.4767	64.1	63 [11]	26.3 [7]	35 [8]	0.209	0.20 [11]	5.9
a-SiO_2	1100 [14]	2.2	591-632 [14]	27.31	0.4561	68	70 [15]	30.4 [16]	33.3 [16]	0.195	0.15 [15]	6.6

[9] Personal correspondance with Poesia

[10] Schott (2013)

[11] Schott (2015)

[12] Schott (2017)

[13] Abrisa Technologies (2014)

[14] Heraeus Quarzglas (2013)

[15] Rouxel (2017)

[16] Sellappan et al. (2013)

Crack resistance is also depended on the bond strength (To et al. 2020), as the stronger the bonds in the network, the more difficult to break. Januchta et al. (2020) also correlate CR to the Bulk modulus[89] stating that flexible glasses can distribute the residual stress in a larger field. At this point, it should be elaborated that Hardness, which quantifies the resistance of a ceramic material to deformation and densification, is not inversely related to CR (see Table 5.4). In other words, the resistance of a glass to crack initiation cannot be predicted by solely reviewing its hardness (a property often and easily tested in glass and ceramics, Table 5.5), as it is the optimum combination of bond strength and atomic packing density that contributes to a high cracking resistance[90].

Table 5.4: Crack resistance, fracture toughness and hardness of soda lime silica and borosilicate glass, as reported in the literature.

Glass Type	Composition (wt%)							CR (N)	K_{ic} (MPa·m$^{0.5}$)	K_{Ic} test method	H_V (GPa)	Source
	SiO_2	B_2O_3	Na_2O	K_2O	CaO	MgO	Al_2O_3					
Soda lime silica	72.6		13.8		9.5	4.1		0.7	0.74	SEPB	6.3	[1]
	80.2		10.4		9.4			1.47	0.75	SEPB	5.6	[2]
	78.3		13.3	1.5	0.9	2.7	3.3	34	0.92	IF	4.7	[3]
Borosilicate	79.2	13.3	5.4				2.1	4.41	0.65/ 0.73	SEPB	6.5	[4], [5], [6]
	73.5	11.4	5.1					9.81	0.76	SEPB	6.1	[2]
	65.6	21.9		7.4				12.75	0.73	SEPB	5.7	[2]

[1] To et al. 2020
[2] Kato et al. 2010
[3] Sehgal & Ito 1998
[4] Limbach et al. 2015
[5] To et al. 2018
[6] Quinn & Swab 2017

[89] For isotropic materials, the Bulk modulus K is related to the Young's modulus and Poisson's ratio as:

$$K = \frac{E}{3(1-2\nu)} \quad (5)$$

[90] As an indication of the parameters influencing the hardness of a glass, the following formula is insightful, developed by Yamane and Mackenzie (1974) for calculating the Vicker's hardness number of glasses from their chemical composition:

$$H_V = 0.051 \cdot E \left(\frac{a}{0.462 + 0.09APF - APF^2}\right)^{1/2} \quad (6)$$

Where a is a factor relating the average single bond strength to Si-O bond strength.

Table 5.5: Vicker's hardness as reported in the literature for common chemical glass compositions.

Glass Type	Composition (wt%)							H_v (GPa)	Indentation load (N)	Source
	SiO_2	B_2O_3	Na_2O	K_2O	CaO	MgO	Al_2O_3			
a-SiO_2	100							6.2	1-3	[1]
	100							8.7	1	[2]
SLS	72.3		12.5	1.6	8.5	3.4	1.7	5.4	1-3	[1]
	74.1		12.2		11	1.9	0.8	6.5	1	[2]
	72		12.9	0.4	9.9	4	0.8	6.3	1	[2]
Modified SLS	76.8		15.2		4.6		3.4	5.8	1-3	[1]
Borosilicate	81.9	12.5	4				1.6	5.5	1-3	[1]
	79.7	14.1	5.3	0.95				6.7	1	[2]

[1] Sehgal & Ito 1999 [2] Sellappan et al. 2013

Proceeding now to the next phase, resisting the propagation of an already created crack, the surface energy (γ) of the material becomes of crucial importance. The fracture surface energy is linked to the surface density of representative structural units and the bond strength (Rouxel 2017)[91]. Experimentally identified (by Wiederhorn 1969, Nakayama 1965) or theoretically calculated (by Rouxel 2017) γ values for glass (Table 5.6) show that borosilicate glass- of a composition similar to DURAN Schott- has a higher γ than SLS glass. This difference is not directly evident if only the K_{Ic}[92] value of these two glass types is considered, and which according to the testing set-up and environmental conditions can be identical (see Table 5.6).

[91] According to Rouxel (2017), the intrinsic γ of a glass can be calculated based on the number and type of bonds involved in the fracture, in the following manner:

$$\gamma = \frac{1}{2} \cdot \left(\frac{1}{V_m}\right)^{\frac{2}{3}} \cdot N^{-\frac{1}{3}} \cdot \langle U_o \rangle \quad (7)$$

Where N is the Avogadro number and Uo is the mean bond strength considered in the fracture process. From the formula it can be derived that strong bonds and small molar volumes increase the surface fracture energy.

[92] Fracture toughness is directly related to the fracture surface energy by the following formula, based on the work of Griffith (1920) and Irwin (1957):

$$K_{Ic} = \sqrt{\frac{2 \cdot E \cdot \gamma}{1 - \nu^2}} \quad (8)$$

Table 5.6: Surface energy and fracture toughness as reported in the literature.

Glass Type	Composition (wt%)							Density (g/cm^3)	E (GPa)	ν	APF	Theoretical γ (J/m^2)	Measured γ (J/m^2), N_2(g), 300°K	K_{Ic} ($MPa \cdot m^{0.5}$)	K_{Ic} measurement method	Source
	SiO_2	B_2O_3	Na_2O	K_2O	CaO	MgO	Al_2O_3									
a-SiO_2	100							2.2	70	0.15	0.456	3.62		0.73	DCC (vacuum)	[1]
	99.8								72.1				4.32-4.42	0.79-0.8	DCC (N_2(g), 300°K)	[2]
	100								73	0.16				0.93	SEPB (N_2)	[3]
SLS	71		13		10	6		2.49	72	0.22	0.496	3.55		0.68-0.72	CN-SEPB	[1]
	72		14	1	7	4	2		73.4				3.82-3.91	0.75-0.76	DCC (N_2(g), 300°K)	[2]
	70-74		12-16	0-0.5	8-13	0-5	0-2		72	0.22				0.76	SEPB (N_2)	[3]
Borosilicate	81	13	4				2	2.23	63.7	0.20	0.478	3.88		0.68	CN	[1]
	80	14	4				2		63.7				4.51-4.75	0.76-0.78	DCC (N_2(g), 300°K)	[2]
	81	13		4			2		64	0.20				0.75	SEPB (N_2)	[3]
a-B_2O_3		100						1.85	17.4	0.26	0.495	4.99		0.95-1.3	IF-SENB	[1]

[1] Rouxel & Yoshida 2017 [2] Wiederhorn 1969 [3] Quinn & Swab 2017

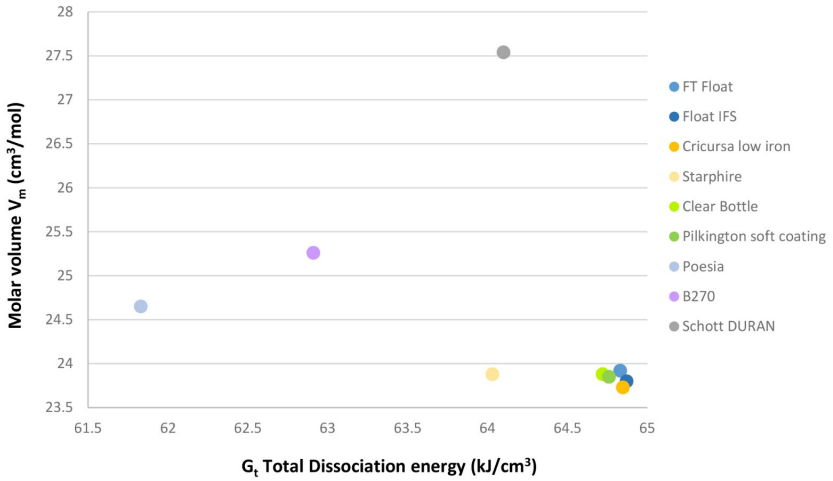

Fig. 5.30 Molar volume in relation to the bond strength (expressed as the Total Dissociation energy) for the glass compositions included in this study.

Therefore, it is concluded that for a high resistance to fracture, a balanced combination of flexibility (empty space) in the network and strong bonds are required. By evaluating the glasses included in this study according to their molar volume V_m and dissociation energy G_t (calculated based on Inaba et al. 1999) in Figure 5.30, it can be predicted which glass types will show higher resistance to crack initiation due to low V_m (Poesia, B270), which will show higher resistance to crack propagation due to high G_t (SLS) and which will perform well in both cases (Borosilicate).

Nonetheless, the above argumentation only takes into account the chemical composition of the glass, and neglects its thermal history and flaw population. A faster cooling and annealing scheme can reduce the polymerization of the SLS glass network leading to lower hardness (Gross and Tomozawa 2008), E modulus and brittleness (Ito and Taniguchi 2004). Moreover, surface flaws and residual stress weaken the glass and decrease the crack initiation load.

The fused specimens included in this study, due to their prolonged dwell time at the crystallization-risk temperature range, develop crystalline zones at the surface (and bulk) of the cast components that change the way the glass interacts with the toolbit. The harder structure or gradient between glassy and crystalline material (e.g. “Clear bottle cullet 1070ºC, heat-treated”) decreases the crack initiation load, leading to a lower fracture resistance load. To an even greater extent, the porous crystalline SLS glass specimen, due to its extensively open/broken network, has a lower resistance to fracture. Glasses with a slower cooling scheme (-50ºC/hr) showed more resistance to fracture (e.g. Poesia cast variants), while the “Low-iron float 1050ºC” specimen, cast above the liquidus point then heat-treated below the crystallization peak showed less crushing and lateral cracking than its fast-cooled “Low-iron 1120ºC” variant (Figure 5.31). Such differences in the thermal history need to be systematically explored to identify how the different parameters affect the densification and crack propagation resistance mechanisms.

The variation in the results shows that the further exploration of surface treatments and the design of composite glasses (e.g. consisting of a more flexible surface yet a tougher core to stop crack propagation) is meaningful in creating less brittle cast glass components.

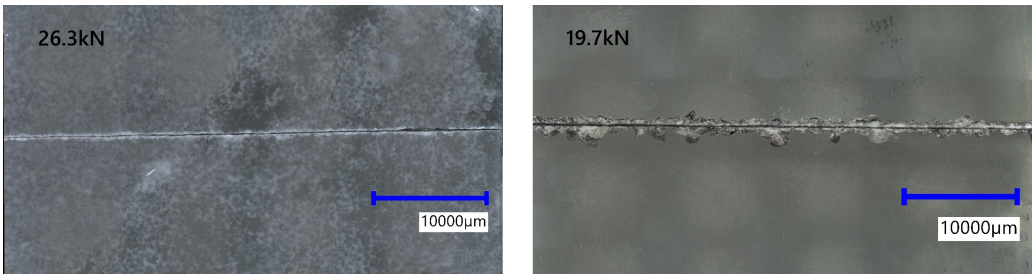

Fig. 5.31 Bottom surface of a heat-treated "Cricursa low-iron float" specimen (left) and a simply cooled and annealed "Cricursa 1120ºC" specimen (right). Although the failure load of the heat-treated specimen was higher (26.3kN versus 19.7kN), the extent of crushing (70-140µm) and lateral damage (max. 747µm) is significantly less than in the normal specimen, where the crushing zone extends from 200-360µm and the maximum lateral damage is 1837µm.

5.4.3 Relevance of the Results to the Engineering Practice

The splitting experiment intensifies -for testing purposes- a typical loading scenario in cast glass structures that involves the development of contact peak stresses. Cast components are often employed in compressive structures, where contact stresses are more critical than far-field stresses. Therefore, relying only on flexural strength data -a common approach in the engineering practice for the design and calculation of a glass structure- can lead to false estimations, as different defects and deformation mechanisms dominate the failure process during bending compared to compression. Even when the direct contact of the glass components to other hard materials (e.g. glass, steel) is avoided, with the use of a soft rubber interlayer for example, the development of peak stresses is not cancelled. Oikonomopoulou (2019) has experimentally proven that during the compressive static loading of dry-stacked interlocking (osteomorphic) cast glass components with polyurethane (PU) intermediaries, the creeping of the interlayer in combination with manufacturing unevenness in the cast components would lead to peak stresses and eventual failure of the glass components. Aurik et al. (2018) showed as well that, during the compression under a constant load of a column assembly out of orthogonal Poesia bricks with PU interlayers inbetween, the insufficient contact between the bricks (due to manufacturing tolerances) will lead to unexpected failures. It is therefore crucial to approach the engineering of cast glass structures in a more integral manner, considering as well the crack initiation and crack propagation resistance of glass, apart from its flexural/tensile strength. Although the splitting test cannot substitute the testing of a prototype section of the cast glass structure envisioned (this test should always take place at the final stages of the design), it can inform the initial steps of the design and choice of glass type.

Also important is to shift the attention of structural engineers from the concept of glass strength to that of "glass flexibility". High hardness and stiffness does not guarantee a long-lasting glass

structure; it is rather the low brittleness (high crack initiation load) or larger scratch resistance according to Seghal and Ito (1999). This is directly evident by the brittleness (B) formula[93] proposed by Quinn and Quinn (1997), which can predict wear:

$$B = \frac{H \cdot E}{(K_{Ic})^2} \tag{10}$$

Thus the ability of a glass to resist surface damage by accommodating contact stresses by deformation, reduces the appearance of cracks, prolonging in that manner its service life.

5.5 Conclusion

This study aims to investigate the fracture resistance of cast glass by means of a customized splitting test. For the purposes of the splitting test, triplets of 50mm cubic specimens are kiln-cast using various different glass cullet types and firing schedules. According to the cullet specifications and imposed thermal history, different inhomogeneities such as bubble veils, cord, crystalline interfaces or randomly spread stones appear in the glass, which are often linked with the creation of internal stress. The splitting test reveals information about the resistance of glass to catastrophic fracture but also about the influence of the occurring flaws in the bulk to the overall structural performance of the glass.

The tests show that the borosilicate specimens (1120 ºC, 970ºC) fail at the highest splitting force, followed by the soda lime silica float specimens (1120ºC), while the fused or porous specimens have a significantly lower resistance to fracture. The ranking of the different glass compositions based on the splitting test is contradictory to the results of previously conducted four-point bending tests in cast glass specimens of similar composition and thermal profile. This occurs because different fracture mechanisms are highlighted when a glass specimen is subjected to a contract stress (sharp toolbit) and to a far-field stress (bending). Specifically, the fracture resistance of the glass specimens is governed, first by the ability of the glass to deform around the pressing sharp toolbit in order to relief the stresses, and then by the bond strength of the glass and the quality of the glass network (e.g. network non damaged/broken by inclusions and flaws). For a high resistance to fracture, a good balance between glass network flexibility (sufficient empty space in molecular level) and high bond dissociation energy is required. The tested borosilicate glass may have a lower stiffness than soda lime silica float glass -which is reflected to its lower flexural strength- yet its higher molar volume and higher fracture surface energy allow for a higher fracture resistance. On the other hand, the low molar volume in combination with low dissociation energy characterizing the Poesia glass, leads to a much lower resistance to

[93] Various formulae exist for quantifying the brittleness of ceramics, with the one developed by Lawn and Marshall (1979) being the most widely used:

$$B = \frac{H}{K_{Ic}} \tag{9}$$

fracture. The contradictory results between different testing methods, highlight the fact that relying on flexural strength data alone is not sufficient for the safe and reliable engineering of cast glass structures.

By studying the manner the crack propagates through the material, the influence of the defects situated in the bulk on the structural performance can be observed. Overall, bubble veils and cord situated in parallel to the crack front, do not form weak zones to the extent of altering the path of a fast moving crack. In a similar fashion, perpendicular to the crack front crystalline interfaces, may momentarily arrest the crack but are not found sufficient to completely cease the catastrophic propagation of the crack. The encountered flaws in the bulk, as long as they are not inducing stresses that lead to immediate fracture upon cooling, they are neither deteriorating nor improving the properties of the glass components to a significant level. If such defects are not situated at the process zone around the toolbit, they seem to have a negligible contribution to the fracture resistance of the glass specimens. In other words, inhomogeneous zones can exist in the bulk of the glass component, without significantly affecting its mechanical properties, as long as they are not exposed to tensile stresses above the tolerable maximum.

5.6 Recommendations

This study involved a minimum number of tested specimens, being indicative for the fracture resistance of cast glass but not conclusive. For obtaining reliable statistical data, extended testing is suggested. To increase the accuracy of the results, fine polished and perfectly parallel bottom and top surfaces are required to avoid misalignments of the specimens with the toolbit and loading head. This should allow to detect minor differences in the performance which are caused by the use of different chemical compositions or thermal profiles (e.g. a slower cooling leading to a more densified network). Also testing of the specimens at different loading rates is advised, as a faster rate will probably lead to a reduced fracture resistance. In addition, the subjection of the cubes to a constant load that can lead to eventual slow crack growth (in combination with environmental humidity) and failure, may reveal different information about the interaction of the inhomogeneities in the bulk with the crack path. Finite element analysis should be conducted in parallel to the physical experiments, in order to quantify the ultimate tensile strength that develops around the toolbit.

The splitting test is advised to be combined with micro-hardness and fracture toughness experiments. These tests will help to determine the contribution of each mechanical property to the fracture resistance of the cast glasses, and therefore engineer cast glasses of higher fracture resistance.

Further experimentation is required regarding the heating, cooling and annealing schemes followed, and the glass properties obtained. It is worth exploring, for example, if a much thicker crystalline zone in the middle of a specimen can arrest a propagating crack travelling perpendicular to it. Or if a faster cooling scheme can add more “flexibility” to the external surface due to the more open space in a molecular scale. As the defects in the meso-level structure seem

to have a minimal role in comparison to the critical role of the surface, efforts in improving or even strengthening the surface of cast glass become crucial for ensuring safe and strong structural components. Various techniques can be investigated such as the chemical or heat-treatment of the surface or the application of a purer/stronger/more flexible glass around a weaker contaminated core. The splitting test is a relatively easy and fast testing method that can detect differences in the surface quality and help in this process of identifying the most suitable strengthening methods and designing efficient composite glasses.

References

Abrisa Technologies: SCHOTT Duran® Lab Glass (Tubed) (2014). abrisatechnologies.com/products-services/glass-products/borosilicate/schott-duran/

Anagni, G.M., Bristogianni, T., Oikonomopoulou, F. Rigone, P., Mazzucchelli, E.S.: Recycled Glass Mixtures as Cast Glass Components for Structural Applications, Towards Sustainability. Paper presented at the Challenging Glass 7: Conference on Architectural and Structural Applications of Glass, Ghent University (2020). doi: 10.7480/cgc.7.4482

ASTM: Designation: C496/C496M − 11. Standard Test Method for Splitting Tensile Strength of Cylindrical Concrete Specimens. US (2011). www.astm.org/Standards/C496

Aurik, M., Snijder, A., Noteboom, C., Nijsse, R., Louter, C. : Experimental analysis on the glass-interlayer system in glass masonry arches. Glass Structures & Engineering 3, 335-353 (2018). doi:10.1007/s40940-018-0068-7

Bristogianni, T., Oikonomopoulou, F., Yu, R., Veer, F.A., Nijsse, R.: Investigating the flexural strength of recycled cast glass. Glass Structures & Engineering 5(3), 445-487 (2020). doi:10.1007/s40940-020-00138-2

Bristogianni, T., Oikonomopoulou, F., Veer, F.A.: On the flexural strength and stiffness of cast glass. Accepted for publication in Glass Structures & Engineering (2021).

Fluegel, A.: Global Model for Calculating Room-Temperature Glass Density From the Composition. Journal of The American Ceramic Society 90, 2622-2625 (2007a). doi:10.1111/j.1551-2916.2007.01751.x

Fluegel, A.: Glass Viscosity Calculation Based on a Global Statistical Modeling Approach. Glass Technology - European Journal of Glass Science and Technology Part A 48, 13-30 (2007b). Corpus ID: 55834711

Gopalakrishnan, K., Mecholsky, J.J.: Quantitative fractography of mixed mode fracture in glass and ceramics. Journal of the European Ceramic Society 34(14), 3247-3254 (2014). doi: doi.org/10.1016/j.jeurceramsoc.2014.03.019

Griffith, A.A.: The phenomena of rupture and flow in solids. Philosophical Transactions of the Royal Society of London. 221(582-593), 163-198 (1920). doi:10.1098/rsta.1921.0006

Gross, T.M., Tomozawa, M.: Fictive temperature-independent density and minimum indentation size effect in calcium aluminosilicate glass. 104(6), 063529 (2008). doi:10.1063/1.2985907

Heimerl, W.: Chemical Resistance and Corrosion, and Ion Release. In: Bach, H., and Krause, D. (ed.) Analysis of the Composition and Structure of Glass and Glass Ceramics. Springer-Verlag Berlin Heidelberg, New York (1999). doi: 10.1007/978-3-662-03746-1

Heraeus Quarzglas: Base Materials (2013). www.base-materials.heraeus-quarzglas.com

Inaba, S., Fujino, S., Morinaga, K. : Young's modulus and compositional parameters of oxide glasses. Journal of the American Ceramic Society 82, 3501-3507 (1999). doi:10.1111/j.1151-2916.1999.tb02272.x

Irwin, G.R.: Analysis of Stresses and Strains near the End of a crack Traversing a Plate. Journal of applied Mechanics Vol. 24, pp. 361-364 (1957).

Ito, S., Taniguchi, T.: Effect of cooling rate on structure and mechanical behavior of glass by MD simulation. Journal of Non-Crystalline Solids 349, 173-179 (2004). doi:10.1016/j.jnoncrysol.2004.08.180

Januchta, K., Smedskjaer, M.M.: Indentation deformation in oxide glasses: Quantification, structural changes, and relation to cracking. Journal of Non-Crystalline Solids: X 1, 100007 (2019). doi:10.1016/j.nocx.2018.100007

Januchta, K., Liu, P., Hansen, S.R., To, T., Smedskjaer, M.M.: Indentation cracking and deformation mechanism of sodium aluminoborosilicate glasses. 103(3), 1656-1665 (2020). doi:10.1111/jace.16894

Kato, Y., Yamazaki, H., Kubo, Y., Yoshida, S., Matsuoka, J., Akai, T. : Effect of B2O3 content on crack initiation under Vickers indentation test. Journal of the Ceramic Society of Japan 118, 792-798 (2010). doi:10.2109/jcersj2.118.792

Kato, Y., Yamazaki, H., Yoshida, S., Matsuoka, J.: Effect of densification on crack initiation under Vickers indentation test. Journal of Non-Crystalline Solids 356(35), 1768-1773 (2010). doi:10.1016/j.jnoncrysol.2010.07.015

Kschinka, B.A., Perrella, S., Nguyen, H., Bradt, R.C.: Strengths of Glass Spheres in Compression. 69(6), 467-472 (1986). doi:10.1111/j.1151-2916.1986.tb07447.x

Lawn, B.R., Marshall, D.B.: Hardness, Toughness, and Brittleness: An Indentation Analysis. 62(7-8), 347-350 (1979). doi:10.1111/j.1151-2916.1979.tb19075.x
Lei, C.O.S.: Structural cast glass-ceramic components: The potential of recycling soda-lime-silica glass into cast glass-ceramic components and its mechanical behaviour. Delft University of Technology (2019). http://resolver.tudelft.nl/uuid:f9a77112-cbe7-445b-a9fe-36285f3b9381
Limbach, R., Winterstein-Beckmann, A., Dellith, J., Möncke, D., Wondraczek, L.: Plasticity, crack initiation and defect resistance in alkali-borosilicate glasses: From normal to anomalous behavior. Journal of Non-Crystalline Solids 417-418, 15-27 (2015). doi:10.1016/j.jnoncrysol.2015.02.019
Makishima, A., Mackenzie, J. D.: Direct calculation of Young's modulus of glass. Journal of Non-Crystalline Solids 12(1), 35-45 (1973). doi:10.1016/0022-3093(73)90053-7
Makishima, A., Mackenzie, J.D.: Calculation of bulk modulus, shear modulus and Poisson's ratio of glass. Journal of Non-Crystalline Solids 17(2), 147-157 (1975). doi:10.1016/0022-3093(75)90047-2
Mellor, M., Hawkes, I.: Measurement of tensile strength by diametral compression of discs and annuli. Engineering Geology 5(3), 173-225 (1971). doi:10.1016/0013-7952(71)90001-9
Nakamura, H., NAP: Optical Glass House. www.nakam.info/en/works/optical-glass-house/ (2012).
Nakayama, J.: Direct Measurement of Fracture Energies of Brittle Heterogeneous Materials. 48(11), 583-587 (1965). doi:10.1111/j.1151-2916.1965.tb14677.x
Nyounguè, A., Bouzid, S., Dossou, E., Azari, Z.: Fracture characterisation of float glass under static and dynamic loading. Journal of Asian Ceramic Societies 4(4), 371-380 (2016). doi:10.1016/j.jascer.2016.07.004
Oikonomopoulou, F., Bristogianni, T., Veer, F.A., Nijsse, R.: The construction of the Crystal Houses façade: challenges and innovations. Glass Structures & Engineering 3(1), 87-108 (2018). doi:10.1007/s40940-017-0039-4
Oikonomopoulou, F., Bristogianni, T., Barou, L., Veer, F.A., Nijsse, R.: The potential of cast glass in structural applications. Lessons learned from large-scale castings and state-of-the art load-bearing cast glass in architecture. Journal of Building Engineering 20, 213-234 (2018). doi:10.1016/j.jobe.2018.07.014
Oikonomopoulou, F.: Experimental and numerical investigation of an interlocking system out of osteomorphic cast glass components. In: Unveiling the third dimension of glass: Solid cast glass components and assemblies for structural applications. A+BE | Architecture and the Built Environment, (2019). doi: 10.7480/abe.2019.9
Parascho, S., Han, I., Walker, S., Beghini, A., Bruun, E., Adriaenssens, S.: Robotic vault: a cooperative robotic assembly method for brick vault construction. Construction Robotics 4 (2020). doi:10.1007/s41693-020-00041-w
Quinn, G.D., Swab, J.J.: Fracture toughness of glasses as measured by the SCF and SEPB methods. Journal of the European Ceramic Society 37(14), 4243-4257 (2017). doi:10.1016/j.jeurceramsoc.2017.05.012
Quinn, J.B., Quinn, G. D.: Indentation brittleness of ceramics: a fresh approach. Journal of Materials Science 32(16), 4331-4346 (1997). doi:10.1023/A:1018671823059
Rouxel, T.: Designing Glasses to Meet Specific Mechanical Properties. Paper presented at the Challenging Glass, Conference on Architectural and Structural Applications of Glass, Delft (2008). https://hal.archives-ouvertes.fr/hal-01148241/
Rouxel, T.: Fracture surface energy and toughness of inorganic glasses. 137, 109--113 (2017). doi:10.1016/j.scriptamat.2017.05.005
Rouxel, T., Yoshida, S.: The fracture toughness of inorganic glasses. Journal of the American Ceramic Society 100(10), 4374-4396 (2017). doi:10.1111/jace.15108
Schott: B 270®i (2013). www.schott.com/en-us/products/b-270
Schott: Tubular Glass Photobioreactors (2015). www.schott.com/tubing/english/special_glass/industry_environment/pbr.html
Schott: DURAN Technical Data (2017). www.schott.com/d/tubing/9d60ae04-a9db-4b63-82b3-7aebd5bad71e/1.6/schott-tubing_brochure_duran_english-en.pdf
Sehgal, J., Ito, S.: Brittleness of glass. Journal of Non-Crystalline Solids 253(1), 126-132 (1999). doi:10.1016/S0022-3093(99)00348-8
Sellappan, P., Rouxel, T., Celarie, F., Becker, E., Houizot, P., Conradt, R.: Composition dependence of indentation deformation and indentation cracking in glass. Acta Materialia 61(16), 5949-5965 (2013). doi:10.1016/j.actamat.2013.06.034
Shannon, R.D.: Revised effective ionic radii and systematic studies of interatomic distances in halides and chalcogenides. 32(5), 751-767 (1976). doi: 10.1107/S0567739476001551
Sheikh, M.Z., Wang, Z., Du, B., Suo, T., Li, Y., Zhou, F., Wang, Y., Dar, U.A., Gao, G., Wang, Y.: Static and dynamic Brazilian disk tests for mechanical characterization of annealed and chemically strengthened glass. Ceramics International 45(6), 7931-7944 (2019). doi:10.1016/j.ceramint.2019.01.106
To, T., Célarié, F., Roux-Langlois, C., Bazin, A., Gueguen, Y., Orain, H., Le Fur, M., Burgaud, V., Rouxel, T.: Fracture toughness, fracture energy and slow crack growth of glass as investigated by the Single-Edge Precracked Beam (SEPB) and Chevron-Notched Beam (CNB) methods. Acta Materialia 146, 1-11 (2018). doi:10.1016/j.actamat.2017.11.056
To, T., Jensen, L.R., Smedskjaer, M.M.: On the relation between fracture toughness and crack resistance in oxide glasses. Journal of Non-Crystalline Solids 534, 119946 (2020). doi:10.1016/j.jnoncrysol.2020.119946

Vitro Architectural Glass: Starphire® Technical Product Data (2020). www.vitroglazings.com/media/gpvmzllx/vitro-starphire-vitro-technical-pds.pdf
Wada, M., Furukawa, H., Fujita, K. : Crack resistance of glass on Vickers indentation. In: Proceedings of the 10th International Congress on Glass (1974).
Wiederhorn, S.M.: Fracture Surface Energy of Glass. 52(2), 99-105 (1969). doi:10.1111/j.1151-2916.1969.tb13350.x
Yamane, M., Mackenzie, J.D.: Vicker's Hardness of glass. Journal of Non-Crystalline Solids 15(2), 153-164 (1974). doi:10.1016/0022-3093(74)90044-1
Yun, Y.H., Bray, P.J.: Nuclear magnetic resonance studies of the glasses in the system $Na_2O{\cdot}B_2O_3{\cdot}SiO_2$. Journal of Non-Crystalline Solids 27(3), 363-380 (1978). doi:10.1016/0022-3093(78)90020-0

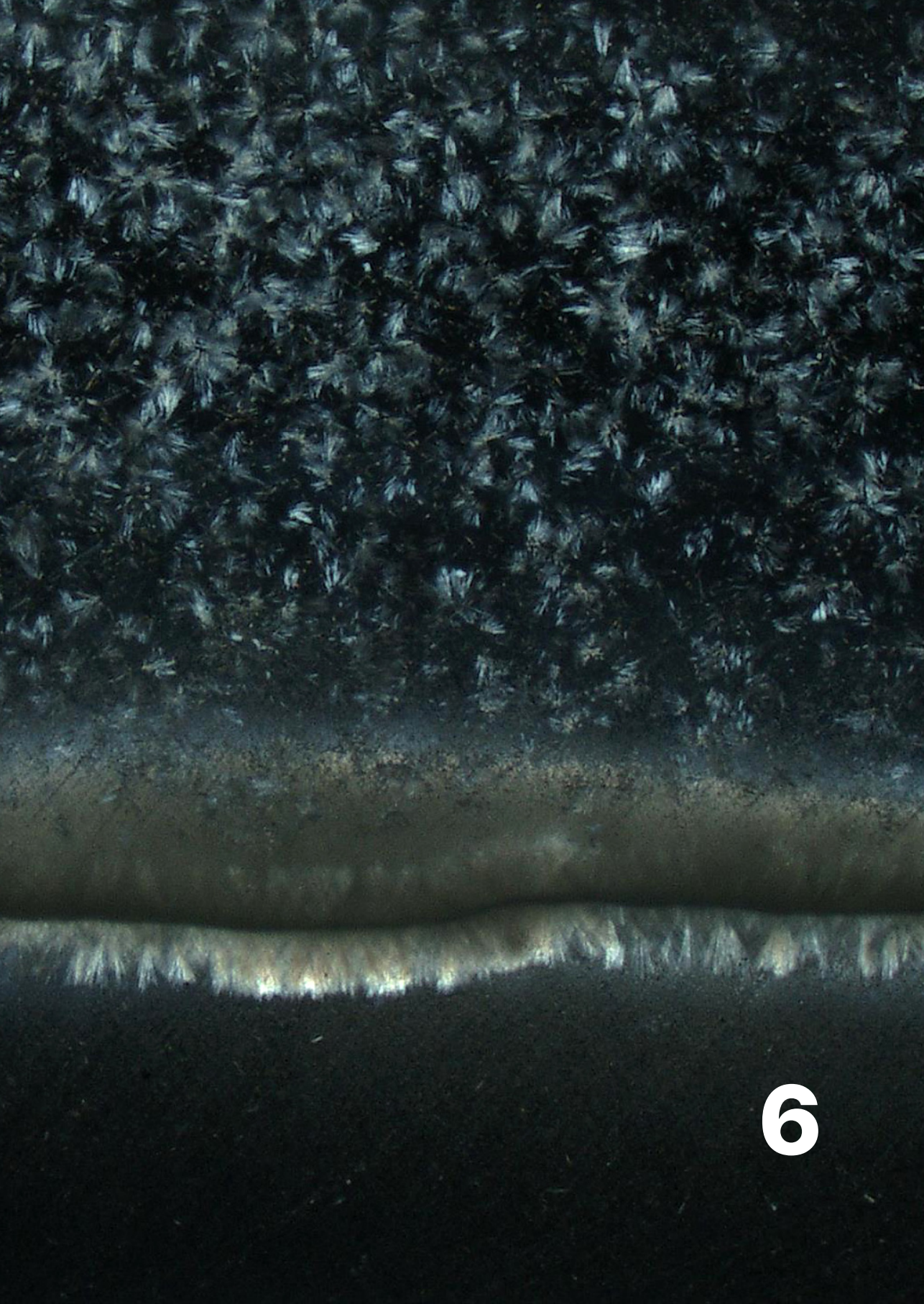
6

Previous page: Linear crystalline interface and loose devitrite crystal formations observed in a recycled float glass specimen, kiln-cast at 970ºC.

Chapter 6: Discussion

This dissertation studies casting flaws in glass and their correlation to the strength, stiffness and fracture resistance of cast components. The initially posed research questions are answered in a "framing the essence" manner, while the depth of the missing scientific knowledge and the systematic research required to fundamentally answer these questions is outlined. Thoughts, remarks, doubts and important factors that surfaced are listed below, opening a critical discussion on the casting procedures, mechanical properties and engineering of cast glass.

Chemical composition

The conventional "hot-pouring at room temperature" technique is used by most glass foundries. This technique requires a glass with a chemical composition formulated to facilitate the particular casting process. This usually translates to a modified soda lime silica glass of lower required pouring temperature (e.g. 1100°-1200°C) in order to ease the casting process by reducing the radiating heat (often craftsmen will ladle molten glass without any protective equipment), and allow for longer working times so there is enough time for the glass to flow and fill up the entire mould. Therefore, such glass compositions usually contain an increased amount of alkali oxides (often a combination of two, e.g. Na_2O and K_2O) that reduces the melting point, and a decreased amount of lime to prevent crystallization (Figure 6.1). Studio glass, specifically purposed for kiln-casting, is further formulated to work at even lower temperatures (the mould material imposes a temperature restriction, often at 900°-1000°C) and be even more resistant to crystallization, by further substituting lime with magnesium, barium and aluminum oxides. Thus, the easy casting requires a preferable chemical composition that subsequently determines -to an extent- the mechanical properties of the cast glass components. For example, the increased alkali-to-lime ratios, compared to typical soda lime silica (SLS) recipes, are beneficial in accommodating local peak stresses during bending, while the addition of aluminum oxide increases the bond strength. In addition, the decreased viscosity of these glasses compared to standard SLS glasses helps to avoid several common casting flaws. This in return results in more homogeneous -and thus stronger- components. On the other hand, some of these casting glass compositions have reduced crack resistance due to their lower surface energy, as observed during the splitting experiments.

Glass type	SiO_2	Na_2O	CaO	Al_2O_3	K_2O	MgO	ZnO	B_2O_3	Other
Float, clear (PPG Starphire)	74	12.5	10	0.1		3			
Bottle, clear	73.5	12	11	1.5		2			
Blowing, clear (Sprucespine)	74.5	13.5	7	2			1	*	0.5 BaO
Casting, clear (Poesia)	72	16	6		2			2.5	1 Sb_2O_3
Optical, clear (B270)	72	10	5	2	6		2	*	2 TiO_2
Studio, clear (Bullseye)	74	16	4	5	1			*	

*Amount of B_2O_3 possible, yet unknown

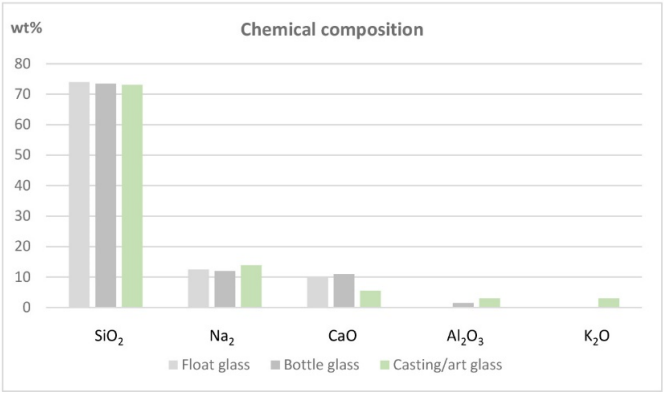

Fig. 6.1 Minor compositional differences within the soda lime silica family to accommodate different glass manufacturing techniques.

From an engineering point of view, interesting design possibilities would arise if we could create cast glass products with a variable range of physical and mechanical properties that could be adjusted on demand, escaping the limitations currently posed by the casting process. Breaking the relationship between a casting-friendly composition and the accompanied properties assigned to the final component is not a simple task; obtaining a hot-poured glass component made out of an SLS composition destined for standard float or glass containers products for example, would demand a pouring temperature above 1450ºC while still having questionable results considering the poor flowability of this type of glass inside the mould. At this point, kiln-casting – either by depositing cullet inside a mould, or by pouring molten glass within a controllable, hot-air environment, can provide a workable solution to this problem. The within-the-kiln pouring method takes advantage of the element of the long pouring time, allowing melts of higher viscosity to slowly fill up the mould. In this manner, typical SLS compositions can be formed inside the mould at temperatures some 300º-400ºC lower than required for the conventional hot-pouring technique. The same applies for other compositional families used in standard commercial glass products, such as borosilicate or aluminosilicate glass. The kiln-casting method thus allows for the casting of a much wider range of compositions and, in addition, enables increased recycling by casting of various types of commercial glass waste. Moreover, larger components can be produced with this manufacturing method, as the pouring is not limited to the volume capacity of the ladle and lifting strength of the worker, but by the size of the oven. Another benefit of this method is the possibility to experiment with different heating and cooling schedules. Forming procedures at temperatures below the liquidus point and at the crystallization

peak region, can lead to –partially- crystallized components. Experimentation with the cooling rate prior to annealing can also lead to different degrees of network compactness, and subsequently to variations in the hardness and E modulus. The thermal history colours the effect of chemical composition on the mechanical properties, and in this manner increases the palette of material properties one can achieve by kiln-casting.

Correlation of the chosen casting parameters to the resulting casting defects

According to the applied heating conditions and the corresponding viscosity of the glass, defined by the chemical composition and shear rate (if applicable), meso-level structures will form in the glass component. Considering the bonding process of individual glass cullet pieces in a mould/crucible, it is important to focus on the consecutive transformations occurring at the connecting interfaces beyond the softening point and as the viscosity decreases with the increase of temperature. Specifically, as seen in Figure 6.2, these interface transformations involve the following structures, and/or their combination in case of uneven heat exposure:

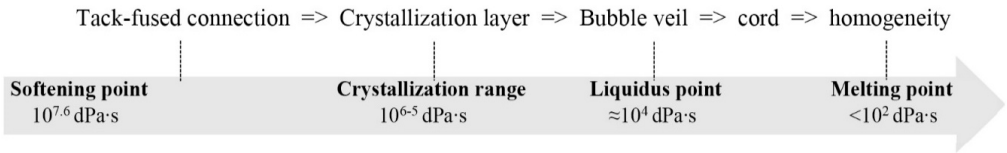

Fig. 6.2 Transformations occurring at the interface between glass cullet pieces or poured glass threads with the increase of temperature above the softening point. The word "point" to describe the viscosity status of glass is used in correlation to the literature and for simplification purposes. However, these transformations take place in a range of temperature/viscosity and not abruptly at an exact point. In addition, other factors such as gravity, pressure or dwell time can cause temperature shifts to these transformation ranges. The extent of each range depends as well on the characteristics of the chemical composition.

Even if entirely pure glass batch or cullet is employed in the casting process, these interfacial structures will be formed at casting viscosities higher than ≈10^{2} dPa·s, as these are related to the chemical reactions within the melt and not to external factors such as contamination. In this sense, such structures can be considered intrinsic, and show a high level of compositional similarity to the parent glass. Some chemical compositions will further promote such formations more than others; for instance if they contain volatile elements that intensify the inhomogeneities along the interfaces, or compounds that spontaneously crystallize. Moreover, a batch can be refined into a fully homogenized melt of low kinematic viscosity, however, if pouring takes place at a lower temperature –and especially at room temperature conditions- some of these intrinsic structures will still form. The manner in which the glass will be poured or positioned as cullet inside a mould will define the location of these structures. A form of shape memory therefore applies to cast glass as a result of the high viscosity of the melt during casting. This shape memory is linked to the number and morphology of the original interfaces existing in the glass object, therefore is relatable to the original size and shape of the cullet or the pouring movement of molten glass inside a mould.

Extrinsic casting flaws can also be found in cast glass components. These are linked to external contamination present in the batch material or the cullet, a poorly melted and/or badly refined batch, and to contamination by the refractory walls or crucible, the mould, and the kiln-environment. Especially in the case of glass recycling, this type of defects can significantly increase due to possible alien material present in the cullet such as coatings, fritting, glass of different compositions or glass ceramics, and traces of ceramic/stone/porcelain or metal. These defects cover a wide range of crystalline, gaseous and glass inhomogeneities, but this time their role can be more invasive, related to the resulting deviation from the thermal expansion coefficient, stiffness and fracture toughness of the parent glass. Extrinsic defects present in the bulk are mainly linked to external contamination and their location is not only relevant to the imposed shape memory, but also to the relation of physical properties between the parent glass and the alien material. For example, differences in the viscosity or density will lead to the sedimentation or volatilization of a contaminant. It is overall much more challenging to predict the location of these flaws, especially in the case of stones caused by refractory reaction, poor batch homogenization or random cullet contamination. The size and shape of such extrinsic flaws is however linked to the original shape characteristics of the contaminant. A higher temperature may assist with dissolving the contaminant within the glass. This is often the case with soft and hard coatings that dissolve into bubble veils and cord structures. Yet heat-resistant coatings, enamels and fritting require temperatures well above the typical glass forming temperatures in order to melt-in. Therefore planar layers of partially molten particles and surrounding colour-sacks are observed in the glass. Extrinsic surface flaws can result from a combination of mould/kiln contamination and external contaminants in the batch/cullet. Post-processing is not always 100% effective in removing such surface flaws, while it can also expose new, possibly critical, flaws to the surface (e.g. micro-cracks, cutting of bubbles leading to surface voids with sharp edges, etc).

Classification of defect severity

Based on the casting defect categorization in intrinsic and extrinsic flaws, a general classification of their severity is made, based on the experimental results of Chapters 2-4. This is schematically portrayed in Figure 6.3. This graph roughly shows the impact that the different types of defects may have on the strength, however such relationships can easily change. This because they are based on the size and distribution of a defect type, as well as its combination with other defect types.

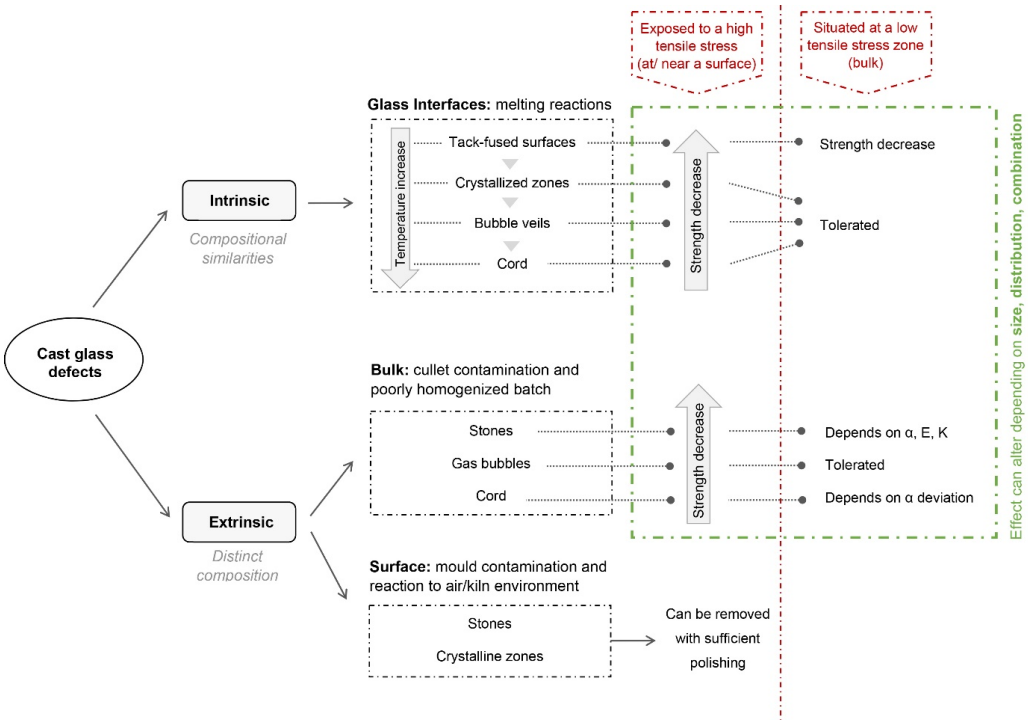

Fig. 6.3 Classification of casting defects and assessment of their severity based on their characteristics and location in the glass specimen.

Considering the intrinsic flaws first, these are mostly well tolerated by the glass network when located in the bulk- as they are rarely subjected to peak stresses, with the only exception being tack-fused surfaces. If, however, these structures are exposed in a zone of high tensile stress, usually at or near the surface, they will decrease the strength. Ranking their effect, cord is the least severe and tack-fused surfaces are the most severe. The combination of intrinsic flaws at the surface plays of course an important role in the reduction of strength and fracture resistance. As an extreme example, glass specimens produced from powdered (pure) cullet at $\approx 10^5$ dPa·s viscosity, were found to be significantly weaker due to the increased porosity (i.e. high population of bubbles) and overall crystallized structure.

Extrinsic flaws also show an increasing severity from cord to bubbles to stones. Yet, this relationship is highly dependent on the extent of the occurring deviations between the physical and mechanical properties of the defect and the glass matrix (Fig 6.4), with the size of the defect being the most crucial. Indeed, experiments with mixing borosilicate and soda lime silica cullet of <2mm size lead to integral components while the mixing of ø10mm rods of the two compositions had catastrophic results. Similar observations were made with minor traces of metal versus the insertion of metal components of considerable size such as ø6mm rods. In fact, for a contaminant of considerable size, a difference in thermal expansion of $1x10^{-6}$ K^{-1} is sufficient for

fracture to be observed, especially if the contaminant has higher stiffness and toughness than the glass matrix. Glass ceramics, due to their much lower thermal contraction than the parent glass, would almost always lead to catastrophic failure of the specimens, even if introduced in the form of small-sized cullet. Extrinsic flaws with considerable deviations from the glass matrix properties and of significant size, are crucial regardless if they are situated in the bulk or at the surface. Even if they do not lead to immediate fracture upon cooling, they will promptly induce fracture to the glass matrix upon even minor subjection to a thermal gradient or mechanical shock.

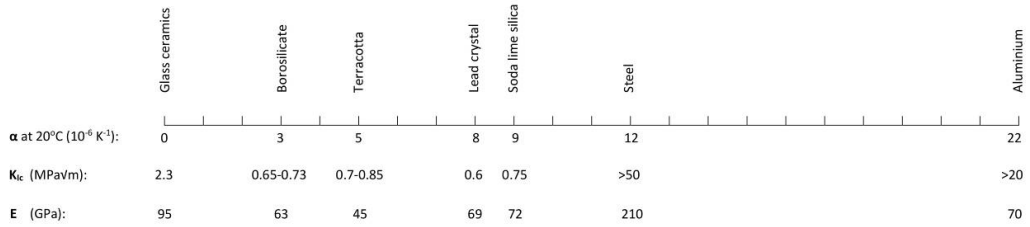

Fig. 6.4 Typical materials that can be traced in a recycled soda lime silica (SLS) cullet provided by the glass recycling industry, and their approximate thermal expansion coefficient (α), fracture toughness (K_{Ic}) and Young's modulus (E) in relation to SLS. The extent of difference in thermal expansion in combination with the size of a contaminant play the most crucial role in the probability of fracture of the glass matrix.

Combination of flaws and mapping techniques

The merging of flaws in one point of the glass surface (e.g. kissing bubbles, stone combined with cord) and the existence of various defect types at different locations of a glass specimen are common examples of defect combinations in cast glass. In fact, cast glass -especially recycled glass, cast at relatively low temperatures- is characterized by combinations of defects that form distinct meso-level structures. The flexural bending tests conducted showed that fracture will not always initiate from the most defect populated zone or from the most suspicious singularity or from a merging of flaws. This phenomenon is on the one hand linked to stress gradients present in the specimen during loading that may leave critically defective areas unexposed to tensile stresses. On the other hand, for defects equally exposed to tensile stress, again the size and combination characteristics will determine the overall severity of each defective spot. This fact reflects an engineering challenge for real-world applications of cast glass, as the subjection of the components to dynamic loading can turn an initially negligible defect (including defects in the bulk) into the weakest link. The structural performance of a cast glass component is therefore a multi-criteria function, based on the specific combination of loadcase, defect characteristics and the local response of the glass network against a tensile stress being subjected around a defect or combination of defects (Figure 6.5). The glass network is a function of the chemical composition and thermal history that defines its compactness and level of frozen-in stresses.

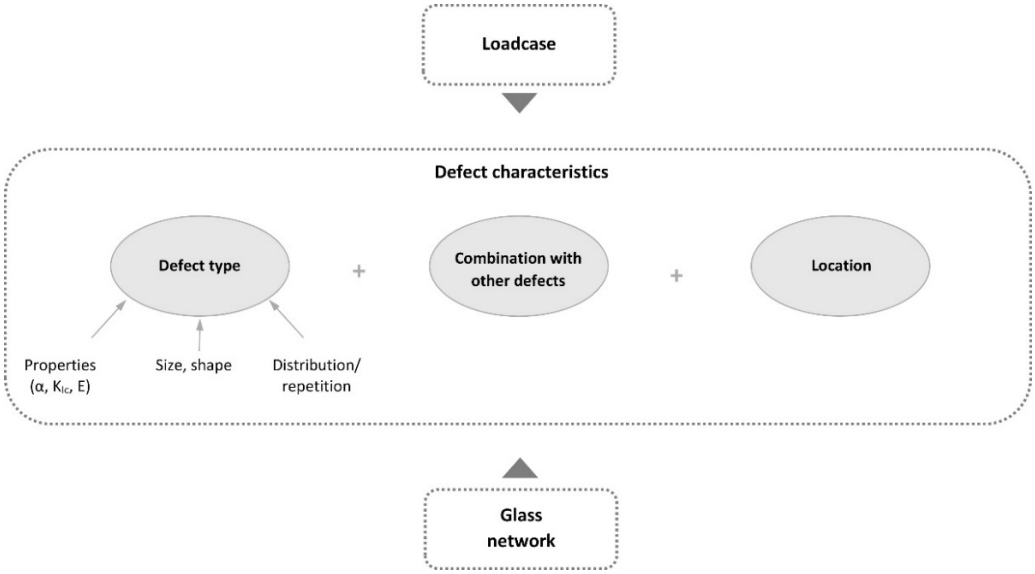

Fig. 6.5 The structural performance of cast glass is a multi-criteria function, based on the loadcase acting upon the defect characteristics of the glass, and the response of the glass network to the imposed stress around these defects.

Important for the development of safe structural cast glass components is the systematic mapping of the formed glass meso-level structures and their correlation to the results of different mechanical testing techniques. However, there is no mature technique for 3D mapping defects in a volume of cast glass. Neither is there a technique for activating defects in the bulk (comparable in effect to activating defects at the surface) through mechanical testing. During this dissertation, the use of a digital microscope employing high magnification 3D image compilation technologies (Keyence VHX-7000) significantly contributed to the characterisation of the different casting defects, in respect to both their morphology and the 3D distribution. With the same microscope, the 3D morphology of non-reflective surfaces[94] could also be studied. Thus the depth of infolds, grinding damage and scratches could be determined with considerable accuracy[95]. The microscope however captures only a small surface (50x50mm with photo-stitching) and thus the mapping of an entire component is a time-consuming process. Moreover, there are accuracy limitations when glossy, transparent surfaces are studied, due to glare. Basic fractographic techniques were employed to study the interaction of these defects with an imposed stress. However, the 3D mapping into something resembling a CAD drawing of these meso-level structures is not yet possible and the complexity of such a venture increases considerably in the case of non-transparent, crystallized glass. CT-scanning techniques were tested and found to work well in defining density differentials within a transparent or opaque glass object. However, the

[94] Glass surfaces ground and polished up to a 600 grit are not reflective nor transparent, and thus their 3D morphology can be easily captured by the microscope without noise caused by glare.

[95] Accurate characterization of surface flaws by microscopic analysis can be often seen in research work concerning the evaluation of the edge quality of float glass, for example in the work of Veer (2022), Bukieda et. al (2020), Müller-Braun et al. (2020) and Lindqvist (2013).

technique failed to detect cord, as in most cases the chemical composition of cord differs minimally from that of the glass matrix. Cord within a transparent cast glass could be detected with an Ilis Flex Polariscope and its shape, distribution within the bulk and stress intensity could be partially defined if images were taken from all sides of the object. Therefore the mapping of different types of defects in cast glass currently relies on a combination of techniques, which however, does not result yet in an integral 3D-representation. Yet, even if such mapping would be possible, it would still lack the additional information required about the severity of each flaw, which breaks down to the differences in composition and structure which result in deviations of E modulus, α and K_{Ic} between each flaw and the glass matrix. Such information can be obtained if the cast component is sliced and fine polished into multiple sections that are further studied with a SEM microscope to derive compositional variations, and systematically indented with a Berkovich nano-indenter to obtain local information on the E modulus and hardness variations. Then, the measured variations would need to be assigned to the 3D-mapping model. The described process is extremely labour intensive and particularly time consuming. More practical, at the moment, is an exact and complete post-mortem fractographic analysis of the fracture origin of a tested specimen. This is the most efficient short-cut for identifying and characterizing critical flaws. In this sense, less critical flaws are by definition excluded from the analysis, which reduces the effort.

Response of the crack path to inhomogeneities

In this work, the effect of singularities and inhomogeneous zones in the bulk on a fast moving crack was studied, during the 4-point bending and splitting experiments. In both sets of experiments, neither major crack front deviations nor complete arrest of a crack was observed, with the exception of the tack-fused specimens. Focusing on the case of the 4-point bending experiments, and given that fracture mirrors were observed in the specimens, we can assume that the crack initially reached a terminal velocity (as proven by the region of mirror and mist hackle), which was later slowed down as it reached the compressive stress zone (compressive curl). The speed and energy of the traveling crack is extremely high[96], and therefore it is not significantly affected by singularities or inhomogeneous zones of similar nature (e.g. cord, thin crystalline layer of compositional proximity to the base glass). Stress gradients within the specimen (e.g. the compressive zone due to bending) are much more dominant in affecting the crack path. Minor local deviations in the crack path are of course observed when inhomogeneities are encountered (e.g. gull-wings when bubbles are reached) and -in accordance with the literature (Quinn, 2016)- it can be assumed that in each of these encounters a miniscule amount of energy is consumed leading to a miniscule reduction of crack velocity. Only in the case of very disruptive flaws, such as extended air-gap zones existing in the interface of tack fused float beams (produced at 650^{o}C), was a significant crack front alteration observed, with the path moving along the weakest zone (air zone at interface), see Figure 6.6. This behaviour supports the prior conclusion that in most of the tested cases, the inhomogeneities encountered did not result in a local significant difference

[96] According to Quinn (2019), the speed of a terminal crack travelling through soda lime silica glass is reported between 1485-1600m/s in the literature.

in the mechanical properties compared to the glass matrix, or were small enough to not affect it (e.g. in the case of bubbles). Indeed, in most cases, the meso-level structure of cast glass had a less critical role than in other materials of, for example, crystalline nature (e.g. metal). The splitting tests on cast glass specimens showed similar results regarding the effect of the meso-level structure. In cases of theoretically weaker zones of bubble veils or crystalline interfaces being situated parallel and in proximity to the crack front, no crack path deviation through these zones was observed, as it was observed in the float glass specimens made for comparison, with their DELO Photobond 4468 adhesive interfaces situated parallel to the crack front.

Total arrest of a fast moving crack was not observed in any of the cast glass samples tested in 4-point bending, only in the comparison specimens made of multiple float layers glued with DELO Photobond 4468 during splitting and when the glue interface was perpendicular to the crack propagation path. There, the low E modulus adhesive interface was found sufficient to stop the running crack, in combination with the fact that the crack initiated from a local peak stress due to contact with a sharp hard object, and thus the tensile stress intensity significantly dropped after the crack departed the crack initiation point. This prevented the crack from propagating further (Figure 6.7).

The response of inhomogeneities in the meso-level structure in the event of slow moving cracks (e.g. low stress fractures due to thermal stress) was not investigated in this work.

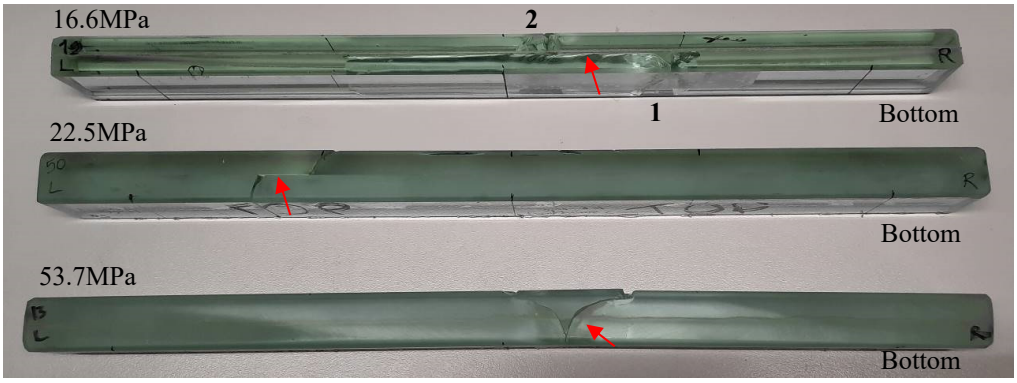

Fig. 6.6 Side view of beams subjected to 4-point bending (20x30x350mm), depicting the occurring crack propagation and the failure stress (MPa). From top to bottom: 2x8mm float laminated, 2x10mm tack fused at 650ºC for 1hr, and 2x10mm fused at 970ºC for 10hr. The first crack at the laminated beam (1) got entirely arrested by the interlayer, and later on a secondary crack started at a different location (2) from the bottom of the second ply, which lead to the complete failure of the beam. The tack fused beam contained air zones within the connective interface, which weakened the beam; failure started at the interface then travelled along the void zones before propagating at the bottom and top ply. The fused beam failed in a continuous manner and without the crystalline interface interacting with the path of crack; the failure pattern and stress was similar to a homogeneous kiln-cast beam.

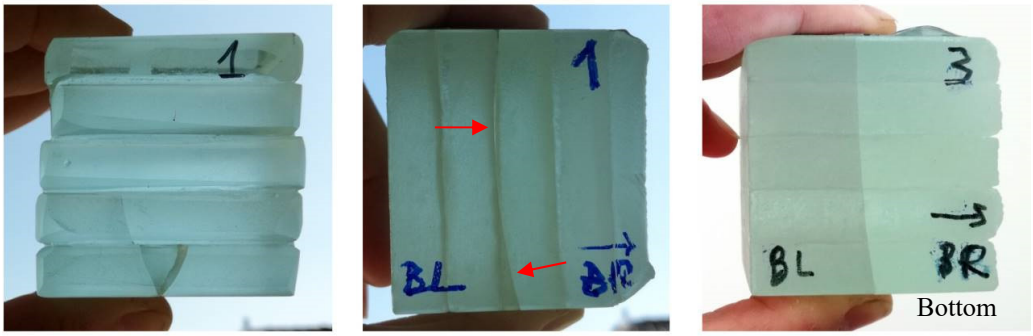

Fig. 6.7 Side view of cubic specimens (50mm) subjected to splitting by a sharp longitudinal indenter, depicting the crack path. From left to right: 5x10mm float glued with DELO Photobond 4468 positioned perpendicular to the force, 5x10mm float fused at 970ºC positioned parallel to the force and 5x10mm float fused at 970ºC positioned perpendicular to the force. The crack is arrested by the adhesive interlayer (left), yet moves unobstructed at the fused version (right) as if the cube were homogeneous. The crack path at the parallel to the force fused cube (middle) reaches the parallel crystalline interface and surpasses it momentarily; it does propagate along the crystalline interface once it is encountered.

Deliberate engineering of meso-level structures

Given that a "shape memory effect" characterizes castings of high viscosity, one can control to a reasonable extent the distribution and form of meso-level structures in a cast glass component. Especially in the case of depositing already formulated glass with a specified cullet shape in a defined manner inside a mould, and kiln-casting the assembly using a viscosity higher than $\approx 10^4$ dPa·s, the resulting meso-level structure can be predicted reasonably well[97]. Controlling the form of meso-level structures in cast glass can contribute to a wide variety of material expressions of aesthetic value. Yet, beyond the visual qualities, zones with mechanical properties distinctive-to-the-matrix can be engineered. These can be either weakening or strengthening zones, with a clear-cut or a gradient transition. Moreover, their nature can be either of intrinsic or extrinsic character.

For example, strengthening zones can be achieved by combining a lower quality recycled glass powder with a small portion of pure glass shards of the same compositional family; with the poorer quality glass positioned to form the bulk which is subjected to lower stresses. Or by combining two glasses with a compatible composition but a distinct strength, and situating the stronger part at the most critical zone of the component. Especially in this latter case of extrinsic strengthening, the relationship between the density and viscosity of the different glasses at a given temperature, in combination with other characteristics such as the tendency to volatize, are of key importance in order to properly engineer the desired meso-level structure.

[97] The "cage principle" for dense liquids applies in high viscosity castings. Specifically, the molecules of a cullet piece are confined by the molecules of the neighbouring cullet pieces and will not diffuse or flow to the other side of the liquid as there is not enough energy for such movement. As a result, we can expect that the majority of the spatial relationships between cullet pieces before casting will be sustained in the final cast component.

The introduction of fused/crystalline intrinsic zones in the glass, however, did not have strengthening attributes, nor the ability to arrest a fast progressing crack. In fact, the different response of the two structures (glass and crystalline material) during loading seems to attract the formation of local peak stresses that can reduce the overall global strength. Specifically, when such zones are exposed to a high tensile stress (e.g. at the lower surface of a bar in bending), they are leading to failure at lower stresses. However, if they would be encapsulated in the core, they would not have an impact on strength or crack propagation. As a conclusion, such structures, as well as other intrinsic structures like bubble veils, can in theory be engineered at specific locations in the component where a weaker strength is desired, to predefine for example the location where the structure will fail, or to reduce the uncertainty about the failure strength; a specified flaw will more or less fail at a predictable load.

Flexural strength of cast glass and size factor

The four-point bending experiments conducted on kiln-cast specimens (30x30x240mm and 20x30x350mm size) and industrially manufactured reference beams presented a flexural strength range of 9-73MPa. The reported strength range is the result of variations in composition, defect type and population, cooling rate, surface quality, and specimen size, and is only indicative given the low number of specimens tested per type. The engineering of the test fixtures used in this study, the loading rate and the humidity level in the surrounding atmosphere, are also determining parameters that affect the reported strength. It is therefore important to not associate a type of cast glass with a mean strength value, as this leads to dangerous and simplified assumptions. Meaningful conclusions can be drawn, however, from the comparison of the qualitative performance of the different types of glass. Average strength values mentioned below only serve as indications.

From the total sample of tested beams, the purer samples allow for the determination of the role of composition, thermal history, and intrinsic flaws on the strength. Highly homogeneous pure cast samples (cast with purer cullet at low viscosities) showed the highest strength and mainly failed due to grinding defects or scratches created after casting. An increase in strength was observed consecutively from the lead silicate specimens (≈35MPa), to the borosilicate (≈44MPa), barium silicate (≈51MPa) and up to the soda lime silica (standard: ≈46-63MPa and modified: ≈59-73MPa) family. Although direct comparisons cannot be made due to the distinct experimental parameters applicable in each scientific study, it can be observed that the obtained values in this dissertation are close to the lower/middle range of reported flexural strength in 4-point bending for annealed soda lime silica float glass in the literature (e.g. 51-71.5MPa by Veer, 2007; 35-170MPa by Veer and Rodichev 2011; 53–129MPa by Yankelevsky et al. 2016; 28-127MPa by Vandebroek et al. 2012; 40.9-56.2MPa by Vandebroek et al. 2014; 35-103.8MPa by Bukieda et al. 2020). The lower reported strength in this work is mainly being linked to the manual post-processing of the specimens' surfaces that induced strength-reducing scratches, and the higher amount of miniscule defects present in the samples due to the kiln-casting of the specimens at a higher viscosity. Among the tested samples, the "Wertheim 1020ºC" specimens showed the highest flexural strength (≈73MPa). It is speculated that, in terms of chemical

composition, the small addition of Al_2O_3 and B_2O_3 and the higher Na_2O to CaO ratio, which alters the standard soda lime silica recipe, increases the bond strength but also the flexibility of the glass network. Moreover, the increased fluidity of this glass at forming temperatures (versus the "short"[98] soda lime silica glass for float or container products) contributes to a smooth surface and thus higher strength. As the chosen forming temperature would decrease, a higher population of flaws would arise (e.g. bubble veils) that would negatively affect the strength. Already a 50°C reduction in the kiln-forming temperature of borosilicate beams caused a 30% drop in flexural strength, due to the presence of bubble-veils at the surface. The strength of borosilicate beams would be reduced by 75% at even lower processing temperatures (as low as 10MPa in beams processed at 970°C), where the created fused interfaces were exposed to a high tensile stress. The testing of other specimens, where such fused interfaces were only present in the bulk of the component, however, showed a similar flexural strength to their homogeneous variants.

The extrinsically contaminated glass specimens showed a lower flexural strength (≈35-42MPa) than their purer counterparts, produced at the same forming temperature. These were specimens produced using float glass cullet with heat-resistant coatings (e.g. oven door glass), enamel or ceramic fritting, where the coating could not dissolve at the processing temperature, or with car-windshield cullet sorted by a recycling factory and thus contaminated with traces of stones and other non-glass materials. In cases such as the heavily contaminated car glass, using a blend of ≈ 30% pure compatible SLS cullet and a 70% of the initial cullet mixture resulted in an improvement in flexural strength by 29%. A 19% strength improvement was also observed in similar composite beams from glass shards which came from fully tempered float glass. The engineering of composite glasses can thus lead to stronger components. These can be made from initially poorer quality, contaminated cullet, provided that no significant stress is developed between the mixed glasses.

In terms of the effect of size on bending strength, this was not clearly observed in all specimen types from the tested purer beams, while a maximum 27% reduction was observed in the more contaminated samples. This is related with the type of flaws responsible for fracture in the two different scenarios. Purer samples fractured mainly from grinding flaws, of similar nature, while the more contaminated samples, failed from stones and other contamination inclusions at the surface. This suggests that different types of flaws have a different impact factor during the scaling up of the component. From a statistical point of view looking at the Weibull size-scaling relationship[99] (Davies, 1973), this implies that stone inclusions would have a lower Weibull modulus m than scratches, and thus weaken the component much more as the size increases.

[98] Glass artists use the term "short glass" to describe a fast stiffening glass during forming, which makes hand-processing difficult, but favours machine-processing. In antithesis, a "sweet or long glass" is a glass with a shallow temperature/viscosity curve that facilitates manual formulation by allowing more time for manipulation (Stone, 2000).

[99] The impact in strength can be predicted using the formula below:

$$\frac{\sigma_1}{\sigma_2} = \left(\frac{V_{E2}}{V_{E1}}\right)^{\frac{1}{m}} \quad (1)$$

It must be noted though that the size difference between the tested short and long series is rather minor, due to manufacturing difficulties that prevented kiln-casting longer components at the lab. The size factor between the maximum tensile area of the two beam sizes (100x30mm in the 1st test series versus 140x30mm in 2nd) is only 1.4, while Kinsella and Persson (2016) observe that at least a factor of 2 between studied surface areas is required to detect a size effect. However this guideline is targeted on the testing of float glass, which by definition has a much lower population of flaws of all types. It is suspected that the size effect is much more dramatic and prominent in cast glass given that different types of flaws can coexist, in random orientations, and often acting concurrently. Later testing at the TU Delft lab (not included in this dissertation) using industrially cast glass by Poesia (i.e. glass frame cut to size) showed that an increase in size by a factor of 2.3 (max. tensile area of 250x39mm versus 140x30mm) caused a reduction in strength by 46%. Although systematic testing[100] is required to allow for hard conclusions, it is strongly suspected that much lower Weibull moduli (e.g. 1-4) are to be expected in cast glass compared to the ones reported for float glass (e.g. 7 by ASTM E 1300, 25 by prEN13474-1). This statement is only made to visualize to engineers the dramatic effect that the size factor of cast glass can have. In fact statistical prediction in cast glass is much more complicated, dealing on the one side with the profile of different defects (type, size, shape, location, orientation) and their distribution and interaction, with the strength of the glass network (chemical composition and thermal history), the stress field, and the mechanism of crack growth. So rough estimates can always be performed to inform the initial design, but full-scale testing of the final cast glass component is mandatory, to reduce risks in the structural application of cast glass.

Young's modulus of cast glass

The E modulus of glass is defined by the compactness of its network and the strength of its bonds[101]. In that sense, the chemical composition plays the most critical role in determining the

---

with σ representing the mean strength, V_E the effective volume and m the Weibull modulus. In the case of the 4 point bending test of a rectangular beam, we can substitute the V_E with the Area of maximum tension, at the bottom surface of the beam (w·2·a). As an indication of typical m values of glass, Datsiou and Overend (2017) tested multiple series of SLS float, annealed glass, and found a 3.4-4.2 Weibull modulus for naturally aged glass (large coefficient of variation) versus a 9.4 for as received, newly produced float.

[100] A minimum number of 30 data points is required for a 95% confidence interval for σ (Lau, 2017), which means 30 samples per type of cast glass would need to be tested in series of different sizes, to be able to predict the size effect in a satisfactory manner.

[101] Makishima and Mackenzie (1973) developed the following equation to describe this relationship:

$$E = 2 \cdot Cg \cdot Gt \quad (2)$$

Where Cg is the atomic packing density and Gt the total dissociation energy per unit volume.

stiffness of the material. The measured E moduli in this work correspond to the values reported in the literature for the different compositional families of glass, justifying the above fact. Specifically, the stiffness ranking found experimentally can be seen below:

$$E_{\text{Potassium Soda Lead-silicate}} \leq E_{\text{Borosilicate}} < E_{\text{BaO/SrO-Silicate}} < E_{\text{Soda Lime Silica}}$$

This ranking corresponds to theoretical calculations of the E modulus based on the chemical composition of the tested glass, as found by XRF analysis. In general, the measurements of stiffness via 4-point bending experiments using Digital Image Correlation (DIC) to detect the maximum displacement, and via the Impulse Excitation Technique (IET), were both found to be accurate and in agreement with each other. The values reported were 60-62GPa for Borosilicate samples, 69-72GPa for Poesia glasses, 70-76GPa for SLS glasses, and 79GPa for the Wertheim glass. An increase in the E modulus upon prolonged cooling and annealing (kiln-cast glass versus the original glass cullet) was detected in the order of 2-3GPa, strongly suggesting that the thermal history and the resultant atomic packing density are affecting the stiffness of cast glasses.

Regarding other measuring methods, the detection of displacement during 4-point bending using LVDT sensors was found to be inaccurate, reporting a much higher displacement and as a consequence returning a lower E value. The measurement of stiffness by ultrasonic wave techniques was not producing reliable results due to improper contact of the ø40mm transducers with the (smaller and rough) side surface of the cast glass beams. Prior testing using 50mm cubic glass samples (see Appendix C) worked better but still with an error of 1-2GPa between different cross sections of the same cube. Much larger samples are perhaps required to reduce the sensitivity error of the ultrasound testing caused by different distributions of internal defects.

Still, considering the rather inhomogeneous character of cast glass, questions arise, on whether and to what extent the meso-level structure of defects in cast glass affects the Young's modulus. The proximity of the experimental data to the reported values in the literature corresponding to homogeneous glass suggests that the impact of the tested meso-level structures on the stiffness is rather negligible and that the chemical composition is the dominant determinant. This is related to the ratio and type of existing defects to the pure glass network, which in the tested cases is still low. It is unknown how a much higher content of stones, cord or gas bubbles in the meso-level structure would affect the E modulus, but a more noticeable impact would be expected.

Impact of micro-level alterations in the glass structure due to thermal history on the macro-level performance of the glass component

A slower cooling rate and longer annealing period contributes to the compactness of the glass network, and leads to an increase of the stiffness, hardness and brittleness of the glass component (Ito and Taniguchi 2004, Smedskaer et al. 2010, Striepe et al. 2013), while the network still retains its amorphous character. Indication of such microscale modifications were detected in the Differential Scanning Calorimetry tests, where kiln-cast specimens of slower cooling rate and longer annealing showed an increase in the Glass Transition Temperature (T_g) and a decrease in the Fictive Temperature (T_f) in comparison to as received specimens with identical chemical

composition. Moreover, a higher E modulus by 2-3GPa was reported between kiln-cast and as received specimens, during the 4-point bending and Impulse Excitation experiments. Regarding the flexural strength, however, the impact the thermal history had on the meso-level structure of the glass and the formation of defects, particularly at its surface, was found to be more influential than the impact it had on the micro-level structure, provided that all samples were sufficiently annealed. In other words, the role of the compactness level of the glass network was obscured in the presence of a much bigger flaw or a more dense population of defects that could be invoked by a certain thermal history. Indirect effects of the micro-scale alterations to the meso-level structure and strength could also be observed; as an example, the higher hardness of a more compacted glass would increase the difficulty of machining, making in this manner the probability of the presence of scratches due to improper grinding (meso-level defect) more frequent and increase the overall chances of failure. The most determining parameters were found to be the forming temperature and corresponding dwell time. As previously mentioned, only a 50^{o}C decrease in temperature could lead to a 30% reduction in strength in kiln-cast borosilicate samples, due to the clustering of miniscule bubbles at the proximity of the surface. Shorter dwell times at forming temperature further revealed the problem of bubble entrapment. Moreover, the casting below the liquidus point introduced crystalline particles or planes in the glass that significantly reduced its strength when these were located at the surface and thus exposed to tension. The above suggests that the impact of the thermal history on the micro-level structure should be of less concern to cast glass manufacturers and engineers than the impact it has on the level of inhomogeneity at, and in proximity, to the glass surface.

Fracture resistance of cast glass

During the splitting experiments on 50mm cubic specimens, a two-step process was identified as governing the fracture resistance of cast glass against a sharp indenter (longitudinal toolbit). The first step involves the resistance to crack initiation, which, in silicate glasses, is controlled by the extent to which the glass network can densify around the pressing toolbit. Glasses with a more open structure, reflected by a lower Atomic Packing Factor (and thus lower Poisson's ratio) and a higher Molar Volume, will have more space within their network to permanently deform by densification and thus relief the local peak stress. This increases crack resistance. Nonetheless, with the increase of pressure, in the second step the crack will initiate. Thus, the resistance to crack propagation dominates here. In this step, the fracture surface energy and the bond strength of the network are the determining properties. To achieve a high resistance to fracture, a good balance between glass network flexibility (sufficient empty space in molecular level) and high bond dissociation energy is required. The results of experimental testing were in accordance to the above conditions, with the borosilicate glass specimens of higher molar volume and higher fracture surface energy compared to soda lime silica glass showing the highest fracture resistance.

Differences in the fracture resistance of specimens with altered thermal history were also observed. For example, a homogeneous glassy specimen heat-treated below the crystallization peak temperature showed less crushing and lateral cracking than its fast-cooled alternative. Glasses cooled at a slower rate (e.g. Poesia specimens) showed more resistance to fracture. On

the other hand, fused specimens heat-treated at the crystallization peak temperature showed a decreased crack initiation load and lower fracture resistance, caused by the increased surface hardness and/or by the co-existence of glass and crystalline zones at the surface and thus altering hardness values.

The splitting test proved the governing role of the pressing sharp toolbit in causing failure, overruling the role of defects in the fracture resistance. Nonetheless, defects at, or close to, the surface were found to contribute to failure, by invoking lateral damage due to stress concentration in the first response step (crack initiation), and by weakening the strength of the glass network in the second step (fracture propagation). As an extreme example, highly porous crystallized glass specimens failed at a considerably lower load. Defects in the bulk however, did not seem to have a positive (e.g. total crack arrest) or negative (e.g. strength reduction) effect on the glass specimens.

Far field versus contact stress

The bending and splitting experiments showed that a glass type- as defined by its chemical composition and thermal history- can have a high flexural strength but low fracture resistance and vice versa. This difference in performance highlights the distinct mechanisms activated during an applied far field stress versus a sharp contact stress. In the first case, of far field stress (due to flexure), the type/shape/orientation/distribution of flaws at the critical surface are activated by inducing a stress concentration to the surrounding glass. The strength of the glass is therefore interrelated to the flaw population characteristics and the quality of its network (chemical composition and thermal history). The response of the network to the bending action is determined by its stiffness, for which a high bond strength and a high atomic packing density is required, but with a certain balance; a slightly more open structure in silicate glasses was found beneficial by allowing for minor deformations around the flaws and thus the relief of stresses during loading. In the case of a contact stress, induced by a pressing sharp indenter, the defects play a secondary role versus the crushing and lateral damage caused by the indenter. In this stress condition, the fracture resistance of the glass specimens is governed, first by the ability of the glass to deform around the sharp indenter in order to relief the stresses and resist crack initiation, then by the bond strength of the glass and the quality of the glass network to resist crack propagation. For a high resistance to fracture, a good balance between glass network flexibility (sufficient empty space in a molecular level) and high bond dissociation energy is required. As an example, the tested borosilicate glass specimens may have a lower stiffness than soda lime silica float glass -which is reflected to its lower flexural strength- yet their higher molar volume/lower Poisson's ratio and their higher fracture surface energy allow for a higher fracture resistance.

This performance shift proves that one type of test alone may be insufficient when engineering a cast glass structure. It is necessary to consider the governing loadcase upon which, a suitable chemical composition can be chosen to best fit the structural requirements.

Putting facts into perspective

The experimental work highlighted a sequence showing how different parameters affect the strength of cast glass. The surface quality (due to mould contact, pouring method, post processing and handling) and the presence of extrinsic and intrinsic defects seem to be the most critical factors, followed by the chemical composition. Differences in the thermal history of a glass type are –on the one hand– crucial when leading to zones/interfaces/localized events of altered properties (e.g. local crystallization within the glass matrix) at the surface, or intensify the presence of surface defects (e.g. higher content of bubbles due to higher viscosity of the melt). On the other hand, a thermal history leading to small structural changes in the glass network is only of secondary importance (provided that sufficient annealing is achieved), as such changes are masked by the far greater effects the surface defects have on the mechanical properties of the cast glass components. As a general observation, the defects present in the bulk of the cast glass specimens –unless responsible for the immediate fracture of the surrounding glass upon annealing due to a considerably contrasting thermal expansion coefficient- seem to be tolerated by the glass and do not degrade its performance. Given the above, a certain amount of defects can be acceptable at the bulk or even surface of a cast glass component, provided that the engineer is aware of the resulting characteristics of this product and its corresponding range of design strengths. It is also acceptable, if reliable data exists, to design and produce cast glass products of lower strength (e.g. due to higher contamination), as not all applications have equally demanding pre-requisites on strength (e.g. a masonry wall). This fact discharges the severity of the existence of a network of specific defects in cast glass products, opening up opportunities for recycling by the casting of challenging glass waste streams with embedded or difficult to remove contaminants. It also places a realistic framework around the production of cast glass, accepting that a flawless product would imply a considerably higher investment in facilities, tools, resources, moulds and energy, resulting to an increase in market price which is not proportional to the increase in performance. This would render the whole venture unrealistic in the majority of cases. So learning to work with flaws, supported by an ongoing research on defining the properties of cast glass products as a relation to their presence, is perhaps the only way to proceed. More importantly, opting for manufacturing the perfect cast glass product at a material level is useless if the component design, the engineering of the overall cast glass structure and/or the assembly method of the components are erroneous. In fact, these factors can equally -if not more- contribute to component failure: insufficient annealing due to abrupt changes in the cross-sectional thickness of a complex shape, trapping of air leading to infolds due to undercuts in the design, sharp corners prone to impact, optimistic estimation of the design strength used in structural simulations, engineering of tensile structures rather than compressive ones, application of stiff adhesives, or connections that introduce peak stresses are common errors observed. For the success of cast glass structures, a comprehensive approach is crucial, tackling all steps from material design, component shaping, structure and assembly method engineering, manufacturing and quality control, and construction.

References

Bukieda, P., Lohr, K, Meiberg, J., Weller, B.: Study on the optical quality and strength of glass edges after the grinding and polishing process. Glass Structures & Engineering 5(3), 411-428 (2020). doi:10.1007/s40940-020-00121-x

Datsiou, K.C., Overend, M.: Artificial ageing of glass with sand abrasion. Construction and Building Materials 142, 536-551 (2017). doi:https://doi.org/10.1016/j.conbuildmat.2017.03.094

Davies, D.C.S.: A statistical approach to engineering design in ceramics. Proceedings of the British Ceramic Society 22, 429-452 (1973)

Ito, S., Taniguchi, T.: Effect of cooling rate on structure and mechanical behavior of glass by MD simulation. Journal of Non-Crystalline Solids 349, 173-179 (2004). doi:10.1016/j.jnoncrysol.2004.08.180

Kinsella, D., Persson, K.: On the applicability of the Weibull distribution to model annealed glass strength and future research needs. In: 2016

Lau, A.T.C.: Why 30? A Consideration for Standard Deviation. ASTM Standardization News (2017)

Lindqvist, M.: Structural Glass Strength Prediction Based on Edge Flaw Characterization. École Polytechnique Fédérale de Lausanne (2013)

Makishima, A., Mackenzie, J. D.: Direct calculation of Young's moidulus of glass. Journal of Non-Crystalline Solids 12(1), 35-45 (1973) doi:10.1016/0022-3093(73)90053-7

Müller-Braun, S., Seel, M., König, M., Hof, P., Schneider, J., Oechsner, M.: Cut edge of annealed float glass: crack system and possibilities to increase the edge strength by adjusting the cutting process. Glass Structures & Engineering 5(1), 3-25 (2020). doi:10.1007/s40940-019-00108-3

Quinn, G.D.: NIST Recommended Practice Guide: Fractography of Ceramics and Glasses, 2nd edition. (2016)

Quinn, G.D.: On terminal crack velocities in glasses. 10(1), 7-16 (2019). doi:https://doi.org/10.1111/ijag.13042

Smedskjaer, M.M., Jensen, M. and Yue, Y.: Effect of thermal history and chemical composition on hardness of silicate glasses. Journal of Non-Crystalline Solids 356(18), 893-897 (2010). doi:https://doi.org/10.1016/j.jnoncrysol.2009.12.030

Stone, G.: Firing Schedules for Glass- The Kiln Companion. Igneous Glassworks, (2010)

Striepe, S., Potuzak, M., Smedskjaer, M.M., Deubener, J.: Relaxation kinetics of the mechanical properties of an aluminosilicate glass. Journal of Non-Crystalline Solids 362, 40-46 (2013). doi:https://doi.org/10.1016/j.jnoncrysol.2012.11.017

Vandebroek, M., Belis, J., Louter, C., Van Tendeloo, G.: Experimental validation of edge strength model for glass with polished and cut edge finishing. Engineering Fracture Mechanics 96, 480-489 (2012). doi:https://doi.org/10.1016/j.engfracmech.2012.08.019

Vandebroek, M., Louter, C., Caspeele, R., Ensslen, F., Belis, J.: Size effect model for the edge strength of glass with cut and ground edge finishing. Engineering Structures 79, 96-105 (2014). doi:https://doi.org/10.1016/j.engstruct.2014.08.004

Veer, A.F.: Looking at the foundations of structural glass with a digital microscope. In: Marie Frier Hvejsel, F.M., Cruz, J. S. P. (ed.) Fifth International Conference on Structures and Architecture (ICSA), Aalborg, Denmark 2022. CRC Press

Veer, F.A.: The strength of glass, a nontransparent value. Heron 52, 87–104 (2007)

Veer, F.A., Rodichev, Y.: The structural strength of glass: hidden damage. Strength Mater. 43, 302–315 (2011). https://doi.org/10.1007/s11223-011-9298-5

Yankelevsky, D., Spiller, K., Packer, J., Seica, M.: Fracture characteristics of laboratory-tested soda lime glass specimens. Can. J. Civ. Eng. (2016). https://doi.org/10.1139/cjce-2016-0374

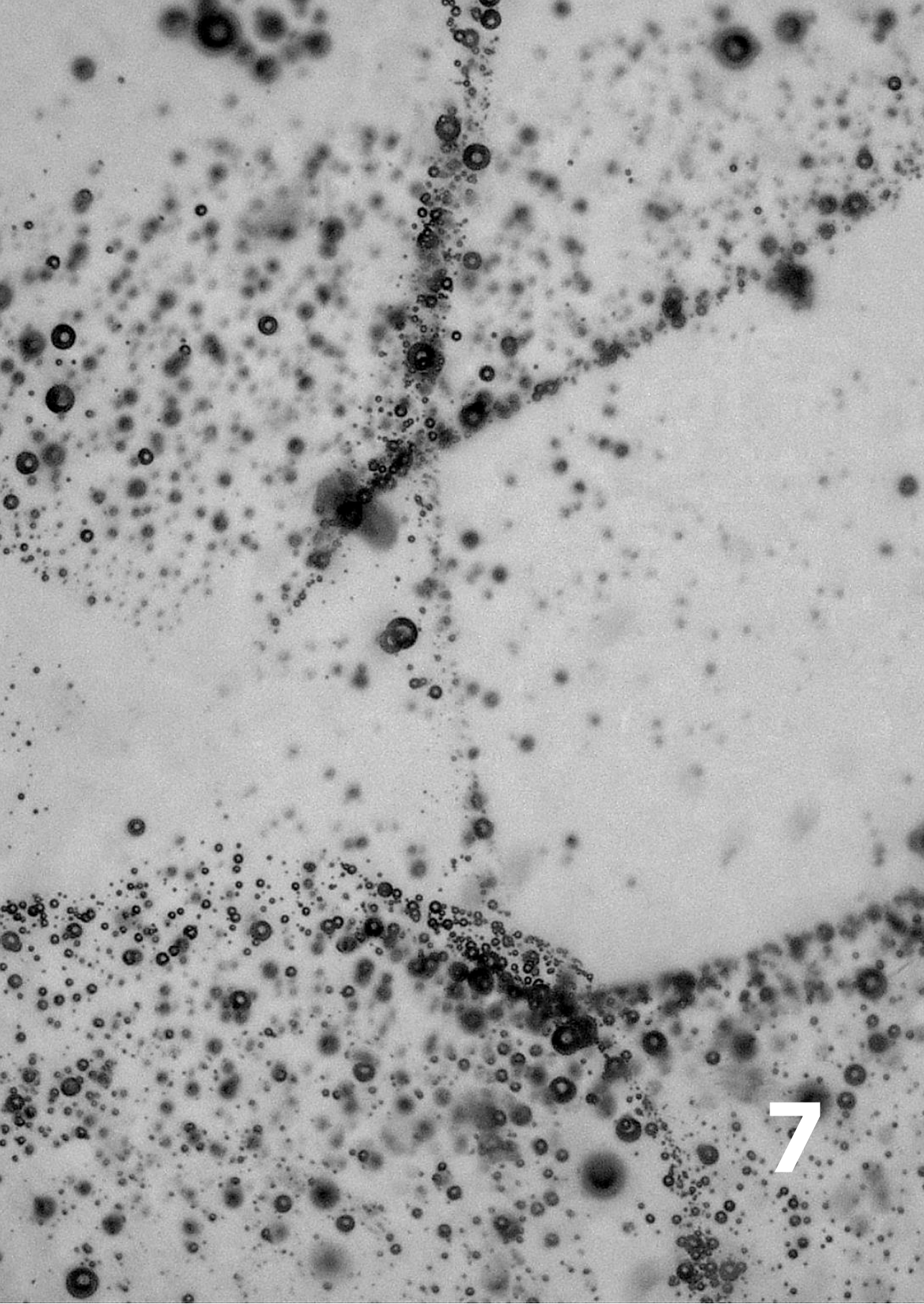
7

Previous page: Bubble veils in a recycled borosilicate glass, kiln-cast at 1120ºC.

Chapter 7: Conclusions

Given the limited number of experimental data, all results obtained in this dissertation are indicative only and are not statistically valid for design purposes. Nonetheless, the obtained data are useful in establishing relationships between the flexural strength, stiffness and fracture resistance of the tested cast glass types, and their chemical composition, thermal profile and defect network. Quantitative assessment of these relationships is omitted from the conclusions, but provided in the discussion chapter (Chapter 6). The derived conclusions of this work are summarized below:

- Compared to conventional soda lime silica glass, typical chemical compositions formulated for casting with higher alkali content, small addition of boron trioxide and alumina, reduce the occurrence of casting flaws due to their fluidity at the forming temperatures. Their more open, yet still strong, structure of the resulting network allows for micro-deformations around a flaw during loading, which prove beneficial in resisting flexure and crack initiation, but may reduce the overall fracture resistance of the component.
- Kiln-casting, in comparison to hot pouring, allows the casting of a larger variety of chemical compositions at relatively low processing temperatures (e.g. 820º-1120ºC), thus circumventing the barrier of high viscosity exhibited by many typical compositions (e.g. soda lime silica, aluminosilicate). Forming glass directly in moulds offers, additionally, compositional flexibility, as the kiln is not bound to the melting of one specific glass recipe. The kiln-casting process bypasses main obstacles that currently prevent the recycling of glass waste other than bottles and food containers (Figure 7.1). It can therefore be a great contribution in the open-loop recycling of the large amount of currently discarded glass waste, provided that other related legislative, logistic and infrastructure challenges are overcome by the industry.
- Above the glass transition temperature, consecutive interface transformations occur as the temperature rises, between deposited glass cullet pieces in a mould or within an accumulated coiling stream of poured glass inside a mould. These interface reactions form a network of intrinsic defects in the cast glass, based on the chosen forming temperature. By increasing temperature, these reactions are: tack fusion -> crystallization -> bubble veils -> cord. The network of intrinsic defects retains a shape memory of the original cullet or pouring sequence, unless much higher temperatures are imposed leading towards homogenization by diffusion.
- Defects can be classified as intrinsic and extrinsic, with the latter being potentially more critical and leading to immediate catastrophic fracture upon cooling, depending on the variation in thermal expansion between the defect and the glass matrix. Extrinsic defects can be avoided by increasing the purity of the batch/cullet, while intrinsic defects are more challenging to avoid as they are inherently linked to the casting process.
- Combinations of different defects, grouped in meso-level structures, are commonly found in cast glass. Such structures in the bulk are tolerable, but if exposed at the surface, they

play a strength reducing role according to their type, shape, orientation and interaction to other defects.

- Meso-level structures can be deliberately engineered within a glass component in a beneficial manner, if higher forming viscosities are employed. Inhomogeneous zones at the meso-level structure level in the form of cord, bubble veils or crystalline zones are not a barrier sufficient to arrest cracks. Crystalline zones and tack fused zones can locally redirect a low energy crack.
- The flexural strength of cast glass is defined mainly by its chemical composition and defect characteristics. The quality of the surface (and proximity zone) is of most crucial importance while the inhomogeneities in the bulk are rarely contributing to the performance (unless a high defect population is examined for example in the case of porous glass). Subtle network alterations due to thermal history will not usually be noticed, but distinct defects related to the chosen thermal profile, such as crystallization or bubble veils, can significantly reduce the strength if exposed to the surface. The flexural strength of pure, fairly homogeneous glass silicate-based compositions ranks as following, covering as indication a 35-73MPa range:
  Lead silicates < borosilicate < barium silicate < soda lime silica (float) < modified soda lime silica (higher alkali/lime ratio). Increasing the size of the casting will reduce the strength, but the effect is different for each type of flaw.
- The Young's modulus of cast glass is determined mainly by the chemical composition, which defines the bond strength and network packing density. Experiments showed the following increasing sequence: Potassium Soda Lead-silicate $\leq$ Borosilicate < BaO/SrO-Silicate < Soda Lime Silica, with the obtained indicative values spanning from 60-79GPa. The Young's modulus can be affected by the inhomogeneities in the glass, but not to an extent relevant for structural applications. However, the firing schedule may impose a noteworthy change; an increase in the order of 2-3GPa (≈3%) was detected in kiln-cast specimens, versus faster-produced industrial specimens.
- The fracture resistance of cast glass under a concentrated sharp load is mainly dependent on the chemical composition and thermal history, and consists of two steps: crack initiation resistance -where an open network is favourable- and fracture propagation resistance -where a high surface fracture energy is required. The experiments showed a reverse to the flexural strength ranking for pure glass silicate based specimens: modified soda lime silica < soda lime silica < borosilicate. This is due to the different fracture mechanisms involved between contact and far field stresses. Defects at the surface deteriorate the fracture resistance by invoking additional lateral damage and by weakening the response line in contact with the sharp indenter.
- Improvement of the surface by engineering composite glasses improves both the flexural strength and fracture resistance of cast glass.
- Glass waste cullet and lower melting temperatures (e.g. 820ºC-1120ºC) can still produce reliable glass components. Lower quality cast products can be mechanically evaluated and used according to their properties in applications of lower demand. This as long as they do not fail instantly from internal stresses or thermal shock.

- Safe cast glass applications require a comprehensive approach that takes into account the material properties, component design, structural engineering, assembly technique, manufacturing process, quality control, and construction method.

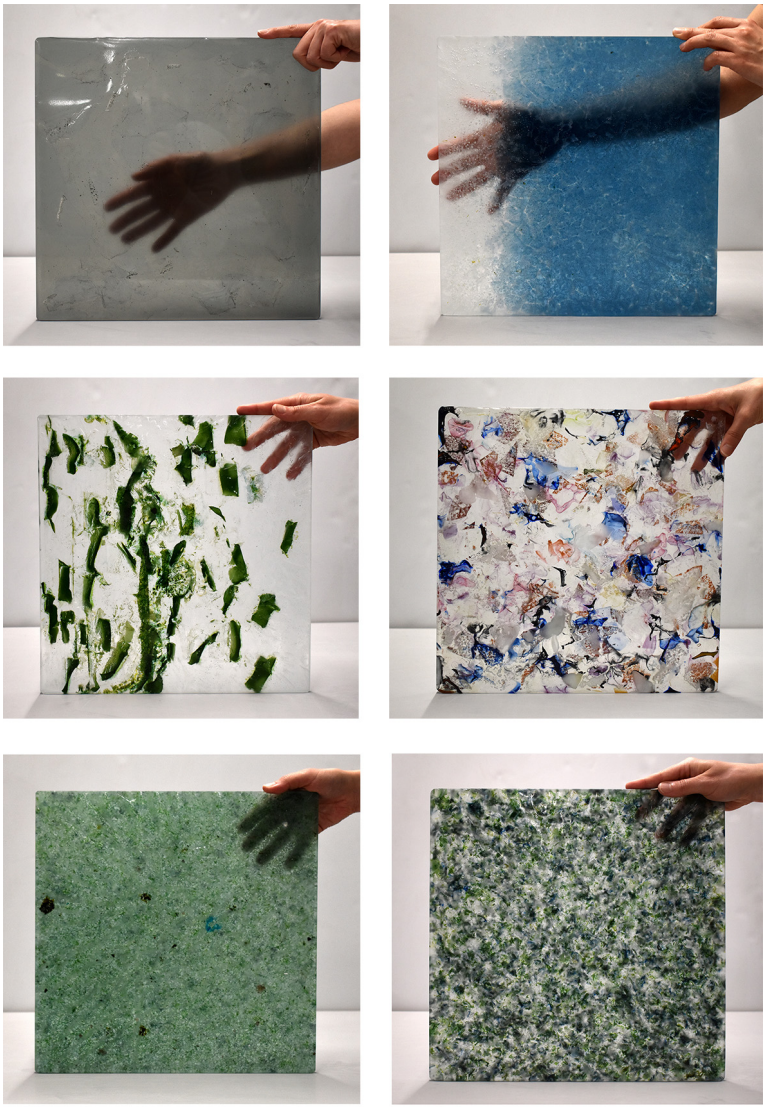

Fig. 7.1 Kiln-cast panels (35x35x1cm) made from glass waste cullet (from top left, clockwise: Cathode-Ray Tube (CRT) front screen, AGC transition float glass from clear to blue, CRT back screen and Leerdam crystal coloured glass, oven doors with heat resistant fritting (Coolrec), car windshields (Maltha Glasrecycling), and enamel float glass (AGC). A fine balance can be achieved between the amount of acceptable defects in a cast glass product and maintaining a reliable strength. Learning to work with glass defects stretches the aesthetical potential of glass, while enabling the recycling of currently landfilled glass waste streams.

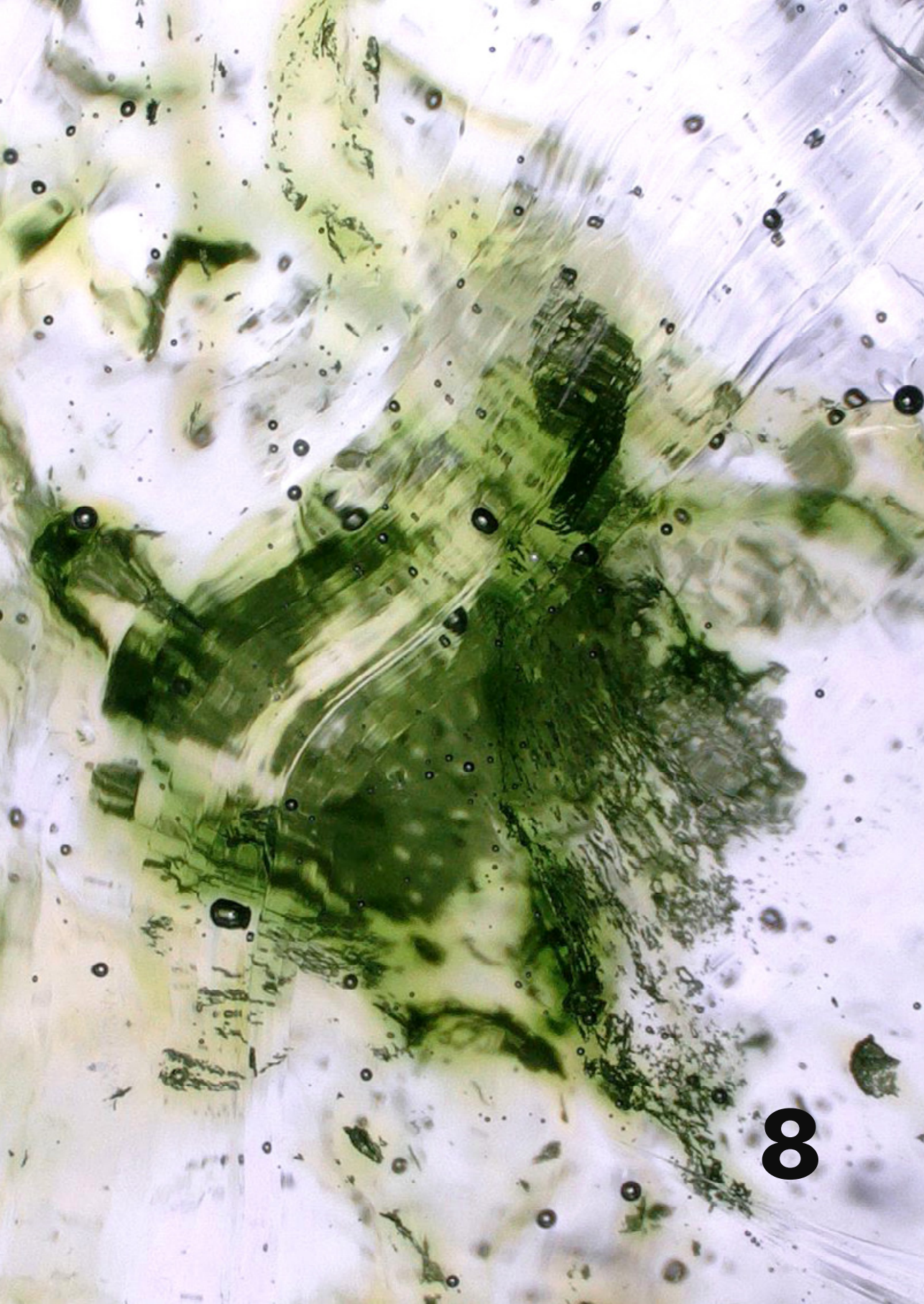
8

Previous page: Crystalline flakes, cord and colour streaks in a recycled oven-door glass (float with heat-resistant coating), kiln-cast at 1120ºC.

Chapter 8: Recommendations

8.1 Limitations of this research

The main limitation of this research lies in the type and number of tested specimens, as well as the methods of testing. Given the diverse character of the family cast glass, particularly the variability in chemical composition and casting flaws from one foundry to another, this dissertation could only study a small variety of types, mainly due to the lack of tested industrialized specimens. Even though in terms of chemical composition a considerable variety was experimentally validated, these specimens were mainly produced at the laboratory using the same casting technique (i.e. kiln-casting using silica-plaster investment moulds). This process allowed the freedom to experiment with the cullet source and the casting parameters in order to correlate the resulting defects to the casting process, yet, condemned the specimens to a set of particular flaws linked with this process, e.g. surface contamination by investment mould contact, larger population of bubbles due to higher viscosity of the melt, etc. Furthermore, the manual post-processing of the specimens did not exceed the 600grit step, which introduced several scratches that are uncommon for industrialized products. Given the laborious and time consuming process required to cast and post-process these specimens, only a limited number of repetitions (1-5) per glass type was possible within the scope of this dissertation, and in only a small variation of sizes and shapes. As a consequence, neither a statistical analysis of the strength per type could be made, as a minimum number of 30 specimens for each type would be required to give a reliable indication, nor a good prediction on the size factor could be reached. The same issue of limited testing applies for other experiments as well, such as the measurement of the Young's modulus or the investigation of the thermal history by Differential Scanning Calorimetry measurements. The obtained results are strongly indicative but cannot be conclusive at this stage. Regarding the splitting test, which was introduced as a testing method in this dissertation, uncertainties arose on the mathematical formula that could be used for calculating the fracture resistance, and attempts with the aid of FEM simulations were not fruitful. Several challenges were also encountered in the process of mapping the 3D meso-level structure of cast glass, as none of the tested technologies were able to capture all types of defects into a 3D point cloud. Other experiments such as a nano-hardness test were unsuccessful due to the unevenness of the surface of the specimen as well as the presence of pores and other defects. Defect characterization using a Scanning Electron Microscope was not possible either.

Considering the encountered limitations, several areas of future work are highlighted during this research, in the field of defect mapping and characterization, and the testing of mechanical properties. In addition, judging on the potential of several prototypes created in the lab, future directions in product development are highlighted. The derived recommendations are provided below.

8.2 Defect mapping and characterization, and testing of voluminous cast glass components

- Repetitive testing in bending is required, employing both laboratory made and industrially produced specimens, to derive design strength values within the 0.8% Probability of Failure confidence guideline (ASTM E1300). This testing should include specimens of various sizes, and especially of larger scale than currently tested, to investigate the size factor in relation to the presence of different types of defects. Testing at different loading rates -and particularly of lower speed than currently tested, and different atmospheric humidity levels are also required to shed light on the slow-crack growth effect on cast glass, and investigate whether there is resistance to stress-assisted corrosion if the thermal history -and thus the network characteristics, of the specimens is altered. Within this context, the testing of linearly indented specimens according to the Single-Edge Pre-cracked Beam (SEPB) test will further provide information on the fracture toughness. Overall, more attention should be given to perfecting the experimental fixtures, so common errors such as friction at the rollers-specimen interface, or improper contact of the rollers to uneven specimens, can be avoided.
- Thermal shock testing is necessary to holistically define the role of different types and sizes of flaws in the bulk of cast glass elements. Cast glass components with different meso-level structure characteristics need to be subjected to abrupt and gradient temperature variations of relevance to typical building applications, particularly exterior ones.
- Testing the chemical durability and weathering resistance of kiln-cast and fused glass, especially of recycled cullet origin, is of particular importance, prior to applying these glass types to exterior building applications. Depletion of volatile compounds (e.g. alkali oxides) and other melting reactions at the surface of the components or along the fused interfaces, alter the stable chemical composition of the original glass cullet in a yet undefined manner. Resistance to corrosion by water vapour can be evaluated in static and cyclic conditions, employing an environmental chamber for exposing the specimens to heat and high relative humidity (e.g. 50°C 75% RH).
- Micro-indentation testing is suggested at the surface and along selected cross sections of cast glass specimens, to understand the variations in hardness due to the presence of inhomogeneities. Comparative hardness testing between specimens of the same chemical composition but of different thermal history can reveal the extent of network alterations and if these are traceable in a micro or macro-scale.
- A new mechanical testing method for the evaluation of voluminous cast glass components needs to be developed. Common mechanical testing methods either: (i) measure the properties of the surface without exposing defects in the bulk to tension (e.g. flexural test, ring on ring test), (ii) lead to pulverized specimens that prevent fractographic analysis to determine the critical flaw (e.g. uniaxial compression test), (iii) require elaborate specimen shaping not relevant to the shaping process –and corresponding defects- of cast glass (e.g. compression on “Theta” specimens) or (iv) although they aim to subject the defects in the bulk to maximum tensile stresses, fail to do so in the case of cast glass, either due to

specimen shape deviations that lead to fracture from contact stresses (e.g. Brazilian disk test), or improper specimen gripping (e.g. direct tensile test). Yet, even if the latter two tests could be redesigned to fit the specifications of cast glass, given that they impose a uni-axial stress field, of even limited range in the case of the Brazilian test (concentrated at the middle strip), they would lead to over-optimistic strength results, as many defects may be oriented in parallel direction to the stress field, or situated outside of that field. An interesting direction to explore is the diametral compression test on spherical cast glass elements. Hiramatsu and Oka (1966) studied the stresses developed in a sphere diametrically pressed between two steel plates, by conducting photoelastic experiments on clear epoxy spheres and mathematically analysing the stress components, with the aim to rationalize the stress distribution occurring in a diametrically compressed rock of irregular shape. Further on, experimental validation on rocks of 25-90mm in the minor dimension showed failure of the specimens in 2-3 pieces by tension within a range of approximately 1-15MPa. Kshinka et al. (1986) conducted diametral compression testing on a series of soda lime silica spheres of 0.51mm-3.68mm diameter, which failed by tensile stress in the bulk. However, this was in an explosive manner due to the much higher stresses (435MPa-143MPa tensile strength respectively) developed in the considerably smaller size glass spheres that subsequently contained a smaller population of flaws than conventional glass products. Considering the above, a diametral compression test that develops radial tensile stresses parallel to the compressive plates can be a solution for subjecting defects of different orientations in the bulk of cast glass spherical specimens to a tensile scenario which is more relevant to compressive applications, but requires lower force than the typical compression test, thus increasing the chances of a clear fracture that can be studied by fractographic analysis. In such experiments, special attention must be given in avoiding crushing and end splitting at the steel/glass contact points, to allow for failure due to tension in the bulk. Such tests could allow not only the studying of the effect of different flaws in the bulk to the strength of cast glass, but also reveal valuable information on the performance of composite cast glasses, of higher quality surface and lower grade bulk, which cannot be easily evaluated currently with the available experimental methods (e.g. flexural testing).

- Focusing on studying the material properties alone- in a generic specimen shape- may be leading to over-optimistic strength estimations. Considering the shaping freedom of cast glass and its potential in building applications, it is important to study the strength of cast components of complex shapes, as any given shape is linked with a characteristic set of defects. These could be trapped bubbles in mould undercuts, surface depressions (“suckers”) caused by differences in temperature during cooling, insufficient stress annealing due to abrupt variations in the cross-section, etc., which can significantly lower the strength, but will not appear in rectangular beam specimens employed in a standard 4-point bending experiment.
- A profound study on the characteristics of different types of flaws and how these affect the performance of a cast glass component is required. This asks for a threefold approach:

a) Defect mapping: 3D mapping techniques for determining the flaw distribution and residual stresses in the meso-level structure of voluminous cast components need to be developed. As a first step, this could be achieved by combining, calibrating and developing currently available techniques such as computed tomography scanning (detecting density gradients/stones and gaseous inhomogeneities) and Real-Time Imaging Polarimetry (detecting cord and residual stresses). As a later development step, a 3D-scanning system that captures the surface morphology and inhomogeneities in the meso-level structure of a cast glass (especially complexed shaped) component and exports the data in a point cloud, would be a significantly contributing method, not only to the scientific research on defining the mechanical properties of cast glass, but also in the quality control process of cast glass products. 3D-scanning technologies are advanced enough to create point clouds of opaque materials with an accuracy of even 0.1mm (e.g. Artec 3D Leo) but do not perform equally well with transparent and glossy materials, an issue that needs to be resolved (Figure 8.1). Advances in digital microscopy can further on be a base for developing a meso-level structure capturing tool, given that 3D image compilation and measuring within the depth of a transparent material is already possible (e.g. Keyence VHX-7000).
b) Defect characterization: meticulous characterization of the typically encountered inhomogeneities must be performed, using a scanning electron microscopy (SEM) that can define the chemical composition of these defects. X-Ray Diffraction (XRD) analyses can further help with identifying the crystalline structures encountered. The above information can be linked to already existing data in the literature and help identify the variations in thermal expansion, stiffness and toughness of the defects in relation to the glass matrix. Consequently, this should inform the level of risk related to each type of defect and if some types of contaminants need to be avoided already from the cullet/batch step.
c) Mechanical testing: Defect mapping and characterization prior to destructive testing, can be of outmost value, to study if a prediction of the failure strength and most critical flaws can be made already from the product quality control stage. Systematic defect documentation and fracture origin correlation upon testing is therefore required.


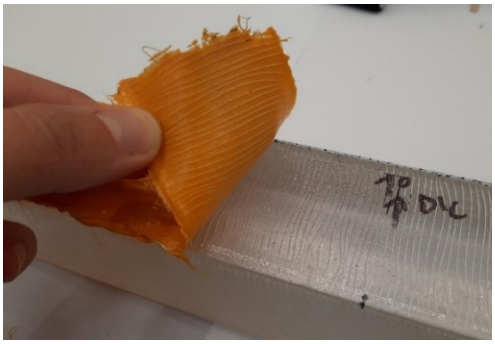

Fig. 8.1 Trials on documenting surface defects on cast glass prior to testing. Left: The 3D scanner Artec 3D Leo can be rotated around the object (volume capture zone 0.16m^3), producing a 3D point cloud of 0.1mm accuracy, yet renders inaccurate results in the case of glossy transparent materials, even if these are coated with an antiglare spray. Right: Replicas of cast glass surfaces – in combination with high-res photography- can be useful for tracing back to the fracture origin site, upon destructive testing. Polyvinylsiloxane, commonly used in dentistry as a fast-curing and highly accurate impression material, can effectively replicate scratches and indents found on the cast glass surface.

- Based on the data collected through the above described threefold approach on determining the criticality of different defects, Artificial Intelligence techniques can be implemented to assist with defect inspection and strength prediction of cast glass components during quality control. Research on the use and benefits of machine learning algorithms as a quality control tool for commercial glass products can be found in the recent literature; Park et al. (2020) developed a deep-learning neural network (DLNN)-based defect inspection system for display glass covers of a 99% detection rate, Drass et al. (2021) used neural networks for the detection of cracks at the cut edge of glass, while Riedel et al. (2021) worked on a deep-learning computer vision system for classifying the surface damage at Vacuum Insulated Glazing units. Machine learning can have a superior detection rate, over conventional human-based judgement inspection or camera-based machine vision methods in cast glass, given the complexity of defect inspection, as this is linked to the characteristics of each defect (mechanical and physical properties, size, shape, location, orientation), its percentage of occurrence and its combination with other types of defects into a 3D meso-level structure.
- The combined outcome of extensive mechanical testing and defect characterization should aim to compile a cast glass material properties database, which reflects the variety of different cast glass types, as these occur from the casting technique, chemical composition, thermal history and defect profile. Further on, the experimental data should be used to compose and inform guidelines on cullet recycling, cast glass production and quality control, and structural cast glass engineering.

8.3 Product development

- The development of composite cast glasses is a promising idea that allows for the combination of low and high grade compatible glasses, without compromising the resulting strength. Given that defects situated in the bulk of voluminous components are rarely activated during loading, impure cullet sources can be safely situated in the bulk. Stronger, purer glass streams can be used to form the surface layer and are anticipated to be at a great extent responsible for the strength and fracture resistance of the component (Figure 8.2). This functional grading can be achieved by using to our advantage the shape memory of cast glass, when this is formed at higher viscosities (e.g. 10^5 dPa·s). Specifically, this functional grading can be obtained by either structuring the different glass cullet grades inside a mould, or encapsulating an already formulated bulk shape with a stronger glass. This concept would allow the recycling of currently discarded glass streams such as glass powder (ø<1mm) separated in a typical glass recycling plant, which is almost entirely rejected by the glass industry due to its size (e.g. corrodes the furnaces, leads to high content of bubbles, etc.) and contamination level (e.g. loss on ignition, organics, etc). Simultaneously, it would reduce the raw resources required for founding high-quality pure glass, as these would only be required for the surface volume. The idea of composite glasses can be explored further outside of the scope of structural performance, targeting the thermal or visual performance of architectural components. As an example, cast glass panels of gradient opacity or colour alterations can be produced, for the purposes of shading or privacy.

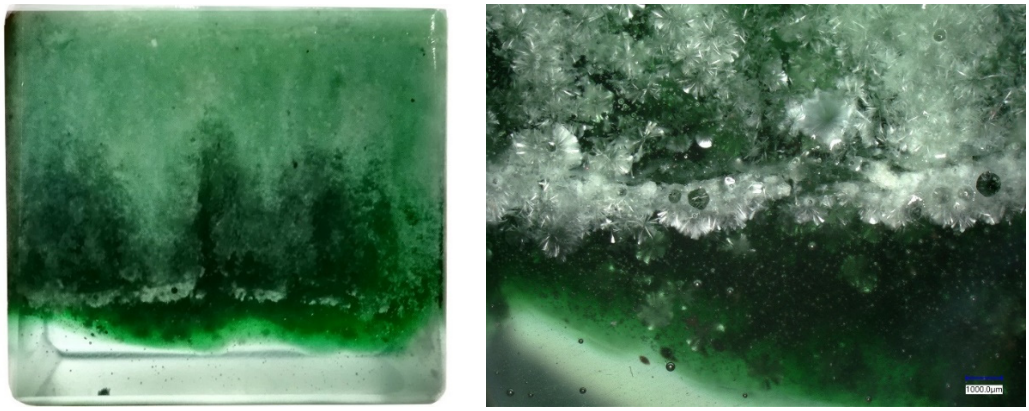

Fig. 8.2 Concept of a composite glass, consisting of a pure, stronger surface and a contaminated core. The particular specimen consists of pure float glass and glass powder contaminated with organics and CSP, a recycling by-product provided by Maltha Glasrecycling. The microscope image to the right shows the co-existence of glassy (bottom) and crystalline (top) parts, and their transition zone.

- Improving the quality of the cast glass surface should be a research focus. Apart from creating composite glasses with a surface layer of increased fracture toughness and minimum quantity of defects, other processes and solutions can be considered, such as improving the quality of the mould and release agents, employing automated grinding and

polishing systems (especially in the case of complex shapes), fire polishing, applying nano-coatings, and chemical strengthening.

- Research should be conducted on methods of fully arresting a propagating crack within the glass bulk, aiming to engineer cast glass components with an inherent safety mechanism. Perhaps the introduction of –compatible to the glass matrix- crystalline zones of larger thickness or higher fracture toughness than the ones experimentally produced and validated in this dissertation, could be an effective means in arresting a crack and providing a visible warning mechanism, allowing for the replacement of the damaged component prior to total failure.
- Reinforced cast glass is another research path worth exploring. Hybrid glass-steel systems, where the metal reinforcement is introduced in laminated float beams either at the tensile edge, on both tensile and compressive edges, or as a surrounding metal strip, have been developed by among other Veer et al. (2003), Nielsen and Olesen (2007), Belis et al. (2009), Louter (2011), Martens et al. (2016) and Cupać et al. (2017, 2021). In prior art, the reinforcement is responsible for the ductile behaviour of the hybrid float glass components, and is activated upon glass fracture; it retains the fractured glass pieces connected, carries the tensile forces, and increases the residual resistance of the beam. Based on this concept, and in a similar fashion to reinforced concrete, metal components of identical thermal expansion to the glass matrix can be introduced in a cast glass component during casting (Figure 8.3, Bristogianni and Oikonomopoulou 2022). Although uncertain if such embedment could increase the tensile strength of the cast glass component, it could provide a warning mechanism well before the ultimate failure stress is reached, and contribute to the component's post-fracture resistance by keeping the glass fragments connected upon failure (Figure 8.4). Embedded metal inserts can also be adapted to fit in complex cast glass shapes; at the same time they could be used as connective elements between components.

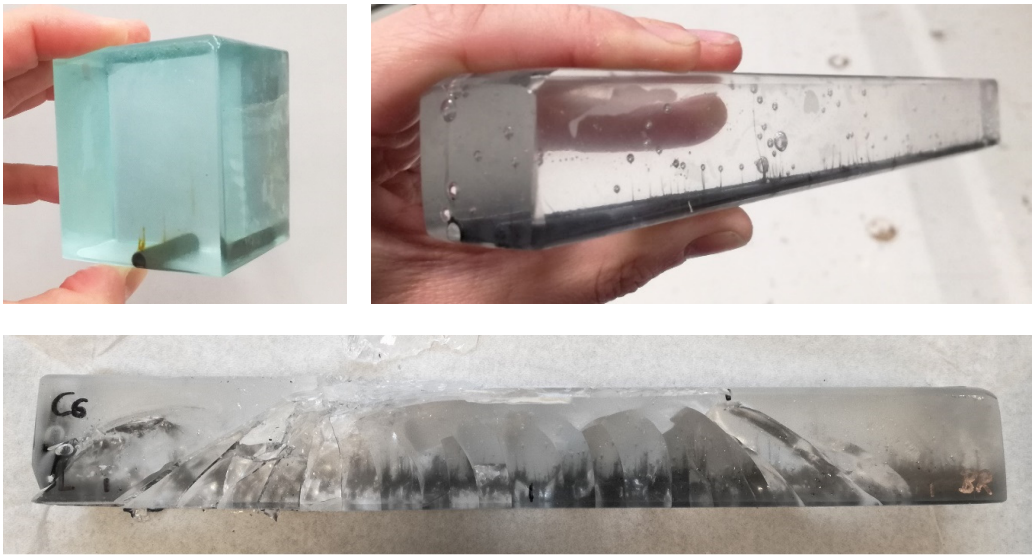

Fig. 8.3 Prototyping and testing of reinforced cast glass components. Top, left image shows a soda lime silica glass with an embedded titanium bar during casting, while the right image shows a borosilicate cast beam reinforced with 2 kovar bars. The image on the bottom shows the side-view fracture of a reinforced cast beam upon flexure. The breaking pattern is similar to typical failure patterns observed in reinforce concrete beams.

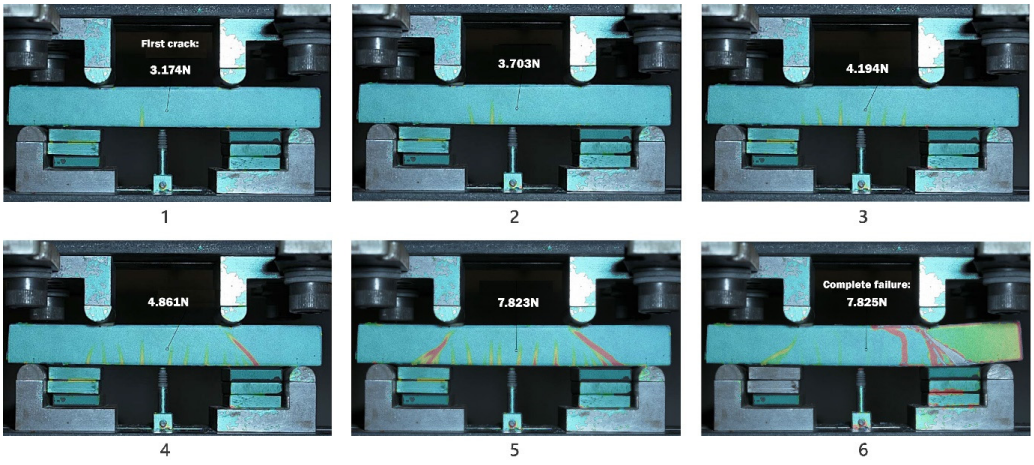

Fig. 8.4 Four-point bending test of a borosilicate beam reinforced with one Kovar bar along its bottom surface. Digital Image Correlation depicts the deformation of the beam during loading. As seen from the consecutive images, the specimen undergoes progressive failure and provides a visible warning mechanism half-way before reaching the critical load.

- The investigation of a chemical composition that can facilitate casting (e.g. low pouring temperature, minimum tendency of crystallization, easy escape of bubbles) and simultaneously lead to cast components of high strength and fracture resistance, is of importance as well. Such a composition could be an improvement of already existing commercial glass recipes, adjusted to the requirements of casting technology. As an

example, the chemical composition of C-glass fibres[102] could be a starting base for such development, given its increased fluidity at common glass processing temperatures and its increased strength in comparison to typical soda lime silica glass.

- Regarding the research on recycling by casting, further exploration should be made in the recycling of a wider variety of commercial glass waste streams, including specialty glasses, glass ceramics, quartz, aluminosilicate, and wired glass (Figure 8.5). Especially glass ceramics and aluminosilicate glasses are ever-increasing electronic waste streams, which are particularly challenging to recycle due to their much higher melting point and inherent tendency to crystallize. From this research, new flaw types will arise, which should be classified and have their criticality assessed. Further on, efforts should be made in scaling up the proposed glass recycling method to an industrial level. This step should involve the readjustment of the firing schedules and mould materials (especially in case corrosive glasses are recycled such as aluminosilicate) and must be supported by manufacturing guidelines, test data and product certifications.

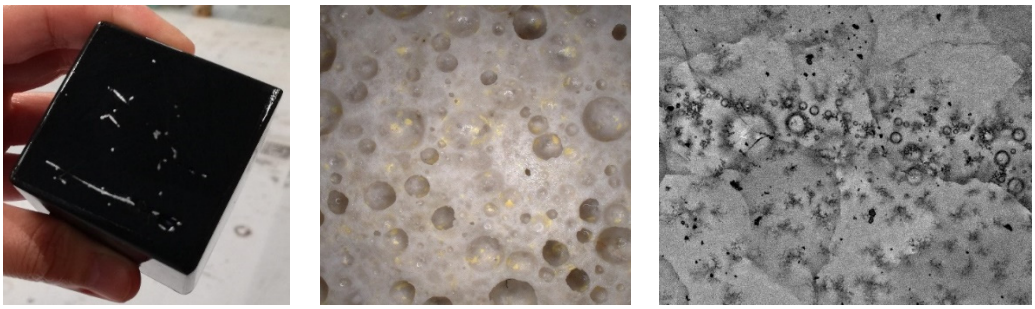

Fig. 8.5 New materials and their corresponding mechanical properties and defects, can evolve from the recycling by casting of a variety of commercial glass waste. Left: specimen produced by kiln-casting wired glass at 1120ºC; the metal wire has been incorporated in the glass and partially molten, giving a black colour to the component (high iron content). Middle: foam structure produced from a recycled phone back-screen. Right: crystal formations developed in a fused phone screen sample, as seen under a digital microscope.

- Exploring further the idea that voluminous cast glass components can tolerate a higher amount of defects without a significant strength reduction, and considering the flexibility of small/medium cast glass foundries in experimenting with different glass recipes compared to the rigidity of larger mass-production glass lines (e.g. float line), the use of more impure sources of raw materials becomes plausible. Assessing if lower-grade batch materials can still lead to cast glass products of acceptable quality and strength is important, to escape the restrictions the glass industry faces with material sourcing (Figure 8.6).

[102] Modified soda lime silica glass with mixed alkali content, higher alkali/lime ratio, and ≈5% addition of alumina and of boron trioxide.

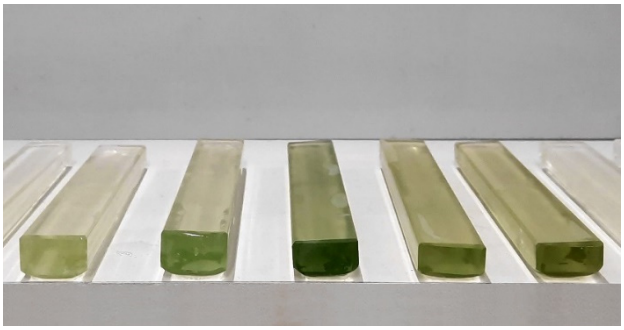

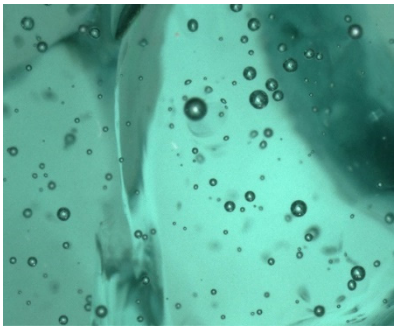

Fig. 8.6 Using impure sand sources from various parts of the world can lead to a variety of new glass recipes and properties. Soda lime silica glass founded using a mixture of pure and volcanic sand (>20% alumina, >15% iron oxide), as seen under a digital microscope; apart from gaseous inhomogeneities, no other defects are observed.

- The introduction of novel cast glass products in the market should be supported by extensive scientific research and validation, the collaboration of the industry and the support of governmental institutions. Guidelines, certifications and regulations must be established to guarantee safe and reliable cast glass structures, and to reduce the risk to be taken by manufacturers, engineers, investors and end-users when engaging with the application of a novel product. This should concern all involved steps from batch material sourcing/cullet recycling to casting methodology, mechanical testing and certification, product quality control, structural engineering, assembly process and maintenance.

References

Belis, J., Callewaert, D., Delincé, D., Van Impe, R.: Experimental failure investigation of a hybrid glass/steel beam. Engineering Failure Analysis 16(4), 1163-1173 (2009). doi:https://doi.org/10.1016/j.engfailanal.2008.07.011

Bristogianni, T., Oikonomopoulou, F.: Reinforced glass: Structural potential of cast glass beams with embedded metal reinforcement In: Zingoni, A. (ed.) Current Perspectives and New Directions in Mechanics, Modelling and Design of Structural Systems. CRC Press, London (2022)

Cupać, J., Martens, K., Nussbaumer, A. Belis, J., Louter, C.: Experimental investigation of multi-span post-tensioned glass beams. Glass Structures & Engineering 2(1), 3-15 (2017). doi:10.1007/s40940-017-0038-5

Cupać, J., Louter, C., Nussbaumer, A.: Flexural behaviour of post-tensioned glass beams: Experimental and analytical study of three beam typologies. Composite Structures 255, 112971 (2021). doi:https://doi.org/10.1016/j.compstruct.2020.112971

Drass, M., Berthold, H., Kraus, M.A., Müller-Braun, S.: Semantic segmentation with deep learning: detection of cracks at the cut edge of glass. Glass Structures & Engineering 6(1), 21-37 (2021). doi:10.1007/s40940-020-00133-7

Hiramatsu, Y., Oka, Y.: Determination of the tensile strength of rock by a compression test of an irregular test piece. International Journal of Rock Mechanics and Mining Sciences & Geomechanics Abstracts 3(2), 89-90 (1966). doi:https://doi.org/10.1016/0148-9062(66)90002-7

Kshinka, B.A., Perrella, S., Nguyen, H., Bradt, R.C.: Strengths of Glass Spheres in Compression. 69(6), 467-472 (1986). doi:https://doi.org/10.1111/j.1151-2916.1986.tb07447.x

Louter, P.C.: Fragile yet Ductile: Structural Aspects of Reinforced Glass Beams. Delft University of Technology (2011)

Martens, K., Caspeele, R., Belis, J.: Experimental investigations of statically indeterminate reinforced glass beams. Construction and Building Materials 119, 296-307 (2016). doi:https://doi.org/10.1016/j.conbuildmat.2016.04.151

Nielsen, J.H., Olesen, J.F.: Mechanically reinforced glass beams. In: The Third International Conference on Structural Engineering, Mechanics and Computation, Cape Town, South Africa 2007. Millpress

Park, J., Riaz, H., Kim, H., Kim, J.: Advanced cover glass defect detection and classification based on multi-DNN model. Manufacturing Letters 23, 53-61 (2020). doi:https://doi.org/10.1016/j.mfglet.2019.12.006

Riedel, H., Mokdad, S., Schulz, I., Kocer, C., Rosendahl, P., Schneider, J., Kraus, M., Drass, M.: Automated Quality Control of Vacuum Insulated Glazing by Convolutional Neural Network Image Classification. Pre-print, (2021)

Veer, F.A., Gross, S., Hobbelman, G.J., Vredeling, M., Janssen, M.J.H.C., Van der Berg, R., Rijgersberg, H.A.: Spanning structures in glass. In: Vitkala, J. (ed.) Glass Processing Days, Tampere, Finland 2003. tamglass ltd.Oy


A

Previous page: Top surface crystallization created at the interface between a copper bearing blue Bullseye glass and a sulphur bearing green Bullseye glass (both modified soda lime silica glasses), fused together at 845ºC.

Appendices

Appendix A: Diffusion experiments

Appendix A consists of the following tables:

A1a-e: Diffusion experiments between clear and coloured transparent or opaque glasses

A2: Flow experiments with clear and red transparent spheres within a 50mm cubic mould

Table A1a: Diffusion experiments, clear and coloured tranparent glass

Glass 1 (clear)	**B270**				
Chemical composition	71.8% SiO_2, 10.3%Na_2O, 6.3% K_2O, 5.1% CaO, 2.2% ZnO, 2.1% Al_2O_3, 1.7% TiO_2, 0.4% Sb_2O_3				
Density (kg/m^3)	2550				
Flow point in °C (viscosity = 10^3 in dPa·s)	915				
Shape	Lenses cut in half, diam. 75mm (320gr)	Lenses cut in half, one full on top (330gr)	Lenses cut in half (≈318gr)	Lenses cut in half (≈318gr)	Lenses cut in half (569gr)
Glass 2 (colour)	**Red transparent**				
Chemical composition	69.1% SiO_2, 12.5%NaO, 9.7% ZnO, 3.8% Al_2O_3, 2.6%K_2O, 1.1% CaO, 0.45% CdO, 0.29% SeO_2, 0.13% S				
Shape	Medium-coarse cullet ≈3*3*6mm (17gr)	Medium-coarse cullet ≈3*3*6mm (21gr)	Medium-coarse cullet ≈3*3*6mm, 17gr	Medium-coarse cullet ≈3*3*6mm, 17 gr	Flat (cast), ≈3mm thick, 50*50mm, 28gr
Glass 1 vs 2					
Position of colour	Bottom	Top	Bottom	Middle/ top	Bottom
Side view					
Density differential	Red glass slightly denser than B270 (White colour in CT scanner indicates higher density over grey colour)				
Viscosity differential	Red glass less viscous and more volatile				
Arrangement of cullet inside the mould (top view)		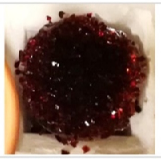			
Max. temperature (°C)	870	870	970	970	970
Hold at max. temp. (hr)	10	10	10	10	10
Hold at 750C at heating (hr)	1	1	1	1	-
Kiln-cast specimen (side view)			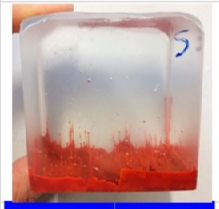		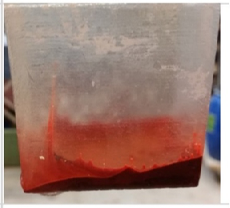
Cross polarized side view (Strainscope Ilis)	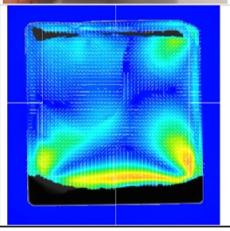	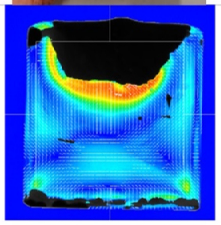	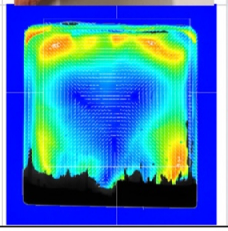	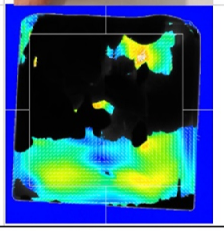	

Table A1b: Diffusion experiments, clear and coloured tranparent glass

Glass 1 (clear)	**B270**				
Chemical composition	71.8% SiO_2, 10.3% Na_2O, 6.3% K_2O, 5.1% CaO, 2.2% ZnO, 2.1% Al_2O_3, 1.7% TiO_2, 0.4% Sb_2O_3				
Density (kg/m^3)	2550				
Flow point in °C (viscosity = 10^5 in dPa·s)	915				
Shape	Lenses cut in half (318gr)	Lenses cut in half, 1 full on top (317gr)	Lenses cut in half (316gr)	Lenses cut in half, 1 full on top (316gr)	Lenses cut in half (317gr)
Glass 2 (colour)	**Red transparent**				
Chemical composition	69.1% SiO_2, 12.5% NaO, 9.7% ZnO, 3.8% Al_2O_3, 2.6% K_2O, 1.1% CaO, 0.45% CeO, 0.29% SeO_2, 0.13% S				
Shape	Medium-coarse cullet (17.3gr)	Medium-coarse cullet (17.1gr)	Medium-coarse cullet (17.2gr)	Medium-coarse cullet (17.2gr)	Medium-coarse cullet (17.5gr)
Glass 1 vs 2					
Position of colour	Bottom	Top	Bottom	Top	Bottom
Side view					
Density differential	Red glass slightly denser than B270 (White colour in CT scanner indicates higher density over grey colour)				
Viscosity differential	Red glass less viscous and more volatile				
Arrangement of cullet inside the mould (top view)				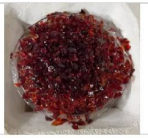	
Max. temperature (°C)	970	970	1120	1120	1200
Hold at max. temp. (hr)	20	20	10	10	10
Hold at 750C at heating (hr)	1	1	-	-	-
Kiln-cast specimen (side view)	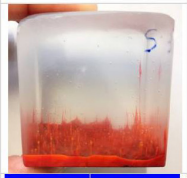		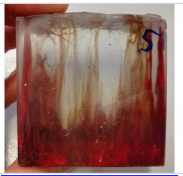		
Cross polarized side view (Strainscope IIIs)	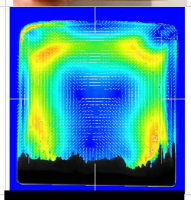	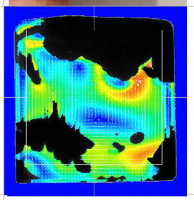	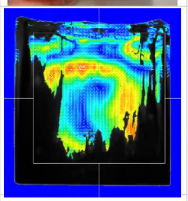	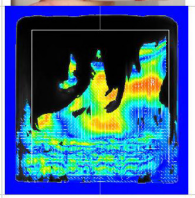	
CT scanner					

Table A1c: Diffusion experiments, clear and coloured tranparent glass

Glass 1 (clear)	**Poesia clear**			
Chemical composition	75.6%SiO_2, 15.8Na_2O, 5.1%CaO, 1.8% K_2O, 0.8% Sb_2O_3, 0.4% CuO, 0.16% Al_2O_3 (& estimated ≈2.5% B_2O_3)			
Density (kg/m^3)	2477			
Flow point in °C (viscosity = 10^3 dPa·s)	877			
Shape	16*50*50mm 2 pieces	16*50*50mm 2 pieces	16*50*50mm 2 pieces	16*50*50mm 2 pieces
Glass 2 (colour)	**Poesia yellow amber transparent**			
Chemical composition	76.9%SiO_2, 17.1%Na_2O, 5.4%CaO, 0.12% K_2O, 0.1% Al_2O_3, 0.08% S (& estimated ≈2.5% B_2O_3)			
Shape	16*50*50mm	16*50*50mm	16*50*50mm	16*50*50mm
Glass 1 vs 2				
Position of colour	Middle vertical layer	Middle horizontal layer	Middle horizontal layer	Middle vertical layer
Side view				
Density differential	Yellow glass seems slightly lighter and more volatile			
Viscosity differential	Yellow glass seems slightly less viscous			
Max. temperature (°C)	970	970	1120	1120
Hold at max. temp. (hr)	10	10	10	10
Hold at 750C at heating (hr)	0.5	0.5	-	-
Arrangement of cullet inside the mould (top view)			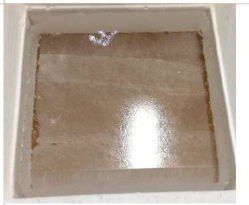	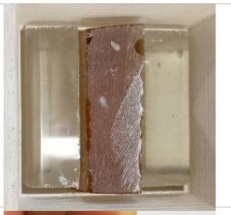
Kiln-cast specimen (side view)	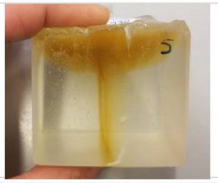		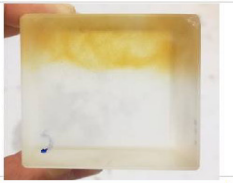	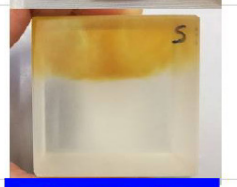
Cross polerized side view (Strainscope Ilis)	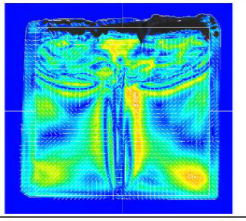	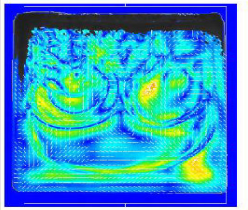	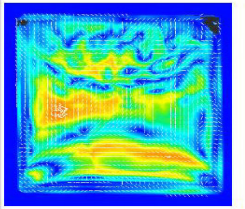	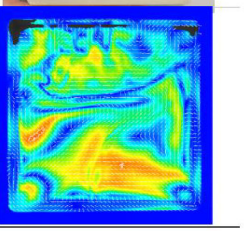

Table A1d: Diffusion experiments, clear and opaque glass

Glass 1 (clear)	**Bullseye tekta clear**			
Chemical composition	74.1% SiO_2, 16.2% Na_2O, 4.5% Al_2O_3, 3.9% CaO, 0.8% K_2O			
Density (kg/m^3)	2500			
Flow point in ^{0}C (viscosity = 10^5 in dPa·s)	835			
Shape	3*50*50mm 14 layers horizontally placed above the green plate	3*50*50mm, 14 layers (7 layers from each side of the green plate)	4 layers 3*50*50mm horizontally placed above the frit , 3mm plates of irregular shape vertically placed on top	3*50*50mm, 14 layers (7 layers from each side of the green plate)
Glass 2 (colour)	**Bullseye Spring Green Opal 0126**			
Chemical composition	76% SiO_2, 9.8% ZnO, 7% Al_2O_3, 4.9% CaO, 0.6% CdO, 0.6% K_2O, 0.2% S			
Shape	3*50*50mm	3*50*50mm	Coarse frit (17.45gr)	3*50*50mm
Glass 1 vs 2				
Position of colour	Bottom	Middle, vertical	Bottom	Middle vertical
Side view				
Density differential	Green glass is denser than tekta clear (White colour in CT scanner indicates higher density over grey colour)			
Viscosity differential	Green glass is more viscous			
Arrangement of cullet inside the mould (top view)	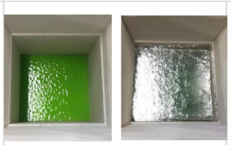	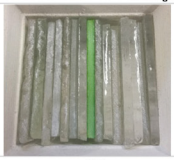		
Max. temperature (^{0}C)	970	970	970	1120
Hold at max. temp. (hr)	10	10	10	10
Hold at 750C at heating (hr)	-	-	-	-
Kiln-cast specimen (side view)	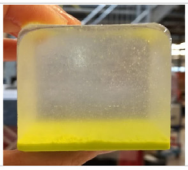	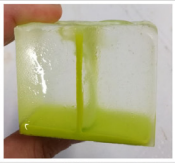	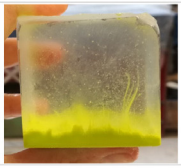	
Kiln-cast specimen (side view)		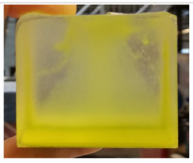		
Cross polarized side view (Strainscope Ilis)				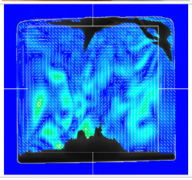
CT scanner				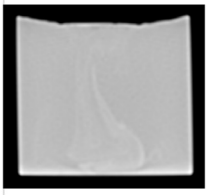

Table A1e: Diffusion experiments, clear and opaque glasses

Glass 1 (clear)	**Bullseye tekta clear**		
Type	74.1% SiO_2, 16.2% Na_2O, 4.5% Al_2O_3, 3.9% CaO, 0.8% K_2O		
Density (kg/m3)	2500		
Flow point in °C (viscosity = 10^5 in dPa·s)	835		
Shape	3mm plates, irregular shape (371gr)	18 layers of 3*50*50mm (296 gr)	3mm plates, irregular shape (412gr)
Glass 2 (colour)	**Bullseye white opal 0013**		**Bullseye Orange opal 0125**
Type			contains selenium, sulfur
Shape	Medium frit (17.3gr)	Medium frit (20.5 gr)	Coarse frit (20.5gr)
Glass 1 vs 2			
Position of colour	Bottom	Top	Bottom
Side view			
Density differential	White glass seems to be denser than tekta clear		
Viscosity differential	White opal glass is more viscous than tekta clear		Orange glass more volatile, less viscous
Arrangement of cullet inside the mould (top view)	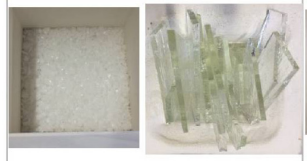		
Max. temperature (°C)	970	970	970
Hold at max. temp. (hr)	10	10	10
Hold at 750C at heating (hr)	1	1	1
Kiln-cast specimen (side view)	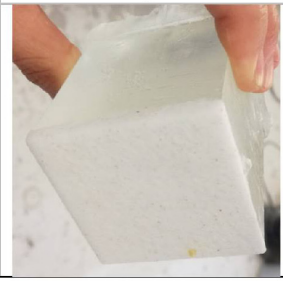	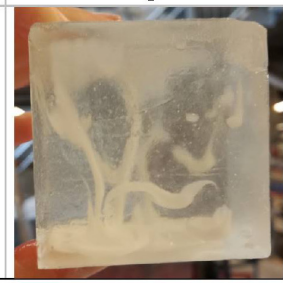	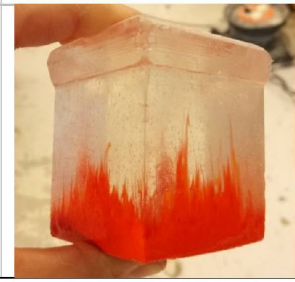

A2: Glass flow experiment, clear and red transparent spheres within a 50mm cubic mould						
Clear glass composition	77.2% SiO_2, 12.9% Na_2O, 6.2% CaO, 1.6% Al_2O_3, 0.4% K_2O					
Red glass composition	69.8% SiO_2, 17% Na_2O, 8.7% ZnO, 3.3% K_2O, 0.4% CdO					
Size	25mm diameter spheres	25mm diameter spheres	25mm diameter spheres, red: 10mm	25mm diameter spheres	25mm diameter spheres	25mm diameter spheres
Initial configuration top layer	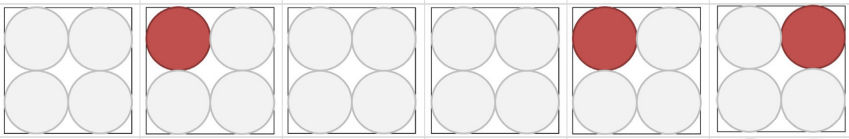					
Initial configuration bottom layer	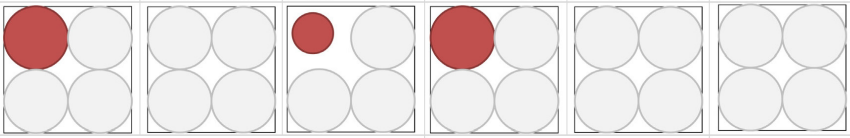					
Top temperature (°C)	**970**			**970**		**1120**
Dwell (hrs.)	10			10		10
Quenching rate (°C/hr)	-160 (down to 600°C)			-160 (down to 560°C)		-150 (down to 560°C)
Top						
Bottom (picture mirrored along y axis)						
Western side						
Northern side	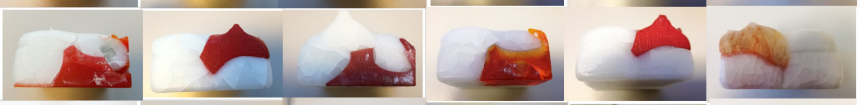					
3D view						
Crystallization	Yes			Red mostly transparent, white crystallized	Yes	Yes

Appendix B: Casting of freeform shapes

Appendix B consists of the following conference papers:

1) Bristogianni, T., Oikonomopoulou, F., Veer, F.A., Nijsse, R.: Design and production of a structural cast glass element for a transparent dome. In: Zingoni, A. (ed.) Insights and Innovations in Structural Engineering, Mechanics and Computation : Proceedings of the 6th International Conference on Structural Engineering, Mechanics and Computation, SEMC, Cape Town, pp. 1662-1667. CRC Press (2016)

2) Bristogianni, T., Oikonomopoulou, F., Veer, F., Snijder, A., Nijsse, R.: Production and Testing of Kiln-cast Glass Components for an Interlocking, Dry-assembled Transparent Bridge. Glass Performance Days 2017 Conference Proceedings, Tampere, Finland (2017)

Design & production of a structural cast glass element for a transparent dome

T. Bristogianni & R. Nijsse
TU Delft, Civil Engineering and Geosciences, Delft, The Netherlands

F. Oikonomopoulou & F. A. Veer
TU Delft, Faculty of Architecture, Delft, The Netherlands

ABSTRACT: In this paper the preliminary study of a novel all-transparent glass dome will be presented. Aim is the design of an elegant and structurally safe transparent large-span dome out of cast glass bricks. These are bonded with a clear, Ultraviolet (UV) curing, acrylic-based adhesive resulting to the maximal transparency and coherence of the structure. With the aid of parametric tools special attention is given to the development of the dome's components in order to minimize the number of different glass bricks required, and thus simplify the production and assembly process. Scale models of the component are produced in the laboratory, to assess its configuration and further study its production method and structural performance. This paper follows the component's production process from the laser-cutting of a reference model, to the construction of a fire-resistant mould via the lost-wax technique, and the kiln-casting of the glass element.

1 INTRODUCTION

In the course of maximizing the incoming daylight in large buildings, glass domes have been realized ever since the Industrial Revolution enabled the use of iron in structures (Schittich, 2007). Since the very first examples, as the wrought-iron glazed dome over the Halle au Blé in Paris in 1889 (Schittich, 2007), a long way has been travelled towards the elegant large-span glass domes of today. However, the prevailing norm is still the construction of domes using steel for the main structure and glass for the cladding. The presence of such steel grids reduces, as a result, the transparency of the dome. Nonetheless, advances over the past 30 years have turned glass into a structural material that can lead to safe, highly transparent structures. Even more, glass by being extremely strong in compression yet weak in tension, is suitable for dome applications, where the structural elements are mainly subjected to compression and only minimum tensile forces appear due to the buckling of the plates or asymmetrical loading by snow or wind load (Wurm, 2007). To that direction, a dome implementing only 8mm float glass, joined with glued aluminum strips, has been realized at TU Delft in 2002, spanning 5,5m (Veer, 2003). Taking the research a step further, the ILEK glass dome spanning 8,5m, constructed at the University of Stuttgart in 2003, eliminates any metal components by the use of an opaque epoxy adhesive to join the 10mm thick glass plates together (Blandini, 2005, 2008).

However, by significantly increasing the span, structures of such high slenderness ratio require either stiffening elements that reduce the transparency to prevent buckling failure, or a total increase of the glass thickness that could clash with the manufacturing standards of float glass. A solution to this challenge can be found in the implementation of adhesively bonded cast glass components in the entire dome structure, which allow for thicker cross-sections and complex three-dimensional configurations while being entirely transparent. A characteristic example of a self-supporting structure out of adhesively bonded cast glass elements is that of the Crystal Houses in Amsterdam, completed in 2016. In this project, a completely transparent UV-curing acrylate of high compression shear strength is used for bonding together the solid cast glass blocks, resulting in a strong glass brick structure that functions monolithically under loading (Oikonomopoulou, 2015). Using this structural system as a starting point, in this paper a concept for a highly transparent dome is proposed, with adhesively bonded cast glass components for the structural grid and cladding.

2 GLASS BRICK DESIGN

2.1 *Design criteria and parameters*

For the development of the cast glass dome concept, a 20m span dome is designed. To achieve a stiff structure with components of comparable size, the configuration of the Buckminster Fuller's Geodesic dome is preferred to a horizontal ring division. Goal is the realization of the dome structure out of the minimum possible number of different hexagonal and pentagonal components with stiffening ribs and flat cladding. For ease of production and assembly, the components' mass should not exceed 10kg. The mass limitation is especially crucial when considering the annealing time of the components, as an increase in mass can exponentially increase the time required for the controlled cooling of the cast component. As an example, the 4kg cast soda-lime glass bricks used at the Crystal Houses required 8 hours of controlled cooling for the relief of the internal stresses. In comparison, bricks of double the mass required 30 hours more (Oikonomopoulou, 2016). This process turns even more complicated when there is unevenness in the component's thickness or sharp angles that lead to different shrinkage and thus to cracks.

2.2 *Setup of parametric model and final design*

A parametric 3D model is made in Rhino3D computer-aided design (CAD) application software with the aid of the plug-in tools Grasshopper for the basic parametric model and BullAnt for the calculation of the geodesic dome. The parameters set in number sliders include the radius of the dome, the order of divisions of the icosahedron on which the dome is based, and the sizing of the ribs and glazing at the bottom and top of the dome. The generated geometry is then evaluated according to the resulting number of different components, the total number of components and the size and mass of the bottom and top piece. The setup of the parameters and output as well as the final design are shown below (Fig.1).

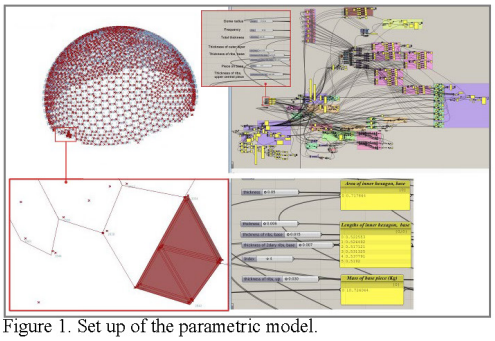

Figure 1. Set up of the parametric model.

3 PRODUCTION TECHNIQUE

3.1 *Experimental approach*

In order to further develop and validate the design, a simplified configuration of a characteristic component in 1:5 scale models is chosen to be reproduced in the laboratory. Purpose of these models is not only to test their mechanical properties but also to give insight into the shape of the bricks in relation to the casting process of the component and the allocation of possible residual stresses.

A simplified geometry of a half hexagonal piece of maximum 89*189*18mm dimensions was chosen for materialization in the laboratory. For the first experiments, the glass ribs along the perimeter are not tapered but considered of constant thickness, and all ribs are slightly enlarged so that they are feasibly cast in 1:5 scale. All sides of the hexagonal component are assumed equal as well.

The production technique of the moulds also varies from the final method to facilitate the low-cost reproduction of several initial test models. At this stage, the moulds are preferred to be inexpensive and disposable in comparison to the final steel precision moulds that should be used for the realization of the dome bricks. For these reasons, the kilncasting method is chosen, where the melting, pouring and annealing of the glass takes place in the same kiln, with the mould kept inside the kiln at all stages.

3.2 *Construction of the moulds*

The technique followed at the TU Delft Glass Lab for the production of the experimental moulds is the so called lost-wax investment casting. With this technique, both the mould as well as the model used as a basis, are disposable by the end of the process. The steps of this process (Fig. 2, 3) are explained below:

1 Production of an accurate model out of 4mm thick Medium-Density Fibreboard (MDF). The 1:5 scaled 3D digital model is horizontally sliced in layers of 4mm thickness, which are further laser-cut and assembled together.
2 Formation of a silicone mould around the MDF model. The two component silicone Siliconenrubber Kapra of 15Pa•s mixed viscosity and 520% elongation at break after curing (De Beeldhouwwinkel 2012) is mixed and poured over the model and let to cure for 16 hours. For easier release, the MDF model is coated with Vaseline.
3 Creation of a removable rigid case around the silicone mould. This is required in order to prevent the silicone mould from deforming when molten

wax is introduced. The rigid case is made out of Supraduro modelling gypsum mixed with water in a volume ratio of 1,75:1 and is let to harden for 1 hour.

4 Casting a wax model of the dome brick by pouring molten wax at 70°C inside the encased silicone mould. When the wax is solidified it can be removed from the silicone mould.

5 Making a heat-resistant mould around the wax model. For the mould, the investment powder Crystalcast M248 is selected, which is composed by Crystalline Silica CAS 14808-60-7 and plaster (SRS, 2003), and can withstand temperatures up to 900°C (Gold Star). The powder is mixed with water in a volume ratio of 2,5:1 and is poured over the wax mould. At least 10mm of thickness are accounted around the wax model, to prevent the mould from cracking. The mixture is stirred to allow the ascend and escape of air-bubbles and is let to cure for 1 hour.

6 Dewaxing the wax model. The cured Crystalcast mould is placed upside down above boiling water and the wax is melt away by the produced steam. The moulds are then cleaned from wax residue with hot water.

7 Calculating the glass volume. The shape to be cast in glass is filled with water and then the volume of the used water is measured by weighing its mass. Using the density equation (1) and applying the density of the glass to be used, the mass of the glass can be found.

$$m_g = V_w \rho_g \quad (1)$$

where m_g = mass of glass; V_w = volume of water; and ρ_g = density of glass.

8 Firing the moulds to remove moisture. The moulds are placed in a ROHDE ELS 200 S Kiln and fired at 125°C for 16 hours, with the ventilation outlet left open for water vapour to escape the kiln.

Upon these steps, the heat-resistant moulds are ready to be used for the kilncasting of the glass components.

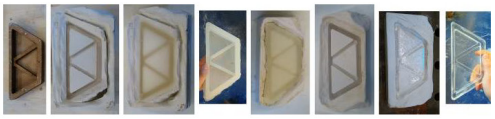

Figure 2. Consecutive steps from base-model to glass: MDF model; silicone mould and rigid plaster case; molten wax pouring; wax model; Crystalcast mould around the wax model; Crystalcast mould after dewaxing; cast glass in Crystalcast mould; final glass product.

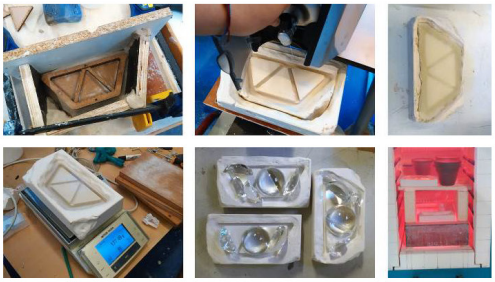

Figure 3. Mould making process and kilncasting: Preparing MDF model for silicone pouring; pouring wax; Crystalcast mould with wax model; calculating the glass volume; free set glass on moulds; kilncasting.

3.3 *Selected type of glass*

B 270® i Ultra-White Glass by Schott is chosen as the raw material for glass casting. This is an optical, highly transparent crown glass (modified soda-lime glass) of 2,55gr/cm^3 density and 91,7% luminance transmittance for 2mm material thickness (Knight Optical) that results in crystal clear castings due to minimum impurities (Desai, 2009).

In Figure 4 a graph of the viscosity of B270 glass as a function of temperature is presented, indicating the working and annealing range of the used type of glass (Knight Optical). In short, glass forms a viscous melt at a viscosity range of 10^5-10^3 Pa•s, which for B270 corresponds to a temperature range of 827-1033°C respectively. Below this temperature, at 724°C and $10^{6.6}$ Pa•s viscosity, we encounter the Littleton softening point, where glass starts to visibly deform under its own weight. During the cooling down of the B270 melt, a critical temperature range is faced between 780- 660°C, which is the dangerous zone for glass crystallization to initiate. At this temperature range the glass has to be subjected to rapid cooling to not allow for sufficient time for the formation of crystals that can result in a cloudy glass of reduced transparency (Shelby, 2005). Upon this point, key temperatures are also the annealing and the strain point, at 541°C and 10^{12} Pa•s, and at 511°C and $10^{13,5}$ Pa•s respectively. At this range the glass has to be subjected to slow and controllable cooling, to release the residual stresses that have occurred during the previous rapid cooling phase. Such stresses develop due to the uneven cooling- thus shrinkage- of the glass object and make the glass susceptible to cracks under small thermal or mechanical shocks. It is therefore crucial to anneal the glass long enough at this range where its viscosity is still sufficient for the glass to keep its shape, while simultaneously it enables molecular rearrangements that result in the release of stresses. The above key temperatures are taken into account for the programming of the firing schedules.

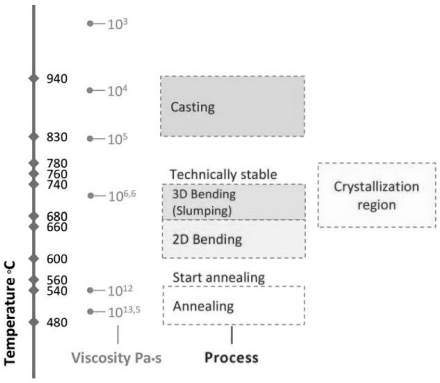

Figure 4. Temperature dependence of viscosity, and corresponding workability for B270 glass.

3.4 *First firing: set-up and results*

For the kilncasting of the glass components, a ROHDE ELS 200 S Kiln is used, with 5-sided heating. For a more even heat distribution at the bottom where no heating elements are present, an elevated ceramic plate is installed, on top of which the moulds are placed. At Firing 1, two moulds, A and B are introduced, with free-set pieces of B270 glass on top, of a mass of 359gr and 322gr respectively. The glass pieces are previously cleaned and oil-free. The heating and cooling rates and dwelling times are presented in Figure 5.

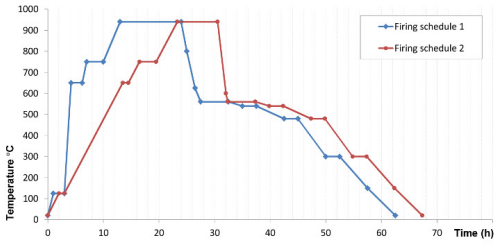

Figure 5. Temperature to time graph for firing schedule 1 & 2.

After the first firing is completed and the moulds are at room temperature, they are immerged in water and let to soak for 20 minutes. This facilitates the removal of the moulds from the glass objects. Once the glass is released from the mould and cleaned, post-processing is required to eliminate the skin left on the glass surfaces in contact with the mould. It should be noted that both moulds presented minor cracks where the mould thickness was close to 10mm, and thus a more robust mould construction should be preferred next time.

In general both glass samples are transparent and without visible air-bubbles. Sample A has a void at its top surface indicating that the mass of the glass pieces placed at this region was not sufficient for covering the full area. Both samples show at their top surface, which was not in direct contact with the mould, signs of crystallization and phase separation. These manifest in opaqueness, rough skin that resembles ice crystals, and droplets that populate the surface. The phenomenon of crystallization, which also affects the phase separation of the melt, occurs by the nucleation and growth mechanism. It initiates with the formation of a nucleus, either spontaneously from the melt (homogeneous) or from the presence of an impurity (heterogeneous) from the mould or air, and grows to a detectable crystal (Shelby, 2005). In our case, the crystallization patterns and milky surfaces seem to initiate from the edges in contact to the mould and are not found in the core of the glass, showing that impurities from the mould and dirt circulating in the air inside the kiln are mostly responsible for this phenomenon rather than the composition of the glass itself. Both samples also present creases at their top surface, especially at the glossy, non-crystallized areas. This pleating of the top surface can be linked to the sudden cooling to which the glass was subjected, which led the skin to contract in a faster rate than the core. Yet, the creasing is mostly located at the perimeter of the samples and at the glazing part, rather than above the ribs. As these areas are in close contact to the mould, the higher shrinkage rate of Crystalcast compared to glass seems to be influencing this phenomenon as well.

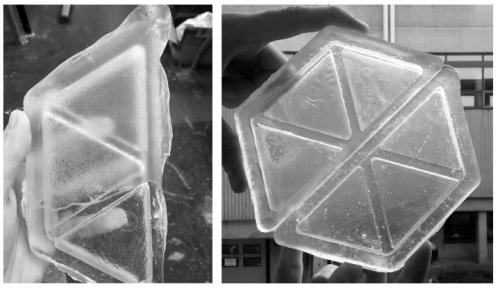

Figure 6. From left to right: Samples A, B and C

3.5 *Second firing: set-up and results*

For firing 2, the prepared moulds are more robust with a higher Crystalcast M248 to water volume ratio of 2,75:1 and thicker walls of minimum 15mm thickness. A slower drying of the moulds is preferred, using a Memmert drying oven, and letting the moulds at 60°C for 2 days. Two moulds, containing samples C and D, are then placed on the elevated ceramic plate of the ROHDE ELS 200 S Kiln. To lower the risk of crystallization and phase separation,

sample D is chosen to be cast via the flowerpot technique and not by placing the glass pieces at the mould, as in sample C. That way, we allow for the glass to melt in the crucible and to flow down into the mould, resulting in a more homogeneous mixture. The glass is also not in contact with the mould during the heating up, therefore is less susceptible to contamination from the vapours exhausting from the mould (Bullseye Glass Co., 2014). To minimize contamination, the terracotta flowerpot used is cleaned before use and the outlet is filed to avoid dirt falling in the glass melt. The flowerpot is placed 250mm above the top surface of the mould. Sample C is fed with 423gr of clean B270 glass while for sample D 446gr of glass are placed in the flowerpot, plus a 10% extra surplus (45gr) that accounts for the material inevitably attached on the surface of the flowerpot (Bullseye Glass Co., 2014). The firing schedule is presented in Figure 5.

From the second firing, certain differences are observed between the results of the free-set and the flowerpot method. Although sample C closely resembles the samples of the first firing with an extensively crystallized opaque top surface, sample D (flowerpot casting) is highly transparent. Yet, the latter has numerous air-bubbles in its volume, trapped during the pouring of molten glass from the flowerpot. This shows that the viscosity of the glass at 940°C is not sufficiently low for the complete release of the trapped air. Also a few minuscule dirt inclusions are found in the sample that could be related to residue dirt from the flowerpot. Creases at the top surface (glossy area) are observed in both samples but in lower extent and magnitude than in the samples of the first firing.

3.6 *Analysis of residual stresses*

A qualitative analysis of the strain concentration and the uniform stress regions is made using a polarized white light source and a crossed polarized film that blocks the transmission of light. Stress-free glass is an isotropic material, so the glass object placed between the polarized light and the polarizing film is seen equally bright through the polarizer. However, when glass is subjected to stress, it exhibits optical anisotropy or birefringence, which corresponds to two refractive indices (McKenzie, 2011). When polarized light passes through the thickness of the glass, it splits into two plane polarized components that travel in two different speeds due to the two different refraction indices. The light beams exert the glass object with a phase difference that results in the presence of colours when seen through the polarizer, called isochromatic fringes. Occasionally, when the principal stress direction at a location is parallel to the plane of polarization, the light exerts the glass object unchanged and thus gets blocked by the polarizing filter. This results in dark areas in the glass sample, called isoclinic fringes. The isoclinic fringes, unlike the isochromatic ones, are independent of the magnitude of the stresses and only mark a path of points with same principal stress. (McKenzie, 2011).

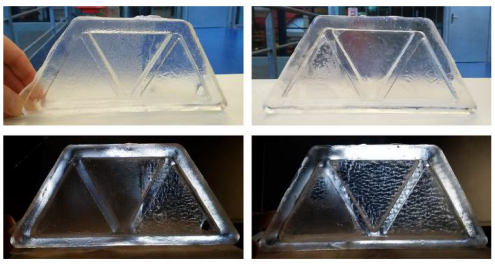

Figure 7. Samples A (left) and B (right) under diffused lighting (above) and as seen through the crossed polarized film (below).

Samples A, B and C present isoclinic fringes when subjected to the polarization test, with the brightest zones mostly being located at the peripheral ribs and around acute angles. The samples show a couple of sharp transition areas from dark to bright that could be attributed to the fusion plane of two broken glass pieces together. The areas of crystallization on the skin surface form repetitive light crosses, a pattern that results from the creation of tensile stress around the crystallized particles (Zschimmer, 2013). This stress is induced by the different expansion coefficient of the amorphous glass and the crystal. In sample C, also isochromatic fringes of yellow tint are present in the top and bottom peripheral rib. Sample D, cast with the flowerpot technique, presents, however, some differences from the above samples. In this case, bright lines cover the entire thickness of both the glazing and the ribs of the sample. These seem to be solidified traces of the swirling of molten glass in the final form of the material. In this sample, we do not see sharp bright areas though, as found in the rest of the specimens.

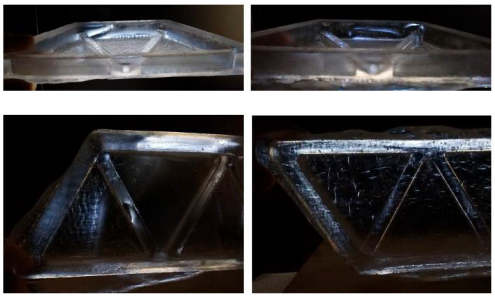

Figure 8. Results of polarization test. Above: Abrupt bright lines found in samples B (left) and C (right). Below: Sample C (left) and D (right).

All the above observations indicate the presence of internal stresses but cannot give a quantitative result. Moreover, it should be taken into account that the rough texture of the glass skin in contact with the moulds, the variations in the thickness of the shape, the translucent areas at the top surface, as well as the presence of air-bubbles, are all parameters that could influence the path of the refracted light, and thus affect the accuracy of the polarization test results. A quantitative analysis was attempted using a Scattered Light Polariscope (SCALP) 04 but the above parameters led to parasitic scattering of the Polariscope's laser beam, and to the inaccuracy of the measurements.

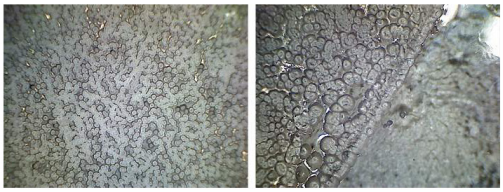

Figure 9. Magnified image of Sample's C top surface using a dnt DigiMicro Scale 2.0 microscope. To the right, the transition from the crystallized to the transparent area can be seen.

4 CONCLUSIONS AND FURTHER STUDY

The conducted research highlights the implications of kiln-casting glass in disposable Crystalcast moulds. The risk of crystallization of the top surface of the samples due to contamination from the mould and the kiln environment is reduced when the flowerpot method is used, yet higher temperatures (≈1050°C) need to be achieved in order for the samples to be air-bubble free. In this context, a more heat-resistant investment powder needs to be tested. Although sudden cooling to the annealing temperature is essential for avoiding the formation of crystals, it bears the risk of creasing at the top surface. Thus, a balance needs to be found in the cooling rate. Regarding the residual stresses, the polaroid test showed probable stress heterogeneity in the samples but this could not be quantified due to the rough finishing surfaces. Both the qualitative and quantitative polarization test should be repeated after the fine polishing of the samples and the results should be compared. The module shape should be optimised towards a more organic form, avoiding sharp edges and acute angles that act as stress concentrators. Following steps include the refinement of the casting technique and the production of the updated design in 1:3 scale models, for the testing of individual and grouped components under compression.

ACKNOLEDGEMENTS

We would like to thank Hein van de Water (SiO_2) and Dawn Bendick (Inside Out Glass Studios) for their guidance and valuable input on the mould-making and kiln-casting process. We are also very grateful to Kees Baardolf (BK, TU Delft) for the technical support, Ate Snijder (BK, TU Delft) for the help with the MDF model, and Kees van Beek (DEMO, TU Delft) and Han de Visser (CiTG, TU Delft) for helping with the polarization test set-up.

REFERENCES

Blandini, L. 2005. The Glass Dome. Glass Processing Days 2005. Tampere, Finland.

Blandini, L. 2008. Structural Use of Adhesives in Glass Shells. Challenging Glass, Conference on Architectural and Structural Applications of Glass. Delft, The Netherlands.

Bullseye Glass, CO. 2014. TIPSHEET 8: Basic Lost Wax Kilncasting. [Online]. http://www.bullseyeglass.com.

De Beeldhouwwinkel. 2012. Siliconenrubber Kapra [Online]. http://www.beeldhouwwinkel.nl.

Desai, J. N. 2009. Advances and processes in Precision Glass Polishing. University of Florida.

Gold Star. Gold Star Powders [Online]. www.siamcasting.com/download/SCP.pdf.

Knight Optical. Technical / Sheet Glasses TSG-B270 [Online]. http://www.knightoptical.com/technical-library/sheet-and-technical-glasses/.

McKenzie, H. W., & Hand, R.J. 2011. *Basic Optical Stress Measurement in Glass*, Sheffield, UK, Society of Glass Technology.

Oikonomopoulou, F., Veer, F., Nijsse, R., & Baardolf, K. 2015. *A completely Transparent, Adhesively Bonded Soda-Lime Glass Block Masonry System.* Journal of Façade Design and Engineering 2, 201-221.

Oikonomopoulou, F., Bristogianni, T., Veer, F., & Nijsse, R. Challenges in the Construction of the Crystal House Façade. In: Louter, C., Bos, F., & Belis, J., ed. Challenging Glass 5, 2016 Gent, Belgium.

Schittich, C., Staib, G., Balkow, D., Schuler, M., & Sobek, W. 2007. *Glass Construction Manual*, Munich, Birkhäuser.

Schott. 2013. B 270® i Ultra White Glass [Online]. http://www.schott.com/advanced_optics/english/products/optical-materials/thin-glass/ultra-white-glass-b-270-i/index.html.

Schott. 2014. TIE-27: Stress in optical glass [Online]. http://www.schott.com/advanced_optics/english/knowledge-center/technical-articles-and-tools/tie.html.

Shelby, J. E. 2005. *Introduction to Glass Science and Technology*, Cambridge, UK, The Royal Society of Chemistry.

SRS. 2003. MSDS Glass Investment Powder [Online]. http://artisanfoundry.co.uk/product_info.php?products_id=131.

Veer, F. A., Wurm, J., & Hobbelman, G.J. 2003. The Design, Construction and Validation of a Structural Glass Dome. Glass Performance Days 2003. Tampere, Finland.

Wurm, J. 2007. *Glass Structures: Design and Construction of Self-supporting Skins*, Germany, Birkhäuser.

Zschimmer, E. 2013. *Chemical Technology of Glass*, Sheffield, UK, Society of Glass Technology.

Production and Testing of Kiln-cast Glass Components for an Interlocking, Dry-assembled Transparent Bridge

Authors

Telesilla Bristogianni 1, Faidra Oikonomopoulou 2, Fred A. Veer 2, Ate Snijder 2, Rob Nijsse 1,2
1 TU Delft, Civil Engineering and Geosciences
2 TU Delft, Faculty of Architecture

Keywords

Cast glass, interlocking components, kiln-casting, glass bridge, dry-assembled transparent load-bearing structures

Abstract

A pedestrian glass bridge, located at the TU Delft campus site, is being designed by the TU Delft Glass & Transparency Group. Specifically, the arch-formed bridge consists of cast, dry-assembled, interlocking glass components. To validate the shape of the components, glass mock-ups in 1:2 scale have been kiln-cast and tested. This paper follows the elements' production process from the 3D milled MDF model and the construction of disposable moulds via the lost-wax technique, to the kiln-casting at 940ºC with the "flowerpot method". Steps are taken towards the refinement of the production technique, with emphasis in minimizing the occurrence of air bubbles, surface flaws and internal stresses that can reduce the load-bearing capacity of the components. Polarisation techniques are employed to define the residual stress distribution of the cast elements as well as to map the consolidated flow of molten glass and the areas of inhomogeneity or non-cohesion. The structural performance of the components and their interlocking behaviour are studied by conducting shear tests on three series comprising three glass bricks with a transparent PU interlayer in-between. The fracture patterns of the specimens are analysed and correlated with the flaws and internal stresses resulting from the kiln-casting process.

1. Introduction

The high compressive strength of glass renders the material suitable for load-bearing applications in structures subjected to compression. In that sense, and inspired by the logic of the Roman arches, a completely transparent glass masonry bridge has been designed by Snijder et al. [1], to be located at the Green Village at TU Delft. The potential of glass masonry systems, comprising adhesively bonded solid glass bricks is well demonstrated by the completion of the Crystal Houses in Amsterdam in 2016 [2]. Developing this innovative glass system a step further, the bridge circumvents the need for an adhesive connection between the glass bricks. Thus it is composed of curved interlocking cast glass components, compressed together to form a stable arch (Figure 1). In-between the glass bricks, a transparent Polyurethane (PU) rubber interlayer is placed, to avoid stress concentrations. Such dry-connections allow for the easy assembly and disassembly of the structure and favour the reuse and/or easy recycling of the individual components. These design decisions result in a more sustainable application of structural glass.

Figure 1 Aspect of the Glass Masonry Bridge and the brick shape

Previous research by [1], [3], [4] led to the current interlocking brick shape that limits the contact of the bricks to the upper and bottom zone of the bridge. This choice leads to a minimum generation of tensile forces in the case of asymmetrical loading. The current paper focuses on the study of the interlocking behaviour of these components. For the purposes of the presented research, a series of glass components have been kiln-cast at the TU Delft Glass & Transparency Laboratory in scale 1:2 and tested in shear. The production of these components differs from the conventional hot-pour casting process which will be used for the final bricks for the bridge, as in kiln casting the glass is cast at a lower temperature and thus with a higher viscosity. The paper studies the production process, to determine the influence on the strength and structural behaviour of the bricks.

2. Production of the components

2.1. Mould production

Disposable investment moulds are prepared for the casting of the glass specimens. The lost-wax technique is- at this initial development stage- preferred, as it allows for the fast and low-cost production of moulds, and thus the easy experimentation with various shapes. The process consists of a series of steps (Figure 2), starting with the accurate milling of the desired brick model in medium-density fibre board (MDF). Based on the MDF model, a silicone counter-mould is produced that serves for the shaping of the brick model in wax. An investment slurry consisting of

Figure 2 Production steps from MDF mould to final glass model

B 270® i Ultra-White Glass by Schott			
Before casting		After casting	
Compound name	Content (wt%)	Content (wt%)	Difference in %
SiO2	71.802	71.883	0.081
Na2O	10.138	9.629	-0.509
K2O	6.275	6.122	-0.153
CaO	5.168	5.575	0.407
ZnO	2.198	2.452	0.254
Al2O3	2.083	1.777	-0.306
TiO2	1.765	1.622	-0.143
Sb2O3	0.403	0.444	0.041
MgO	0.041	0.042	0.001
BaO	0.03	0.286	0.256
Cl	0.022	-	
S	0.018	0.058	0.04
Er2O3	-	0.043	
P2O5	0.017	0.014	-0.003
Fe2O3	0.016	0.018	0.002
ZrO2	0.008	0.009	0.001
SrO	0.006	0.008	0.002
Rb2O	0.005	0.005	0
NiO	-	0.004	
CuO	-	0.004	
PbO	0.005	0.003	-0.002

Table 1 Composition of B 270® before and after kiln-casting

1 part water to 2.8 parts Crystalcast M248- a powder mixture of Cristobalite, Quartz and Gypsum [5]- is poured around the wax and left to cure. The steaming out of the wax model results in a heat-resistant mould, suitable for glass casting up to 900°C temperature. After the casting is completed, the mould is removed by submerging it in to water, which dissolves down the investment material. A more detailed description of the above process is described in [6].

2.2. Selected type of glass

The selected glass for the castings is B 270® i Ultra-White Glass by Schott, an optical highly transparent crown glass used for optical applications [7]. Zschimmer [8] stresses the importance of such potash-lime-silica systems -the base of crown glass- in glass technology, due to their lack of colour when compared to typical soda-lime-silica systems. The glass used is shaped in the form of lenses of 70mm diameter.

The exact glass composition is analysed with a Panalytical Axios Max WD-XRF spectrometer and the data are evaluated via SuperQ5.0i/ Omnian software. As seen in [Table 1] Zinc oxide is also included in the recipe, a compound contributing, as well, in the colourlessness of the glass [8].

[Figure 3] provides insight to the viscosity of the glass used as a function of the temperature. In short we encounter the softening point at 724°C, the annealing point at 541°C and the glass's strain point at 511°C [9]. The forming temperature starts from 827°C.

Firing no	10		11			14		19	
Brick number	a	b	1	2	3	a	c	c	f
Position in the kiln (door at bottom)									
Flowerpot arrangement									
Distance flowerpot-mould (mm)	40	40	30	30	40	0	0	25	40
Diameter of flowerpot (mm)	20	20	14	14	14	12, 14	12	14	14
Air bubbles									
Air-bubble size (mm)	≤ 3	≤ 2,5	≤ 1	≤ 1	≤ 1	≤ 1	≤ 1,5	≤ 1 (2 bubbles: 3,5)	≤ 1 (2 bubbles: 3,5)
Surface crystallisation	no	no	yes	yes	yes	no	no	no	no
Internal stresses (front side)	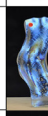								
Internal stresses (concave side)									

Table 2 Variables and results regarding Firings 10, 11, 14 and 19

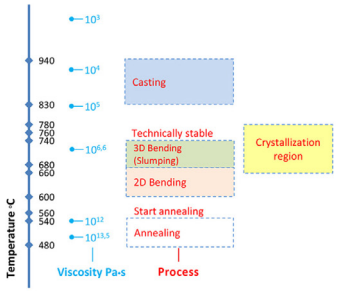

Figure 3 Viscosity of B 270® glass as a function of temperature

2.3. Casting set-up and firing schedules

The glass bricks studied in this paper are produced by kiln-casting [Figure 4]. This production technique employs a single kiln for the melting of the glass into the moulds and for the subsequent annealing process. As the investment moulds remain in the kiln throughout the whole process, they define the maximum heating rate [50°C/hr] and maximum temperature [900°C] that can be reached [10]. These specifications are tested by the authors and adjusted up to a heating rate of 75°C/hr and a maximum temperature of 950°C. The maximum temperature reached corresponds to a glass of 10^5 dPa•s viscosity [9]. This viscosity value is considerably higher than in the hot-pour casting method, which is planned for the final production of the bricks. Indeed in such a method, viscosities of around 10^3 dPa•s or less are achieved [11], to guarantee a homogeneous and air-bubble free mixture. Questions are therefore raised regarding the homogeneity, cohesion and strength of the glass components produced by the kiln-casting method. The above mentioned aspects will be examined below. The "flowerpot" casting method is employed for the feeding of the glass into the moulds. This method suggests the positioning of terracotta flowerpots filled with glass above the moulds. At forming temperatures, the glass drops down through the flowerpot hole and fills the mould [Figure 5].

Figure 4 Kiln-casting method

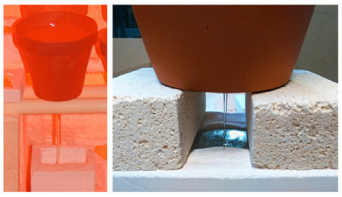

Figure 5Glass flowing from the flowerpot down to the mould

Firing schedule 10		
Temperature (°C)	Ramp (°C/h)	Dwell time (h)
25		
	50	
750		2
	50	
850		2
	30	
950		7
	-160	
870		1
open door	-105	
606		
	-160	
580		4
	-2	
540		12
	-2	
510		12
	-2	
480		4
	-30	
300		2.5
150	-30	0
20	-25	0

Firing schedule 11		
Temperature (°C)	Ramp (°C/h)	Dwell time (h)
25		
	75	
750		2
	75	
850		1
	40	
940		28.5
	-160	
870		2
open door	-113	
616		
	-160	
580		4
	-2	
540		12
	-2	
510		12
	-2	
480		4
	-30	
300		2.5
150	-30	0
20	-25	0

Firing schedule 14		
Temperature (°C)	Ramp (°C/h)	Dwell time (h)
25		
	50	
350		1
	50	
750		1.5
	50	
850		2
	30	
940		9
	-160	
870		2
open door	-125	
600		
	-160	
560		12
	-2	
540		12
	-2	
510		12
	-2	
480		4
	-30	
300		2.5
150	-30	0
20	-25	0

Firing schedule 19		
Temperature (°C)	Ramp (°C/h)	Dwell time (h)
25		
	50	
750		1
	50	
850		1
	50	
940		8
open door	-260	
617		
	-160	
560		6
	-2	
540		12
	-2	
510		12
	-2	
480		6
	-30	
300		0
150	-30	0
20	-30	0

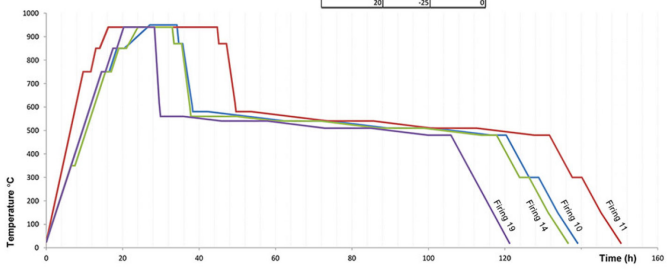

Table 3 Firing schedules 10, 11, 14 and 19

Four firings- Firing 10, 11, 14 and 19- are conducted for the production of the glass bricks, using a ROHDE ELS 200 S Kiln with 5-sided heating. Different variables regarding the casting set-up are presented in [Table 2]. The position of the mould in the kiln, the number of used flowerpots, the distance of the flowerpots from the mould and the radius of the flowerpot hole are documented so that their influence to the final product is examined. The four firing schedules followed are presented in [Table 3]. Although the schedules are mainly similar, a few alternations do occur between them. Regarding the heating up of the moulds and glass, Firing 10 has the slowest process, lasting 27hrs while Firing 11 has the fastest, lasting 16hrs. At top temperature, Firing 11 has a considerably higher dwell, reaching 28.5 hrs while the rest of the firings have a dwell between 7-9hrs. Regarding the temperature drop from the forming temperature to the annealing point, in Firing 10, 11 and 14, this occurs in two steps, one from 940°C to 870°C at -160°C/hr rate (including 1-2hrs dwell at 870°C) and a second step at approx. -105 to 125°C/hr rate (executed by consecutively opening and closing the kiln door). In Firing 19, the intermediate step at 870°C is avoided, and the cooling down occurs at a -260°C/hr rate (aided by the opening of the kiln door). Finally, in Firings 10 and 11, the annealing soak starts at 580°C while in Firings 14 and 19 it starts lower, at 560°C. In Firing 19, the annealing soak time is half that applied in Firing 14.

3. Assessment of the cast components

3.1. Contamination

An X-ray fluorescence (XRF) analysis is conducted with a Panalytical Axios Max WD-XRF spectrometer on a glass specimen resulting from Firing 11. The resulting composition, seen in [Table 1] is compared to the original glass recipe. The difference in content of the main compounds is not exceeding the percentage of +-0.5, therefore significant alternations in the glass recipe are not observed. Impurities due to contamination from the Crystalcast mould do appear, in percentages below 0.05, namely Nickel Oxide (NiO=0.004%), and Copper Oxide (CuO=0.004%). The content of Barium Oxide (BaO) and Sulfur (S) is also increased due to contamination from the mould. Especially interesting is the presence of Erbium Oxide (Er_2O_3=0.043%) after casting. This is an expensive element often used in soda-lime silicate glasses as a luminescent dopant or to create optical amplifiers [12], [13]. Since optical glass lenses are used for melting, it is possible that Erbium traces exist in the original recipe and were not traced in the XRF test. An XRF analysis of the Crystalcast is required to define which of the above impurities are indeed attributed to the investment material.

3.2. Air-bubble entrapment

In [Table 2] the distribution and sizing of the entrapped air is seen. It can be observed that the most influential parameters for the size and spreading of the air-bubbles is the size of the flowerpot hole and its distance from the mould. The least air-content is seen in Firing 14, where the minimum flowerpot hole diameter and distance from the mould is found. This can be explained if we focus on the melting and pouring process, as this occurs from the flowerpot to the mould [Figure 6]. First, the glass starts to melt from the boundaries of the flowerpot towards its interior. As the lenses start to fuse together, big bubbles are formed due to the initial existing voids from the stacking of the lenses. Then, the molten glass- with the big bubbles present- starts to flow down the mould and mix with the existing air, creating a new series of big bubbles. The more the level of the molten glass rises in the mould, the less the impact the glass has when dropping and thus the smaller the created air-bubbles. Considering the above, the reduction of the path to be travelled by the molten glass stream (flowerpot closer to the mould) creates less turbulence and thus less air-bubbles. This is also the case with a smaller stream diameter (smaller flowerpot hole). Moreover, a small flowerpot hole prevents the big bubbles formed in the flowerpot to pass through together with the glass. In Firing 14, the use of two smaller flowerpots instead of one bigger further contributes, as less voids occur while stacking the glass lenses inside the smaller pots. The increase of the dwell time at top temperature seems to be less decisive than the above variables in the content of air. This is observed in the samples of Firing 11 -kept at top temperature for approx. 20hrs more than the other samples- that still have a high content of air-bubbles. In Firing 19- the only firing that has one abrupt cooling stage directly from 940°C to 617°C at -260°C/hr rate- an intense swirling of miniature air-bubbles is seen. It should be noted that this firing schedule also

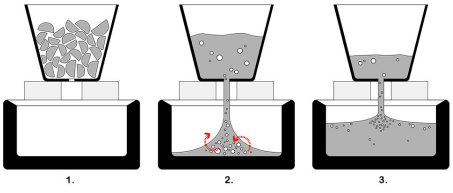

Figure 6 Air-entrapment during kiln-casting

has the fastest heating rate from the start of the forming temperature towards the top temperature. This fast heating implies that the glass is dropping in a faster rate and while larger differentiations in the temperature of the melt occur. This is expected to intensify the swirling of the molten glass inside the mould. Moreover, the fast cooling abruptly "freezes" the air-bubbles in place. At the top surface of both bricks, two bubbles of larger diameter were about to escape when they got trapped in the glass by the abrupt cooling. This shows that similar bigger bubbles (caused at the initial melting step) that existed in the samples of the other firings had enough time to escape with a slower cooling rate. In principle, such bubbles have a bigger volume that creates a bigger upward force, making their escape easier than in the case of the smaller bubbles (that even after 28.5hrs at 940°C in Firing 11, they were still present). Finally, the position of the moulds in the kiln has negligible influence in the formation of air-bubbles.

3.3. Surface crystallization

Crystallization at the top surface is only observed in the samples of Firing 11. This crystallization appears in the perimeter of the bricks, where the glass surface is in contact with the mould. The nucleation is thus linked to the mould material and possibly to the contamination of the air circulating inside the kiln. Although the dangerous crystallization zone of B 270 glass is empirically located between 780-660°C, the prolonged presence of the samples at top temperature and the extra hour of dwell at 870°C seems to affect the growth from the nuclei. As the temperature range of crystallisation can differ with the nucleating agent [14] an analysis of the percentage of crystallinity should be conducted in order to identify the present crystal.

3.4. Internal stresses

A qualitative estimation of the strain concentration and the uniform stress regions is made by projecting a polarized white light source behind the bricks and photographing them with a crossed circular polarized filter. Areas subjected to stress exhibit optical birefringence, causing the polarized light beam to exert the glass object with a phase difference that corresponds to the presence of isochromatic fringes [15]. In [Table 2] the results of the polarized pictures can be seen and compared. In general, regardless the firing schedule, the location of the moulds in the kiln, and the number of flowerpots used, all bricks seem to have the same stress distribution [Figure 7]. The geometry of the brick is thus catalytic in the arrangement of these stress regions. The polarized images suggest that these regions are linked with the manner the molten glass is flowing from the flowerpot stream inside the specific shape of the mould. This is especially evident when studying the polarized images of the concave side of the bricks [Figure 8]. The regions imply that the flowing glass mass - due to its relatively high viscosity at the top temperature- does not entirely cohere throughout the total volume, resulting thus to the occasional appearance of fusion lines/strips. The described layering is particularly evident in the bricks of Firing 19 that are abruptly cooled to the annealing point. Regarding the quantity of the stresses, the bricks of Firing 10, as well as the bricks 11-1 and 19c have higher internal stresses. Other factors -for example the location of the moulds in the kiln and therefore their proximity to the kiln-door, the heating elements or other moulds- seem to interfere with the cooling schedule of the bricks, causing the observed irregularities. The samples presented in this paper are not sufficient for drawing conclusions on the exact effect of these factors.

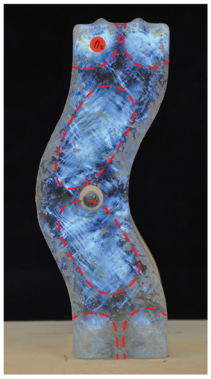

Figure 7 Typical stress zones after the kiln-casting of the bricks (Polarized image)

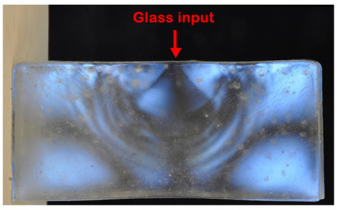

Figure 8 The polarized images show the flow patterns of the glass

4. Experimental validation

4.1. Experimental set up

The bricks with the least internal stresses, layering and air-bubbles are chosen for the shear experiment. Regarding the experimental set up, three glass bricks with a 2mm thick PU rubber sheet of hardness 70A in between, are framed by two steel L-shaped frames [Figure 9]. The frames are fixed on the base of a Zwick Z100 displacement controlled universal testing machine. Two extra steel plates welded at the frames prevent the side bricks from moving downwards. In between the compression head and the middle brick, an aluminium profile is placed that fits the dimensions of the brick. Loose acrylic parts shaped to match the brick's geometry are placed on the one side for support. The L frames are bolted together until the bricks are fixed in place. Between the horizontal surfaces of the glass components and the elements of the setup, 2mm thick sheets of neoprene are placed. Three shear tests are conducted until failure, with a displacement speed of 10mm/min. The bricks are lit with white polarized light and photographed during the experiment with a crossed circular polarisation filter.

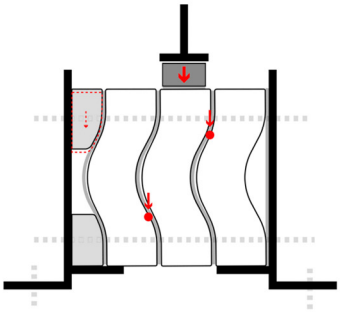

Figure 9 Experimental set-up

4.2. Results

In [Figure 10] the load is plotted versus the displacement. Since the contact area between the bricks is limited to their upper and lower part, two point loads develop at the side bricks [Figure 9] during the loading of the middle brick. All tests terminate with the failure of the brick on the right that is confined between the middle glass brick and the L-shaped frame. The loose acrylic parts in contact with the brick on the right allow, in fact, for minor adjustments in the position of this brick and therefore the development of a more favourable load case. The point load acting on the right brick subjects it to bending, creating a zone of tension at its concave surface, from where eventually all bricks start to crack. In [Figure 11], the gradual increase of the number of isochromatic fringes in proportion to the

increase of the external loading can be seen [16]. In [Figures 12] the correlation between the areas where the isochromatic fringes appear during the experiments and the fracture zone of the bricks is seen. In addition, the fracture patterns are linked with the initial polarized images of the bricks, to determine possible defects that could affect the crack path. It is observed that within the weakest zone dictated by the load case, possible flaws found in the glass from the casting become the origins of fracture. This is particularly evident in Test 2/ Brick 14a, where the crack originates from an impurity cluster combined with an air-bubble. Such clusters are not directly observed in the other two cracked bricks (11-3, 14c) which could explain why these bricks failed at double the load. Regarding the path of the cracks, they tend to follow fusion lines and internal stress regions found in the initial polarized images. In brick 11-3 (side view) for example, the crack spread corresponds to a cone region formed exactly below the flowerpot. In the case of brick 14a, when removing the initially attached flowerpot, a damaged glass zone around the terracotta traces was created, which acts as an attraction to the crack path. In [Figures 13] a wave is seen at the crack travelling through brick 11-3 and 14c. Such local deviations can be caused by internal stresses or in-homogeneities [17]. Areas of lower fracture toughness could occur due to the kiln-casting process, introducing weaker zones that divert

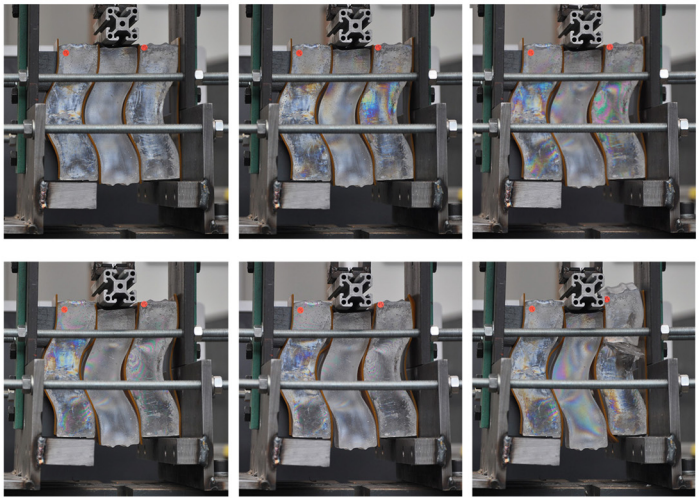

Figure 11 Polarized pictures of Test 1, showing the increase of the stresses developed in the glass

Figure 12 Superposition of the fracture paths of the broken bricks and the polarized images of the bricks before and during testing (prior to failure)

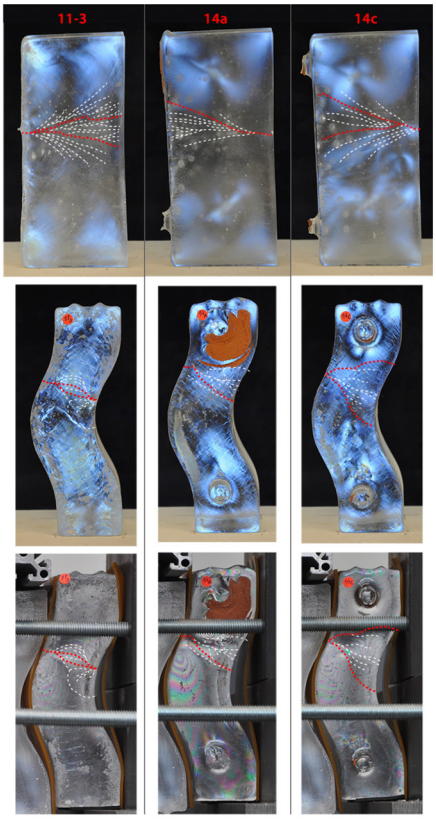

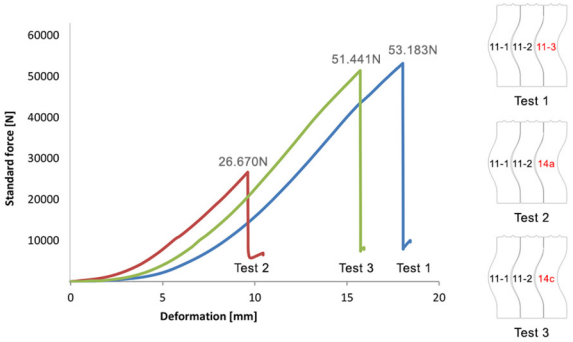

Figure 10 Load versus displacement diagram

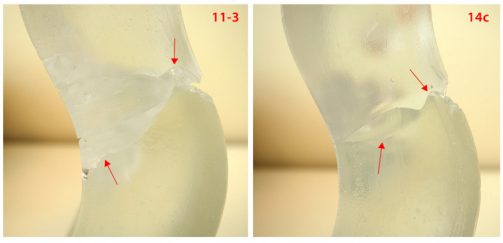

Figure 13 Fracture paths of bricks 11-3 and 14c

the crack. An indentation test should be conducted to define possible differences in the fracture toughness along the glass mass.

5. Conclusions

In this paper, interlocking kiln-cast glass components are produced and tested, to define their structural performance. The analysis of the kiln-casting method and its results highlights the influential factors on the quality of the glass components. The process can be optimized when a slower heating rate is adopted, in combination with the use of smaller flowerpots placed directly above the moulds. This is crucial, as flaws generated during the casting stage can initiate failure when subjected to tension. The polarized images of the bricks indicate zones of fusion and inhomogeneity in the glass, due to casting at a relatively high viscosity. Upon brick failure, these are considered weak zones that attract the path of the crack. The kiln-cast bricks -produced for the first experimental phase- form therefore the worst case scenario, as the final hot-poured bricks are not expected to contain these flaws in such extent. Nonetheless, the governing factor in the failure mode of the bricks is the applied load case. In that sense, questions arise whether the partial contact of the bricks at their bottom and top surface- which introduces point loads- is desired. The redesign of the bricks so they achieve full contact along their height could enhance the structural performance of the system and should be experimentally validated in the next research phase.

References

[1]. Snijder, A., Smits, J., Bristogianni, T. & Nijsse, R., Design and Engineering of a Dry Assembled Glass Block Pedestrian Bridge in Challenging Glass 5, B.L. Belis, Editor. 2016: Ghent.
[2]. Oikonomopoulou, F., Bristogianni, T., Veer, F., and Nijsse, R., The construction of the Crystal Houses façade: challenges and innovations. Glass Structures & Engineering, 2017: p. 1-22.
[3]. Sombroek, I., Structural cast glass; A research process of design and experiment towards a feasible geometry for a cast glass element, in Architecture and The Built Environment. 2016, TU Delft.
[4]. Aurik, M., Structural Aspects of an Arched Glass Masonry Bridge, in Civil Engineering and Geosciences 2017, TU Delft.
[5]. SRS. MSDS Glass Investment Powder. 2003; Available from: http://artisanfoundry.co.uk/product_info.php?products_id=131.
[6]. Bristogianni, T., Oikonomopoulou, F. Veer, F. A. & Nijsse, R,. Design and production of a structural cast glass element for a transparent dome. in Proceedings of the 6th International Conference on Structural Engineering, Mechanics and Computation, SEMC 2016. 2016. Cape Town, South Africa: CRC Press.
[7]. SCHOTT. B 270® i Ultra White Glass. 2013; Available from: http://www.schott.com/advanced_optics/english/products/optical-materials/thin-glass/ultra-white-glass-b-270-i/index.html.
[8]. Zschimmer, E., Chemical Technolodgy of Glass, ed. M. Cable. 2013, Sheffield, UK: Society of Glass Technolodgy.
[9]. KNIGHT, OPTICAL. Technical / Sheet Glasses TSG-B270. Available from: http://www.knightoptical.com/technical-library/sheet-and-technical-glasses/.
[10]. Gold, Star. Gold Star Powders. Available from: www.siamcasting.com/download/SCP.pdf.
[11]. SCHOTT, Technical Glasses, Physical and Technical Properties. 2014: Germany.
[12]. Krsmanović, R., Bertoni, G. & Van Tendeloo, G. Structural Characterization of Erbium doped LAS Glass Ceramic Obtained by Glass Melting Technique. in Eighth Yogoslav Materials Research Society Conference "YUCOMAT 2006". 2006. Herceg-Novi.
[13]. Lægsgaard, J., Dissolution of rare-earth clusters in SiO2 by Al codoping: A microscopic model. Physical Review B (Condensed Matter and Materials Physics), 2002. Vol. 65(No. 17): p. p. 174114.
[14]. Thieme, K., Avramov, I. & Rüssel, C., The mechanism of deceleration of nucleation and crystal growth by the small addition of transition metals to lithium disilicate glasses. Scientific Reports, 2016. 6: p. 25451.
[15]. McKenzie, H.W., & Hand, R.J., Basic Optical Stress Measurement in Glass. 2011, Sheffield, UK: Society of Glass Technology.
[16]. Post, D., Photoelasticity, in Manual on Experimental Stress Analysis, J.F. Doyle, Phillips, J. W. & Post, D., Editor. 1989, Society for Experimental Mechanics: Michigan.
[17]. Quinn, G.D., Fractography of Ceramics and Glasses. 2007: National Institute of Standards and Technology.

Acknowledgements

The authors would like to thank Hein van de Water (SiO2) and Dawn Bendick (Inside Out Glass Studios) for their guidance on the mould-making and kiln-casting process, Lida Barou (CiTG, TU Delft) for assisting with the artwork, Kees Baardolf (BK, TU Delft) for the experimental set-up, Remko Siemerink (BK, TU Delft) for the milled MDF model, Ruud Hendrikx (3mE, TU Delft) for the XRF analysis, and Clarissa Justino de Lima (CiTG, TU Delft) for her insight in glass chemistry.

Appendix C: Ultrarsonic measurements of E modulus

C: Ultrasonic measurements in cast glass 50mm cubes

Sensor 54KHz Proceq Transducer, Gain 1*, Voltage 50V, lubricant DC4 electrical compound by Dow Corning

Specimen name		Mirror (blue)	Fully tempered window	Maltha flat glass mix (black cube)	Poesia glass transparent+amber	B270 optical lenses	B270 optical lenses + red cullet	SIU gaffer glass	Leerdam dark amber
Glass description		Soda lime silica (float), barium/zinc coating	Soda lime silica (float)	Soda lime silica (float), various coatings or tints	Soda lime silica, 5% CaO, 2.5% B_2O_3	Potassium soda lime silica	Potassium soda lime silica + floating red glass	Soda silica, ZnO	Lead crystal, various colours
Cube	Mass (gr)	312.41	312.17	314.06	309.03	319.98	323.95	363.23	393.79
	Volume (ml)	120.86	120.14	123.98	120.71	125.29	129.31	125.87	122.42
	Density (Kg/m^3)	2584.89	2598.39	2533.15	2560.10	2553.91	2505.22	2885.76	3216.71
Side A	Distance (mm)	49.96	49.95	50.62	50.27	50.25	50.52	50.34	50.04
	Transmission time (µs)	9.1	9.2	9.3	9.7	9.5	9.5	10.4	11.4
	Velocity (m/s)	5490.11	5429.35	5443.01	5182.47	5289.47	5317.89	4840.38	4389.47
	E modulus (GPa)	**77.91**	**76.59**	**75.05**	**68.76**	**71.45**	**70.85**	**67.61**	**61.98**
Side B	Distance (mm)	50.29	50.21		49.6	50.51	51.32	50.2	51
	Transmission time (µs)	9.3	9.2		9.7	9.5	9.6	10.5	11.5
	Velocity (m/s)	5407.53	5457.61		5113.40	5316.84	5345.83	4780.95	4434.78
	E modulus (GPa)	**75.59**	**77.39**		**66.94**	**72.20**	**71.59**	**65.96**	**63.26**

*E modulus= density*velocity^2*

Curriculum Vitae

Photo by F. Oikonomopoulou

Telesilla Bristogianni

Born in Athens on July 24, 1984

Education

2016-2022	**PhD Candidate** TU Delft, Faculty of Civil Engineering and Geosciences, 3Md Department
2010-2012	**MSc in Building Technology** (Cum Laude) TU Delft, Faculty of Architecture and the Built Environment
2002-2009	**MArch in Architectural Engineering** (Excellent, Class rank: 5th of 212) National Technical University of Athens School of Architecture

Work Experience

2021-now	**Post-doc researcher and lecturer** TU Delft, Faculty of Architecture and the Built Environment, AE+T Department
2014-2020	**Researcher** TU Delft, Faculty of Civil Engineering and Geosciences, Engineering Structures Department, 3Md Department
2012-2014	**Architect / Research Assistant** at SHAU Rotterdam
2008-2010	**Junior Architect** at Zerefos Tessas Architects, Athens

Key Projects

2021-now	**Mirage Sculpture at Apple Cupertino Headquarters**
2017-now	**Re^3 Glass research project**

Partially funded by 3TU. Bouw Lighthouse 2016, 4TU. Bouw Lighthouse 2017

2021 **Recyclability of glass display screens** (industrially funded)

2021 **Qaammat UNESCO Pavilion**, Greenland

2014-2016 **Crystal Houses Façade,** Amsterdam, NL

Awards

2022 **Young Researcher Award SGAMR-YRA-2021**
by the Editorial Board of the International Journal of Structural Glass and Advanced Materials Research

2022 **AE+T Photography Competition Award.** Winner in the computer image category.

2022 **Architizer A+Awards, Popular Choice Winner: Pavilion Category** for the Qaammat Pavilion. Conjoint award: Konstantin Arkitekter and TU Delft

2021 **Best paper award 2020 Glass Structures & Engineering**
by the Editors in Chief of the Glass Structures & Engineering Journal. Conjoint award with Oikonomopoulou, F., Yu, R., Veer, F., Nijsse, R.

2021 **Architect Magazine's 2021 R+D Award** for the Glass Vault project. Conjoint award with SOM, Princeton University and TU Delft

2020 **STARTS prize 2020 Nominee**
by Ars Electronica for the Re^3 Glass project. Conjoint nomination with Oikonomopoulou F.

2019 **Honourable Award by Bouwend Nederland**
for the contribution to innovative research on structural glass of the Glass & Transparency Research Group of TU Delft

2018 **New Material Award 2018 Nominee**
by Het Nieuwe Instituut, Fonds Kwadraat & Stichting Doen for the Re^3 Glass project. Conjoint nomination with Oikonomopoulou F.

2017 **Talent met Toekomst, Nederlandse Bouwprijs 2017**
for the Crystal Houses Façade. Conjoint award with Oikonomopoulou F.

2016	**Outstanding Innovation Award 2016 by the Society of Façade Engineers** for the Crystal Houses Façade. Conjoint award: TU Delft and ABT
2016	**Innovation Award, Glas Award 2016** for the Crystal Houses Façade. Conjoint award: MVRDV, TU Delft, ABT, Poesia
2016	**Public Award, Dutch Design Awards 2016** for the Crystal Houses façade. Conjoint award: MVRDV, TU Delft, ABT, Poesia

Key Exhibitions

2022	**LWL-Industriemuseum Glashutte Gernheim** Exhibition of recycled glass panels in walk-in sculpture "Transparent Things" at Gernheim Glassworks (Germany), in collaboration with FUTUR21 and TH OWL.
2021-now	**Parlamentarium** (European Parliament's Visitor Centre in Brussels). Exhibition of Re^3 Glass recycled components at the Topics Media Station, as representative project for the topic of Climate Change
2020	**Bozar**, Brussels Exhibition of the "Re^3 Glass" project as part of the STARTS PRIZE 2020 nomination
2020	**Anatomy of Structure: The Future of Art and Architecture**, London. SOM exhibition in collaboration with Princeton University, TU Delft, and Global Robots
2019-now	**Vitra Design Museum, Schaudeport Lab,** Germany Exhibition of prototypes from the "Re^3 Glass" project at the material library
2019	**Salone del Mobile 2019**, Alcova, Milan Exhibition of the "Re^3 Glass" project as part of the New Material Award nomination
2018	**Dutch Design Week 2018**, Eindhoven Exhibition of the "Re^3 Glass" project as part of the New Material Award nomination
2018	**Venice Design at Palazzo Michiel**, Venice 16th International Architecture Exhibition | La Biennale di Venezia 2018. Exhibition of the "Re^3 Glass" project, TU Delft BK Booths

List of Publications

Journal Papers as first author

Bristogianni, T., Oikonomopoulou, F.: Glass up-casting: A review on the current challenges in glass recycling and a novel approach for recycling “as-is” glass waste into volumetric glass components. Accepted for publication in Glass Structures & Engineering, T.I.: Glass Circularity (2022).

Bristogianni, T., Oikonomopoulou, F., Veer, F., Nijsse, R.: Exploratory Study on the Fracture Resistance of Cast Glass. International Journal of Structural Glass and Advanced Materials Research 5, 195-225 (2021). doi:10.3844/sgamrsp.2021.195.225

Bristogianni, T., Oikonomopoulou, F., Veer, F.A.: On the flexural strength and stiffness of cast glass. Glass Structures & Engineering 6(2), 147-194 (2021). doi:10.1007/s40940-021-00151-z

Bristogianni, T., Oikonomopoulou, F., Yu, R., Veer, F.A., Nijsse, R.: Investigating the flexural strength of recycled cast glass. Glass Structures & Engineering 5(3), 445-487 (2020). doi:10.1007/s40940-020-00138-2

Bristogianni, T., Oikonomopoulou, F., Justino de Lima, C.L., Veer, F.A., Nijsse, R. : Structural cast glass components manufactured from waste glass: Diverting everyday discarded glass from the landfill to the building industry. Heron 63 (1/2 Special issue: Structural Glass), 57-102 (2018)

Other Journal Papers

Oikonomopoulou, F., Bristogianni, T.: Adhesive solutions for cast glass assemblies: ground rules emerging from built case studies on adhesive selection and experimental validation. Glass Structures & Engineering 7(2), 293-317 (2022). doi:10.1007/s40940-022-00178-w

Oikonomopoulou, F., Bristogianni, T., van der Velden, M., Ikonomidis, K.: The adhesively-bonded glass brick system of the Qaammat Pavilion in Greenland: From research to realization. Architecture, Structures and Construction 2(1), 39-62 (2022). doi:10.1007/s44150-022-00031-2

Justino de Lima, C., Aldinger, B., de Haan, P., Bristogianni, T., Veer, F.: Effects of composition on the durability and weathering of flat glass. Glass Structures & Engineering 7(2), 139-155 (2022). doi:10.1007/s40940-022-00175-z

Damen, W., Oikonomopoulou, F., Bristogianni, T., Turrin, M.: Topologically optimized cast glass: a new design approach for loadbearing monolithic glass components of reduced annealing time. Glass Structures & Engineering 7(2), 267-291 (2022). doi:10.1007/s40940-022-00181-1

Oikonomopoulou, F., Bristogianni, T., Veer, F.A., Nijsse, R.: The construction of the Crystal Houses façade: challenges and innovations. Glass Structures & Engineering 3(1), 87-108 (2018). doi:10.1007/s40940-017-0039-4

Oikonomopoulou, F., Bristogianni, T., Barou, L., Veer, F.A., Nijsse, R.: The potential of cast glass in structural applications. Lessons learned from large-scale castings and state-of-the art load-bearing cast glass in architecture. Journal of Building Engineering 20, 213-234 (2018). doi:https://doi.org/10.1016/j.jobe.2018.07.014

Oikonomopoulou, F., Bristogianni, T., Barou, L., Jacobs, E., Frigo, G., Veer, F.A., Nijsse, R.: Interlocking cast glass components, Exploring a demountable dry-assembly structural glass system. Heron 63 (2018)

Oikonomopoulou, F., van den Broek, E. A. M., Bristogianni, T., Veer, F. A., Nijsse, R.: Design and experimental testing of the bundled glass column. Glass Structures & Engineering 2(2), 183-200 (2017). doi:10.1007/s40940-017-0041-x

Veer, F.A., Bristogianni, T., Baardolf, G.: A case study of apparently spontaneous fracture. Glass Structures & Engineering 3(1), 109-117 (2018). doi:10.1007/s40940-017-0047-4

Veer, F., Bristogianni, T., Justino de Lima, C.L.: An overview of some recent developments in glass science and their relevance to quality control in the glass industry. Heron 63, 15-30 (2018)

Barou, L., Oikonomopoulou, F., Bristogianni, T., Veer, F. and Nijsse, R.: Structural glass: A new remedial tool for the consolidation of historic structures. Heron 63 (2018)

Heinzelmann, F., Bristogianni, T., Teuffel, P.: Adaptive Liquid Lens and Sunlight Redirection. International Journal of Architectural Computing 12(2), 129-153 (2014). doi.org/10.1260/1475-472X.12.2.129

Conference Papers as first author

Bristogianni, T., Oikonomopoulou, F.: Reinforced glass: Structural potential of cast glass beams with embedded metal reinforcement In: Zingoni, A. (ed.) Current Perspectives and New Directions in Mechanics, Modelling and Design of Structural Systems. CRC Press, London (2022)

Bristogianni, T., Oikonomopoulou, F., Veer, F.A., Nijsse, R.: The effect of manufacturing flaws in the meso-level structure of cast glass on the structural performance. In: Zingoni, A. (ed.) Advances in Engineering Materials, Structures and Systems: Innovations, Mechanics and Applications. pp. 1703-1708. CRC Press, Leiden (2019)

Bristogianni, T., Oikonomopoulou, F., Justino de Lima, C.L., Veer, F.A. & Nijsse, R.: Cast Glass Components out of Recycled Glass: Potential and Limitations of Upgrading Waste to Load-bearing Structures In: Louter, Bos, Belis, Veer, Nijsse (Eds.) Challenging Glass 6 Conference, Delft, NL. TU Delft Open (2018)

Bristogianni, T., Oikonomopoulou, F., Veer, F., Snijder, A., Nijsse, R.: Production and Testing of Kiln-cast Glass Components for an Interlocking, Dry-assembled Transparent Bridge. Glass Performance Days 2017 Conference Proceedings, Tampere, Finland (2017)

Bristogianni, T., Oikonomopoulou, F., Veer, F.A., Nijsse, R.: Design and production of a structural cast glass element for a transparent dome. In: Zingoni, A. (ed.) Insights and Innovations in Structural Engineering, Mechanics and Computation: Proceedings of the 6th International Conference on Structural Engineering, Mechanics and Computation, SEMC, Cape Town, pp. 1662-1667. CRC Press (2016)

Other Conference Papers

Oikonomopoulou, F., Koniari, A.M., Damen, W., Koopman, D., Stefanaki, I.M., Bristogianni, T.: Topologically optimized structural glass megaliths: Potential, challenges and guidelines for stretching the mass limits of structural cast glass. In: Zingoni, A. (ed.) Current Perspectives and New Directions in Mechanics, Modelling and Design of Structural Systems. CRC Press, London (2022)

Barou, L., Oikonomopoulou, F., Bristogianni, T., Veer, F., Nijsse, R.: Fill-in-Glass Restoration: Exploring Issues of Compatibility for the Case of Schaesberg Castle. In: Roca, P., Pelà, L., Molins, C. (Eds) 12th International Conference on Structural Analysis of Historical Constructions (SAHC) (2021)

Oikonomopoulou, F., Bhatia I.S., Damen, W., van der Weijst, F., Bristogianni, T. : Rethinking the Cast Glass Mould. Challenging Glass 7, Ghent University, Belgium. (2020)

Yu, R., Bristogianni, T., Veer, F. A., & Nijsse, R.: The Application of Waste Float Glass, Recycled in Structural Beams made with the Glass Casting Method. In: Louter, C., Bos, F. & Belis, J. (ed.) Challenging Glass Conference: Conference on Architectural and Structural Applications of Glass, CGC 7, Ghent University, Belgium (2020)

Anagni, G.M., Bristogianni, T., Oikonomopoulou, F. Rigone, P., Mazzucchelli, E.S.: Recycled Glass Mixtures as Cast Glass Components for Structural Applications, Towards Sustainability. Challenging Glass Conference 7: Conference on Architectural and Structural Applications of Glass, Ghent University, Belgium (2020). doi: 10.7480/cgc.7.4482

Eskes, A., de Krom, D., Bristogianni, T., Veer, F., Rammig, L., Nijsse, R.: The Production and Performance of Heat Bonded Glass Connections, an experimental study Paper presented at the

Challenging Glass 7: Conference on Architectural and Structural Applications of Glass, Ghent University, Belgium (2020)

Oikonomopoulou, F., Bristogianni, T., Barou, L., Veer, F.A.: Dry interlayers out of cast polyurethane rubber for interlocking cast glass structures: experimental exploration and validation. In: Zingoni, A. (ed.) Advances in Engineering Materials, Structures and Systems: Innovations, Mechanics and Applications. pp. 1709-1714. CRC Press, Leiden (2019)

Oikonomopoulou, F., Bristogianni, T., Louter, C., Veer, F., Nijsse, R.: Education on Structural Glass Design: Redefining glass through the design of innovative, full-glass structures. In: Cruz, J.S.P. (ed.) Structures and Architecture: Bridging the Gap and Crossing Borders. Proceedings of the Fourth International Conference on Structures and Architecture (ICSA 2019), Lisbon, Portugal. CRC Press (2019)

Oikonomopoulou, F., Bristogianni, T., Barou, L., Jacobs, E., Frigo, G., Veer, F., Nijsse, R.: A Novel, Demountable Structural Glass System Out of Dry-Assembly, Interlocking Cast Glass Components In: Louter, Bos, Belis, Veer, Nijsse (Eds.) Challenging Glass 6 Conference, Delft, NL. TU Delft Open (2018)

Veer, F., Bristogianni, T., Justino de Lima, C.L.: A Re-evaluation of the Physiochemistry of Glass on the Basis of Recent Developments and its Relevance to the Glass Industry In: Louter, Bos, Belis, Veer, Nijsse (Eds.) Challenging Glass 6 Conference, Delft, NL. TU Delft Open (2018)

Barou, L., Oikonomopoulou, F., Bristogianni, T., Veer, F. and Nijsse, R.: Dematerialization of the Ruins: Glass as a Promising Restorative Material for the Consolidation of Historic Structures In: Louter, B., Belis, Veer, Nijsse (Eds.) Challenging Glass 6 Conference, Delft, NL. TU Delft Open (2018)

Barou, L., Bristogianni, T., Oikonomopoulou, F.: Transparent Restoration. Paper presented at the IABSE Bath 2017: Creativity and collaboration: Instilling imagination and innovation in structural design, Bath, UK (2017)

Oikonomopoulou, F., Bristogianni, T., Veer, F. & Nijsse, R.: Developing the bundled glass column. In: Cruz, J.S.P. (ed.) Structures and Architecture Beyond their Limits. Proceedings of 3rd International Conference on Structures and Architecture (ICSA 2016), Guimaraes, Portugal, pp. 1014–1021. CNC Press (2016)

Oikonomopoulou, F., Bristogianni, T., Karron, K., Groot, C., Veer, F., Nijsse, R.: Restoring and structurally reinforcing historic monuments by glass. In: Zingoni, A. (ed.) Proceedings of the 6th International Conference on Structural Engineering, Mechanics and Computation, Cape Town, South Africa (2016)

Snijder, A., Smits, J., Bristogianni, T. & Nijsse, R.: Design and Engineering of a Dry Assembled Glass Block Pedestrian Bridge. In: Belis, J., Louter, C. & Bos, F. (eds.) Conference on

Architectural and Structural Applications of Glass (CGC5), Ghent, Belgium. Universiteit Gent (2016)

Oikonomopoulou, F., Bristogianni, T., Nijsse, R., Veer, FA.: Innovative structural applications of adhesively bonded solid glass blocks. In: Glass Performance Days (GPD), Tampere, Finland (2015)

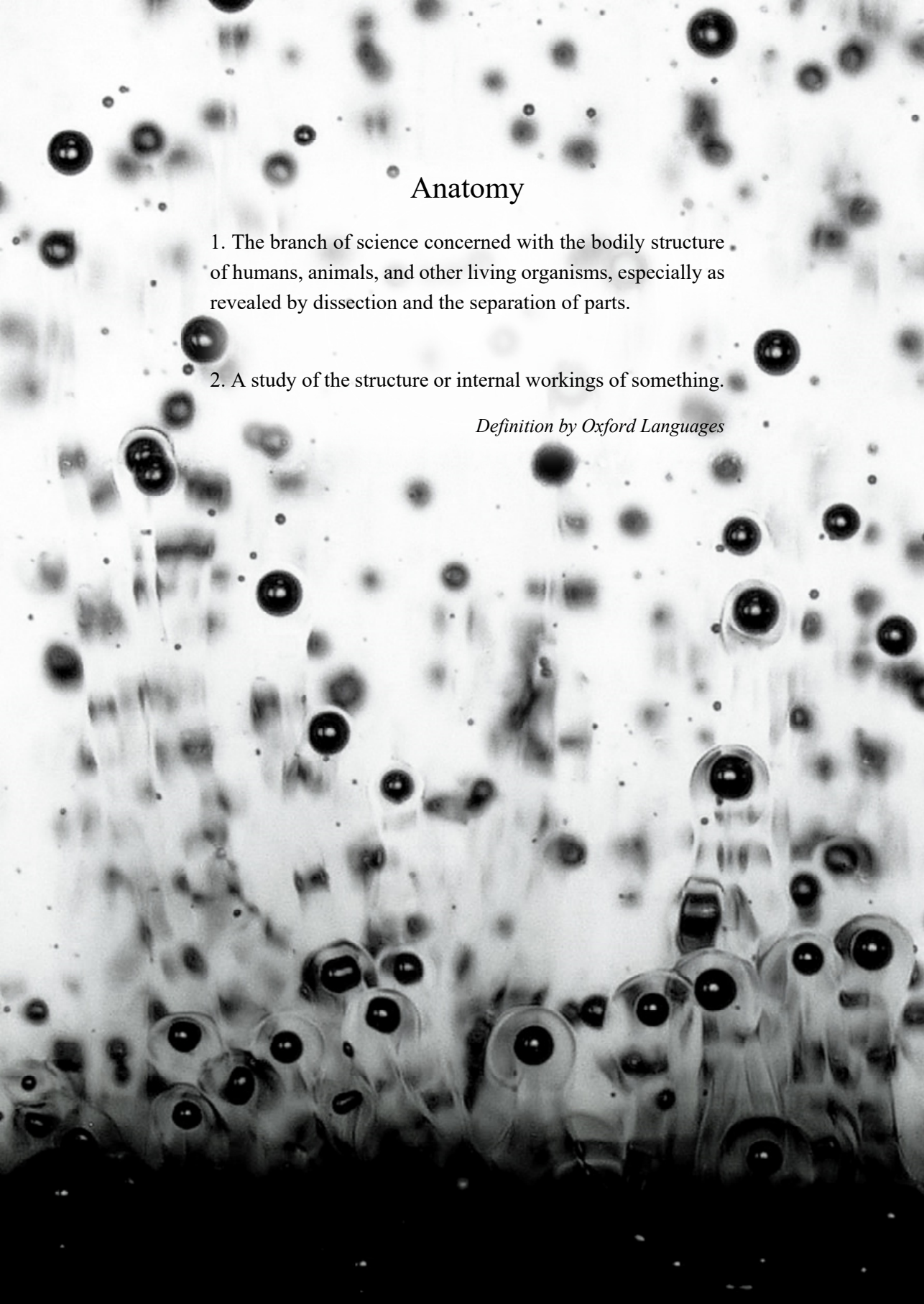

Anatomy

1. The branch of science concerned with the bodily structure of humans, animals, and other living organisms, especially as revealed by dissection and the separation of parts.

2. A study of the structure or internal workings of something.

Definition by Oxford Languages

Previous page: Frog eggs detected in cast glass…or literally, escaping bubbles surrounded by cord in a recycled soda lime silica glass, kiln-cast at 1120ºC.

Glass, in our daily experience, is clear, perfect, flawless.
By habit, our eyes pass through the material and focus on the object behind, as if glass itself is absent, devoid of substance.

What a surprise to our eyes, when encountering a piece of cast glass for the first time! A multitude of imperfections creates pathways for our eyes to follow and marks for our eyes to stop. This world of imperfections, threaded into the amorphous structure of cast glass, forms unique identities and reminds us of the way each piece of glass was made. Imperfections are inherent to cast glass, adding beauty and subtracting strength; properties will vary per identity.

Through this dissertation, you are presented with a study of anatomy. Hundreds of cast glass specimens were created, sliced and observed, in search of these identities and the strength of cast glass. And though we may be far from mastering this knowledge, through the learning process, the wonderful potential of cast glass is starting to unfold in front of us.

9 789068 240740